Elucidating the involvement of thermosensitive ion channels (TRPV4 and TRPM8) in mitochondrial structure-function relationship: Significance in physiology and diseases

By

Tusar Kanta Acharya
LIFE11201704006

National Institute of Science Education and Research (NISER) - Bhubaneswar

A thesis submitted to the
Board of Studies in Life Sciences
In partial fulfillment of requirements
for the Degree of

DOCTOR OF PHILOSOPHY

of

HOMI BHABHA NATIONAL INSTITUTE



December, 2022

HOMI BHABHA NATIONAL INSTITUTE

RECOMMENDATIONS OF THE VIVA VOCE COMMITTEE

As members of the Viva Voce Committee, we certify that we have read the dissertation prepared by **Tusar Kanta Acharya** entitled **"Elucidating the involvement of thermosensitive ion channels (TRPV4 and TRPM8) in mitochondrial structure-function relationship: Significance in physiology and diseases"** and recommend that it may be accepted as fulfilling the thesis requirements for the award of Degree of Philosophy.

Chairman – Dr. Asima Bhattacharyya		Date: 8th June 2023
Guide / Convener – Dr. Chandan Goswami	Chandan Goswami 8th June 2023	Date: 8th June 2023
Examiner – Prof. Pradeep Kumar G		Date: 8th June 2023
Member 1 – Dr. Praful Singru		Date: 8th June 2023
Member 2 –Dr. Kishore CS Panigrahi		Date: 8th June 2023
Member 3 – Dr. Sanjib Kar	Sanjib Kar	Date: 8th June 2023

Final approval and acceptance of this thesis is contingent upon the candidate's submission of the final copies of the thesis to HBNI.

I/We hereby certify that I/we have read this thesis prepared under my/our direction and recommend that it may be accepted as fulfilling the thesis requirement.

Chandan Goswami

Date: 8th June 2023

Place: NISER, BHUBANESWAR

Dr. Chandan Goswami

(Thesis Supervisor)

STATEMENT BY AUTHOR

This dissertation has been submitted in partial fulfillment of requirements for an advanced degree at Homi Bhabha National Institute (HBNI) and is deposited in the library to be made available to borrowers under the rules of the HBNI.

Brief quotations from this dissertation are allowable without special permission, provided that accurate acknowledgment of the source is made. Requests for permission for extended quotation from or reproduction of this manuscript in whole or in part may be granted by the Competent Authority of HBNI when in his or her judgment the proposed use of the material is in the interests of scholarship. In all other instances, however, permission must be obtained from the author.



Tusar Kanta Acharya

DECLARATION

I, hereby declare that the investigation presented in the thesis has been carried out by me. The work is original and has not been submitted earlier as a whole or in part for a degree/ diploma at this or any other Institution / University.

Tusar Kanta Acharya

Tusar Kanta Acharya

List of Publications arising from the thesis

1. Acharya, T.K., Pal, S., Ghosh, A., Kumar, S., Kumar, S., Chattopadhyay, N., Goswami, C. (2023) TRPV4 regulates osteoblast differentiation and mitochondrial function that are relevant for channelopathy. *Frontiers in Cell and Developmental Biology*. 11, p1066788.

2. Acharya, T.K., Kumar, S., Rokade, T.P., Chang, Y.T. and Goswami, C. (2023) TRPV4 regulates mitochondrial Ca2+-status and physiology in primary murine T cells based on their immunological state. *Life Sciences*, 318, p.121493.

3. Acharya, T.K., Kumar, A. Kumar, S. Goswami, C. (2022) TRPV4 interacts with MFN2 and facilitates endoplasmic reticulum-mitochondrial contact points for Ca $^{2+}$-buffering. *Life Sciences*, 310: 121112.

4. Acharya, T.K., Kumar, A., Majhi, R.K., Kumar, S., Chakraborty, R., Tiwari, A., Smalla, K.H., Liu, X., Chang, Y.T., Gundelfinger, E.D. and Goswami, C. (2022) TRPV4 acts as a mitochondrial Ca^{2+}-importer and regulates mitochondrial temperature and metabolism. *Mitochondrion*. 67: 38-58.

5. Acharya, T.K., Sahu, R.P., Kumar, S., Rokade, T.P., Chakraborty, R., Dubey, N.K., Shikha, D., Chawla, S. and Goswami, C. (2022) Function and regulation of thermosensitive ion channel TRPV4 in the immune system. *Current Topics in Membranes*, 89, pp.155-188.

6. Acharya, T.K., Tiwari, A., Majhi, R.K. and Goswami, C. (2021) TRPM8 channel augments T-cell activation and proliferation. *Cell Biology International*, 45, pp.198-210.

7. Acharya, T.K., Kumar, S., Tiwari, N., Ghosh, A., Tiwari, A., Pal, S., Majhi, R.K., Kumar, A., Das, R., Singh, A. and Maji, P.K., Chattopadhyay, N., Goswami, L., Goswami, C. 2021. TRPM8 channel inhibitor-encapsulated hydrogel as a tunable surface for bone tissue engineering. *Scientific Reports*, 11, pp.1-16.

Other Publications

8. Mohapatra, A., Kumar, S., **Acharya, T.K.**, Goswami, C. and Bhaumik, S. (2023) Highly stable multi-encapsulated red-emitting cesium lead halide nanocrystals for efficient copper ion detection and imaging in live cells. *Journal of Alloys and Compounds*, *947*, p.169453.

9. Kar, M.R., Kumar, S., **Acharya, T.K.**, Goswami, C. and Bhaumik, S. (2023) Highly water-stable, luminescent, and monodisperse polymer-coated CsPbBr 3 nanocrystals for imaging in living cells with better sensitivity. *RSC advances*, *13*(9), pp.5946-5956.

10. Singh, A., Kumar, S., **Acharya, T.K.**, Goswami, C. and Goswami, L. (2022) Application of nanohydroxyapatite-polysaccharide based biomaterial for bone cell mineralization in tissue engineering. *Materials Today Communications*, p.103783.

11. Chakraborty, R*, **Acharya, T.K***, Tiwari, N., Majhi, R.K., Kumar, S., Goswami, L. and Goswami, C., (2022) Hydrogel-mediated release of TRPV1 modulators to fine tune osteoclastogenesis. *ACS Omega*. (* **Equal First Author**)

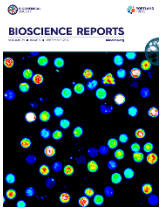
12. Kar, M.R., Chakraborty, R., Patel, U., Ray, S., **Acharya, T.K**., Goswami, C. and Bhaumik, S. (2022) Impact of Zn-doping on the composition, stability, luminescence properties of silica coated all-inorganic cesium lead bromide nanocrystals and their biocompatibility. *Materials Today Chemistry*, *23*, p.100753.

13. Das, M., Maity, D., **Acharya, T.K.,** Sau, S., Giri, C., Goswami, C. and Mal, P. (2021) Lowest aqueous picomolar fluoride ions and *in vivo* aluminum toxicity detection by an aluminum (iii) binding chemosensor. *Dalton Transactions*, *50*(8), pp.3027-3036.

14. Sahoo, S.S., Majhi, R.K., Tiwari, A., **Acharya, T.K**., Kumar, P.S., Saha, S., Kumar, A., Goswami, C. and Chattopadhyay, S. (2019) Transient receptor potential ankyrin1 channel is endogenously expressed in T cells and is involved in immune functions. *Bioscience Reports*, *39*(9). **Coverpage article**.

15. Kumar, A., Majhi, R.K., **Acharya, T.K**., Smalla, K.H., Gundelfinger, E.D. and Goswami, C. (2018) TRPV4 interacts with mitochondrial proteins and acts as a mitochondrial structure-function regulator. *BioRxiv*, p.330993.

Cover page Article



Conference Presentations

Oral Presentation:

* Selected for oral presentation at Asia-Pacific Microscopy Conference-2020, organized by Electron Microscopy Society of India, at Hyderabad, 3-7 February 2020.

* Best Oral Presentation award in Medical Biotechnology at Annual Meeting of Society of Biotechnologists India (SBTI), 22-23 January 2021.

* Selected for oral presentation at International conference on Materials for the millennium-MATCON organized by Cochin University of Science and Technology, 15-19 March 2021.

Poster Presentation:

* Presented a poster at International conference on Mitochondria in human disease organized by Journal of Internal Medicine and Karolinska Institute, 16-18 September, 2019, Stockholm, Sweden.

* Presented a poster at 2nd International Online Meeting of the Junior European Calcium Society, 23-24 November 2021.

* Presented poster at "Insights into the key trends in Biomaterial Research", organized by DBT-Institute of Life Sciences, Bhubaneswar, Odisha on 27th and 28th, September 2022.

Tusar Kanta Acharya

Tusar Kanta Acharya

Dedicated to…

My Parents

&

Friends

ACKNOWLEDGEMENTS

I want like to express my deep and sincere gratitude to my thesis supervisor Dr. Chandan Goswami for his unprecedented support, guidance, and patience. His comprehensive knowledge in this field and enthusiasm for science have constantly encouraged me to learn and strive harder. I will be eternally grateful to him for the scientific skills he taught me. This work would have been seemingly difficult without his cooperation. I would also like to thank him for his patience while critically editing this thesis. I want to thank my doctoral committee members Dr. Asima Bhattacharyya (NISER, Bhubaneswar), Dr. Praful Singru (NISER, Bhubaneswar), Dr. Kishore CS Panigrahi (NISER, Bhubaneswar), Dr. Sanjib Kar (NISER, Bhubaneswar) for their constant support and scientific suggestions and feedback during my research work. I am thankful to the current and former chairpersons of School of Biological Sciences, NISER. I acknowledge all the faculties and staff of biological sciences for their constant help and support. Support from SBS CIF, imaging facility, CIS for SEM, and Raman spectroscopy facility is greatly acknowledged. I also want to thank the animal house facility of NISER and especially Dr. Saurabh Chawla and all the animal house staff for helping me conduct *in vivo* experiments.

This work would not have been possible without the support of collaborative scientists who provided constructs and samples. In this regard, I want to thank Prof. Young Tae Chang (POSTECH, Korea) for providing MTY, ETY, ATP red, and GTP green dye for my research work. Prof. Eckart D, Gundelfinger, and Dr. Karl-Heinz Smalla (Leibniz Institute, Magdeburg, Germany) for providing synaptosomal fractions of the rat brain for some critical experiments. I want to thank Dr. Rikke Katrine Olsen (Aarhus University, Denmark) for helping us to analyze the critical information and data. I want to thank Dr. Luna Goswami (KIIT Deemed To Be University, Bhubaneswar) for providing us with hydrogels for our research work, Dr. Mamoni

Dash (ILS, Bhubaneswar) for providing us MC3T3-E1 and K7M2 cell lines for our work, Dr. Saikat Bhoumik (ICT, Bhubaneswar), Dr. Prasenjit Mal (NISER, Bhubaneswar) for some collaborative research work.

I am highly obliged to all the funding agencies like DAE, DBT, ICMR and UGC for providing fellowship and all financial assistance during my research tenure.

My heartfelt thanks to all my present and past lab members, namely, Dr. Ashutosh Kumar, Dr. Manoj Yadav, Dr. Rakesh Kumar Majhi, Dr. Ankit Tiwari, Dr. Somdatta Saha, Dr. Rashmita Das, Nikhil, Arijit, Ranabir, Srujanika and present lab members Dr. Satish Kumar, Ramprasad, Nishant, Sushama, Deepsikha, Barsha didi, Parnashree, Shamit, Tejas, Harshit, Shreya, Subham, Nilesh, Raima, Ramijur, Vikash and all other lab members. I want to especially thank Satish bhai, Shamit, Tejas and Ranabir for helping me complete my pending thesis experiments. They were not only labmates but also acted like my family whenever I needed to talk and share my frustration.

Apart from lab members I would like to extend my gratitude towards my batchmates and friends namely, Dhyan, Umesh, Raktim, Sohini, Debasis, Prakash, Jyoti, Asish, Giri, Basu, Rishi, Aditya, Pratyush, Surya, Sukanya, Rojalin, Saumya, Kewal, Binayak, and all other friends for encouraging and motivating throughout my journey.

I am grateful to my mother and sister who have been the strength in this journey. I want to express my special gratitude to my wife Pooja who took all the suffering and sacrifices for my stake and always supported throughout my journey. I also want to thank all my family members and in laws for their support and believe in me. It would have been impossible to reach here without the support, love and affection of my family and friends.

Tusar Kanta Acharya

Tusar Kanta Acharya

Table of Content

Summary		i-iii
List of figures		iv-ix
List of Tables		x
List of Abbreviations		xi-xiii
Chapter 1: Introduction		
1.1	**General introduction on TRP ion channel super family**	1
1.1.1	Discovery of TRP channel	1
1.1.2	Classification of TRP channel	2
1.1.3	Structure of TRP channel	4
1.1.4	Tissue-specific distribution and physiological functions of different TRP channels in vertebrate	7
1.2	**Differential regulation of TRP channels by endogenous and exogenous ligands**	**11**
1.2.1	Pharmacological modulation of TRP channels by exogenous ligands	12
1.2.1.1	TRPV channels	12
1.2.1.2	TRPA1 channel	15
1.2.1.3	TRPM channels	16
1.2.1.4	TRPC channels	18
1.2.2	Modulation of TRP channels by endogenous compounds	22
1.3	**Sub-cellular distributions of TRP channels**	**23**
1.4	**Overall architecture and structure of TRPV4**	**24**
1.4.1	Expression and function of TRPV4 in different tissue and cells	27
1.4.2	TRPV4 mutation mediated genetic disorders	30
1.5	**Specific introduction of TRPM8**	**34**
1.5.1	General architecture and structure of TRPM8	34
1.5.2	Expression and function of TRPM8 in different tissue and cellular systems	36
1.5.3	TRPM8 in pathophysiology	37
1.6	**Important aspects of mitochondrial research**	**39**
1.6.1	Mitochondria acts as a cellular sensor	40
1.6.2	Mitochondrial Ca^{2+} regulation	42
1.6.3	Regulation of mitochondrial membrane potential	44
1.6.4	Mitochondrial heterogeneity	46
1.6.5	Mitochondrial communication with other organelles	48

1.6.6 Mitochondria function as a thermostat 50

1.7 Specific objectives of this study 52

Chapter 2: Results

2.1 Characterization of TRPV4 channel in intracellular organelles 55

2.1.1 TRPV4 is present in mitochondria endogenously 55

2.1.2 TRPV4 colocalizes with mitochondrial markers in isolated mitochondria 57

2.1.3 Localization of TRPV4 in mitochondrial membrane 57

2.1.4 TRPV4 contributes in mitochondrial Ca^{2+}-influx in cell-free system 59

2.1.5 TRPM8 is localized in mitochondria endogenously 61

2.2 If and how TRPV4 regulates mitochondrial metabolism? 64

2.2.1 TRPV4 regulates mitochondrial Ca^{2+}-dynamics 64

2.2.2 Presence of TRPV4 enhances the basal level Ca^{2+} within mitochondria 67

2.2.3 TRPV4 affects both mitochondrial Ca^{2+}-levels and mitochondrial numbers 67

2.2.4 TRPV4 regulates mitochondrial ATP & GTP production 72

2.2.5 TRPV4-expressing cells display an altered mitochondrial morphology 74

2.2.6 Endogenous TRPV4 colocalized with endogenous MFN2 77

2.2.7 TRPV4 regulates mitochondrial fusion 79

2.2.8 TRPV4 is present in the ER-mito contact site 81

2.2.9 TRPV4 modulation regulates the number of ER-mito contact points 82

2.2.10 Presence of TRPV4 regulates basal mitochondrial Ca^{2+}-levels 88

2.3 If and how TRPM8 regulates mitochondrial metabolism? 91

2.3.1 Long term Menthol treatment elevates cytosolic and mitochondrial Ca^{2+}-levels 91

2.3.2 Menthol alters the mitochondrial morphology 93

2.3.3 Menthol causes instantaneous rise in mitochondrial Ca^{2+} 93

2.3.4 Menthol affects sub-population dynamics based on the Ca^{2+}-status of individual mitochondria 96

2.3.5 Menthol affects mitochondrial membrane potential and ATP levels 98

2.3.6 Menthol elevates the mitochondrial superoxides and Cardiolipin levels 100

2.3.7 Menthol regulates the ER-mito contact points 100

2.3.8 Menthol regulates the mitochondria but not ER temperature is osteosarcoma cells 100

2.3.9 TRPM8 regulates mitochondrial morphology 104

2.3.10 TRPM8 regulates mitochondrial Ca^{2+}-dynamics 105

2.3.11 TRPM8 modulates both mitochondrial Ca^{2+} level and mitochondrial numbers 108

2.3.12 Chronic TRPM8 modulation affects both basal cytosolic and mitochondrial Ca^{2+}-status in Saos-2 cells 111

2.3.13	Regulation of mitochondrial membrane potential and ATP level by TRPM8	112
2.3.14	TRPM8 modulates mitochondrial ROS generation	113
2.3.15	TRPM8 activation changes mitochondrial Cardiolipin status	114
2.3.16	TRPM8 regulates mitochondrial and ER temperature	115
2.3.17	TRPM8 activation decreases ER-mito contact points	117
2.3.18	TRPM8 regulates basal mitochondrial Ca^{2+} and membrane potential in MSCs	120
2.3.19	TRPM8 modulation decreases mitochondrial Cardiolipin status in MSCs	121
2.3.20	TRPM8 regulates mitochondrial temperature in MSCs	122
2.3.21	TRPM8 regulates mitochondrial Ca^{2+} and temperature in isolated mitochondria	123
2.4	**TRPV4 mediated mitochondrial regulation: impact on bone cell functions and application in bone tissue engineering**	**126**
2.4.1	Hydrogel containing TRPV4 modulating drugs regulates the expression and functionality of TRPV4 channel in MSCs	127
2.4.2	Hydrogel containing TRPV4 modulator drug effects morphology and physiology of MSCs	129
2.4.3	Hydrogel containing TRPV4 modulatory drugs effectively regulate mitochondrial Reactive Oxygen Species (ROS), cytosolic NO and mitochondrial Cardiolipin status in MSCs	131
2.4.4	Hydrogel encapsulated with TRPV4 drugs regulates cellular parameters during osteoblast differentiation	134
2.4.5	Hydrogel containing TRPV4 modulator drugs enhance metabolic state of MSCs during osteoblast differentiation	136
2.4.6	TRPV4 modulator containing hydrogel enhance *in vitro* osteogenesis in MSCs	138
2.4.7	Effect of TRPV4 modulators containing hydrogel in *in-vivo* bone repair	139
2.4.8	*In vivo* analysis for biosaftey	143
2.4.9	Osteointegration analysis by SEM	145
2.4.10	Assessment of the quality of the newly formed bone	146
2.5	**TRPM8-mediated mitochondrial regulation: impact on bone cell functions and application in bone tissue engineering**	**149**
2.5.1	TRPM8 channel modulates intracellular Ca^{2+}-dynamics in osteoblasts	149
2.5.2	CMT: HEMA hydrogel act as suitable surface for growth of MSCs	150
2.5.3	CMT: HEMA encapsulated with TRPM8-specific compounds regulate cellular morphology	151
2.5.4	CMT: HEMA encapsulated with TRPM8-specific compounds induce differential ROS signaling	153

2.5.5	CMT: HEMA encapsulated with TRPM8-specific compounds affect mitochondrial membrane potential	153
2.5.6	CMT: HEMA encapsulated with TRPM8-specific inhibitor enhances bone differentiation and mineralization and osteogenic markers	155
2.6	**TRPV4- mediated mitochondrial regulation: impact on T cell activation**	**161**
2.6.1	TRPV4 regulates mitochondrial Ca^{2+}-status and physiology in primary murine T cells based on its immunological state	161
2.6.2	TRPV4 colocalizes with mitochondria in Tcells	162
2.6.3	TRPV4 regulates basal cytosolic and mitochondrial Ca^{2+}-load in T cells	164
2.6.4	TRPV4 activation causes instantaneous Ca^{2+}-influx in primary murine Tcells	167
2.6.5	Activation of TRPV4 causes instant increase in mitochondrial Ca^{2+} amount	169
2.6.6	Mitochondrial superoxide and mitochondrial membrane potential are affected by TRPV4 in resting and in TCR treated T cells	174
2.6.7	TRPV4 activation affects mitochondrial ATP production and Cardiolipin status differently in resting and in TCR- treated T cells	176
2.6.8	Mitochondrial and ER temperature of T cells is affected by TRPV4 modulation	178
2.6.9	TRPV4 modulation regulates the ER number, mitochondrial number and their co- localization in primary T cells	180
2.7	**TRPM8- mediated mitochondrial regulation: impact on T cell activation**	**184**
2.7.1	TRPM8 is localized in plasma membrane as well as in mitochondria endogenously	184
2.7.2	TRPM8 is functional in $CD3^+$ T cells	185
2.7.3	TRPM8 regulates mitochondrial Ca^{2+}-levels and dynamics	188
2.7.4	TRPM8 modulation increases basal mitochondrial and cytosolic Ca^{2+}-level	192
2.7.5	TRPM8 regulates mitochondrial ATP production and membrane potential	195
2.7.6	Regulating TRPM8 affects Cardiolipin and mitochondrial superoxides levels	197
2.7.7	Mitochondrial and ER temperature are regulated by TRPM8 specific modulations	199
2.7.8	ER-mito contact points increases upon TRPM8 inhibition	201
2.8	**Characterization of TRPV4-mediated channelopathies in the context of mitochondrial abnormalities**	**205**
2.8.1	Mitochondrial morphology is altered by TRPV4 mutants	205
2.8.2	Expression of different TRPV4 mutation induce mitochondrial ROS	211
2.8.3	Novel mutation at the N-terminal of TRPV4 alters mitochondrial structure and metabolism	214
2.8.4	TRPV4-S372L mutation regulates cytosolic Ca^{2+}-level	221
2.8.5	TRPV4-S372L mutation alters mitochondrial Ca^{2+}-level	223
2.8.6	TRPV4-S372L mutation alters mitochondrial ROS and ATP level	223

2.8.7 Expression of TRPV4-S372L mutation regulates mitochondrial Cardiolipin and ER temperature level 224

Chapter 3 Discussion

3.1 Physical presence of TRP channels in the mitochondria 227

3.1.1 Localization of TRPV4 channel in mitochondria 227

3.1.2 TRPV4 as a part of MAM 229

3.1.3 Localization of TRPM8 channel in mitochondria 230

3.1.4 Functional characterisation of TRP channels in mitochondrial function in T cell 230

3.1.5 Presence of endogenous TRPV4 in the mitochondria of T cell has immunological consequence 231

3.1.6 TRPM8 regulates mitochondrial function in T-cells 232

3.2 Importance of TRP channels in mitochondria: Regulation of mitochondrial Ca^{2+} -homeostasis 233

3.2.1 TRPV4 regulates mitochondrial Ca^{2+}-influx and mitochondrial membrane potentiality 233

3.2.2 TRPV4 as positive regulator for mitochondrial Ca^{2+} and negative regulator for ER-mito contact points 235

3.2.3 Mitochondrial Ca^{2+} as a factor for determining the ER-mito contact points 237

3.2.4 TRPV4 makes close contact with lysosome for Ca^{2+}-mobilization too 238

3.2.5 Menthol regulates mitochondrial Ca^{2+} and metabolism in osteogenic cell 241

3.2.6 TRPM8 regulates mitochondrial Ca^{2+}-metabolism 241

3.2.7 TRPM8 activation decreases ER-mito contact sites 242

3.2.8 TRPV4 is involved in the maintenance of mitochondrial Ca^{2+}-level in T-cell 243

3.2.9 TRPV4 regulates ER-mito contact points in T-cells 244

3.2.10 TRPM8 activation increases cellular and mitochondrial Ca^{2+} in T cells 245

3.2.11 TRPM8 activation increases ER-mito contact points in resting and TCR treated cells 246

3.3 Importance of TRP channels in regulation of mitochondrial metabolism 247

3.3.1 TRPV4 interacts with mitochondrial proteins 247

3.3.2 TRPV4 activation regulates mitochondrial protein level 248

3.3.3 To counteract mitochondrial stress, TRPV4 triggers the UPR pathway 250

3.3.4 Menthol regulates mitochondrial metabolism 251

3.3.5 Menthol has some indirect effect independent of TRPM8 252

3.3.6 TRPM8 regulates mitochondrial membrane potential and ATP level 253

3.3.7 TRPM8 induces mitochondrial ROS and changes Cardiolipin level 254

3.3.8 TRPV4 regulates mitochondrial metabolism relevant for T cell activation 254

3.3.9	TRPV4 regulates Cardiolipin levels in T-cells through complex Ca^{2+}-signaling	255
3.3.10	TRPM8 regulates mitochondrial function in T-cells	257
3.3.11	TRPM8 increases mitochondrial ATP level in TCR treated T cell	258
3.3.12	Regulation of mitochondrial membrane potential and Cardiolipin level by TRPM8	258
3.3.13	TRPM8 regulates mitochondrial ROS level in T-cell	259
3.4	**TRP channels as regulators of mitochondrial temperature and quality**	**259**
3.4.1	TRPV4 as mitochondrial temperature sensor	259
3.4.2	TRPV4 at mitochondria is relevant for regulation of body temperature	261
3.4.3	Menthol decreases mitochondrial temperature	261
3.4.4	TRPM8 activation increases mitochondrial temperature but not ER temperature	264
3.4.5	TRPV4 regulates temperature of subcellular organelles of T cell in context-dependent manner	266
3.4.6	TRPM8 modulates mitochondrial and ER temperature in T-cells	267
3.5	**TRP channels at mitochondria: Implications in health and pathophysiology**	**268**
3.5.1	Importance of TRPV4 in ER-mitochondrial contact point regulation in neuropathic pain and other diseases	268
3.5.2	Importance of mitochondrial TRPV4 in pathophysiology	268
3.5.3	TRPV4 mutants alter mitochondrial morphology	269
3.6	**Fine regulation of TRP channel as a future therapeutics**	**270**
3.6.1	Regulation of bone mineralization *in vitro* and *in vivo*: TRPV4 and TRPM8 as suitable targets for bone tissue engineering	270
3.6.2	TRPV4 modulator-encapsulated hydrogel can be used as a possible target for bone tissue engineering	271
3.6.3	TRPV4-modulatory drug-based hydrogel provides a suitable microenvironment for bone differentiation	272
3.6.4	TRPV4 regulates ossification *in vitro* by modulating the mitochondrial activity	273
3.6.5	Involvement of TRPV4 activator encapsulated hydrogel in *in vivo* bone repair	274
3.6.6	TRPM8 inhibitor encapsulated hydrogel as a tunable surface for bone tissue engineering	274
3.6.7	TRPM8 drug encapsulated hydrogels regulate cellular Ca^{2+}-level and organellar function in MSCs	275
3.6.8	TRPM8 drug-encapsulated hydrogel acts as a suitable surface for the growth of osteogenic cells	276
3.6.9	Differential expression of TRPV4 and TRPM8 in Mesenchymal stem cells growing over the TRPM8 drug encapsulated hydrogel surface	277
3.6.10	TRPM8 inhibitor AMTB-loaded hydrogels promote osteogenesis in MSCs *in vitro*	277

Chapter 4 Conclusion

Conclusion and future prospects 279

Chapter 5 Materials and Methods

5.1 Materials 282

5.1.1 Chemicals used 282

5.1.2 Kits Markers and Enzymes 284

5.1.3 Primary Antibodies 284

5.1.4 Secondary Antibodies 285

5.1.4 Constructs Used 285

5.1.5 Cell lines and primary cells 286

5.2 Methods 286

5.2.1 Methods related to Molecular Biology 286

5.2.1.1 Construct Preparation 286

5.2.1.2 Polymerase Chain Reaction (PCR) 286

5.2.1.3 Site Directed Mutagenesis and construct preparation 287

5.2.1.4 Agarose Gel Electrophoresis 289

5.2.1.5 Restriction digestion 290

5.2.1.6 Ligation of insert and vector 290

5.2.1.7 Transformation 290

5.2.1.8 Competent Cell Preparation by RbCl method 291

5.2.2 Biochemical techniques 293

5.2.2.1 SDS-PAGE 293

5.2.2.2 Coomassie staining 295

5.2.2.3 Western blot analysis 295

5.2.3 Methods related to cell biology 297

5.2.3.1 Cell culture, transfection and pharmacological modulation of TRPV4 297

5.2.3.2 Immunocytochemistry, live-cell imaging and microscopy 297

5.2.3.3 Isolation of mitochondria from mammalian brain and CHO-K1 cells 298

5.2.3.4 Mitochondrial Ca^{2+}-imaging 299

5.2.3.5 Fluorescence labelling and antibody staining of Mesenchymal stem cells & isolated mitochondria 300

5.2.3.6 JC-1 (Ratiometric dye) staining in adherent cells and isolated mitochondria 301

5.2.3.7 Labelling of Mito Thermo Yellow (MTY) and ER Thermo Yellow (ETY) 302

5.2.3.8 Mitochondrial image analysis and quantification 303

5.2.3.9 Measurement of Mitochondrial ATP level and ATP release assay 304

5.2.3.10 Measurement of GTP level 305

5.2.3.11	Hypotonic treatment to the cell and ER-mito contact point quantification	305
5.2.3.12	Docking of MFN2 with TRPV4	306
5.2.3.13	Detection of mitochondrial superoxides and Cardiolipin	307
5.2.3.14	Animal procurement and Primary cell isolation	307
5.2.3.15	Growing cells on hydrogel-coated surface	308
5.2.3.16	Quantification of Reactive Oxygen Species (ROS)	308
5.2.3.17	Mineralization assay	309
5.2.3.18	Implantation of hydrogel in rat femur	309
5.2.3.19	Histopathological study of organs	310
5.2.3.20	Assessment of newly formed at defect site by SEM (Scanning Electron Microscopy)	311
5.2.3.21	RAMAN Spectroscopic analysis	311
5.2.3.22	Isolation and activation of murine T-cell	311
5.2.3.23	Live cell mitochondrial and cellular Ca^{2+}-imaging of T cells	312
5.2.3.24	Basal cytosolic and mitochondrial Ca^{2+} detection in T cell	313
5.3	**Statistical tests and Correlation analysis**	**313**
5.4	**Bibliography**	**314**

Summary

Ca^{2+}signaling plays a major role in regulating many cellular processes, including cell proliferation, cell death, neurotransmitter release etc. There are a plethora of ion channels present on the cell surface which mediate the process of calcium ion entry inside the cell. Among different ion channels, Transient Receptor Potential channels (TRP) are the ion channels that contribute to regulating cellular calcium by mediating calcium entry from extracellular and intracellular sources (Pedersen SF, 2005). TRP channels are present in singlecell eukaryotes to humans but absent in plants. These channels are classified into 7 subfamilies based on their amino acid sequence and homology. These are TRPC (canonical), TRPM (melastatin), TRPV (vanilloid), TRPA (ankyrin), TRPML (mucolipin), and TRPP (polycystin). These channels are primarily nonselective cation channels mediating the transmembrane influx of different divalent cations down their electrochemical gradient (Clapham DE, 2001). Among all the vanilloid family members, TRPV1-V4 are thermosensitive andcan be activated by different temperatures ranging from 27-52º C. whereas other members of the TRPV family as TRPV5 and TRPV6, are not thermosensitive. Still, they are highly selective towards calcium (Hofmann T, 2002). Transient Receptor Potential Vanniloid sub type 4 (TRPV4) is a non-selective cation channel functionally expressed in different tissues including respiratory airways, skin, vasculature, kidney, bone, sperm, immune cells, cardiac cells, brain, adipose tissue, muscle, cartilage and many other systems where it modulates various cellular physiology (Voets T, 2005; Chung MK, 2003; Jia Y, 2002; Liedtke W, 2000; Strotmann R, 2000; Kumar A, 2016). TRPV4 is a polymodal receptor and can be activated by a range of physical and chemical stimuli such as 4αPDD (4α-Phorbol 12, 13-didecanoate), endocannabinoids, different metabolites, steroids, arachidonic acid, temperature, mechanical force, pH, osmolarity (Majhi RK, 2015). TRPV4 is a unique channel with many naturally

occurring point mutations among all the TRP channels. These mutations correlate very well with the development of several pathophysiological conditions, including *Brachyolmia*, *Charcot-Marie-Tooth disease type-2C (CMT2C), skeletal dysplasia, spondylometaphyseal dysplasia Kozlowski (SMDK), cystic fibrosis* and many other diseases (Watanabe H, 2002).

TRPM8 is one of the members of the melastatin TRP channel subfamily of the TRP superfamily. TRPM8 is a non-selective cation channel that senses cold temperature and can be activated by Menthol, icilin, and temperature below 30 ºC.TRPM8 is also known as the "Menthol receptor" or "cold-sensitive receptor". Although TRPM8 is critical for the transduction of thermal stimuli to the peripheral nervous system, it is also expressed in other cellular systems. The expression of TRPM8 has been reported in the prostate, sperms, male genital tract, urinary bladder, and T-cells. TRPM8 expression increases in different types of cancer such as prostate cancer, breast, skin, colon, and lung. (Nilius B, 2013; Tsavaler L, 2001; McKemy DD, 2007; Acharya TK, 2021).

Previously it was a common notion that TRP channels are expressed only on the plasma membrane and regulate intracellular calcium homeostasis. But, in recent decades, intracellular localization of TRP channels has been a hot research topic. Indeed recent reports reveal the localization of TRP channels in intracellular organelles, and the functionality of these channels has been demonstrated (McKemy DD, 2002). Among TRPV channels, TRPV1 and TRPV3 are functionally expressed in ER and regulate its function (Dong XP, 2010). It has also been reported that TRPV1 is present in the mitochondria and regulates mitochondrial calcium levels (Gallego-Sandín S, 2009). Besides TRPV1, another TRP channel, such as TRPC3, also reported in mitochondria (Lang H, 2015). Recently it was shown that TRPM8 is present at the mitochondria-associated membrane (MAM) region and regulates ER-mitochondrial calcium transfer (Feng S,

2013). Although various studies suggest the localization of different TRP channels in subcellular organelles, no single report suggests the functional localization of TRPV4 and TRPM8 in mitochondria. In our work, we hypothesize that TRPV4 and TRPM8 are present in mitochondria in various endogenous systems and modulate mitochondrial structure, Ca^{2+}-metabolism, ATP level, membrane potential, Cardiolipin level, ER-mito contact sites and most importantly, we are first time proposing TRPV4 and TRPM8 regulates mitochondrial and ER temperature. An interesting observation of this thesis is TRPV4/TRPM8 activation increases mitochondrial temperature, and inhibition decreases mitochondrial temperature. These channels act as a cellular switches for managing mitochondrial temperature in our bodies. However, their function might differ in different cellular and organ systems, which opens a new field of study.

This work has also studied the importance of mitochondrial TRPV4 and TRPM8 in T-cell function in resting and T-cell activated conditions. Notably, mitochondrial Ca^{2+}-levels remain elevated during TCR activation, compared to cytosolic Ca^{2+}-levels.

As it has been reported that any changes in TRPV4 and TRPM8 induce skeletal deformities, we targeted these channels *in vitro* and *in vivo* by using hydrogel-based drug delivery system as a translational approach to improve the bone health and to understand the underlying mechanisms.

List of Figures

Sl. No.		Page No.
1.	Phylogenetic tree of mammalian TRP channel	4
2.	General structure of TRP members	6
3.	Differential regulation of Thermosensitive TRP ion channels	19
4.	Cryo-EM structure of TRPV4	26
5.	Ion permeation pathway of TRPV4	27
6.	Schematic diagram showing different sites of occurrence of TRPV4 mutation	30
7.	Structure of mouse TRPM8 (MmTRPM8)	34
8.	Steps of Mitochondrial information processing system (MIPS)	40
9.	General model of mitochondrial Ca^{2+}-transport in intact cell	43
10.	Model of cristae as individual bioenergetics unit	45
11.	Schematic diagram of mitochondrial heterogeneity within a cell	47
12.	Interaction of mitochondria with different organelles	49
13.	Different signaling pathways of mitochondria	51
14.	TRPV4 is endogenously present in mitochondria	56
15.	TRPV4 is endogenously present in isolated mitochondria	57
16.	Localization of TRPV4 in mitochondrial membrane	58
17.	TRPV4 regulates Ca^{2+}-levels in isolated mitochondria	60
18.	Time series of Ca^{2+}-influx in isolated mitochondria	61
19.	TRPM8 is endogenously localized at the mitochondria	62
20.	TRPV4 regulates mitochondrial Ca^{2+}-influx	65
21.	TRPV4 regulates mitochondrial Ca^{2+}-levels	66
22.	TRPV4 regulates mitochondrial Ca^{2+}-levels and mitochondrial numbers	69
23.	TRPV4 regulates mitochondrial Ca^{2+}-levels and mitochondrial numbers	71
24.	TRPV4 modulation regulates mitochondrial ATP and GTP level	73
25.	Effect of BAPTA-AM or Thapsigargin on mitochondrial morphology	75
26.	Changes in mitochondrial morphology due to TRPV4 activation in Saos-2 cell	76

27.	TRPV4 colocalizes and interacts with MFN1 and MFN2	78
28.	TRPV4 regulates the rate of mitochondrial fusion	80
29.	TRPV4 is present at the ER-mito contact site	81
30.	Modulation of TRPV4 regulates ER-mito contact points	84
31.	Modulation of TRPV4 regulates ER-mito contact points in cytosolic Ca^{2+}-depleted conditions	85
32.	Modulation of TRPV4 regulates ER-mito contact points in ER Ca^{2+}-depleted conditions	86
33.	TRPV4 regulates ER-mito contact points	87
34.	TRPV4 regulates mitochondrial Ca^{2+}-status	89
35.	Menthol increases mitochondrial Ca^{2+} and alters mitochondrial morphology	92
36.	Menthol causes instantaneous mitochondrial Ca^{2+}-influx	95
37.	Preventing Ca^{2+}-mobilization from different sources protects mitochondria from Menthol-induced Ca^{2+}-overloading	97
38.	Menthol regulates mitochondrial membrane potential and metabolism	99
39.	Menthol enhances ER-mito contact points	101
40.	Menthol cools mitochondria, but not the ER	102
41.	Regulation of mitochondrial morphology by TRPM8	104
42.	Activation of TRPM8 causes instantaneous mitochondrial Ca^{2+}-influx	107
43.	TRPM8 regulates mitochondrial Ca^{2+}-level and mitochondrial number	108
44.	Preventing Ca^{2+}-mobilization from different sources protects mitochondria from WS12-induced Ca^{2+}-overloading	110
45.	Chronic modulation of TRPM8 changes the cytosolic and mitochondrial Ca^{2+}-level differentially	111
46.	TRPM8 regulates mitochondrial membrane potential and metabolism	113
47.	Modulation of TRPM8 increases mitochondrial superoxide level	114
48.	TRPM8 modulation affects mitochondrial membrane potential and metabolism	115
49.	TRPM8 activation by WS12 raises ER temperature but not for the mitochondrial temperature	116

50.	Modulation of TRPM8 regulates ER-mito contact points	118
51.	TRPM8 regulates ER-mito contact points	119
52.	TRPM8 regulates mitochondrial Ca^{2+} and membrane potential in MSCs	120
53.	TRPM8 modulation decreases mitochondrial Cardiolipin level in MSCs	121
54.	TRPM8 inhibition decreases mitochondrial temperature in MSCs	122
55.	TRPM8 modulation changes mitochondrial Ca^{2+} and temperature in purified mitochondria	124
56.	Hydrogel-mediated drug release altersTRPV4 expression and basal Ca^{2+}-load of bone marrow derived Mesenchymal stem cell population	128
57.	Hydrogel-mediated drug release alters the morphology of bone marrow-derived Mesenchymal stem cell population	130
58.	Hydrogel-mediated drug release regulates cellular and mitochondrial physiologies of bone marrow derived MSCs population	132
59.	Hydrogel-mediated drugs regulate cellular physiologies during osteoblast differentiation	135
60.	Hydrogel-mediated released drugs regulate mitochondrial function during osteoblast differentiation	137
61.	Hydrogel (CMT: HEMA)-mediated release of TRPV4 agonist and antagonist modulates osteoblasts functions	138
62.	Hydrogel (CMT: HEMA)-mediated release of TRPV4 agonist and antagonist modulates *in vivo* bone healing	140
63	Hydrogel (CMT: HEMA)-mediated release of TRPV4 agonist or antagonist modulates *in vivo* bone repair and increases osteogenic markers	142
64.	*In vivo* toxicity assay	144
65.	Assessment of bone healing and quality of new bone	146
66.	TRPM8 activation increases cellular Ca^{2+}-level	149
67.	Hydrogel (CMT: HEMA) as a suitable surface for drug coating and growing of Mesenchymal stem cells	150
68.	Hydrogel-mediated drug release alters the morphology of bone marrow derived Mesenchymal stem cell population	152
69.	Hydrogel coated with TRPM8 activators but not with inhibitor specifically	154

stimulates ROS signaling by decreasing mitochondrial oxidative potential
70. Hydrogel (CMT: HEMA)-mediated release of TRPM8 agonist and antagonist modulates osteoblasts functions 156
71. Osteopontin expression in MSCs is induced when grown on different surfaces with TRPM8 modulatory drugs 158
72. Osteocalcin expression in MSCs is induced when grown on different surfaces with TRPM8 modulatory drugs 159
73. TRPV4 colocalizes with mitochondria in T-cells 163
74. TRPV4 regulates the basal cytosolic and mitochondrial Ca^{2+}-levels in T-cells 165
75. TRPV4 activation increases cytosolic Ca^{2+}-influx instantly in murine $CD3^{+}$ T-cells 168
76. TRPV4 activation cause instant mitochondrial Ca^{2+}-influx in murine $CD3^{+}$ T-cells 171
77. TRPV4 activation increases mitochondrial Ca^{2+}-influx in murine $CD3^{+}$ T-cells 172
78. TRPV4 regulates mitochondrial ROS and membrane potential 175
79. TRPV4 regulates mitochondrial ATP and Cardiolipin levels 177
80. TRPV4 regulates mitochondrial and ER-temperature 179
81. TRPV4 regulates ER-mito contact sites 181
82. TRPM8 is localized in mitochondria 185
83. TRPM8 activation by synthetic activator increases intracellular Ca^{2+}-levels in T cells 186
84. TRPM8 activation by Menthol increases intracellular Ca^{2+}-levels in T cells 187
85. TRPM8 activation by specific synthetic activator increases mitochondrial Ca^{2+}-status in murine $CD3^{+}$ T-cells 189
86. TRPM8 activation by Menthol a natural activator increases mitochondrial Ca^{2+}-status in murine $CD3^{+}$T-cells 191
87. TRPM8 modulation increases basal cytosolic and mitochondrial Ca^{2+} in murine $CD3^{+}$T-cells 193
88. Correlation study between basal Cyto Ca^{2+} and mito Ca^{2} 194

89. TRPM8 regulates mitochondrial ATP and membrane potential 196
90. TRPM8 regulates mitochondrial Cardiolipin and ROS levels 198
91. TRPM8 regulates mitochondrial and ER-temperature 200
92. TRPM8 regulates ER-mito contact sites 202
93. TRPV4 mutants affects mitochondrial morphology-based parameters and have different translocation efficiencies 206
94. TRPV4 mutants alter mitochondria shape and size 207
95. TRPV4 mutants differentially affect mitochondrial function in MC3T3-E1 cells 209
96. TRPV4 mutants alter mitochondria shape and size 210
97. TRPV4 mutants increase mitochondrial ROS in Saos-2 cells 212
98. TRPV4 mutants increase mitochondrial ROS in MC3T3-E1 cells 213
99. Schematic representation of the site of occurrence of the S372L point mutation 214

100. TRPV4-S372L mutation changes mitochondrial morphology in bone cells 216
101. TRPV4-S372L mutant differentially affect mitochondrial function in bone cells 217
102. TRPV4-S372L mutation changes mitochondrial morphology in neuronal, keratinocyte and fibroblast cells 219
103. TRPV4-S372L mutant differentially affect mitochondrial function in neuronal, keratinocyte and fibroblast cells 220
104. TRPV4-S372L mutant modulates cytosolic Ca^{2+}-influx in human osteosarcoma cells (Saos-2) 222
105. TRPV4-S372L mutant modulates mitochondrial Ca^{2+}-influx in human osteosarcoma cells (Saos-2) 223
106. TRPV4-S372L mutant increases mitochondrial ROS and ATP-level in human osteosarcoma cells (Saos-2) 224
107. TRPV4-S372L mutant alters mitochondrial Cardiolipin and ER temperature level in human osteosarcoma cells (Saos-2) 225
108. Schematic model depicting the TRPV4- and Ca^{2+}-dependent regulation of mitochondrial structures, numbers and temperature 234

109.	Involvement of TRPV4 in the ER-mito contact mediated Ca^{2+}-buffering	238
110.	TRPV4 inhibition increases mitochondria-lysosomal contact sites	240
111.	Correlation study among different mitochondrial parameters	244
112.	TRPV4 regulates HSP60, MFN1, DRP1 levels	248
113.	TRPV4 regulates MFN2 degradation	249
114.	TRPV4 induces Mitochondrial UPR	251
115.	Regulation of mitochondrial physiology and heterogeneity by TRPM8	256
116.	Plausible molecular mechanism of Menthol-mediated mitochondrial Ca^{2+}-increment	263
117.	Schematic model depicting the TRPM8-mediated mitochondrial regulation	266
118.	Schematic model of possible involvement of both “hot and cold-sensitive TRP channels” in mitochondrial “heating up” and “cooling down” processes	281

List of Tables

Sl. No.		Page No.
1.	Tissue specific distribution of different vertebrate TRP ion channels	7
2.	Structure of some of the modulators of TRP channels	20
3.	List of endogenous compounds that modulate different TRP channels	22
4.	Expression and localization of different TRP channels in sub cellular organelles	23
	Specific introduction of TRPV4	
5.	Mutation list of natural occurring TRPV4 mutations	31
6.	Expression and function of TRPM8 in human cancers	38
7.	Chemicals used	282
8.	Kits, Markers and Enzymes	284
9.	Primary Antibodies	284
10.	Secondary Antibodies	285
11.	Constructs Used	285
12.	Cell lines and primary cells	286
13.	PCR for Site Directed Mutagenesis	288
14.	PCR reaction conditions for SDM	288
15.	Composition of TFBI buffer	292
16.	Composition of TFBII buffer	292
17.	12% SDS-PAGE gel composition	294
18.	10X SDS Running buffer	294
19.	5X Laemmli buffer	294
20.	Composition of staining solution	295
21.	Composition of de-staining solution	295
22.	Composition of TBS	296
23.	Composition of Western Blot Transfer Buffer	296

List of abbreviations

3-T1AM	3-iodothyronamine
4αPDD	4-Phorbol 12,13-didecanoate
Amp	Ampicillin
AMTB	N-(3-aminopropyl)-2-[(3-methylphenyl)methoxy]-N-(2-thienylmethyl)-benzamide hydrochloride (1:1)
APS	Ammonium persulphate
ARS	Alizarin Red staining
ATP	Adenosine triphosphate
AU	Arbitrary Unit
BAPTA-AM	1,2-bis-(2-aminophenoxy)ethane-N,N,N',N'-tetraacetic acid tetra(acetoxymethyl) ester
BFP	Blue Fluorescence Protein
BGP	β-Glycerophosphate
BMM	Bone Marrow Macrophage
Bp	Base pair
BSA	Bovine serum albumin
CBB	Coomassie Brilliant Blue G250
CCCP	Carbonyl cyanide m-chlorophenyl hydrazine
CHOK1-Mock	Chinese Hamster Ovary K1-Mock
CHOK1-V4	Chinese Hamster Ovary K1-TRPV4
CHOP	C/EBP Homologous Protein
CMT	Carbox Methyl Tamarind
CPC	Cetyl Pyridinium Chloride
Cyt C	Cytochrome C
DAPI	4',6-diamidino-2-phenylindole
DIC	Differential Interference Contrast
DMSO	Dimethyl Sulfoxide
DNA	Deoxyribonucleic acid
dNTP	deoxy Nucleotide Tri Phosphate
ECM	Extra Cellular Matrix
EDTA	Ethylenediaminetetraacetic acid
EGTA	Ethylene glycol bis(2-aminoethyl ether)tetraacetic acid
ER	Endoplasmic Reticulum

EtBr	Ethidium Bromide
ETY	ER Thermo Yellow
FBS	Fetal Bovine serum
GFP	Green Fluorescence Protein
GTP	Guanosine 5′-triphosphate
H&E	Hematoxylin and Eosin
H2DCFDA	2',7'-dichlorodihydrofluorescein diacetate
HRP	Horseradish Peroxidase
IMM	Inner Mitochondrial Membrane
JC-1	5,5′,6,6′-tetrachloro-1,1′,3,3′-tetraethylbenzimidazolocarbocyanine iodide
Kan	Kanamycin
Kb	Kilo base
kDa	Kilo Dalton
KO	Knock out
LAA	L-Ascorbic Acid
LB	Luria-Bertani
LICV	Large Intracellular Vesicles
MAM	Mitochondria-associated membrane
MFN 1	Mito Fusion 1
MFN2	Mito Fusion 2
Min	Minutes (Time unit)
Mito	Mitochondria
MSC	Mesenchymal stem cell
MTG	Mito Thermo Green
MTY	Mito Thermo Yellow
NA	Numerical aperture
NaCl	Sodium Chloride
NAO	Nonyl Acridine Orange
NOS	Nitric oxide synthase
OB media	OsteoBlast media
OCN	Osteocalcin
OMM	Outer Mitochondrial Membrane
OPN	Osteopontin

PAGE	Poly Acrylamide Gel Electrophoresis
PBS	Phosphate buffer saline
PCR	Polymerase Chain Reaction
PFA	Paraformaldehyde
PI	Protease inhibitor
PVDF membrane	Polyvinylidene difluoride membrane
RFP	Red Fluorescence Protein
RN1734	2,4-Dichloro-N-isopropyl-N-(2-isopropylaminoethyl)benzenesulfonamide
ROI	Region of Interest
ROS	Reactive oxygen species
RPM	Revolution-Per-Minute
RT	Room temperature
RUNX-2	Runt-related transcription factor 2
SDM	Site Directed Mutagenesis
SDS	Sodium Dodecyl Sulphate
SEM	Scanning Electron Microscopy
Sirt 3	Sirtuin 3
SMDK	Spondylometaphyseal dysplasia (SMD) Kozlowski type
TAE	Tris-Acetic Acid-EDTA
TCR	T-Cell Receptor
TEMED	N,N,N′,N′-Tetramethylethylenediamine
TMRM	Tetramethylrhodamine, methyl ester
Tris	Transient Receptor Potential
UPR	Unfolded Protein Response

Chapter 1

Introduction

1.1 General introduction on TRP ion channel superfamily:

1.1.1 Discovery of TRP channel:

In 1969, a *Drosophila melanogaster* mutant was found by Cosens and Manning. When exposed to bright light, this mutant acted as though it was blind. *Drosophila melanogaster*'s chromosome 3 is the location where the mutation was identified. Electroretinogram (ERG) of the mutant *Drosophila* eyes revealed that, after prolonged exposure to intense light, the mutant Drosophila flies' receptor potential soon returns to normal. But in the case of the Wild Type (WT) flies, these changes occur more gradually. WT flies consistently react to light pulses, regardless of the duration of the gaps between consecutive and/or repetitive stimuli. On the other hand, this mutant is presumably blind to a second flash of light and requires a brief interval of darkness to regain its light sensitivity (Cosens DJ, 1969). As these visually impaired mutant flies exhibited a transient response to consistent light pulses in contrast to sustained responses of WT flies, these mutants were designated as "*Transient Receptor Potential*" or *trp* mutants (Minke B, 1975). Even 20 years after the *trp* gene was discovered in 1989, it was still unclear whether or not the *trp* protein could function as a channel. The *trp* gene was later cloned, and the derived amino acid sequence indicates that this gene may function as an ion channel. (Montell C, 1985; Montell C, 1989). The hydrophobicity plot of TRP protein suggested a more definitive character of TRP protein. Craig Montell and his colleagues proposed that "*TRP proteins function as ion channels"* because this protein includes 6-8 transmembrane domains (Montell C, 2011). Subsequently, a number of transient receptor potential (TRP) channels have been discovered, and these channels are engaged in a wide variety of sensory and physiological processes across a widerange of organisms. TRPV1 was the first discovered member of the TRPV sub-family of ions. The TRPV1 was discovered from screening the rat cDNA library using "Capsaicin response" as the read-out system (Caterina

MJ, 1997). Most mammalian TRPV1 member's response to Capsaicin in a variety of heterologous conditions, leading to a strong Ca^{2+}-influx upon Capsaicin application. The first molecular cloning and characterization of TRPV1 was reported in 1997 by Prof. D. Julius group (Caterina MJ, 1997). The discovery of TRPV1 was a milestone towards the study of pain. Because of the identification and characterization of TRPV1, Prof. D. Julius was awarded Nobel Prize in the year of 2021 (Nobel press report).

1.1.2 Classification of TRP channel:

Since the discovery of TRP channels in Drosophila, homologues from other organisms belonging to various phyla, from Caenorhabditis elegans to mammals, have been cloned. (Clapham DE, 2001). TRP channels are differentiated by homology rather than ion selectivity or ligand preference because their activities are diverse, and the majority are still uncharacterized (Clapham DE, 2003). Based on sequence homology, the mammalian TRP channel superfamily has been categorized into six subfamilies, namely TRPC (Canonical), TRPM (Melastatin), TRPV (Vanilloid), TRPA (Ankyrin), TRPML (Mucolipin), TRPP (Polycystin) **Fig. 1** (Clapham DE, 2001; Clapham DE, 2003; Ramsey IS, 2006; Himmel NJ, 2020). The first four subfamilies are categorized as group I, and the last two subfamilies constitute group II. In addition to mammalian TRP channels, numerous subfamilies of TRP channels have been found in many other organisms. For example, TRPY, also known as yeast TRPs, is distantly related to the conventional mammalian subfamilies and is responsible for hypertonicity sensing (Cai X, 2012). Mammals lack TRPN channels, however some vertebrates, including zebrafish, express them. Members with the greatest sequence similarity to *Drosophila* TRP have been classified to the TRPC or canonical subfamily. So far, TRPC1–7 have been found in mammals, but TRPC2 is not found in humans. All of the other TRPCs are found in different parts of cells. There are 8 members of the subfamily TRPM in

mammals. There are 6 members of the TRPV family, and some of these channels are thermosensitive in nature. TRPA1 is the only member of TRPA1 sub-family. TRPA1 is formerly known as ANKTM1 due to the presence of several ankyrin repeats located at the N-terminal (Montell C, 2005). The TRPM subfamily in mammals comprises eight members (TRPM1-8). Mucolipin-1 (TRPML1) was the first member of the ion channel family known as the TRPML. TRPML1 and TRPML2 channels have lysosomal-targeting signals which helps in Lysosomal membrane localization (Kiselyov K, 2005; Venkatachalam K, 2006). TRPP is the earliest group of TRPs. TRPP2 is the archetype (microbial homolog), and yeast cells also have it. Autosomal dominant polycystic kidney disease (ADPKD) was the first thing that linked TRPP2 to a protein disruptor. (Mochizuki T, 1996; Palmer CP, 2001).

Notably, TRP channels are primarily found in animal kingdom. Genome sequences from multiple plants suggests that TRP channels are largely absent in plants, though with some exceptions. So far, only *Chlamydomonus* has certain TRP channels (Fujiu K, 2011). TRP channels have also been identified in different fungus (Lange M, 2016; Wang, H 2021).

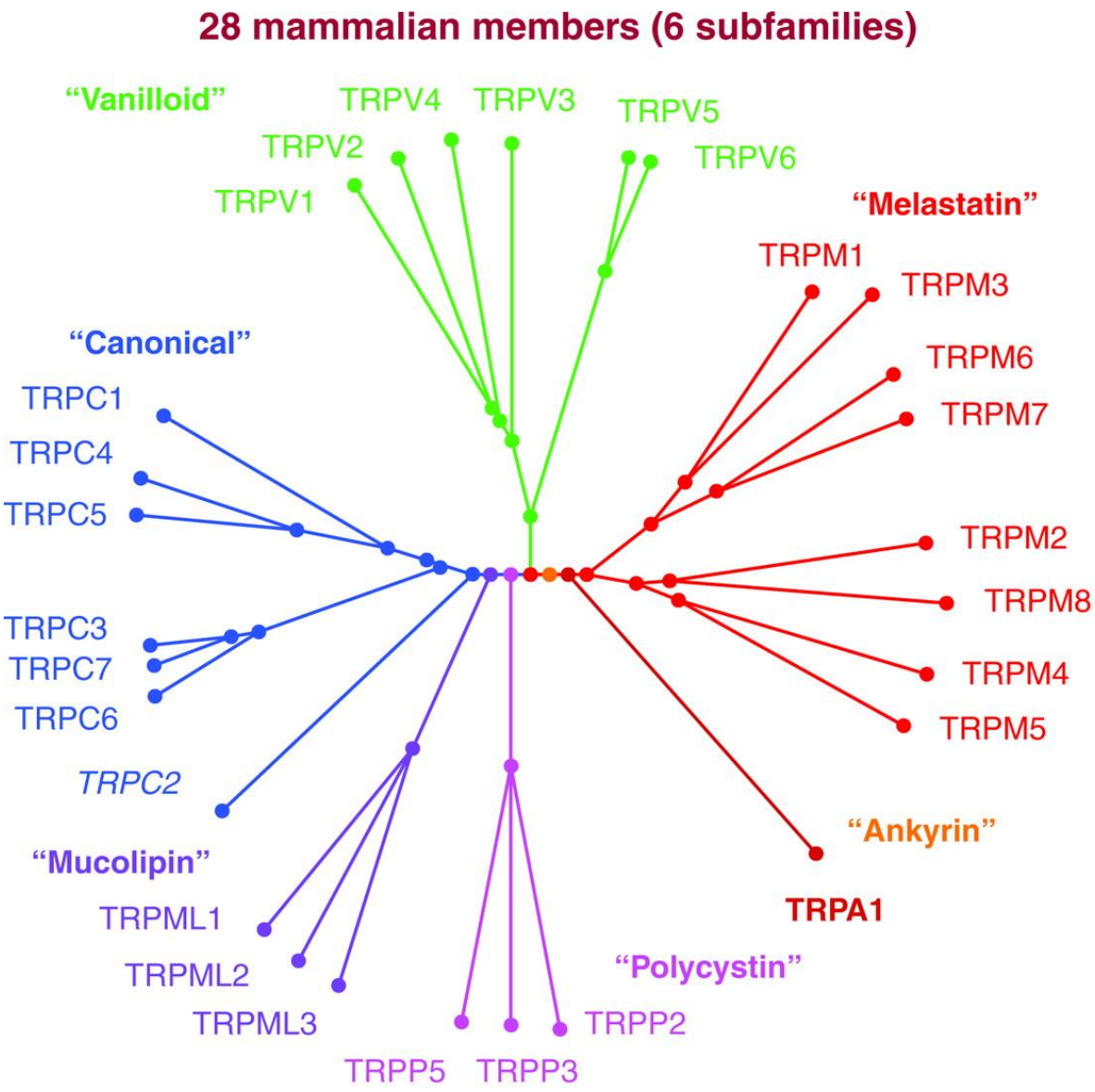


Fig. 1. Phylogenetic tree of mammalian TRP channel. The only recognized subfamilies in mammals are TRPC (canonical), TRPM (melastatin), TRPV (vanilloid), TRPA (ankyrin), TRPP (polycystin), and TRPML (mucolipin). The image taken from (Nilius B, 2012).

1.1.3 Structure of TRP channel:

TRP channels are comprised of six transmembrane helices (6TM), and the pore domain located between the 5th (S5) and 6th (S6) transmembrane regions. The N- and C-termini, both are located at the intracellular sides of the cell (Clapham D, 2003). Multiple members of the TRP superfamily

have an N-terminal ankyrin-like repeat domain (ARD) and several additional domains/motifs in the C-terminus, such as the TRP-box, a coiled-coil domain, an enzymatic domain, an ER-retention-signaling domain, Ca^{2+}-binding motif (EF hand) sequence, etc. (**Fig. 2**). The transmembrane region can be divided into two sections: the "sensor region," which is made up of S1–S4 and the "pore area," which is made up of S5–S6. The pore contains a “selectivity filter” that determines nature of ions that are permitted to pass through the channel pore based on the electrostatic and stereochemical characteristics. The “gate area” of the channel is another crucial component, as it controls “pore opening” or “pore closing” in response to information (i.e. conformational change) from the sensor region that detects signal(s), (Gaudet R, 2006). The majority of TRP channels contain the "TRP-box", a conserved region of 25 amino acids which is found at the cytosolic side and right after the sixth transmembrane segment (S6). The TRP-box is a typical structural feature detected in several TRP channels. In case of TRPC, TRPV, and TRPM members, the TRP-box is highly conserved. Even though it's not clear what “TRP-box” actually does, recent research has shown that the TRP-box regions of TRPM8, TRPV5, and TRPM5 can sense phosphatidylinositol 4, 5-bisphosphate (PIP_2) levels (Gaudet R, 2006).

TRP channels come together to make a homo- or heterotetramer, and these tetramers is the functional unit able to conduct ion influx. Different TRPs, such as TRPM6/TRPM7, TRPV5/TRPM6, TRPC1/TRPC3, TRPC1/TRPC4, TRPC1/TRPC5, TRPC3/TRPC4, and TRPC4/TRPC5, are reported to co-assemble together to produce functional hetero-tetrameric channels (Zheng J, 2013). The structural determination and comparison of different TRP channels are essential for elucidating their diverse various functions. Members of this family have a similar transmembrane structure but significant diversity at the N- and C-termini, where they interact with the different cytoplasmic factors. TRP channels are able to detect a wide variety of external and

intracellular stimuli, mostly due to the diversity of their extracellular and intracellular domains. So far, the structure of many members belong to the TRP super family, including TRPV1, TRPV2, TRPV3, TRPV4, TRPV5, TRPV6, TRPA1, TRPP2, TRPML1, TRPML3, TRPM4, TRPM7, TRPM8, TRPN, TRPC3, TRPC4, TRPC5, and TRPC6, have been resolved by cryo-EM (Huffer KE, 2020; Zhao Y, 2021; Koivisto AP, 2022).

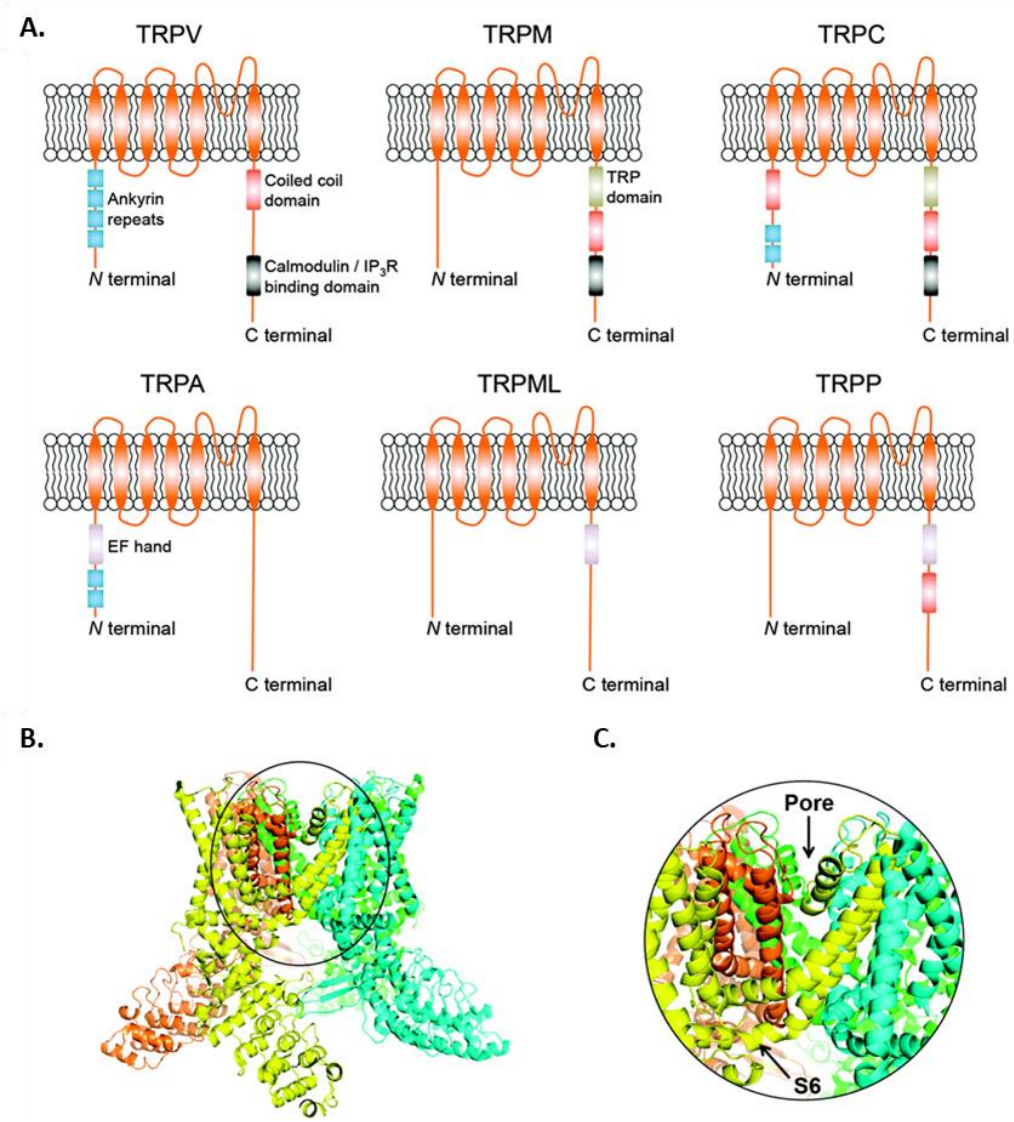


Fig. 2. General structure of TRP members. A. Schematic diagram showing different domain organization as observed in different TRP subfamilies. **B**.The 3D structure of TRPV1 is used to illustrate an overview of a functional TRPV channel. **C**. The "pore-S6 domain" of TRPV1 channel is shown in detail. Figure is taken from (Rodrigues T, 2016).

1.1.4 Tissue-specific distribution and physiological functions of different TRP channels in vertebrate:

Different tissues express different TRP channels, mostly in a spatio-temporal manner. mRNA profiling, protein expression studies such as western blot analysis, immunohistochemistry, ligand binding assay as well as functional studies such as patch clamping and Ca^{2+}-imaging, and, all confirm the presence of different TRP proteins in their cellular environments. Although many TRP channels are expressed ubiquitously, some are found only in selected tissue and cells, that too under certain conditions. The major types of tissue in which different TRP channels have been detected and their physiological functions are described are provided (**Table-1**). A detained description of the distribution of all TRP channels is beyond the scope of this thesis report. However, the updated tissue-specific expression of individual TRP channels is accessible on the website of the protein atlas (https://www.proteinatlas.org/ENSG00000196689-TRPV1).

Table 1

Channel subunit	Chromosomal location	Cellular expression	Physiological functions
TRPC subfamily			
TRPC1	Human: 3q22-q24; mouse: 9 E4	Ubiquitous	Generation of the excitatory postsynaptic potential in brain; netrin-1 and brain-derived neurotrophic factor (BDNF)-mediated growth cone guidance; connections to sleep/wakefulness states, alertness and appetite; brain development (together with TRPC5); glutamate signaling in hippocampus; regulation of smooth muscle contraction pulmonary system; platelet function; skeletal muscle differentiation; mechano-sensation?
TRPC2	Human: 11p15.4-p15.3 (pseudogene); mouse: 7 F1	Dendritic tips of the vomeronasal sensory neurons and spermatozoa	Pheromone detection that regulates sexual and social behaviors, such as gender

		(mouse)	recognition and male-male aggression (mouse)
TRPC3	Human: 4q25-q27; mouse: 3 B	Central nervous system (CNS) and smooth and cardiac muscle cells	BDNF-mediated growth cone guidance (TRPC1-independent); spine formation in brain; γ aminobutyric acid signaling in striatum; astrocyte function; moto-control in cerebellum; cerebral vasomotor control; erythropoietin function; functional coupling to orexin receptor
TRPC4	Human: 13q13.1-q13.2; mouse: 3 D	Placenta, adrenal gland, CNS, endothelium, smooth muscle cells, kidney, intestinal cells of Cajal	Endothelium-dependent vasorelaxation and regulation of transcellular permeation of the endothelial layer; cell-cell adhesion in endothelium through junctional proteins; hypoxia sensing together with TRPC1
TRPC5	Human: Xq23-q24; mouse: X F2	Brain, especially in fetal brain and very weak expression in other tissues	Brain development (together with TRPC1); neurite growth, growth cone guidance and morphology; anxiety, fear and reward processing in nucleus accumbens
TRPC6	Human: 11q21-q22; mouse: 9 A1	Smooth muscle cells, lung, brain, placenta, kidney (podocyte foot processes), spleen, ovary and small intestine, neutrophils	Vaso-motor regulation; α1-signaling in smooth muscle; smooth muscle proliferation; angiogenesis; endocannabinoid signaling in the brain; promotion of dendrite growth and synapse forming in the developing brain; glomerular filter integrity in the kidney; platelet function; redox sensor; mechano-sensor?
TRPC7	Human: 5q31.2; mouse: 13 B2	Pituitary glands, kidney and CNS (human); heart and lung; weak in CNS and kidney (mouse)	Controls respiratory rhythm activity in pre-Bötzinger complex in the brain
TRPV subfamily			
TRPV1	Human: 17p13.3; mouse: 11 B3	Dorsal root and trigeminal ganglia; spinal and peripheral nerve terminals, brain, skin (cutaneous	Thermo-sensation (heat); autonomic thermoregulation; nociception; pain management; synaptic plasticity in the brain (long-

		sensory nerve fibers, mast cells, epidermal keratinocytes, dermal blood vessels, the inner root sheet and the infundibulum of hair follicles, differentiated sebocytes, sweat gland ducts, and the secretory portion of eccrine sweat glands), pancreas, bladder (urothelium, smooth muscle, blood vessels and neurons)	term depression); endocannabinoid signaling in the brain; food intake regulation; growth cone guidance in the brain; osmosensing in the brain by a particular TRPV1 variant; multiple functions in the gut
TRPV2	Human: 17p11.2; mouse: 11 B2	Dorsal root ganglia and CNS neurons, gastro-intestinal tract, spleen, mast cells, smooth, cardiac and skeletal muscle cells	Thermo-sensation (noxious heat); nociception; axon outgrowth in spinal motor neurons; critical for phagocytosis in macrophages
TRPV3	Human: 17p13.3; mouse: 11 B4	Dorsal root and trigeminal ganglion neurons, brain, keratinocytes, hair follicles, tongue and testis	Thermo-sensation (moderate heat); nociception; skin integrity, wound healing, hair growth and sebocyte function
TRPV4	Human: 12q24.1; mouse: 5 F	CNS (large neurons), trigeminal ganglia, heart, liver, kidney, skin (keratinocytes), osteoblasts, blood vessels (endothelium), bladder (urothelium) and testis, cochlea (inner and outer hair cells, marginal cells of the cochlear stria vascularis), kidney (epithelial cells of tubules and glomeruli)	Thermo-sensation (moderate heat); mechano-sensation; osmo-sensation; nociception; modulation of cell migration; endothelium vaso-motor control and possible shear stress sensor; mechano-receptor in urothelium (important for voiding control); osteogenesis and osteoclast function; important in human bone and neurodegenerative diseases; control adherens junctions in skin; cochlea
TRPV5	Human: 7q35; mouse: 6 B2	High in kidney; lower in gastro-intestinal tract, pancreas, testis, prostate, placenta, brain and salivary gland	Ca^{2+}-(re)absorption channel in kidney and intestines
TRPV6	Human: 7q33-q34; mouse: 6 B2	High in gastro-intestinal tract; lower in kidney, pancreas, testis, prostate, placenta, brain and salivary gland	Ca^{2+}-(re)absorption channel in intestines and kidney; key player in Ca^{2+}/1,25-dihydroxyvitamin D3 induced keratinocyte development in the skin
TRPM subfamily			
TRPM1	Human: 15q13-q14; mouse: 7 C	Skin melanocytes, retinal bipolar ganglia	Light response in ON bipolar retinal ganglia cells; tumor repressor

			in melanoma cells
TRPM2	Human: 21q22.3; mouse:10 C1	Brain, bone marrow, peripheral blood cells (neutrophils), lung, spleen, eye, heart and liver	Oxidative and nitrosative stress response; activation of granulocytes; pancreas insulin release; critical in apoptosis
TRPM3	Human: 9q21.13; mouse: 19 C1	Primarily in kidney; lower in brain, sensory neurons, testis, ovary, pancreas and spinal cord	Steroid hormone (pregnanolon) sensor; possible regulator in endocrine pancreas, glia cells and cerebellar Purkinje cells
TRPM4	Human: 19q13.32; mouse:7 B4	Heart, exo- and endocrine pancreas, mast cells, smooth muscle, macula densa, lung and placenta	Mast cell degranulation (histamine release) and migration as a critical Ca-impermeable cation channel regulating Ca^{2+}-entry; catecholamine release from chromaffin cells; vasopressin release from paraventricular and supraoptic hypothalamic nuclei
TRPM5	Human: 11p15.5; mouse: 7 F5	Tongue (taste bud cells), lungs, testis, digestive system, brain, endocrine pancreas	Taste (sweet, bitter, umami); positive regulator of glucose-induced insulin release; trigeminal nasal chemoreception
TRPM6	Human: 9q21.13; mouse: 19 B	Kidney, colon and intestine	Mg^{2+} homeostasis and reabsorption in kidney and intestine
TRPM7	Human: 15q21; mouse: 2 F2	Ubiquitous	Mg^{2+} homeostasis and reabsorption in kidney and intestine; cell cycle control; gastrulation; development of thymocytes (thymopoiesis); cell migration; shear stress sensor?; skeletogenesis?
TRPM8	Human: 2q37.1; mouse: 1 C5	Sensory dorsal root and trigeminal ganglia neurons, nodose ganglion cells innervating the upper gut, vascular smooth muscle cells, liver, gastric fundus, bladder (urothelium) and different tissues of the male genital tract; high in tumors from prostate, breast, colon, lung and skin	Thermo-sensation (cold); sperm motility, acrosome reaction
TRPA1 subfamily			
TRPA1	Human: 8q13; mouse: 1 A3	Hair cells, sensory dorsal root and trigeminal ganglia neurons, fibroblasts	Thermo-sensation (noxious cold); the most versatile chemo-sensor;

			mechano-sensation?; nociception; olfactory responses; cold-induced contraction in colon and bladder
TRPML subfamily			
TRPML1	Human: 19p13.3-13.2; mouse: 8 A1.1	Ubiquitous; intracellular ion channel	Essential for endocytosis and endosomal/lysosomal function; regulation of autophagy
TRPML2	Human: 1p22; mouse: 3 H3	Ubiquitous; intracellular ion channel	Endosomal/lysosomal function
TRPML3	Human: 1p22.3; mouse: 3 H3	Hair cells (stria vascularis, stereocilia); intracellular ion channel	Endosomal/lysosomal function; autophagy; hair cell maturation?
TRPP subfamily			
TRPP2	Human: 4q22; mouse: 5 E4	Ubiquitous; mostly in ovary, fetal and adult kidney, testis, and small intestine in both motile and primary cilia	Cardiac, skeletal and renal development; integrity of the vessel wall; negative regulator of endogenous mechano-sensitive channels; mechano-receptor and flow-sensor in endothelium; apoptosis
TRPP3	Human: 10q24-q25; mouse: 19 D1	Adult heart, skeletal muscle, brain, spleen, testis, retina and liver	Renal development; part of putative sour sensor
TRPP5	Human: 5q31; mouse: 18 B3	Testis, brain and kidney	Spermatogenesis?

Table-1. Tissue specific distribution of different vertebrate TRP ion channels (Nilius B, 2011**).**

1.2 Differential regulation of TRP channels by endogenous and exogenous ligands:

TRP channels are biological sensors. TRP channels are involved in a wide variety of physiological processes, and understanding how they are modulated and regulated is crucial for understanding these processes. TRP channels have polymodality, i.e. these channels have the ability to respond to a spectrum of physical stimuli such as temperature, voltage, light, osmolality, pH, mechanical pressure, and chemical stimuli such as noxius stimuli, synthetic compounds, protons, natural products, endogenous ligands, and different ions etc (**Fig. 3**). (Zheng J, 2013; Belvisi MG, 2011)

1.2.1 Pharmacological modulation of TRP channels by exogenous ligands:

1.2.1.1 TRPV channels:

The vertebrate TRPV subfamily has only six members i.e. TRPV1, TRPV2, TRPV3, TRPV4, TRPV5 and TRPV6. All these TRPV channels are non-selective cation ion channels. TRPV1 to TRPV4 is the Ca^{2+}-permeable channel and can also be activated by temperature in a wide range of cells. TRPV5 and TRPV6 are highly Ca^{2+}-selective and low thermosensitive (Clapham DE, 2003). TRPV1-V4 are mainly involved in nociception and thermosensation and also activated by wide range of chemical stimuli (Voets T, 2005). TRPV1 is the founding member of the TRP superfamily and was discovered due to its sensitivity towards apsaicin (the active compound present in hot chili pepper and the plants of capsicum genus). Capsaicin and there are other analogs of Capsaicin collectively termed as Capsaicinoids or capsinoids. The most well studied capsinoid is "Capsaicin" which is a well-documented natural irritant. In 1997 Julius and colleagues have discovered that TRPV1 is a potential receptor for Capsaicin (Caterina MJ, 1997). Piperine is a natural alkaloid found in plants belong to *piperaceae* family which are commonly known as black pepper. It has various medicinal value as well as anti-inflammatory properties. Piperine is similar to Capsaicin and has effect on TRPV1. McNamara et al. has concluded that piperine is similar to Capsaicin and exhibits a greater efficacy than Capsaicin for both activation and desensitization of TRPV1 (McNamara FN, 2005). Eugenol is a phenolic compound, a major constituent of clove or clocimum oil obtained mainly from *Eugenia carophyllata* and *Ocimum gratissimum.* Eugenol is referred as a TRPV1 agonist and is able to activate hTRPV1 in HEK293 cells and TG neurons (Yang BH, 2003). Eugenol can also activate TRPV3 and TRPA1 (Xu H, 2006). Resiniferatoxin is a very important and specific agonist of TRPV1. Resiniferatoxin is an extremely irritant compound found in the dried latex of a cactus-like plant *Euphorbia resinifera*. Resiniferatoxin is commonly coded

and known as RTX. TRPV1 is activated by RTX at a concentration of 10 nM (Raisinghani M, 2005). RTX shows a much higher affinity towards TRPV1 in comparison to Capsaicin (Elokely K, 2016; Yadav M, 2019). Capsaicin and RTX are analogues and share a homovanillyl group as a structural motif. There are certain compounds that are isolated from ginger plants (*Zingiber officinale*) like gingerols, shogaol, zingerone and paradol. These compounds, specifically gingerols and shogaol increase intracellular Ca^{2+}-concentration by activating TRPV1 in HEK293 cells (Iwasaki Y, 2006). In this case, shogaol is more efficient than gingerols. Cannabinoids are the secondary metabolite found in the cannabis plant (*Cannabis sativa*). These are also known as cannabidiol (CBD), and it has a similar effect as Capsaicin having anti-inflammatory and analgesic effects (Malfait AM, 2000; Lorton D, 2000). There are reports that cannabidiol inhibits the binding of RTX to the TRPV1 and increases intracellular Ca^{2+}-concentration (Bisogno T, 2001). Camphor is a compound isolated from camphor laurel tree (*Cinnamomum camphora*) has recently reported as an activator of TRPV1. Camphor is less potent, less specific than Capsaicin, and the camphor requires more concentration to activate TRPV1 (Xu H, 2005). Apart from various plant products that effect TRPV1 there are some venoms or toxins which have a robust effect on TRPV1. Venom from the North American funnel spider *Agelenopsis aperta* has an inhibitory effect on TRPV1. AG489 and AG505 are the purified toxins which inhibit TRPV1 from the extracellular side of the membrane (Kitaguchi T, 2005; Vennekens, R, 2008). A tarantula species, namely *Psalmopoeus cambridgei* from West Indies, has venom which contains three peptides which interact with TRPV1 (Siemens J, 2006).

TRPV2 is another member of the TRPV family having sequence similarity with TRPV1. TRPV2 also acts as a pain receptor and gets stimulated by noxious high temperatures (>50 °C). The physiological function of TRPV2 is still unclear. There are different natural and synthetic

compounds which interact with TRPV2 and modulate its function/s (Caterina MJ, 1999; Tominaga M, 2004). The first natural modulator of TRPV2 was discovered by Neeper MP, 2007 and the compound is Δ^9-tetrahydrocannabinol (THC), derived from the Marijuana plant *Cannabis sativa.* But this compound is not specific as Capsaicin. THC also interacts with CB2, TRPA1 and activates it in a similar concentration (Jordt SE, 2004; Akopian AN, 2008). Probenecid is a very specific TRPV2 agonist which can activate at a less concentration (Bang S, 2007).

TRPV3 is the third member of the TRPV family, reported to be expressed in keratinocytes, DRG neurons, as well as in the brain and spinal cord (Peier AM, 2002; Xu H, 2002). TRPV3 shares 40% similarity with TRPV1 and is activated at the normal temperature range of 32 -39 ˚C (Peier AM, 2002; Xu H, 2002). The natural compound Camphor extracted from *Cinnamomum camphora* also acts as an activator of TRPV3 (Moqrich A, 2005). TRPV3 is also activated by Carvacrol, a major compound of oregano (*Origanum majorana*), thymol, an important constituent of thyme (*Thymus vulgaris*), Vanillin, and the major ingredient of vanilla (*Vanilla planifolia*) (Xu H, 2006).

TRPV4 is the fourth and most important member of the TRPV family and the TRP super family. TRPV4 was initially discovered as an osmolarity sensor (Liedtke W, 2000). TRPV4 is activated at the normal body temperature (> 25 °C). TRPV4 is widely expressed in the tissue including DRG neurons, osteoblasts, osteoclasts, reproductive cells, immune cells, and regulate the diverse physiological processes of the body (Plant TD, 2007; Everaerts W, 2009). 4α-phorbol 12, 13-didecanoate (4αPDD) is a phorbol ester that belongs to the family of tetracyclic diterpenoid compounds and is a potent activator of TRPV4 (Vriens J, 2007). Another chemical compound is GSK3527497 which is a very specific inhibitor of TRPV4 (Brooks CA, 2019). In contrast, GSK1016790A is a very potent and specific agonist of TRPV4 and regulates intracellular Ca^{2+}-levels (Baratchi S, 2019). RN-1734, a synthetic small molecule, is the TRPV4 antagonist first

reported by Vincent et al. RN-1734, which binds to S2 and S3 domains of TRPV4, blocks the effect of TRPV4 agonist 4αPDD (10 µM of RN1734 has been administered) (Vincent F, 2009). Bisandrographolide A (BAA) is a natural compound derived from a herbaceous plant *Andrographis paniculata* is found to be an activator of TRPV4 (Smith PL, 2006).

1.2.1.2 TRPA1 channel:

TRPA1 is an important member of the TRP superfamily. TRPA1 is heterogeneously expressed in different tissues system, including DRG neurons. TRPA1 is also expressed in immunological cells as T-cells and regulates the Ca^{2+}-signaling in the T-cell (Sahoo SS, 2019). The "temperature" as a stimuli relevant for TRPA1 and of TRPA1 can act as a cold-receptor that is still unclear. TRPA1 is widely regulated by natural as well as synthetic compounds. Isothiocyanate-derived compounds, such as Allyl isothiocyanate (AITC) are an active compound present in mustard oil. This compound interacts with TRPA1 and activates TRPA1. Sahoo et al. have found that in the presence of AITC, the intracellular Ca^{2+}-level increases in T-cells (Sahoo SS, 2019). There are certain chemical compounds as A967079 and HC-030031 acts as an inhibitor of TRPA1 and decreases the Ca^{2+}-influx in T cell (Sahoo SS, 2019). Unlike isothiocyanates, there are thiosulfinate compounds which also act as TRPA1 activators. These are natural plant-derived compounds available in the plant of the *allium* genus. Allicin is the major constituent of garlic and onion plant, which activates TRPA1 (Bautista DM, 2005). Bandell et al. 2004 reported that TRPA1 is activated by cinnamaldehyde, the major component of cinnamon oil isolated from *Cinnamomum cassia*. CHO cells expressing TRPA1 exposed to cinnamaldehyde show a sharp increment of the intracellular Ca^{2+}-level. They have also used eugenol (from clove oil), gingerol (from ginger), methyl salicylate (from wintergreen oil) and isothiocyanate as TRPA1 activators and observed the same Ca^{2+}-spike in the cell (Bandell M, 2004). Camphor is a secondary metabolite from

Cinnamonum camphora, which activates both TRPV3 and TRPV1, but on the contrary, it desensitizes TRPA1 (Xu H, 2005). Nicotine is an alkaloid present in the tobacco plant (*Nicotiana tabacum).* Nicotine acts as a neuroinflammatory reagent and is a potent activator of TRPA1 (Andre E, 2008).

1.2.1.3 TRPM channels:

The TRPM (melastatin) subfamily of ion channels are the member of the TRP superfamily and has eight members. These eight members are again subdivided into four groups TRPM1/TRPM3, TRPM6/TRPM7, TRPM4/TRPM5, and TRPM2/TRPM8, based on their structural similarity (Zholos A, 2011). TRPMs are heterogeneously expressed and diversely activated, involving osmolarity, pH, and temperature (Zholos A, 2011). Regarding the ion selectivity nature of TRPMs, TRPM4 and TRPM5 channels are permeable only to monovalent cations (Na+, K+, Cs+) and TRPM6 and TRPM7 are permeable to divalent cations (Ca^{2+}, Mg^{2+}). TRPM8 is known as the "cold receptor" as it can be activated by low temperature. TRPM8 have the highest P_{Ca}: P_{Na} selectively values at 3:3 (McKemy DD, 2002). For the members of the TRPM family, the natural compounds and synthetic compounds are very less studied. TRPM2 is modulated by nicotinamide adenine dinucleotide, arachidonic acid (Togashi K, 2006; Beck A, 2006; Vetter I, 2011). There is a synthetic compound known as 2-minoethoxydiphenyl borate (2-APB), which has been reported as a blocker of TRPM2 (Togashi K, 2008). 2-APB acts on TRPM channels in a dose-dependent manner and in micromolar concentration, yet differently. 2-APB activates TRPM6 but inhibits TRPM7. But on the contrary, in higher doses, i.e. at milimolar concentration, 2-APB activates heteromultimer of TRPM6-TRPM7 and TRPM7 (Li M, 2006). Carvacrol is a major component of *Origanum vulgare* and is found to be a TRPV3 activator, but it inhibits TRPM7 (Parnas M, 2009). Indeed there are very few natural compounds have been discovered for these channels.

However, the selectivity and specificity of the natural compounds for the TRPM channels remain debatable questions.

TRPM8 is the most studied ion channel in the TRPM subfamily, certainly due to its cold sensitivity. TRPM8 is "the cold-sensitive" ion channel and gets activated by low temperatures. TRPM8 can be activated at ≤25 °C (McKemy DD, 2007). TRPM8 is heterogeneously expressed in different tissues as DRG neurons and highly expressed in the prostate, sperm cell, and liver (Fonfria E, 2006; Majhi RK, 2015). The important and specific natural compound activating TRPM8 is Menthol. Menthol is a cyclic monoterpenoid compound (which is the common peppermint) chiefly found in the mint species plants, such as *Mentha piperita*. For its high sensitivity towards Menthol, TRPM8 is also known as "the Menthol receptor" (McKemy DD, 2002; McKemy DD, 2005). In addition to Menthol, there are other natural compounds like ethanol, icilin, 1, 8-cineole, eucalyptol, and peppermint oil which provide a cold sensation and activates TRPM8 (Takaishi M, 2012; McKemy DD, 2005; Namer B, 2005; Majhi RK, 2015). Decarboxylated and deiodinated thyroid hormone (TH) derivative, 3-iodothyronamine (3-T1AM) has been reported as an endogenous modulator of TRPM8 (Khajavi N, 2017). Behrendt et al has described the order of efficacy and potency of different monoterpenoid natural compounds that activate TRPM8. As per the findings, the efficacy is in this order: Icilin>WS-3>Menthol>WS-23>geraniol (a component of essential oil)>eucalyptol (constituent of *Eucalyptus sp*)>linalool (found in the plants of *Lamiaceae* family)>hydroxyl-citronellal (found in the plants of genus *Cymbopogon*) (Behrendt HJ, 2004; Vetter I, 2011). Interestingly, there are certain synthetic compounds discovered which also modulate the activity of TRPM8 channels. AMTB (N-(3-aminopropyl)-2-[(3-methylphenyl) methoxy]-N-(2-thienylmethyl)-benzamide hydrochloride) is a synthetic compound which acts as a TRPM8 blocker (Lucius A, 2016; González-Muñiz R, 2019).

AMTB is considered as a specific inhibitor of the TRPM8 ion channel, but the action of AMTB on other ion channels is not explored yet. In addition to synthetic antagonist like AMTB, there are selective derivatives of Menthol, such as WS12 and CPS-369, which activates the TRPM8 and induce Ca^{2+}-influx inside the cell (Grolez GP, 2019).

1.2.1.4 TRPC channels:

TRPC channels are PLC-activated Ca^{2+}-permeable channels. In mammals, the TRPC family have seven TRP homologs. On the basis of sequence homology and functional similarities, TRPC channels can be divided into four subgroups, TRPC1, TRPC4, TRPC5, TRPC3, TRPC6, TRPC7, and TRPC2 (Clapham DE, 2002). The naturally occurring ligands for different TRP channels, likely the TRPV channel, TRPM channel, and TRPA channels, have been discovered, but there is very insufficient information about the ligands of TRPC channels.

Hyperforin is the first naturally occurring plant product of the TRPC family. Hyperforin is the bicyclic polyprenylated acylphloroglucinol derivative and is the main constituent of "St. John´s wort extract", which is widely used as a herbal medicine for the treatment of depression. Hyperforin is the selective modulator of TRPC6. Leuner et al. reported hyperforin as a TRPC6 modulator for the first time, and they have shown that it has a specific activity towards TRPC6 but is insensitive to TRPC3 (Leuner K, 2007; Harteneck C, 2011). TRPC5 is also activated by a natural compound Adenophostin A isolated from *Penicillium brevicompactum.* Though Adenophostin act as a potent agonist, the exact nature of its action is unclear. If it interacts with the IP3 receptor or works independently, that remains to be established (Kanki H, 2001; Vetter I, 2011).

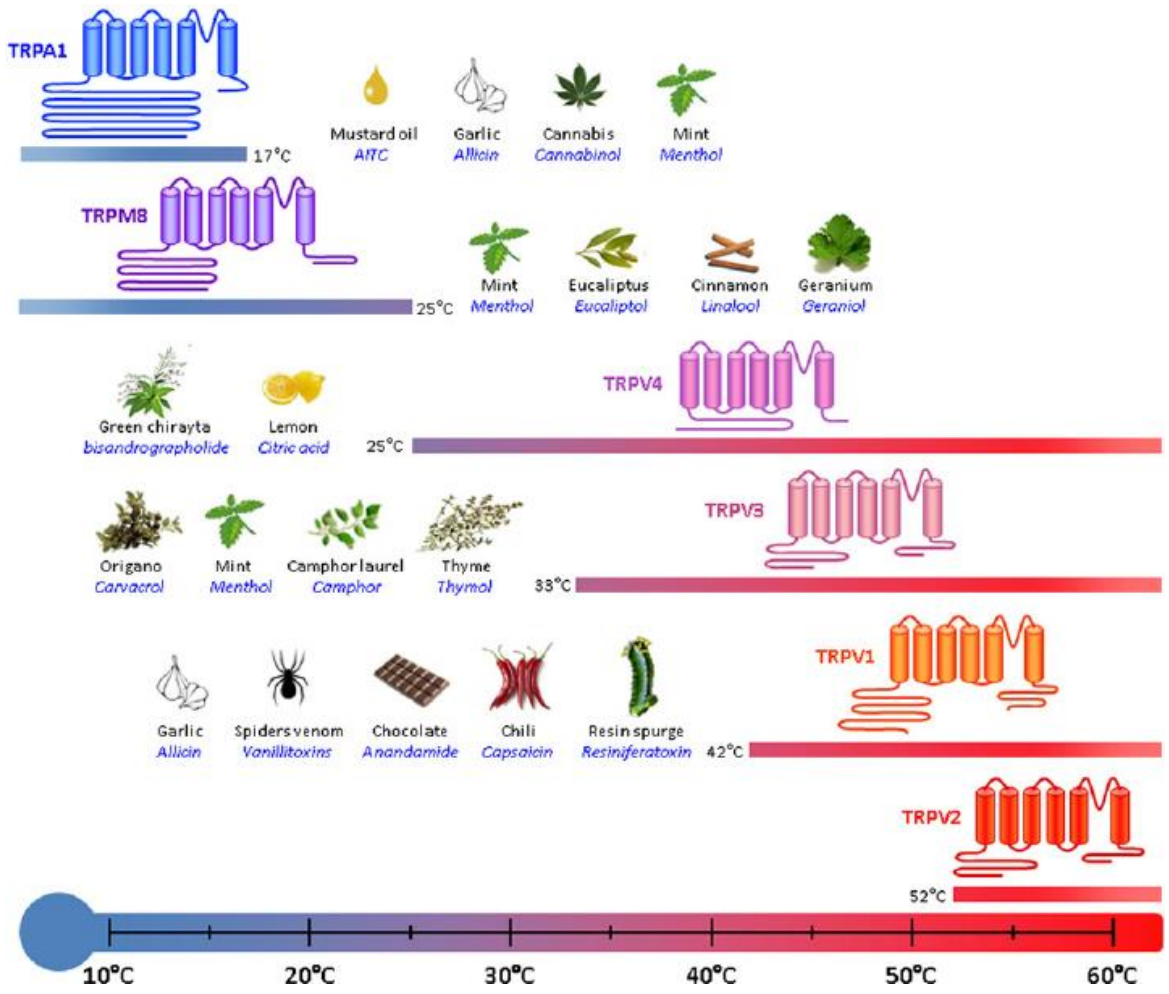
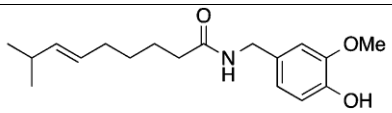
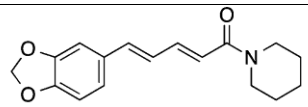
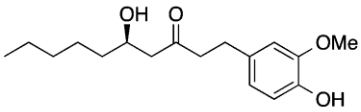
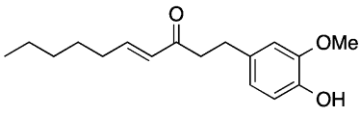
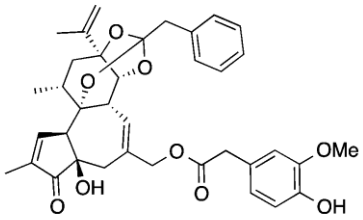
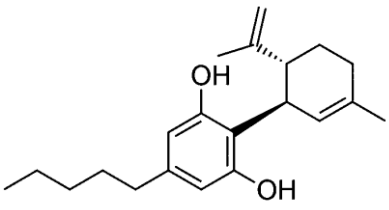


Fig. 3. Differential regulation of thermosensitive TRP ion channels: TRP channels are regulated by various natural compounds. The image is adapted from Belvisi MG, 2011.

A peptide toxin GsMTx-4 purified from Chilean Rose tarantula *Grammostola spatulata* has been reported as the pharmacological target for multiple TRPC channels. TRPC1, TRPC5 and TRPC6 are the potential targets for the toxin, and GsMTx-4 inhibits the effect of these channels (Suchyna TM, 2000; Gottlieb P, 2006). SKF-96365 is an organic synthetic compound which blocks the activity of receptor-mediated as well as store-operated Ca^{2+}-entry. The initial characterization of SKF-96365 shows that it blocks the activity of TRPC3 and TRPC6 in human myometrial cells (Boulay G, 1997; Shlykov SG, 2003). 2-minoethoxydiphenyl borate (2-APB) is a synthetic compound was initially used for the blocking of the store-operated Ca^{2+}-signaling and blocking of

IP_3-mediated Ca^{2+}-signals. There are reports that 2-APB has an effect on the activity of TRP channels. Mostly TRPC channels are blocked by 2-APB. Specifically TRPC1, TRPC3, TRPC5, TRPC6 and TRPC7- mediated Ca^{2+}-signaling was blocked by 2-APB (Xu SZ, 2005; Harteneck C, 2011)

Chemical structure of some of the TRP channel modulators:

TRPV1	 Capsaicin  Piperine  6-Gingerol  6-Shogaol  Resiniferatoxin Capsaicin (EC_{50} = 40 nM), Piperine (EC_{50} = 38 µM), 6-Shogaol (EC_{50} = 770 nM), Resiniferatoxin (EC_{50} = 1 nM),
TRPV2	 Cannabidiol

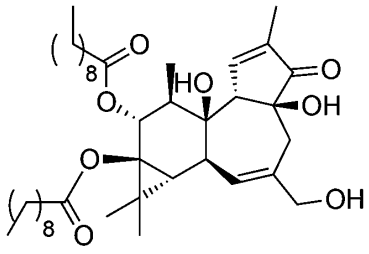
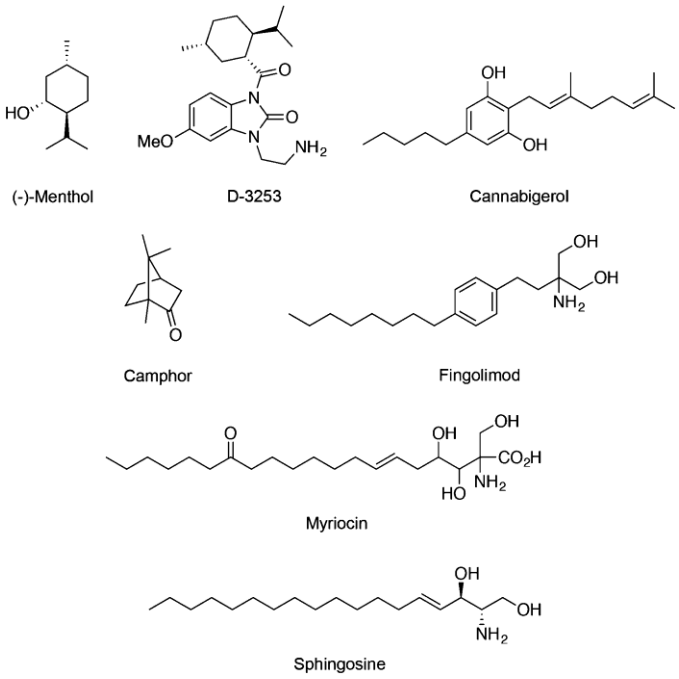
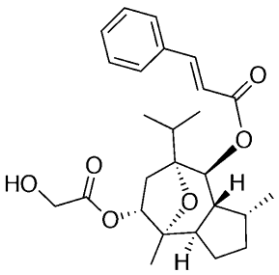
TRPV4	 4α-PDD 4αPDD (EC_{50} = 200 nM)
TRPM7/TRPM8	 (-)-Menthol D-3253 Cannabigerol Camphor Fingolimod Myriocin Sphingosine Menthol (EC_{50} =4–80μM), Cannabigerol(IC_{50} =0.11±0.02μM), Sphingosine (IC_{50} = 0.72 and 0.59 μM)
TRPC4/5	 (-)-Englerin A Englerin (IC_{50} = 10 nM)

Table-2. Structure of some of the modulators of TRP channels. This table is adapted from Rodrigues T, 2016.

1.2.2 Modulation of TRP channels by endogenous compounds:

Several endogenous ligands can also regulate TRP channel activity in addition to exogenous modulators. Some of these compounds and their activities are presented in **Table-3**.

Table-3

TRP channel	Endogenous ligands	Effect
TRPV1	Anandamide	Direct intracellular binding vasodilatation, activation, sensitization
	(S)HPETE, 15-(S)HPETE, LTB4	Activation, sensitization
	9-HODE, 13-HODE	Activation, sensitization
	Bradykinin	Indirect activation, and sensitization via HPETE production
	Serotonin	Sensitization (PKC)
	PGS	Sensitization (PKA
	Histamine	Sensitization (PKC)
	OEA	PKC-dependent stimulation
	NADA	Activation, sensitization
	OLDA	Activation
	AA-5-HT	FAAH and TRPV1 blockade
	OA-NO2	Activation, desensitization
	n-3 fatty acids	Phosphorylation-dependent interaction potentiates responses to protons, displace binding of [3 H] resiniferatoxin, inhibit the responses of vanilloid agonists
TRPV3	FPP	Direct channel interaction
TRPV4	EET	Direct channel gate
	AEA, AA	Indirect activation by CYP450 epoxygenase–induced conversion to EETs
	DMAPP	Activation
TRPM8	PIP2	Direct channel activates, restores rundown activity
	LPI, LPC, LPS	Activation and potentiation of cold response
TRPA1	PGA1, PGA2, 8-iso-PGA2, 15-deoxy- 12,14-PGJ2, 12-PGJ2	Direct channel gate
	OA-NO_2	Activation, desensitization

	Bradykinin	DAG, AA-dependent activation
	HNE	Activation
	PAR2	Sensitization
	NGF	Increased expression
TRPC	DAG, PIP_2, lysophospholipids oxidized phospholipids, AA and its metabolites, sphingosine-1-phosphate, cholesterol, steroidal derivatives, and gangliosides.	Indirect modulation

Table-3. List of endogenous compounds that modulate different TRP channels. This table is adapted from Palazzo E. 2013**.**

1.3 Sub-cellular distributions of TRP channels:

TRPs have a wide variety of activation mechanisms and subcellular localizations, both of which contribute to their extensive functional diversity in cells. The majority of TRPs are found in the plasma membrane, although some may play essential roles in organelle biology and signal transmission as organellar channels. Recent advances in research techniques, including organellar Ca^{2+}-imaging and organellar electrophysiology, have assisted in validating the roles of organellar TRPs. Several TRP channels are also thought to be in organelles inside cells. A list of these organelles is given (**Table 4**).

Table 4

TRP channels	Organelle	References
TRPA1	PM, Mitochondria, late endosome and lysosome, Secretory vesicles	(Shang S, 2016) (Zhang X, 2018) (Liu J, 2020)
TRPV1	PM, Mitochondria, ER, Golgi, Intracellular vesicles	(Turner H, 2003) (Morenilla-Palao C,2004) (Hurt CM, 2016) (Miyake T, 2015)
TRPV2	PM, Early endosomes	(Saito M, 2007)
TRPV3	PM, Lysosomes	(Yadav M, 2017) (Sahu RP, 2022)
TRPV4	PM, Mitochondria	(Acharya TK, 2022a) (Acharya TK, 2022b)
TRPV5	PM, Secretory vesicles	(Van de Graaf SFJ, 2006) (Zhang X, 2018)
TRPV6	PM, Secretory vesicles	(Van de Graaf SFJ, 2006) (Zhang X,2018)
TRPC1	PM, ER, intracellular vesicles	(Nesin V, 2014)

TRPC2	PM	(Zhang X, 2018)
TRPC3	PM, Mitochondria, secretory vesicles, (TGN) Trans Golgi Network, Golgi stack	(Singh BB, 2004), (Feng S, 2013), (Lavender V, 2008)
TRPC4	PM, Secretory vesicles	(Zhang X, 2018)
TRPC5	PM, Intracellular vesicles	(Bezzerides VJ, 2004)
TRPC6	PM	(Zhang X, 2018)
TRPC7	PM, TGN (trans-Golgi network) and the Golgi stack	(Lavender V, 2008)
TRPM1	PM, Melanosomes	(Zhang X, 2018)
TRPM2	PM, Late endosome, and lysosome	(Lange I, 2009) (Zhang X, 2018) (Dong XP, 2008)
TRPM3	PM,	(Zhang X, 2018)
TRPM4	PM	(Zhang X, 2018)
TRPM5	PM	(Zhang X, 2018)
TRPM6	PM, vesicles	(Zhang X, 2018) (Dong XP, 2008)
TRPM7	PM, Synaptic vesicles	(Brauchi S, 2008) (Krapivinsky G,2006) (Dong XP, 2010)
TRPM8	PM, ER, mitochondria,	(Thebault S, 2005) (Bidaux G, 2018)
TRPML1	PM, Late endosome and Lysosome, tubulovesicles.	(Dong XP, 2008) (Zhang X, 2018)
TRPML2	PM, Recycling endosomes, Late endosome, and Lysosome	(Zhang X, 2018)
TRPML3	PM, Early endosomes, Late endosome, and Lysosome	(Zhang X, 2018)
TRPP1	PM, cilia, ER	(Zhang X, 2018)
TRPP2	PM, cilia	(Zhang X, 2018)
TRPP3	PM, cilia	(Zhang X, 2018)
TRPY1	Yeast Vacuole	(Denis V, 2002) (Palmer CP, 2001) (Zhou XL, 2003)

Table-4. Expression and localization of different TRP channels in sub-cellular organelles Specific introduction of TRPV4

1.4 Overall architecture and structure of TRPV4:

Due to its crucial physiological and clinical significance, TRPV4 has been one of the most extensively investigated TRP channels. Crystallographic studies of isolated cytoplasmic domains and a cryo-EM model at 35Å resolution are the only sources of structural information so far (Inada

H, 2012; Shigematsu H, 2010). TRPV4 from *Xenopus tropicalis* shares 78% of sequence similarity with the human protein. Recently the cryo-EM structure of *Xenopus* TRPV4 resolved at 3.8Å resolution (Deng Z, 2018). X-ray crystallographic investigations of the ion-binding sites in the pore have been reported (Deng Z, 2018). For efficient crystallization, the full-length TRPV4 channel was shortened by deleting specific regions of the N- and C-terminal fragments and a truncated construct consisting residues of 133-797 was considered. The proline-rich domain (PRD), ankyrin-repeat domain (ARD), linker domain, transmembrane domain, and transient receptor potential (TRP) domain are all present in this construct. The glycosylation site was further removed by adding the point mutation N647Q to enhance X-ray diffraction. This allowed cryo-EM structural identification of $TRPV4_{cryst}$ (133-797 N647Q) to nearly atomic resolution. TRPV4 shares its symmetric tetrameric structure with other TRPV channels, such as TRPV1, TRPV2, and TRPV6. Four S1–S4 domains surround the central ion-conduction pore formed by S5 and S6, and the intervening pore loops from four identical subunits. TRPV4 exhibits a domain-swapped arrangement between the S1–S4 domain and the pore domain S5–S6, similar to TRPV1, TRPV2, and several VGICs. The S4–S5 linker, which connects the two domains, has a different structure than TRPV1 and TRPV2. Instead of a helix, it is made up of ordered-loops. Similar to other types of TRPV channels, the tetrameric TRPV4 channel's intracellular domains are composed of an N-terminal ARD, a linker domain, and then an S1-S4 domain. The amphipathic TRP-helix is oriented with its long axis parallel to the membrane and makes close contact with the ordered S4-S5 linker that joins the S1-S4 and pore domains. As a result, the TRP-helix is positioned between the cytosolic and transmembrane domains, where different physical or chemical stimuli exert their pressures (**Fig. 4**).

The ion permeation pathway of TRPV4 contains a single restriction at the bottom, making the "lower gate". The narrowest point of the channel is defined by the side chains of M714, with a diameter of 5.3 Å. Yet, this is large enough to block the passage of ions, indicating that the structure reflects a closed conformation of the channel (**Fig. 5**).

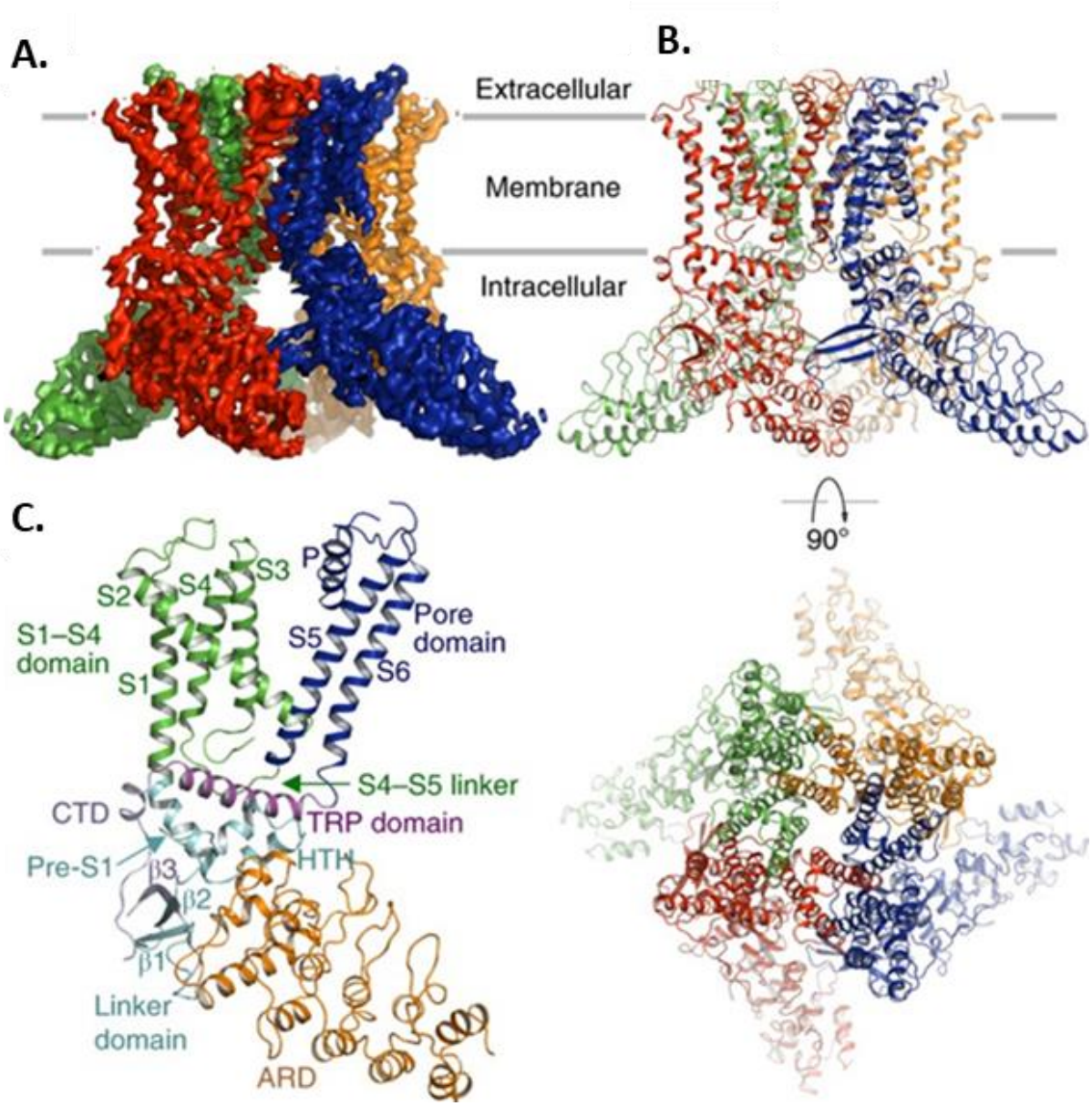


Fig. 4. Cryo-EM structure of TRPV4. **A-B.** Cryo-EM structure of the tetrameric channel. Each sub-unit is labeled in a different color. **C**. structure of a single subunit. Each sub-unit is represented in a different color. (Deng Z, 2018)

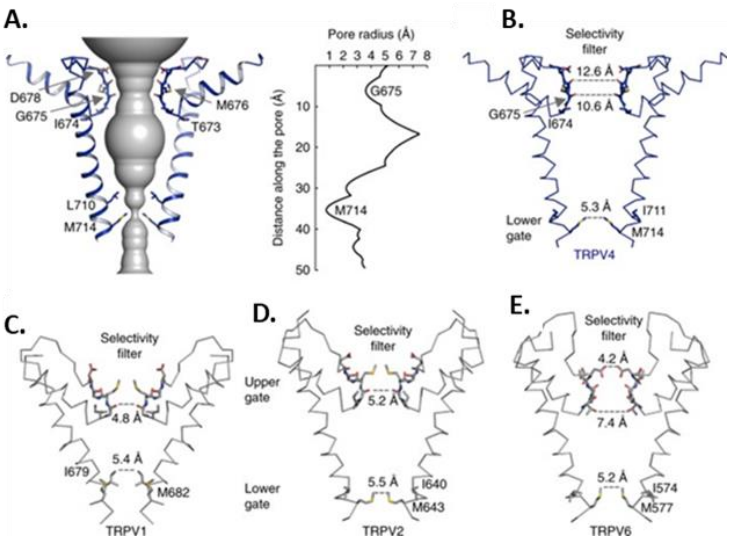


Fig. 5. Ion permeation pathway of TRPV4. A. The ion-conduction pore of TRPV4. Single constriction formed by M714 residues defines the intracellular gate in S6. **B**. Details of TRPV4 pore**. C-E**. Comparison with other TRPV pore structures reveals a closed "lower gate" and the absence of a typical "upper gate" in TRPV4 (Deng Z, 2018).

1.4.1 Expression and function of TRPV4 in different tissue and cells:

TRPV4 is expressed in a broad range of tissues. TRPV4 is highly expressed in the cilia of the bronchial epithelium and the lungs, where it controls the rate of ciliary beating and the delivery of mucus (Lorenzo IM, 2008). TRPV4 is also expressed in pulmonary fibroblasts, lung endothelium, alveolar macrophages, bronchial epithelium, and alveolar epithelium (Pairet N, 2018). TRPV4 has been functionally involved in several respiratory diseases, including asthma, cystic fibrosis, and acute respiratory distress syndrome (ARDS) (Scheraga RG, 2017). Recently it has been reported that the TRPV4 function is involved in the maintenance of blood pressure. TRPV4 conduct Ca^{2+}-influx stimulated by shear stress resulting due to blood flow and changes in vessel diameter, and changes in blood viscosity (Baratchi S, 2017). TRPV4 has been shown to play a part in a variety of vascular processes, including vasodilation, vasoconstriction, vascular permeability, vascular remodelling, and vascular injury (Liu L, 2021). Upon exposure to hypo-osmotic stress, TRPV4 expression and localization in acutely isolated rat ventricular myocytes shifted from nuclear/peri-

nuclear to sarcolemmal distribution, indicating a complex and dynamic cellular localization of TRPV4 (Zhao Y, 2012). The mechanosensitive and nociceptive behavior of TRPV4 is postulated based on the evidence that TRPV4$^{-/-}$ mice show abrogated tail responses to pressure and acid-induced pain (Desai BN, 2005). Pharmacological suppression of TRPV4 function or genetic knock-down of TRPV4 reduced the abnormally high stretch sensitivity observed in iPSCs derived from patients with dilated cardiomyopathy (DCM) (Lu J, 2017). Kidney function relies heavily on TRPV4 because it regulates cellular water balance. Its expression is high in the kidneys, where it responds to hypotonicity (Liedtke W, 2000). The mechanosensitivity of TRPV4 activation is ideally suited for sensing changes in renal tubule flow rates. Consistent with this, high levels of TRPV4 mRNA and protein expression were observed in the early distal convoluted tubule, the connecting tubule, and the collecting duct (Berrout J, 2012; Janas S, 2016). Another study using gene expression analysis found that TRPV4 was highly expressed in the ascending loop of Henle, a section of the renal tubule that does not allow water to pass through. (Tian W, 2004). Primary cultured proximal tubule cells from wild-type and TRPV4 knockout mice (*Trpv4*$^{-/-}$) were activated by the selective TRPV4 agonist GSK1016790A. As expected, the agonist stimulated the whole cell currents in wild-type cells but not in cells derived from *Trpv4*$^{-/-}$ (Gualdani R, 2020). TRPV4 expression is reported in the urothelium lining of the urinary bladders, namely in the basal and in the intermediate urothelial cells of mice and rats (Gevaert T, 2007). TRPV4 is a viable target for over-active-bladder (OAB) and possibly other bladder disorders because agonists appear to increase bladder hyperactivity, and antagonists appear to reduce it (Janssen D, 2011).

There are many different types of immune cells, mainly T-cells, mast cells, macrophages, leukocytes, neutrophils, and monocytes; all express TRPV4 ion channels (Parenti A, 2016; Majhi RK, 2015; Acharya TK, 2022a). TRPV4 is also expressed in mouse CD11c+ bone marrow-derived

DCs (BMDCs). In CD11c+ BMDCs, TRPV4 is predominantly expressed in the plasma membrane, and pharmacological activation by GSK1016790A (TRPV4-specific agonist) increases intracellular Ca^{2+}-levels. The cells were unresponsive to the agonist in the presence of TRPV4 antagonist HC067047. Similarly, in TRPV4 knockout cells, GSK1016790A could not increase the Ca^{2+}-levels confirming the functional importance of TRPV4. Moreover, TRPV4 channels are downregulated in mature DCs. During the differentiation process of immature to mature DCs, the activity and expression of TRPV4 were downregulated in the presence of lipopolysaccharide (LPS). TRPV4 deficient cells did not lower the nuclear translocation of NF-κB in response to LPS. Accordingly, the lack of TRPV4 did not prevent the upregulation of pro-inflammatory cytokines, IL-6, IL-12 or maturation markers like CD40, CD80, and CD86 (Naert R, 2019). Recently from our lab, we have reported that TRPV4 and TRPM8 are expressed in rat primary microglia and microglial cell line N9 and regulate cellular Ca^{2+}-level, cellular morphology, migration and motility (Chakraborty R, 2022).

TRPV4 protein is expressed in all vertebrate sperm cells ranging from fishes to mammals. In fishes, amphibians, reptiles, birds, and several mammals, including humans, expression of TRPV4 remains conserved, suggesting its role in sensing temperature, osmolarity, and different other chemicals relevant to reproduction (Kumar A, 2016). In addition, a sperm motility test utilizing a TRPV4 knock-out mouse model revealed that the TRPV4 channel plays a role in thermotaxis in mice sperm (Hamano K, 2016; Kumar A, 2016).

Ionic concentrations in muscle cells, including vascular smooth muscle, skeletal muscles, and endothelial cells, are mostly controlled by transient receptor potential vanilloid 4 (TRPV4) (Brinkmeier H, 2011; Filosa JA, 2013). Several reports have suggested that TRPV4 plays a crucial role in bone production and resorption, mechanical stimulation of bones, joint inflammation, and

bone pain. Further significance of TRPV4 in bone health is supported by several point mutations in TRPV4 causing bone defects. In fact, mutation or deletion in TRPV4 causes a wide variety of bone-related illnesses, usually known as skeletal dysplasias and arthropathies. Bone abnormalities are also observed in TRPV4 knockout animals (Hu F, 2019; McCray BA, 2020).

1.4.2 TRPV4 mutation mediated genetic disorders:

During the course of evolution, TRPV4 remained conserved in all vertebrates. However, several mutations have been reported that cause different TRPV4-mediated pathophysiologies. These mutations are mostly "gain-of-functions" by nature. Most of these missense and nonsense point mutations are linked to genetic diseases in humans. Notably, most of these mutations are "tolerable" (i.e. not lethal), and thus the patients carrying these individual mutations are viable and often show genetic transmission of the mutant gene.

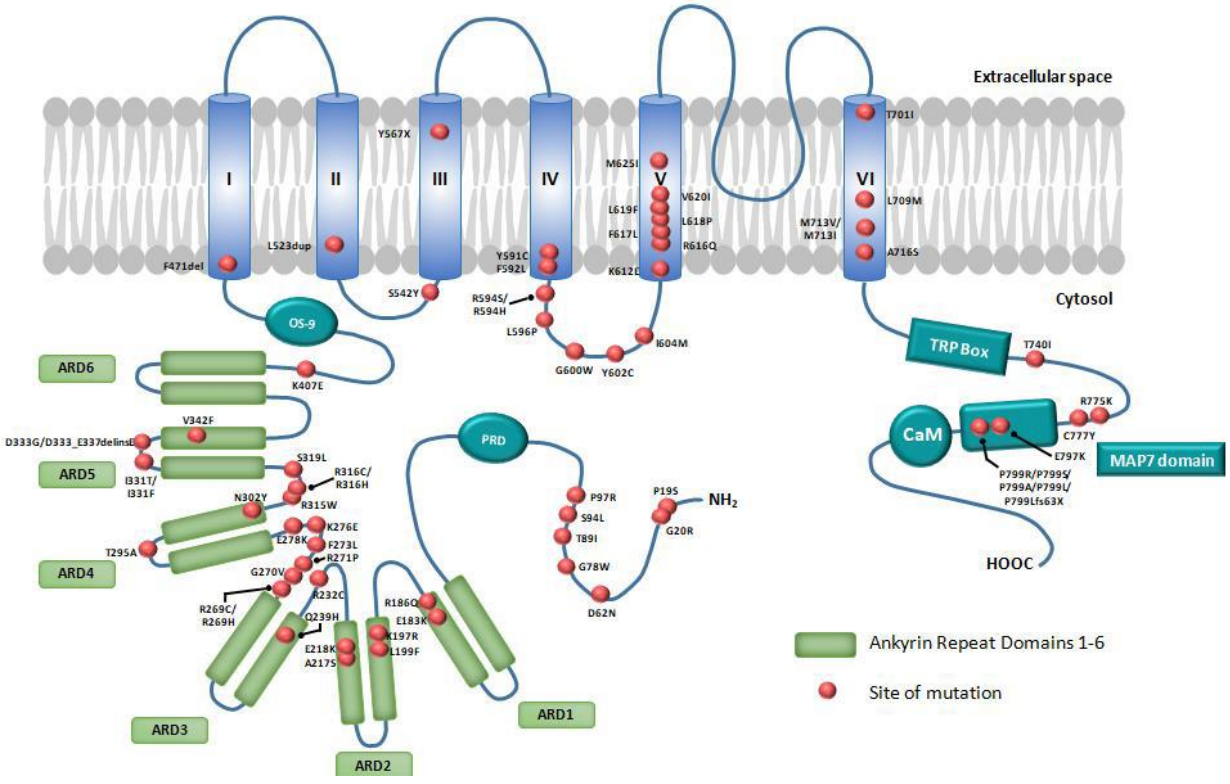


Fig. 6. Schematic diagram showing different sites of occurrence of TRPV4 mutation (Das R, 2022).

However, there are certain mutations that cause embryonic lethality. A detailed list of naturally occurring TRPV4 mutations and the diseases have been represented in **Fig. 6** and **Table 5**. The figure and table are adapted from Das R, 2022.

Table 5

Mutation	Residue	Disease	Effects on ion conductivity
	P19S	Hyponatremia (reduced response to hypotonic stress)	Loss of channel function
58G>A	G20R	Distal hereditary motor neuropathy (dHMN)	
184G>A (exon 2)	D62N	Phenotype is compatible with CMT type 2C and presented with intra-cytoplasmic basophilic inclusions besides the neurogenic changes.	
C366>T (Exon 2)	G78W	Dual phenotype of metatropic dysplasia and fetal akinesia.	
	T89I	Neonatal lethal metatropic dysplasia	Elevated basal Ca^{2+}
281C>T	S94L	Congenital spinal muscular atrophy and arthrogryposis(CSMAA)	Increase in the channel activity
290C>G (Exon 2)	P97R	Distal muscular atrophy (dSMA) and vocal cord paralysis	Loss-of-function
547G>A (exon 3)	E183K	SEDM-PM2	
557G>A	R186Q	Charcot–Marie–Tooth disease type 2C	Slight increase in Ca^{2+}
A590>G	K197R	Metatropic dysplasia	
597G>C (exon 4)	L199F	Metatropic dysplasia	
649G>T	A217S	SMDK and a neurological phenotype compatible with scapulo-humeral spinal muscular atrophy	
652G>A	E218K	CMT2 with Complex neurological syndrome with demyelinating neuropathy	
694C>T (Exon 4)	R232C	HMN with vocal fold paralysis, SPSMA, HMSN2	
717G>C (Exon 5)	Q239H	Metatropicdysplaisa	
805C>T (exon 5)	R269C	HSMN type IIC, with SPSMA and also with distal congenital non-progressive SMA.	
G806A (exon 5)	R269H	SMA, CMT2C, SPSMA	Gain-of-function
c.809G>T (exon 5)	G270V	Familial digital arthropathy-brachydactyly (FDAB)	Reduced response to agonist

c.812G>C (exon 5)	R271P	Familial digital arthropathy-brachydactyly (FDAB)	Reduced response to agonist
c.819C>G (exon 5)	F273L	Familial digital arthropathy-brachydactyly (FDAB)	Reduced response to agonist
	K276E	Dual phenotype of metatropic dysplasia and fetal akinesia	
832G>A (exon 5)	E278K	SMDK	
883A>G (Exon 6)	T295A	Metatropic dysplasia	
904A>T	N302Y	Charcot–Marie–Tooth disease type 2C (CMT2C)	
943C>T (Exon 6)	R315W	CMT2C	
C946T (exon 6)	R316C	HMSN2C	Gain-of-function
G947>A (exon 6)	R316H	Charcot–Marie–Tooth disease type 2C	Increased intracellular Ca^{2+}
c.956C>T	S319L	Isolated scapular winging	
A991>T (Exon 6)	I331F	Severe Metatropic dysplasia	Constitutive open channels
992T>C (Exon 6)	I331T	Metatropic dysplasia	
cA992!G (Exon 6)	D333G	SMDK	Increased Ca^{2+}-influx
1024G>T (Exon 6)	V342F	Metatropic dysplasia	
1219A>G (Exon 7)	K407E	Metatropic dysplasia (MD)	
1412_1414del (Exon 8) 471	F471del	Metatropic dysplasia (MD)	
1566_68dup; p. L523dup (Exon 9)	L523dup	SMDK	
1625C>A (Exon 10)	S542Y	CMT2C	
1701C>A	Y567X	Charcot–Marie–Tooth disease type 2C	
1772A>G (Exon 11)	Y591C	Brachyolmia, SMDK	
1780C>A (Exon 11)	R594S	Metatropic dysplasia (MD)	
1774T>C (Exon 11)	F592L	Metatropic dysplasia	
1781G>A (Exon 11)	R594H	SMDK, Parastremmatic dysplasia	Increased Ca^{2+}-influx
c.1787T>C (Exon 11)	L596P	SMDK	
1798G>T (Exon 11)	G600W	SMDK	
c.1805A>G (Exon 11)	Y602C	SEDM-PM2	

C1812>G (Exon 11)	I604M	Metatropic dysplasia	
1834A>G (Exon 12)	K612E	Metatropic dysplasia	
1847G>A (Exon 12)	R616Q	Brachyolmia	Increased Ca^{2+}-influx
C1851>A (exon 12)	F617L	Metatropic dysplasia	
T1853>C (Exon 12)	L618P	Metatropic dysplasia	
1855C>T	L619F	Metatropic dysplasia (accelerated chondrogenic differentiation of dental pulp stem cells)	Enhanced intracellular Ca^{2+}-level
1858G>A (Exon 12)	V620I	Brachyolmia	Increased Ca^{2+}-influx
1875G>A (Exon 12)	M625I	SMDK	
2102C>T	T701I	Charcot–Marie–Tooth disease type 2C	
2125C>A (Exon 13)	L709M	SMDK/BO	
	M713V/I	Central Giant cell lesions of the jaw (GCLJ)	Increased channel activity
c.G2146!T (Exon 13)	A716S	SMDK	Same as WT
	T740I	Dual phenotype of metatropic dysplasia and fetal akinesia	
2324G>A (Exon 14)	R775K	Metatropic dysplasia	
2330G>A (Exon 14)	C777Y	SMDK	
c.2389G>A (Exon 15)	E797K	Spondylo epimetaphyseal dysplasia Maroteaux—pseudo-Morquio type 2 (SEDM-PM2), SMDK and Metatropic dysplasia	
2396C>G (Exon 15)	P799R	Metatropic dysplasia	
2395C>T (Exon 15)	P799S	Metatropic dysplasia	
2395C>G (Exon 15)	P799A	Metatropic dysplasia	
C2396>T (Exon 15)	P799L	Metatropic dysplasia, SEDM-PM2	Constitutive open channels
999_1010del (Exon 6)	D333_E337delinsE	Mild Metatropic Dysplasia	
2396_2412del17	Pro799Lfs63X	SEDM-PM2	
c.1846C > G	p.R616G	congenital CMT2C neuropathy	Increased Ca^{2+}-influx

Table-5. Mutation list of naturally occurring TRPV4 mutations (Das R, 2022**)**

1.5 Specific introduction of TRPM8:

1.5.1 General architecture and structure of TRPM8:

TRPM8 is a non-selective cation channel and acts as a "cold receptor" in humans which gets activated by moderately cool temperatures (15-28 °C) (Bautista DM, 2007). Recent studies have characterised the structures of TRPM8 from two birds, *Parus major* (PmTRPM8) and *Ficedula albicollis* (FaTRPM8), which share 91% sequence similarity and 82% sequence identity with mouse TRPM8 (MmTRPM8) in the absence of a ligand as well as in the presence of an agonist or antagonist (Yin Y, 2018; Diver MM, 2019; Yin Y, 2019).

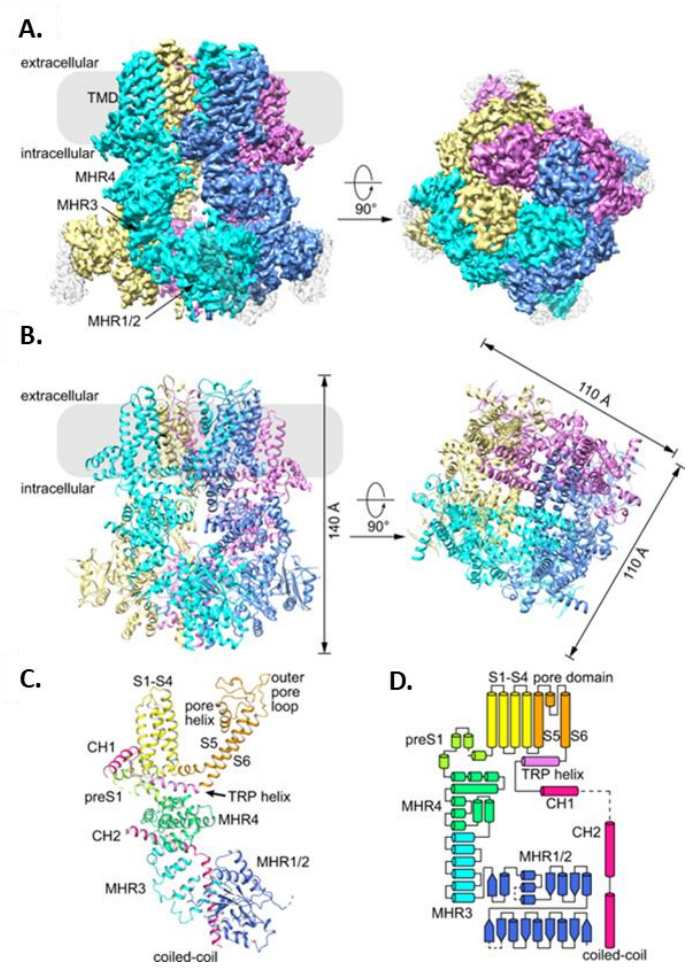


Fig.7. Structure of mouse TRPM8 (MmTRPM8). A-B. 3D reconstruction of MmTRPM8 where each subunit is colored differently. **C**. Image represents one subunit of MmTRPM8. **D**. Simplified topology of the TRPM8 channel.

Further validation of the conservation of these bird TRPM8 structures and the postulated ligand modulation mechanisms is required because they differ from those of other mammalian TRPM channels. To address this, Zhao et al. 2022 recently conducted an in-depth structural analysis of mouse TRPM8 (MmTRPM8) and revealed its cryo-EM structures both in the presence and absence of ligands, as well as in the presence of both icilin and Ca^{2+}. (Zhao C, 2022). The dimensions of the homotetramer MmTRPM8 are 140×110×110 Å. An entire tetrameric assembly, including the N-terminal area, the transmembrane domain, and the C-terminal region, is required for channel function. Every MmTRPM8 subunit comprises numerous domains, including the N-terminal 4 TRPM homology repeats (MHR1 to MHR4), the S1-S6 six transmembrane helices in a domain swap arrangement, the TRP helix, and the C-terminal coiled-coil. (**Fig.7**).

The MmTRPM8 structure is generally similar to the TRPM4, TRPM5, and TRPM7 structures found in other mammalian TRPM channels. (Zhao C, 2022). The MmTRPM8 ion conduction pore, including S5, the pore-helix, the selectivity filter, the outer pore-loop, and S6, are resolved at high resolution. The long exterior pore loop (Val915-Pro952) that connects the filter to S6 creates an extracellular turret that encompasses a deep vestibule at the channel's outer entrance. There are numerous negatively charged residues on the inner surface of the vestibule, which enables cations to move into the pore efficiently. Ion conduction pathway is composed of Phe912 and Gly913 backbone carbonyls and Gln914 side chain. There is a minimum distance of 9Å between the carbonyl oxygen atoms of Phe912 and Gly913. The similarity between MmTRPM8 and MmTRPM4 (the mouse TRPM4) in sequence and structure is particularly strong in the filter region (Zhao C, 2022).

1.5.2 Expression and function of TRPM8 in different tissue and cellular systems:

TRPM8 is highly expressed in primary sensory neurons in the dorsal root and trigeminal ganglia, as shown by functional and morphological investigations (McKemy DD, 2002; Peier AM, 2002). The sensory and afferent neurons that innervate the oesophagus, stomach, intestines, and colon have been extensively studied for their expression and functional relevance of TRPM8 (Yu X, 2016). Additional tissues such as dorsal root ganglia, thalamus, liver, nodose ganglion, bladder and the male genital tract, the tongue, the fundus of the stomach, the vascular smooth muscle of the lungs, the brain, and the petrosal and jugular ganglia, all are known to express TRPM8 (Liu Y, 2011). Wild-type mice that have been induced with colitis by Trinitrobenzene sulfonic acid (TNBS) and/or DSS respond favorably to icilin (which activates TRPM8) therapy, whereas TRPM8-deficient mice are extremely vulnerable to the disease (De Jong PR, 2015). The expression of TRPM8 in human bronchial epithelial cells and nerves innervating the lungs have been reported (Sabnis AS, 2008). TRPM8 modulators have been suggested as prospective therapeutics for the management of a number of airway-related diseases, including asthma, cough, and COPD (Chronic Obstructive Pulmonary Disease). (De Logu F, 2016; Preti D, 2012). It has been demonstrated that TRPM8 is also important for the excretory system. Inhibition of TRPM8 decreases overactive bladder while increasing micturition intervals, volume, and bladder capacity. (Mistretta FA, 2016). TRPM8 regulates the endocrine system as well. For example, mice lacking TRPM8 exhibit high insulin clearance rates (McCoy DD, 2013). Functional characterization of TRPM8 has been demonstrated in human bone marrow Mesenchymal stem cells (hBM-MSCs). Treating the cells with TRPM8 agonists, namely with Menthol or icilin increases osteogenic differentiation and in contrast, inhibition of TRPM8 by BCTC decreases osteogenic differentiation (Henao JC, 2021). Recently we have also reported the expression of TRPM8 in various bone cell

lines as well as in mouse bone marrow-derived Mesenchymal stem cells and in rat calvarial osteoblasts (Acharya TK, 2021). Using electrophysiological patch clamp analysis, expression of functional TRPM8 channels in the macrophage RAW-264.7 cell line was reported, and later on, it became evident that TRPM8 plays a role in immune cell functions (Wu SN, 2011). The functional expression of TRPM8 has also been observed in macrophages derived from mouse peritoneum (Khalil M, 2016). Apart from macrophages, the expression of TRPM8 has also been established in human and mouse T-cells (Kume H, 2019). Recent research has established that the TRPM8 protein acts as a testosterone receptor. These investigations further established that testosterone directly binds to the TRPM8 protein and triggers TRPM8-mediated currents and Ca^{2+}-responses (Asuthkar S, 2015).

1.5.3 TRPM8 in pathophysiology:

Initial findings suggested a significant elevation of TRPM8 in prostate cancer and other malignancies (Tsavaler L, 2001). Several other reports also supported the expression profile of TRPM8 in prostate cancer cell lines (Bidaux G, 2005; Prevarskaya N, 2007; Valero M, 2011). According to a recent investigation, the mRNA for the transcription factor TRPM8 has also been found in male bodily fluids (Bai VU, 2010). Patients with metastatic cancer had significantly higher mRNA levels of TRPM8 in their blood and urine compared to those with localized prostate cancer, providing a diagnostic tool for differentiating between the two phases of cancer (Bai VU, 2010). Present data show that TRPM8 is expressed in many solid tumors, and the functional roles of TRPM8 in cancer cells have been revealed. So far, there are several cancers where TRPM8 expression has been studied (**Table 6**).

Table 6

Cancer	Expression	Functional Role
Prostatic carcinoma	Up-regulated in tissues and androgen receptor-expressing cell lines (LNCaP, VcaP, C4-2B, NCI-H660).	Cell proliferation, survival, migration, hypoxic growth, xenograft growth, angiogenesis
Pancreatic carcinoma	Up-regulated in cell lines (PL45, MIA PaCa-2, PANC-1, HPAF-II, BxPC-3, Capan-1, Panc 02.03). Over-expressed in pancreatic adenocarcinoma. Also aberrantly expressed in chronic pancreatitis, pancreatic intraepithelial neoplasm, intraductal papillary mucinous neoplasm, solid pseudopapillary neoplasm, adenosquamous carcinoma, and neuroendocrine tumor.	Cell proliferation, cell cycle progression, replicative senescence, survival, migration, and invasion.
Breast adenocarcinoma	Over-expressed in cell line (MCF-7, T47D, MDA-MB231, BT549, SKBR3, ZR-75-30). Over-expressed in breast adenocarcinoma tissues.	Cell migration, invasion
Lung carcinoma	Expressed in tissues and cell lines (LLC-1, LLC-2, LLC-3).	Cell proliferation, adhesion, migration, invasion, resistance to hypothermia
Colorectal adenocarcinoma	Expressed in tissues and cell lines (Caco-2, HCT 116).	Cell growth, survival, xenograft tumor growth, chemically-induced cancer growth.
Melanoma	Expressed in tissues and cell lines (G-361, A-375, Mel 202, Mel 270, 92.1, omm 2.3)	Cell survival
Urinary bladder carcinoma	Expressed in cell line (T24). Over-expressed in urothelial carcinoma tissues.	Cell survival
Neuroblastoma	Up-regulated expression in cell line (IMR-32) in response to 5-bromo-2-deoxyuridine induced differentiation.	Not reported
Glioblastoma multiforme	Expressed in cell line (DBTRG) and tissues.	Cell migration, survival
Neuroendocrine tumor	Expressed in neuroendocrine tumor cell line (BON) and tissues.	Secretion of neurotensin.
Oral squamous cell carcinoma	Expressed in cell lines derived from tongue (HSC3 and HSC4).	Cell migration and invasion.
Osteosarcoma	Expression in osteosarcoma cell lines (U2OS, MG-63, SaoS2, HOS); increased expression in osteosarcoma as compared to osteochondroma	Cell proliferation, cell cycle progression, survival, migration, and invasion.

Table-6. Expression and function of TRPM8 in human cancers. This table has been adapted from Yee NS, 2015.

Apart from cancer, TRPM8 is also involved in several other diseases. Several studies show that TRPM8 may be involved in both normal and abnormal painful cold sensations (M Knowlton W, 2011; Fernández-Peñam C, 2013). Capsazepine, a TRPM8 blocker, dramatically reduces cold allodynia in neuropathic pain animal models, while mice lacking TRPM8 exhibit diminished thermal sensitivity in neuropathic cold pain in animal models (Xing H, 2007; Zuo X, 2013; Dhaka A, 2007; Colburn RW, 2007). In growth cones of cultured DRGs, TRPM8 is implicated in Ca^{2+}-entry caused by a mutant type of transthyretin. This study provides further evidence that TRPM8 may play a role in the development of familial amyloidotic polyneuropathy, in which a mutant, insoluble form of transthyretin is a key factor (Gasperini RJ, 2011). Multiple genome-wide association studies have linked TRPM8 expression in the brain meninges to an increased risk of migraine headaches. Migraine researchers are actively exploring both agonists and antagonists of TRPM8 as treatment options due to the fact that cold can stimulate migraine in certain people while Menthol can relieve headaches (Dussor G, 2016).

1.6 Important aspects of mitochondrial research:

Due to the recent findings, the conventional understanding of mitochondria as "the powerhouse of the cell" has been changed. As per thecurrent understanding, mitochondria have been defined as a living, dynamic, maternally inherited, energy transforming, biosynthetic, social, and signaling organelle which actively transduces biological information by making contact with the nucleus, ER, and other organelles and develops the "mitochondrial information processing system" (MIPS) (Picard M, 2022). As a whole, mitochondrial functions can be differentiated into three steps. First, through morphological and functional modification, mitochondria "sense" and "respond" to both endogenous and environmental cues. Second, integration of information through network-based physical interactions and diffusion. Third, it provides output signals that influence the functioning

of other organelles and systemic physiology (Picard M, 2022). In addition, this approach provides novel insights into mitochondria's role in mediating the inter-organ activities that underpin human health. MIPS (mitochondrial information processing system) is an elaboration of the conventional process of receptor-mediated detection of extracellular signals, signal amplification, and transduction into downstream second messengers (**Fig. 8**).

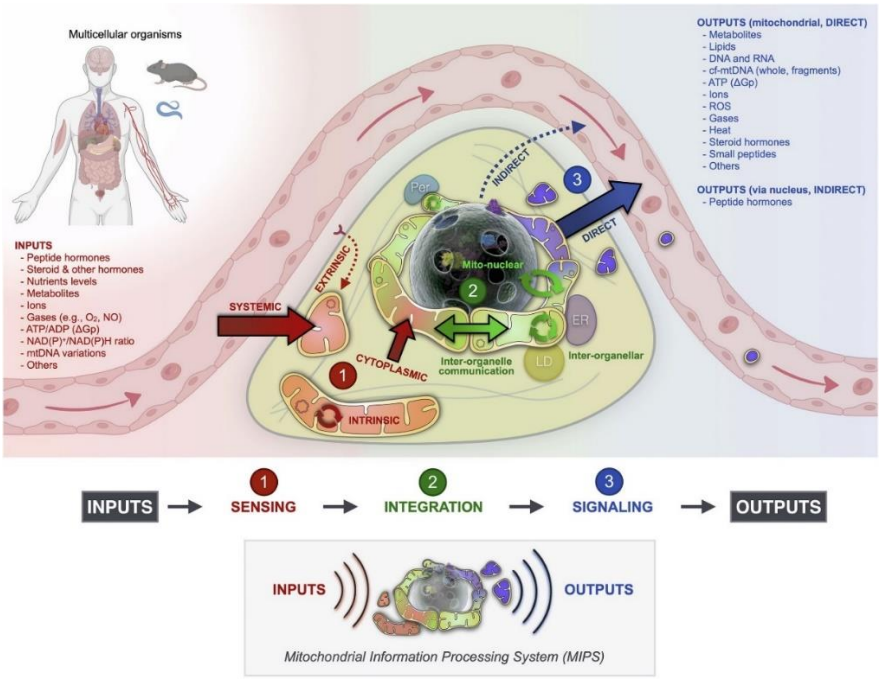


Fig. 8. Steps of mitochondrial information processing system (MIPS). This model has been adapted from Picard M, 2022.

Mitochondria are located at the topological interface between signals from the extracellular space and the nucleus, the cell compartment of the cell that stores the genome. All mitochondria can sense, integrate and generate signal/s that contribute to cellular functions (Picard M, 2022). In the next few sections, some of the crucial functions of mitochondria are discussed.

1.6.1 Mitochondria acts as a cellular sensor:

The mitochondrial sensing pathway consists of ligand-activated receptors, transporters, ion channels, the mitochondrial genome, oxidative phosphorylation, and other biochemical events

within the outer and inner mitochondrial membranes (OMM and IMM). Mitochondria have a vast range of receptors and molecular characteristics that allow them to detect various components, including hormones, metabolic products, ions and many other ligands (Picard M, 2022). Nuclear receptors (which are ligand-activated transcription factors that are usually found in the nucleus), are also found in the mitochondria. However, the localization of these receptors are still debatable which need further investigation. Thyroid hormones (T3 and T4) have dual action on nuclear gene expression and mitochondrial function. It has been discovered that mitochondria have two different types of thyroid hormone receptors. These receptors are p28 and p43 which are likely to be present in the IMM. These receptors have a high affinity towards T3 (triiodothyronine). In isolated mitochondria, the respiratory chain activity is modulated by T3 without altering the protein synthesis (Wrutniak-Cabello C, 2001; Sterling K, 1984; Sterling K, 1978; Sterling K, 1977). In a similar manner, two isoforms of estrogen receptors, ERα and ERβ, have been reported in mitochondria. ERα activates nuclear gene expression and regulates mitochondrial biogenesis. In contrast, ERβ translocates to mitochondria and executes an antiapoptotic effect (Mosselman S, 1996; Klinge CM, 2017; Yang SH, 2004; Solakidi S, 2005). Mitochondria sense androgenic hormones by its androgen receptor (AR). In prostate cells fraction of the AR localize to the mitochondria. The mitochondrial AR impacts mtDNA levels, mtDNA transcription and translation (Bajpai P, 2019). In order to respond to glucocorticoid hormones such as cortisol and corticosterone, mitochondria possess glucocorticoid receptors (GR). Mitochondria sense glucocorticoid by GRγ (Morgan DJ, 2016; Demonacos C, 1995).

G protein-coupled receptors are a relatively recent evolutionary development that are a part of the mitochondrial sensory system (GPCRs). Mitochondrial GPCRs, specific for angiotensin II, melatonin, endocannabinoids, and purines, are located in the outer mitochondrial membrane

(OMM) and inner mitochondrial membrane (IMM). These mitochondria-localized GPCRs have a wide range of potential effects, as evidenced by their ability to modulate a variety of mitochondrial processes, including ion absorption, OxPhos, nitric oxide generation, apoptotic signaling, and reactive oxygen species (ROS) production (Abadir PM, 2011; Suofu Y, 2017; Bénard, G, 2012). Another ligand-gated channel, namely α7 nicotinic Acetylcholine receptor (nAchR), is localized at the OMM, which senses acetylcholine and nicotine (Lykhmus O, 2014).

1.6.2 Mitochondrial Ca^{2+}-regulation:

At the intracellular level, Ca^{2+}-regulation is a very well-orchestrated process mainly governed by mitochondria and ER. Under homeostatic conditions, mitochondrial Ca^{2+}-concentration remains the same as cytoplasm (100-200 nM), but when the cells such as a neuron, cardiomyocytes, and other excitable cells are stimulated, the mitochondria can accumulate 10-20 fold more Ca^{2+} than the cytoplasm (Giorgi C, 2018). Mitochondrial Ca^{2+}-regulation can be divided into two pathways i.e. the way mitochondria will uptake Ca^{2+} from the cytosol and many other sources and the other pathway where the Ca^{2+} will extrude from it. In terms of uptake, the cytosolic Ca^{2+} should cross the outer mitochondrial membrane (OMM) and inner mitochondrial membrane (IMM) to reach the matrix. The OMM has high permeability due to the localization of VDAC (Voltage-dependent anion channel). VDAC is of three types: VDAC1, VDAC2 and VDAC3, that are present ubiquitously (Shoshan-Barmatz V, 2012; Messina A, 2012). After reaching the intermembrane space (IMS), Ca^{2+} travel through the inner mitochondrial membrane (IMM) predominantly by the mitochondrial calcium uniporter complex (MCU). Cell death, energy production, and cytosolic Ca^{2+}-signaling are all regulated by mitochondrial uptake of Ca^{2+} via the mitochondrial calcium uniporter complex (MCU). MCU is made up of four main parts: the pore-making protein MCU, the gatekeepers MICU1 and MICU2, and another part called EMRE, which is needed for Ca^{2+}-

transport (Fan M, 2020). Ca^{2+}-influx through the MCU is a predominant mechanism for mitochondrial Ca^{2+}-uptake. Nevertheless, MCU-independent Ca^{2+}-entry routes have been found. TRPC3 is a member of the TRP ion channel superfamily that resides in mitochondria and permits Ca^{2+} to enter the matrix. (Feng S, 2013). In accordance with that, several other TRP channels, such as TRPV1 and 4TM-TRPM8 and TRPV4, present in mitochondria and regulate mitochondrial Ca^{2+}-influx (Lang H, 2015; Bidaux G, 2018; Acharya TK, 2022a).

There are two major groups of transporters that have been discovered which transport Ca^{2+} from the matrix to the IMS (Inter Membrane Space). These are the mitochondrial Na^{+}/Ca^{2+}-exchanger (mNCX) and the mitochondrial H^{+}/Ca^{2+}-exchanger (HCX).

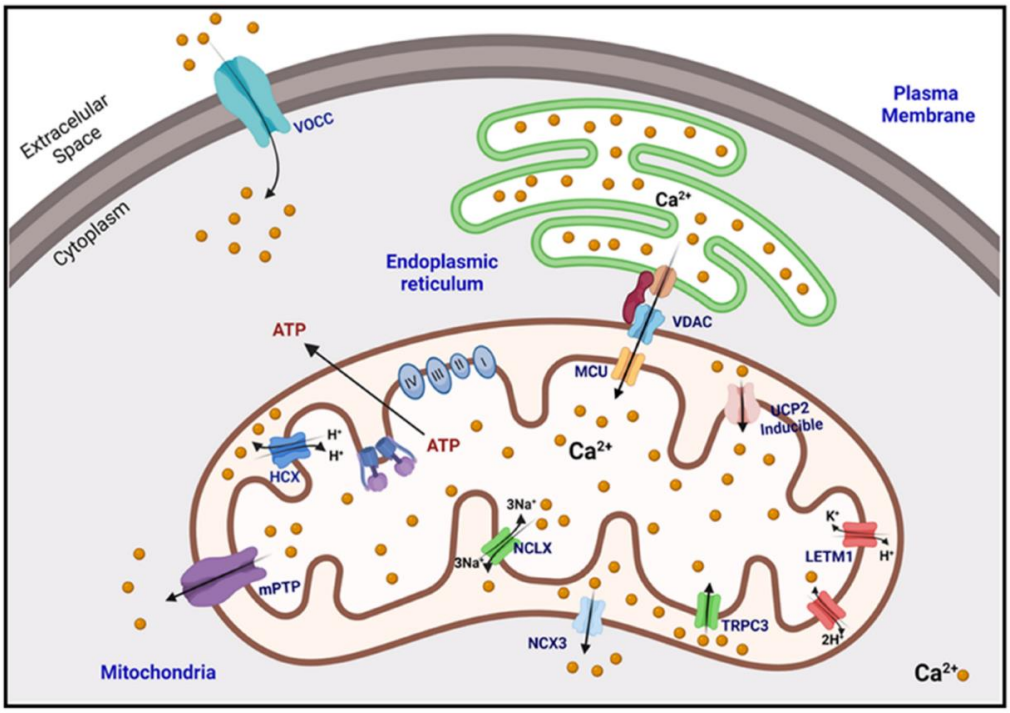


Fig. 9. General model of mitochondrial Ca^{2+}-transport in the intact cell. This image has been adapted from Matuz-Mares D, 2022.

Initially, mitochondrial NCX was simply defined as a Na+/Ca^{2+}-antiporter. However, it was discovered that it transported lithium (Li^{+}) or sodium (Na^{+}) in exchange for calcium (Ca^{2+}). As a result, it was later given the designation NCLX, which stands for (Na/Li/Ca exchanger) (Palty R,

2004). In excitable tissues such as the heart and brain, NCLX is the major antiporter, whereas HCX is mainly found in non-excitable tissues such as the kidney and liver. The NCLX transporter has a stoichiometry of three (or four) Na^+/Li^+ for each Ca^{2+}, whereas HCX exchanges two H^+ for one Ca^{2+} (**Fig. 9**) (Jung DW, 1995; Dash RK, 2008; Gunter KK, 1991; Matuz-Mares D, 2022).

1.6.3 Regulation of mitochondrial membrane potential:

Mitochondria create membrane potential (ψm) across the inner mitochondrial membrane (IMM) by using nutrients and molecular oxygen. The mitochondrial membrane potential (ψm) is the primary factor that controls the oxidative phosphorylation reaction (OXPHOS) and other mitochondrial metabolic activities. Therefore depolarization directly impacts mitochondrial physiology and decreases energy availability or ATP generation. The inner mitochondrial membrane (IMM) consists of cristae and an inner boundary membrane (IBM), which is expected to have uniform membrane potential (Wolf DM, 2019). As per the conventional understanding, the mitochondrial membrane potential is "homogeneous across the IMM". However, recent advanced microscopic techniques established that individual cristae within the same mitochondrion have disparate membrane potential and any impairment causing depolarization affects some cristae but not all. Notably, cristae within the same mitochondrion behave as an "independent bioenergetics unit", and any dysfunction of any cristae does not alter the function of other cristae directly or immediately (Wolf DM, 2019). The ψm is higher at the cristae compared to IBM, and when mitochondria were treated with oligomycin and FCCP, the ψm is altered across the IMM. In a similar manner, deletion of MICOS (mitochondrial contact site and cristae organizing system) complex components and OPA1 decreases the intra-mitochondrial heterogeneity of ψm (Wolf DM, 2019). Imaging at high or super-resolution of the inner membrane matrix (IMM) stained with ψm -dependent dyes is consistent with a notion of cristae as separate

batteries interconnected with one another. The ψm is not uniform along the IMM, but it does show substantial variances between the Cristae and the IBM. Because of the mitochondrion's "hetero-potential structure", various cristae can carry out various tasks. Some cristae in this scenario might be more specialized for ATP production, whereas other cristae in the vicinity might be involved in ROS-signaling. A graphical illustration of the hetero-potential of mitochondria cristae and IBM is summarized (**Fig. 10**).

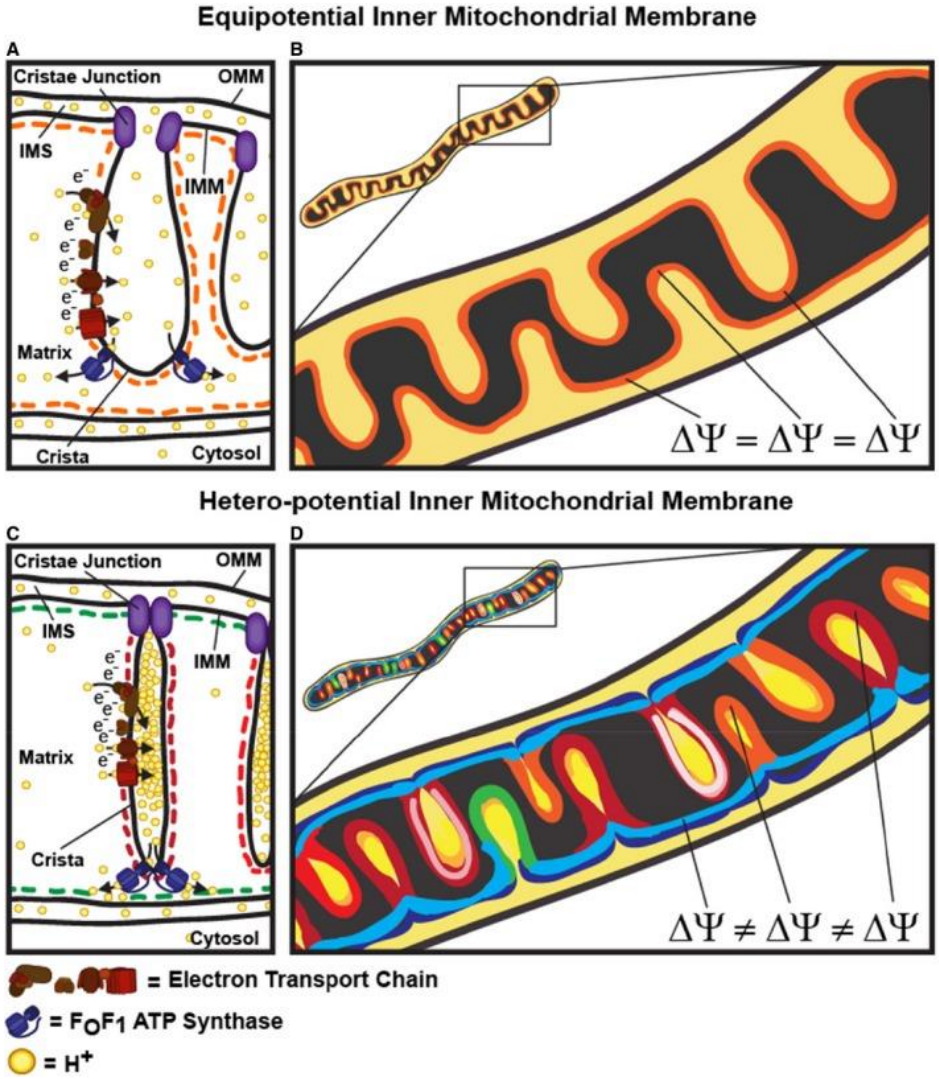


Fig. 10. Model of cristae as individual bioenergetics unit. A-B showing equipotential of IMM. **C-D**. Cartoon represents IMM is hetero-potential. This image has been adapted from Wolf DM, 2019.

1.6.4 Mitochondrial heterogeneity:

In an organ, neighboring cells of the same type may look and act differently because they are at different stages of differentiating, maturing, or facing challenges from the outside world. Similarly, a group of mitochondria in a single cell may represent different stages of development as well as varied response to the cellular environment, representing mitochondrial heterogeneity (Aryaman J, 2019). Both genetic and non-genetic factors contribute to mitochondrial heterogeneity. Mitochondrial DNA (mtDNA) sequence variation offers genetic sources of intracellular heterogeneity that affect processes, including reactive oxygen species (ROS) generation, protein structure conformation, and electron transport chain capacity (Palmer JW, 2004). Yet, post-translational processes, including phosphorylation and ubiquitination of mitochondrial proteins, also regulate structural and functional diversity. The molecular machinery determining the mitochondrial life cycle (biogenesis, mitochondrial motility, fusion and fission, and clearance of damaged mitochondria) can also produce mitochondrial heterogeneity (Ngo J, 2021). Mitochondrial heterogeneity is caused by a mitochondrial subpopulation having a different shape, Ca^{2+}-level, membrane potential, cell localization or proximity to other organelles. At the physiological state, subcellular Ca^{2+}-levels promote mitochondrial Ca^{2+}-heterogeneity in two ways: through dense Ca^{2+}-microdomains and Ca^{2+} -tunnelling (Hüser J, 2000). Intracellular mitochondrial Ca^{2+}-heterogeneity has been demonstrated to alter the mitochondrial shape, motility, and mitophagy in a variety of cell types, including HeLa, PAEC, COS-7, HUVEC, hepatocytes, astrocytes, and neuronal cells (Collins TJ, 2002; Georgiadou E, 2020; Kremneva E, 2013). Mitochondria subpopulations have been categorized as perinuclear, peripheral, ER-bound, and peridroplet. Even while subpopulation-specific functions have been observed, it remains unclear if these functions are a result of location-specific requirements or intrinsic features (**Fig.**

11) (Ngo J, 2021). Perinuclear mitochondria localized to the nucleus and represent higher membrane potential and reduced mitochondrial length. The peripheral mitochondria cover the plasma membrane display increases mitochondrial length. ER-bound mitochondria tethers to the ER consists of higher mitochondrial Ca^{2+}-load. Peridroplet mitochondria make close contact with lipid droplets and the length is elongated compared to cytosolic mitochondria (Ngo J, 2021).

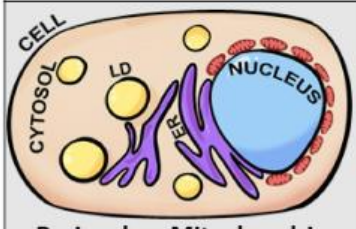
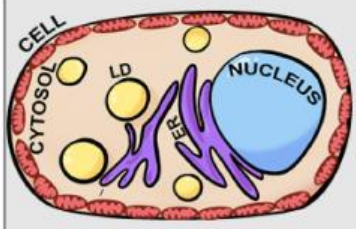
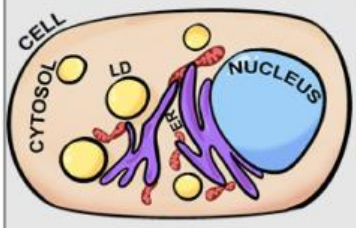
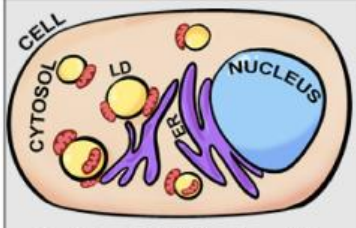
	Localization	Morphology	Membrane Potential	$\frac{ATP}{ADP}$	$_{mt}Ca^{2+}$
A	 Perinuclear Mitochondria	Shorter	Higher ΔΨ	Lower	Lower
B	 Peripheral Mitochondria	Elongated	Lower ΔΨ	Higher	Higher
C	 ER-Bound Mitochondria	Intermediate	Higher ΔΨ	No Change	Higher
D	 Peridroplet Mitochondria	Elongated	Undetermined	Higher	Undetermined

Fig. 11. Schematic diagram of mitochondrial heterogeneity within a cell. This figure has been adapted from Ngo J, 2021.

1.6.5 Mitochondrial communication with other organelles:

Mitochondria regulate cellular processes such as energy metabolism, biosynthetic processes, apoptosis, and cell turnover through a variety of interactions with the endoplasmic reticulum, lysosomes, cytoskeleton, and peroxisomes. These interactions can take place through signal transduction, vesicle transport, and membrane contact sites (Audano M, 2020). The contact sites between mitochondria and endoplasmic reticulum (ER) are essential for the regulation of a wide variety of cellular functions, such as Ca^{2+}-homeostasis. Ca^{2+} enters mitochondria from the endoplasmic reticulum via MAMs and serves a crucial function in the mitochondrial division and apoptosis control (Xia M, 2019). Mitochondria also make close contact with the peroxisomes. The crosstalk between mitochondria and peroxisomes is vital for a number of different metabolic activities, and the beta-oxidation of fatty acids is one of the most well-known examples of the communication that takes place between these two organelles (Poirier Y, 2006). Mitochondria and peroxisomes function together in lipid metabolism, but they also exchange information for various signaling pathways. Peroxisomal and mitochondrial metabolisms are closely linked to the production of reactive oxygen and nitrogen species (ROS and RNS). They have antioxidant systems and play a crucial role in controlling cellular redox state (Diogo CV, 2018). Recent discoveries also suggest that mitochondria make contact with lysosomes to import Ca^{2+} and other metabolites. Furthermore, voltage-dependent anion channel 1, the mitochondrial Ca^{2+}-uniporter, other channels present in the outer and inner mitochondrial membranes, respectively, regulate mitochondrial Ca^{2+}-uptake at mitochondria-lysosome contact points (Peng W, 2020). Recent reports suggest that lysosomal Ca^{2+}-efflux channel Transient Receptor channel mucolipin 1 (TRPML1) acts as an important regulator of mito-lyso contact points. Loss of TRPML1 results in lysosomal storage disorder, i.e. mucolipidosis type IV (MLIV) which is due to alteration in

mitochondria-lysosome contact dynamics and improper mitochondrial Ca^{2+}-uptake (Peng W, 2020). In order to understand the mitochondrial diseases and mitochondrial stress signaling, more and detailed investigation is required to identify how different organelles communicate and interact with each other. Any perturbation in intra-organelle communication can affect the structure and function of these organelles, which leads to different pathophysiology.

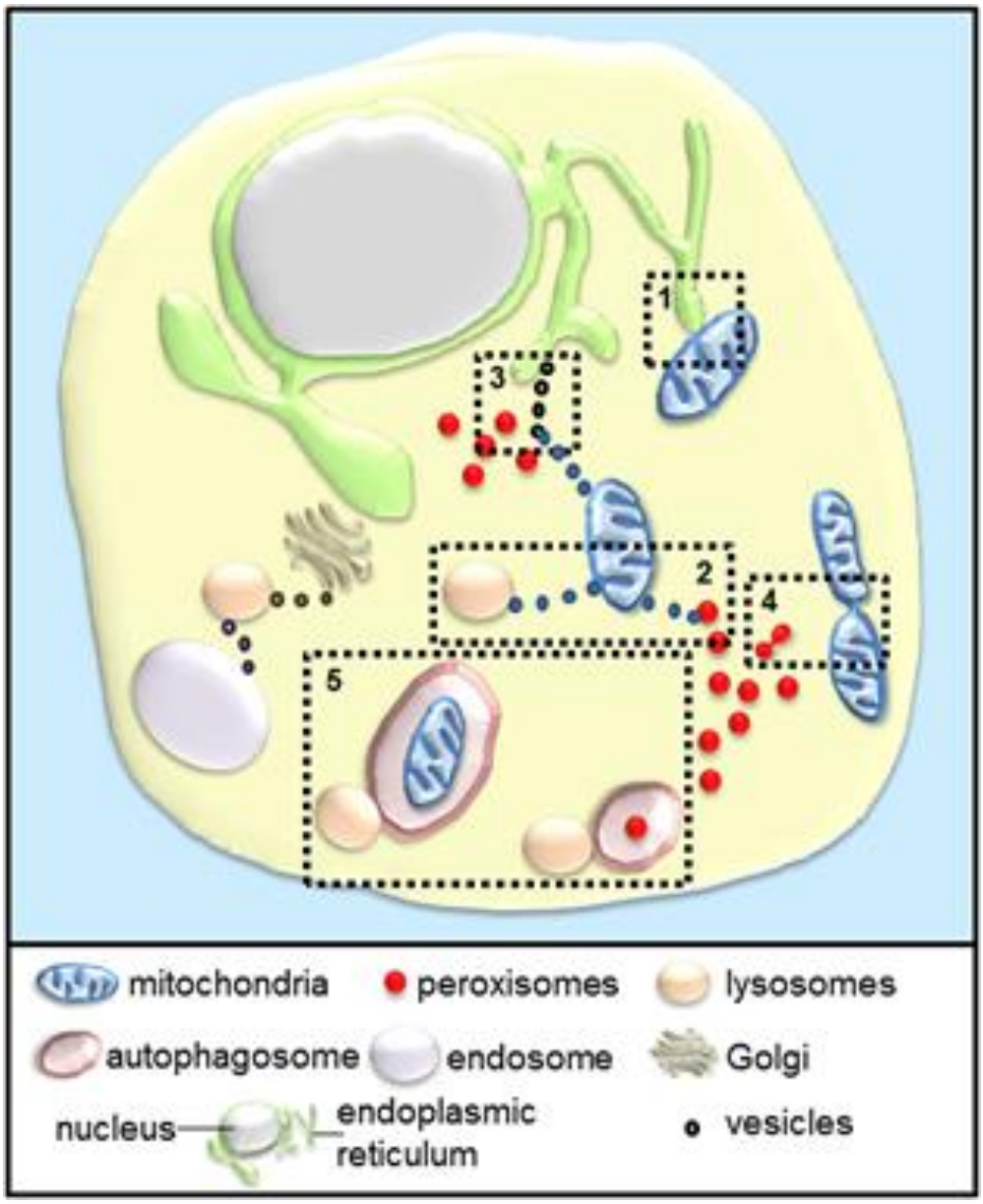


Fig. 12. Interaction of mitochondria with different organelles. This schematic representation of different organelles with whom mitochondria make contact. This scheme has been adapted from Diogo CV, 2018.

1.6.6 Mitochondria function as a thermostat:

The thermostat is a device that controls the temperature of a house or a device by switching on and off according to convenience**.** In a cellular system, mitochondria are the warmest compartment and hottest component of the cell. Endotherms obtain their body temperature mostly from respiratory chain activity (Nicholls DG, 1984; Picard M, 2022). The second law of thermodynamics states that the direction of heat movement is always from warmer to colder areas. Therefore, the diffusion of heat and changes in biochemical activities represent a form of signaling. The heat-mediated signaling is transferred from one organelle to other sub-cellular compartments. In a cellular environment, mitochondria act as a thermostat and regulate cellular functions. Recent reports suggest that mitochondria maintain their temperature at 50 °C (Chretien D, 2018). Uncoupling of OxPhos by FCCP increases mitochondrial matrix temperature by 6-9 °C (Nakano M, 2017). Consequently, the temperature difference between mitochondria (the warmest compartment) and other subcellular structures designate mitochondria a thermodynamically advantageous and regulatory position in signal transduction than other subcellular organelles.

Multiple well-established and evolving signaling mechanisms connect mitochondrial activity to nuclear gene expression also. Accordingly, so far, several components of mitochondrial signaling, including apoptotic signaling, ROS-mediated signaling, and metabolic signaling, mitochondrial genome signaling, mitochondrial innate immunity signaling, synthesis of stress and steroid hormones, have been identified, all of which can modulate the nuclear gene expression (Picard M, 2022). Therefore, understanding mitochondrial functions in diverse cellular contexts is important. In this context, the importance of thermosensitive ion channels is extremely important as these channels can be crucial for several of these mitochondrial sensory and regulatory abilities.

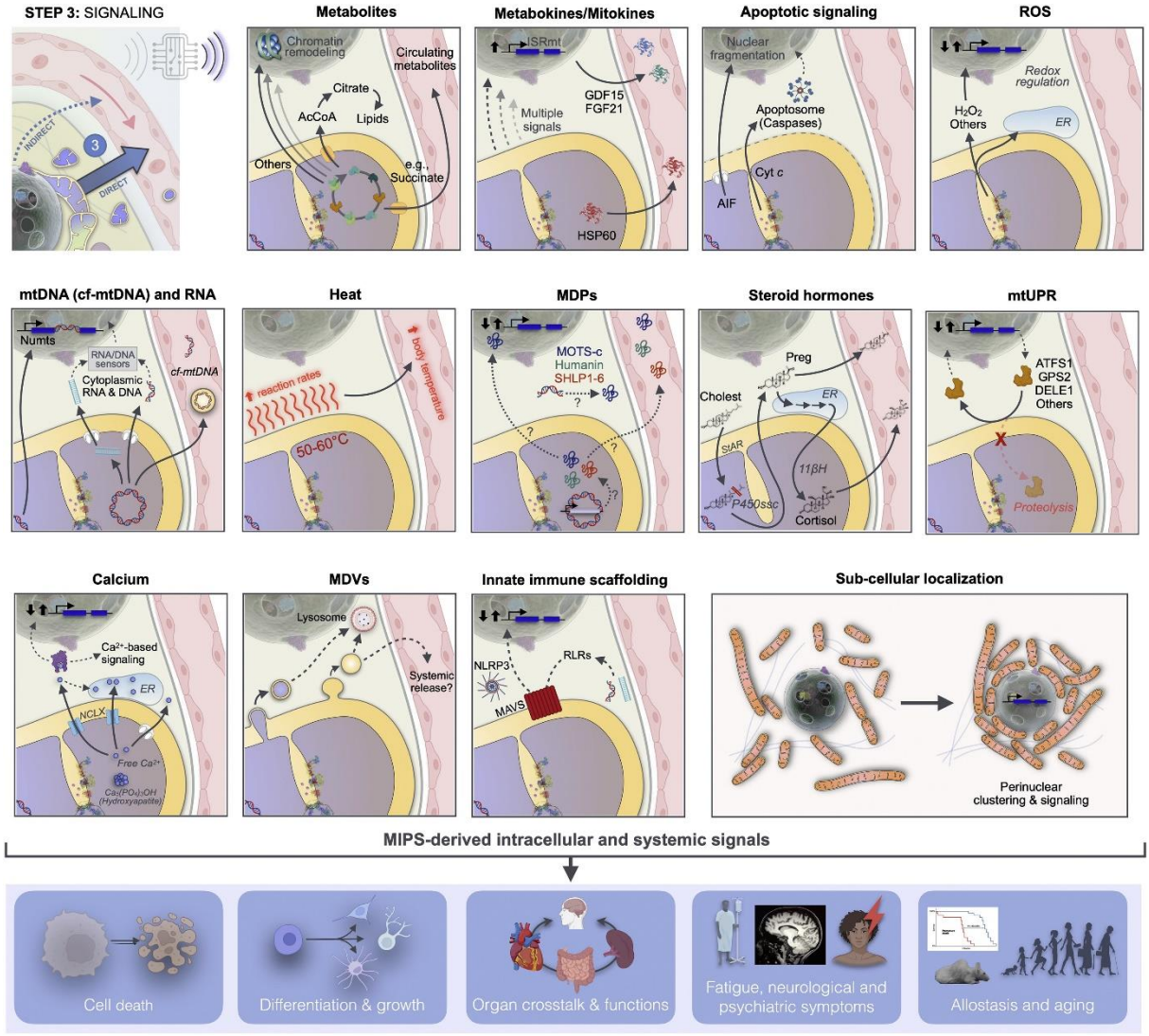


Fig. 13. Different signaling pathways of mitochondria. This image has been adapted from Picard M, 2022.

1.7 Specific objectives of this study:

This thesis aims to characterize the functionality of two ion channels i.e. TRPV4 and TRPM8, representing "heat-sensing" and "cold-sensing" ion channels, respectively, in the context of mitochondrial biology. TRPV4 and TRPM8 channels are non-selective cation channels that permeate Ca^{2+} favorably inside the cell. These channels are ubiquitous and present in almost all the tissue and organ systems that have been explored. Notably, point mutations in specific (but not all) TRP channels induce complex disorders and diseases with numerous manifestations, commonly termed as "Channelopathies". In this context, TRPV4 is very important as, so far, at least ~60 point mutations have been identified with different penetration levels, and all these are linked to disorders with pathophysiological phenotypes ranging from very mild, context dependent to embryonic lethality. Similarly, different pathophysiologies related to TRPM8 have been reported. Mostly in various types of cancer and other diseases, the role of TRPM8 has been studied. Previously it was a common notion that TRP channels are expressed only on the plasma membrane and regulate intracellular calcium homeostasis. But, in recent decades, intracellular localization of TRP channels has been reported by several labs. Indeed, recent reports revealed the localization of TRP channels in sub-cellular organelles, such as in lysosomes and in mitochondria. The functionality of these channels within the context of these sub-cellular organelles has been demonstrated.

Among TRPV channels, TRPV1 and TRPV3 are functionally expressed in ER and regulate its function (Dong XP, 2010). It has also been reported that TRPV1 is present in the mitochondria and regulates mitochondrial calcium levels (Gallego-Sandín S, 2009). Besides TRPV1, there is another TRP channel, such as TRPC3, which is also reported to be present in mitochondria (Lang H, 2015). Recently it was shown that TRPM8 is present at the mitochondria-associated membrane

(MAM) region and regulates ER-mitochondrial Ca^{2+} transfer (Feng S, 2013). Recent reports have also shown that TRPV4 has sub-cellular localization in the nucleus and the endoplasmic reticulum (ER) (Bidaux G, 2018). However, it was revealed that when TRPV4 is mutated, its surface localization reduces, and it purportedly localizes in the cytoplasm as a puncta. The functional characterization of these puncta were unknown (Becker D, 2008). Although several studies demonstrate the functional localization of multiple TRP channels in subcellular organelles, no evidence that suggests the functional localization of TRPV4 and TRPM8 in mitochondria. In our work, we postulate that TRPV4 and TRPM8 are present in mitochondria in many endogenous systems and govern the mitochondrial structure, Ca^{2+}-metabolism, ATP level, membrane potential, Cardiolipin level, ER-mito contact sites, and most importantly, mitochondrial and ER temperature. Since it has been shown that mutations in TRPV4 and TRPM8 cause skeletal deformities and other bone-related disorders, we used a hydrogel-based drug delivery system to specifically target these channels *in vitro* and *in vivo* as a translational strategy for enhancing bone health and better comprehend their underlying mechanisms.

AIMS OF THE PRESENT STUDIES:

1. Functional localization of TRPV4 and TRPM8 in mitochondria in different cellular systems
2. If and how TRPV4 regulates mitochondrial metabolism?
3. If and how TRPM8 regulates mitochondrial metabolism?
4. TRPV4 mediated mitochondrial regulation: impact on bone cell functions and application in bone tissue engineering
5. TRPM8-mediated mitochondrial regulation: impact on bone cell functions and application in bone tissue engineering
6. TRPV4- mediated mitochondrial regulation: impact on T cell activation
7. TRPM8-mediated mitochondrial regulation: impact on T cell activation
8. Characterization of TRPV4-mediated channelopathies in the context of mitochondrial abnormalities.

Chapter 2

Results

2.1 Characterization of TRPV4 channel in intracellular organelles:

Mostly TRP channels are localized in the plasma membrane in various neuronal and non-neuronal tissues and carry out various cellular functions. However, recent reports suggest that TRP channels are not only present in the plasma membrane but also localized in intracellular organelle membranes. For example, TRPV1, TRPM8, and TRPV3 are physically present at the ER membrane and regulate its metabolism (Gallego-Sandin S, 2009; Lo IC, 2016; Bidaux G, 2018). Similarly, TRPML1 (mucolipin 1) channels are present in the late endosome and lysosome membrane and mutations in this channel cause mucolipidosis type IV disease (Dong XP, 2008). Nevertheless, the molecular characterization of these channels in the intracellular compartments is not fully understood. Previously we have reported that in case of overexpression, TRPV4 as well as TRPV4-GFP localize to the plasma membrane in F11 cells. In addition, a considerable fraction of TRPV4 also localizes to specific intracellular organelles (Goswami C, 2010). To characterize this intracellular fraction in detail, recently, we performed immunolocalization on TRPV4 overexpressing conditions (HaCaT, COS-7, HeLa, F11, CHO-K1 cells) and in endogenously expressing HUVEC cells. In all cases, we observed TRPV4 in the plasma membrane and in separate intracellular organelles (Acharya TK, 2022a). Here we observed that indeed TRPV4 localized to mitochondria and did not localize to other organelles such as ER, lysosomes, and Golgi (Acharya TK, 2022a).

2.1.1 TRPV4 is present in mitochondria endogenously:

From our previous studies, we had an idea that TRPV4 colocalizes with different mitochondrial proteins in other cellular systems. Next, we sought to confirm that TRPV4 is endogenously present in mitochondria. We immunostained Mesenchymal stem cells and bone marrow macrophages isolated from mouse bone marrow for that purpose. For the immunostaining

method, we stained with specific TRPV4 antibodies and HSP60 was used as a mitochondrial marker. We observed colocalization of TRPV4 with HSP60 in these cells confirming that TRPV4 is indeed present in a subpopulation of mitochondria (**Fig. 14 A-B**). We have represented the colocalized spots as white points along with scattered plots were shown in **Fig. 14 C-D** to depict the extent of colocalization in the cell.

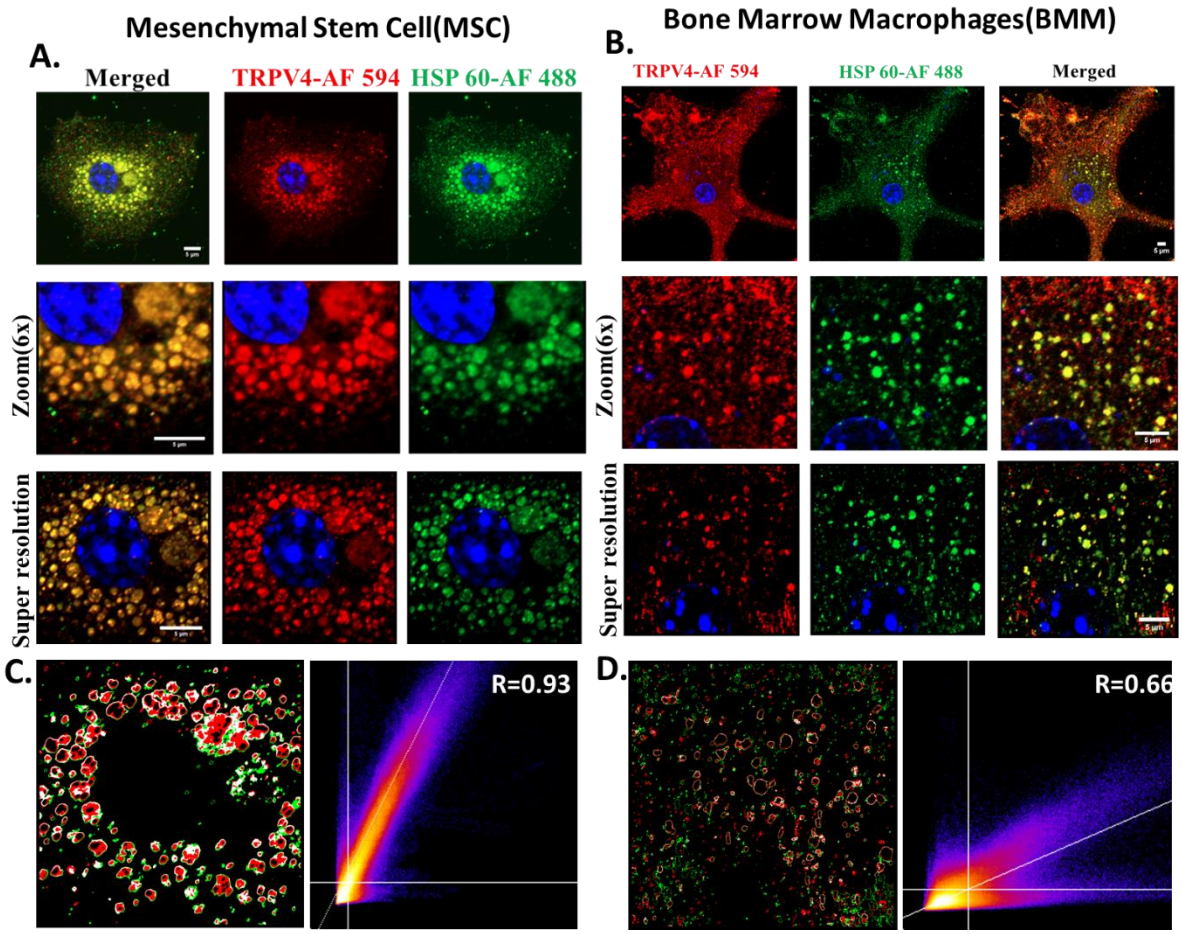


Fig. 14. TRPV4 is endogenously present in mitochondria. A-B. TRPV4 colocalizes with HSP60 in Mesenchymal stem cells (MSC) (**A**) and Bone marrow macrophages (BMM) (**B**) isolated from mouse bone marrow. Cells were immunostained for TRPV4 and HSP60. **C-D.** The colocalized spots were represented as white spots and scattered plots for the extent of colocalization were represented. Scale bar is 5 μm. (Published figure. Acharya TK. et al. 2022, *Mitochondrion*)

2.1.2 TRPV4 colocalizes with mitochondrial markers in isolated mitochondria:

To further confirm this, freshly isolated mitochondrial fractions from rat brain were labelled *ex vivo* with the mitochondria-specific dye MitoTracker Red. After fixation, the isolated mitochondria were stained for TRPV4 and analyzed by super-resolution microscopy (**Fig. 15**). In the same way, isolated mitochondria were double stained for both HSP60 and TRPV4 (**Fig. 15**). In both cases, TRPV4 was detected in a subset of mitochondria, but not in all of them.

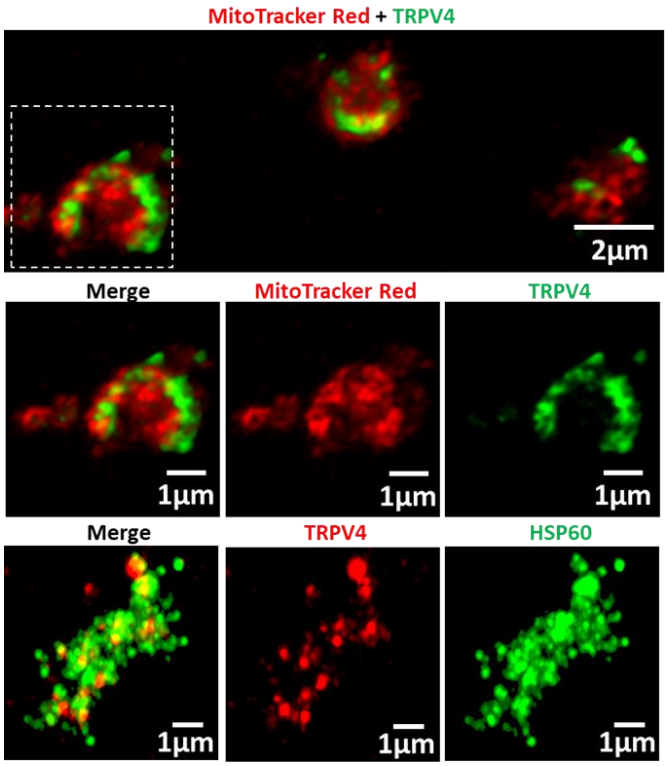


Fig. 15. TRPV4 is endogenously present in isolated mitochondria. Shown are the super-resolution images of mitochondria isolated from rat brains and immunostained for TRPV4 (green). Isolated mitochondria were labelled with MitoTracker Red (upper and middle panel) or immunostained for Hsp60 (green, lower panel). TRPV4 is present in a subset of mitochondria but not in all. (Published figure. Acharya TK. et al. 2022, *Mitochondrion*).

2.1.3 Localization of TRPV4 in the mitochondrial membrane:

We tested the presence of TRPV4 in the mitochondria by immunoblot analysis. TRPV4 is present and enriched in the isolated mitochondria from rat brains. Mitofusin-2 has been used as a positive mitochondrial control to show the purity of the mitochondrial membrane fraction. Next,

we attempted to explore if TRPV4 is present in the inner or outer membrane of mitochondria. For that purpose, we isolated the inner membrane and outer membrane and analyzed the presence of TRPV4 there. We noted that TRPV4 is present in both inner and outer membranes when isolated from rat brains, where tentatively more TRPV4 seems to be present in the inner membrane (**Fig. 16A, C**).A similar observation was made for mitochondria isolated from CHO-K1-Mock and CHO-K1-V4 cells where TRPV4 seems to be more abundant in the outer than in the inner membrane (**Fig. 16 B-C**).

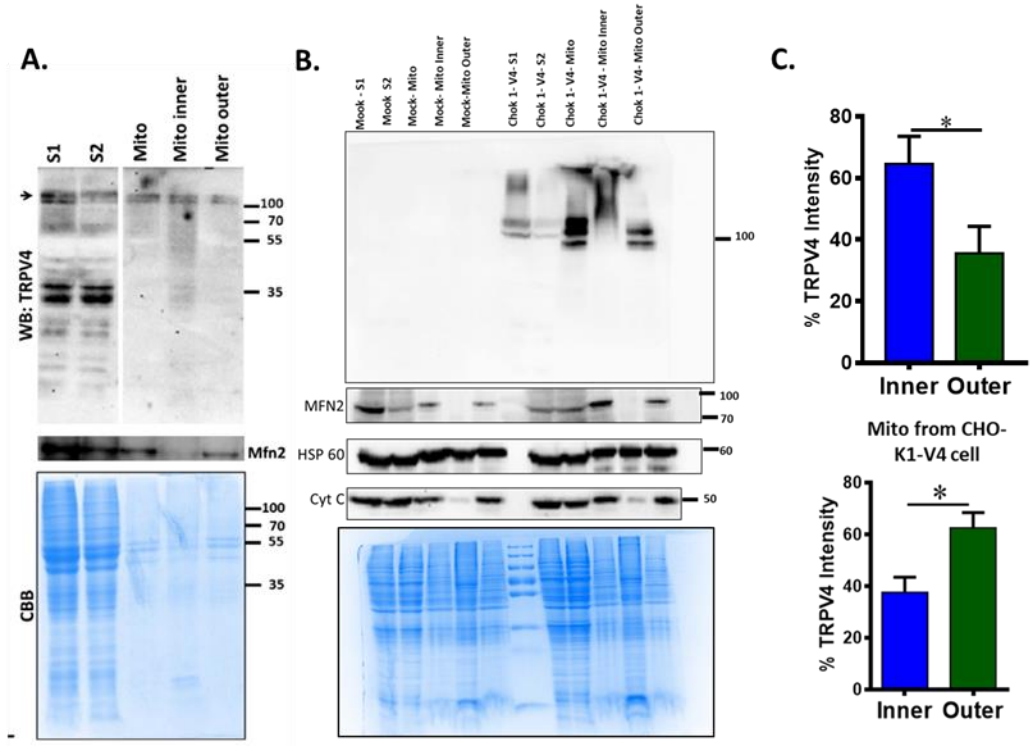


Fig. 16. Localization of TRPV4 in the mitochondrial membrane: **A**. Western blot analysis of different mitochondrial fractions (S1, S2 and Mitochondrial fraction) isolated from rat brains are shown. Endogenous TRPV4 is present in isolated mitochondrial fractions as well as in both inner and outer membrane fractions. **B**. Western blot analysis of mitochondrial fraction isolated from CHO-K1-Mock and CHO-K1-V4 cells are shown. TRPV4 is present mostly in the outer membrane fraction. **C**. Quantification of relative abundance of TRPV4 in outer and inner mitochondrial membrane is shown (total mitochondrial TRPV4 is considered as 100%). The majority of the endogenous TRPV4 is present in the inner membrane rather than in the outer membrane of mitochondria isolated from the brain (ns = non-significant, n = 4, P value = 0.1181). In contrast, the majority of the TRPV4 is present in the outer membrane rather than in the inner membrane of the mitochondria isolated from CHO-K1-Mock and CHO-K1-V4 cell (n = 6, P value = 0.0141, n = 6). (Published figure. Acharya TK. et al. 2022, *Mitochondrion*)

2.1.4 TRPV4 contributes in mitochondrial Ca^{2+}-influx in cell-free system:

To substantiate the results of Ca^{2+}-influx through TRPV4 into mitochondria, we performed Ca^{2+}-imaging with isolated mitochondria in a cell-free system using Rhod-3-AM dye. Mitochondria were purified from mouse brain and treated with 4αPDD (5 µM, 0.5 µM and 0.05 µM), RN1734 (10 µM), ionomycin (5 µM) or CCCP (100 µM). Ca^{2+}-influx inside mitochondria increases significantly after the addition of 4αPDD in comparison to control at all the concentrations tested. In contrast, in the presence of RN1734, mitochondrial Ca^{2+}-level decreased. Ionomycin treatment caused a strong influx of Ca^{2+} into mitochondria, and as a result, mitochondria formed large clusters. In the presence of CCCP, Ca^{2+}-level was reduced drastically. These data suggest that TRPV4 regulates mitochondrial Ca^{2+}-influx even in a cytosol-free condition as well (**Fig. 17A-B**).

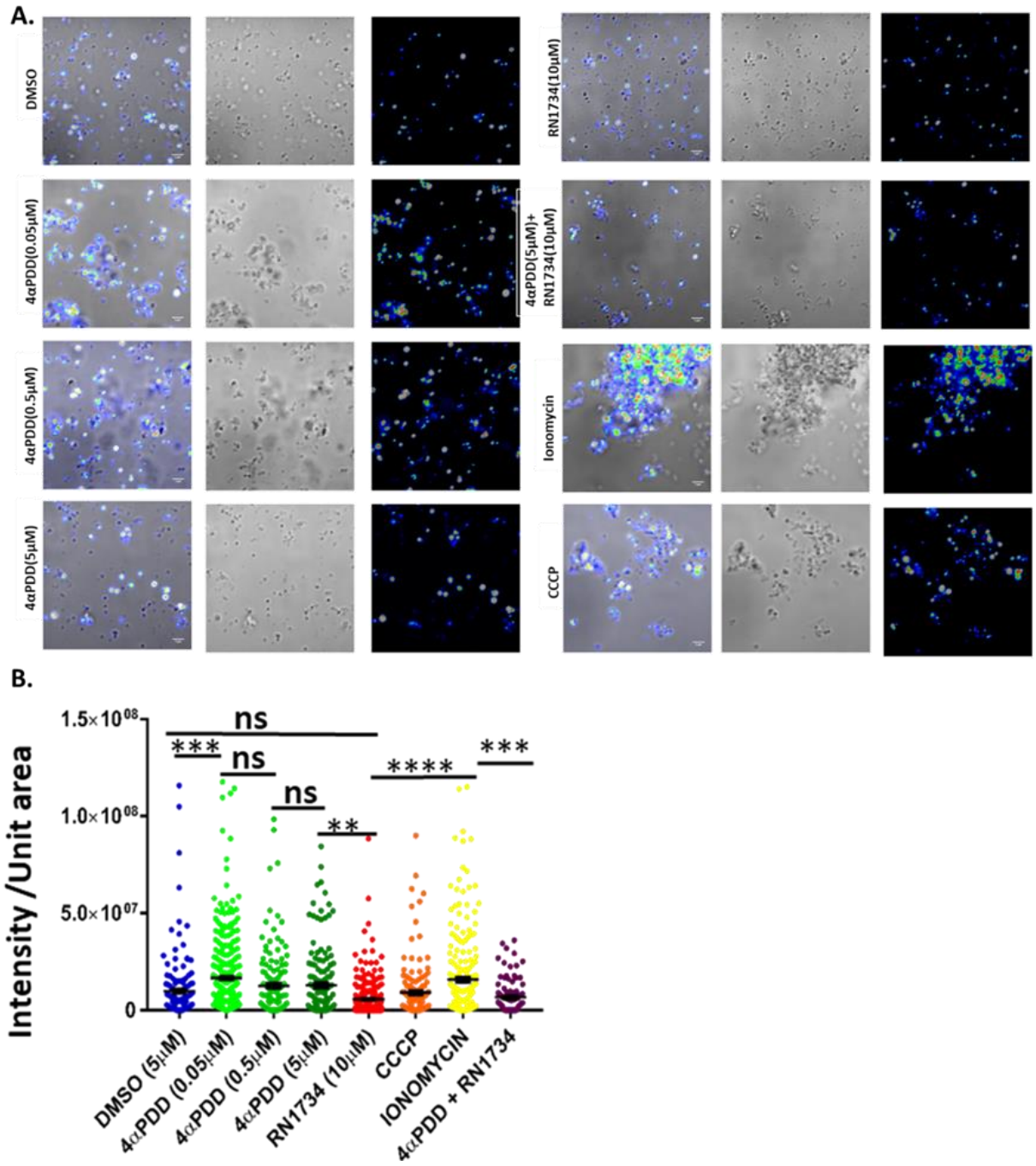


Fig. 17. TRPV4 regulates Ca^{2+}-levels in isolated mitochondria. A. Mitochondria were purified from mouse brain and treated with 4αPDD (5 μM, 0.5 μM and 0.05 μM), RN1734 (10 μM), Ionomycin (5 μM), or CCCP (100 μM). Ca^{2+}-levels inside the mitochondria increase after the addition of 4αPDD in comparison to the control. In the presence of RN1734, the mitochondrial Ca^{2+}-levels goes down significantly (N = 2, scale bar is 1 μm). **B.** The fluorescence intensity indicating the relative Ca^{2+}-levels in each condition is represented (one-way ANOVA, ns = non-significant *** = $p<0.001$, **** = $p<0.0001$). (Published figure. Acharya TK. et al. 2022, *Mitochondrion*).

We also performed kinetic imaging in isolated mitochondria from mouse brains. As mitochondria are highly mobile, it is very difficult to track the same mitochondrial particle for a period, and we considered a view field saturated with mitochondria. We observed that upon addition of 4αPDD, mitochondria became aggregated, and the fluorescence intensity increased (**Fig. 18**).

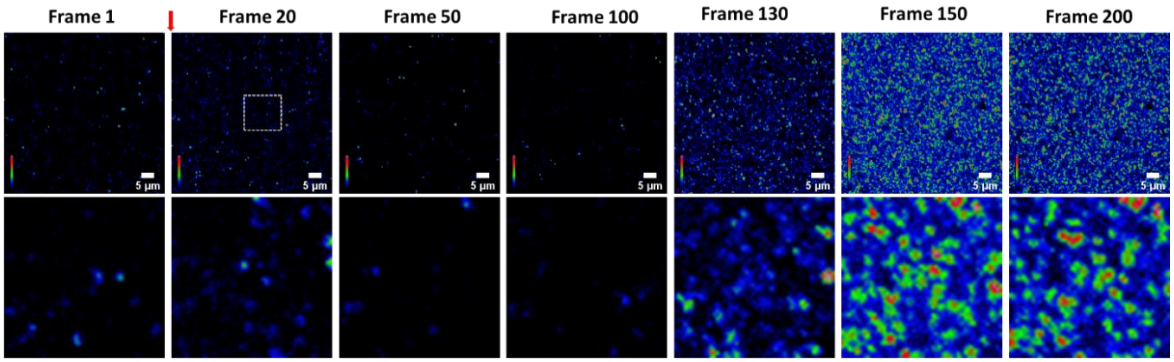


Fig. 18. Time series of Ca^{2+}-influx in isolated mitochondria. The isolated mitochondria ware activated by 4αPDD added at 20th frame (indicated by red arrow). Increase in Ca^{2+}-intensity within the mitochondria is observed at later points (after 125th frames). (Un-published Figure).

2.1.5 TRPM8 is localized in mitochondria endogenously:

Previously it has been demonstrated that truncated 4TM-TRPM8 is present at the ER and ER-mito contact site (Bidaux G, 2018). We explored the localization of endogenous TRPM8 in mitochondria. For that purpose, we performed immunofluorescence study in Saos-2 cells (human osteosarcoma cell), mouse bone marrow derived Mesenchymal stem cell and purified mitochondria from mouse brain. MitoTrackerRed CMXRos, OPA-1 and Cyt C were used as mitochondrial markers. From the immunostaining study, we found that there is a subset of mitochondria where TRPM8 co-localize with different mitochondrial markers (**Fig. 19A, C**). This data support the previous finding, which mentioned the localization of truncated 4TM-TRPM8 in mitochondria (Bidaux G, 2018). To explore the role of TRPM8 in mitochondrial physiology, we used Menthol (a natural and non-specific agonist of TRPM8) and also specific synthetic modulators of TRPM8, such as WS12 (TRPM8 agonist) and AMTB (TRPM8 antagonist).

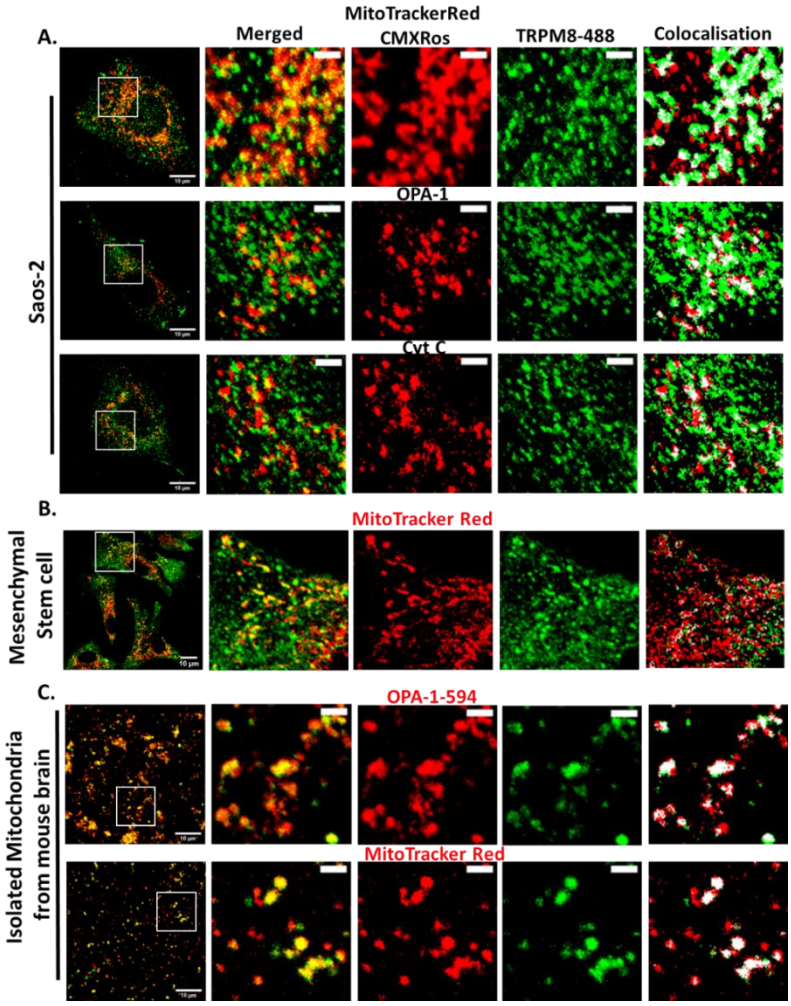


Fig. 19. TRPM8 is endogenously localized at the mitochondria. A. TRPM8 colocalizes with mitochondrial markers (mitoTrackerRed, OPA1, CytC) in Saos-2 cells. **B.** TRPM8 colocalizes with mitoTracker Red in primary mouse bone marrow derived Mesenchymal stem cells. **C.** Mitochondria isolated from mouse brains were immunostained for TRPM8 (green). Isolated mitochondria were labelled with MitoTracker Red or immunostained for OPA1 (red). TRPM8 colocalizes with these mitochondrial markers in a subset of mitochondria but not in all. Colocalized points were represented as white spots. (Un-published figure).

Summary: TRPV4 and TRPM8 are group of thermosensitive ion channels associated with the development of neuropathic pain, sensory defects, muscular dystrophies, neurodegenerative disorders, Charcot Marie Tooth and skeletal dysplasia. In all these cases, mitochondrial abnormalities are prominent. Here, we demonstrate that TRPV4 and TRPM8 localize to a subpopulation of mitochondria in various cell lines, primary cells (mouse bone marrow derived Mesenchymal stem cells and bone marrow macrophages) and isolated mitochondria from mouse brain. In all these conditions, TRPV4 and TRPM8 colocalizes with mitochondrial markers. The topology of this channels in the mitochondrial membrane is not clearly known yet. However, through our biochemical fractional experioments, TRPV4 has been detected both in the inner as well as outer mitochondrial membrane.

2.2 If and how TRPV4 regulates mitochondrial metabolism?

2.2.1 TRPV4 regulates mitochondrial Ca^{2+}-dynamics:

While the outer mitochondrial membrane allows for relatively free entry of Ca^{2+}-ions via VDAC and other yet unidentified ion channels, passage of Ca^{2+}-ions across the inner membrane is tightly controlled (Rosencrans WM, 2021; Hoppe UC, 2010). We explored if TRPV4 is involved in the control of Ca^{2+}-influx into mitochondria. Live-cell imaging was performed on CHO-K1-V4 and CHO-K1-Mock cells expressing Mito-Pericam, to assess the mitochondrial Ca^{2+}-dynamics in the presence of TRPV4 activator or inhibitors. Ca^{2+}-influx into mitochondria increases within seconds after the addition of 4αPDD in CHO-K1-V4 cells, but not to a similar extent in CHO-K1-Mock cells (**Fig. 20A, D**). Addition of the inhibitor RN1734 results in a gradual reduction of mitochondrial Ca^{2+}-levels both in CHO-K1-V4 and in CHO-K1-Mock cells, though to different extents, as indicated by fluorescence intensities of Mito-Pericam. (**Fig. 21A**).

Further, cells were pre-incubated with RN1734 for 1 hour and subsequently were activated by 4αPDD. In this case, the Ca^{2+}-level also increases, but more modestly than without inhibitor, upon addition of 4αPDD in CHO-K1-V4 cells. A slight increase in Ca^{2+} is observed in CHO-K1-Mock cells (**Fig. 20B, D**). Notably, in CHO-K1-V4 cells, 4αPDD-induced Ca^{2+}-influx is significantly lower in the presence of RN1734 than in the control condition. In another experiment, cells were pre-treated with BAPTA-AM for 1 hour to chelate intracellular $Ca^{2+,}$ and subsequently Ca^{2+}-influx was recorded by adding 4αPDD. In this condition, mitochondrial Ca^{2+}-levels are higher in CHO-K1-V4 than in CHO-K1-Mock cells (**Fig. 20C, D**). This suggests that BAPTA-AM-mediated intracellular Ca^{2+}-chelation limits the Ca^{2+}-influx in mitochondria in response to TRPV4 activation.

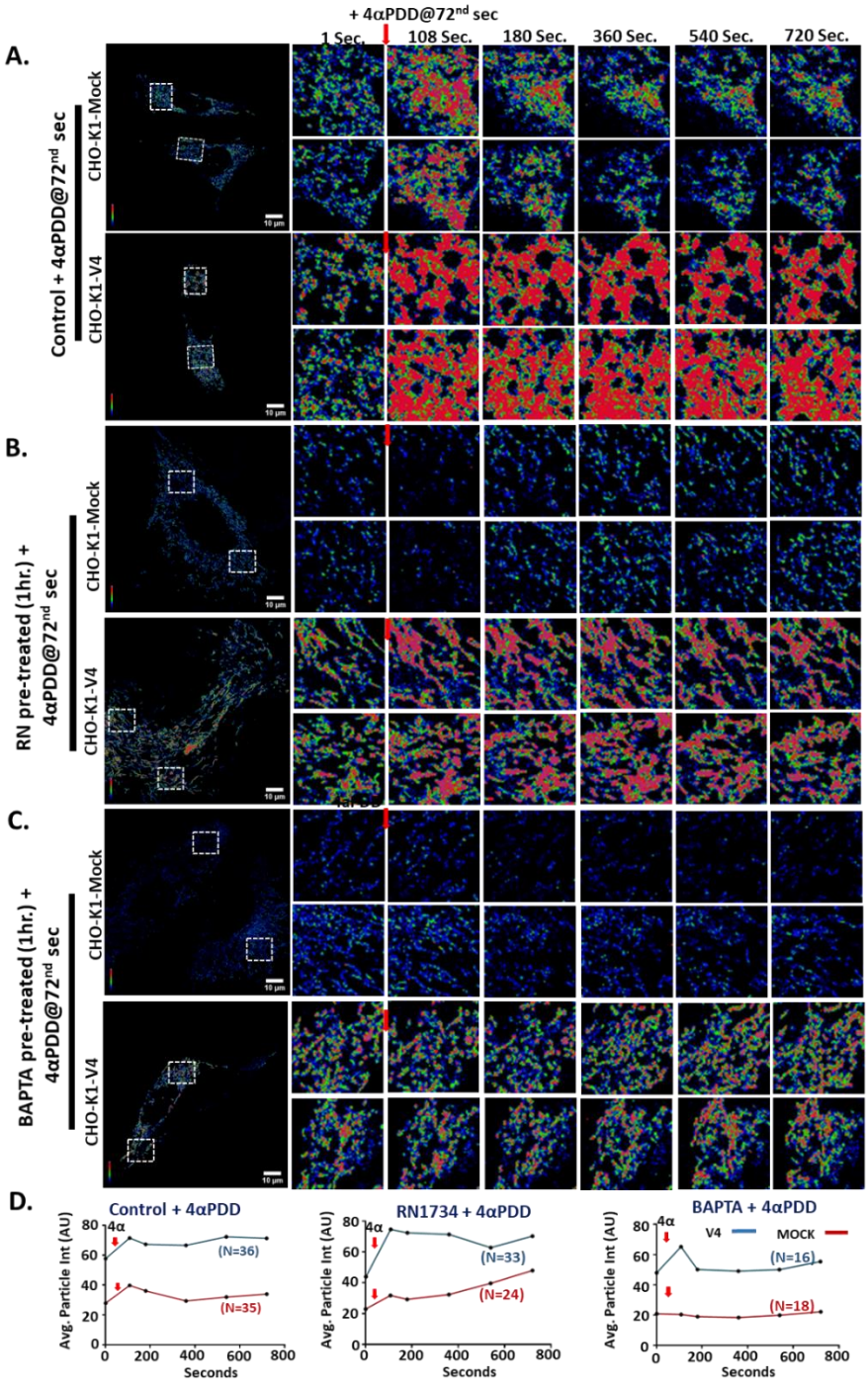


Fig. 20. TRPV4 regulates mitochondrial Ca^{2+}-influx. A-C. Mito-Pericam was transiently expressed in CHO-K1-V4 or CHO-K1-Mock cells, and live-cell imaging was performed to monitor the effect of TRPV4 activation (4αPDD, 5 μM) on mitochondrial Ca^{2+} in untreated cells (**A**), or cells pre-treated with RN1734 (10 μM) (**B**) and BAPTA-AM (10 μM) (**C**). The red arrow indicates the time of addition of the 4αPDD (72nd seconds). The addition of 4αPDD causes mitochondrial Ca^{2+}-influx in CHO-K1-V4 cells prominently. The fluorescence intensity of Mito-Pericam is shown in rainbow color (pseudo scale, red indicates highest intensity and blue indicates the lowest intensity). The average particle intensity in different time points

have been represented as a time series graph. Scale bar: 10μm. **D.** Quantified average mitochondrial Ca^{2+}-levels and their time-dependent changes in different conditions are shown. The arrow indicates the time of addition of 4αPDD. The number of cells are indicated next to each graph (blue indicates CHO-K1-V4 and Red line indicates CHO-K1-Mock cells). (Published figure. Acharya TK. et al. 2022, *Mitochondrion*)

We explored if the TRPV4-mediated Ca^{2+}-influx can be blocked by Ruthenium red (RR). For that, we pre-incubated the cells with RR for 1 hour and monitored the Ca^{2+}-influx by adding 4αPDD (**Fig. 21B)**. In the presence of RR, the Ca^{2+}-level increased very marginally in CHO-K1-V4 cells but not in CHO-K1-Mock cells. Notably, the 4αPDD-mediated Ca^{2+}-influx in CHO-K1-V4 cells upon RR-pre-treatment was significantly lower when compared with the 4αPDD-mediated Ca^{2+}-influx in control conditions (**Fig. 21B**). Similar changes in the mitochondrial Ca^{2+} in response to activation of endogenous TRPV4 is also observed in cell and cell-free systems.

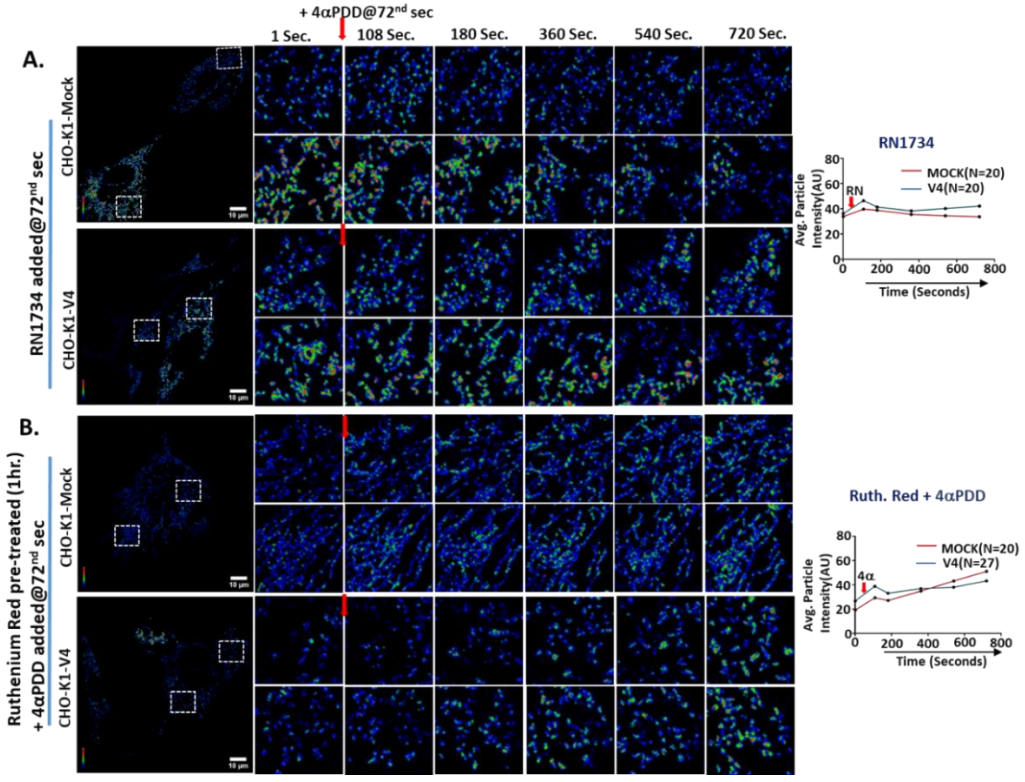


Fig. 21. TRPV4 regulates mitochondrial Ca^{2+}-levels. A. CHO-K1-Mock or CHO-K1-V4 cells expressing Mito-Pericam were treated with TRPV4 inhibitor RN1734 (10 μM) at 72nd seconds, and live cell Ca^{2+}-influx recorded up to 720 secconds. **B.** Cells were pre-incubated with Ruthenium red (10 μM) for 1 hour,

and mitochondrial Ca^{2+}-level is monitored by treating with 4αPDD added at the 72nd frame. (Published figure. Acharya TK. et al. 2022, *Mitochondrion*)

Taken together, these data suggest that in all the conditions, TRPV4 activation increases mitochondrial Ca^{2+} more (~2-fold increase) in CHO-K1-V4 than in CHO-K1-Mock cells. Ca^{2+}-entry can be reduced by intracellular chelation of Ca^{2+} or by inhibiting TRPV4.

2.2.2 Presence of TRPV4 enhances the basal level Ca^{2+} within mitochondria:

Next, we quantified the Ca^{2+}-intensity of each mitochondrion (at basal level, i.e. at 1 sec) and compared the total mitochondrial Ca^{2+} in CHO-K1-V4 as well as in CHO-K1-Mock cells in control conditions, or when pre-treated with RN1734, RR, or BAPTA-AM (**Fig. 22A**). The total mitochondrial Ca^{2+}-levels are significantly higher in CHO-K1-V4 than CHO-K1-Mock in the control condition, this holds true also in RN1734 and BAPTA-AM pre-treated conditions. In the case of RR pre-treatment, CHO-K1-V4 cells have more mitochondrial Ca^{2+} than CHO-K1-Mock cells.

2.2.3 TRPV4 affects both mitochondrial Ca^{2+}-levels and mitochondrial numbers:

We noted that the average number of mitochondria per cell is ~18% lower in CHO-K1-V4 cells than in CHO-K1-Mock cells, suggesting that the expression of TRPV4 contributes to the regulation of mitochondrial numbers. Therefore, we analyzed the effect of TRPV4 activation on mitochondrial Ca^{2+}-dynamics by comparing the individual mitochondrial numbers as well as the respective Ca^{2+}-levels. To this end, we plotted all the fluorescence intensities of individual mitochondria in ascending order and compared the changes at different time points (i.e. at 1st, 108th, 180th, 360th, 540th, 720th seconds) after TRPV4 activation by 4αPDD (**Fig. 22B-C**). In all cases, biphasic plots were observed, suggesting the presence of at least two populations of mitochondria where Ca^{2+}-level differs dramatically (the absolute values of individual

mitochondrial fluorescence indicating Ca^{2+}-levels range from 1 to more than 1000 AU). In all cases, the fraction of mitochondria with very low (1-10 AU) or low (10-100 AU) fluorescence intensities representing "very low" to "low" Ca^{2+}-levels remain majority in numbers. Only a minor fraction had "high" (100-1000 AU) or "very high" (more than 1000 AU) fluorescence intensity. We noted that in both CHO-K1-V4 and CHO-K1-Mock cells, the total number of mitochondria decreases in a time-dependent manner after TRPV4 activation. Interestingly, the changes are more prominent in CHO-K1-V4 cells than in CHO-K1-Mock cells **(Fig. 22B-C**). A sudden increase in mitochondrial Ca^{2+}-level is observed in CHO-K1-Mock cells, but that Ca^{2+}-level reduces quickly in these cells suggesting a better Ca^{2+}-buffering ability in these cells. In contrast, in CHO-K1-V4 cells, the Ca^{2+}-level increases and stays high suggesting compromised Ca^{2+}-buffering abilities, and therefore CHO-K1-V4 cells need longer duration than CHO-K1-Mock cells to adjust mitochondrial Ca^{2+}-level. Under conditions of continuous activation by 4αPDD, the total number of mitochondria is reduced by 19.7% within ~12 min in CHO-K1-Mock cells. In contrast, in CHO-K1-V4 cells, the sudden increase in mitochondrial Ca^{2+}-level is accompanied by a rapid reduction in total mitochondrial number (~33.18% within ~12 min (720 seconds), suggesting a compromised mitochondrial distribution and reduced ability to buffer cytosolic Ca^{2+}.

To understand the relationship between mitochondrial Ca^{2+}-levels and the mitochondria numbers, we classified the mitochondrial particles into 4 groups according to their fluorescence intensities (Gr 1: 1-10 AU, Gr 2: 10-100 AU, Gr 3: 100-1000 AU, and Gr 4: >1000 AU). We observed that in spite of having lower numbers of mitochondria per cell, the fraction of mitochondria having high-level of Ca^{2+} (Gr 3 + Gr 4) is higher in CHO-K1-V4 cells (~8.5%) as compared to the CHO-K1-Mock cells (~4%) at the beginning of the experiment. After ~720th sec., CHO-K1-Mock cells maintain ~4% mitochondria with high or very high Ca^{2+}-levels suggesting

that these cells have better mitochondrial Ca^{2+}-buffering capacities. On the contrary, in CHO-K1-V4 cells, ~7.7% of mitochondria showed high and very high Ca^{2+}-levels (Gr 3 + 4), suggesting fusion of mitochondria, preferably with mitochondria having high Ca^{2+}-levels (**Fig. 22D, F**).

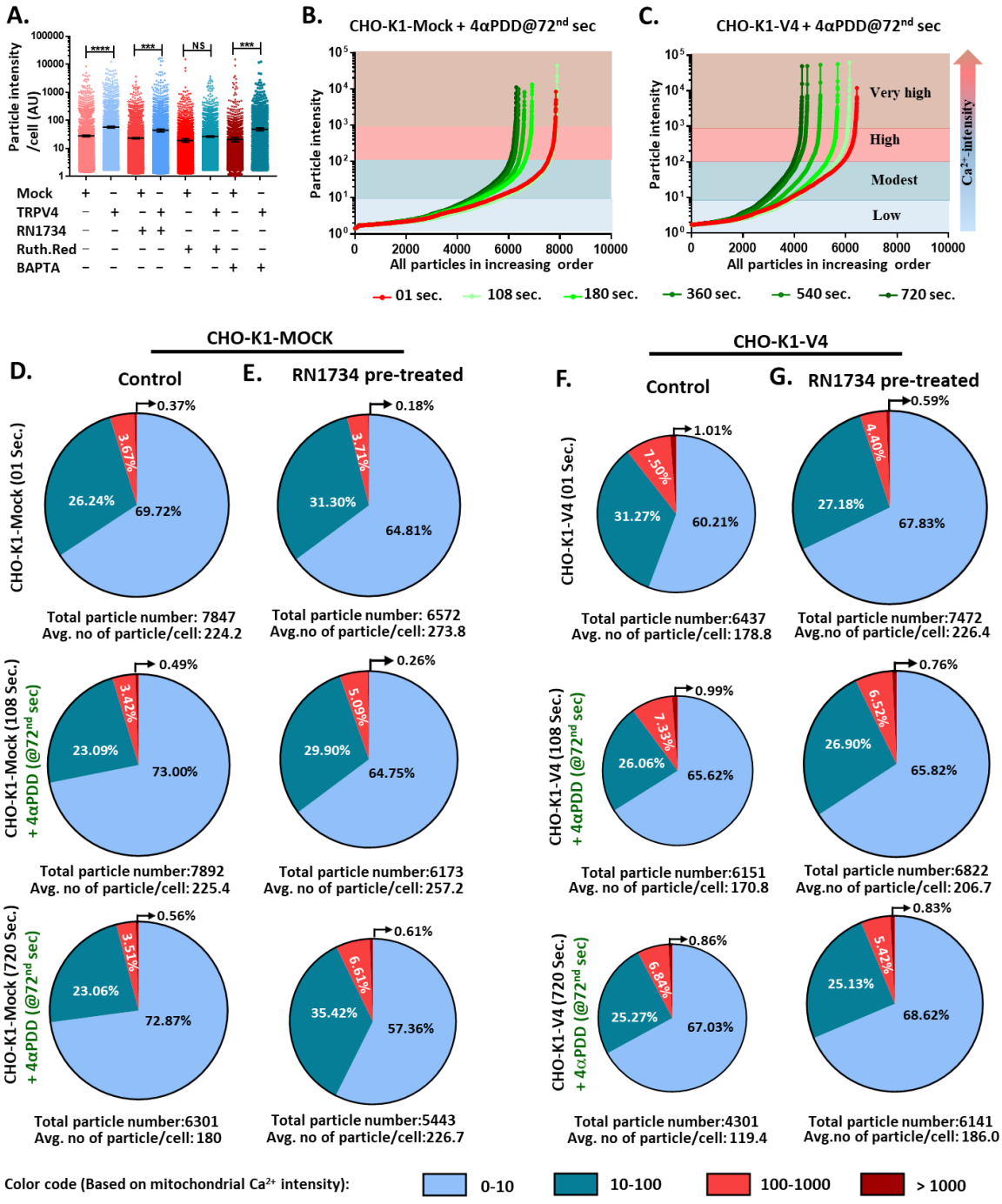


Fig. 22. TRPV4 regulates mitochondrial Ca^{2+}-levels and mitochondrial numbers. Time series images of CHO-K1-V4 or CHO-K1-Mock cells expressing Mito-Pericam were performed, and fluorescence

intensities of individual mitochondria were quantified. **A.** Shown are the basal level fluorescence intensities of Mito-Pericam in cells. Basal level fluorescence intensity is more in CHO-K1-V4 as compared to CHO-K1-Mock cells. Values from 20-35 cells (in each group) and ~6000-7000 mitochondrial particles per condition were analyzed for this quantification. *** = $p<0.001$, **** = $p<0.0001$, ns = non-significant. **B-C.** Fluorescence intensities of individual particles (More than 3000 numbers) from ~35 cells were arranged in an increasing order. Total particles from CHO-K1-V4 or CHO-K1-Mock cells at different time points (01st, 108th, 180th, 360th, 540th, and 720th) are shown. Both changes in total particle number as well as in the mitochondrial Ca^{2+}-level is observed due to TRPV4 activation. In each case, TRPV4-specific agonist 4αPDD was added at the 72nd sec. **D-G.** Presence as well as activation of TRPV4 alters the total mitochondrial number as well as intra-mitochondrial Ca^{2+}-distribution. Shown are the pie charts of mitochondrial particle numbers of CHO-K1-V4 or CHO-K1-Mock cells with RN1734 pre-treatments and treatment with agonist in three different time points. In all graphs, the sizes of the pie charts are represented as per the total mitochondrial numbers observed in those conditions. In all cases, the mitochondrial Ca^{2+}-level remain within a range of 10^1 to 10^4 (AU). Mitochondrial particles were classified based on their level of Ca^{2+} (light blue = 10^0-10^1, dark blue = 10^1-10^2, light red 10^2-10^3, dark red = $<10^3$ AU). (Published figure. Acharya TK. et al. 2022, *Mitochondrion*)

In the RN1734, pre-treated condition in CHO-K1-V4 cells, the average mitochondrial number increases with compared to control cells. The percentage of mitochondria having a high and very high level of Ca^{2+} is also reduced (~5%), and upon activation by TRPV4 agonist, these percentages gradually increase. (**Fig. 22E, G**). CHO-K1-Mock or CHO-K1-V4 cells, when treated with RN1734 (added at the 72nd frame) and checked the mitochondrial number. We observed interestingly in RN1734 treated CHO-K1-V4 cells, the mitochondrial number increases with compared to mock cells (**Fig. 23A**). CHO-K1-Mock and CHO-K1-V4 cells that are pre-treated with Ruthenium red (1 hour) and BAPTA-AM (1 hour), subsequently treated with TRPV4 activator 4αPDD (at 72nd sec) and we plotted the mitochondrial number in Pie charts (**Fig. 23B-C**). We noticed that in both the condition, the mitochondrial number reduced in CHO-K1-V4 cells when compared to mock cells. However, the percentage of mitochondria having high to very high Ca^{2+}-increased significantly.

Taken together, these mitochondrial particle-based quantification data suggest that TRPV4 plays a role in the regulation of mitochondrial Ca^{2+}-levels, mitochondria numbers, and overall Ca^{2+}-buffering abilities.

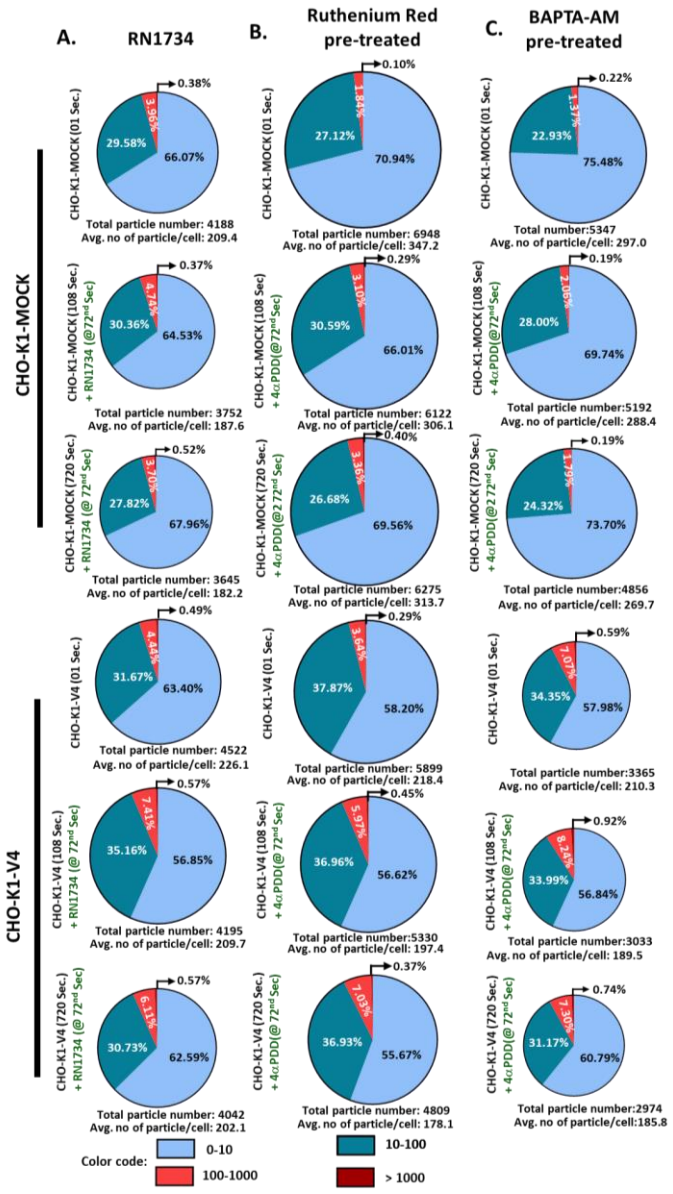


Fig. 23. TRPV4 regulates mitochondrial Ca^{2+}-levels and mitochondrial numbers. A. Pie charts depicting mitochondrial particle number as well as Ca^{2+}-intensities (at 01st sec, 108th sec and 720th sec) of CHO-K1-Mock or CHO-K1-V4 cells when treated with RN1734 (added at the 72nd frame). In the treatment of TRPV4 inhibitor, the Ca^{2+}-influx goes down in both CHO-K1-V4 and CHO-K1-Mock cells. **B.** Pie charts showing the mitochondrial particle counts and the Ca^{2+}-intensities (01st sec, 108th sec and 720th sec) in CHO-K1-Mock and CHO-K1-V4 cells that are pre-treated with Ruthenium red (1 hour) and subsequently

treated with TRPV4 activator 4αPDD (at 72nd second). Here the Ca^{2+}-level increases marginally in CHO-K1-V4 cells. **C**. Pie charts showing the mitochondrial particle counts and the Ca^{2+}-intensities (01st , 108th and 720th seconds) in CHO-K1-Mock and CHO-K1-V4 cells that are pre-treated with cytosolic Ca^{2+}-chelator BAPTA-AM (1 hour) and subsequently treated with TRPV4 activator 4αPDD (at 72nd sec). Here Ca^{2+}-level increases in CHO-K1-V4 cells. In all cases, the mitochondrial Ca^{2+}-level is observed to be ranged within 10^1 to 10^4 (AU). Mitochondrial particles were classified based on their level of Ca^{2+} (Mitochondrial Ca^{2+}-intensities are: light blue = 10^0 to 10^1, dark blue = 10^1 to 10^2, light red 10^2 to 10^3, dark red = more than 10^3). (Published figure. Acharya TK. et al. 2022, *Mitochondrion*).

2.2.4 TRPV4 regulates mitochondrial ATP & GTP production:

Ca^{2+}-based signaling and ATP-based energetics are often interlinked (Petersen OH, 2016). As activation of TRPV4 decreased the activity of the complex IV and inhibition restored its activity, using ATP-Red, we explored the amount of ATP release in CHO-K1-Mock and CHO-K1-V4 cells (Wang L, 2016). In CHO-K1-V4 cells, mitochondrial ATP level decreased significantly when treated with 4αPDD, which was increased in the presence of RN1734. In contrast, in CHO-K1-Mock cells, the ATP level decreased in activated condition, but in the presence of inhibitor the ATP level further goes down (**Fig. 24A-B**).

To further validate this, we performed a similar experiment with mitochondria purified from CHO-K1-Mock and CHO-K1-V4 cells. Using a luciferase-based detection system (Invitrogen), we measured the ATP release from these isolated mitochondria upon incubation with TRPV4 modulators. In control conditions, the amount of ATP release is low in mitochondria isolated from CHO-K1-V4 cells as compared to CHO-K1-Mock cells. The ATP release becomes low in the presence of 4αPDD (5 μM) as compared to the control, both in CHO-K1-Mock cells and in CHOK1-V4 cells. However, RN1734 (10 μM) increases the ATP release in mitochondria isolated from CHO-K1-V4 cells. On the other hand, in mitochondria isolated from CHO-K1-Mock cells, ATP release is less as compared to control and activated condition. This result suggests that TRPV4 activation might change the activity of complex V as well as the ATP release from the

mitochondria (**Fig. 24C**). The trend of ATP release remains similar in both whole cells as well as in isolated mitochondria.

As we observed that TRPV4 activation decreases mitochondrial ATP level, we further investigated the change in GTP level if any, due to modulation of TRPV4. For that, we used GTP green dye in CHO-K1-Mock and CHO-K1-V4 cells in the presence of TRPV4 agonist and antagonist. We observed that in the presence of TRPV4 agonist, the GTP level increases in both the CHO-K1-V4 and CHO-K1-Mock cells. In the presence of antagonist, the GTP level decreased significantly (**Fig. 24D-E**).

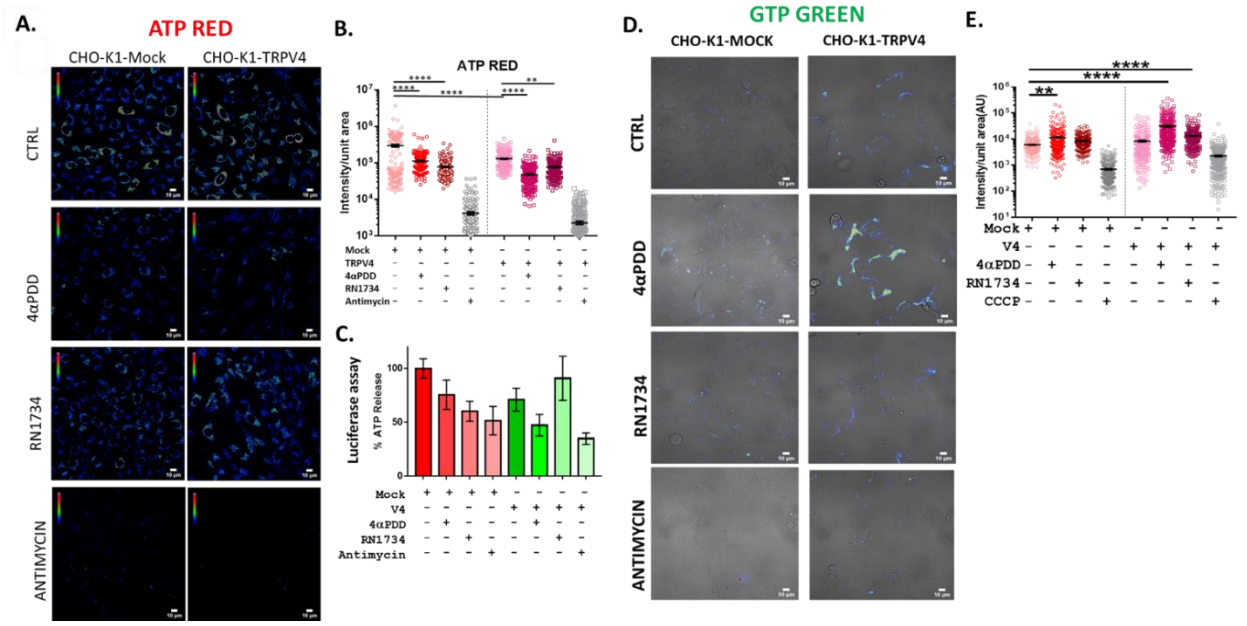


Fig. 24. TRPV4 modulation regulates mitochondrial ATP and GTP levels. A-B. CHO-K1-Mock and CHO-K1-V4 cells were treated with 4αPDD (5 μM) and inhibitor RN1734 (10 μM) for 6 hours, and cells were stained with ATP-Red for 15 minutes. TRPV4 activation decreases the mitochondrial ATP release in both cell types. In contrast, TRPV4 inhibition restores the ATP level in CHO-K1-V4 cells but not in the CHO-K1-Mock cells, where the ATP level decreases further. **C.** ATP release assay has been performed in isolated mitochondria from CHO-K1-Mock and CHO-K1-V4 cells. Isolated mitochondria were treated with TRPV4 activator and inhibitor for 1 hour. ATP level decreases in the 4αPDD-treated cells. The luminescence values have been plotted as % values (N=3). Antimycin has been taken as a positive control for this assay. **D-E**. CHO-K1-Mock and CHO-K1-V4 cells were treated with 4αPDD (5 μM) and inhibitor RN1734 (10 μM) for 6 hours, and cells were stained with GTP green (10 μM) for 30 minutes. TRPV4 activation increases the mitochondrial GTP level in both cell types, and TRPV4 inhibition decreases the

GTP level. One-way ANOVA ** = p<0.01, **** = p<0.0001, ns = non-significant. (Published figure. Acharya TK. et al. 2022, *Mitochondrion*).

2.2.5 TRPV4-expressing cells display an altered mitochondrial morphology:

Previously in our lab, we have explored the change in mitochondrial morphology by treating the TRPV4 activator (4αPDD, 5 µM) or inhibitor (RN1734, 10 µM) for 8 hours CHO-K1-V4 and CHO-K1-Mock cells and checked various morphological parameters. In CHO-K1-Mock cells, mitochondrial morphology remains normally elongated and/or tubular in shape, even when cells were treated with TRPV4 activator or inhibitor for the same duration. However, in CHO-K1-V4 cell, 4αPDD treatment cause aggregation of spherical-shaped (small) mitochondria (Acharya TK, 2022a, Acharya TK, 2022b). In accordance with that, we explored the effect of BAPTA-AM and Thapsigargin in mitochondrial morphology in CHO-K1-Mock and CHO-K1-V4 cells. We observed that mitochondria become circular and aggregated in TRPV4 expressing cells mostly (**Fig. 25**). In a similar experiment, we explored the changes in mitochondrial morphology in another cell line, i.e. in Saos-2 (human osteosarcoma cell) cells by expressing TRPV4-GFP and mitoDsRed. In TRPV4-GFP expressing cells, the mitochondrial circularity and aggregation increase due to activation by 4αPDD. In contrast, in control and RN1734 treated cells, the mitochondrial morphology remains unchanged (**Fig. 26**).

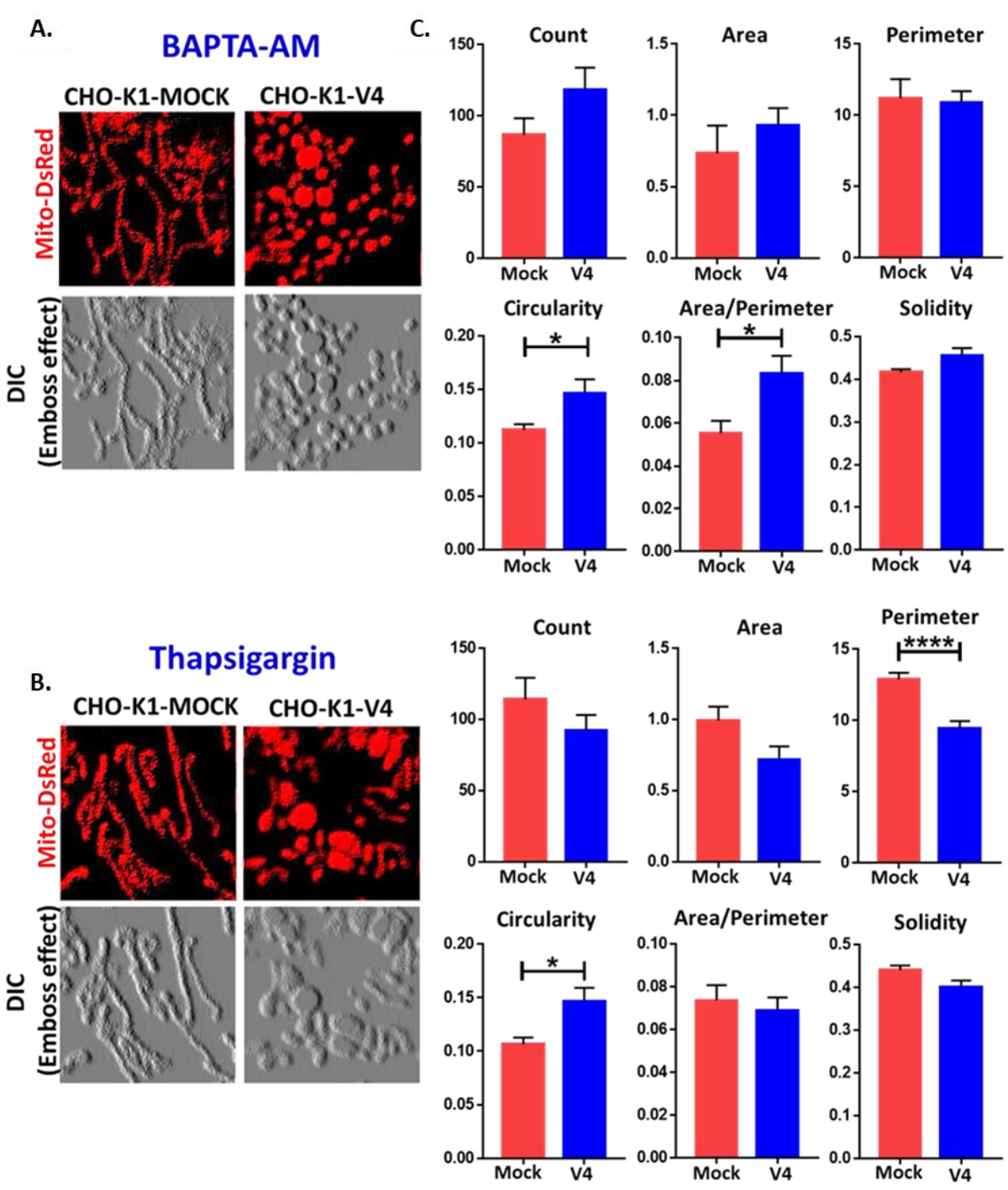


Fig. 25. Effect of BAPTA-AM or Thapsigargin on mitochondrial morphology. A-B. CHO-K1-Mock and CHO-K1-V4 cells were treated with BAPTA-AM and Thapsigargin for 6 hours, and different mitochondrial morphological parameters were quantified. In both condition, there is more mitochondrial circularity and aggregation observed in TRPV4-expressing cells. For quantification, More than 15 cells were used. Student's t-test was performed by Graph-pad, * = p <0.05, **** = p <0.0001, ns = non-significant. (Published figure. Acharya TK. et al. 2022, *Life Sciences*).

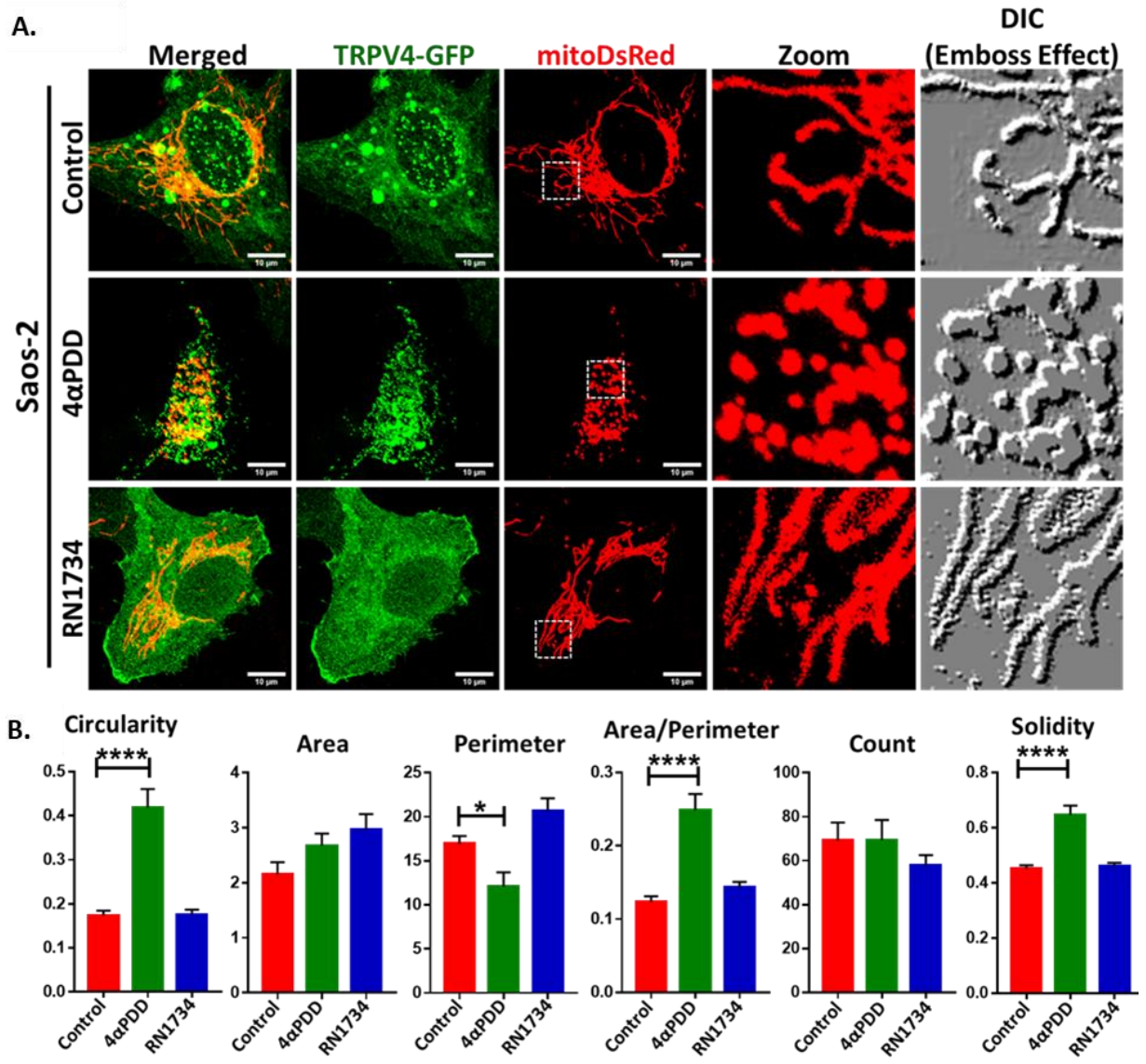


Fig. 26. Changes in mitochondrial morphology due to TRPV4 activation in Saos-2 cell. A-B. TRPV4-GFP was expressed in Saos-2 cells and subsequently treated with 4αPDD and RN1734 for 6 hours. The morphometric analysis suggests that activation of TRPV4 increases mitochondrial circularity and aggregation in TRPV4 expressing cells, and the mitochondrial morphology remains normal in control and RN1734 incubated cells. For this quantification, more than 15 cells were used. Onaway ANOVA was performed by Graph-pad, * = $p<0.05$, **** = $p<0.0001$, ns = non-significant. (Published figure. Acharya TK. 2022, *Life Sciences*).

2.2.6 Endogenous TRPV4 colocalized with endogenous MFN2:

We explored if endogenous TRPV4 colocalizes with endogenous MFN1/2. For that, we isolated and cultured the primary Mesenchymal stem cells (MSC) from mouse bone marrow. We observed colocalization of TRPV4 with MFN1 as well as MFN2 (**Fig. 27A**). To ensure that TRPV4 is indeed colocalized with these mitochondrial proteins, we also isolated mitochondria from mouse brain, fixed those mitochondria and performed immunostaining. We observed colocalization of TRPV4 along with MFN1 and MFN2 in a subset of mitochondria (**Fig. 27B**). Quantitative assessment of colocalization of TRPV4 with MFN1 or MFN2 in both MSCs and isolated mitochondria suggest TRPV4 colocalizes with both MFN1 and MFN2 (**Fig. 27C-D**). These findings indicate the localization of TRPV4 in the mitochondria and possibly at the MAM area, as MFN2 is also known to be present at the MAM.

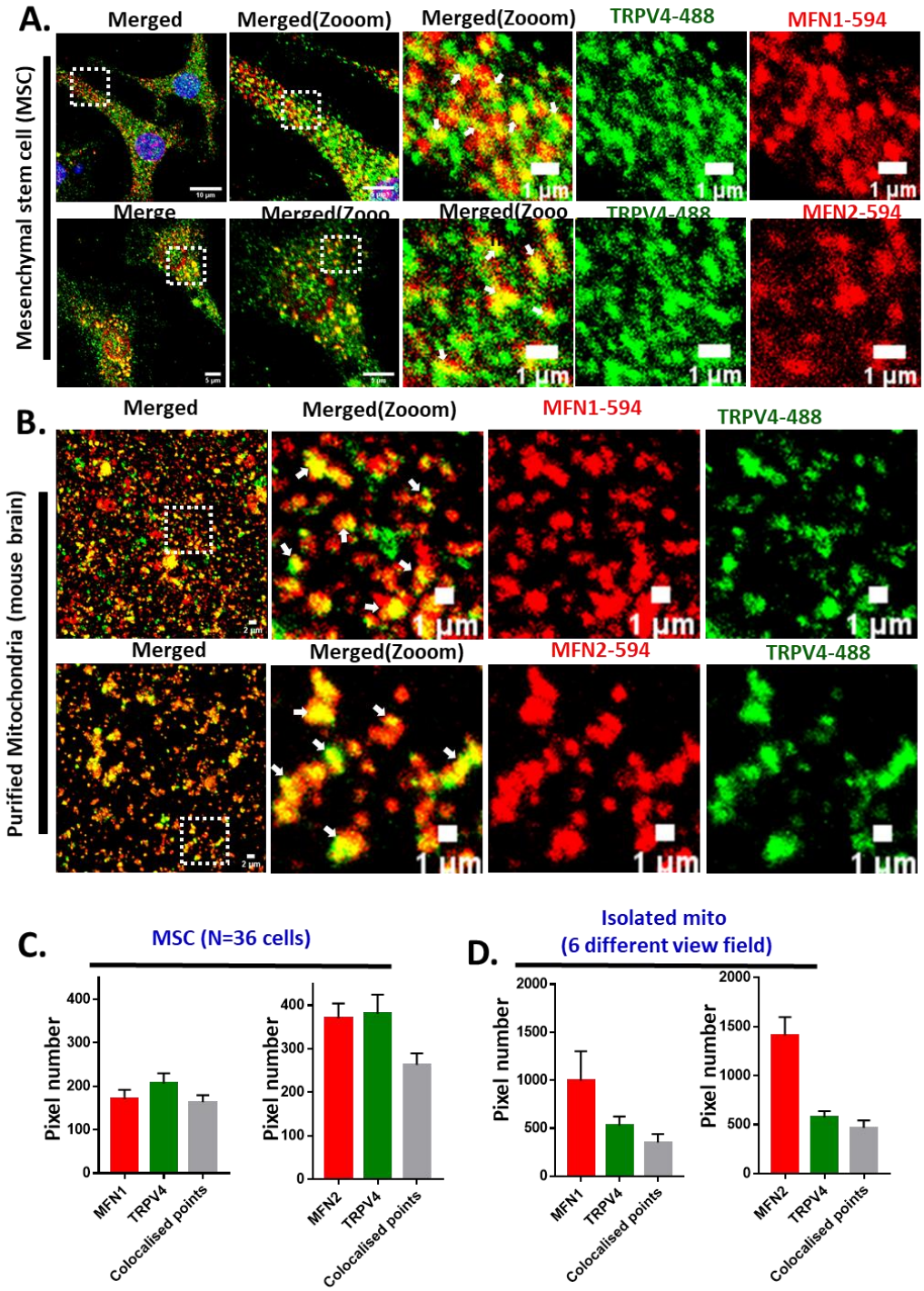


Fig. 27. TRPV4 colocalizes and interacts with MFN1 and MFN2: **A**. TRPV4 colocalizes (indicated by white arrows) with MFN1 or MFN2 in Mesenchymal stem cells isolated from mouse bone marrow. Scale bar: 1µm. **B**. TRPV4 colocalizes (indicated by white arrows) with MFN1 or MFN2 in mitochondria purified from the mouse brain. Distinct colocalization is observed in some but not in all mitochondria. Scale bar: 1µm. **C**. Graph represents quantification of colocalization of TRPV4 with MFN1 or MFN2, in MSCs (N=36) **D**. Quantification of colocalization between TRPV4 with MFN1 or MFN2 in isolated mitochondria (6 different view fields). (Published figure. Acharya TK. et al. 2022, *Life Sciences*).

2.2.7 TRPV4 regulates mitochondrial fusion:

As we identified, mitochondrial morphology could be altered by chronic activation of TRPV4, which prompted us to monitor mitochondrial dynamics in live cells. Recently we also demonstrated that activation of TRPV4 results in quick reduction in the mitochondrial numbers (Acharya TK. 2022a). Here we performed a photo-activable GFP-based fusion assay as described before (Karbowski M, 2004). A mitochondrial matrix-targeted photo-activable GFP (termed as mito-PAGFP) was used to monitor the change in mitochondrial fusion-fission as well as distribution in CHO-K1-Mock and CHO-K1-V4 cells. Here cells were co-transfected with mito-PAGFP and mitoDsRed. After 16-20 hours post-transfection, the cells were treated with TRPV4 activator and inhibitor for a period of another 6 hours. Photo-activation of a small region of interest (ROI, 37.5μm^2) was carried out by using 405 nm laser. The photo-activated ROI was monitored subsequently for next 30 minutes. The fusion and, therefore, dilution of green fluorescence within the red-labelled mitochondrial network were tracked with respect to time (**Fig. 28A**). The decrease in green fluorescence intensity within the selected ROI was measured during different time points to estimate the rate of mitochondrial fusion/diffusion (Karbowski M, 2004) We observed that there is a change in mitochondrial fusion rate in CHO-K1-Mock and CHO-K1-V4 cells in the control condition itself. The change in the intensities suggests that in CHO-K1-Mock cells, the mitochondrial diffusion rate is steady in control and TRPV4-activated condition, and there is no significant change was seen in the rate of mitochondrial diffusion. But, the diffusion rate is a bit slower in the inhibited condition. In contrast, in the CHO-K1-V4 cells, there is a considerable change in the mitochondrial diffusion in the control and RN1734-treated condition. Nevertheless, in the presence of 4αPDD, the change in the green intensity becomes slower, suggesting that in the activated condition, the rate of mitochondrial diffusion decreases (**Fig. 28B, E**).

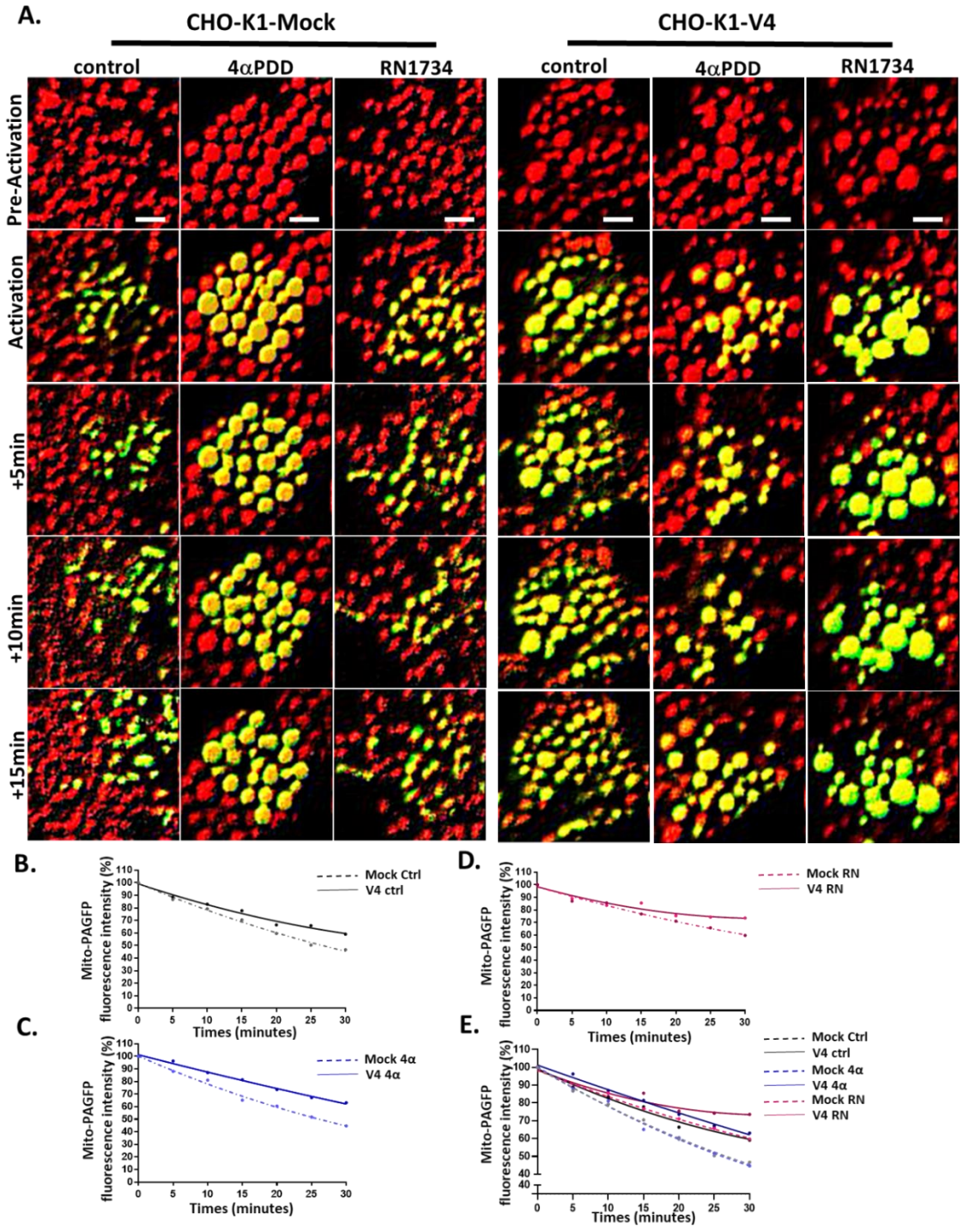


Fig. 28. TRPV4 regulates the rate of mitochondrial fusion: **A**. Representative images demonstrating the "rate-of-diffusion" of mito-PAGFP along with mitoDsRed in different experimental conditions in CHO-K1-Mock and CHO-K1-V4 cells. The cells were treated with 4αPDD and RN1734 for 6 hours. For the photoactivation experiment, a region of interest was photoactivated, and those mitochondria were tracked for 30 minutes continuously. Scale bar 2μm. **B-E.** Graph represents the rate of change in average green mitochondria intensity in 30 minutes after photoactivation. In CHO-K1-Mock cells, there is no significant

changes in the rate of mitochondrial fusion. In contrast, in CHO-K1-V4 cells in the chronic inhibited condition, the rate of mitochondrial fusion decreased with respect to control and activated states. For the quantification in CHO-K1-Mock, control (15 cells), 4αPDD (18 cells), RN1734 (14 cells) and in CHO-K1-V4 control (11 cells), 4αPDD (17 cells) and in RN1734 (12 cells) were taken. The graphs are represented as the best-fit line. (Un-published figure).

Taken together, the results suggest that TRPV4 activation as well as inhibition causes changes in the rate of mitochondrial diffusion.

2.2.8 TRPV4 is present in the ER-mito contact site:

We explored the localization of TRPV4 (by using an antibody raised against the C-terminus of TRPV4) in CHO-K1-V4 cells that are also labelled by KDEL-BFP (ER marker), mitoDsRed (mitochondrial marker). We could detect TRPV4 at the ER-mito contact points also (**Fig. 29A**). In addition, there are certain cases where TRPV4 localizes to mitochondria and present adjacently to ER (data not shown). All these results suggest the presence of TRPV4 at the ER-mito contact points. In accordance to that, we treated the cells with 4αPDD or RN1734 for 6 hours and quantified the triple colocalized points (ER, Mitochondria and TRPV4). Colocalization of these three markers are less in 4αPDD-treated cells and there were no changes observed between control and RN1734-treated cells (**Fig. 29B**).

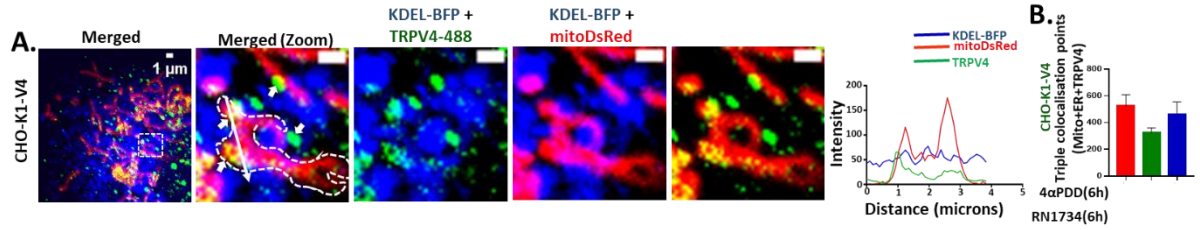


Fig. 29. TRPV4 is present at the ER-mito contact site. **A.** Triple color labelling of ER (by using KDEL-BFP, blue), mitochondria mitoDsRed, red) along with TRPV4 (using anti-TRPV4 antibody) in CHO-K1-V4 cells. TRPV4 is present at the ER-mito contact sites (indicated by arrows). The intensity profile at the right indicates the presence of TRPV4 at the ER-mito contact point, as shown in the line drawing. Scale bar: 1µm. **B.** Graph represents quantification of triple colocalized points (ER+Mito+TRPV4) in CHO-K1-V4 cells in resting, activated and inhibited conditions. Activation of TRPV4 reduces triple colocalized points (N=16). (Published figure. Acharya TK. et al. 2022, *Life Sciences*).

2.2.9 TRPV4 modulation regulates the number of ER-mito contact points:

Mitochondrial ability to buffer cellular Ca^{2+} also depends on the status of ER and Ca^{2+}-buffering ability of the ER. Notably, the ER-mito contact points are also important for Ca^{2+}-buffering and the exchange of metabolites. Therefore, we estimated the ER-mito contact points. For that purpose, we modulate the activities of TRPV4 by using a specific activator (4αPDD) and inhibitor (RN1734) in CHO-K1-Mock and CHO-K1-V4 cells. To overcome the technical challenges and limitations to study the ER-mito contact points (the contact sites have complex shape, regulation, and dynamics in live cell), we characterized the ER-mito contact points by using hypotonic media, as established before (Jaiswal A, 2019; King C, 2020). For that purpose, we have replaced the cell media with a 5% hypotonic media for 5 minutes only. The ER and mitochondria produce large intracellular vesicles (LICV) because of swelling, but the tethering points remain intact. In parallel experiments, cells were pre-incubated with 4αPDD and RN1734 for 6 hours before this hypotonic media was applied (**Fig. 30**). We also used BAPTA-AM to chelate cytosolic Ca^{+2}, in order to study the status of cytosolic Ca^{2+}-chelation on the ER-mito contact points, especially in this TRPV4-modulated conditions. For that, the cells were treated with 4αPDD and RN1734 for 6 hours and treated with BAPTA-AM for last 1 hour (**Fig. 31**). We further examined the effect of Thapsigargin (as it depletes the Ca^{2+} from ER), which is known to increase the ER-mito contact points (Bravo R, 2011). For that purpose, CHO-K1-Mock or CHO-K1-V4 cells were pre-treated with 4αPDD and RN1734 (for 6 hours) and treated with Thapsigargin for last 1hour (**Fig. 32**). We observed that chelation of intracellular Ca^{2+} or depleting ER Ca^{2+} or blocking TRPV4 by pharmacological means results in alteration of ER-mito contact points.

We quantified the total mitochondria particle and ER particle in all conditions. We noted that there is a significant change in the ER particle number in CHO-K1-Mock or CHO-K1-V4 in control conditions but not in all states. By contrast, the mitochondrial number is highly variable in different conditions. In the control condition and in BAPTA-AM treated cells (but not in Thapsigargin treated cells), the mitochondrial number decreases in CHO-K1-V4 cells when compared to mock cells (**Fig. 33A, C**). The results also suggest that both Ca^{2+}-levels and the presence of TRPV4 affect the ER and mitochondrial particle number.

We next quantified the extent of ER-mito contact points in all these conditions. For that, we quantified the ER-mito colocalized pixels, as described previously (Dagda RK, 2009). We observed that in the case of long-term inhibition of TRPV4, there is a significant increase in the ER-mito contact points as compared to the control condition. In CHO-K1-Mock, cells in the activated condition, there is 25% reduction in colocalized pixels and the number rescued in the inhibited state. On the other hand, in CHO-K1-V4 cells, the colocalized pixel number increased up to 20% in the presence of 4αPDD and in the presence of RN1734, there is an increment of about 30% colocalized pixels compared to the control condition.

Similarly, we also quantified the number of colocalized points in the BAPTA-AM and Thapsigargin-treated condition. Interestingly, in both situations, the colocalized pixel number is significantly reduced compared to the 6-hour drug treatment and control conditions in both CHO-K1-Mock and CHO-K1-V4 cells. However, in both the conditions, the ER-mito contact point is higher in CHO-K1-Mock cells with respect to CHO-K1-V4 cells. This data suggests that the ER-mito contact point is highly dependent on the mitochondrial and cellular Ca^{2+}-load (**Fig. 33D**). Overall, the results indicate that inhibition of TRPV4 increases ER-mito contact points, however,

to a different extent. However, in the case of cytosolic Ca^{2+}-chelation or ER Ca^{2+}-depleted condition, the extent of colocalization decreases further.

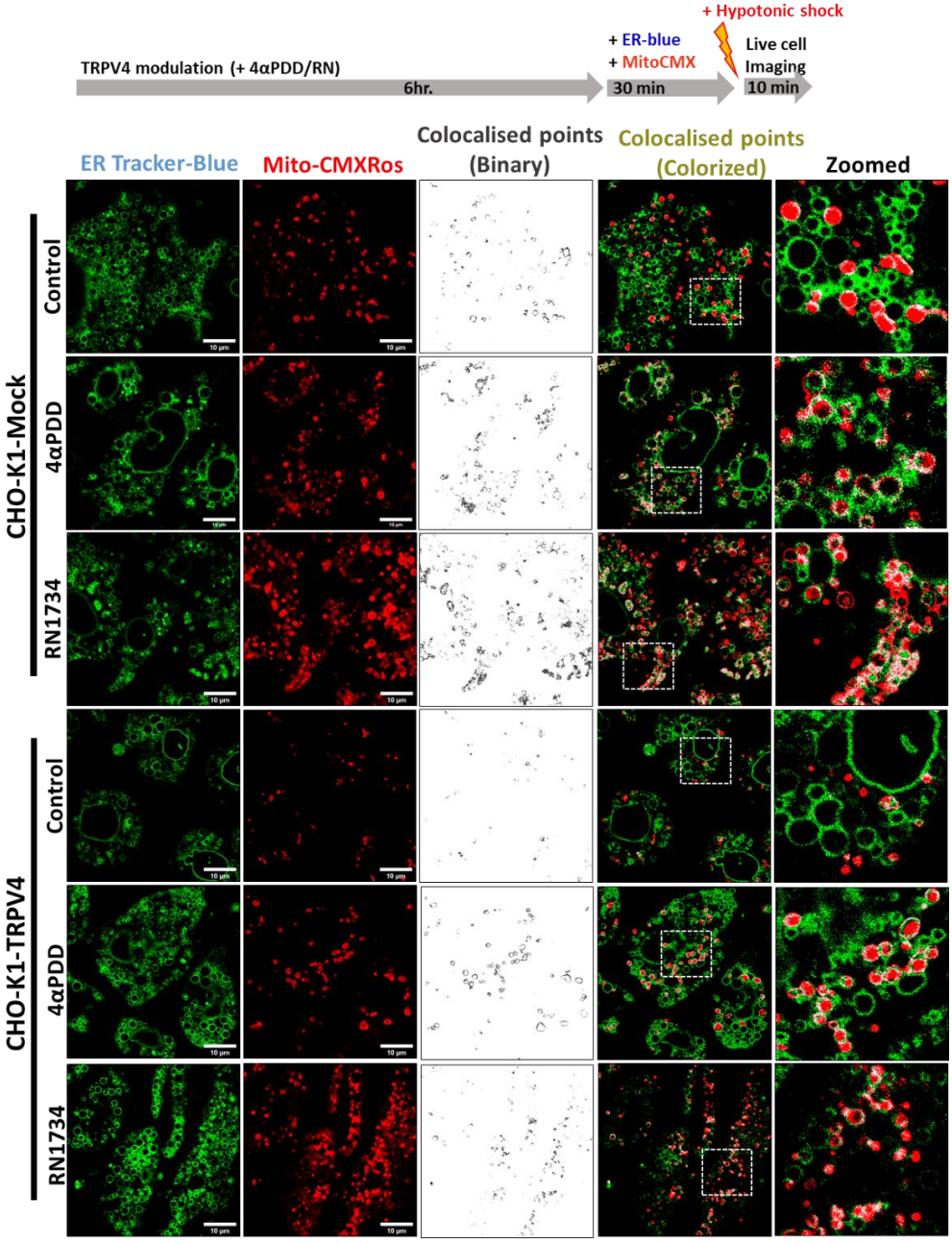


Fig. 30. Modulation of TRPV4 regulates ER-mito contact points. CHO-K1-Mock and CHO-K1-V4 cells were incubated with 4αPDD and RN1734 for 6 hours, and post-incubation cells were stained with ER-Tracker Blue and MitoTracker Red CMXRos and subsequently incubated with 5% hypotonic stimulus to allow the cells to produce large cellular vesicles of ER and mitochondria. Representative images showed pseudo color green for ER for better visualisation. The colocalized points are represented as white. The portion of colocalized points is digitally zoomed. The scale bar is 10µm. (Published figure. Acharya TK. et al. 2022, *Life Sciences*).

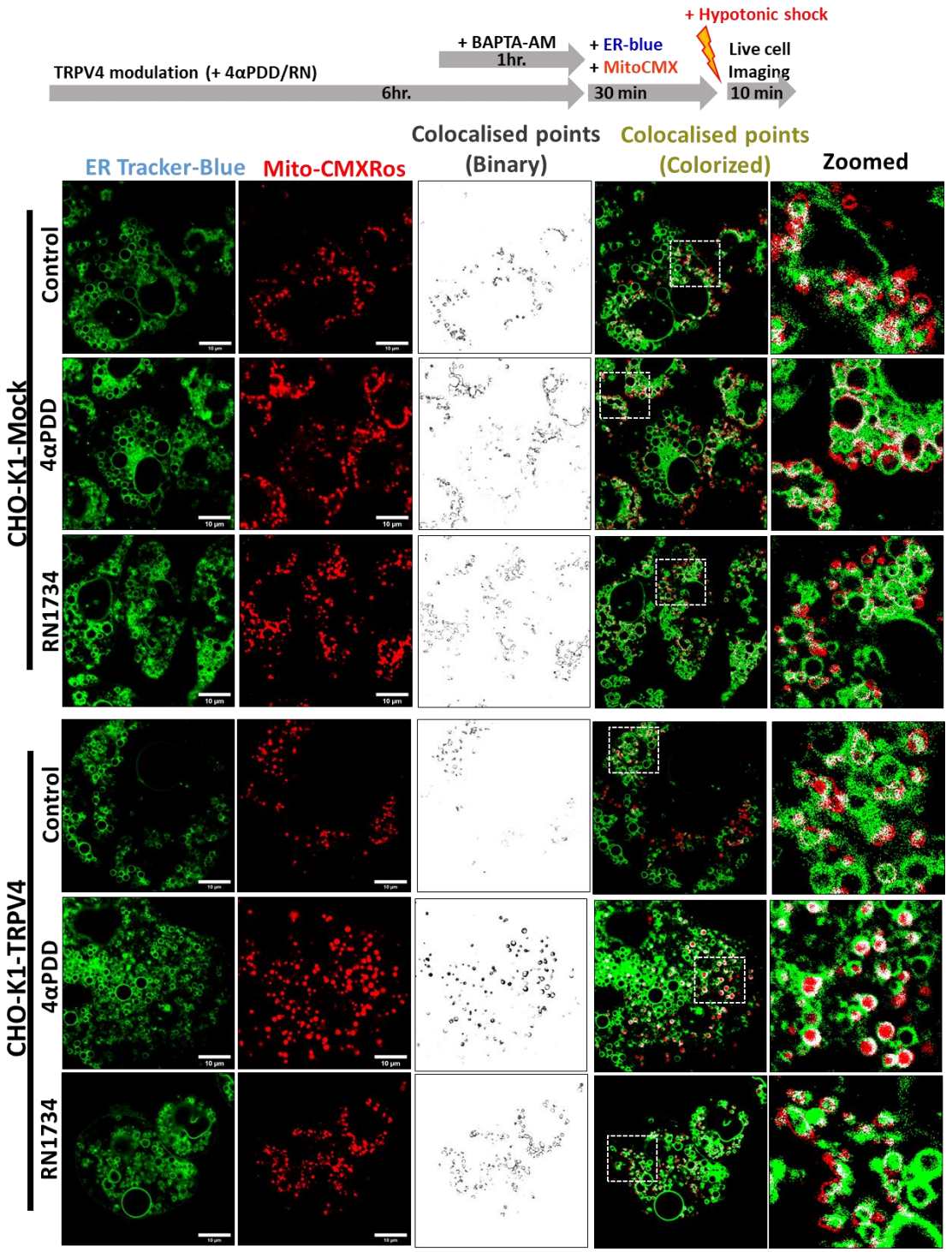


Fig. 31. Modulation of TRPV4 regulates ER-mito contact points in cytosolic Ca^{2+}-depleted conditions. CHO-K1-Mock and CHO-K1-V4 cells were treated with 4αPDD and RN1734 for 6 hours, and the cytosolic Ca^{2+} was chelated using BAPTA-AM for the last 1 hour. After incubation, cells were stained with ER-Tracker Blue and MitoTracker Red CMXRos and subsequently incubated with 5% hypotonic stimulus to allow the cells to produce large cellular vesicles. The ER is represented as green (pseudocolor), and the colocalized points are represented as white. The scale bar is 10µm. (Published figure. Acharya TK. et al. 2022, *Life Sciences*).

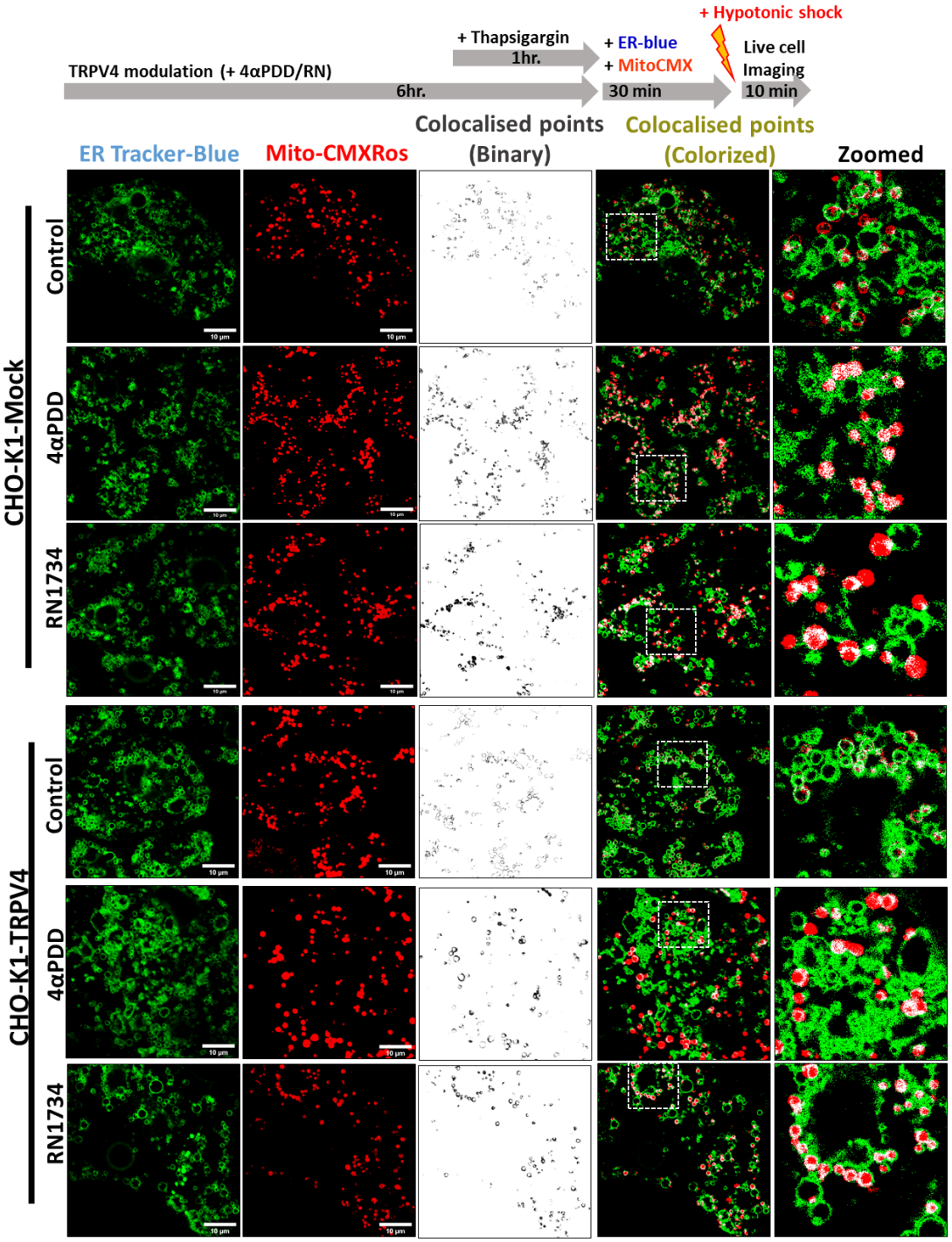


Fig. 32. Modulation of TRPV4 regulates ER-mito contact points in ER Ca^{2+}-depleted conditions. CHO-K1-Mock and CHO-K1-V4 cells were modulated with 4αPDD and RN1734 for 6 hours and the ER Ca^{2+} was depleted by using Thapsigargin for last 1 hour. After incubation, cells were stained with ER-Tracker Blue and MitoTracker Red CMXRos and subsequently incubated with 5% hypotonic stimulus to allow the cells to produce large cellular vesicles. The ER is represented as green (pseudo color) and the colocalized points are represented, as white. The scale bar is 10µm. (Published figure. Acharya TK. et al. 2022, *Life Sciences*).

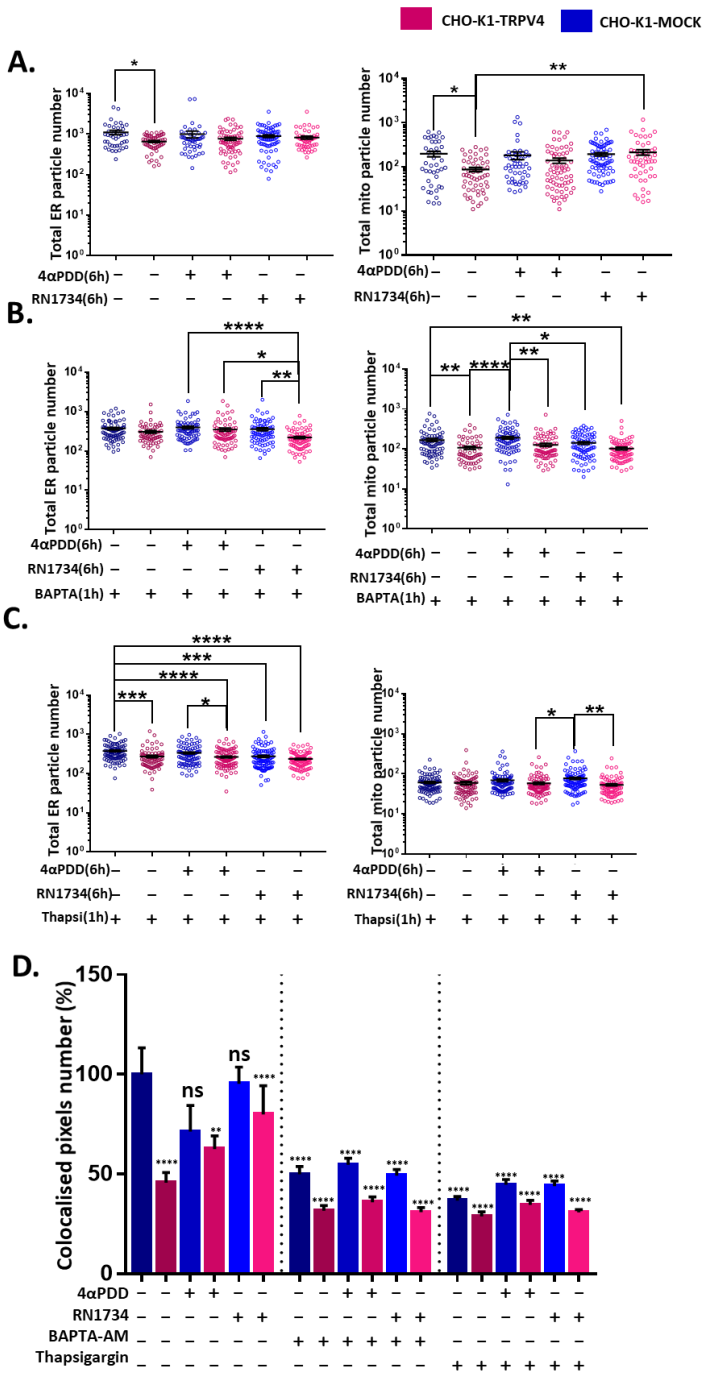


Fig. 33. TRPV4 regulates ER-mito contact points. **A-C**. Quantitative representation of the total ER particle and total mitochondrion particle in different conditions. This analysis inferred that insignificant change happened in ER particle number in most cases (except in the Thapsigargin-treated condition). In BAPTA-AM-mediated cytosolic Ca^{+2}-chelated condition, there is a significant change occurred in the mitochondria particle number. **D**. Graph represents the percentage of colocalized pixels in different treatment conditions. The percentage change was quantified considering mock control as 100%. There is overall significant reduction in the colocalized pixels when cells were treated for cytosolic Ca^{+2}-chelation (by BAPTA-AM) and ER Ca^{2+}-depletion (by Thapsigargin). Particle quantification was done from a

minimum of 40 cells in each group. One-way ANOVA was performed by graph-pad, and all the groups were compared with the Mock control group. * = $p<0.05$, ** = $p<0.01$, *** = $p<0.001$ **** = $p<0.0001$, ns = non-significant. (SEM values were plotted in each condition). (Published figure. Acharya TK. et al. 2022, *Life Sciences*).

2.2.10 Presence of TRPV4 regulates basal mitochondrial Ca^{2+}-levels:

Mitochondrial morphology and dynamics are highly dependent on mitochondrial Ca^{2+}-level. In a cell, mitochondria store many folds more Ca^{2+} than the cytosol and help in Ca^{2+}-buffering to maintain cellular homeostasis. To compare the basal level of mitochondrial Ca^{2+} in CHO-K1-Mock and CHO-K1-V4, cells were transiently transfected with Mito-Pericam construct. In the presence of TRPV4, the mitochondrial Ca^{2+} is significantly high compared to mock cells (**Fig. 34A**). We further compared the mitochondrial Ca^{2+}-level in conditions when the cytosolic Ca^{2+} is chelated by using BAPTA-AM (10 μM). We also depleted the Ca^{2+}-from ER by using Thapsigargin (1 μM). In case of Thapsigargin treatment, the mitochondrial Ca^{2+}-level goes down in both CHO-K1-Mock and CHO-K1-V4 cells than in control conditions. However, in all these conditions, mitochondrial Ca^{2+} remain high in CHO-K1-V4 cells as compared to CHO-K1-Mock cell (**Fig. 34B-C**). However, when TRPV4 is inhibited by RN1734 (10 μM), the mitochondrial Ca^{2+}-level increases slightly for CHO-K1-Mock cells and decreases in CHO-K1-V4 cells (**Fig. 34D**). However, under this condition, the difference between CHO-K1-Mock and CHO-K1-V4 cells become minimum. Taken together, the results suggest that the mere presence of TRPV4 has a significant impact on mitochondrial Ca^{2+}-levels in all these tested conditions, and the Ca^{2+}-level remains high in CHO-K1-V4 cells (**Fig. 34E**). Pharmacological inhibition of TRPV4 also results in reduce mitochondrial Ca^{2+}-levels. Considering the absolute average values measured for ER-mito contact points and absolute average values of Mito-Pericam intensities in comparative conditions, data suggests for an inverse relationship between ER-mito contact points with the mitochondrial Ca^{2+}-levels (**Fig. 34F**).

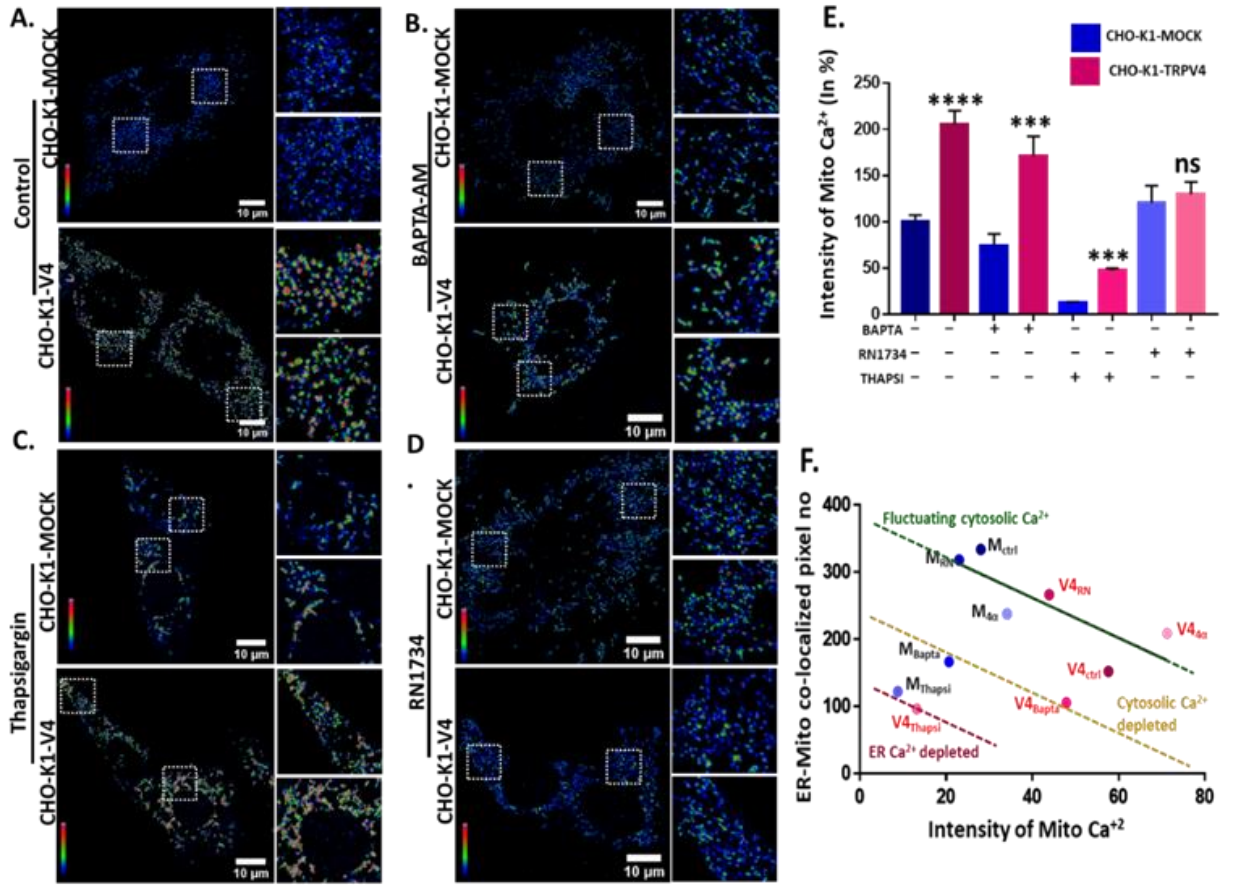


Fig. 34. TRPV4 regulates mitochondrial Ca^{2+}-status. A. Representative image of mitochondrial Ca^{2+}-level in CHO-K1-Mock and CHO-K1-V4 cells. There is more basal level of mitochondrial Ca^{2+} in CHO-K1-V4 cells compared to the mock cells. **B-C**. Cells were pre-incubated with cytosolic Ca^{2+}-chelator BAPTA-AM (B) or ER Ca^{2+}-depletion agent Thapsigargin (C) for 1 hour. In both cases, there is more basal mitochondrial Ca^{2+} in CHO-K1-V4 cells. **D**. Representative image shows pre-incubation with RN1734 for 1hr and the basal mitochondrial Ca^{2+}-level remains unchanged in both mock and V4 cells. **E**. The graph represents the quantitative measurement of the Mito-Pericam intensity in different conditions. The changes are represented as a percentage scale by considering the Mock control condition as 100%. Values from 20-35 cells (in each group) and ~6000-7000 mitochondrial particles were analyzed for this quantification: one-way ANOVA, ** = $p<0.01$, *** = $p<0.001$, **** = $p<0.0001$, ns = non-significant. **F.** The extent of colocalized pixels (representing ER-mito contact points) shares an inverse relationship with the extent of mitochondrial Ca^{2+}, both in CHO-K1-Mock and CHO-K1-V4 cells where cytosolic Ca^{2+}-levels are altered, i.e. in control 4αPDD, and RN1734 treated conditions. However, this relationship differs in case of BAPTA-AM or Thapsigargin-treated conditions, though the slope remains same. (Published figure. Acharya TK. et al. 2022, *Life Sciences*).

Summary: In this work we demonstrate that expression and/or pharmacological modulation of TRPV4 regulates mitochondrial morphologies, Ca^{2+}-level, and mitochondrial temperature. Accordingly, several naturally occurring TRPV4 mutations affect mitochondrial morphology and distribution. TRPV4 interacts with MFN1/MFN2, the key mitochondrial regulatory factors. TRPV4 regulates ER-mito contact points. We used different cellular conditions where cytosolic or ER Ca^{2+}-levels were pharmacologically altered. Analysis of ~55000 mitochondrial particles, ~125000 ER-mito contact points from ~900 cells in 10 different cellular conditions suggest that ER-mito contact points are inversely regulated with mitochondrial Ca^{2+}-levels where TRPV4 always elevates mitochondrial Ca^{2+}-levels. These findings link TRPV4 with MFN2-mediated diseases and suggest that different TRPV4-induced channelopathies are likely due to mitochondrial abnormalities.

2.3 If and how TRPM8 regulates mitochondrial metabolism?

By immunofluorescence study, we have demonstrated the localization of TRPM8 in mitochondria in Saos-2 cells, mouse Mesenchymal stem cells, and isolated mitochondria. For the functional characterisation of TRPM8 in mitochondrial physiology, we have used the Saos-2 cell (human osteosarcoma cell). We used Menthol, WS12, and AMTB as pharmacological modulators of TRPM8 in this study. Though transient receptor potential melastatin sub-type 8 (TRPM8) has been named as "Menthol-receptor", reports from several labs have demonstrated that Menthol has several other targets (Oz M, 2017). These other molecular targets suggest that other than TRPM8, Menthol can modulate at least 10 or more ion channels and receptors, such as TRPA1, TRPV3, Voltage-dependent L-type calcium channel, Kv7.2/3 channel, Nav1.8 channel, Nav1.9 channel, Ca^{2+}-activated K+ channel, μKappa-type opioid receptor, GABA receptor, 5-HT_3 receptor, Nicotinic receptors, Ryanodine receptors, IP3 receptors and several others (Oz M, 2017). Because of this, we first looked at how Menthol affected the function of mitochondria. Then, we used the TRPM8-specific agonist WS12 and the antagonist AMTB to study mitochondrial function.

2.3.1 Long term Menthol treatment elevates cytosolic and mitochondrial Ca^{2+}-levels:

We tested if and how long term application of Menthol affects the cytosolic and mitochondrial Ca^{2+}-levels. Thus we used Rhod-2-AM and Fluo-4-AM dye respectively. For that Menthol (100 μM) was added for 6 hours and subsequently, the status of cytosolic and mitochondrial Ca^{2+}-levels were evaluated (**Fig. 35A**). In the case of cytosolic Ca^{2+}, Menthol treatment elevates the basal cytosolic Ca^{2+} drastically as seen by increase in Fluo-4-AM intensity. Similar effect, i.e. increase in Ca^{2+}-levels due to Menthol was seen in case of mitochondrial Ca^{2+}-levels too as seen by Rhod-2-AM intensity (**Fig. 35B**).

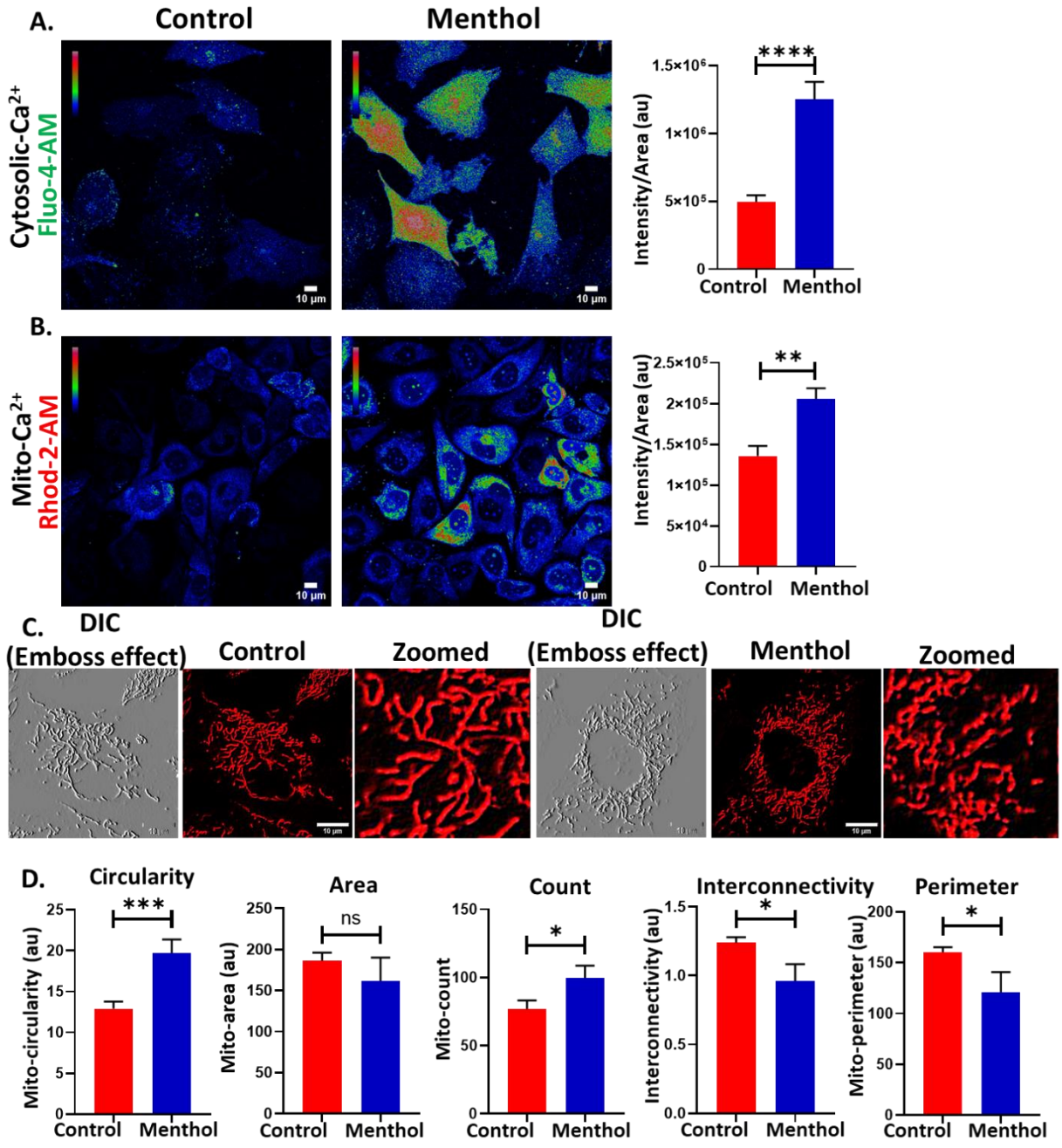


Fig. 35. Menthol increases mitochondrial Ca^{2+} and alters mitochondrial morphology. A-B. Shown are the comparatives of fluorescence intensities (represented in pseudo color) of live Saos-2 cells in control condition or treated with Menthol and labelled with cytosolic Ca^{2+}-indicator dye Fluo-4-AM (a) or mitochondrial Ca^{2+}-indicator dye (Rhod-2-AM) (b). n>60 cells were used in each case. **** = p≤ 0.0001, ** = p<0.01. **C.** Shown are the confocal images of Saos-2 cells labelled with MitoTrackerRed-CMXRos and analyzed for their mitochondrial morphology. **D.** Comparative analysis of mitochondrial parameters such as circularity, area, count, interconnectivity and perimeter are shown. N≥17 cells were used in each case. *** = p<0.001, * = p<0.05, ns = non-significant. (Un-published figure).

2.3.2 Menthol alters the mitochondrial morphology:

It is well known that cytosolic and mitochondrial Ca^{2+} affect mitochondrial morphology (Kowaltowski AJ, 2019). Since Menthol increases both cytosolic and mitochondrial Ca^{2+}, we checked the effect of Menthol on mitochondrial morphology and other parameters. Cells were treated with Menthol for 6 hours, and subsequently, mitochondrial morphological parameters were evaluated (**Fig. 35C**). Treatment of Menthol increases the mitochondrial count (**Fig. 35D**). Moreover, results suggest that Menthol treatment increases the mitochondrial circularity as well (**Fig. 35D**). At the same time, Menthol decreases the mitochondrial perimeter as well as interconnectivity (area/perimeter) significantly. However, the mitochondrial area remains unchanged. Taken together, the data suggest that Menthol regulate mitochondrial morphology and induces mitochondrial circularity.

2.3.3 Menthol causes instantaneous rise in mitochondrial Ca^{2+}:

In order to characterize the effects of Menthol on mitochondrial Ca^{2+}-levels in details, we performed live cell time series mitochondrial Ca^{2+}-imaging using Mito-Pericam construct. Addition of Menthol leads to an instant and continuous rise in the mitochondrial-Ca^{2+}-level observed even at 200th frames (~7.5 minutes) (**Fig. 36A**). Next, we chelated the extracellular Ca^{2+} using EGTA for 1 hour. In case of EGTA pre-treated cells, Menthol addition also shows a slow and sustained increase in mitochondrial Ca^{2+}-levels (**Fig. 36B**). The trend of mitochondrial Ca^{2+}-increase in EGTA-treated cells match well with only Menthol-mediated mitochondrial Ca^{2+}-influx, suggesting that the mitochondrial Ca^{2+} increase due to Menthol is most-likely independent of the Ca^{2+}-influx from extracellular sources. We chelated the cytosolic Ca^{2+} using BAPTA-AM for 1 hour. In contrast to EGTA-treated cells, we observed that in BAPTA-AM pre-treated cells, Menthol addition leads to a sharp rise in mitochondrial-Ca^{2+} (as seen by the slope between Frame

1 and 30) up to 150 frames and then the mitochondrial Ca^{2+}-starts decreasing with time (**Fig. 36C**). This suggests that addition of Menthol may lead to Ca^{2+}-release from some sub-cellular compartment as well.

To evaluate the dependency of Menthol-induced mitochondrial Ca^{2+}-increase on ER as Ca^{2+}-reserve, we used Thapsigargin; a well-known SERCA inhibitor for 1 hour which depletes the Ca^{2+} from ER. In Thapsigargin pre-treated cells, although addition of Menthol shows a sudden increase in mitochondrial-Ca^{2+}, but it starts decreasing from 30th frame. (**Fig. 36D**). This shows the dependency of ER on mitochondria for Ca^{2+} in its chelated state. One of the major target of Menthol is the TRPM8 ion channel (Peier AM, 2002). To evaluate the contribution of TRPM8 on this mitochondrial Ca^{2+}-increment, we incubated the cells with AMTB (10 μM; TRPM8-specific antagonist) for 1 hour and then added Menthol. In AMTB pre-treated cells also, Menthol causes an instantaneous rise in mitochondrial-Ca^{2+} (**Fig. 36E**). However, the basal mitochondrial Ca^{2+}-level is less when cells were pre-treated with AMTB, suggesting endogenous activity of TRPM8 is also involved in the maintenance of mitochondrial Ca^{2+} regulation to some extent (**Fig. 36F**). Notably, reducing the cytosolic Ca^{2+}-levels by either chelating extracellular or cytosolic Ca^{2+} or depleting ER Ca^{2+}, also affect the mitochondrial Ca^{2+} increment due to Menthol application (**Fig. 36G**). On comparing the differences in mitochondrial Ca^{2+}-level increment upon Menthol addition, it is evident that Menthol-induced mitochondrial Ca^{2+}-influx is greatly dependent on ER (**Fig. 36H**). The changes in mitochondrial Ca^{2+} in EGTA is also reduced which is comparable to AMTB-treated condition. Overall, the data suggest that Menthol causes an instantaneous influx of Ca^{2+} in mitochondria, which is partially independent of TRPM8 and partially dependent on Ca^{2+} source from ER, at least in short term application of Menthol.

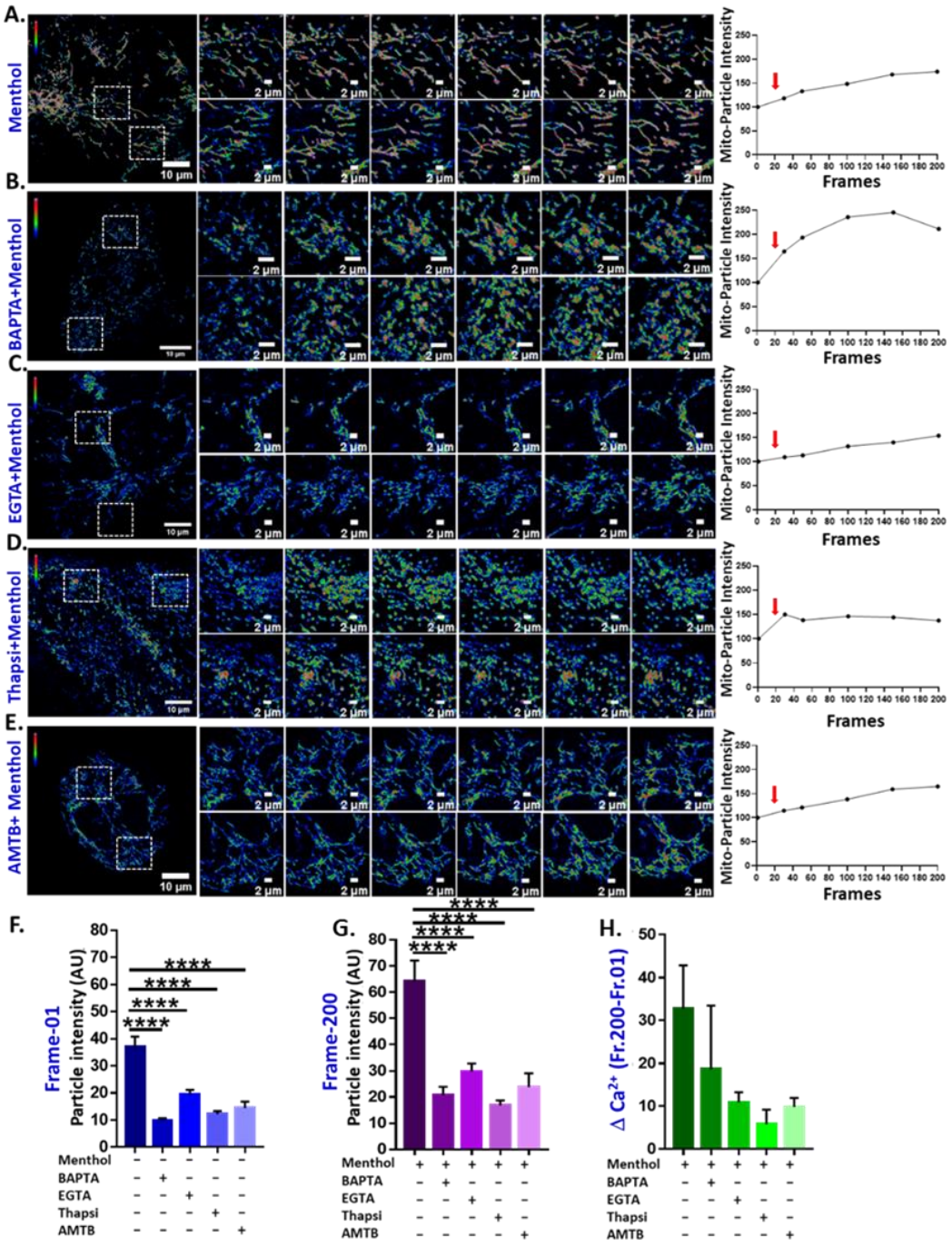


Fig. 36. Menthol causes instantaneous mitochondrial Ca^{2+}-influx. Mito-Pericam was transiently expressed in Saos-2 cells and live cell imaging was performed for 200 frames (~7.5 minutes). Menthol (100 µM) was added at 20th frame of the imaging as shown by the red arrow. **A.** Menthol increases the mitochondrial Ca^{2+} soon after its addition. A time-dependent changes in the mitochondrial Ca^{2+} (average particle intensity, initial value is normalized to 100%) is shown in right side. **B-E.** Cells were pre-treated with EGTA (5 µM); BAPTA-AM (10 µM); Thapsigargin (1 µM) and AMTB (10 µM) for 1 hour for blocking Ca^{2+}-mobilization from different sources and then Menthol was added. The fluorescence intensity of Mito-Pericam is shown in rainbow color (pseudo scale, red indicates highest intensity and blue indicates

the lowest intensity). Similar time-kinetics of mitochondrial Ca^{2+}-levels are shown in the right side. **F.** Graph shows the basal mitochondrial Ca^{2+}-load in cells as seen by intensity at Frame-01. Pre-treatment of cells with different agents reducing Ca^{2+} from different sources reduce the basal level mitochondrial Ca^{2+}. **G.** Graph indicates the total mitochondrial Ca^{2+}-intensity at Frame-200 suggesting the rise in mitochondrial Ca^{2+} upon Menthol addition. Prior chelation of extracellular or cytosolic or ER Ca^{2+} by different means, also affects the mitochondrial Ca^{2+}-status due to Menthol application. **H.** Changes in mitochondrial Ca^{2+}-levels (during last time point from initial time point) upon Menthol addition is shown. The change is least when Ca^{2+} from ER is depleted by prior application of Thapsigargin. TRPM8 inhibition by AMTB also reduce the changes in Menthol-induced mitochondrial Ca^{2+}-levels. One-way ANOVA **** = $p \leq 0.0001$, ns = non-significant. (Un-published figure).

2.3.4 Menthol affects sub-population dynamics based on the Ca^{2+}-status of individual mitochondrion:

Next, we quantified the individual mitochondrial Ca^{2+}-levels per cell using a particle-based quantification approach in each of the above mentioned conditions. This also allowed us to analyze the mitochondrial sub-population dynamics. We quantified >7000 individual mitochondrial particles from ≥14 cells in each condition at different time frames (1st, 30th, 100th and 200th of time points of live cell imaging.), i.e. at initial time point, soon after Menthol treatment, intermediate time point and at the end time point (total events measured is ~7.5 minutes). We categorized total mitochondrial particles into 4 sub-groups, mainly based on their individual Ca^{2+}-intensity. Therefore, the total mitochondrial pool is classified as Gr I: i.e. mitochondria with very low Ca^{2+}-intensity (1-10 AU; indicated by light blue), Gr II: mitochondria with low Ca^{2+}-intensity (10-100 AU; indicated by dark blue), Gr III: mitochondria with high Ca^{2+}-intensity (100-1000 AU; indicated by light red) and Gr IV: mitochondria with very high Ca^{2+}-intensity (≥1000 AU; indicated by dark red). We observed that upon addition of Menthol, the group of mitochondria with high (Gr III) and very high (Gr IV) Ca^{2+}-level increases (0.46% to 0.75%) (**Fig. 37A**). Interestingly, in Ca^{2+}-reduced condition, i.e., in EGTA, BAPTA-AM, Thapsigargin or AMTB pre-

treated condition, the percentage of mitochondria with very low (Gr I) Ca^{2+} is more and those with high (Gr III) and very high (Gr IV) Ca^{2+} become less (F-1) (**Fig. 37B, E**).

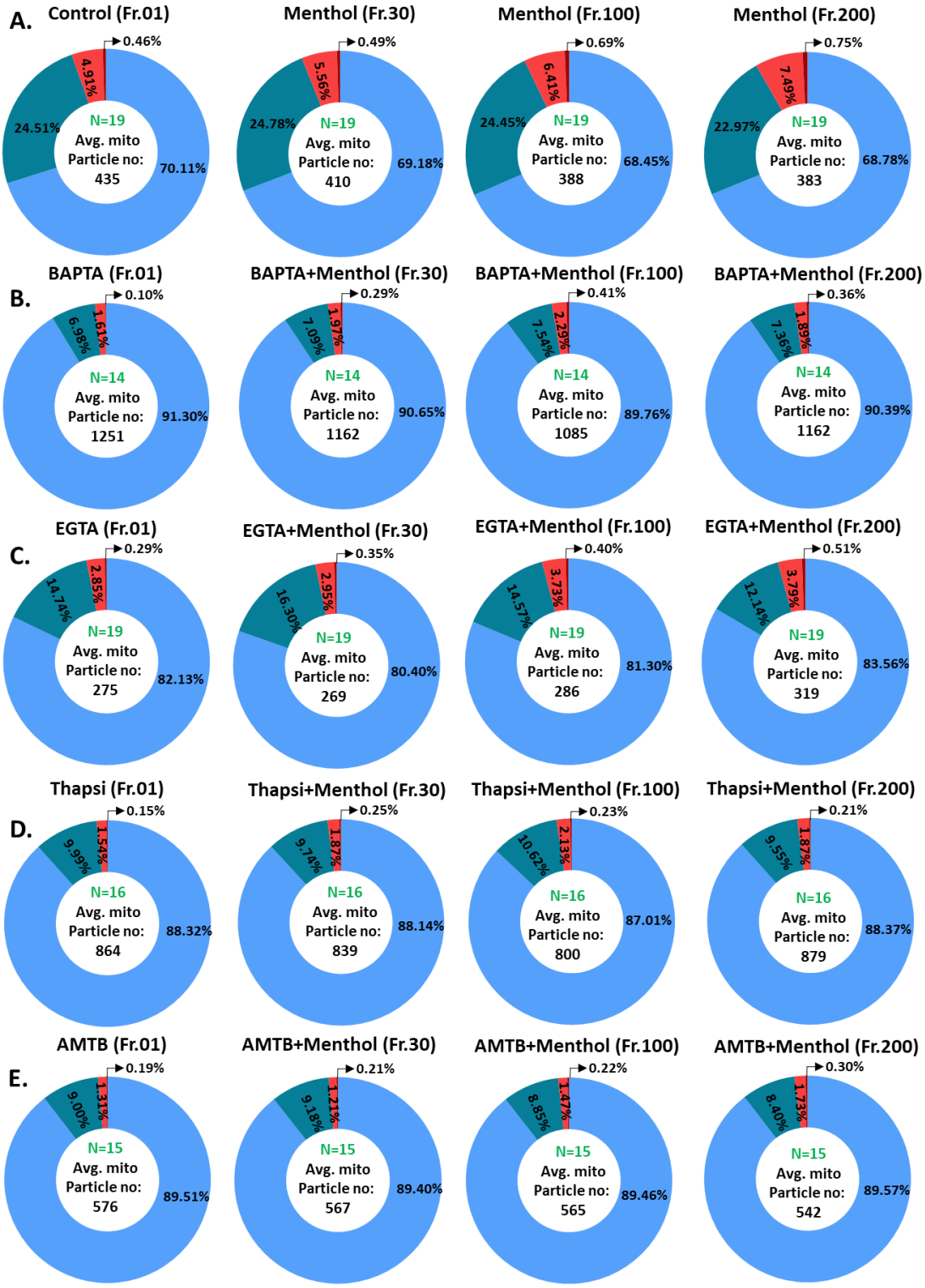


Fig. 37. Preventing Ca^{2+}-mobilization from different sources protects mitochondria from Menthol-induced Ca^{2+}-overloading. Live cell time series imaging was performed using Saos-2 cells expressing Mito-Pericam and Menthol (100 μM) was added at Frame-20. Fluorescence intensity of individual mitochondrial particles were quantified at different time points. **A-E.** Shown are the pie charts of mitochondrial particle numbers (represented in %) in different conditions and time points. In all the conditions, mitochondrial Ca^{2+} fluctuates within a range of 10^1 to 10^4 (AU). Mitochondrial particles are classified based on their Ca^{2+}-levels (Gr I: light blue = 10^0-10^1, Gr II: dark blue = 10^1-10^2, Gr III: light red 10^2-10^3, Gr IV: dark red = $\geq 10^3$ AU). Menthol addition leads to changes in mitochondrial particle numbers belongs to Gr III and Gr IV (red and dark red). Chelation of Ca^{2+} from extracellular media, or cytosol or depleting Ca^{2+} from ER or inhibiting TRPM8 by AMTB, all reduces the numbers of mitochondria in Gr III and Gr IV, and increases the mitochondria belongs to Gr I and Gr II. (Un-published figure).

In each of the situation, upon addition of Menthol the mitochondria with very high (Gr IV) Ca^{2+}-levels generally increase. However, in AMTB-treated condition, this increment in this group (Gr IV) is less (~2.3 fold less) and in Ca^{2+}-depleted from ER (Thapsigargin-treated) condition, this population is even more reduced (~4.8 fold less in Gr IV). We also quantified the basal mitochondrial Ca^{2+}-levels in different conditions where Ca^{2+}-mobilization from different sources were blocked (**Fig. 37F**). The end-point measurements after short-term Menthol treatment in different pre-treated cells also suggest that chelating of extracellular Ca^{2+}, or cytosolic Ca^{2+} or depleting ER Ca^{2+} or inhibiting TRPM8, all affects the extent of mitochondrial Ca^{2+}-levels induced by Menthol (**Fig. 37G, H**). Overall, the data suggest that Menthol addition causes an instantaneous rise in mitochondrial Ca^{2+}. Data also indicates that this Menthol-induced mitochondrial Ca^{2+}-influx is at least partially dependent on the presence of Ca^{2+} in ER.

2.3.5 Menthol affects mitochondrial membrane potential and ATP levels:

To confirm that Menthol indeed causes changes in the mitochondria, we evaluated multiple and specific mitochondrial functions. Mitochondrial membrane potential (ΔΨm) is a status of mitochondrial health and its activity (Zorova LD, 2018). Menthol changes the mitochondrial Ca^{2+} which is further shown to affect the mitochondrial membrane potential (Mito-MP) (Storey NM,

2017). We analyzed mitochondrial membrane potential (ΔΨm) by using TMRM dye. Menthol addition causes a decrease in the TMRM intensity which corresponds to a reduction in mitochondrial membrane potential (**Fig. 38A**). Mitochondrial Ca^{2+} is even reported to regulate the ATP production (Tarasov AI, 2012). Saos-2 cells were treated with Menthol for 6 hours and then evaluated for mitochondrial-ATP using BioTracker ATP-Red dye. Treatment of Menthol causes an increase in intensity of ATP-Red dye suggesting the rise in ATP production in Menthol-treated cells (**Fig. 38B**).

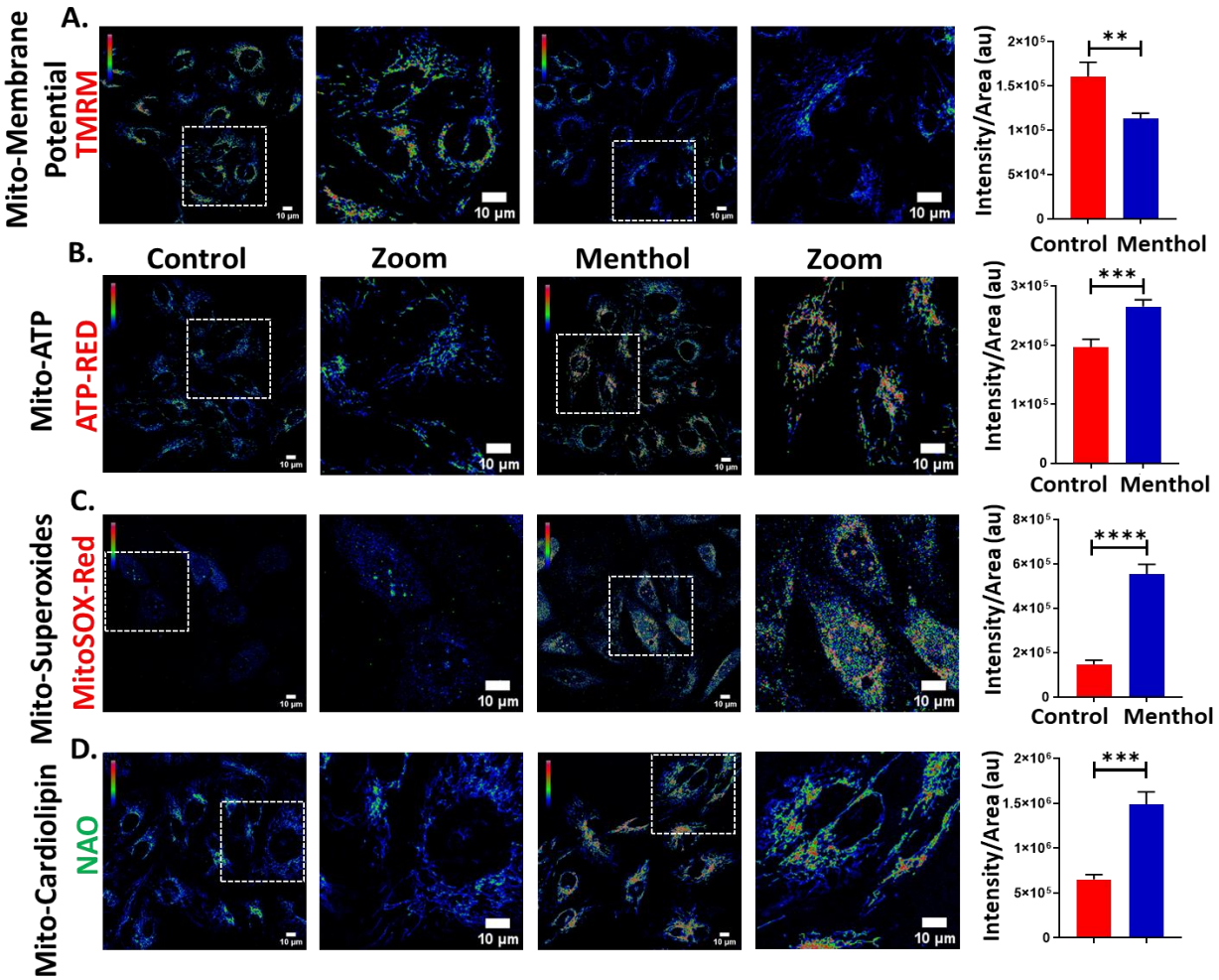


Fig. 38. Menthol regulates mitochondrial membrane potential and metabolism. A. Saos-2 cells were labelled with TMRM dye for analysing the mitochondrial membrane potential. Menthol application reduces the mitochondrial membrane potential. n>50 cells ** = p<0.01. **B-D.** Saos-2 cells were labelled with ATP-red (for mitochondrial ATP levels) (b), or MitoSOX-Red (for mitochondrial superoxide levels, c) or NAO dye (for mitochondrial Cardiolipin levels, d). Confocal images were acquired (represented in pseudo color)

and analyzed for Menthol effect. Menthol application increases mitochondrial ATP levels, superoxide levels and Cardiolipin. n>50 cells in each case Students t test, **** = p≤ 0.0001, *** = p<0.001. (Un-published figure).

2.3.6 Menthol elevates the mitochondrial superoxides and Cardiolipin levels:

We further investigated the involvement of Menthol in the regulation of mito-superoxides and Cardiolipin levels. For that purpose, we used MitoSOX-Red and NAO dye. Treatment of cells with Menthol for 6 hours leads to a sharp elevation of mito-superoxides than the control condition (**Fig. 38C**). Also, due to Menthol treatment, the amount of Cardiolipin increases drastically than normal cells (**Fig. 38D**). Altogether, our data suggest that Saos-2 cells, Menthol treatment causes increased mitochondrial Ca^{2+}-levels that in turn causes a significant change in several mitochondrial parameters.

2.3.7 Menthol regulates the ER-mito contact points:

Menthol-mediated increment in mitochondrial Ca^{2+} is affected by Thapsigargin, suggesting Ca^{2+} from ER is also contributing to the mitochondrial Ca^{2+}-increment, indicating that Menthol might also alter the ER-mito contact points as well. For that purpose, we labelled the cells with ER-Tracker Blue-White DPX and MitoTracker RedCMXRos, and quantified the total mitochondrial particles total ER particles, and compared the ER-mito contact points. We observed that Menthol does not increase the mitochondrial or ER particle numbers but increases the ER-mito contact points (**Fig. 39A**).

2.3.8 Menthol regulates the mitochondria but not ER temperature is osteosarcoma cells:

To evaluate the effects of the cooling agent Menthol on the mitochondrial and ER temperature, we used the MTY and ETY dyes, respectively. An increase in the intensity of ETY or MTY dye corresponds to decrease in the temperature of ER or mitochondria respectively (Arai

S, 2014; Arai S, 2015). Menthol addition for 6 hours does not change the ER temperature as compared to the untreated cells (**Fig. 40A**). Whereas the addition of Menthol elevated the MTY fluorescence intensity suggesting the reduction in the mitochondrial temperature upon treatment of Menthol (**Fig. 40B**).

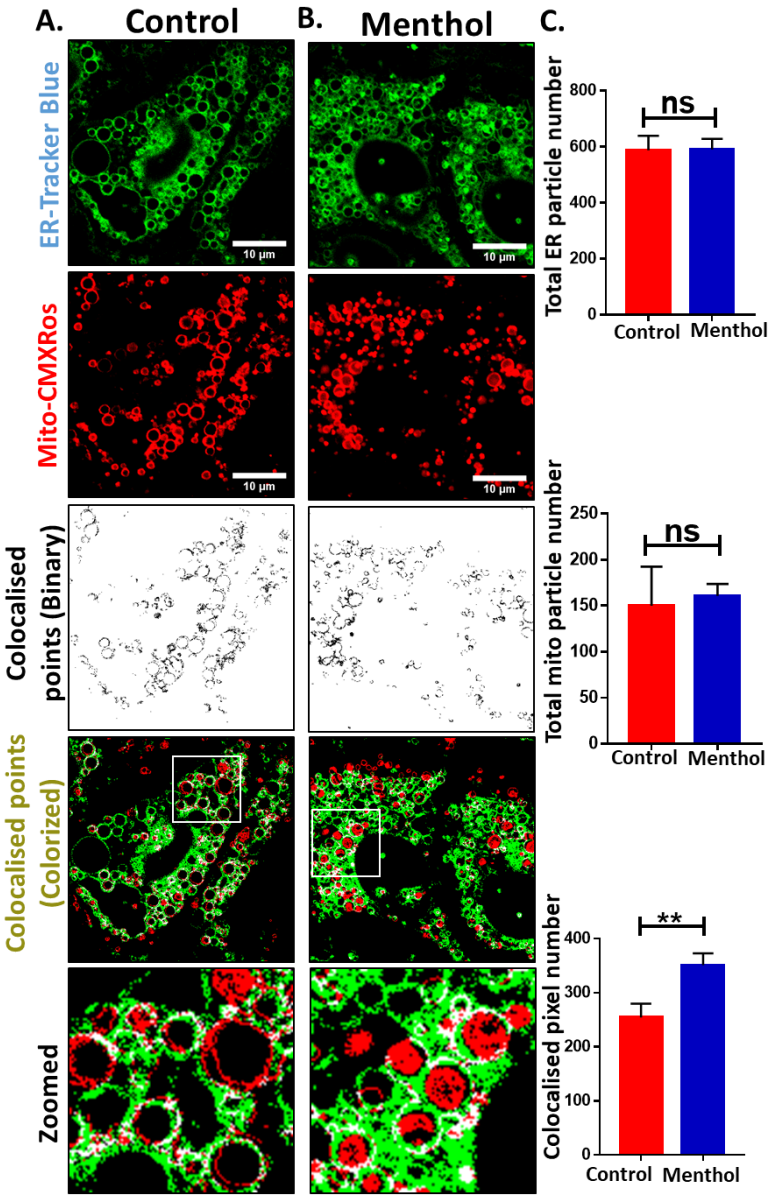


Fig. 39. Menthol enhances ER-mito contact points. A-C. Shown are the confocal images of Saos-2 cells where ER-blue (pseudo color green) and mitochondrial (red) are labelled with specific dyes. Cells were treated with hypotonic shock to evaluate the ER-mito contact points, and in this analysis, colocalized pixels are indicated as white areas. Menthol does not alter total particle numbers of ER or mitochondria but increases ER-mito contact points significantly. N≥20 cells in each condition, ** = p<0.01, ns = non-significant. (Un-published figure).

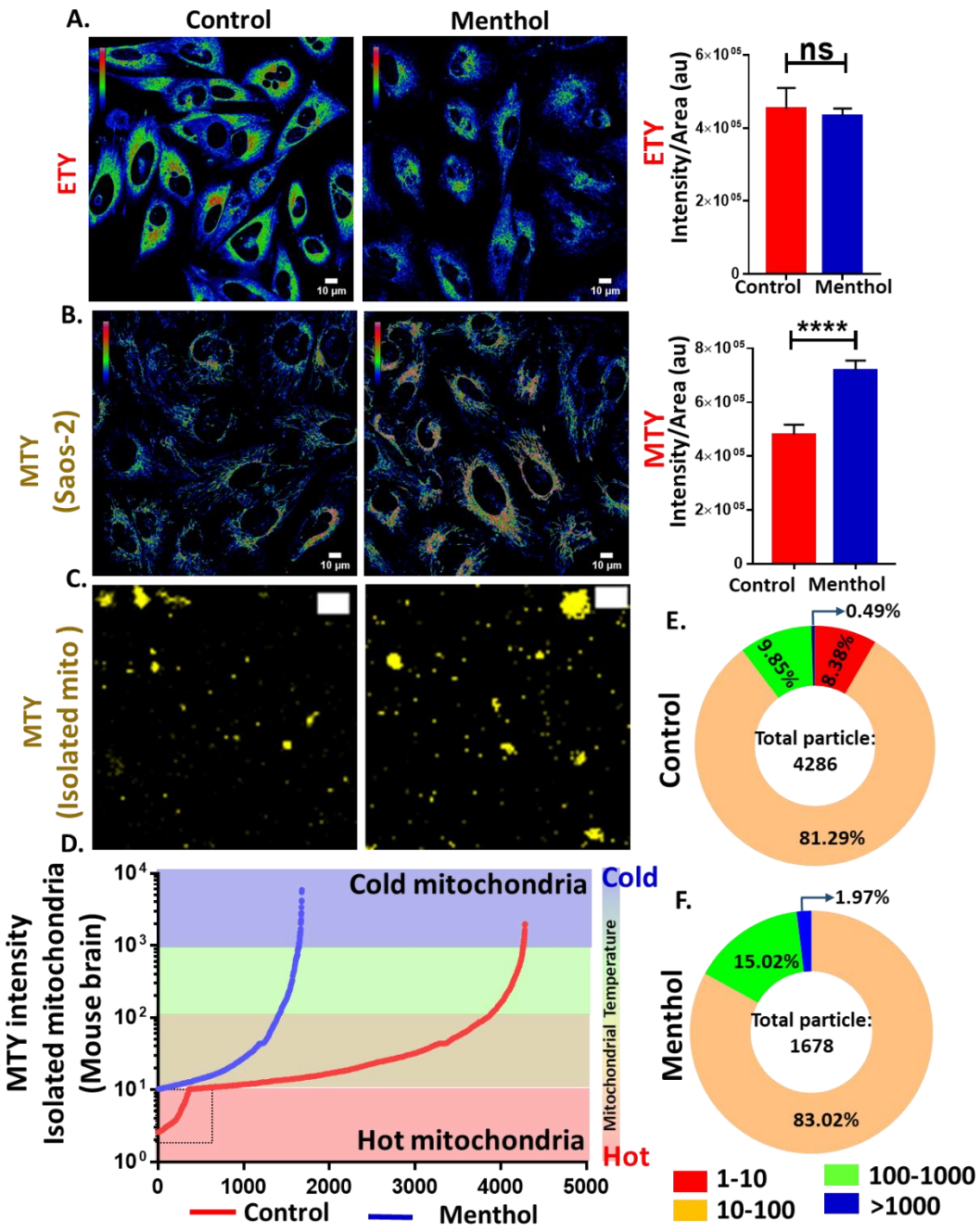


Fig. 40. Menthol cools mitochondria, but not the ER. A. Shown are the confocal images of Saos-2 cells loaded with ER temperature sensitive dye (ETY). The ETY fluorescence in control cells and Menthol-treated cells were recorded. No change in ER temperature is observed (quantified graphs were shown right side of the image). **B.** Saos-2 cells were loaded with mitochondrial temperature sensing dye Mito-Thermo Yellow (MTY). The MTY fluorescence in cells in control conditions and in Menthol-treated condition were acquired. Treatment of Menthol increase in MTY fluorescence intensity (i.e. decreases mitochondrial temperature). More than 50 cells were quantified in each condition. Student's t test. **** = $p \leq 0.0001$, ns = non-significant. **C.** Shown are the comparative confocal images of mitochondria isolated from mouse

brains and were labelled with MTY dye and were treated with Menthol (5 µM) or left untreated. Scale bar 5 µm. **D.** Fluorescence intensities of individual mitochondrial particles from the same preparation that are labelled with MTY dye and treated with Menthol were compared. Both changes in particle number and MTY intensity were observed due to Menthol treatment. More than 4000 particles in the control condition and 1500 in Menthol-treated condition as observed from 6 different view fields in each condition, were arranged in an increasing order. In all the cases, mitochondrial MTY intensity ranges from 10^0 to 10^4. Mitochondrial particles were classified based on their MTY intensity (Red-10^0-10^1 = very hot mitochondria, yellow-10^1-10^2 = slightly hot mitochondria, green-10^2-10^3 = moderate hot temperature mitochondria, and blue-10^3-10^4 = cold mitochondria). In the case of Menthol-treatment, the number of hot mitochondria with MTY fluorescence intensity in the range of 10^0 to 10^1 is reduced (indicated by dotted square) and number of cold-mitochondria with MTY fluorescence intensity in the range of 10^3 to above is increased. **E-F.** Shown are the pie charts of mitochondrial number in isolated mitochondria in control and Menthol-treated cells labelled with MTY dye. In Menthol treated condition, mitochondria having low intensity of MTY (very hot mitochondria) is not observed. (Un-published figure).

To check this crucial phenomenon, we performed a similar experiment in isolated mitochondria from mouse brain. We observed the same trend. In isolated mitochondria also, the MTY fluorescence intensity was elevated upon treatment with Menthol (**Fig. 40C**). Over all, the fluorescence intensity increased ~2 folds due to Menthol treatment, suggesting a cooling effect of mitochondria. To fully comprehend the change, we measured the fluorescence intensity of each mitochondrial using Image J's particle-based quantification method. Based on their fluorescence intensity, we classified the mitochondrial particle into four groups (Gr 1:10^0-10^1 AU, Gr 2:10^1-10^2 AU, Gr 3:10^2-10^3 AU and Gr 4: greater than 10^3 AU). We noticed that overall mitochondrial particle is low in Menthol-treated condition. We found that in the control condition, ~8.38% of mitochondria (Group-I) have low MTY intensity (thus represents hot mitochondria) and this group of mitochondria is absent in the Menthol-treated condition, suggesting that these hot mitochondria become cold. When we compare the highest MTY intensity mitochondria (Group III + Group IV) in the control and Menthol-treated condition, we observed that in the control condition, the percentage is ~10.34%, and in Menthol treated condition, it raised up to ~17%. Taken together,

the mitochondria particle based quantification data suggest that Menthol treatment causes rapid cooling of the hot mitochondria in particular.

2.3.9 TRPM8 regulates mitochondrial morphology:

As we have mentioned that Menthol has various other off targets other than TRPM8 which compelled us to check other specific modulators of TRPM8 namely WS12 and AMTB to confirm the specific functionality of TRPM8 in mitochondrial parameters if any. Previously we observed that Menthol causes mitochondrial fragmentation and causes change in the mitochondrial morphology. Therefore, we tested the effect of specific agonist and antagonist of TRPM8 i.e. WS12 (5µM) and AMTB (10µM) on mitochondrial morphology. We quantified different mitochondrial morphometric parameters after TRPM8 modulation.

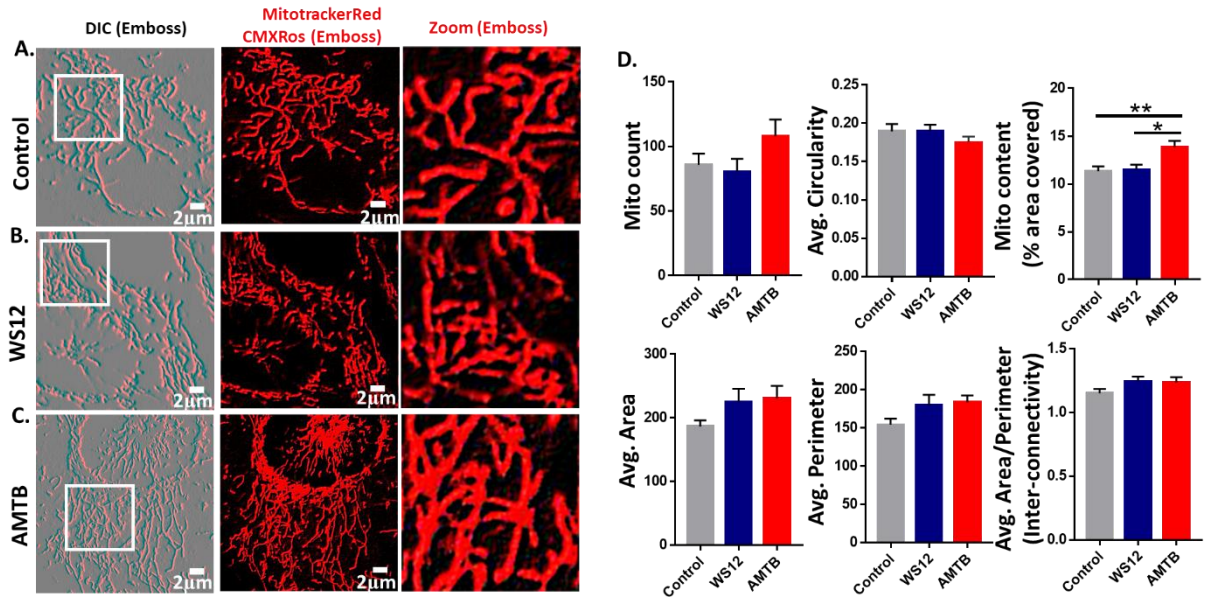


Fig. 41. Regulation of mitochondrial morphology by TRPM8. A-C. Shown are the confocal images of Saos-2 cells labelled with MitoTracker Red CMXRos and analyzed for their mitochondrial morphology. Images are represented in emboss effect. **D.** Comparative analysis of mitochondrial parameters such as circularity, area, count, interconnectivity and perimeter are shown. N≥17cells in each case. ** = $p<0.01$, * = $p<0.05$, ns = non-significant. (Un-published figure).

We quantified mitochondrial numbers, average area and perimeter, area-to-perimeter ratio (Interconnectivity), mito-content, i.e. percentage of area covered (mitochondrial distribution

within the cell), average circularity and solidity in different cells. Data suggests that there is no significant change observed in mitochondrial morphology in control as well as in treated conditions. Albeit, there is a significant decrease in mitochondrial distribution in WS12-treated cells, and mitochondrial distribution is increased in AMTB-treated cells. Similarly, the mitochondrial interconnectivity increased in AMTB treated cells (**Fig. 41A-D**).

2.3.10 TRPM8 regulates mitochondrial Ca^{2+}-dynamics:

Mitochondrial Ca^{2+}-level is directly associated with cytoplasmic Ca^{2+}-level (Finkel T, 2015). TRPM8 activation increases cytosolic Ca^{2+} in Saos-2 cells, which we reported earlier (Acharya TK, 2021). Nevertheless, the propensity of change in mitochondrial Ca^{2+} is not explored yet. Here we investigated the role of TRPM8 on mitochondrial Ca^{2+}-homeostasis using Mito-Pericam and performed live cell imaging for 200 frames (~07 mins), and added the drug at 20th frame (**Fig. 42**). Sustained increase in mitochondrial Ca^{2+}-level was observed seconds after addition of WS12 (**Fig. 42A**). In contrast, upon addition of AMTB, the mitochondrial Ca^{2+}-level declines gradually after an initial spike (**Fig. 42B**). Furthermore, we pre-incubated the cells with AMTB for 1hour and then added WS12. Here also, we observed a continuous rise in mitochondrial Ca^{2+} (**Fig. 42C**). In another experiment, we pre-treated the cells with either BAPTA-AM, Thapsigargin or EGTA for 1 hour to chelate the intra-cellular, ER Ca^{2+}, and extra-cellular Ca^{2+} respectively. In each of the cases (BAPTA-AM, Thapsigargin and EGTA), addition of WS12 results in an increment in mitochondrial Ca^{2+}-level instantly (**Fig. 42D, F**). Taken together, our results suggest that activation of TRPM8 causes an instantaneous mitochondrial Ca^{2+}-influx in Saos-2 cells.

We further quantified the basal mitochondrial Ca^{2+}-level (Mito-Pericam intensity at Frame 01) of each of the above conditions (**Fig. 43A**). In all the pre-treatment conditions (AMTB,

BAPTA-AM, Thapsigargin and EGTA), the basal mitochondrial Ca^{2+}-load reduces as compared to control cells but with different extent. Specifically, a population of mitochondria with very low Ca^{2+} is not observed in control condition, but detected in all other pre-treated conditions (**Fig. 43A**). In AMTB or EGTA-pre-treated conditions, the reduction in mitochondrial Ca^{2+} is less and similar (~0.77-fold less for both). However, pre-treatment of cells by BAPTA-AM or Thapsigargin decreases the mitochondrial Ca^{2+} to a greater extent (~0.46-fold and ~0.31-fold less respectively). We also quantified the change in mitochondrial Ca^{2+}-level (ΔMito Ca^{2+} = Mito-Pericam intensity at Frame 200 – Frame 01) of each condition (**Fig. 43B**). Addition of WS12 in cells without any pre-treatment has the maximum change in mitochondrial Ca^{2+} content whereas, AMTB addition showed no such changes in mitochondrial Ca^{2+}-level of these cells (**Fig. 43B**). Interestingly, in AMTB pre-treated cells, the change is mitochondrial Ca^{2+} due to WS12 stimulation is greater than only AMTB-stimulated cells. Also, in case of EGTA, BAPTA-AM, or Thapsigargin-pre-treated conditions, the extent of mitochondrial Ca^{2+}-influx is lesser than only WS12 stimulated condition (**Fig. 43B**). A similar pattern was also observed when we compared the fold change in the intensity values (**Fig. 43C**). All in all, the results suggest that TRPM8-mediated mitochondrial Ca^{2+}-influx is partially dependent on all the three Ca^{2+}-reservoirs, i.e., intra-cellular, extra-cellular and Thapsigargin.

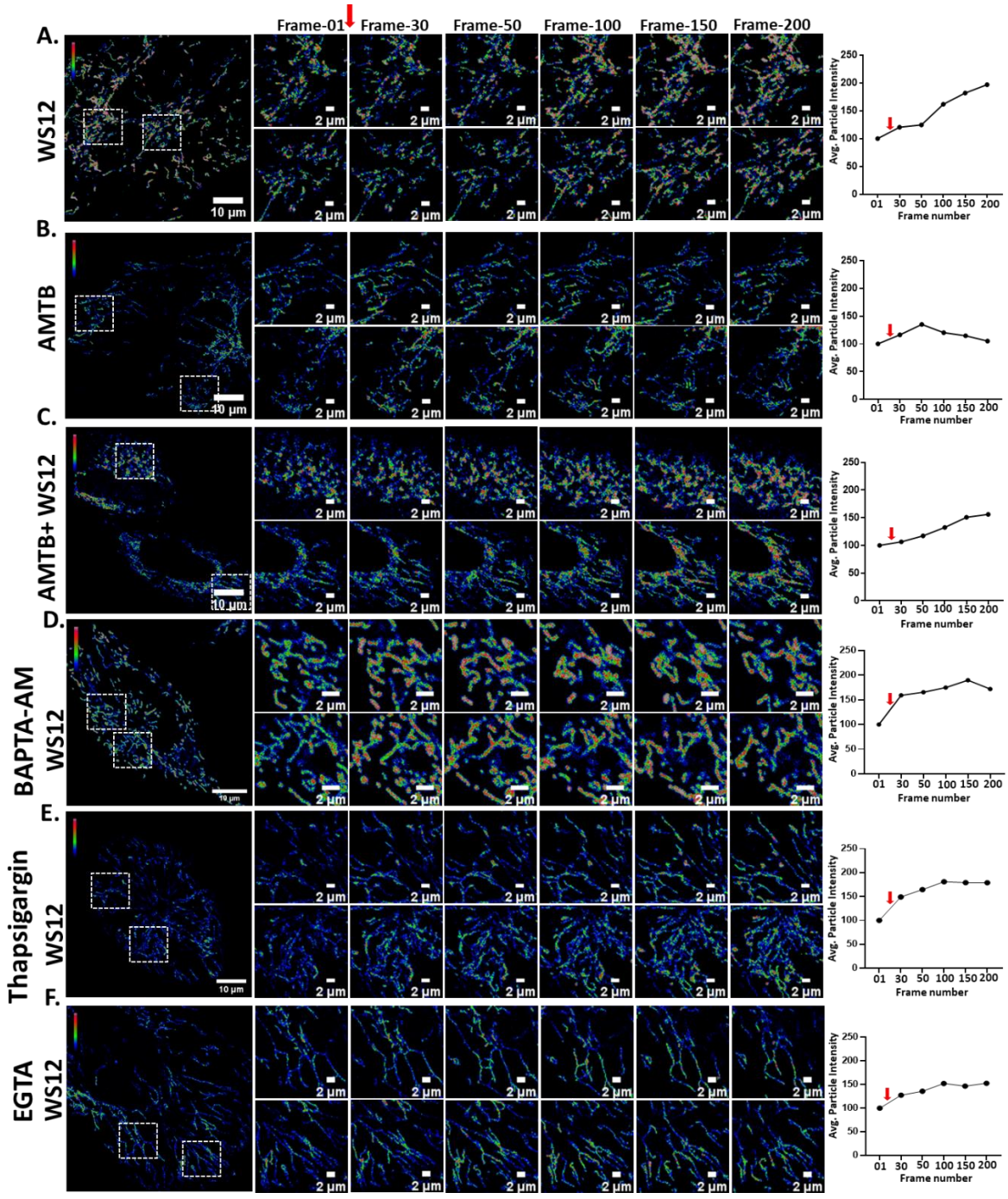


Fig. 42. Activation of TRPM8 causes instantaneous mitochondrial Ca^{2+}-influx. Mito-Pericam was transiently expressed in Saos-2 cells, and live cell imaging was performed for 200 frames (~7.5 minutes). **A.** WS12 (5 µM) was added at 20th frame of the imaging as shown by the red arrow. A time-dependent changes in the mitochondrial Ca^{2+} (average particle intensity, initial value is normalized to 100%) is shown in right side. **B-F.** Cells were pre-treated with EGTA (5 µM); BAPTA-AM (10 µM); Thapsigargin (1 µM) and AMTB (10 µM) for 1 hour for blocking Ca^{2+}-mobilization from different sources and then WS12 (5 µM) was added. The fluorescence intensity of Mito-Pericam is shown in rainbow color (pseudo scale, red indicates highest intensity and blue indicates the lowest intensity). Similar time-kinetics of mitochondrial Ca^{2+}-levels are shown in the right side. (Un-published figure).

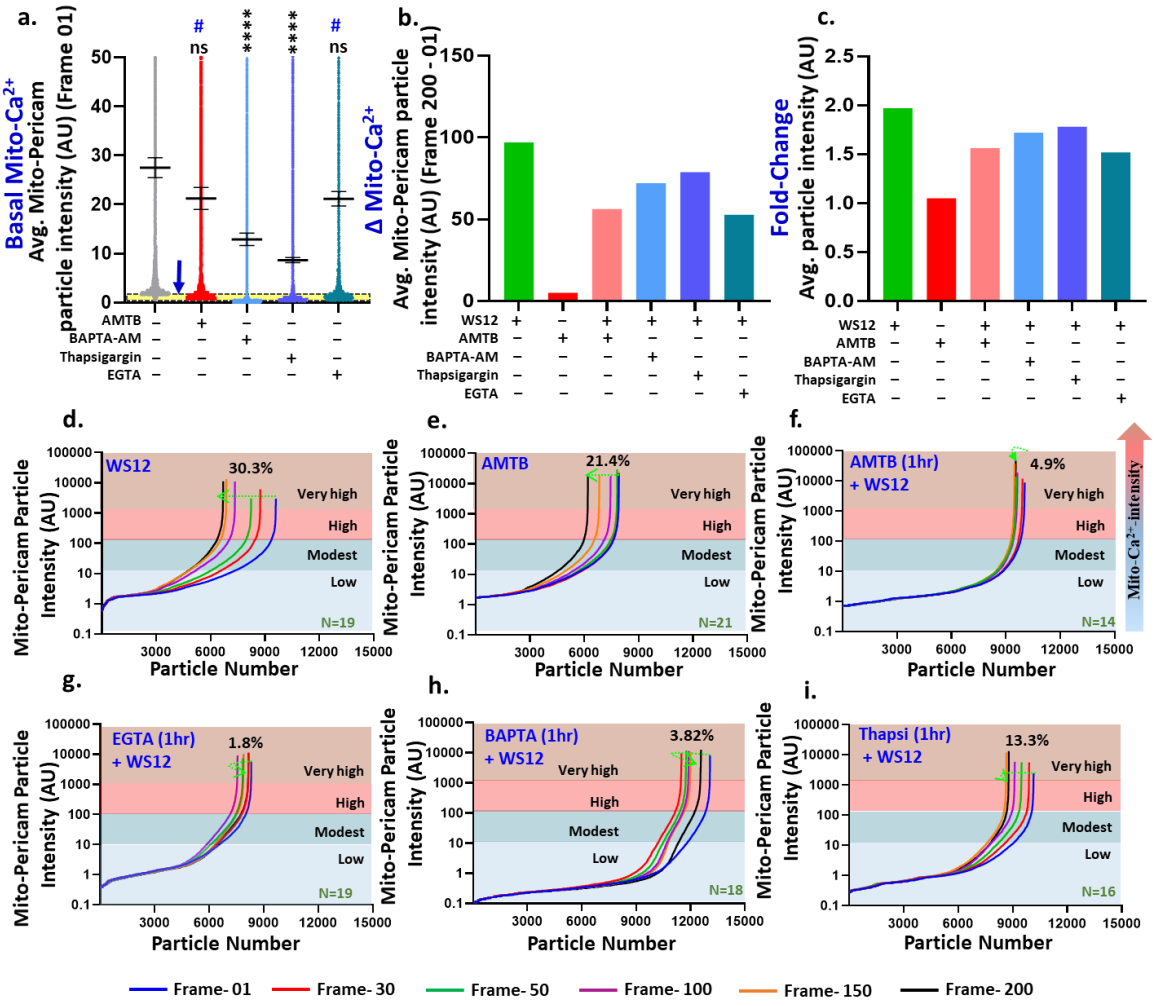


Fig. 43. TRPM8 regulates mitochondrial Ca^{2+}-load and mitochondrial number. Quantification of basal Ca^{2+} level in each experimental condition. Here we quantified ~7000 mitochondrial particles of different time points (i.e. Frame 01, 30, 50, 100, 150 and 200). The yellow highlighted box and the blue arrow indicate the population of mitochondria with very low level of Ca^{2+} which is absent in the control condition but is detected in all other pre-treated conditions. **B-C**. Quantification of delta change of mitochondrial Ca^{2+} (intensity at Frame 200 – Frame 01) and fold-change in the Ca^{2+}-intensity in different experimental conditions. **D-I.** Fluorescence intensities of individual mito-particles were arranged in increasing order. Total particles from Saos-2 cells at different time points are shown. Both changes in total particle number as well as in the mitochondrial Ca^{2+}-level is observed due to TRPM8 activation. In each case, TRPM8-specific agonist WS12 was added at the 20th frame. **** = $p<0.0001$, ns = non significant. (Un-published figure).

2.3.11 TRPM8 modulates both mitochondrial Ca^{2+}-level and mitochondrial numbers:

We quantified mitochondrial number and Ca^{2+}-intensity by particle based quantification in each of the above experimental conditions. Here we quantified ~7000 mitochondrial particles of

different time points (i.e. Frame 01, 30, 50, 100,150 and 200). Upon plotting the mitochondrial particle number along with its intensity, we observed biphasic plots suggesting the presence of at least two populations of mitochondria where Ca^{2+}-level differ dramatically. Modulation of TRPM8 leads to a decrease in the total amount of mitochondria. However, the reduction was minimum in the case of AMTB (**Fig. 43D, I**). For a detailed analysis of changes in mitochondrial number, we categorised four groups of mitochondria based upon their Ca^{2+}-intensity. The fraction of mitochondria with very low Ca^{2+}-intensity (0.1-10 AU, light blue), low (10-100 AU, dark blue), high (100-1000 AU, red) and very high (≥1000 AU, dark red). We noted that upon activation of TRPM8, the average mitochondrial number and mitochondria with very low Ca^{2+} decreases gradually and simultaneously, the group of mitochondria having high to very high Ca^{2+}-load increases (**Fig. 44A**). Interestingly, upon addition of AMTB, the mitochondrial distribution (based on Ca^{2+}) does not change much and remains close to Frame 01 (**Fig. 44B**). Although, a reduction in average mitochondrial number was observed (**Fig. 44B**). This suggest that instantaneous TRPM8 inhibition doesn't alter the mitochondrial Ca^{2+}-status greatly. In the case of AMTB pre-treated cells, the average mitochondrial number increases and the addition of WS12 causes an increment in mitochondria with very low as well as very high Ca^{2+}, however, low and high mitochondria Ca^{2+} number decreases (**Fig. 44C**). Moreover, AMTB treatment causes rise in very low Ca^{2+}-containing mitochondria (87.96%) (**Fig. 44C**). For BAPTA-AM, Thapsigargin and EGTA treated cells, addition of WS12 results in increment of mitochondria with high, very high increases and low and very low Ca^{2+}-mitochondria reduce (**Fig. 44D-F**). Furthermore, the mitochondria with very low Ca^{2+} increases (Frame 01) rises up in these condition suggesting a reduction in the mitochondrial Ca^{2+} of the cells (**Fig. 44D-F**). Altogether the data suggest that

TRPM8 modulation not only affect the mitochondrial Ca^{2+}-status of cell, but also brings about changes in mitochondrial number.

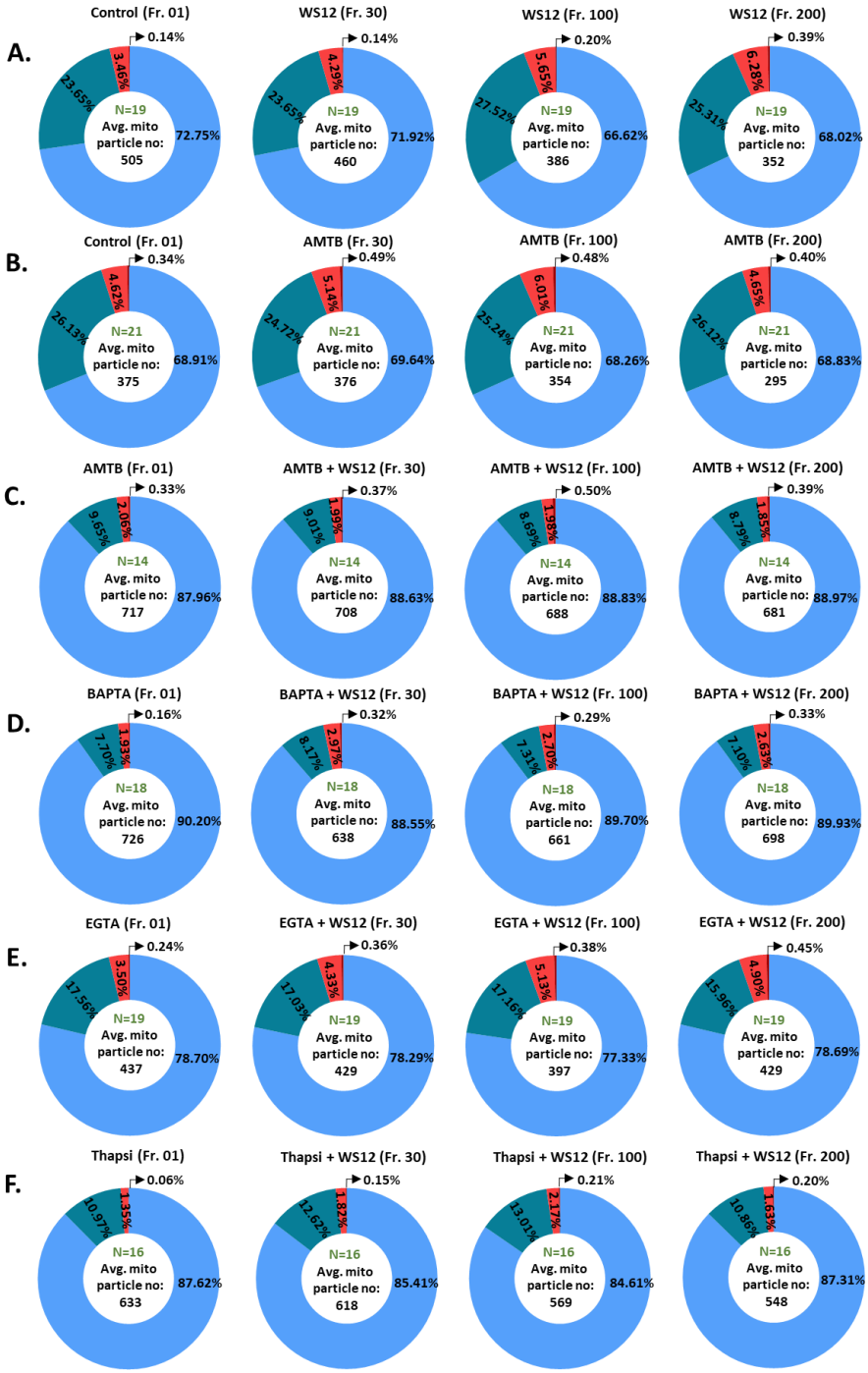


Fig. 44. Preventing Ca^{2+}-mobilization from different sources protects mitochondria from WS12-induced Ca^{2+}-overloading. Live cell time series imaging was performed using Saos-2 cells expressing Mito-Pericam and WS12 (5 μM) was added at Frame-20. Fluorescence intensity of individual mitochondrial particles were quantified at different time points. **A-F.** Shown are the pie charts of

mitochondrial particle numbers (represented in %) in different conditions and time points. In all the conditions, mitochondrial Ca^{2+} fluctuates within a range of 10^1 to 10^4 (AU). Mitochondrial particles are classified based on their Ca^{2+}-levels (Gr I: light blue = 10^0-10^1, Gr II: dark blue = 10^1-10^2, Gr III: light red 10^2-10^3, Gr IV: dark red = $\geq 10^3$ AU). WS12 addition leads to changes in mitochondrial particle numbers belongs to Gr III and Gr IV (red and dark red). Chelation of Ca^{2+} from extracellular media, or cytosol or depleting Ca^{2+} from ER or inhibiting TRPM8 by AMTB, all reduces the numbers of mitochondria in Gr III and Gr IV, and increases the mitochondria belongs to Gr I and Gr II. (Un-published figure).

2.3.12 Chronic TRPM8 modulation affects both basal cytosolic and mitochondrial Ca^{2+}-status in Saos-2 cells:

We next sought to investigate how long term modulation of TRPM8 affects the cytosolic Ca^{2+}-status of cells (**Fig. 45A**). Addition of WS12 for 6 hours resulted in increased (~1.94 fold) cytosolic Ca^{2+}-load of cells, whereas AMTB addition shows reduction (~0.57-fold) in the cytosolic Ca^{2+}-load (**Fig. 45C**). In a similar fashion, we determined the mitochondrial Ca^{2+}-status of TRPM8 modulator treated cells (**Fig. 45B**).

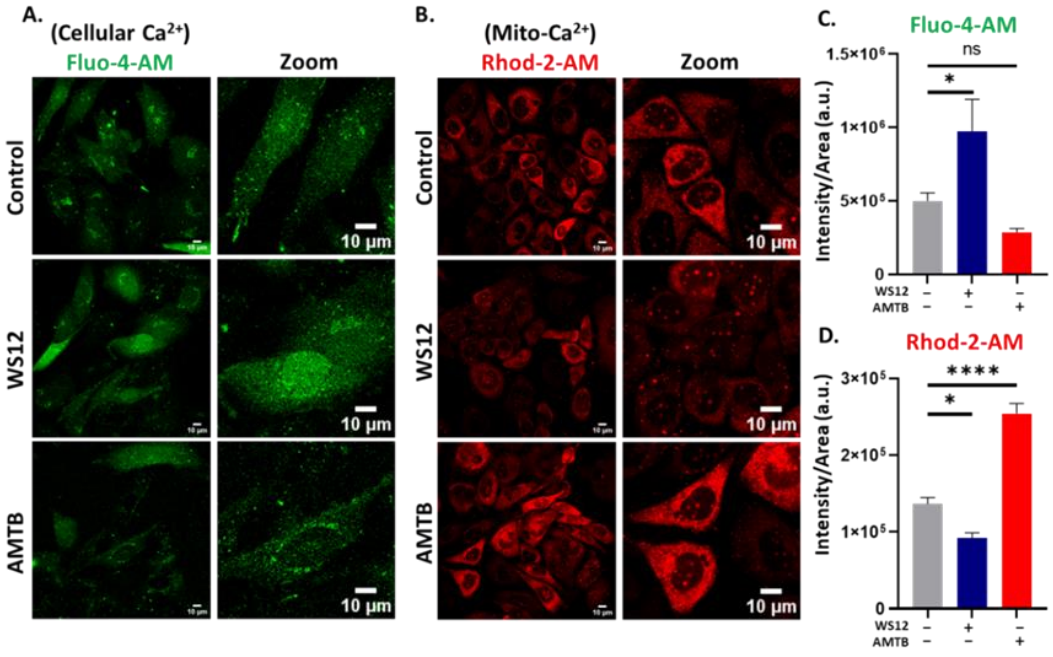


Fig. 45. Chronic modulation of TRPM8 changes the cytosolic and mitochondrial Ca^{2+}-levels differentially. A, C. Saos-2 cells were treated with WS12 and AMTB for 6 hours and cytosolic Ca^{2+} was measured by labelling with Fluo-4-AM dye. Quantitative analysis of Fluo-4-AM fluorescence levels indicates that WS12-treated cells have elevated cytosolic Ca^{2+}. **B, D.** Similarly, the cells were labelled with Rhod-2-AM dye for measurement of mitochondrial Ca^{2+}, and cells treated with AMTB for a longer duration (6hours.) exhibit a greater mitochondrial Ca^{2+}-load than WS12-treated cells. (Un-published figure).

Interestingly, WS12 treated cells have lesser mitochondrial Ca^{2+} (~0.67 fold less Rhod-2-AM intensity), however, AMTB resulted in a significant rise (~1.86 fold) in mitochondrial Ca^{2+} of cells (more Rhod-2-AM intensity) (**Fig. 45D**). Overall, the data suggest that long term modulation of TRPM8 affects the mitochondrial and cytosolic Ca^{2+}-status of cells differently.

2.3.13 Regulation of mitochondrial membrane potential and ATP level by TRPM8:

It has been reported that elevation of mitochondrial Ca^{2+} results collapse of mitochondrial membrane potential (Chalmers S 2008, Talbot J, 2007). Since TRPM8 activation escalates the mitochondrial Ca^{2+}-level it further intrigued us to check the membrane potential in Saos-2 cells. For this purpose, the cells were treated with different TRPM8 modulators for a chronic period of 6hr and subsequently probed with TMRM dye. By quantifying 200 cells in different conditions, we inferred that in the TRPM8 activated cells the membrane potential decreases significantly (~0.8 fold), whereas in the inhibited condition, the membrane potential is generally rescued (~1.43-fold increase in TMRM intensity) (**Fig. 46A, B**). This finding supports our previously reported data where we have measured the mitochondrial membrane potential in mouse bone marrow derived Mesenchymal stem cells. Where in the TRPM8 inhibited condition the mitochondrial membrane potential increased significantly and it got reversed in TRPM8 activated cells (Acharya TK, 2021).

Mitochondrial Ca^{2+} and ATP synthesis is frequently interlinked (Brookes PS, 2004). To execute this experiment, we have used ATP red dye, which binds to the mitochondrial ATP and it can be visualize by confocal microscope. In this experiment, the cells were also pre-treated with TRPM8 drugs and subsequently, they were stained with ATP red dye for 15 min. The intensity of ATP red from 200 cells per condition was quantified by Image J. The ATP level is significantly high in AMTB treated cells (~1.99 fold), whereas in the WS12 treated cells, the ATP level is typically low (**Fig. 46C, D**)

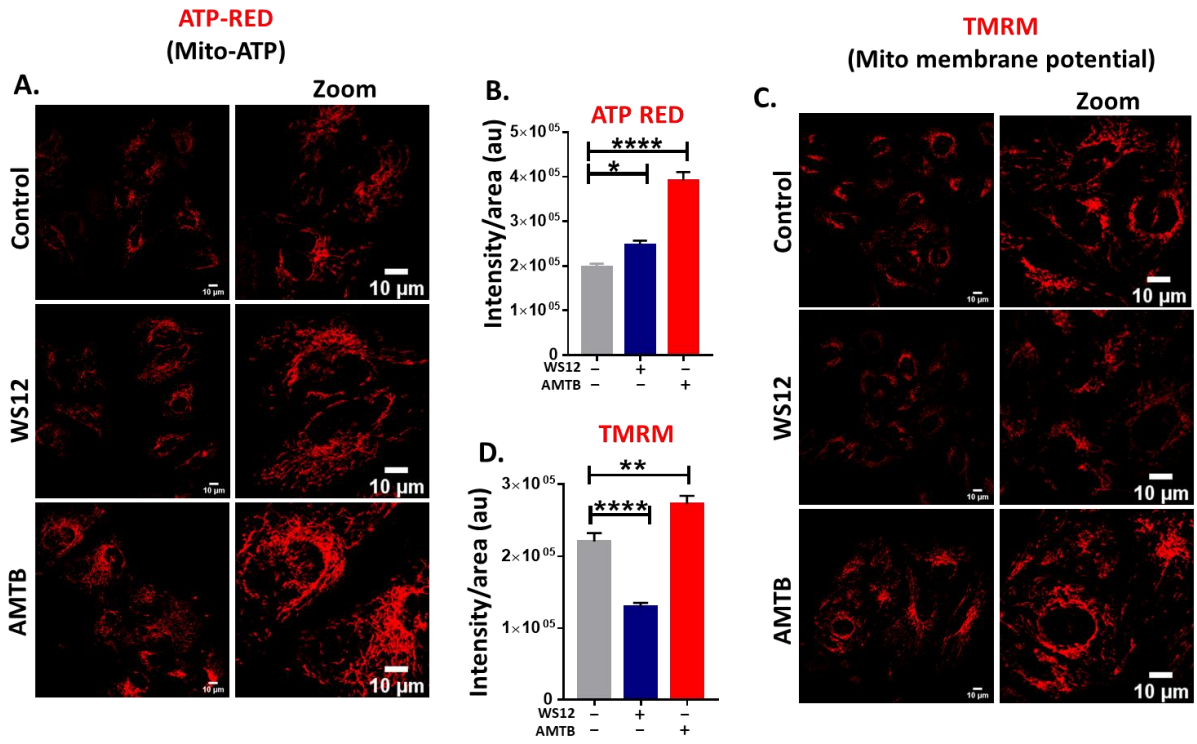


Fig. 46. TRPM8 regulates mitochondrial membrane potential and metabolism. A-B. Saos-2 cells were labelled with TMRM dye for analyzing the mitochondrial membrane potential. WS12 application reduces the mitochondrial membrane potential. n>50 cells ** = p<0.01. **C-D.** Saos-2 cells were labelled with ATP-red (for mitochondrial ATP levels). WS12 application decreases mitochondrial ATP levels and AMTB treatment increases ATP level. n>50 cells in each case. One-way ANOVA, **** = p≤ 0.0001, ** = p<0.01, ns = non significant. (Un-published figure).

2.3.14 TRPM8 modulates mitochondrial ROS generation:

Mitochondrial Ca^{2+} and ROS are mutually interlinked. Calcium and ROS signaling can be considered as a bidirectional phenomenon. Ca^{2+}-signaling is required for ROS generation, and ROS can regulate Ca^{2+}-level (Adam-Vizi V, 2010). As TRPM8 activation increases mitochondrial Ca^{2+}-level and decreases mitochondrial membrane potential, we checked the mitochondrial ROS status in different conditions. For this experiment, the cells were treated with TRPM8 activator and inhibitor for 6 hr and subsequently labelled with MitoSOX red to identify the ROS level. Surprisingly we observed that in all the activated (WS12) and inhibited (AMTB) conditions, the

mitochondrial ROS level increased significantly as compared to the control condition (~2.33 and ~3.79 fold more respectively) (**Fig. 47A, B**). This data suggest that both the activation and inhibition of the channel are crucial for the oxidative metabolism of the cell.

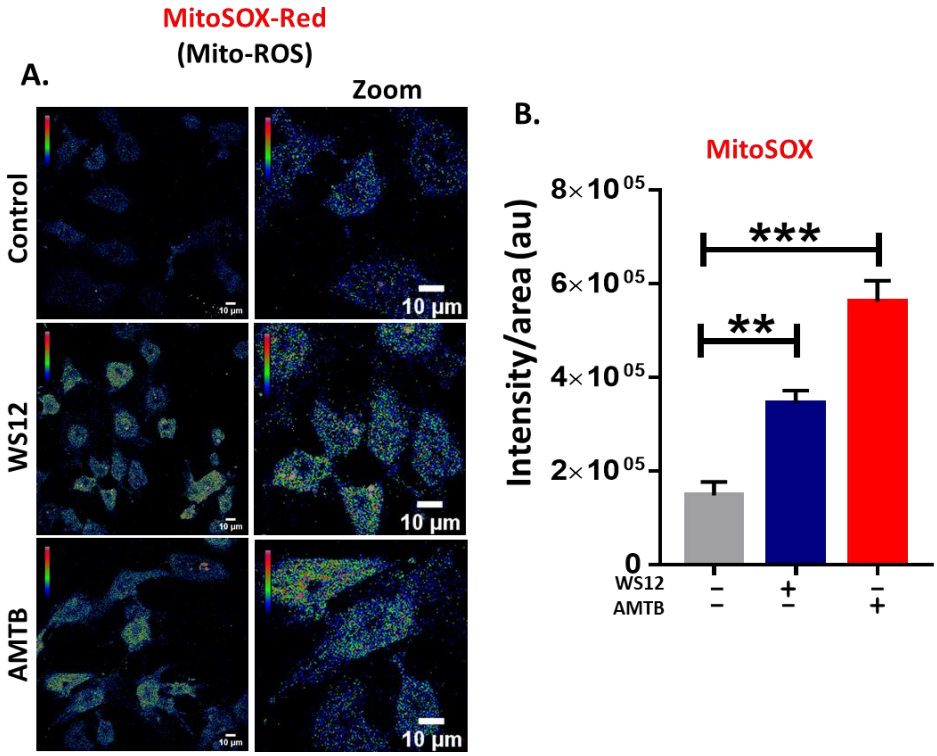


Fig. 47. Modulation of TRPM8 increases mitochondrial superoxide level. A-B. Saos-2 cells were labelled with MitoSOX-Red for the detection of mitochondrial superoxide levels. Confocal images were acquired (represented in pseudo color) and analyzed for WS12 and AMTB effects. Both activation and inhibition elevate superoxide levels n>50 cells in each case. Students t test, **** = p≤ 0.0001, ** = p<0.01. (Un-published figure).

2.3.15 TRPM8 activation changes mitochondrial Cardiolipin status:

Mitochondrial phospholipid Cardiolipin is an essential indicator of mitochondrial health and plays a major role in mitochondrial physiology. We checked the changes in Cardiolipin status in Saos-2 cells by using 10-*N*-nonyl-acridine orange (NAO) indicator. TRPM8 agonist WS12 (5 µM) causes enhanced levels of Cardiolipin (1.97 fold), which results in increased NAO intensity. On the other hand, AMTB (10 µM) did not exhibit any such changes in the Cardiolipin status of

the cells. (**Fig. 48A-B**). Taken together, our data suggest that TRPM8 modulation have no detrimental effect on the mitochondrial Cardiolipin levels in Saos-2 cells

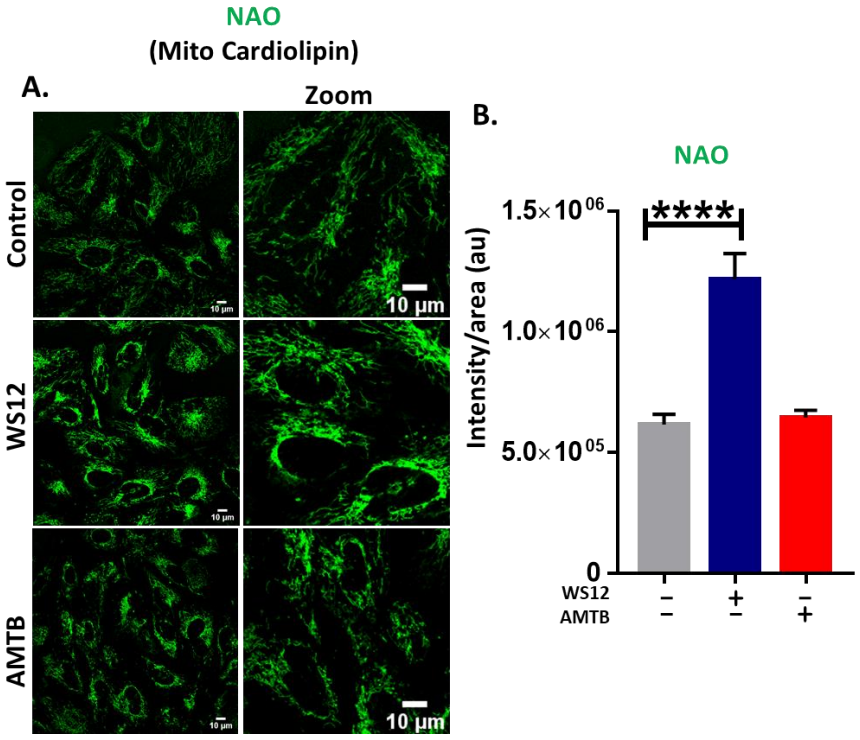


Fig. 48. TRPM8 modulation affects mitochondrial membrane potential and metabolism. A-B. Saos-2 cells were labelled with NAO dye (for mitochondrial Cardiolipin levels). Confocal images were acquired (represented in pseudo color) and analyzed for WS12 and AMTB effect. WS12 application increases mitochondrial Cardiolipin levels. n>50 cells in each case. Students t-test, **** = p≤ 0.0001, ns = non significant. (Un-published figure).

2.3.16 TRPM8 regulates mitochondrial and ER temperature:

Mitochondrial temperature is an outcome of the oxidative phosphorylation of cells. Recently, it was reported that mitochondria are maintained at 50 °C for their proper functioning. Keeping this in mind, we tested whether TRPM8 modulation results in changes in mitochondrial temperature. We used mitochondria-specific MTG dye (an increase in intensity corresponds to decrease in temperature) (**Fig. 49A, C)**. The addition of WS12 does not alter the mitochondria temperature; however, inhibition by AMTB shows a significant increase (~2.31 fold) in MTG

intensity, suggesting the decrease in the mitochondrial temperature of cells (**Fig. 49A, C**). This may suggest that spontaneous activation of endogenous TRPM8 keeps mitochondria in a warm state and prevents it from cooling.

In a similar manner, we determined the ER temperature using the ETY dye (an increase in intensity corresponds to a decrease in ER temperature) (**Fig. 49B, D**). Interestingly, WS12 addition shows a decrease (~0.68 fold) in ETY intensity corresponding to an increase in ER temperature (**Fig. 49B, D**). Inhibition by AMTB shows no significant change (~1.13 fold) in the ER temperature (**Fig. 49B, D**). Overall, the data suggest that modulation of cold-sensitive ion channel TRPM8 regulates the temperature of ER as well of mitochondria.

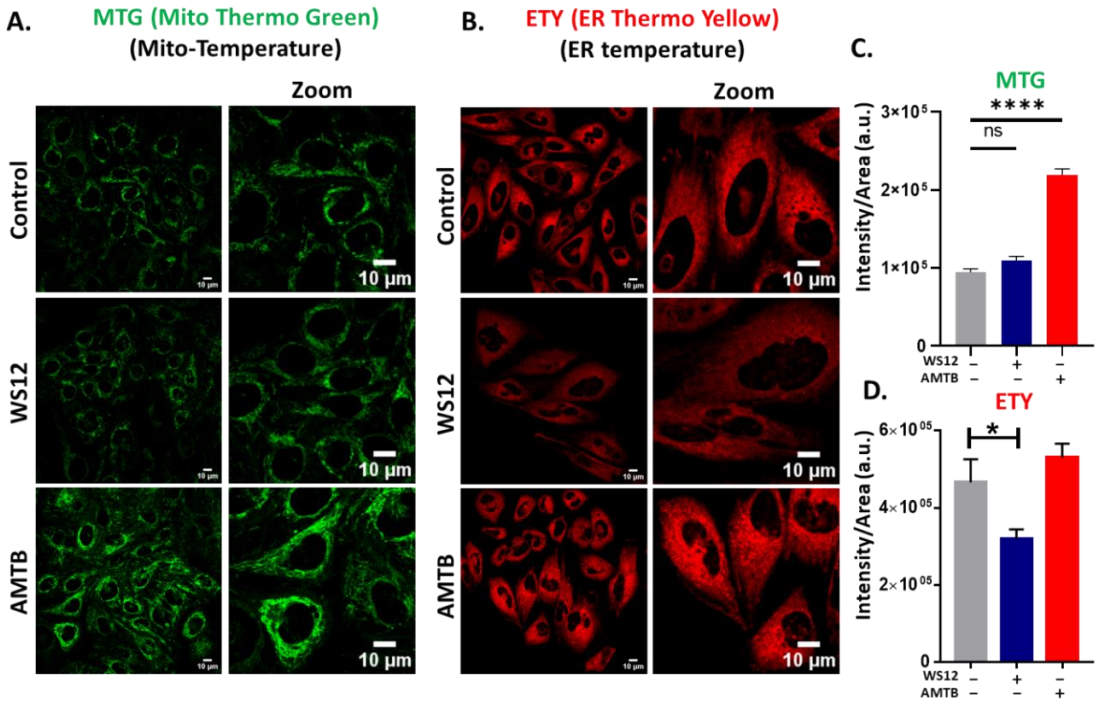


Fig. 49. TRPM8 activation by WS12 raises ER temperature but not for the mitochondrial temperature. A-B. Shown are the confocal images of Saos-2 cells loaded with ER temperature sensitive dye (ETY) and mitochondrial temperature sensitive dye (MTG). MTG fluorescence was measured in cells under control, TRPM8 agonist, and antagonist conditions. (A). **B.** The ETY fluorescence was measured in cells under control, WS12 and AMTB treated conditions were recorded. **C-D.** Quantification of MTG and ETY intensity from more than 50 cells were plotted. Treatment of AMTB increases the MTG fluorescence intensity (i.e. decreases in mitochondrial temperature) (C). The ETY intensity decreases in WS12-treated conditions (increase in ER temperature) (D). One-way ANOVA. **** = $p \leq 0.0001$, ns = non significant. (Un-published figure).

2.3.17 TRPM8 activation decreases ER-mito contact points:

Mitochondria mostly makes a closer contact with the ER for various metabolic functions, such as import of Ca^{2+}, steroids and other metabolites. For cellular Ca^{2+}-buffering ER-mito contact points play a significant role. Therefore, we compared and quantified the ER-mito contact points. For that purpose, we modulated the cells with TRPM8 agonist and antagonist for a longer period of 6 hours. To overcome the technical difficulties to study the ER-mito contact points (The dynamics of live cells, complex shape and regulation), we used a recently developed approach where cells were treated with 5% hypotonic media for 5 minutes only. The ER and mitochondria produce large intracellular vesicles (LICV) because of swelling, yet the tethering points remain intact in this condition. This method is a well-established method and has been successfully used (Jaiswal A, 2019; King C, 2020). The total colocalized points were quantified by particle based quantification as described before (Chidawanyika T, 2021). Representative images from different experimental conditions were given in **Fig. 50A-I**. From this experiment, we observed that the cells treated with WS12 have less ER-mito contact points and in the AMTB-treated cells, the ER-mito contact sites remain unchanged (**Fig. 51A**). This data broadly suggests that an increase in the mitochondrial Ca^{2+} decreases the propensity of mitochondria to make a close contact with ER. We further checked the impact of cellular Ca^{2+} and ER Ca^{2+}-store on ER-mito contact sites. We treated the cells with BAPTA-AM (5 µM) and Thapsigargin (1 µM) for 1 hour along with WS12 (5 µM) and AMTB (10 µM) for 6 hours. After detailed quantification, we observed that BAPTA-AM treatment does not impact on the ER-mito contact sites (**Fig. 51B**). Similarly, in the Thapsigargin treatment condition, there is a significant reduction of colocalized points (**Fig. 51C**). We compared the ER-mito contact points among all these groups and considered the control condition as 100%.

We observed that there is an increment in the contact points in BAPTA-AM treated condition when compared to control and only WS12-/AMTB-treated condition (**Fig. 51D)**

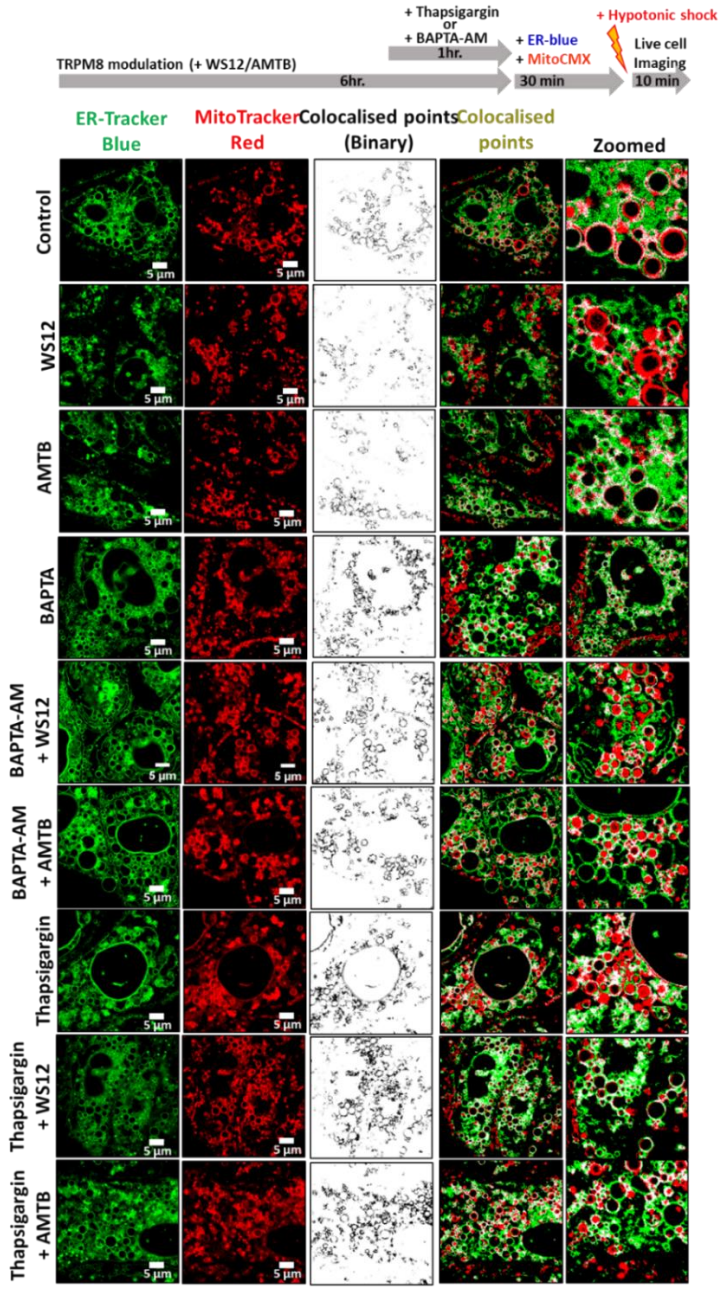


Fig. 50. Modulation of TRPM8 regulates ER-mito contact points. Saos-2 cells were incubated with WS12 (6 hours), AMTB (6 hours), BAPTA-AM (1 hour) and Thapsigargin (1 hour) and post-incubation cells were stained with ER-Tracker Blue and Mito Tracker red CMXRos for 30 minutes, and subsequently incubated with 5% hypotonic stimulus to allow the cells to produce large cellular vesicles of ER and mitochondria. Representative images show ER (pseudo color green for ER for better visualisation) and Mitochondrial labelling (Red). The colocalized points are represented as white. The portion of colocalized points is digitally zoomed. The scale bar is 5µm. (Un-published figure).

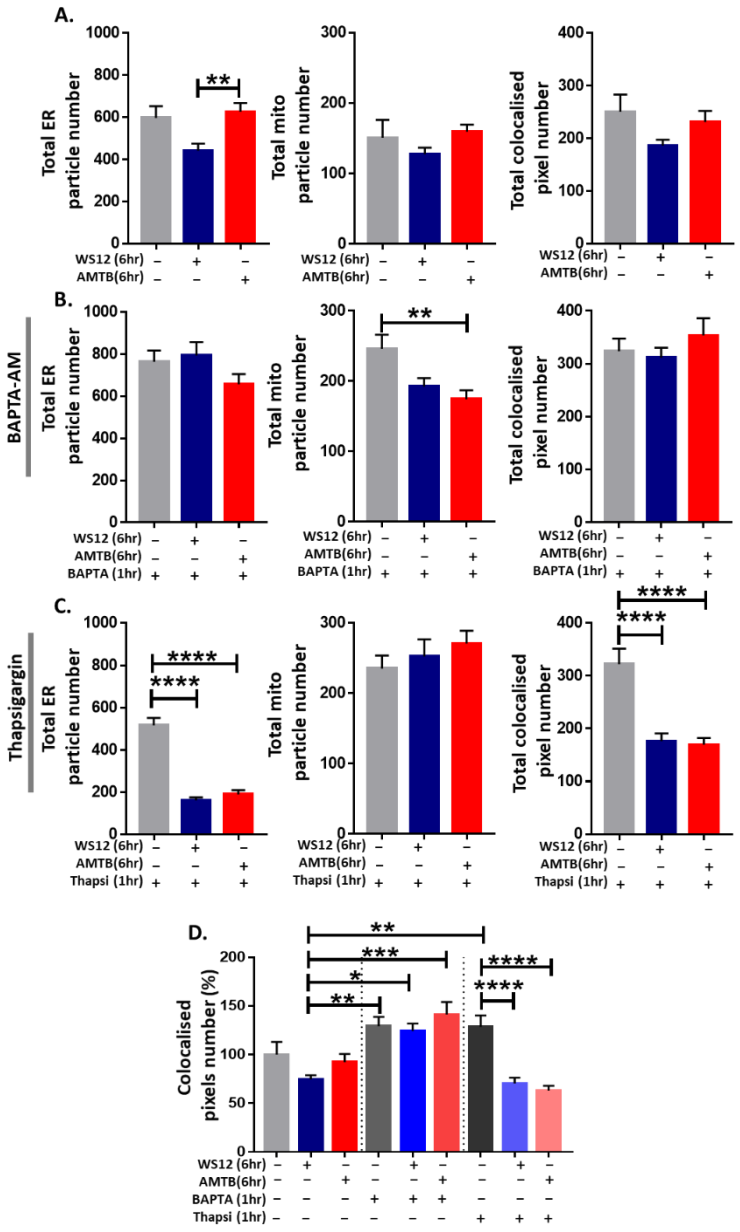


Fig. 51. TRPM8 regulates ER-mito contact points. **A-C**. Quantitative representations of the total ER particles and total mitochondrion particles in different conditions are shown. This analysis inferred that insignificant change happened in ER particle number in most cases but the ER number reduced significantly in Thapsigargin-treated cells. In the case of mitochondrial number in BAPTA-AM-mediated cytosolic Ca^{+2}-chelated conditions, the particle number of mitochondria decreases significantly. **D**. Graph represents the percentage of colocalized pixels in different treatment conditions. The percentage change was quantified, considering control as 100%. There is overall significant increase in the colocalized pixels when cells were treated for cytosolic Ca^{2+}-chelation (by BAPTA-AM) and ER Ca^{2+}-depletion (by Thapsigargin). However, the colocalized pixels decrease when the Thpasi + WS12 and Thapsi + AMTB treated condition. Particle quantification was done from a minimum of 40 cells in each group. One-way ANOVA was performed by Graph-pad, and all the groups were compared with the control group*p<0.05, ** = p<0.01, *** = p<0.001 **** = p<0.0001, ns = non-significant. (Un-published figure).

. However, in the Thapsigargin-treated cells, the contact points reduced in TRPM8-modulated conditions when compared to the control condition. In summary, our results suggest that TRPM8 regulates the extent of ER-mito contact points and both cytosolic as well as ER Ca^{2+} (and possibly also the mito Ca^{2+} due to TRPM8 modulation) are involved in this process.

2.3.18 TRPM8 regulates basal mitochondrial Ca^{2+} and membrane potential in MSCs:

We further validated some of the major findings in primary Mesenchymal stem cells derived from mouse bone marrow. We treated the MSCs with WS12 and AMTB and evaluated the levels of mitochondria Ca^{2+} using Rhod-2-AM (**Fig. 52A-B**). Interestingly, here we observed that long-term activation of TRPM8 results in a significant reduction (~0.31 fold less) in mitochondrial Ca^{2+}-levels, but AMTB-treated cells showed a similar (~0.96 fold) mitochondrial Ca^{2+} as compared to the control group (**Fig. 52A-B**).

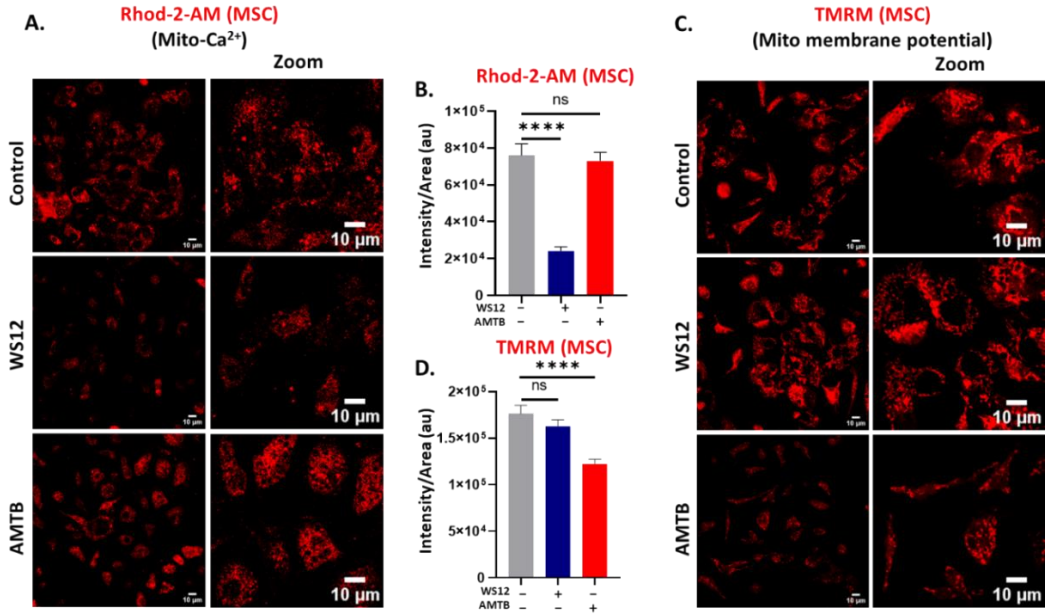


Fig. 52. TRPM8 regulates mitochondrial Ca^{2+} and membrane potential in MSCs. A-B. MSCs were treated with WS12 (5 µM) and AMTB (10 µM) for 6 hours and labelled with Rhod-2-AM for detection of mitochondrial Ca^{2+}-level. WS12 application decreases mitochondrial Ca^{2+}-level and chronic AMTB treatment increases Ca^{2+}-level. n>50 cells in each case One-way ANOVA, **** = p≤ 0.0001. **C-D.** MSCs were labelled with TMRM dye for analyzing the mitochondrial membrane potential. WS12 and AMTB application reduces the mitochondrial membrane potential. n>50 cells. **** = p≤ 0.0001, ns = non-significant. (Un-published figure).

Furthermore, we checked the changes in mitochondrial membrane potential upon modulation of TRPM8 in primary MSCs using TMRM (**Fig. 52C-D**). We observed that inhibition of TRPM8 decreases (~0.69 fold) mitochondrial membrane potential, and in activation, it remains unchanged (~0.92 fold) (**Fig. 52C-D**). Overall, the results suggest that TRPM8 affects mitochondrial Ca^{2+} and membrane potential in primary MSCs. This result is in contrast to the result we obtained in Saos-2 cells, where activation leads to a decrease in membrane potential. This data inferred that TRPM8 regulates mitochondrial membrane potential in cell-specific manner.

2.3.19 TRPM8 modulation decreases mitochondrial Cardiolipin status in MSCs:

We further checked the change in Cardiolipin status in mouse bone marrow derived Mesenchymal stem cells (MSCs) by using 10-*N*-nonyl-acridine orange (NAO). In this experiment, we observed that both the treatment of TRPM8 agonist WS12 (5 µM) and antagonist AMTB (10 µM) decreases mitochondrial Cardiolipin (~0.60 and ~0.39 fold less, respectively). (**Fig. 53A-B**).

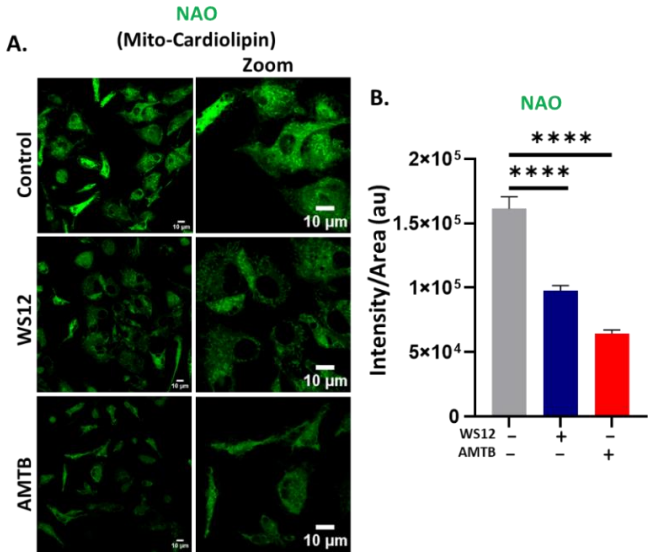


Fig. 53. TRPM8 modulation decreases mitochondrial Cardiolipin level in MSCs. A. MSCs were labelled with NAO dye (for mitochondrial Cardiolipin levels). Shown are the representative confocal images (represented in pseudo color) and analyzed for WS12 and AMTB effect. **B.** Both WS12 and AMTB application decreases mitochondrial Cardiolipin levels. n>50 cells in each case Students t-test, **** = p≤ 0.0001. (Un-published figure).

This data differs from Saos-2 cells, where both agonist and antagonist don't have detrimental effect on Cardiolipin level, whereas in MSCs, we found contrasting results. This may suggest that TRPM8 modulation effects the Cardiolipin status differentially in different cellular systems, especially in immortal cell lines and in primary cells.

2.3.20 TRPM8 regulates mitochondrial temperature in MSCs:

We also checked the effect of TRPM8 modulation on mitochondrial temperature status in primary MSCs using MTG dye (**Fig. 54A-B**). We found that in WS12-treated cells, the MTG intensity decreases non-significantly (~0.62 fold), suggesting a slight increase in mitochondrial temperature (**Fig. 54A-B**). However, the mitochondrial temperature decreases significantly with the presence of AMTB (~1.69 fold) increase in MTG intensity) (**Fig. 54 A, B**).

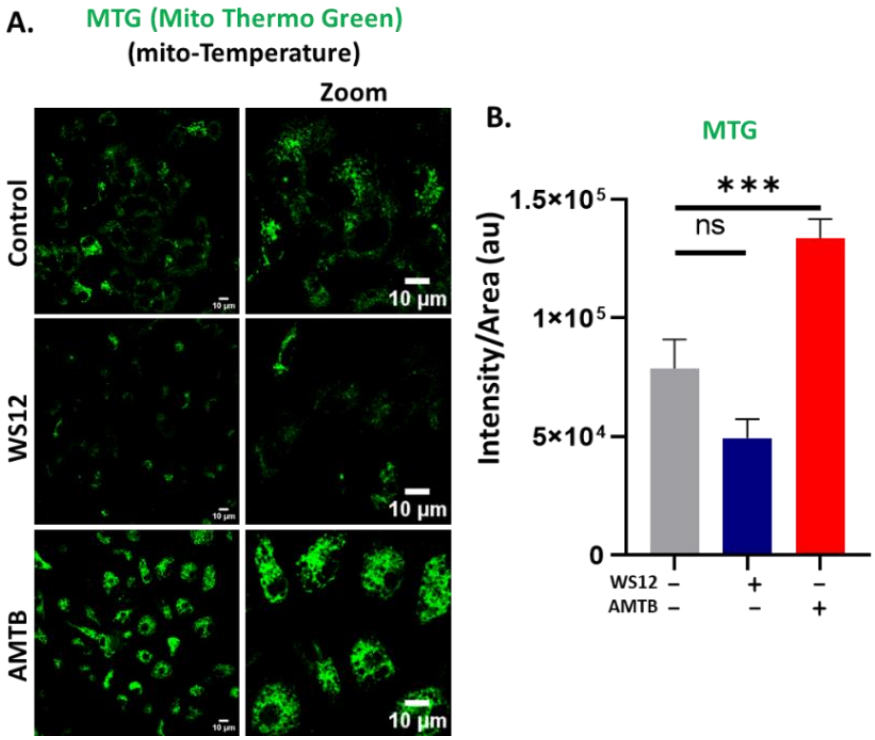


Fig. 54. TRPM8 inhibition decreases mitochondrial temperature in MSCs. A. Shown are the representative confocal images of Saos-2 cells loaded with mitochondrial temperature sensitive dye (MTG) and treated with TRPM8 modulators. **B.** Treatment of AMTB increase in MTG fluorescence intensity (i.e. decreases mitochondrial temperature). More than 50 cells were quantified in each condition. (Quantified graphs were shown right side of the image). One-way ANOVA. *** = $p \leq 0.001$, ns = non significant. (Un-published figure).

Our data suggests the regulation of mitochondrial temperature by TRPM8 in primary MSCs. Notably, this data accords well with our studies using Saos-2 cells, where AMTB lowers the temperature of the mitochondria.

2.3.21 TRPM8 regulates mitochondrial Ca^{2+} and temperature in isolated mitochondria:

We tried to extrapolate the finding of mitochondrial Ca^{2+} using Rhod-3-AM (**Fig 45A**). In the case of mitochondrial Ca^{2+}, cold shock (4 °C) increases the Rhod-3-AM intensity significantly, suggesting a rise Ca^{2+}-levels (**Fig. 55B**). Surprisingly, modulation of TRPM8 by WS12 and AMTB also increases the Ca^{2+}-level of the mitochondria (**Fig. 55B**). Antimycin is used as a control which decreases the mitochondrial Ca^{2+}-level (**Fig. 55B**).

We also tested the dependence of mitochondrial temperature on TRPM8 in isolated mitochondria (**Fig. 55C**) using MTY dye. Cold shock (4 °C) to isolated mitochondria results in a decrease in MTY intensity (increase in mitochondria temperature) (**Fig. 55D**). Also, WS12 addition reduces the MTY intensity, which then increases in the AMTB-treated cells (**Fig. 55D**). Antimycin treatment reduces the MTY intensity significantly as compared to the control condition (**Fig. 55D**). In summary, our result suggest that TRPM8 modulation affects both Ca^{2+} and temperature of isolated mitochondria.

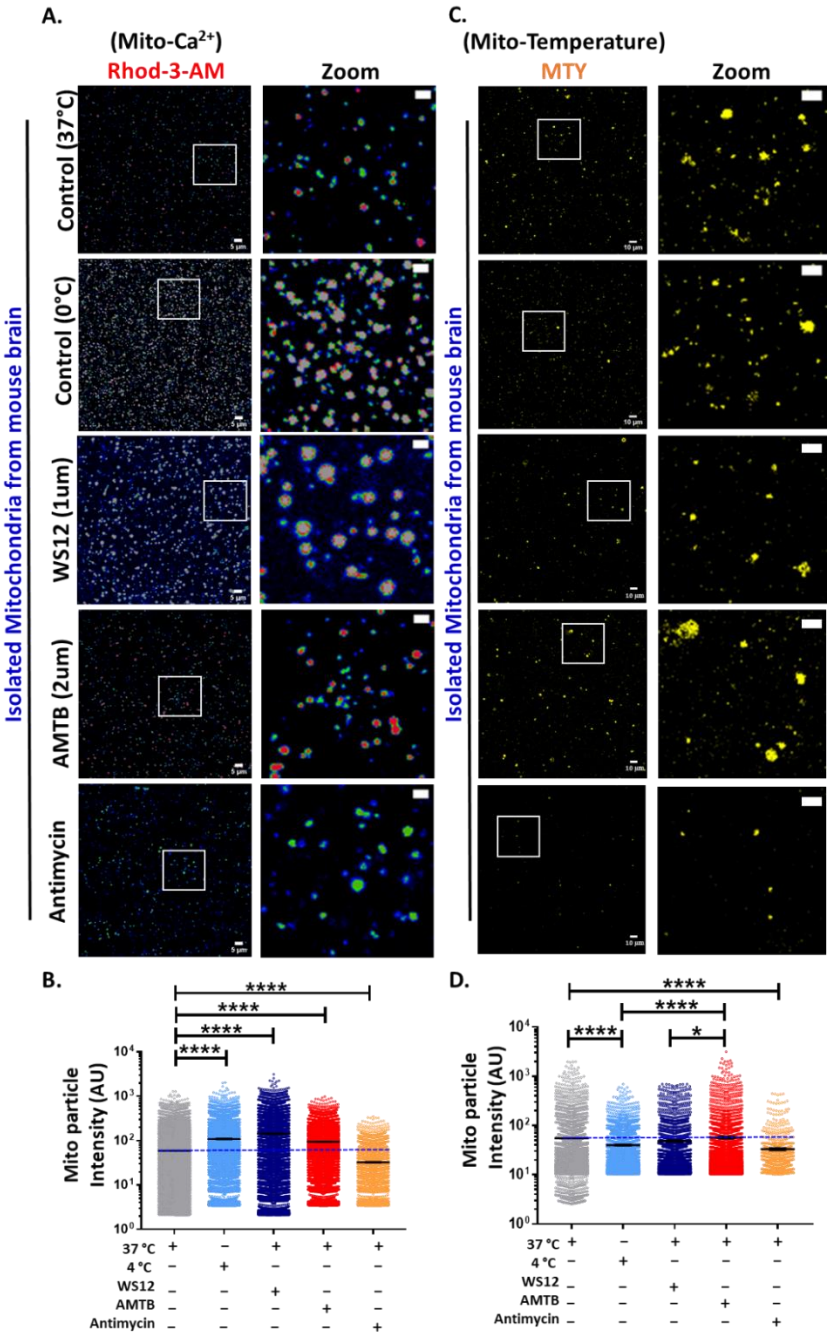


Fig. 55. TRPM8 modulation changes mitochondrial Ca^{2+} and temperature in purified mitochondria. A-B. In order to measure the level of mitochondrial Ca^{2+}-load, isolated mitochondria from mouse brain were subjected to a treatment with WS12 and AMTB for one hour, followed by Rhod-3-AM.WS12-treated cells have a higher Ca^{2+}-load. **C-D**. In a way analogous to this, the purified mitochondria were subjected to treatment with TRPM8 agonist and antagonist, which was then followed by labelling with MTY for the purpose of measuring the temperature of the mitochondria. When mitochondria are incubated at a cool temperature (4 °C) with WS12, the mitochondrial temperature rises (decrease in MTY intensity), but mitochondria that have been treated with AMTB have a higher MTY intensity (decrease in temperature). One way ANOVA. **** = $p \leq 0.0001$, ns = non significant. (Un-published figure).

Summary: Here we demonstrate that Transient Receptor Potential Melastatin member 8 (TRPM8), a cold-sensitive and Ca^{2+}-permeable ion channel is present in a subset of mitochondria of cells from different origins. We demonstrated that Menthol a non specific activator of TRPM8 causes increased mitochondrial Ca^{2+} in a complex manner, which is mainly contributed by intracellular sources including ER. Menthol also changes Ca^{2+}-load of individual mitochondrial particles in different conditions. Menthol increases ER-mito contact points, causes mitochondrial morphological changes, and increases mitochondrial ATP, Cardiolipin, mitochondrial ROS and reduces mitochondrial membrane potential ($\Delta\Psi m$). In addition, Menthol lowers mitochondrial temperature within cell and also serves as a cooling agent for the isolated mitochondria in a cell free system too. Notably, Menthol-induced reduction of mitochondrial temperature is observed in diverse types of cells. Instant as well as long-term modulation of TRPM8 by specific agonist and antagonist of TRPM8, WS12 and AMTB respectively causes influx of Ca^{2+} to the mitochondria of Saos-2 cells and also in isolated mitochondria, i.e. in cell-free system. Accordingly, TRPM8 modulation by WS12 and AMTB affects mitochondrial membrane potential, ROS, ATP levels, mitochondrial morphology as well as ER-mito contact points. TRPM8 modulation also alters temperature of mitochondria and ER. We suggest that TRPM8 plays an important role in determining the thermal gradient between ER and mitochondria affecting flow of Ca^{2+} and other metabolites from these subcellular organelles. Thus, the presence of TRPM8 in mitochondria seem to provide an "additive benefit" to cells. Such findings may have broader implications in understanding of cellular functions, regulation relevant for different diseases

2.4 TRPV4 mediated mitochondrial regulation: impact on bone cell functions and application in bone tissue engineering:

TRPV4 mutations cause skeletal dysplasia and various bone-related disorder (Das R, 2022). In our previous result, we discussed that the expression of various TRPV4 mutants in bone cell induce mitochondrial abnormality and alteration in mitochondrial morphology and physiology. However, the suitable treatment for these genetic skeletal diseases is largely unknown. These results further intrigued us to use a translational approach where we can modify the bone function by using TRPV4 channel activators and inhibitors. All therapies available currently comes with complicated risks such as graft rejection, infection, reoperation, availability of limited bone grafts, etc. However, in the case of growth factor (hormones, cytokines, large proteins etc.)-related therapies, their short half-lives, degradation by biological agents, burst release, limited osteogenic inducing potential, and their high cost hinders their application as a bone regeneration agent. In recent decades, biomaterial-associated therapies have been widely explored in tissue engineering to enhance the regeneration of hard tissues. In the majority of bone-related ailments, ECM (Extracellular matrix), which regulates many cellular functions, is either lost or damaged (Wei Y, 2020). Among the biomaterial constituent component, natural polysaccharide-based biomaterial has given more hope due to their excellent biocompatibility, ECM mimicking and structural manipulation ability, as well as significant benefits in the delivery of bioactive molecules and stem cell fate modulation (Dang M, 2018). Some efforts have been made to design a biomimetic scaffold using natural polymers for providing ECM-like microenvironments or as a biological cue delivering agents at defect sites for accelerated regeneration. However, these strategies have failed in providing satisfactory results. Furthermore, these strategies have been greatly hampered by complications such as tumor formation, non-union bone formation and poor

osteointegration (Willie BM, 2010). In this study, we aim to develop TRPV4 modulators containing a biomimetic hydrogel delivery system, which not only provides native ECM like microenvironment, it also regulates the TRPV4 or TRPM8 activity at the defect site for better osteoinduction and mineralization in a safe manner. Previously we have reported that CMT: HEMA based hydrogel is highly porous in nature and supports the adhesion of osteogenic cells and skin cells (Sanyasi S, 2014). CMT: HEMA hydrogel efficiently delivers TRPM8 and TRPV1 modulators in *in vitro* system and regulates the differentiation of osteoblasts and osteoclasts (Chakraborty R, 2022; Acharya TK, 2018). CMT: HEMA has an uneven rough surfaces in dry conditions and with bigger pores in wet conditions. Such morphology is ideal for the growth and adhesion of cells with osteogenic properties. This hydrogel doesn't have any adverse effects when applied on the skin of live rats, indicating its suitability for *in-vivo* applications (Choudhury P, 2018). In this work, we have encapsulated TRPV4 or TRPM8 modulators in CMT hydrogel and explored the role of TRPV4 and TRPM8 in bone homeostasis and metabolic states in *in vitro* and *in vivo* system.

2.4.1 Hydrogel containing TRPV4 modulating drugs regulates the expression and functionality of TRPV4 channel in MSCs:

We have investigated the expression of TRPV4 in MSCs cultured on glass surface and on TRPV4 modulating drug containing hydrogel (CMT). In all these cases, a consistence positive expression of TRPV4 was observed in mouse bone marrow derived Mesenchymal stem cells, as analyzed by immunofluorescence. When MSCs were exposed towards hydrogel containing different doses of TRPV4 specific agonist (4αPDD at 10 nM and 50 nM), the intensity of TRPV4 expression got increased in the case of 4αPDD at 10 nm exposure, as compared to a higher dose (50 nM) or in comparison to glass and only hydrogel surface. While MSCs show low expression

of TRPV4 upon exposure towards hydrogel containing antagonist (i.e. RN1734 50 nM and 100 nM).

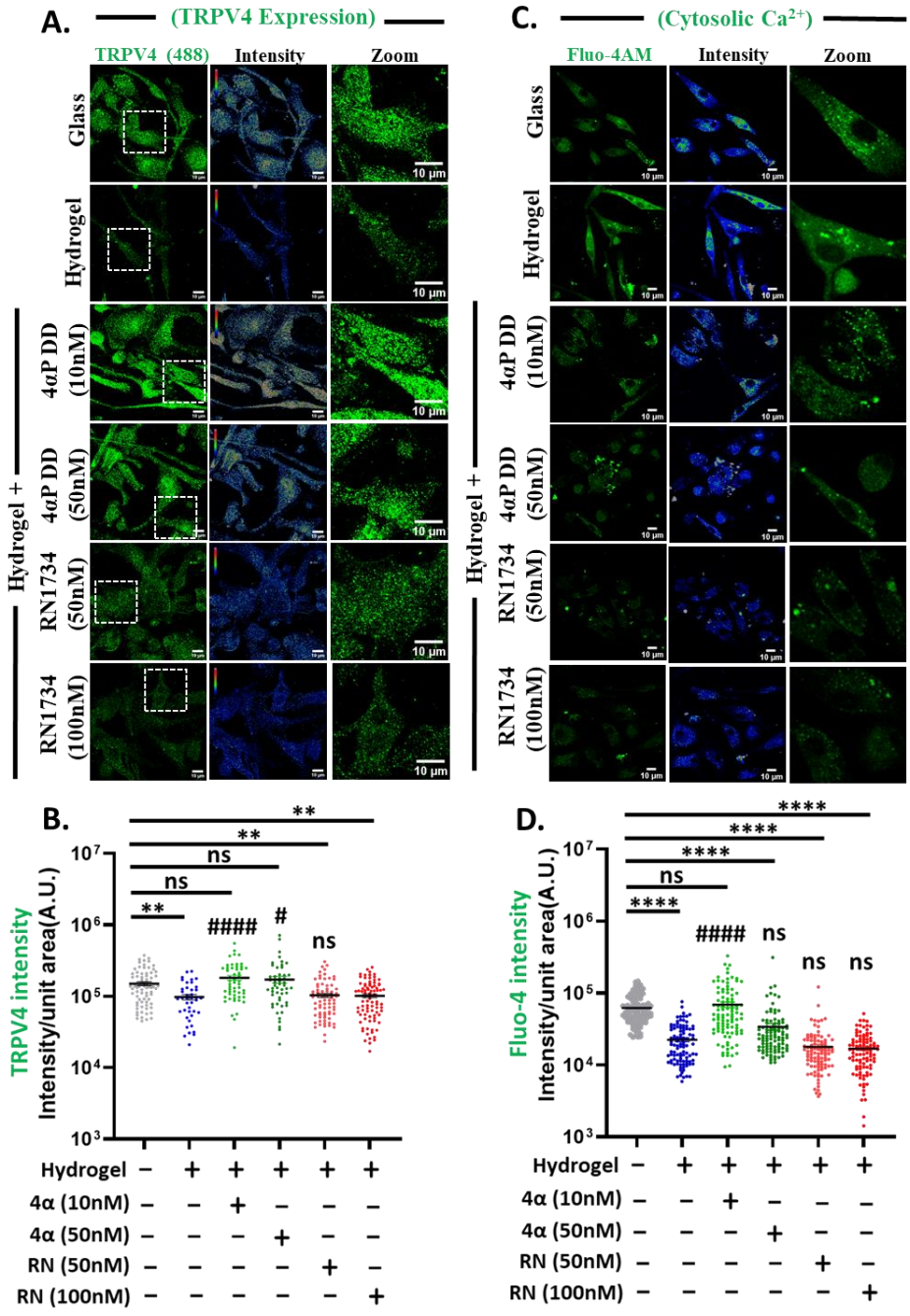


Fig. 56. Hydrogel-mediated drug release altersTRPV4 expression and basal Ca^{2+}-load of bone marrow derived Mesenchymal stem cell population. BM-MSCs were isolated and grown on only glass, only hydrogel or on hydrogel-coated with different drugs affecting the TRPV4 ion channel. **A-B**. Fluorescence intensity of TRPV4 expression is quantified. 4αPDD-treated cells have a higher level of TRPV4 expression. **C-D.** BM-MSCs were grown over the hydrogel encapsulated with various TRPV4

modulators. Basal Ca^{2+}-load was measured by Fluo-4-AM. In general, 4αPDD-treated cells have higher Ca^{2+}-load as compared to control and RN1734-treated condition. The statistical values are: ANOVA test, p values: ns = non-significant, * = <0.05, ** = < 0.01, *** = <0.001, **** = <0.0001. # symbol indicates the comparison of the group with hydrogel only condition. (ANOVA, $^{\#}$ = < 0.05, $^{\#\#\#\#}$ = <0.0001, ns = non significant). (Un-published figure).

These data suggest that the expression of TRPV4 seems to be dependent on the concentration of agonist and antagonist dose (**Fig. 56A-B)**. Next, we analyzed the functionality of TRPV4 by measuring the basal Ca^{2+}-level in MSCs grown on hydrogel containing different doses of agonist and antagonists (**Fig. 56C-D)**. Activation of TRPV4 by a lower dose of 4αPDD induces elevated intracellular Ca^{2+} in MSCs as compared to glass surface and hydrogel surface alone. Inhibition of TRPV4 by antagonist containing hydrogel results in decreased level of intracellular Ca^{2+}. These data clearly indicate that a functional TRPV4 ion channel is present in MSCs, and hydrogel infused with TRPV4-specific drugs effectively modulates the function of channel activity.

2.4.2 Hydrogel containing TRPV4 modulator drug affects morphology and physiology of MSCs:

The morphology of cells on hydrogel surface significantly alters the cellular activity and it determines the fate of differentiations of MSCs. So organization of cytoskeleton filaments of MSCs grown on glass surface, only on hydrogel surface and hydrogel containing different doses of TRPV4-specific agonists and antagonists were investigated. For this, MSCs were cultured on different surfaces for 24 hours, fixed and were stained with rhodamine phalloidin (For actin filament) and DAPI (for Nuclei). MSCs grown on glass, only hydrogel and hydrogel containing TRPV4 agonist (4αPDD 10 nM & 50 nM) surfaces, shows well organized F-actin filaments, while MSCs attached on TRPV4 antagonist hydrogel surfaces contain diminished actin filaments, more significantly in the case of higher dose of TRPV4 antagonist condition (RN1734 100 nM) (**Fig. 57A)**. The intensity of actin filaments was quantified from immunofluorescence images of MSCs

by Image J software. From **Fig. 57B,** it is evident that intensity of F-actin in the case of hydrogel containing 10 nM and 50 nM of 4αPDD was significantly high as compared to glass and hydrogel only surface.

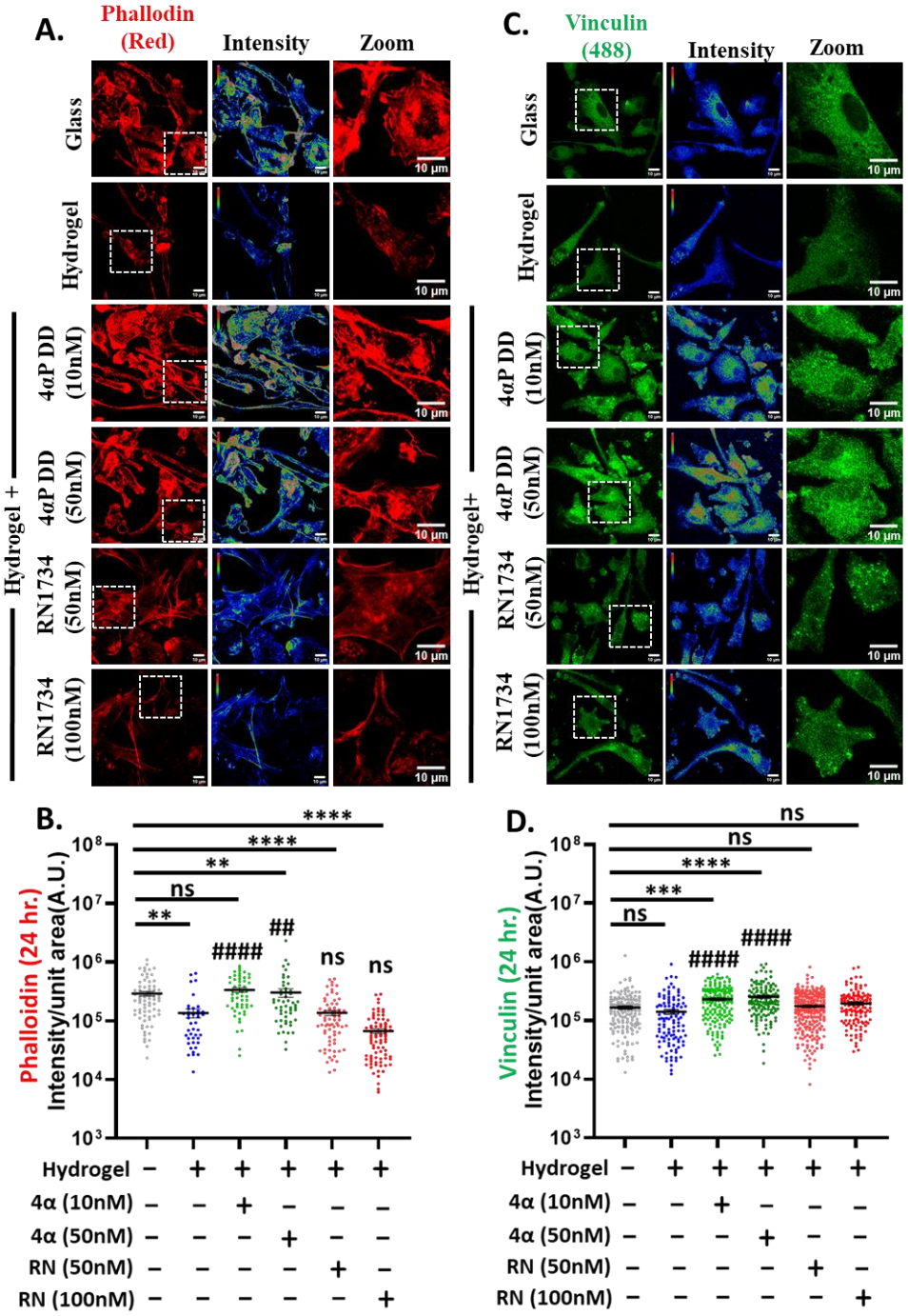


Fig. 57. Hydrogel-mediated drug release alters the morphology of bone marrow-derived Mesenchymal stem cell population. BM-MSCs were isolated and grown on only glass, only hydrogel or

on hydrogel-coated with different drugs affecting TRPV4 ion channel. **A-B**. Morphology of cells grown on different surfaces are shown. Cells were stained with Phalloidin (green) and DAPI (blue). **C-D**. BM-MSCs were immunolabelled with Vinculin as a marker of focal adhesion point. The changes in the intensity of vinculin was measured and plotted. The statistical values are ANOVA test, p values: * = <0.05, ** = < 0.01, *** = <0.001, **** = <0.0001. # symbol indicates the comparison of the group with hydrogel only condition. (ANOVA, $^{\#\#}$ = < 0.01, $^{\#\#\#\#}$ = <0.0001, ns = non significant). (Un-published figure).

Further inhibition of TRPV4 channel activity by RN1734 results in disorganization and lesser formation of F-actin filaments in MSCs. Adhesion of cells on any substrates is regulated by integrins and FACs (focal adhesion complexes), which play a significant role in the integrity & functioning of cells. Vinculin is a key component of FACs which conciliates many essential cellular functions. It has been reported that formation of FACs is dependent on Ca^{2+}-signaling. TRPV4 is mechanosensitive ion channel which plays a critical role in Ca^{2+}-signaling. Thus, effect of TRPV4 activation or inhibition on focal adhesion points was investigated by staining vinculin in MSCs grown on TRPV4 modulator containing hydrogel surfaces. From **Fig. 57 C-D** it is observed that on only hydrogel surface, expression of vinculin in MSCs is less in comparison to glass surface. MSCs grown on hydrogel containing TRPV4 agonist 4αPDD at 10 & 50 nM dose express higher levels of vinculin, and it further increases with higher doses of drug. While in case of MSCs grown on TRPV4 antagonist containing hydrogel, intensity of vinculin is similar to glass surface but less than hydrogel with TRPV4 agonist. The elevated intensity of vinculin in the case of TRPV4 agonist condition may be due to functional activation of ion channel, which in turn regulates the mechanosensing & Ca^{2+}-signaling in MSCs.

2.4.3 Hydrogel containing TRPV4 modulatory drugs effectively regulate mitochondrial Reactive Oxygen Species (ROS), cytosolic NO and mitochondrial Cardiolipin status in MSCs:

When considering the objective of bone tissue regeneration, implanted biomaterials produce elevated levels of reactive oxygen species at the interface of tissue and implanted

biomaterial (Willie BM, 2010). Reports also suggest that activation of TRPV4 by agonist results in enhanced ROS production (Lieben L, 2012). Elevated level of ROS leads to the inflammation, and ultimately in failure of implants. Mitochondria are the most important source of ROS within mammalian cells.

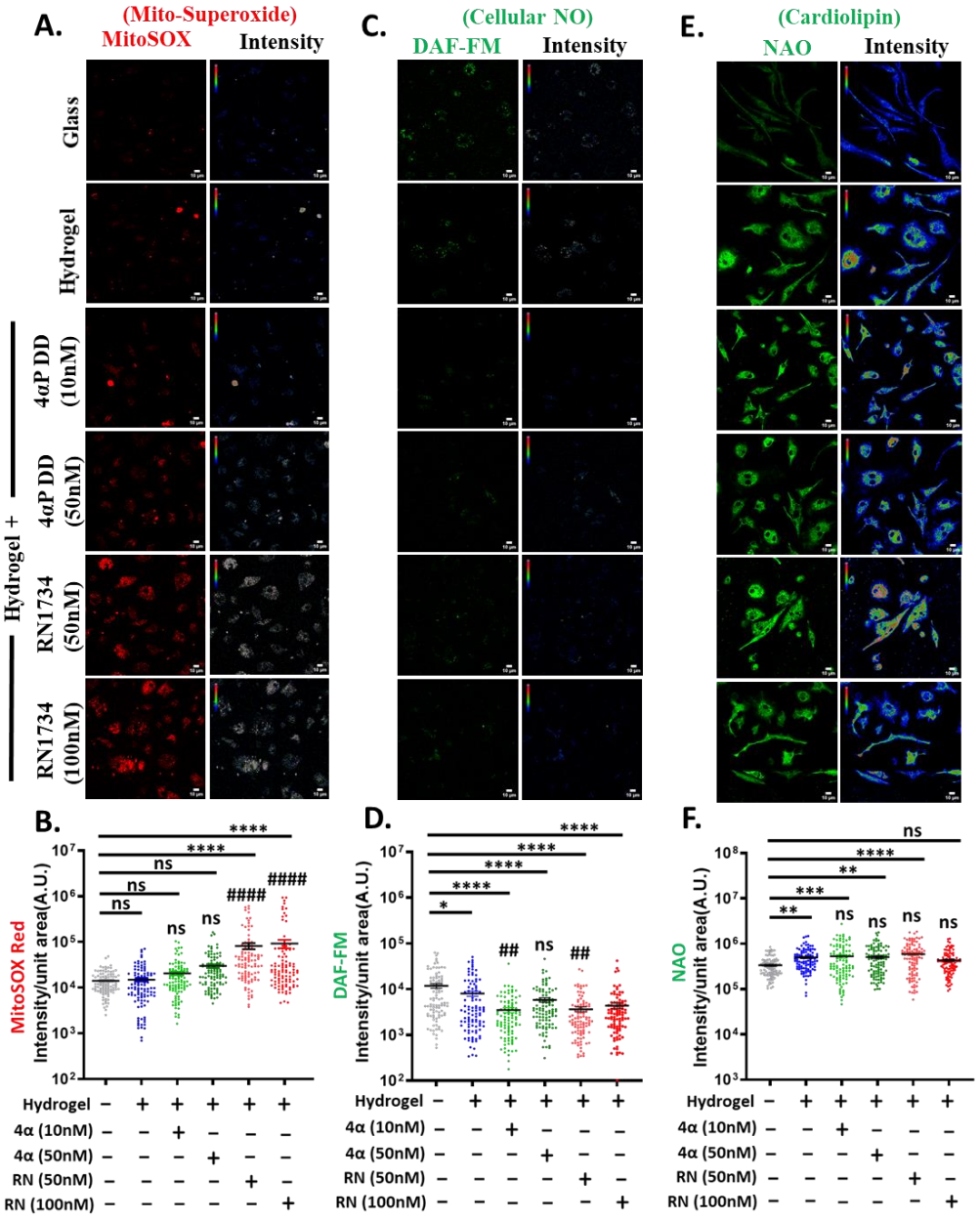


Fig. 58. Hydrogel-mediated drug release regulates cellular and mitochondrial physiologies of bone marrow derived Mesenchymal stem cell population. A-B. Mitochondrial ROS level was measured by using MitoSOX Red in different drug-treated conditions. **C-D**. Changes in the level of cellular NO level was measured by labelling the cells with DAF-FM dye. **E-F.** Quantification of mitochondrial Cardiolipin

level is represented. The mitochondrial Cardiolipin was stained with NAO dye. All these experiments were performed after 24 hours of cell growing on only glass, on hydrogel only, or on the hydrogel loaded with drugs. The statistical values are: ANOVA test, p values: * = <0.05, ** = < 0.01, *** = <0.001, **** = <0.0001. # symbol indicates the comparison of the group with hydrogel only condition. (ANOVA, #### = <0.0001, ns = non significant). (Un-published figure).

Therefore, first mitochondrial ROS levels were analyzed and compared among the MSCs cultured on TRPV4 modulatory drugs containing hydrogels, glass surface and on only hydrogel. For that Mitosox dye was used. As evident from **Fig. 58A-B**, after 24 hours, cells grown on TRPV4 agonist containing hydrogels and on only hydrogel exhibit comparable levels of mitochondrial ROS with respect to cells grown on glass surfaces only. MScs grown on TRPV4 antagonist containing hydrogel (i.e. RN1734 50 &100 nM) exhibit elevated levels of mitochondrial ROS (**Fig. 58A-B**). Apart from ROS, RNS (reactive nitrogen species) in combination with ROS are known to target mitochondrial function and thus affect bone-homeostasis. So, level of nitric oxide (NO) in MSCs grown on TRPV4 modulator containing hydrogels were analyzed and compared. Decreased level of RNS was observed in MSCs exposed towards TRPV4 agonist and antagonist as compared to glass surface and hydrogel only surface (**Fig. 58C-D**). Recent, studies have highlighted the critical role of mitochondrial biogenesis towards the fate of stem cell differentiation. Down regulation of glycolysis and upregulation is oxidative phosphorylation is required for compensating higher demand of energy, which is a characteristic of stem cell differentiation. Regulation of TRPV4 actively regulates mitochondrial homeostasis. So, next, we have investigated the mitochondrial health by analyzing the Cardiolipin level in MSCs seeded on TRPV4 modulators containing hydrogels by staining with 10-N-nonyl-acridine orange (NAO). No significant changes in signal intensity of NAO in MSCs have been observed in case of all these hydrogels (**Fig. 58E-F**)

2.4.4 Hydrogel encapsulated with TRPV4 drugs regulates cellular parameters during osteoblast differentiation:

Overload of Ca^{2+} also imparts elevated cellular ROS in cells, and activation and inhibition of TRPV4 by pharmacological agents results in elevated levels of Ca^{2+} in cells (Brookes PS, 2004; Vellino S, 2021). So, the Ca^{2+}-level in differentiated MSCs grown on hydrogels with a TRPV4 modulator was measured. After 24 hours, it's clear that MSCs grown on TRPV4 agonist-containing hydrogel in the presence of OB media have a much higher level of Ca^{2+} inside their cells than MSCs grown on a glass surface without OB media (Glass only) or with OB media (Positive control). Also, MSCs grown on hydrogel with a TRPV4 antagonist show a lower level of Ca^{2+} compared to all other conditions. (**Fig. 59A-B**). Next, we have analyzed the intracellular Ca^{2+} in osteogenic differentiated MSCs. i.e., after 15 days (**Fig. 59C-D**). The amount of Ca^{2+} inside the cells was comparable for the TRPV4 agonist, the positive control, and the hydrogel condition. While a TRPV4 antagonist exhibits a lower level of Ca^{2+} inside the cell. These observations suggest that TRPV4 modulators containing hydrogel effectively releases drug for longer period of time and effectively regulates the TRPV4 activity in MSCs as well as in mature osteoblasts. As in most of the implanted biomaterial, accumulation of ROS at the implanted site occurs with time. We have analyzed the level of cytosolic ROS in MSCs seeded on different surfaces with the help of H_2DCFA dye. In the TRPV4 agonist condition decreased level of cytosolic ROS was observed, in contrast to the TRPV4 antagonist and control conditions (**Fig. 59E-F**). While in the case of mature osteoblasts (i.e. after 15 days of incubation period), TRPV4 agonist (50 μM) exposed cells displayed a little bit of elevated level of cytosolic ROS as compared to the cells grown in the absence of osteogenic media (Glass only). Cells grown on TRPV4 antagonist containing hydrogels

also show elevated levels of cytosolic ROS (**Fig. 59G-H**). This may suggest that deviation from endogenous activity, both in terms of activation or inhibition, induces stress and cause more ROS.

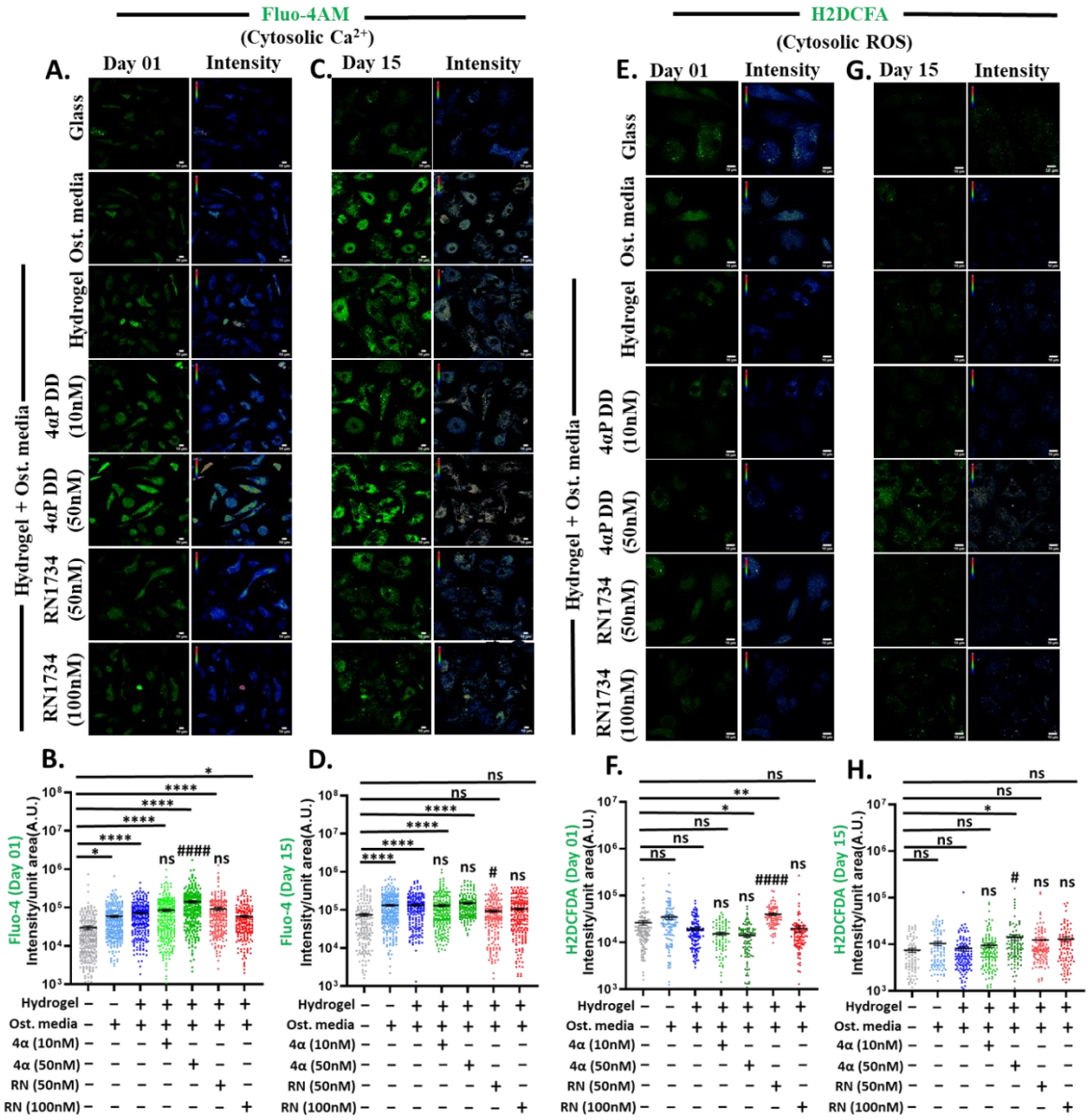


Fig. 59. Hydrogel-mediated drugs regulate cellular physiologies during osteoblast differentiation. BM-MSCs were isolated and grown on only glass, only hydrogel or on hydrogel-coated with different drugs affecting the TRPV4 ion channel. The cells were treated with osteoblast differentiation media for 1 day or 15 days. **A-B**. MSCs were treated with OB differentiation media for 1 day only, and basal Ca^{2+}-load was measured by Fluo-4-AM. **C-D**. Basal Ca^{2+}-load was measured at the 15th day of osteoblast differentiation. 4αPDD-treated cells have a higher cytosolic Ca^{2+}-load. **E-F.** MSCs were treated with OB differentiation media for 1 day and cytosolic ROS was measured by DCFDA. **G-H.** Cytosolic ROS was measured at the 15th day of osteoblast differentiation. There is no significant change in cytosolic ROS (except 4αPDD 10 μM) as observed during the process of bone differentiation. The statistical values are

One-way ANOVA test, p values: * = <0.05, ** = < 0.01, *** = <0.001, **** = <0.0001. # symbol indicates the comparison of the group with hydrogel only condition. (ANOVA, $^{\#}$ = < 0.05, $^{\#\#\#\#}$ = <0.0001, ns = non significant). (Un-published figure).

2.4.5 Hydrogel containing TRPV4 modulator drugs enhance metabolic state of MSCs during osteoblast differentiation:

MSCs seeded on TRPV4 agonist containing hydrogel exhibit lower cytosolic ROS. Thus, it was analyzed if this decreased level of cytosolic ROS generated due to TRPV4 activation, can effects the mitochondrial functions. For evaluating the mitochondrial membrane potential, Tetramethyl rhodamine methyl ester (TMRM) staining was performed. MSCs (after 24 hours) seeding on hydrogel only, or on TRPV4 agonist & antagonist containing hydrogels show higher fluorescence intensity as compared to positive control and control condition (**Fig. 60A-B**). Further, in mature osteoblasts (15 days in OB medium), there was no substantial inhibition of mitochondrial potential by TRPV4 activation in differentiated MSCs was observed. These observations indicate that TRPV4 modulators containing hydrogel elicit higher mitochondrial membrane potential as compared to glass surface (**Fig. 60C-D**).

In addition to higher mitochondrial membrane potential resulting from hydrogel and TRPV4 modulators containing hydrogel, ultimate bioenergetic effect of hydrogel and TRPV4 modulators containing hydrogel was analyzed. For this, ATP level was measured in MSCs grown of different surfaces for short term (24 hours) as well as for long term (15 days with OB media). In accordance with the mitochondrial potential results, the hydrogel only, TRPV4 agonist, and antagonist group showed considerably greater ATP levels after 24 hours (**Fig. 60E-F**). The ATP level of MSCs is elevated following prolonged exposure to a TRPV4 agonist (after 15 days in OB media). While ATP levels are lower in the TRPV4 antagonist group compared to the agonist group and higher compared to the control group. (**Fig. 60G-H**). Together, these metabolites levels

indicate that TRPV4 activity modulation through hydrogel mediated drug delivery elevates mitochondrial potential and generate elevated level of ATP.

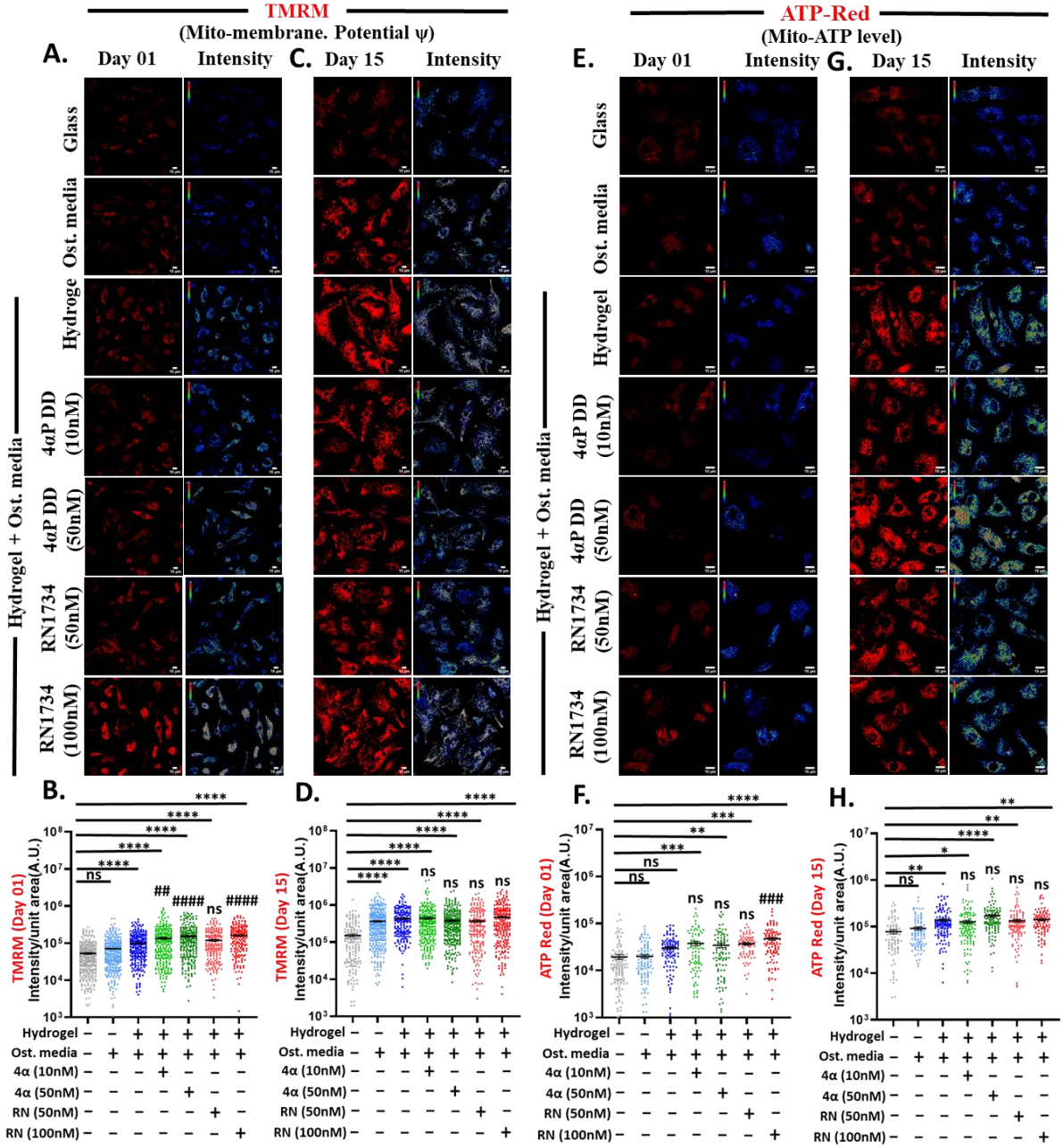


Fig. 60. Hydrogel-mediated released drugs regulate mitochondrial function during osteoblast differentiation. BM-MSCs were isolated and grown on only glass, only hydrogel or on hydrogel-coated with different drugs which affect TRPV4 ion channel. The cells were treated with osteoblast differentiation media for 1 day or 15 days. **A-B**. MSCs were treated with OB differentiation media for 1 day and mitochondrial membrane potential was measured by TMRM dye. **C-D**. Mitochondrial membrane potential was measured at the 15th day of osteoblast differentiation. During the differentiation, mitochondrial membrane potential increases irrespective of any treatment. **E-F.** MSCs were treated with OB

differentiation media for 1 day and mitochondrial ATP was measured by ATP red dye. **G-H.** Mitochondrial ATP was measured at the 15th day of osteoblast differentiation. Significant increase in mitochondrial ATP is observed during the process of bone differentiation. The statistical values are: One-way ANOVA test, p values: * = <0.05, ** = < 0.01, *** = <0.001, **** = <0.0001. # symbol indicates the comparison of the group with hydrogel only condition. (One way ANOVA, $^{\#\#}$ = < 0.01, $^{\#\#\#\#}$ = <0.0001, ns = non significant). (Un-published figure).

2.4.6 TRPV4 modulator containing hydrogel enhance *in vitro* osteogenesis in MSCs:

Regulation of TRPV4 activity by agonist and antagonist maintains mitochondrial health, function and enhances the ATP production in MSCs. Notably, increased extracellular ATP is required for an enhanced osteogenesis process and TRPV4 activation results in enhanced ATP generation. So, next *in vitro* osteogenesis was assessed by implying the ARS (Alizarin Red-S) staining method to investigate the role of TRPV4 activity in the presence of modulators containing hydrogel. MSCs exposed to agonist containing hydrogel show enhanced calcium nodules formation (Intense Red staining) than control (OB media only), as evident from ARS staining (**Fig. 61**). In the case of TRPV4 agonist RN1734 (50 nM), lesser formation of calcium nodules was observed as compared to control and activator groups.

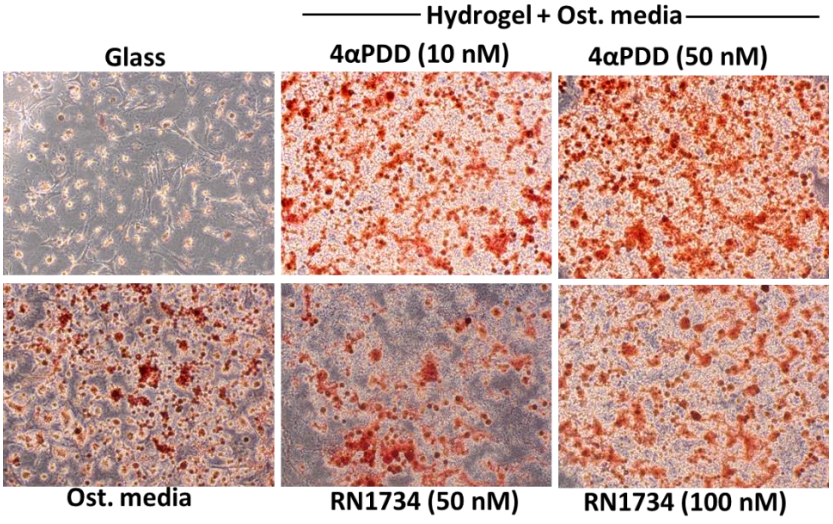


Fig. 61. Hydrogel (CMT: HEMA)-mediated release of TRPV4 agonist and antagonist modulates osteoblasts functions. Representative images represent mineralization nodules of Mesenchymal stem cells

(MSCs) grown for 15 days in the absence or presence of hydrogel (CMT: HEMA) as detected by Alizarin Red staining (n = 3). The extent of mineralization nodules formed when cells were grown on 4αPDD or RN1734 encapsulated CMT: HEMA hydrogel in two different doses are also shown. These images depict the higher mineralization nodules in 4αPDD treated cells with respect to control or RN1734-treated cells. (Un-published figure).

2.4.7 Effect of TRPV4 modulators containing hydrogel in *in-vivo* bone repair:

In vitro, findings show that activation of TRPV4 through the sustained release of agonist from hydrogel enhances the osteogenesis process by elevating intracellular Ca^{2+}-level and by regulating mitochondrial activity. However, hydrogel alone does not show such activity. So, to confirm the enhanced osteogenic efficacy of the TRPV4 modulator containing hydrogel *in vivo,* the "femur hole drill model" was utilized in rats. In this method, 8-week-old male Wistar rats were taken, and ~ 1.2 mm (in size) hole defect was created in the rat femur, which were treated with PBS (control), or TRPV4 modulators containing hydrogel (Hydrogel + 50 nM-4αPDD, Hydrogel + 100 nM RN1734). The surgical methods for the implantation of hydrogels are shown in **Fig. 62A**. Animals subjected to surgery followed by hydrogel implantation were survived throughout the study period, and no sign of any infections or noticeable toxic effects appeared at the implant site. Subsequently, the animal's movement, physiology and behavior were monitored, and no adverse effect was observed. After 8 weeks of implantation, all the animals were sacrificed and their femur were collected and *in vivo,* bone healing efficacy was evaluated by optical imaging, X-ray, histological studies. Optical images of isolated rat femur show enhanced hard tissue content in the case of 4αPDD-treated group as compared to the control and RN1734-treated group. No traces of hydrogel were observed in any group. In the case of PBS and RN1734-treatment group, created defect hole was still visible, while in the case of 4αPDD-treated group, the drilled defect was healed almost completely (**Fig. 62B**).

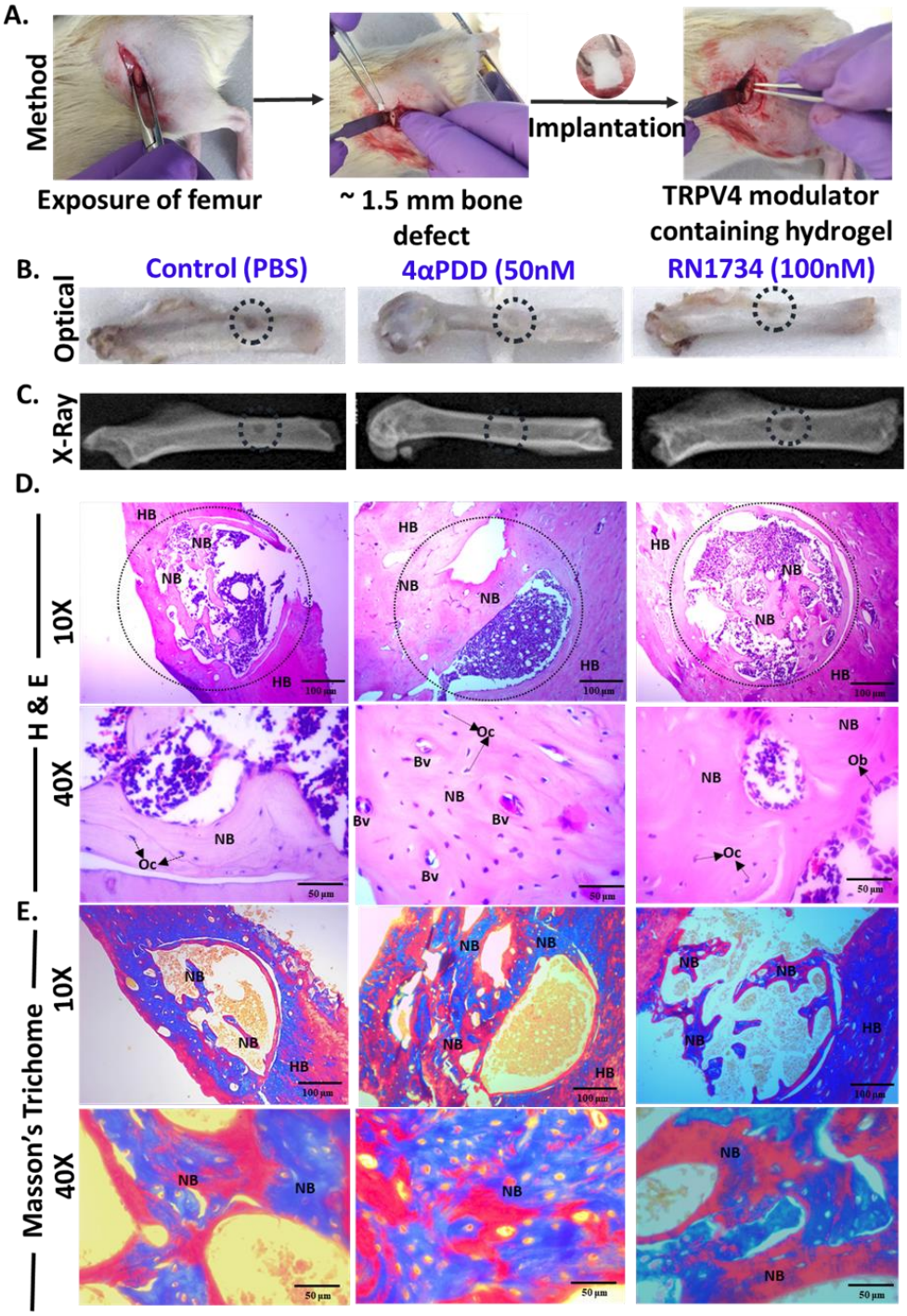


Fig. 62. Hydrogel (CMT: HEMA)-mediated release of TRPV4 agonist and antagonist modulates *in vivo* bone healing. A. The surgical method for the implantation of hydrogel is shown schematically. Animals subjected to surgery were followed by hydrogel implantation and surgical suture was performed. **B-C.** *In vivo* bone healing efficacy was evaluated by optical imaging and X-ray methods. **D-E.** Quality of newly formed bone was further histologically analyzed by H&E (haematoxylin & eosin) and Masson's trichome staining. Sustained release of TRPV4 agonist at defect site from hydrogel enhanced bone tissue regeneration, while TRPV4 inhibition at bone defect site results in delayed bone regeneration process. (Unpublished figure).

X-ray images of bone also show that area of the drilled defect was almost covered by new bone tissue in case of 4αPDD treated group followed by PBS and RN1734-treated group (**Fig. 62C**).

Subsequently, X-ray analysis of the wound bone was performed to assess the quality of newly formed bone and further histologically analysis by H&E (haematoxylin & eosin) and Masson's trichome staining was performed. H&E-stained images of bone revealed absence of necrosis and inflammatory response at the defect site in all the groups as well as almost degradation of hydrogel. 4αPDD-treated group revealed a pronounced amount of newly formed bone tissue, as well as recruitment of osteoblasts, osteocytes and new blood vessels formation at the defect site. While the PBS group shows an island of new bone tissue at the edges of the defect site and no formation of new blood vessels was observed. While in the case of the RN1734 group, a minimal amount of newly formed bone tissue island, mainly at the edges and a certain amount at the center of the defect site, was observed (**Fig. 62D**). Masson's Trichome staining images (**Fig. 62E**) shows 4αPDD-treated group contains significantly dense blue-red stained osteoid island as well as neo-vascularized structure, while PBS-treated group shows less dense blue and red stained osteoid mainly at the edges of the defect. The RN1734-treated group also showed less blue and red stained osteoid. These observations are well corroborated with H&E staining. These results indicate that sustained release of TRPV4 agonist at the defect site from hydrogel enhanced bone tissue regeneration, while TRPV4 inhibition at the bone defect site results in delayed bone regeneration process.

Next, the osteogenic efficacy of TRPV4 modulators containing hydrogel was explored by investigating the expression of TRPV4 in newly formed bone tissue. To understand this regenerative events at cellular and molecular levels, immunofluorescence staining was performed.

Bone tissue samples were decalcified, cut into thin sections, and immunohistochemically stained for the detection of TRPV4 expression and bone-specific markers (Runx-2, OCN & OPN) and SIRT3 (mitochondrial UPR marker). As shown in **Fig. 63A**, the fluorescence intensity of TRPV4 in the 4αPDD treatment group and in host bone is high as compared to PBS- and RN1734-treated group.

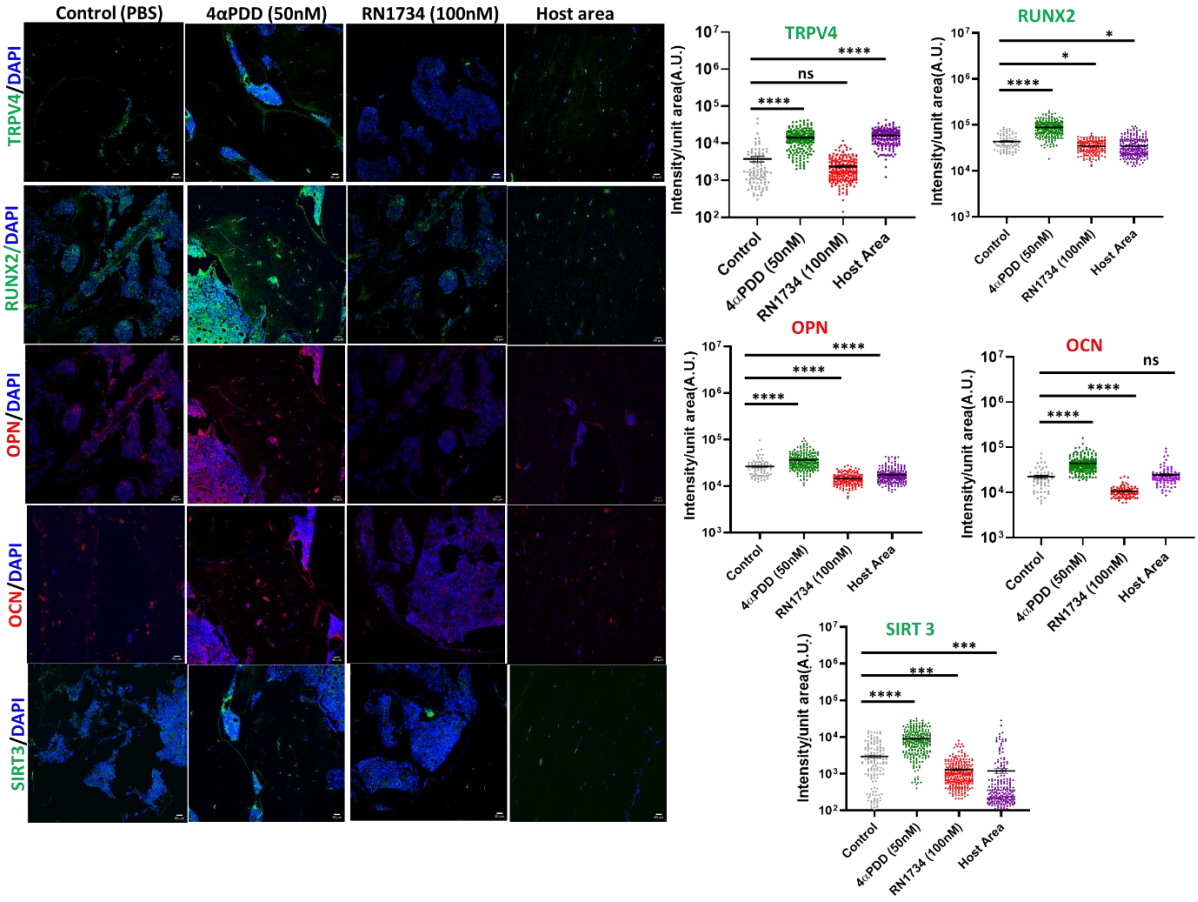


Fig. 63. Hydrogel (CMT: HEMA)-mediated release of TRPV4 agonist or antagonist modulates *in vivo* bone repair and increases osteogenic markers. Bone tissue samples were decalcified, cut into thin sections (5µm) and immunohistochemically stained for the detection of TRPV4 expression, bone formation (Runx-2, OCN & OPN), and SIRT3 (mitochondrial UPR marker). Fluorescence intensity of TRPV4 and other osteogenic markers are high in case of 4αPDD treated group as compared to PBS or RN1734-treated group. The quantified fluorescence intensities have been plotted right side of each image. (N = 3, 4 rats in each group). The statistical values are ANOVA test, p values: * = <0.05, ** = < 0.01, *** = <0.001, **** = <0.0001, ns = non-significant. (Un-published figure).

Fig. 63B-D shows the presence of bone formation related protein RUNX-2, OPN and OCN in the bone defect area and host bone. Generally, RUNX-2 is expressed early in osteogenesis cascades, whereas OPN and OCN come at the middle and late stage of the process. From **Fig. 63B-D** it is observed that the 4αPDD group has significantly higher expression of RUNX-2, OCN & OPN than other groups and host bone. In the PBS group, these markers are expressed only at the defect edges. While in the case of RN1734-treated group, the very diminished intensity of these markers were observed in the newly formed hard tissue. Notably, osteogenic process is highly energy consuming event and mitochondrial health is important for supplying increased demand of ATP. Thus, the expression of mitochondrial stress suppresser marker SIRT3 in the newly developed bone samples were investigated. The intensity of SIRT3 is high in 4αPDD-treated group, followed by the PBS-treated group and RN1734-treated group, show the lowest level of expression (**Fig. 63E**). These observation shows that TRPV4 is present in rat femur and their activation at defect site enhanced osteogenesis process by regulating the osteogenic genes and by maintaining the mitochondrial health.

2.4.8 *In vivo* analysis for biosafety:

In addition to these enhanced osteogenic abilities, the *in vivo*, non-toxic nature of the hydrogel alone or associated with drugs are also crucial factors for their successful practical applications in biological systems. Therefore, we performed H&E staining to investigate the potential toxicity of TRPV4 modulators containing hydrogels *in vivo*. **Fig. 64** shows histologically stained sections of the kidney, liver and spleen collected from hydrogel-implanted sacrificed rats. The findings show that none of the groups had any apparent structural changes or organ abnormalities compared to the control (PBS) group, indicating that implantation of TRPV4 modulatory containing hydrogel or their degraded components did not exert any detectable

adverse effects on the *in vivo* model systems. Overall, these findings further confirm the suitable osteogenic and biocompatibility nature of TRPV4 modulators and hydrogel, which has a potential to be used as a bioactive scaffold for accelerated bone remodeling.

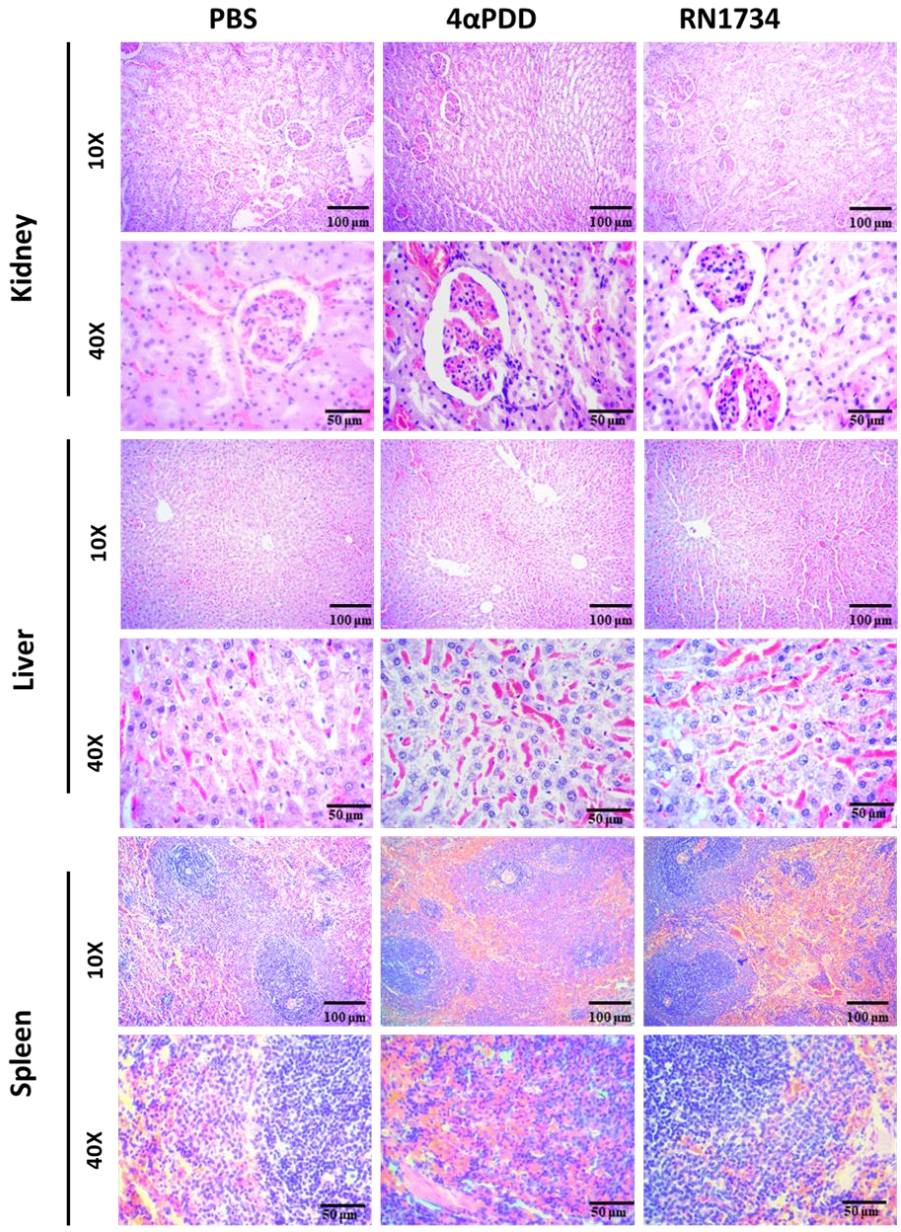


Fig. 64. *In vivo* toxicity assay. Representative images of H&E staining are shown to analyze the potential toxicity of TRPV4 modulators containing hydrogels applied *in vivo*. Kidney, liver and spleen organs were collected from hydrogel implanted sacrificed rats and histological staining were performed on the tissue sections. None of the groups had any apparent structural changes or organ abnormalities as compared to the control (PBS) group. (Un-published figure).

2.4.9 Osteointegration analysis by SEM:

After 8 weeks, bone samples were isolated, and the hydrogel implanted area was analyzed under an optical microscope and SEM. Optical microscope images confirm that the defect site exposed towards hydrogel with 4αPDD was completely covered with hard tissue, while in the case of RN1734 containing hydrogel and self-healing condition (PBS), the defect sites contain a lesser amount of new bone and/or soft tissues (**Fig. 65A**). SEM images of defect site exposed with 4αPDD containing hydrogel exhibits complete reabsorption of hydrogel and accelerated bone growth. RN1734 exposed defect site revealed a clear gap at the interface of the host bone and hydrogel implant. There is irregular growth of new bone tissue, resulting in an aberrant rough surface, as observed. Deposition of collagen fibers at the interface of host bone and implant, and harversian system with rough surface were also observed. In the case of 4αPDD treatment, no gap was observed between the interface of the host bone and implant. In this case, the presence of mature osteoblasts and osteoclasts and the appearance of new blood vessels and harversian system with a smooth surface at the defect site indicates the formation of new hard tissue similar to functional, healthy bone. While in the case of self-healing condition, the gap is not present, but a 'hole-like" pit structure and several cracks at the defect site and irregular deposition of collagen matrix was observed. Collectively these indicate a slow bone healing process in the case of PBS application. These observations suggest that activation of TRPV4 by localized and sustained delivery of 4αPDD from the hydrogel at the defect site accelerates *in vivo* bone healing process while blocking of TRPV4 activity by RN1734 results in slow hard tissue formation at the defect site (**Fig. 65B**).

2.4.10 Assessment of the quality of the newly formed bone:

The rate of bone fracture healing and their respective strength are determined by chemical component constituents and arrangements of mineralized collagen fibers at the defect site. For determining the quality of bone, the physicochemical properties of mineralized crystals and organic matrix were characterized.

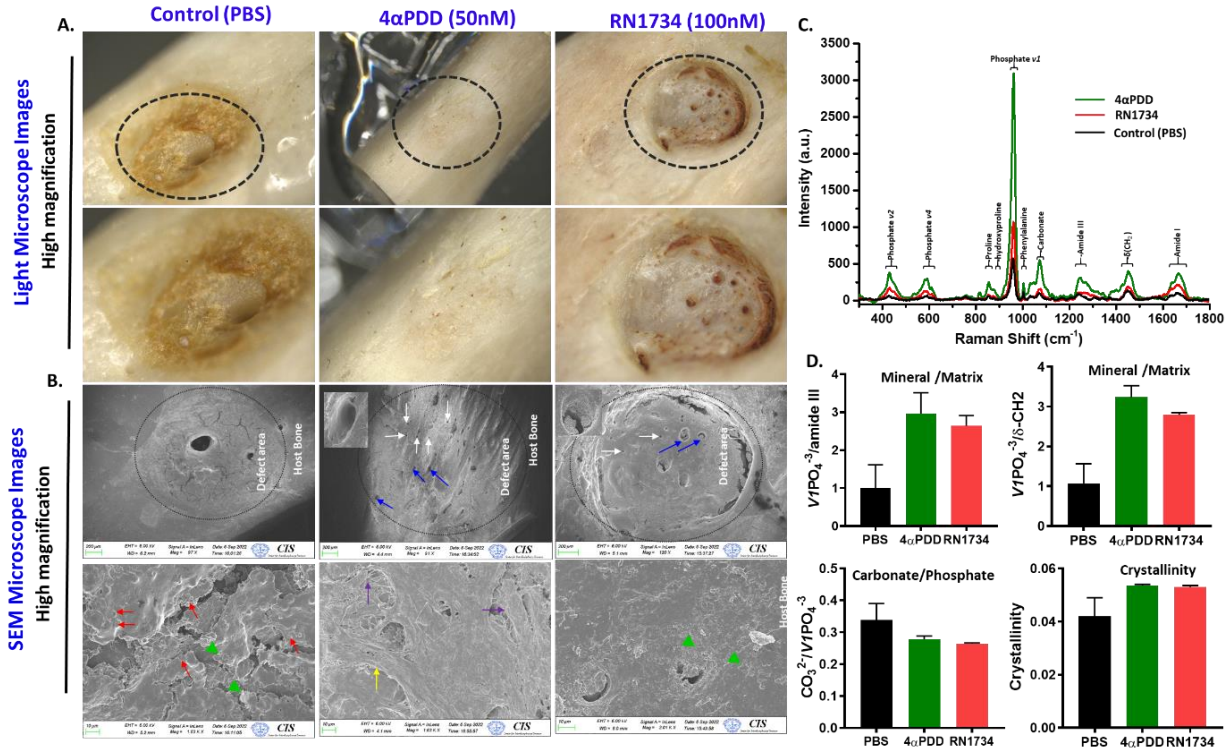


Fig. 65. Assessment of bone healing and quality of new bone. A-B. Hydrogel implanted area were analyzed under an optical microscope and SEM. These images confirm that the defect site exposed towards hydrogel with 4αPDD were completely covered with hard tissue, while in the case of RN1734 containing hydrogel and self-healing condition (PBS), the defect sites contain lesser amount of newly formed bone and soft tissue. **C-D.** For analyzing the quality of newly formed bone tissue at the defect site, Raman spectroscopy study was performed. Raman spectrum intensity were acquired in the range of 400 to 1800 cm^{-1} form all the bone samples. Prominent Raman bands of the mineral phase and organic phase of bone with their respective biomolecular assignments were observed at different peak positions (C). Mineral/ matrix ratio, Carbonate/phosphate ratio and Crystallinity were measured (D). Modulation of TRPV4 activity at the defect site by TRPV4 agonist containing hydrogel results in an enhanced bone healing process and mostly matches with the chemical composition of newly formed bone tissue. (Un-published figure).

Raman spectral bands are highly sensitive in distinguishing the structural, chemical and compositional changes of bone. So, to analyze the quality of newly formed bone tissue at the defect

site, Raman spectroscopy was performed. **Fig. 65C-D** shows and also compares the Raman spectra of bone tissue samples collected from different treated groups. Raman spectrum intensity was acquired in the range of 400 to 1800 cm^{-1} form all bone samples. Prominent Raman band of the mineral phase and organic phase of bone with their respective biomolecular assignments were observed at different peak positions. Mineral phase molecular species of bone samples are presented at following tentative peaks: Appearance of peak at 430 $cm^{-1,}$ and 590 cm^{-1} corresponds to *v2, v4* vibration of PO_4^{3-}, peaks at 590 cm^{-1} and 1070 cm^{-1} represents P-O symmetric stretch of PO_4^{3-} and C-O in plane stretch vibration of CO_3^{-2} respectively. Organic phase: Peaks present at 1003 cm^{-1} represents phenylalanine ring breathing, while the peak at 1246 cm^{-1} and 1667 cm^{-1} are attributed to C-N-H stretch vibration of amide III and C-C-N stretch vibration of amide I, respectively. The peak at 1450 cm^{-1} corresponds to the C-H bending mode of lipid and protein content of the tissue. **Fig. 65D** shows the results of the Raman spectroscopy for the various parameters. Crystallinity and mineral/ matrix ratio depict the rate of mineralization and mechanical strength of newly formed bone tissue. Mineral crystallinity and mineral/ matrix are higher in the case of the TRPV4 agonist-treated group as compared to the antagonist and self-healed group. Another important parameter is the carbonate-to-phosphate ratio, which represents the substitution of carbonate into the phosphate group of apatite lattice. Decreased ratio of carbonate to phosphate results in high mineral crystallinity or *vice versa*. The carbonate to phosphate ratio is higher in the PBS-treated group as compared to the TRPV4 agonist- and antagonist-treated group. From this observation it can be concluded that modulation of TRPV4 activity at the defect site by TRPV4 agonist containing hydrogel results in an enhanced bone healing process, and the chemical composition of newly formed bone tissue resembles with normal healthy bone.

Summary: Treating different types of bone defects are difficult, complicated, time-consuming and expansive. Here we demonstrate that TRPV4, a mechano-sensitive, thermo-gated and non-selective cation channel, is endogenously present in the Mesenchymal stem cells (MSC). TRPV4 regulates both cytosolic Ca^{2+}-levels and mitochondrial health. Accordingly, hydrogel made from a natural biopolymer and encapsulated with TRPV4-modulatory agents affect different parameters of MSCs, such as cell morphology, focal adhesion points, intracellular Ca^{2+}, ROS and NO levels. TRPV4 also regulates cell differentiation and bio-mineralization *in vitro*. We demonstrate that 4α-CMT-Hy (the hydrogel encapsulated with 4αPDD, TRPV4 activator) upregulates the mitochondrial health, i.e., increase in ATP- and Cardiolipin levels, and improves mitochondrial membrane potential. The same scaffold turned out to be non-toxic *in vivo*. 4α-CMT-Hy enhances the repair of bone-drill hole in rat femur, both qualitatively and quantitatively *in vivo*. We conclude that 4α-CMT-Hy acts as a scaffold and is suitable for treating large bone defects at low cost and can be tested for clinical trial.

2.5 TRPM8-mediated mitochondrial regulation: impact on bone cell functions and application in bone tissue engineering:

After determining that TRPV4 had an effect on osteogenesis, we then investigated whether or not TRPM8 also has an effect on osteogenesis. In order to accomplish this, we encapsulated the specific modulators of TRPM8 in the hydrogel (CMT: HEMA) and studied the *in vitro* osteogenesis as well as other aspects of cellular physiology.

2.5.1 TRPM8 channel modulates intracellular Ca^{2+}-dynamics in osteoblasts:

We have previously described the expression of TRPM8 in Saos-2 (human osteosarcoma cell) and primary mouse bone marrow derived Mesenchymal stem cells in our earlier results. In order to probe for the functionality of TRPM8 in bone cells, Ca^{2+}-imaging was performed using Fluo4-AM loaded into Saos-2 cells (Human osteosarcoma cell line).

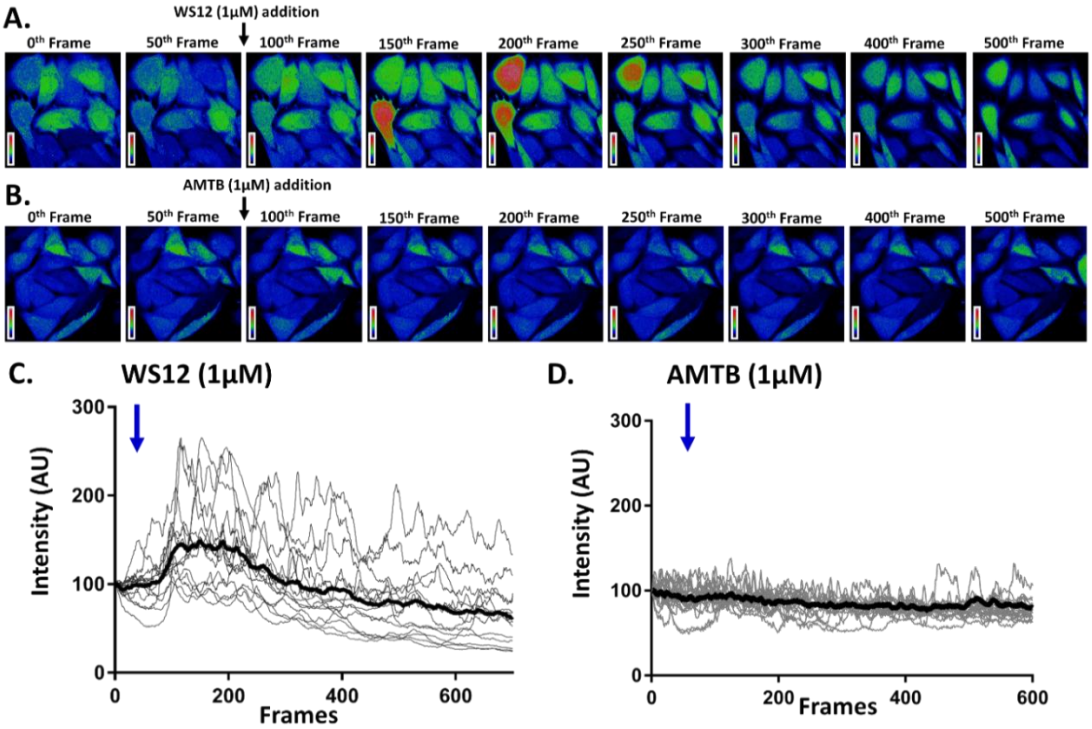


Fig. 66. TRPM8 activation increases cellular Ca^{2+}-level. A-B. Time series images of Ca^{2+}-intensity in live Saos-2 cells. Cells were loaded with Fluo-4-AM and fluorescence intensity is represented in pseudo color (red and blue indicating highest and lowest intensity respectively). Ca^{2+}-imaging was performed at the speed of 2 Frames per second. At the 100th frame, cells were treated with TRPM8 activator WS12 (1

μM) (A) or inhibitor AMTB Hydrate (1 μM) (B). **C-D.** Quantification of Fluo-4-AM intensity (in AU) over 500 frames, with the initial value normalized at 100%. Increased fluorescence intensity is observed in most cells treated with WS12 (C), which declines gradually over time. TRPM8 inhibitor (AMTB) doesn't alter Fluo-4-AM intensity over time (D). (Published figure, Acharya TK. et al. 2021, *Scientific reports*).

TRPM8 activator WS12 (1μM), added at the 50th frame, was able to induce a sharp spike in intracellular Ca^{2+}-levels in most of the osteoblasts. Few osteoblasts remained insensitive to WS12 (**Fig. 66A-B**). This indicated that TRPM8 is functional in Saos-2 cells. However, the addition of TRPM8 inhibitor (AMTB 1μM) didn't alter the intracellular calcium levels in Saos-2 cells as reflected by insignificant changes in Fluo-4-AM intensity with respect to time (**Fig. 66C-D**).

2.5.2 CMT: HEMA hydrogel act as suitable surface for growth of Mesenchymal stem cells:

We explored whether Mesenchymal stem cells can grow on CMT: HEMA as well as drug-coated CMT: HEMA gels. We grew the cells over the drug coated hydrogel surface and performed scanning electron microscopic study to check the morphology of the cells.

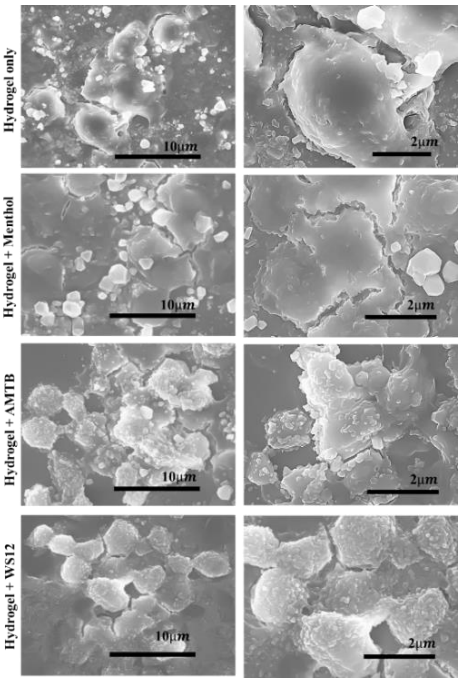


Fig. 67. Hydrogel (CMT: HEMA) as a suitable surface for drug coating and growing of Mesenchymal stem cells. Scanning Electron Microscopic images of Mesenchymal stem cells grown on hydrogel (CMT: HEMA) only and coated with different drugs modulating TRPM8 ion channel. (Published figure, Acharya TK. et al. 2021, *Scientific Reports*).

We observed that Mesenchymal stem cells grow well on these surfaces, yet with different morphologies and roughness in the surface (**Fig. 67**).

2.5.3 CMT: HEMA encapsulated with TRPM8-specific compounds regulate cellular morphology:

Differentiation of MSCs to osteoblasts and subsequent mineralization involves specific changes in the morphology. Such morphological changes are pre-requisite for actual mineralization. We explored if CMT: HEMA hydrogel is able to induce morphological changes in BM-MSCPs. Therefore, BM-MSCPs were grown on the glass surface, hydrogel coated coverslips as well as in hydrogels coated with Menthol, WS12, and AMTB. Cells were stained with Phalloidin-488 as well as with DAPI and images were acquired (**Fig. 68A**). We quantified number of cells grown per unit area. We also quantified the morphological parameters such as length, breadth, area, and parameter are quantified from 100 cells on each coverslips (**Fig. 68B**). While number of cells grown on unit area on CMT: HEMA hydrogel alone is less than only glass, the number of cells grown is significantly higher when either Menthol (TRPM8 activator) or AMTB (TRPM8 activator inhibitor) is used (**Fig. 68B** upper left panel). This suggests that CMT: HEMA alone as well as drug-coated CMT: HEMA, can be used for desired number of cells on unit area (discussed later). There is no significant difference in the cell length, width, cell perimeter or even cell area in most cases (**Fig. 68B**). However, the presence of WS12, an activator of TRPM8 in the CMT: HEMA, causes increased length, increased perimeter, increased cell area but no change in cell width. In contrast, presence of AMTB, an inhibitor of TRPM8 in the CMT: HEMA, causes no change in cell length, width, perimeter, and area when compared to the CMT: HEMA only (**Fig. 68B**). This data suggests that CMT: HEMA with or without TRPM8-specific drugs affect cell adhesion and cell migration differently.

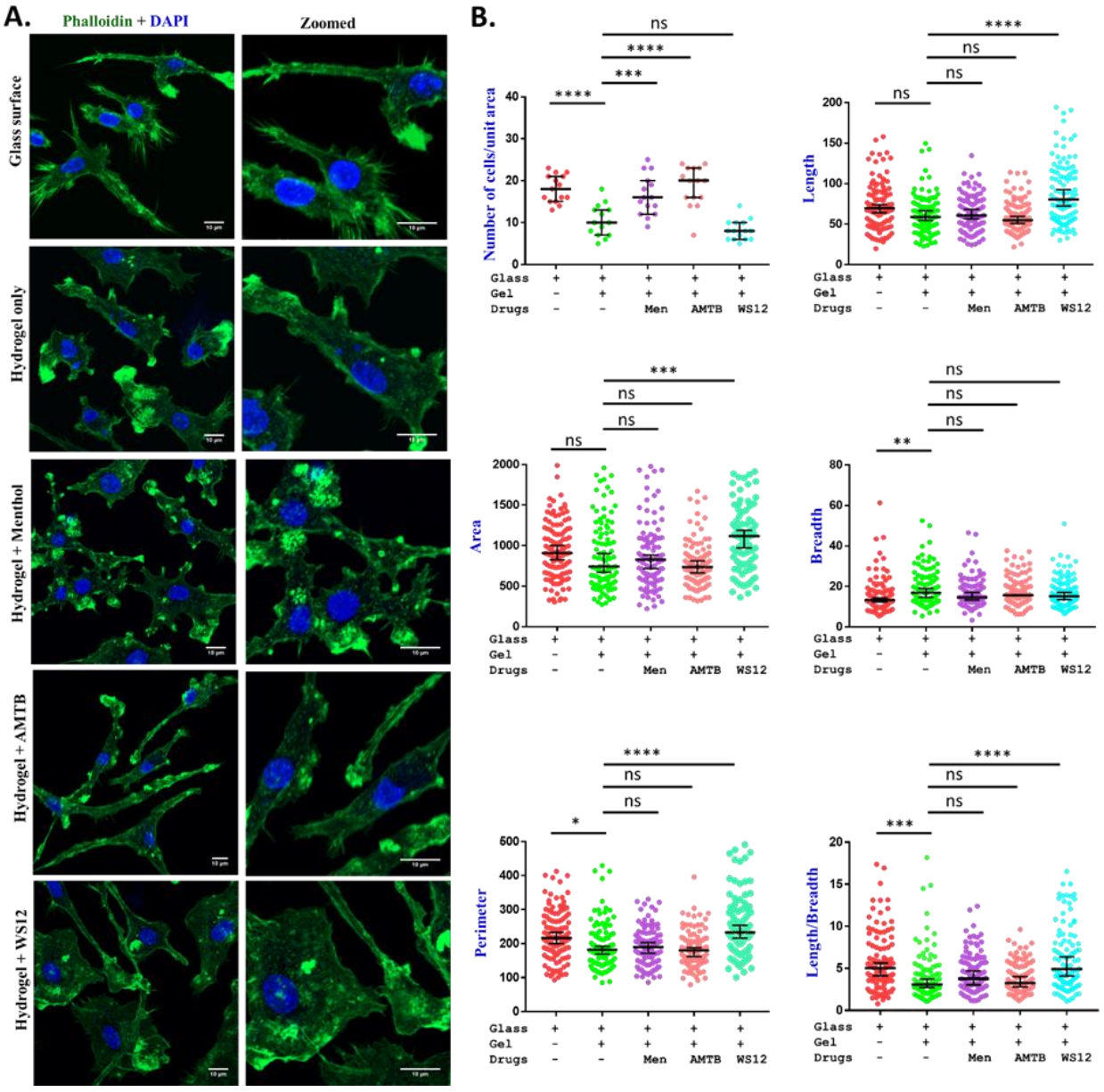


Fig. 68. Hydrogel-mediated drug release alters the morphology of bone marrow derived Mesenchymal stem cell population. BM-MSCPs were isolated and grown on only glass, only hydrogel or on hydrogel-coated with different drugs affecting TRPM8 ion channel. A. Morphology of cells grown on different surface are shown. Cells were stained with Phalloidin (green) and DAPI (blue). B. Different morphology parameters of the cells grown on different surfaces are shown. The statistical values are: ANOVA test, p values: * = <0.05, ** = < 0.01, *** = <0.001, **** = <0.0001, ns = non significant. (Published figure, Acharya TK. et al. 2021, *Scientific Reports*).

2.5.4 CMT: HEMA encapsulated with TRPM8-specific compounds induce differential ROS signaling:

Reactive Oxygen Species (ROS) signaling is important for bone mineralization (Gao J, 2018). Therefore, we analyzed the extent of ROS produced by Mesenchymal stem cells when grown on CMT: HEMA only or CMT: HEMA coated with TRPM8 specific drugs. We used H_2O_2 (20μM) as a positive control, as it is known to generate free radicals and generate ROS. We quantified the relative amount of ROS produced in each condition using Image-J. We did not observe any difference in the fluorescence intensity of ROS in cells grown on glass and only hydrogel (**Fig. 69A, C**). This confirms that the cells that are grown on Hydrogel are producing a negligible amount of ROS. On the other hand, hydrogels coated with Menthol and WS12 are producing modest amount of ROS that is tolerable by cells (**Fig. 69A, C**). In contrast, AMTB-coated hydrogel produces basal level of ROS. This data also demonstrates the CMT: HEMA can be fine-tuned for ROS production applicable to other cells also.

2.5.5 CMT: HEMA encapsulated with TRPM8-specific compounds affect mitochondrial membrane potential:

We explored if TRPM8 activation can cause changes in the mitochondrial membrane potential. For this purpose, Mesenchymal stem cells were grown on hydrogel alone as well as hydrogel-coated with TRPM8 specific activator or inhibitor for 24 hours. Subsequently, cells were labelled with ratiometric dye JC-1. Subsequently, image intensity (Red and Green) was quantified by Image J. The Red intensity (Ex535/Em590) represents higher membrane potential (**Fig. 69B, D**). In the presence of CMT: HEMA hydrogel mitochondrial potential is significantly decreased as compared with only glass as surface.

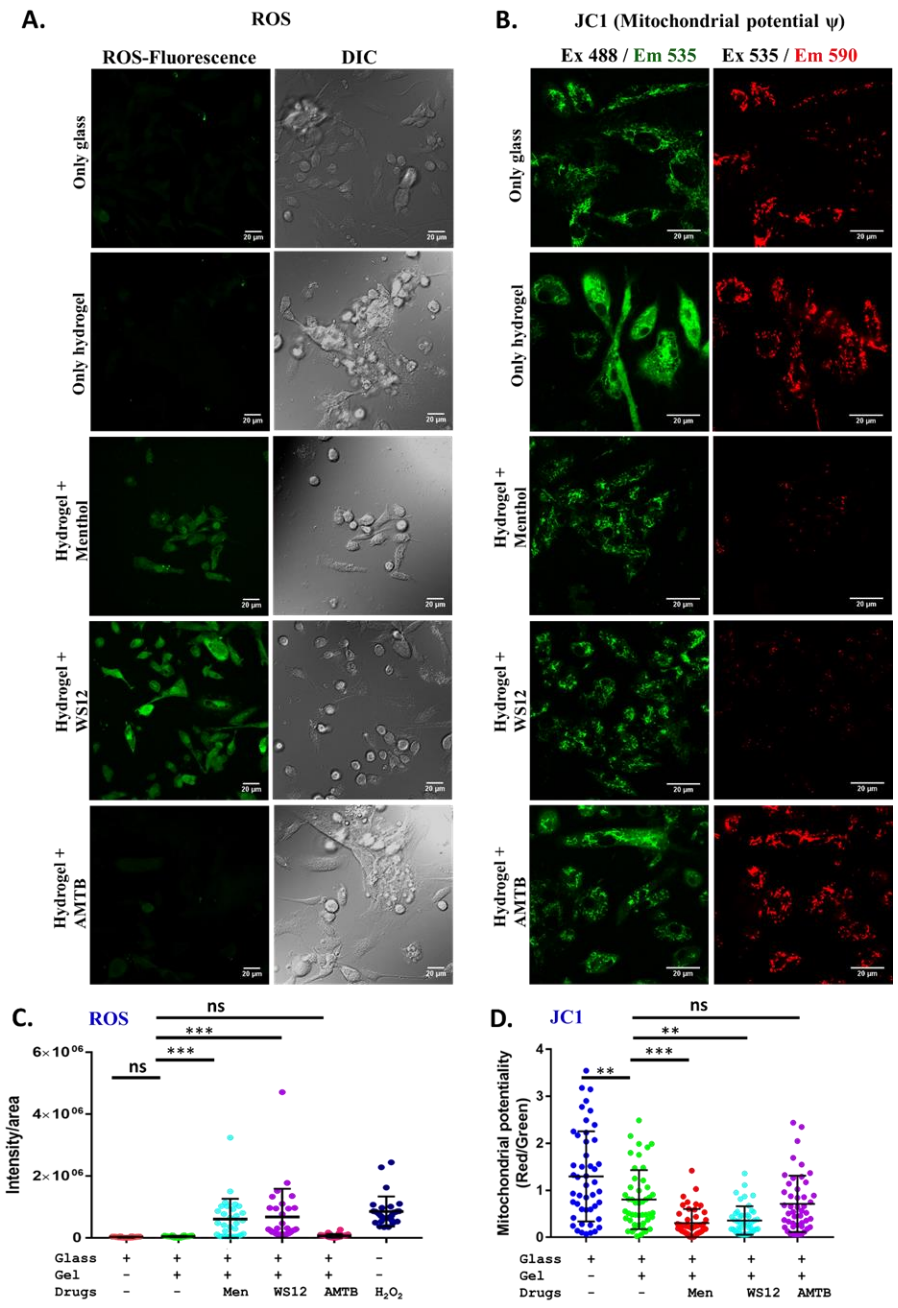


Fig. 69. Hydrogel coated with TRPM8 activators but not with inhibitor specifically stimulates ROS-signaling by decreasing mitochondrial oxidative potential. A-B. Fluorescence microscopic images from cells grown on only glass, only hydrogel or the same hydrogel coated with different activators and inhibitor are shown. ROS signal (green in left panel) and DIC images of the cells are shown in left side (A). Similarly, mitochondrial oxidative potential analyzed by JC1 dye is shown in right side (B). JC1 fluorescence emission at 590 nm (red panel, indicative of high oxidative potential) is reduced in cells when grown on hydrogel coated with TRPM8 activators. **C-D.** Quantified values representing the fluorescence values from individual cells grown on different surface as shown in Fig. A-B. The statistical values are as follows: One-way ANOVA test, p values: ** = < 0.01, *** = <0.001, ns = non-significant. (Published figure, Acharya TK. et al. 2021, *Scientific Reports*).

However, in the presence of TRPM8 activator Menthol (10 μM) or WS12 (1 μM), mitochondrial potential was significantly decreased as compared to CMT: HEMA alone. TRPM8 inhibitor, AMTB (1 μM) did not alter the mitochondrial potential in BM-MSCPs and retained its membrane potential similar to the CMT: HEMA only (**Fig. 69B, D**).

2.5.6 CMT: HEMA encapsulated with TRPM8-specific inhibitor enhances bone differentiation and mineralization and osteogenic markers:

BM-MSCPs grown on plates coated with hydrogels containing TRPM8 specific drugs were viable and proliferated well (data not shown). ALP assay performed after 7 days of culture show a dose-dependent increase in ALP activity in cells grown on AMTB-coated CMT: HEMA hydrogel when compared to cells grown on only CMT: HEMA hydrogel in the presence of differentiating factors (BGP, LAA) (**Fig. 70B**). However, WS12 coated hydrogels didn't significantly affect ALP activity. None of these hydrogels decreased ALP activity, showing that they are suitable for targeting BM-MSCPs as well as Osteoblasts. This was in full agreement with the results obtained upon application of the TRPM8 activator or inhibitor alone, as described above. The hydrogel alone didn't increase or decrease ALP activity, suggesting that the results obtained above are the effects of slow and local release of TRPM8 modulators only (**Fig. 70B**).

Further, we performed mineralization assay after 15 days of culturing BM-MSCPs on hydrogel coated plates in the presence of differentiating factors (BGP, LAA, and Dexamethasone). We observed that very low concentrations of WS12 coated hydrogels (1 nM and 10 nM) induce an increase in mineralization, while higher concentrations either don't affect mineralization (WS12; 100 nM) or decrease mineralization significantly (WS12; 1 μM) (**Fig. 70C**).

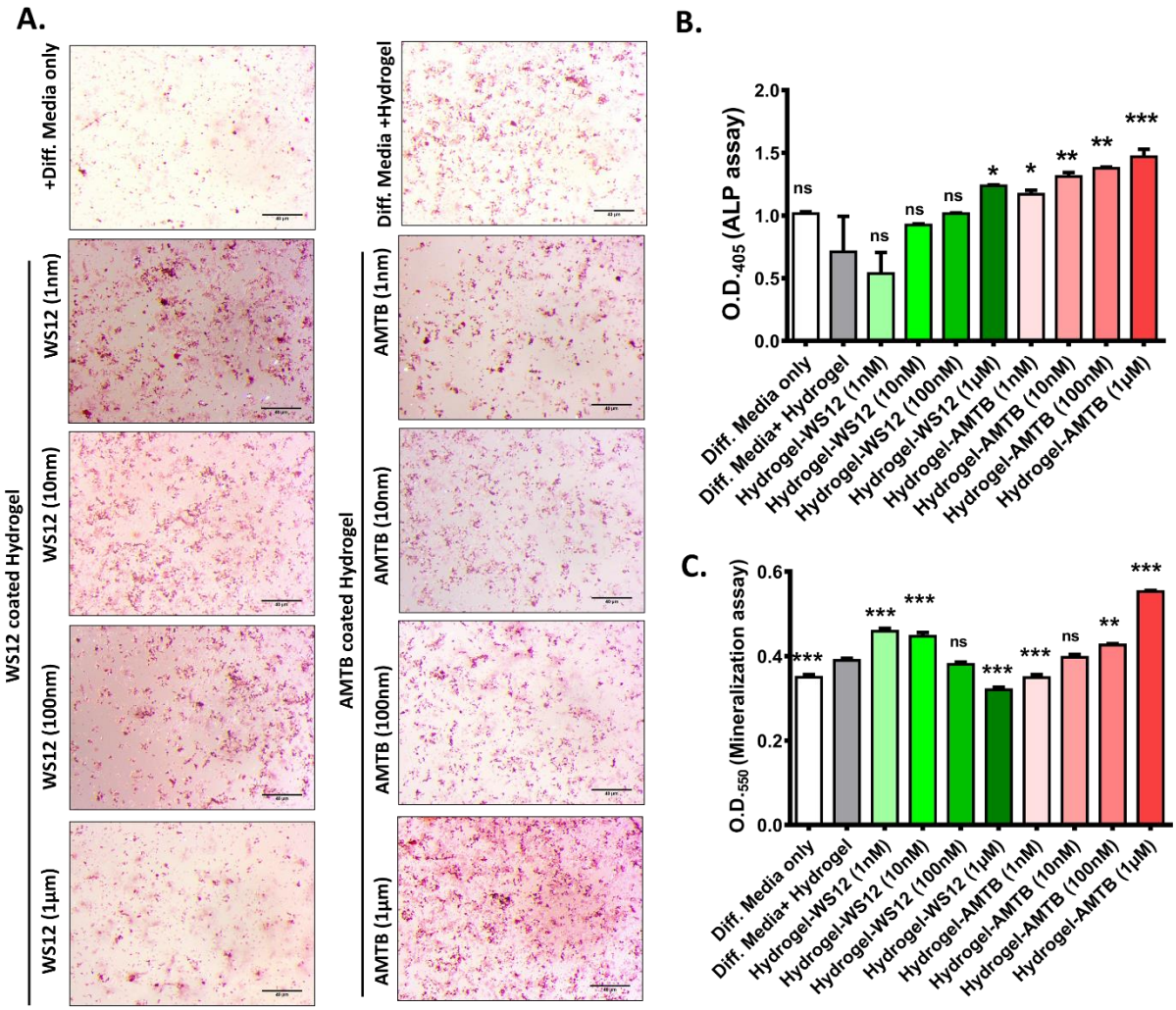


Fig. 70. Hydrogel (CMT: HEMA)-mediated release of TRPM8 agonist and antagonist modulates osteoblasts functions. A. Photographs (upper panel) represent mineralization nodules of Mesenchymal stem cells (MSCs) grown for 15 days in the absence or presence of hydrogel (CMT: HEMA) as detected by Alizarin Red staining (n = 3). The lower panel photographs represent the extent of mineralization nodules formed when cells were grown on WS12 or AMTB encapsulated CMT: HEMA hydrogel. Scale bar 40 µm. **B-C.** Bone marrow-derived Mesenchymal stem cell population (BM-MSCPs) grown on these hydrogels or hydrogels-encapsulated with AMTB or WS12 reveals dose-dependent differentiation (B) and mineralization (C) (n=3). The significance values are as follows: ANOVA test, p values: * = <0.05, ** = < 0.01, *** = <0.001, ns = non-significant. (Published figure, Acharya TK. et al. 2021, *Scientific Reports*).

Opposite effect was observed in case of AMTB coated Hydrogels. Very low concentration of AMTB in hydrogel either decrease mineralization (AMTB 1nM) or don't affect mineralization (10 nM), while higher concentration of AMTB coated hydrogel increase mineralization

significantly (100 nM and 1 μM) (**Fig. 70C**). Higher number of Alizarin-red stained mineralized nodules are visible in WS12 (1 nM) coated CMT: HEMA hydrogel and in AMTB (1 μM) coated CMT: HEMA hydrogel but not in only CMT: HEMA hydrogel (**Fig. 70A**) confirming the results obtained after extraction of Alizarin Red by CPC extraction (**Fig. 70C**).

We further checked the expression of osteogenic markers such as Osteopontin and Osteocalcin during bone differentiation. The Mesenchymal stem cells isolated from mouse bone marrow were grown on the hydrogel coated with different concentrations of AMTB (1 nm, 10 nm, 100 nm, 1 μM) and WS12 (1 nm, 10 nm, 100 nm, 1 μM). After 14 days of growing in mineralization media, the cells were fixed and stained with antibody specific for Osteopontin (OPN) and Osteocalcin (OCN). We observed enhanced expression of these markers in AMTB treated cells (**Fig. 71, 72**).

Taken together, we demonstrate that endogenous and functional TRPM8 is present in osteoblasts and TRPM8 modulators can be utilized pharmacologically for enhanced osteoblast differentiation and mineralization by CMT: HEMA hydrogel-based surfaces.

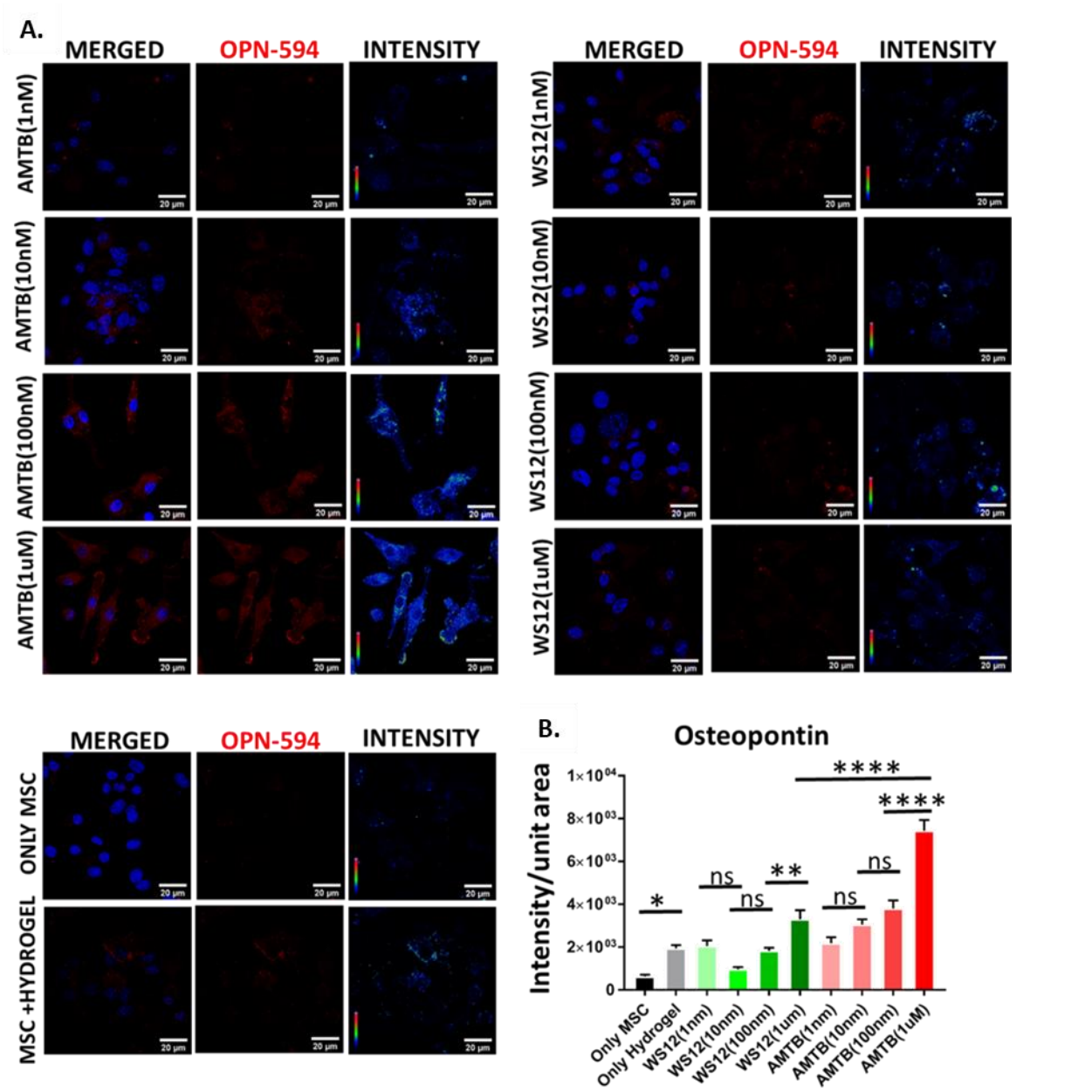


Fig. 71. Osteopontin expression in MSCs is induced when grown on different surfaces with TRPM8 modulatory drugs. **A.** Mesenchymal stem cells isolated from mouse bone marrow were grown on the hydrogel coated with different concentrations of AMTB (1 nM, 10 nM, 100 nM, 1 μM) and WS12 (1 nM, 10 nM, 100 nM, 1 μM). After 14 days of growing in mineralization media the cells were fixed and stained with antibody specific for Osteopontin. Dose-dependent increment in Osteopontin expression is observed in case of AMTB-coated hydrogels. Intensity of Osteocalcin is represented in pseudo rainbow color. **B**. The intensity of Osteopontin is quantified by using Image J software. The expression of OPN is more in AMTB (1μM) in compared to the WS12 and control condition**.** (Published figure, Acharya TK. et al. 2021, *Scientific Reports*).

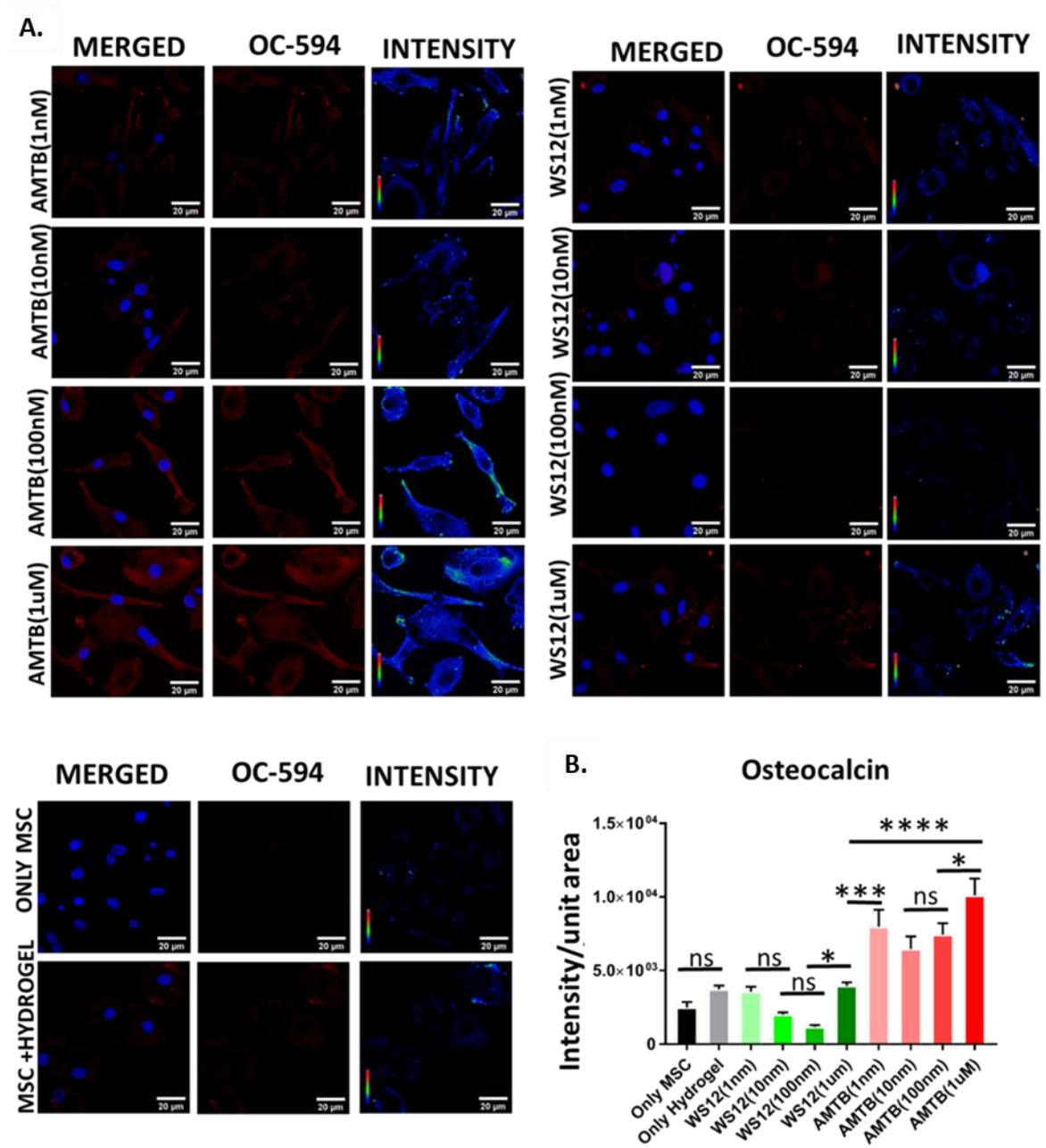


Fig. 72. Osteocalcin expression in MSCs is induced when grown on different surfaces with TRPM8 modulatory drugs. **A.** Mesenchymal stem cells isolated from mouse bone marrow were grown on the hydrogel coated with different concentrations of AMTB (1 nM, 10 nM, 100 nM, 1 μM) and WS12 (1 nM, 10 nM, 100 nM, 1 μM). After 14 days of growing in mineralization media, the cells were fixed and stained with antibody specific for Osteocalcin. Higher levels of Osteocalcin expression is observed in case of AMTB-coated hydrogels. The intensity of Osteocalcin is represented in pseudo rainbow color. **B**. The intensity of Osteocalcin is quantified by using Image J software. The expression of OCN is more in AMTB (1 μM) in compared to the WS12 and control condition**.** (Published figure, Acharya TK. et al. 2021, *Scientific Reports*).

Summary: A major limitation in the bio-medical sector is the availability of materials suitable for bone tissue engineering using stem cells and methodology converting the stochastic biological events towards definitive as well as efficient bio-mineralization. We show that osteoblasts and Bone Marrow-derived Mesenchymal stem cell Pools (BM-MSCP) express TRPM8, a Ca^{2+}-ion channel critical for bone-mineralization. TRPM8 inhibition triggers up-regulation of key osteogenesis factors, and increases mineralization by osteoblasts. We utilized CMT: HEMA, a carbohydrate polymer-based hydrogel that has nanofiber-like structure suitable for optimum delivery of TRPM8-specific activators or inhibitors. This hydrogel is ideal for proper adhesion, growth, and differentiation of osteoblast cell lines, primary osteoblasts, and BM-MSCP. CMT:HEMA coated with AMTB (TRPM8 inhibitor) induces differentiation of BM-MSCP into osteoblasts and subsequent mineralization in a dose-dependent manner. Prolonged and optimum inhibition of TRPM8 by AMTB released from the gels results in the upregulation of osteogenic markers. We propose that AMTB-coated CMT: HEMA can be used as a tunable surface for bone tissue engineering. These findings may have broad implications in different bio-medical sectors.

2.6 TRPV4- mediated mitochondrial regulation: impact on T cell activation:

2.6.1 TRPV4 regulates mitochondrial Ca^{2+}-status and physiology in primary murine T cells based on its immunological state:

T-cells are very specialized immune cells having the unique ability to recruit immunity against pathogens and antigens. T cells are generally maintained at a resting state, but under certain conditions, T cells are activated. Notably, The T cell activation process is largely a Ca^{2+}-driven process. It has been shown that chelation of cytosolic as well extracellular Ca^{2+}-level altered by BAPTA-AM or EGTA respectively reduces IL2-production, IL2-receptor expression and proliferation of naïve T-cell (Acharya TK, 2022c). In recent reports, it has been established that mitochondria translocate to the immune synapse during the onset of T-cell activation and in turn, increase the mitochondrial Ca^{2+}-influx (Quintana A, 2007). T-cell activation and clonal expansion is an energy-driven process, and activated T-cell is highly dependent on mitochondrial Ca^{2+} and ATP levels (Desdín-Micó G, 2018). Inhibition of the mitochondrial Ca^{2+}-influx by CCCP, oligomycin/antimycin decreases cytosolic Ca^{2+}-level and prohibits T-cell activation, suggesting that mitochondria play a critical role in the T-cell activation process, especially in the initial phase (Ledderose C, 2014; Quintana A, 2007). Previously we have reported that TRPV4 is endogenously expressed in the primary human T-cell and primary murine T-cells (Majhi RK, 2015). Notably, inhibition of TRPV4 reduced the ConA-mediated T cell activation process, suggesting that spontaneous function of TRPV4 is involved in the T cell activation process (Majhi RK, 2015). Using CHO-K1 cells that express TRPV4 after a stable selection, recently we have demonstrated that TRPV4 is present in the mitochondria and also in the ER-mitochondrial contact points (Acharya et al. 2022a; Acharya et al. 2022b). We have reported the presence of TRPV4 in the mitochondria of other cellular systems, including primary cells, such as MSCs and also in the

mitochondrial isolated from mammalian brain. Accordingly, TRPV4 activation also results in quick increment of Ca^{2+}-levels within the isolated mitochondria (Acharya TK, 2022a). The presence of TRPV4 in mitochondria and also in the MAM strongly suggests that TRPV4 is involved in intracellular Ca^{2+}-buffering from the cytosol and Ca^{2+}-mobilization from ER-to mito and *vice versa* (Acharya TK, 2022b). The presence of TRPV4 in the mitochondria also suggests the possible involvement of TRPV4 in the temperature-driven events that are biologically relevant. In fact, TRPV4 activation alters mitochondrial temperature (Acharya TK, 2022a). In this context, T cells are highly relevant and offer a suitable cellular system where the function of endogenous TRPV4 can be tested at the mitochondrial level. Therefore, T cells offer a suitable cellular system where the presence and involvement of TRPV4 in the mitochondrial can be investigated in the context of cellular and physiological functions. In this work, we not only demonstrate the presence of TRPV4 in the mitochondria of T cells but also show the function of TRPV4 in the overall cellular and mitochondrial Ca^{2+}-metabolism linked to diverse metabolic functions. Our findings suggest the involvement of mitochondrial TRPV4 in T cell functions.

2.6.2 TRPV4 colocalizes with mitochondria in T-cells:

Recently we have reported the localization of TRPV4 at mitochondria (Acharya TK, 2022a). In order to characterize the TRPV4 colocalization with the mitochondria of T cell, we performed double labelling. Mitochondria were labelled by using MitoTrackerRed-CMXRos in resting T cells, and TRPV4 was labelled by using antibody. We observed TRPV4 colocalization with mitochondria in resting T cells (**Fig. 73A**). Further to validate this qualitative result, we performed the colocalization analysis of TRPV4 with MitoTrackerRed using 'Co-localization' plugin of ImageJ. The colocalized pixels are detected as white spots in resting T cells too.

Further, we analyzed the distribution of TRPV4 in mitochondria, especially with respect to cells. For this purpose, we detected both TRPV4 and mitochondria from multiple small ROIs located at the periphery, middle or at random positions of the cell. We detected more TRPV4 in the peripheral region of the T cells as compared to the middle region (**Fig. 73B-C**).

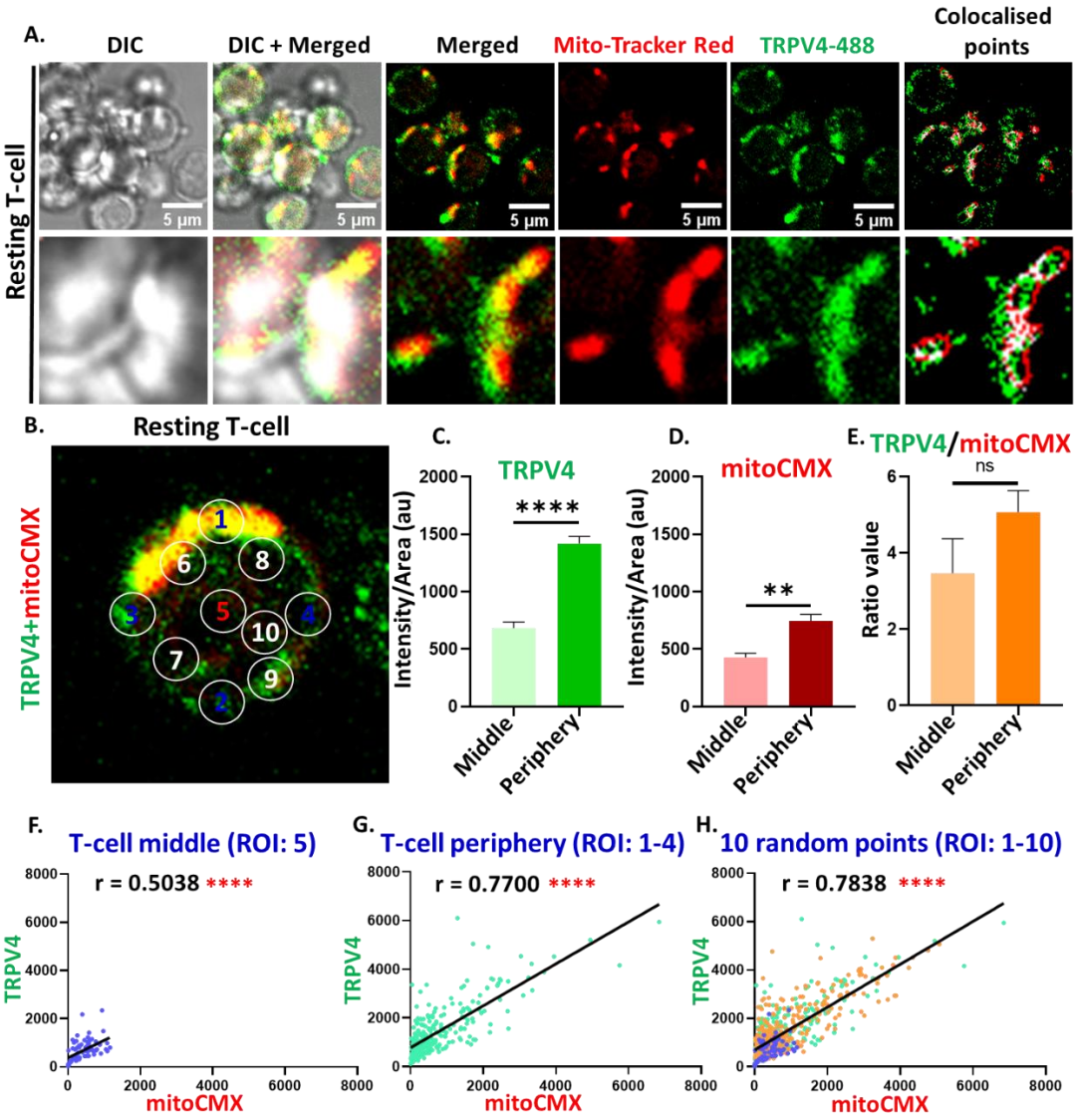


Fig. 73. TRPV4 colocalizes with mitochondria in T-cells: A. Representative Images showing colocalization of TRPV4 with mitochondria. **B-E.** Distribution of TRPV4 in mitochondria by quantifying the intensity of TRPV4 and mitochondria in 10 different ROIs of the cell. TRPV4 is present significantly more in the peripheral region of T cells as compared to the middle region (≥100 cells were quantified). **F-H.** Analysis of the correlation values of TRPV4 and mitoCMX in the middle, periphery and all the random ROIs. Student's t-test, p values: ** = < 0.01, **** = <0.0001, ns = non-significant. (Published figure, Acharya TK. et al. 2023, *Life Sciences*).

Further, results show that the amount of mitochondria is also more in the peripheral region of the T cells than the middle regions (**Fig. 73B, D**). The ratio of TRPV4/mitoCMX is slightly high in the peripheral region than the middle region (though the values remain non-significant) (**Fig. 73B, E**).

Next, we tested the chances of TRPV4 in the mitochondria. For that, we analyze the correlation values of TRPV4 and mitoCMX in the middle, periphery and all the random positions. For that, we selected ROIs from different regions (**Fig. 73F-H**). In case of middle region of the T cells, the R-value is 0.5038 with lesser amount of TRPV4 and mitochondria (**Fig. 73F**). In the periphery region, the R-value increases to 0.77, suggesting the chances of TRPV4 to be in the mitochondria increases in the periphery (**Fig. 73G**). This similar pattern was observed in case of random ROI's from each cell (R = 0.78) (**Fig. 73H**). In all cases, we observed a positive correlation and a positive slope, suggesting the presence of TRPV4 is expected to be more where mitochondria are present.

2.6.3 TRPV4 regulates basal cytosolic and mitochondrial Ca^{2+}-load in T cells:

We aim to determine if and how TRPV4 modulation simultaneously affects cytosolic and mitochondrial Ca^{2+}-levels in T cells. For this purpose, we labelled both resting and TCR-beads treated (12 hours) T cells with Fluo-4-AM and Rhod-2-AM and TRPV4 modulation was performed for 1 hour (**Fig. 74 A, D**). In case of cytosolic Ca^{2+}, both 4αPDD and RN1734 treatment shows no changes in resting T cells (**Fig. 74B**). For T cells treated with TCR for 12 hours, the basal cytosolic Ca^{2+}-load become significantly lesser than resting T cells. Also, in TCR-beads treated cells, inhibition of TRPV4 leads to an increase in the cytosolic $Ca^{2+,}$ whereas activation has no significant changes in cytosolic Ca^{2+}-levels (**Fig. 74C**). This data may suggest that blocking of TRPV4 function by RN1734 may compromise the cytosolic Ca^{2+}-buffering by intracellular

organelles. For resting T cells, both activation and inhibition of TRPV4 results in no changes in levels of mitochondrial Ca^{2+} (**Fig. 74E**).

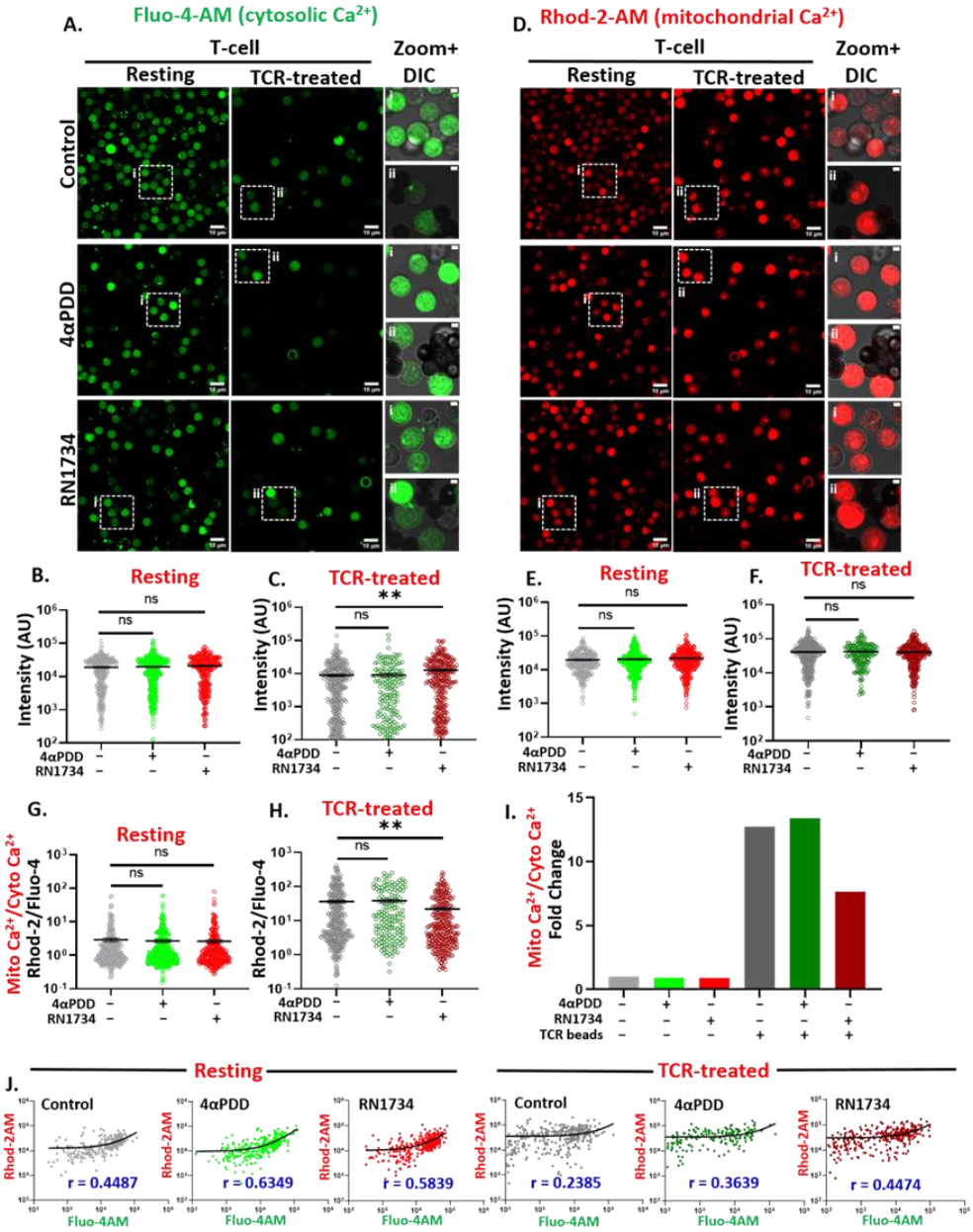


Fig. 74: TRPV4 regulates the basal cytosolic and mitochondrial Ca^{2+}-levels in T-cells. A. Resting and TCR-bead treated (12 hours) T cells were labelled with Fluo-4-AM for the detection of cytosolic Ca^{2+} in the presence of TRPV4 modulators. **B-C.** Quantification of Fluo-4-AM intensity from resting and TCR-bead treated cells (more than 100 cells) is shown. **D-F.** Resting and TCR-bead treated (12 hours) T cells were labelled with Rhod-2-AM for mitochondrial Ca^{2+}-measurement in the presence of TRPV4 modulators. TCR-bead treated cells have higher mitochondrial Ca^{2+}-load as compared to resting cells (≥100 cells were quantified). **G-H**. The ratio of mitochondrial Ca^{2+} to cytosolic Ca^{2+} at individual T cells was measured. **I.** The fold-change in the mito/cyto Ca^{2+} between resting and TCR-bead treated cells were

plotted. TCR-bead treated cells have ~10 fold or more mito/cyto Ca^{2+} as compared to resting T cells. **J.** Analysis of the correlation between cytosolic Ca^{2+} and mitochondrial Ca^{2+} in both resting and TCR-bead treated cells are shown. One-way ANOVA, p values: ** = < 0.01, ns = non-significant. (Published figure, Acharya TK. et al. 2023, *Life Sciences*).

The basal mitochondrial Ca^{2+}-level increases in the TCR-beads treated cells as compared to resting T cells, suggesting that overloading of mitochondrial Ca^{2+} (~2 fold) is an important step towards the T cell activation. Also, 4αPDD and RN1734 cause no changes in the mitochondria Ca^{2+}-levels in TCR-beads treated cells (**Fig. 74F**). We next quantified the ratio of mitochondrial Ca^{2+} to cytosolic Ca^{2+} at individual T cells. Resting T cells show no effect on the ratio of mito/cyto Ca^{2+} by TRPV4 modulation and the values match well with the control group (**Fig. 74G**). However, in TCR-beads treated T cells, the mito/cyto Ca^{2+} ratio decreases significantly in RN1734-treated cells suggesting that TRPV4 inhibition prevents Ca^{2+}-entry to intracellular organelles such as in the mitochondria though cytosolic Ca^{2+}-level is increased (**Fig. 74H**). Also, the mito/cyto Ca^{2+} ratio increases several folds (~10 fold or more) in TCR-beads treated cells as compared to resting the T cells and inhibiting TRPV4 reduces this fold change by almost half (**Fig. 74I**). This data suggests that during TCR-beads mediated T cell activation process, spontaneous activity of TRPV4 is relevant as blocking of TRPV4 function by RN173 reduces the Mito Ca^{2+}/Cyto Ca^{2+} ratios.

Next, we evaluated if the cellular and mitochondrial Ca^{2+} are correlated and if TRPV4 modulation affects this correlation. For resting T cells, the mitochondrial and cellular Ca^{2+} are moderately correlated (R= 0.4487), and this correlation increases with both activation (R= 0.6349) and inhibition (R = 0.5839) of TRPV4 (**Fig. 74J**). In TCR-beads treated T cells, irrespective of any condition, the correlation is always lesser than resting T cells. However, in TCR-bead treated T cells, the correlation of mitochondrial Ca^{2+} to cytosolic Ca^{2+} reduces greatly (**Fig. 74J**). In TCR-beads treated cells, both 4αPDD and RN1734 cause an increment in the correlation value than the

control condition (**Fig. 74J**). Overall, the result indicates that TRPV4 affects the cellular and mitochondrial Ca^{2+}-status differently, as well as their relative ratio and dependency. Data also suggest that during the T cell activation process, apparently TCR-signaling become predominant over TRPV4 modulation.

2.6.4 TRPV4 activation causes instantaneous Ca^{2+}-influx in primary murine T-cells:

To check the effects of TRPV4 activation on cellular Ca^{2+}-status instantaneously, we performed live cell Ca^{2+}-imaging for 400 frames (~07 min) using intracellular Ca^{2+}-sensor Fluo-4-AM. Due to the floating nature of T-cells, tracking of Ca^{2+}-signal as time kinetics in individual cells was not possible. Therefore, we quantified the Ca^{2+}-intensity of the cell population before (Frame-1) and after (Frame-400; ~7 minutes) addition of drug (at Frame-20) (**Fig. 75A).** Addition of 4αPDD (5 μM) causes a rise in intracellular Ca^{2+}-level (**Fig. 75B**). Next, we investigated the effects of activation of TRPV4 in Ca^{2+}-chelated conditions. Chelation of extra-cellular, intra-cellular and ER Ca^{2+} was performed by using EGTA, BAPTA-AM and Thapsigargin, respectively. In EGTA pre-treated cells, the addition of 4αPDD results in no significant changes in intra-cellular Ca^{2+}-levels. However, in BAPTA-AM and Thapsigargin pre-treated cells, 4αPDD addition elevates the cellular Ca^{2+} significantly (**Fig. 75C-E**). Further, we used TCR-bead treated T cells to understand the effect of TRPV4 activation. TRPV4 activation in TCR-bead treated T cells results in a steep rise in the cellular Ca^{2+}-level as indicated by more Flou-4-AM intensity (**Fig. 75F**). We also quantified the basal Ca^{2+}-level (Frame-01; before addition of 4αPDD) in the above conditions (**Fig. 75G**). In EGTA-treated cells, the level of intra-cellular Ca^{2+} reduces non-significantly, but BAPTA-AM treatment reduces the cellular Ca^{2+} to a great extent (**Fig. 75G**). In case of both TCR-bead treated T cells and ER Ca^{2+}-chelated condition (Thapsigargin), the basal

cellular Ca^{2+} increases. Treatment of 4αPDD elevates the cellular Ca^{2+} in each condition (**Fig. 75H**).

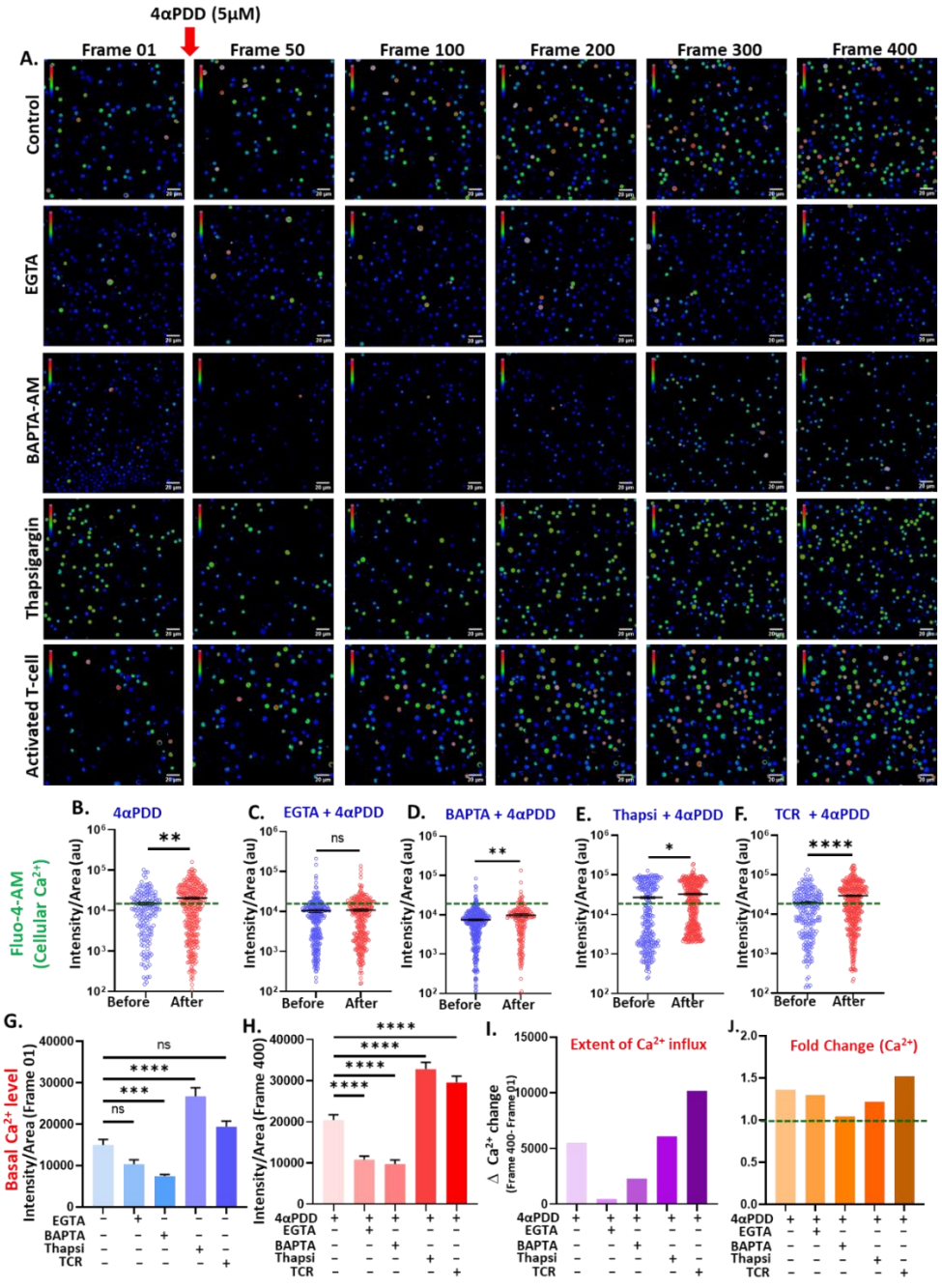


Fig. 75. TRPV4 activation increases cytosolic Ca^{2+}-influx instantly in murine $CD3^+$ T-cells. A. Representative images of different time frames acquired during time-lapse imaging of T-cells loaded with Fluo-4-AM are shown. The Ca^{2+}-intensity is represented in a rainbow scale for better visualisation. T-cells were pre-incubated with BAPTA-AM (5μM), EGTA (5 μM) and Thapsigargin (1 μM) for 1 hour and with TCR-beads for 12 hours where indicated. Scale bar 20 μm. **B-F**. Quantification of Fluo-4-AM fluorescence intensities from frame 01 (before drug addition) and frame-400 (after drug addition) in each condition are

shown. **G-H**. Basal Ca^{2+}-levels in frame 01 and frame-400 were quantified and plotted (≥100 cells in each condition). **I**. Delta change in Ca^{2+}-intensity (Intensity at Frame 400 – Frame 01) in each conditions were plotted. **J**. Fold-change values were measured. TCR-bead treated cells have the highest fold-change in Ca^{2+}, as observed. Student's t-test. p values: * = <0.05, ** = < 0.01, *** = <0.001, **** = <0.0001, ns = non-significant. (Published figure, Acharya TK. et al. 2023, *Life Sciences*).

To understand the dependency of TRPV4-mediated increase in cellular Ca^{2+} on various Ca^{2+} sources, we determined the extent of Ca^{2+}-influx in each condition (Intensity at Frame 400 – Frame 01) (**Fig. 75I**). Interestingly, in case of both EGTA or BAPTA-AM pre-treatment, the basal Ca^{2+}-load is less and change in Ca^{2+}-level after activation is less when compared to only 4αPDD treatment. However, in EGTA-pretreated condition, almost no or slight change in Ca^{2+}-level occurs upon 4αPDD addition, suggesting the high dependency of TRPV4 on extracellular Ca^{2+} for the increment of cytosolic Ca^{2+}-level. Further, in Thapsigargin pre-treated cells, the extent of Ca^{2+}-influx is similar to that of only 4αPDD, indicating that TRPV4-mediated increase in cellular Ca^{2+} are mostly independent of Ca^{2+}-mobilization from ER. In case of TCR-bead treated T cells, the extent of Ca^{2+} is the highest. This depicts that TRPV4 activity goes up in case of TCR-bead treated T cells. This is also seen when the "fold change" in Ca^{2+}-levels upon 4αPDD addition was calculated (**Fig. 75J**). In TCR-bead treated cells, the fold-change in Ca^{2+} become highest, suggesting enhancement in TRPV4 activity in presence of TCR-beads. Taken together, the data suggests that TRPV4 activation causes instant increase in cellular Ca^{2+}, which is dependent greatly on extra-cellular Ca^{2+}-source and presence of TCR-beads.

2.6.5 Activation of TRPV4 causes instant increase in mitochondrial Ca^{2+} amount:

Cellular Ca^{2+}-levels are critical regulators of the mitochondrial Ca^{2+}-status (Finkel T, 2015). Moreover, recently we have shown the presence of TRPV4 on mitochondria where it regulates mitochondrial Ca^{2+}-levels (Acharya TK, 2022a). Therefore, using Rhod-2-AM dye, we

evaluated the effects of TRPV4 activation on mitochondrial Ca^{2+}-levels. An increase in the Rhod-2-AM intensity corresponds to the increase in the mitochondrial Ca^{2+}-level. We performed live cell mitochondrial-Ca^{2+} imaging for 400 frames (~7 mins) and added 4αPDD (5 μM) at the 20th frame of imaging. **Fig. 76** represents the representative confocal images of the time series imaging. Addition of 4αPDD causes an instant rise in the mitochondrial Ca^{2+} (**Fig. 76, 77A, B**). Further, we pre-treated the T cells with either EGTA, BAPTA-AM or Thapsigargin for 1 hour. In each of these Ca^{2+}-chelated conditions, TRPV4 activation results in an increase in the mitochondrial Ca^{2+}-level (**Fig. 76, 77B**). For the TCR-treated T cells also, 4αPDD addition increases the mitochondrial Ca^{2+} (**Fig. 76, 77B**). Furthermore, we evaluated the basal mitochondrial Ca^{2+}-levels (as indicated by intensity of Frame 01) in different condition (**Fig. 77C**). EGTA addition does not affect the mitochondrial Ca^{2+}-level significantly; however, depleting intra-cellular Ca^{2+} by BAPTA-AM reduces the mitochondrial Ca^{2+}. In case of both TCR-bead treated T cells and Thapsigargin, the cells have significantly higher amount of mitochondrial Ca^{2+} as compared to the control condition. 4αPDD treatment shows more mitochondrial Ca^{2+} in each of the above mentioned conditions as depicted by the fluorescence intensity at Frame-400 (**Fig. 77D**). In order to evaluate the dependency of TRPV4-induced mitochondrial Ca^{2+} increment, we determined the extent of change in Ca^{2+}-influx in each condition (Intensity Frame 400 – Frame 01) (**Fig. 77E**). Depleting either extra-cellular, intra-cellular or ER Ca^{2+} resulted in lesser mitochondrial Ca^{2+}-influx suggesting the dependency of TRPV4 in all these Ca^{2+}-reservoirs (extracellular, intracellular and ER) to bring about increase in mitochondrial Ca^{2+}. Interestingly, for mitochondrial Ca^{2+} also, TCR-bead treated T cells have more Ca^{2+} rise than resting T cells. The "fold-change" in Ca^{2+}-levels is almost similar in most of the conditions although slightly lesser for EGTA and Thapsigargin-treated cells (**Fig. 77F**).

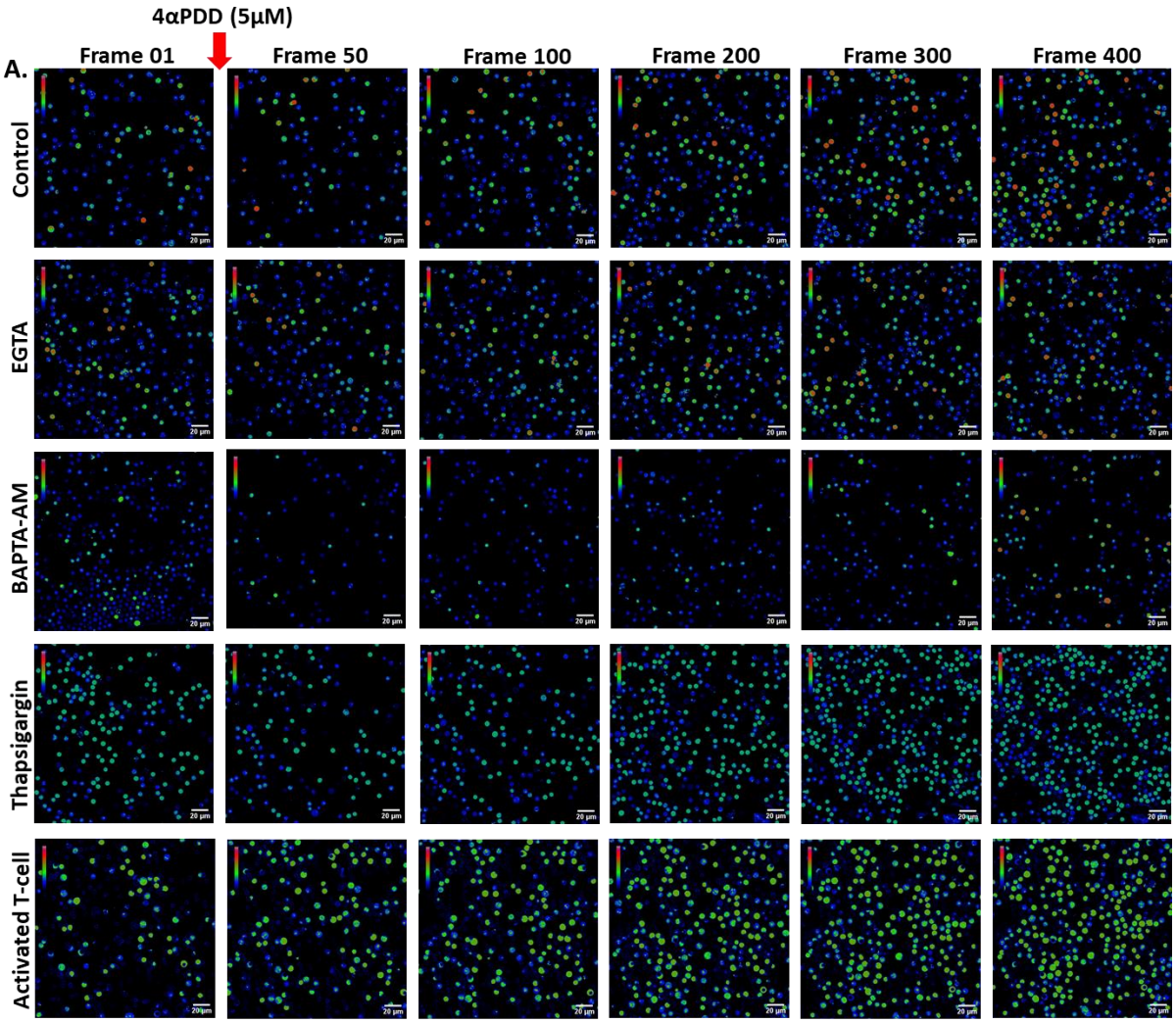


Fig. 76. TRPV4 activation cause instant mitochondrial Ca^{2+}-influx in murine $CD3^{+}$ T-cells. A. Representative images of different time frames acquired during time-lapse imaging of T-cells loaded with Rhod-2-AM are shown. The Ca^{2+}-intensity is represented in a rainbow scale for better visualisation (red and blue indicate high and low cytosolic $Ca^{2+,}$ respectively). Where indicated, T-cells were pre-incubated with BAPTA-AM (5 μM), EGTA (5 μM) and Thapsigargin (1 μM) for 1 hour and TCR-beads for 12 hours. Scale bar 20 μm. (Published figure, Acharya TK. et al. 2023, *Life Sciences*).

Next, we checked whether TRPV4 modulation changes the ratio of mito-cyto Ca^{2+} instantly (**Fig. 77G**). The basal level of mito/cyto Ca^{2+} remains almost unchanged in EGTA and BAPTA-AM treated cells where Thapsigargin and TCR-beads cause a significant (~2.48 and

~2.53 folds, respectively) rise in the ratio of mito-cyto Ca^{2+} suggesting the impaired Ca^{2+}-buffering which is due to either more mitochondrial Ca^{2+} or lesser cytosolic Ca^{2+}.

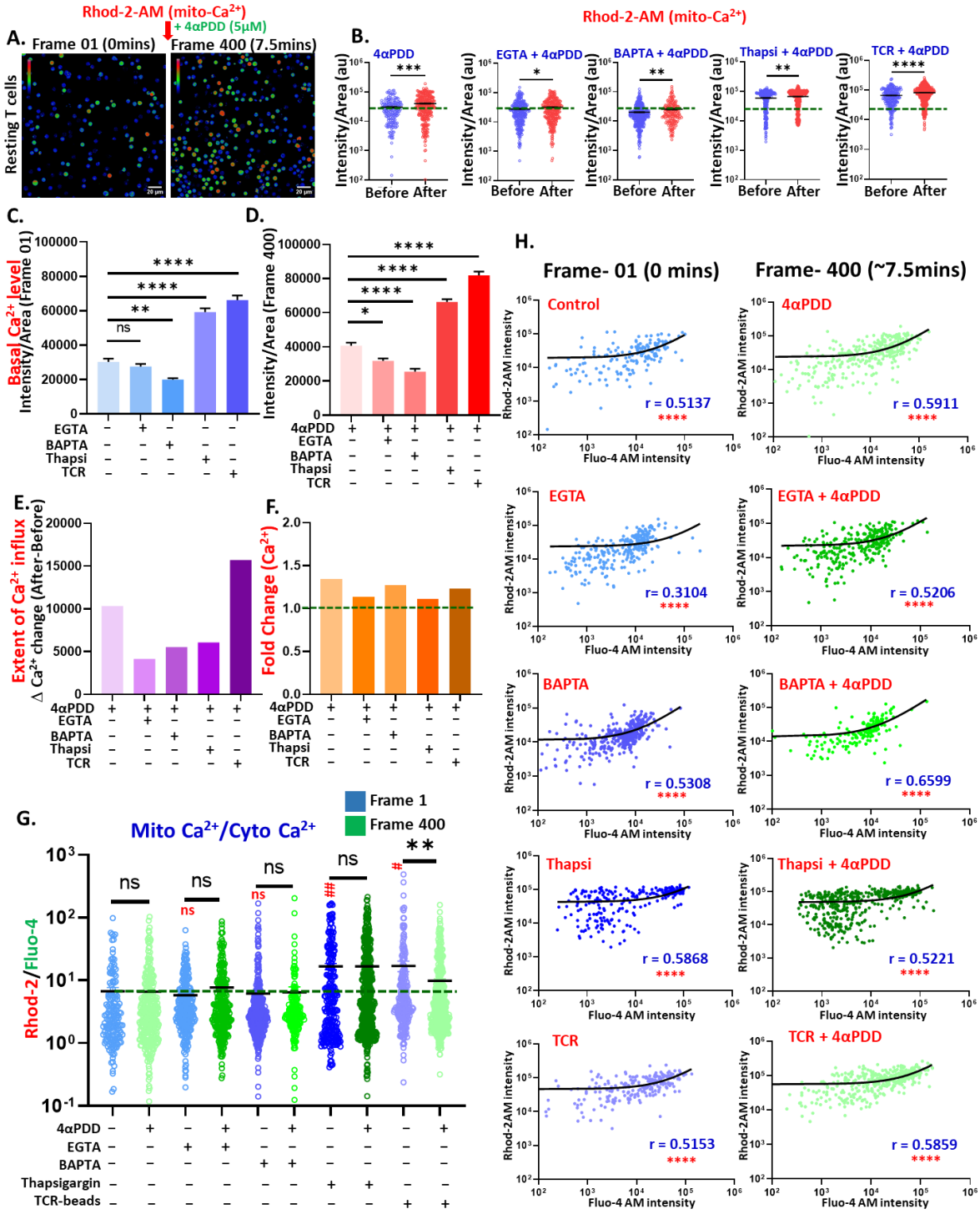


Fig. 77. TRPV4 activation increases mitochondrial Ca^{2+}-influx in murine $CD3^+$ T-cells. A. Representative Images of the time lapse imaging of T-cells loaded with Rhod-2-AM activated by 4αPDD

at 20th frame are shown. **B.** Quantification of Rhod-2-AM fluorescence intensities from frame 01 (before drug addition) and frame-400 (after drug addition) in each condition are shown. Student's t-test. p values: * = <0.05, ** = < 0.01, *** = <0.001, **** = <0.0001, ns = non-significant. **C-D**. Basal Ca^{2+}-level in frame 01 and frame-400 were quantified and plotted (≥100 cells in each condition). **E**. Delta change in Ca^{2+}-intensity (Intensity at Frame 400 – Frame 01) in each condition was plotted. **F**. Fold change values were measured. TCR-bead treated cells have highest fold change in Ca^{2+} as observed. **G.** Ratio of changes in mito-cyto Ca^{2+} instantaneously by TRPV4 modulation in different experimental conditions were plotted. **H.** Correlation of cyto-mito Ca^{2+} at Frame 1 and Frame 400 (after 4αPDD addition) are calculated and plotted. This correlation signifies the dependency of mitochondrial Ca^{2+} on cytosolic Ca^{2+}. # symbol indicates the comparison of that group with resting control that are significntly different (Student's t-test, ## = < 0.01, #### = <0.0001, ns = non-significant). (Published figure, Acharya TK. et al. 2023, *Life Sciences*).

4αPDD addition shows no changes in the mito/cyto Ca^{2+} in each of the treated condition except in presence of TCR-beads where 4αPDD treatment decreases the ratio of mito-cyto Ca^{2+}. Thus TRPV4 causes more cytosolic Ca^{2+}-influx than mitochondrial in TCR-treated cells. The dependency of mitochondrial Ca^{2+}-influx on cytosolic Ca^{2+}-levels were tested and thus correlation of cyto-mito Ca^{2+} for Frame 1 and Frame 400 (after 4αPDD addition) were analyzed. In resting T cells, the mitochondrial and cytosolic Ca^{2+} are moderately correlated (R= 0.5137) (**Fig. 77H upper panel**). 4αPDD-treatment increases the dependency of mitochondrial Ca^{2+} on cytosolic Ca^{2+} than control cells (**Fig. 77H**). However, in EGTA-treated cells, the mito-cyto Ca^{2+}-dependency is reduced (R= 0.3104) but is restored by 4αPDD addition to cells (R= 0.5206) (**Fig. 77H**). In case of intra-cellular Ca^{2+}-chelated condition (BAPTA-AM), the mito-cyto Ca^{2+} -dependency slightly increases (R=0.5308) than the resting T cells, and 4αPDD makes this dependency even higher (R= 0.6599) (**Fig. 77H**). ER, Ca^{2+}-chelation increases the dependency further (R= 0.5868); however, this is the only condition where 4αPDD addition decrease the dependency of mito Ca^{2+} on cyto-Ca^{2+} (R= 0.5221) (**Fig. 77H**). The addition of TCR-beads does not change the correlation much (R= 0.5153) than resting T cells. However, 4αPDD here also increases the correlation of mito-cyto Ca^{2+}-level (R= 0.5859) (**Fig. 77H**). All in all, the data shows that TRPV4 activation elevates mitochondrial Ca^{2+}-instantly and this event is partially dependent on all the three Ca^{2+}-sources

(i.e. extra cellular, intra cellular and ER) of the T cells also this mitochondrial Ca^{2+}-influx is correlated with cytosolic Ca^{2+}-influx.

2.6.6 Mitochondrial superoxide and mitochondrial membrane potential are affected by TRPV4 in resting and in TCR treated T cells:

Mitochondria are one of the major sources of ROS. Although ROS is harmful for the cell, but certain amount of ROS is required for various processes, particularly in immune cells. Large amount of ROS are produced for phagocytosis and it also guides T cell development (Case AJ, 2011) and activation (Belikov AV, 2015). To understand the significance of TRPV4 in mitochondrial ROS production in primary murine T cells, MitoSOXRed dye (which increases its intensity with an increase in mitochondrial superoxide levels) is used (**Fig. 78A**). In resting T cells, addition of 4αPDD shows no significant change in the superoxide level, but inhibiting TRPV4 by RN1734 results in more intensity or mitochondrial superoxide level (**Fig. 78B**). This TRPV4-mediated changes in mitochondrial superoxide levels are only seen in resting T cells but not in TCR-bead treated T cells. In case of TCR-bead treated T cells, although the basal levels of superoxide is significantly more as compared to resting T cells, but further activation or inhibition of TRPV4 cause no changes in the level of mitochondrial superoxide formation (**Fig. 78C**). Also, the level of mitochondrial superoxide by RN1734 treatment in resting T cells is similar to the levels in TCR-treated T cells. All in all, TRPV4 modulation affects the mitochondrial superoxide levels only in resting T cells, where inhibition of TRPV4 increases the mitochondrial superoxide levels that become comparable to TCR-bead treated T cells.

Mitochondrial membrane potential indicates the mitochondrial status and activity. It is related directly to the electron transport chain and oxidative phosphorylation (Lee YX, 2019) which in turn are affected by TRPV4 (Acharya TK, 2022a). Thus, we tested if TRPV4 affects the

mitochondrial status in resting and TCR-bead treated T cells using ratiometric JC-1 dye (**Fig. 78D**).

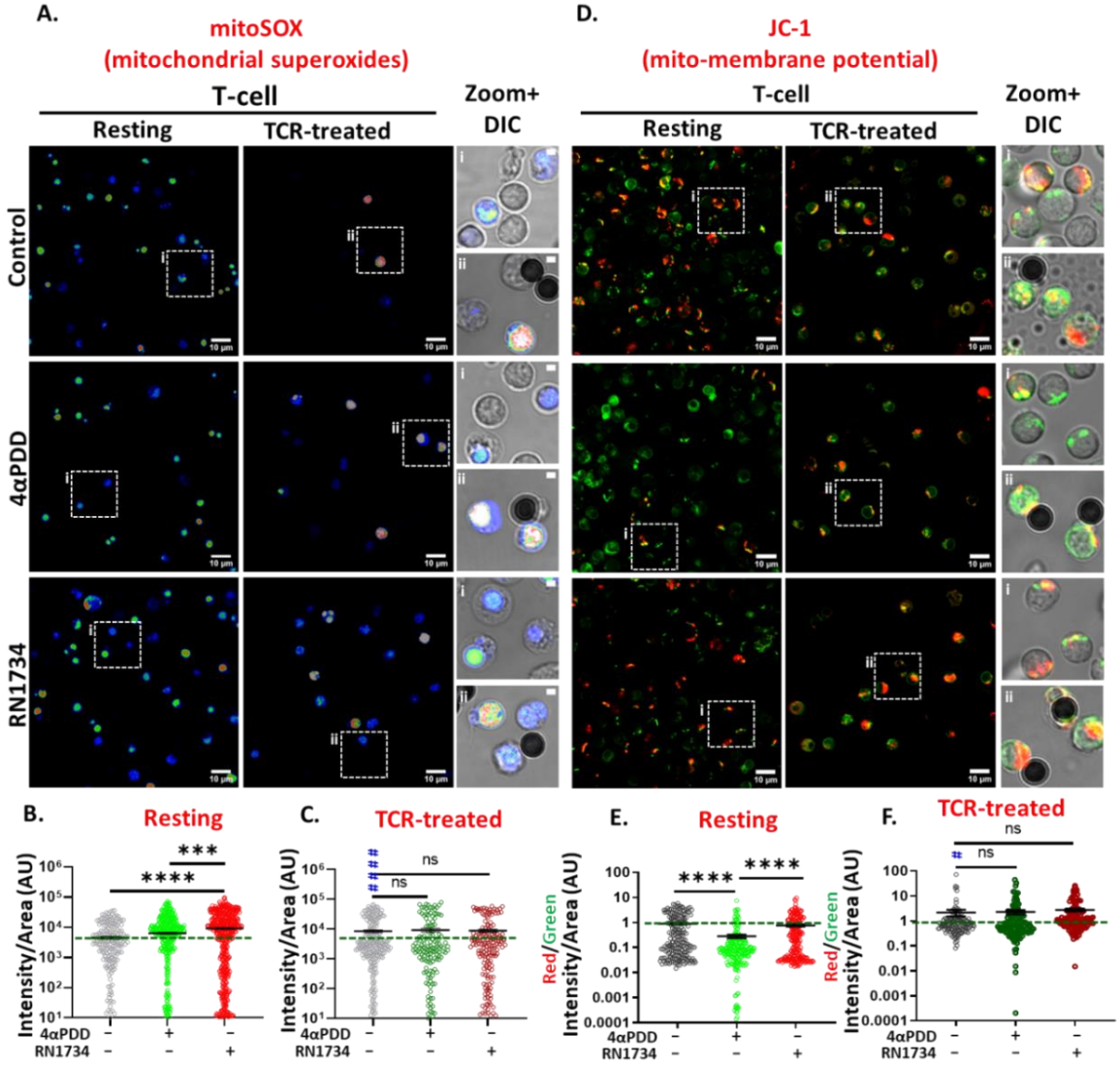


Fig. 78. TRPV4 regulates mitochondrial ROS and membrane potential. A. Resting and TCR-bead treated $CD3^+$ T cells were treated with TRPV4 agonist 4αPDD (5 µM) and TRPV4 antagonist RN1734 (10 µM). **B-C.** Both resting and TCR-bead treated cells were treated with different TRPV4 modulators and subsequently stained with MitoSOX red (2.5 µM) for detection of mitochondrial ROS. Scale bar is 10 µm. **D.** Both resting and TCR-bead treated cells were treated with TRPV4 modulators and subsequently stained with JC1 dye (5 µM). In resting T cells, TRPV4 agonist decreases the membrane potential, whereas in TCR-bead treated cells, the membrane potential increases in all conditions. Scale bar: 10µm. **E-F.** Quantification of fluorescence intensities of MitoSOX and JC1 in resting and TCR-bead treated cells. (n ≥100 cells in each condition were quantified, One way ANOVA, * = $p<0.05$, *** = $p<0.001$, **** = $p<0.0001$). # symbol indicates the comparison between resting control and TCR-bead control condition (Student's t-test, # = $p<0.05$, #### = $p<0.0001$, ns = non-significant). (Published figure, Acharya TK. et al. 2023, *Life Sciences*).

In resting T cells, a decrease in red/green intensity of JC-1 is seen upon activation of TRPV4 by 4αPDD which corresponds to the decrease in mitochondrial membrane potential whereas inhibition of TRPV4 using RN1734 shows no effect on the mitochondrial potential (**Fig. 78E**). Interestingly, this TRPV4-dependent changes in the mitochondrial membrane potential are seen only in resting T cells. Upon addition of TCR-beads, an increase in the basal mitochondrial membrane potential occurs (**Fig. 78F**). But, both activation and inhibition of TRPV4 show no effects in the mitochondrial potential (**Fig. 78F**). Thus, TRPV4 modulation affects the mitochondrial membrane potential only in resting T cells and effect of TRPV4 become redundant in the TCR-treated T cells.

2.6.7 TRPV4 activation affects mitochondrial ATP production and Cardiolipin status differently in resting and in TCR- treated T cells:

Mitochondrial ATP production is crucial to support the specific cellular needs, especially for immune cells to achieve their activity as well as for T cell activation. If TRPV4 has any role in ATP production in T cells that was evaluated by using the ATP-Red dye (**Fig. 79A**). An increase in the fluorescence intensity corresponds to an increase in the ATP levels. In resting T cells, the addition of agonist 4αPDD causes a decrease in the intensity (i.e. decrease in the mitochondrial ATP production), and RN1734 shows no effects on the ATP levels (**Fig. 79B**). Further, the dependency of the ATP levels on TRPV4 in TCR-bead treated T cells was examined. In TCR-bead treated T cells, the basal ATP levels increase (1.33 fold) non-significantly than the resting T cells (**Fig. 79C**). Contrary to unstimulated T cells, 4αPDD addition further increases the intensity or the ATP levels. RN1734 doesn't affect the ATP levels in the TCR-bead treated T cells as compared to the control condition (**Fig. 79C**). Thus, TRPV4 activation regulates the mitochondrial

ATP production differently in a context dependent manner, i.e. in resting and TCR-bead treated T cells.

Cardiolipins are the inner mitochondrial membrane lipids which govern various mitochondrial aspects (Paradies G, 2019). Recently, TRPV1 as a molecular regulator of the Cardiolipin levels has been reported (Chakraborty R, 2022). We used NAO dye to test whether TRPV4 affects the Cardiolipin levels in primary T cells (**Fig. 79D**).

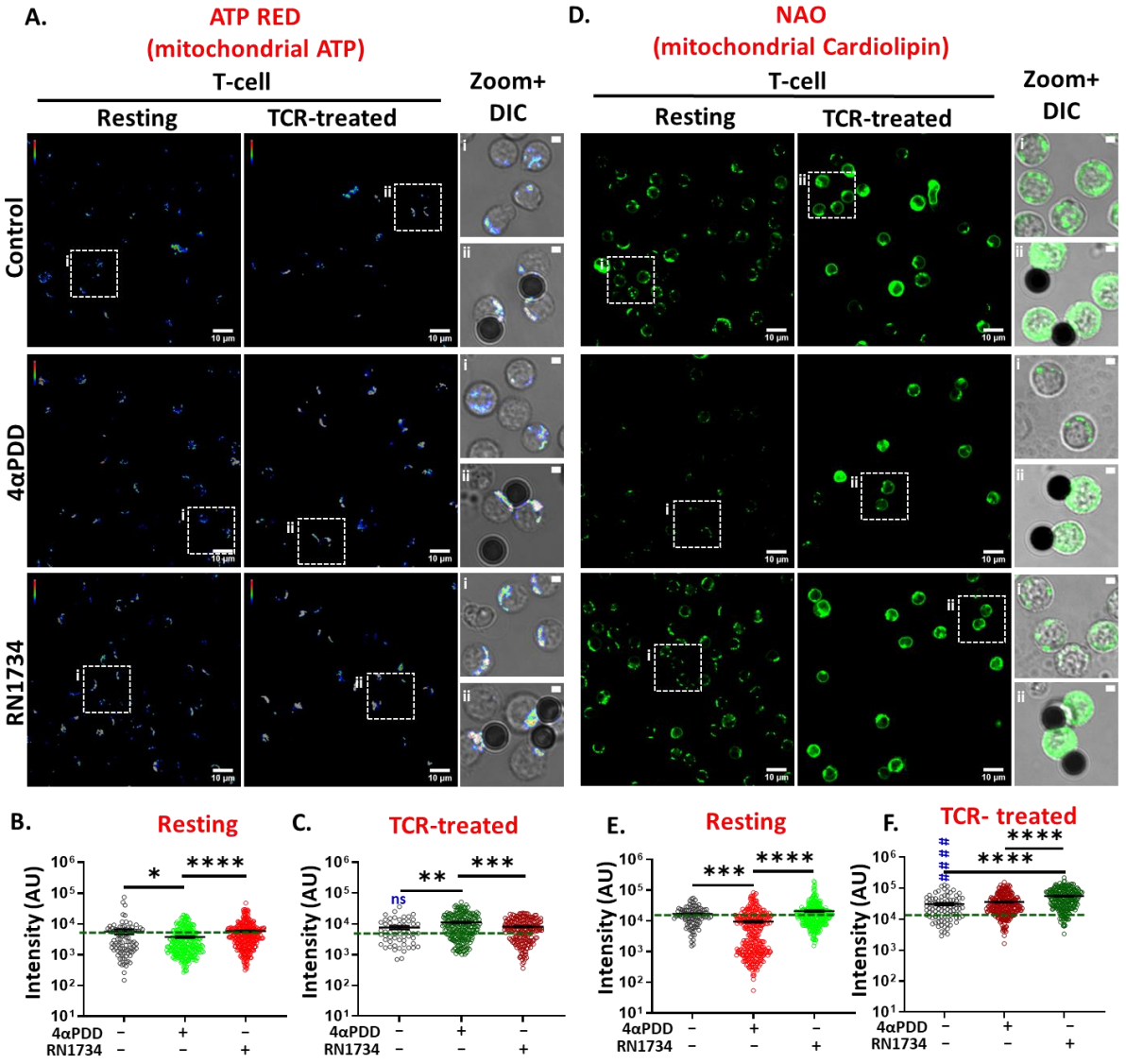


Fig. 79. TRPV4 regulates mitochondrial ATP and Cardiolipin levels. A-C. Murine $CD3^+$ T cells at resting and TCR-bead treated conditions were also treated with TRPV4 agonist 4αPDD (5 μM) or antagonist RN1734 (10 μM). The mitochondrial ATP level was measured by using ATP red dye (5 μM).

ATP level is high in TCR-bead treated cells as compared to resting cells. Scale bar: 10μm. (n ≥100 cells in each condition were quantified). **D-F.** Both resting and TCR-bead treated T-cells were treated with TRPV4 agonist 4αPDD (5 μM) and antagonist RN1734 (10 μM). The mitochondrial Cardiolipin was measured by using NAO (5 μM). The Cardiolipin level elevates in TCR-bead treated cells. Scale bar is 10μm. (n ≥100 cells in each condition were quantified). One way ANOVA, * = p<0.05, ** = p<0.01, *** = p<0.001, **** = p<0.0001, ns = non-significant). # symbol indicates the comparison between resting control and TCR control condition (Student's t-test, ns = non-significant, #### = p<0.0001). (Published figure, Acharya TK. et al. 2023, *Life Sciences*).

In resting T cells, 4αPDD treatment causes slight decrease in the Cardiolipin levels (**Fig. 79E**). No effect of RN1734 is observed (**Fig. 79E**). Cardiolipin levels in TCR-bead treated T cells were also analyzed. Firstly, the NAO intensity increases, indicating that Cardiolipin levels increase in TCR-bead treated T cells (**Fig. 79F**). Also, 4αPDD treatment causes no effect in the Cardiolipin levels whereas antagonist RN1734 leads to an increment in the Cardiolipin levels (**Fig. 79F**). Our data suggests that, dependency of Cardiolipin on TRPV4 in primary T cells changes based on resting or TCR-bead treated T cells. In resting condition, activation of the TRPV4 causes either less Caridiolipin formation and/or enhancers Cardiolipin degradation. In TCR-bead treated condition, endogenous activity of TRPV4 is enhanced, which either prevents Cardiolipin formation and/or enhancers Cardiolipin degradation. As a result, and thus RN1734 treatment increases the Cardiolipin levels in TCR-bead treated conditions.

2.6.8 Mitochondrial and ER temperature of T cells is affected by TRPV4 modulation:

Next, we evaluated if TRPV4 modulation affects the ER-temperature and thus, ETY dye (which increases intensity with decrease in ER temperature) was used (**Fig. 80A**). In resting T cells, TRPV4 activation does not affect the ER temperature, whereas inhibition of TRPV4 by RN1734 causes an increase in the ETY intensity, equivalent to the reduction in the ER temperature (**Fig. 80B**). Albeit, this TRPV4 inhibition-dependent reduction in ER temperature is not seen in case of TCR-bead treated T cells where antagonist RN1734 treatments has no effect on ER

temperature, but activation of TRPV4 leads to increase in ETY intensity (equivalent to reduction of the ER temperature) (**Fig. 80C**). Also, the basal ER temperature decreases in TCR-bead treated T cells. Therefore, based on the immunological status, whether resting or TCR-bead treated, TRPV4 regulates the ER temperature differently in primary murine T cells.

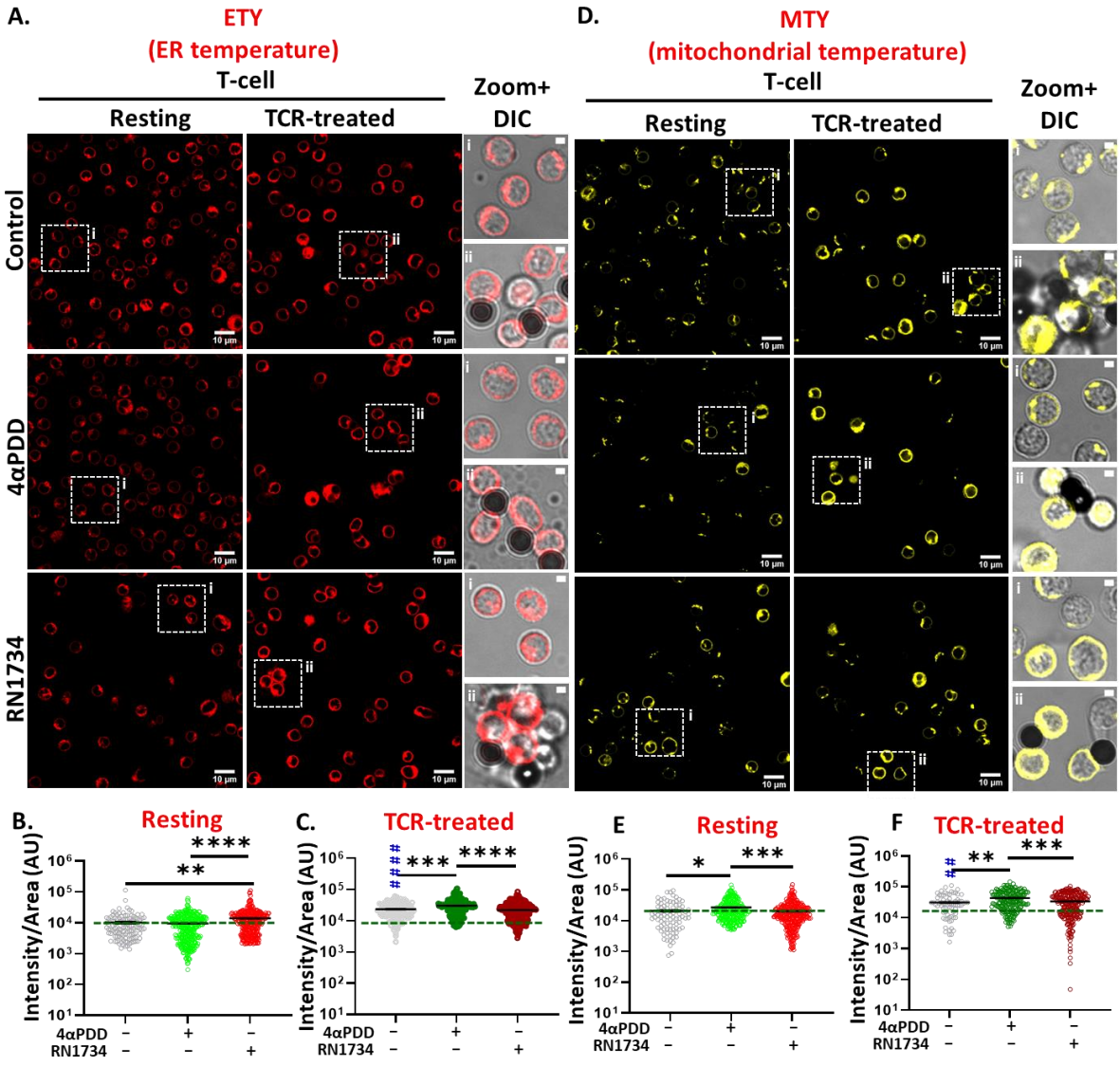


Fig. 80. TRPV4 regulates mitochondrial and ER-temperature. A-C. Both resting and TCR-bead treated cells were treated with different TRPV4 modulators and subsequently stained with ETY (0.5 µM). In resting T cells, the ER temperature does not change in 4αPDD-treated cell and the ER temperature decreases (increase in ETY intensity) in RN1734-treated cells. In TCR-bead treated cells, the ER-temperature is decreased (increase in temperature) in case of both agonist-antagonist treatments. Scale bar

10µm. **D-F.** Resting and TCR-bead treated murine $CD3^+$T cells were treated with TRPV4 agonist 4αPDD (5 µM) and TRPV4 antagonist RN1734 (10 µM). The mitochondrial temperature was measured by MTY (0.5 µM). In TCR-bead treated cells, the mitochondrial temperature decreased (increase in intensity). Scale bar 10µm. Fluorescence intensities of individual cells were represented in the graph (n ≥100 cells in each condition, One way ANOVA, * = $p<0.05$, ** = $p<0.01$, *** = $p<0.001$, **** = $p<0.0001$, ns = non-significant). The # symbol denotes the comparison between resting control and TCR-bead control condition (Student's t-test, ## = $p<0.01$, #### = $p<0.0001$, ns = non-significant). (Published figure, Acharya TK. et al. 2023, *Life Sciences*).

Elevated temperature is shown to help T cell responses in a mitochondria-dependent manner (O'Sullivan D, 2021). Recently it has been shown that mitochondrial temperature affects due to TRPV4 modulation. In order to determine if TRPV4 modulates mitochondrial temperature in primary T cells, we conducted an experiment utilising the mitochondrial thermo sensing dye MTY. (**Fig. 80D**). An increase in MTY intensity corresponds to the decrease in the mitochondrial temperature. In resting T cells, activation of TRPV4 by 4αPDD leads to an increase in MTY intensity or decrease in the mitochondrial temperature, whereas treatment with RN1734 has no effect (**Fig. 80E**). In TCR-bead treated T cells, the MTY intensity increases as compared to the control condition, suggesting that mitochondrial temperature decreases in the presence of TCR-beads (**Fig. 80F**). In TCR-bead treated T cells, MTY intensity increases due to activation of TRPV4, but remains unchanged in case of RN1734 treatment (**Fig. 80F**). Overall, our data suggests that activation of TRPV4 leads to a decrease in the mitochondrial temperature in T cells irrespective of their immunological status.

2.6.9 TRPV4 modulation regulates the ER number, mitochondrial number and their co-localization in primary T cells:

It is shown that TRPV4 activation leads to Ca^{2+}-influx in primary T cells. ER-mito contact points are crucial in maintaining the Ca^{2+}-levels inside the cell. Also, recently we have reported that TRPV4 regulates the ER-mito contact points (Acharya TK, 2022b). We quantified the

mitochondrial number, ER number and ER-mito colocalized points using a particle-based quantification approach (**Fig. 81A-B**).

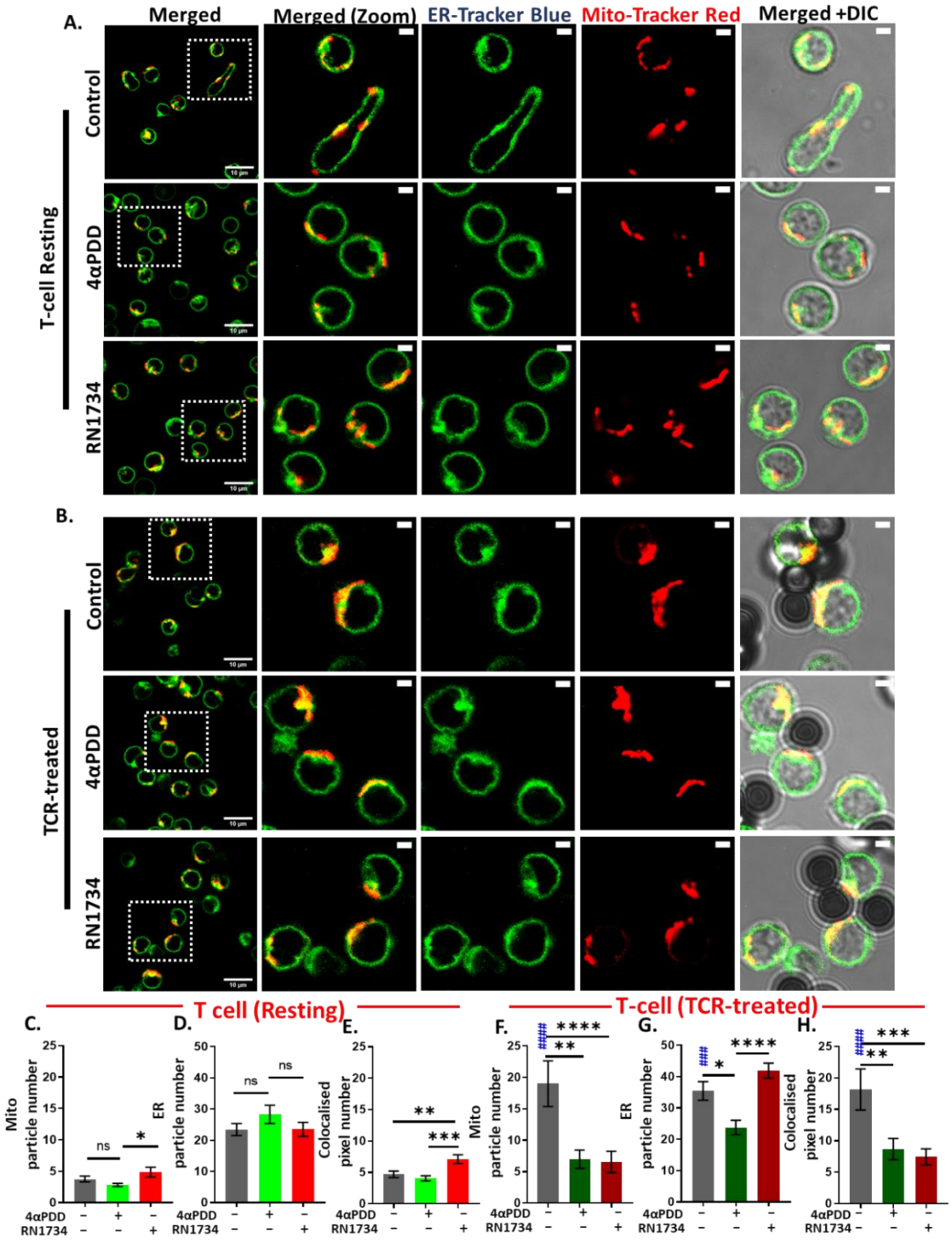


Fig. 81. TRPV4 regulates ER-mito contact sites. Resting and TCR-bead treated CD3^{+}T cells were treated with 4αPDD (5 µM) or RN1734 (10 µM) and were labelled by mitoCMXros (0.5 µM) and ER-tracker blue

(0.5 μM). **A-B.** Representative confocal images of ER-mito contact points in resting and TCR-bead treated cells**. C-E.** The total mitochondrial, total ER and colocalized particles were quantified by ImageJ. In resting T cells, the number of mitochondrial particles increased in RN1734-treated condition and the ER-particles remain unchanged in both 4αPDD and RN1734-treated condition. The total colocalized particle number is increased at the RN1734-treated cells. Scale bar 2μm. **F-H.** In TCR-bead treated cells, both mitochondrial and ER-particle numbers increase as compared to resting T cells. In this condition, the colocalized particle number decreased significantly in both 4αPDD and RN1734 treated cells. Scale bar 2μm. (n ≥30 cells in each condition were quantified). ER–Tracker blue is represented in pseudocolor green in all the representative images. One way ANOVA, * = $p<0.05$, ** = $p<0.01$, *** = $p<0.001$, **** = $p<0.0001$). The # symbol indicates the comparison between resting control and TCR-bead control condition (Student's t-test, ### = $p<0.001$, #### = $p<0.0001$, ns = non-significant). (Published figure, Acharya TK. et al. 2023, *Life Sciences*).

In case of resting T cells, activation of TRPV4 by 4αPDD shows no changes in the mitochondrial numbers, ER numbers, nor in colocalized points (**Fig. 81C-E**). RN1734 treatment increases the mitochondria numbers, which also leads to an increment in ER-mito colocalization points (**Fig. 81C-E**).

Similar analysis for TCR-bead treated T cells reveals that the particle numbers for mitochondria and ER are significantly more in the control condition (**Fig. 81F-G**). This accords with the rise in ER-mito colocalization in control TCR-bead-treated T cells. (**Fig. 81H**). Further, treating the TCR-bead treated T cells with agonist 4αPDD shows a reduction of ER and mitochondrial particle numbers (**Fig. 81F-G**). Notably, RN1734 application in TCR-bead treated T cells also lead to a decrease in the mitochondrial number but does not change the ER number significantly (**Fig. 81F, G**). Also, both activation and inhibition of TRPV4 leads to a notable decrease in the ER-mito colocalization (**Fig. 81H**). Thus, our data shows that TRPV4 modulation regulates both mitochondria and ER number in T cells, which further affects the ER-mito contact points.

Summary: The T cell activation process is critically affected by temperature and intracellular Ca^{2+}-signaling. Yet, the nature and the key molecules involved in such complex Ca^{2+}-signalling is poorly understood. It is mostly assumed that ion channels present in the plasma membrane primarily regulate the cytosolic Ca^{2+}-levels exclusively. TRPV4, a non-selective Ca^{2+} channel, endogenously express in T cells. TRPV4 is involved in several physiological and pathophysiological processes as well as different forms of pain. Here we demonstrate that TRPV4 can also be activated at physiological temperature, is present in the mitochondria of T cells. TRPV4 activation increases mitochondrial Ca^{2+}-levels, and alters mitochondrial temperature as well as specific metabolisms. The TRPV4-dependent increment in the mitochondrial Ca^{2+} is context-dependent and not just passively due to the increment in the cytosolic Ca^{2+}. Our work also indicates that mitochondrial Ca^{2+}-level correlates positively with a series of essential factors, such as mitochondrial membrane potential, and mitochondrial ATP production negatively correlates with certain factors, such as mitochondrial temperature. We propose that TRPV4-mediated mitochondrial Ca^{2+}-signaling and other metabolisms has implications in the immune activation process, including immune synapse formation. Our data also endorse the re-evaluation of Ca^{2+}-signalling in T cell, especially in the light of mitochondrial Ca^{2+}-buffering. Thus the presence of TRPV4 in the mitochondria of T cells is relevant for immune response, thus provides evolutionary adaptive benefit. These findings may also have broad implications in different pathophysiological processes, neuro-immune cross-talks, and channelopathies involving TRPV4.

2.7 TRPM8- mediated mitochondrial regulation: impact on T cell activation:

2.7.1 TRPM8 is localized in plasma membrane as well as in mitochondria endogenously:

After understanding the effect of TRPV4 in $CD3^+$ T-cell function, we went ahead to check the effect of another thermosensitive ion channel TRPM8 on T-cell function. In our previous reports from our lab, we have shown the presence of TRPM8 in T cells and modulation of TRPM8 changes the T-cell activation and proliferation (Acharya TK, 2021). However, the localization of TRPM8 in mitochondria in T-cells is not established. Localization of truncated 4TM-TRPM8 in mitochondria and MAM (Mitochondria Associated membrane) in different cellular systems have been reported (Bidaux G, 2018). With this notion, we explored the localization of TRPM8 in mitochondria in resting and TCR-bead treated $CD3^+$ T cells. For this study, we used mitoTracker Red and OPA1 as mitochondrial markers. By immunostaining with TRPM8 in these cells, we found distinct colocalization of TRPM8 with mitochondrial markers. However, the areas of the colocalizations are heterogeneous in different T cells (**Fig. 82A-B**).

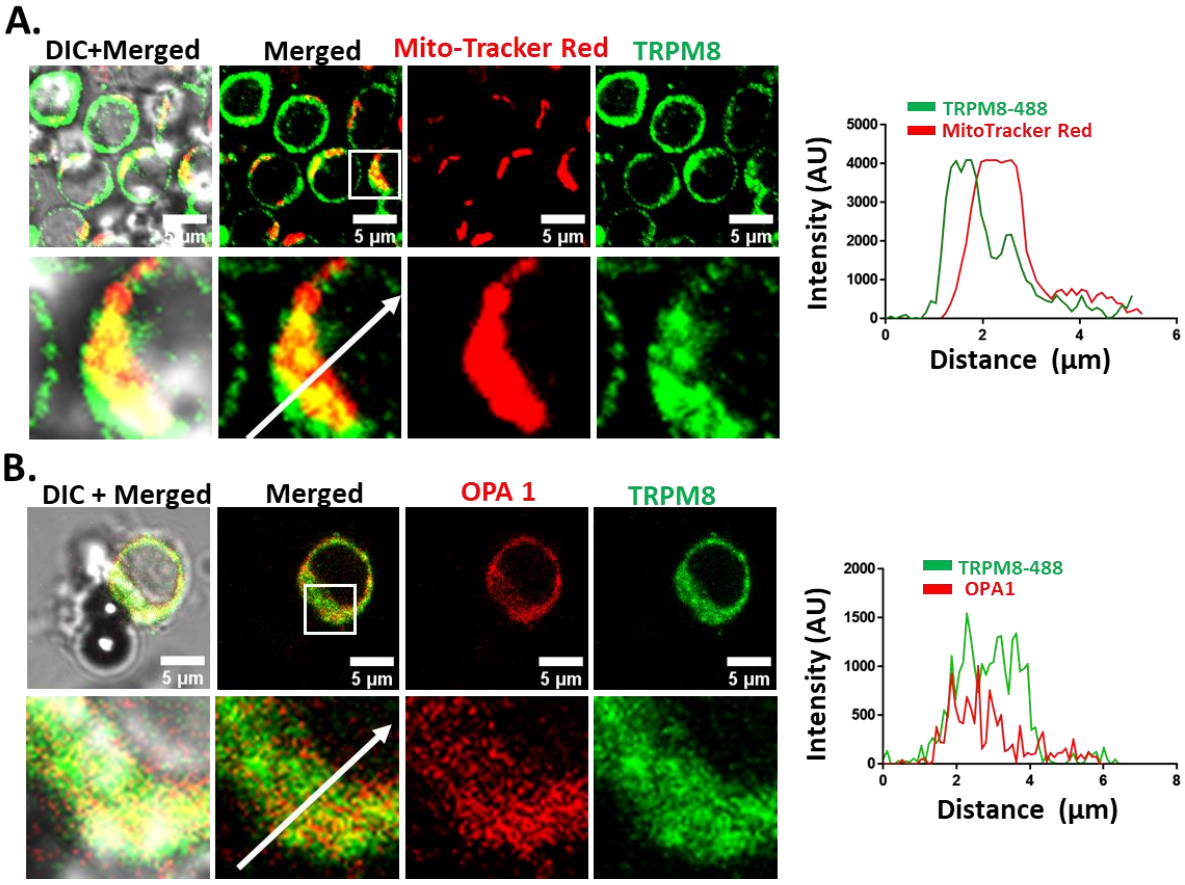


Fig. 82. TRPM8 is localized in mitochondria. A. Representative image demonstrating the colocalization of TRPM8 with Mito-Tracker red in $CD3^+$T-cells in resting condition. The intensity profile (at the right side) across the line indicates the possible presence of TRPM8 at the mitochondria**. B.** TRPM8 colocalizes with Opa1 (mitochondrial marker) in TCR-treated $CD3^+$T-cells. These cells were immunostained with antibodies specific for TRPM8 and OPA1. The intensity profile (at the right side) across the line indicates the colocalization between TRPM8 and Opa1 in TCR-treated T-cells. (Un-published figure).

2.7.2 TRPM8 is functional in $CD3^+$ T cells:

To verify the functionality of TRPM8, intracellular Ca^{2+}-levels of murine $CD3^+$ T cells were probed by labelling with Ca^{2+}-sensor dye Fluo-4-AM. Representative confocal images of time-lapse imaging are shown (**Fig. 83, 84A**). Due to the floating nature of T cells, continuous time course tracking of individual T cells over time is not possible.

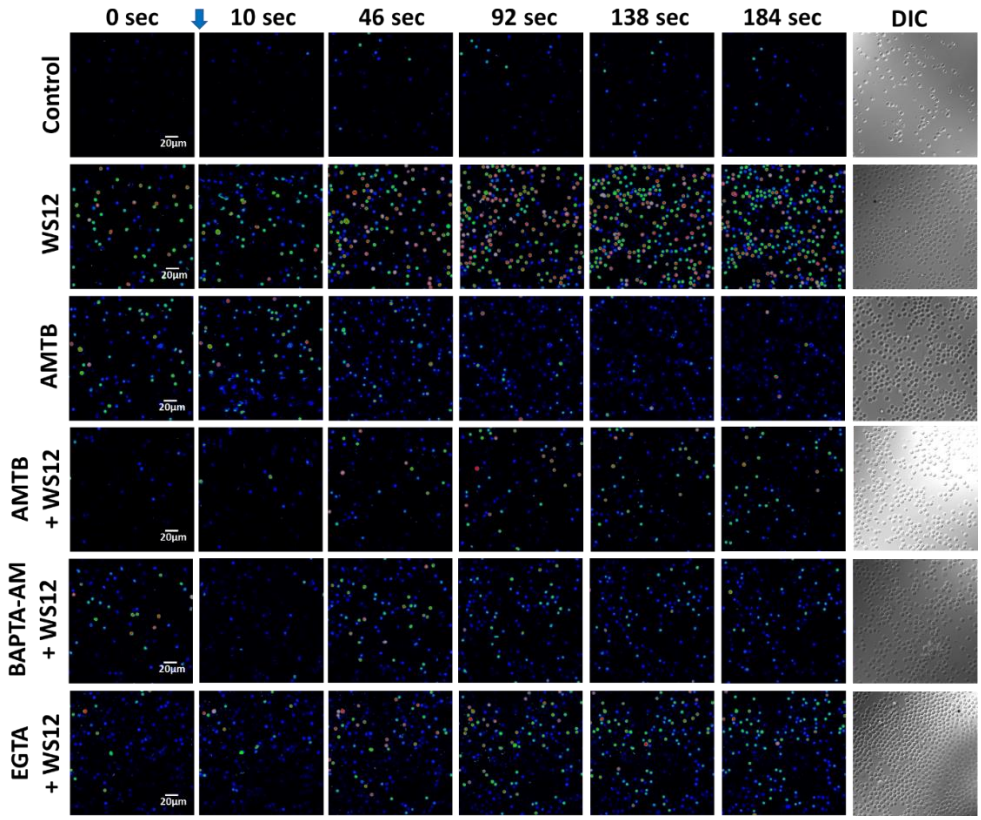


Fig. 83. TRPM8 activation by synthetic activator increases intracellular Ca^{2+}-levels in T cells. A. Representative images acquired during time lapse imaging of murine CD3+ T cells loaded with Ca^{2+}-sensing dye Fluo-4-AM are shown. Intracellular Ca^{2+}-levels (coded blue to red) represent increasing Fluo-4-AM intensity upon addition of synthetic TRPM8 activator WS12 (5 µM) at 10th second to either Resting (untreated) or cells pre-treated with the indicated inhibitors. Where indicated, T cells were pre-incubated with either AMTB (10 µM, specific inhibitor of TRPM8), BAPTA-AM (5 µM, to chelate intracellular Ca^{2+}), or EGTA (5 µM, to chelate extracellular Ca^{2+}). Scale bar 20µm. (Un-published figure).

Therefore, the intensity quantification of individual T cells presents in the view-field at the end of the time series (in 2 independent experiments) is quantified (**Fig. 84B, C**). The addition of TRPM8 synthetic activator WS12 (5 µM) or the natural activator Menthol (50 µM) causes a rapid and significant increase in intracellular Ca^{2+}, whereas TRPM8 inhibitor AMTB (10 µM) treatment doesn't increase Ca^{2+}-levels beyond the basal (resting) levels (**Fig. 83, 84**). AMTB is effectively able to block WS12 or Menthol induced increase in Ca^{2+}-levels confirming the presence of

functional TRPM8 in T cells (**Fig. 83, 84**). We investigated if the intracellular Ca^{2+}-increase is due to extracellular Ca^{2+}-influx or by the release of Ca^{2+} from intracellular stores.

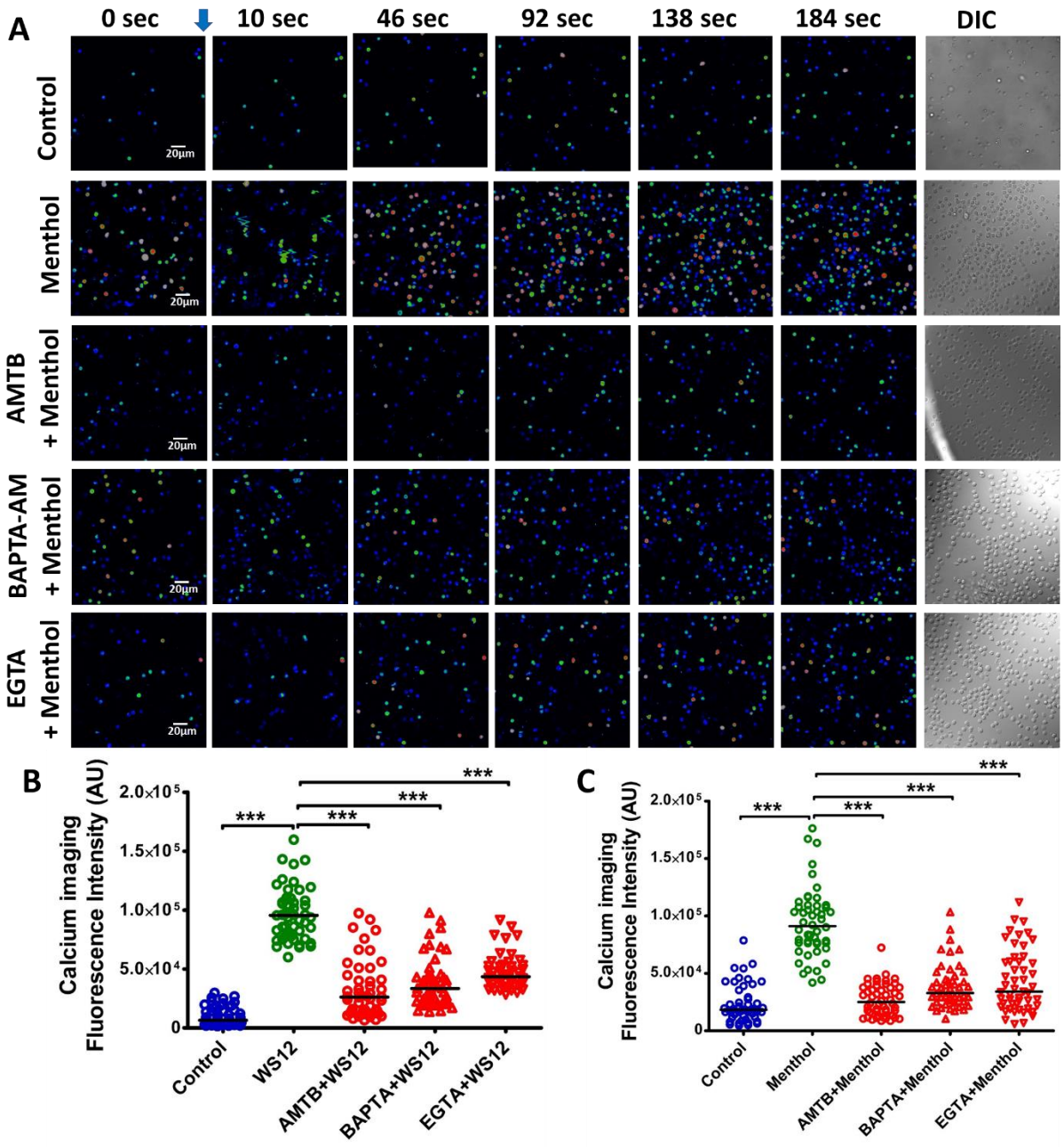


Fig. 84. TRPM8 activation by Menthol increases intracellular Ca^{2+}-levels in T cells. A. Representative images acquired during time lapse imaging of murine CD3+ T cells loaded with Ca^{2+}-sensing dye Fluo-4 -AM are shown. Intracellular calcium levels (coded blue to red) represent increasing Fluo-4-AM intensity upon addition of natural TRPM8 activator Menthol (50 µM) at 10th second to either Resting (untreated) or cells pre-treated with the indicated inhibitors. Where indicated, T cells were pre-incubated with either AMTB (10 µM, specific inhibitor of TRPM8), BAPTA-AM (5 µM, to chelate intracellular Ca^{2+}), or EGTA (5 µM, to chelate extracellular Ca^{2+}). Scale bar 20µm. **B-C.** Quantification of Fluo-4-AM fluorescence

intensities (intracellular Ca^{2+}-levels) in T cells treated and imaged as depicted in Fig. 3, 4A above. Ca^{2+}-sensor dye Fluo-4-AM intensities from individual cell intensity at the end-point of the experiment (approximately 184 sec) are represented by dots, and median values are shown from 1 field each from two independent experiments. The P-values are ns = non-significant; *** = < 0.001. (Un-published figure).

Application of EGTA (5 µM), which chelates extracellular Ca^{2+} and BAPTA-AM (5 µM), which chelates intracellular Ca^{2+}, effectively blocks WS12 and Menthol-mediated increase in the cytosolic Ca^{2+}-levels. This reinforces that the TRPM8 activation mediated Ca^{2+} increase is mainly due to Ca^{2+}-influx from the extracellular source. The predominant localization of TRPM8 at the surface justifies this observation. However, the contribution of trace amount of functional TRPM8 in the intracellular organelles of T cells, especially in the Ca^{2+}-stores like endoplasmic reticulum and mitochondria cannot be ruled out.

2.7.3 TRPM8 regulates mitochondrial Ca^{2+}-levels and dynamics:

Mitochondrial Ca^{2+} plays a prime role in Tcell activation, proliferation and functions. Mitochondrial Ca^{2+} is highly dependent on cytosol and ER. TRPM8 activation by WS12 and Menthol increases cytosolic Ca^{2+} in T cells as reported earlier (Acharya TK, 2021). Here we monitor the instant changes in mitochondrial Ca^{2+} (by using Rhod-2-AM dye) upon modulation of TRPM8 in different cellular conditions. Mitochondrial Ca^{2+}-level escalates upon addition of WS12 in resting and in TCR-treated cells (**Fig. 85A-B**). We further explored the changes in intracellular Ca^{2+}-level by treating the cells with BAPTA-AM (cytosolic Ca^{2+}-chelator), EGTA (extra cellular Ca^{2+}-chelator) and Thapsigargin (SERCA inhibitor, which depletes ER Ca^{2+}) for 1 hour. We observed that mitochondrial Ca^{2+}-level rises in all these conditions, yet at different extents suggesting that T cells use multiple Ca^{2+}-sources and TRPM8 contributes in all these sources (as blocking any of these sources does not abolish the mitochondrial Ca^{2+}-increment) (**Fig. 85A-B**). We further quantified the change in fluorescence intensity of Rhod-2-AM in individual

T cells in each condition by considering the initial time point (before stimulation) and at the end of the experiment (after stimulation) of the time series.

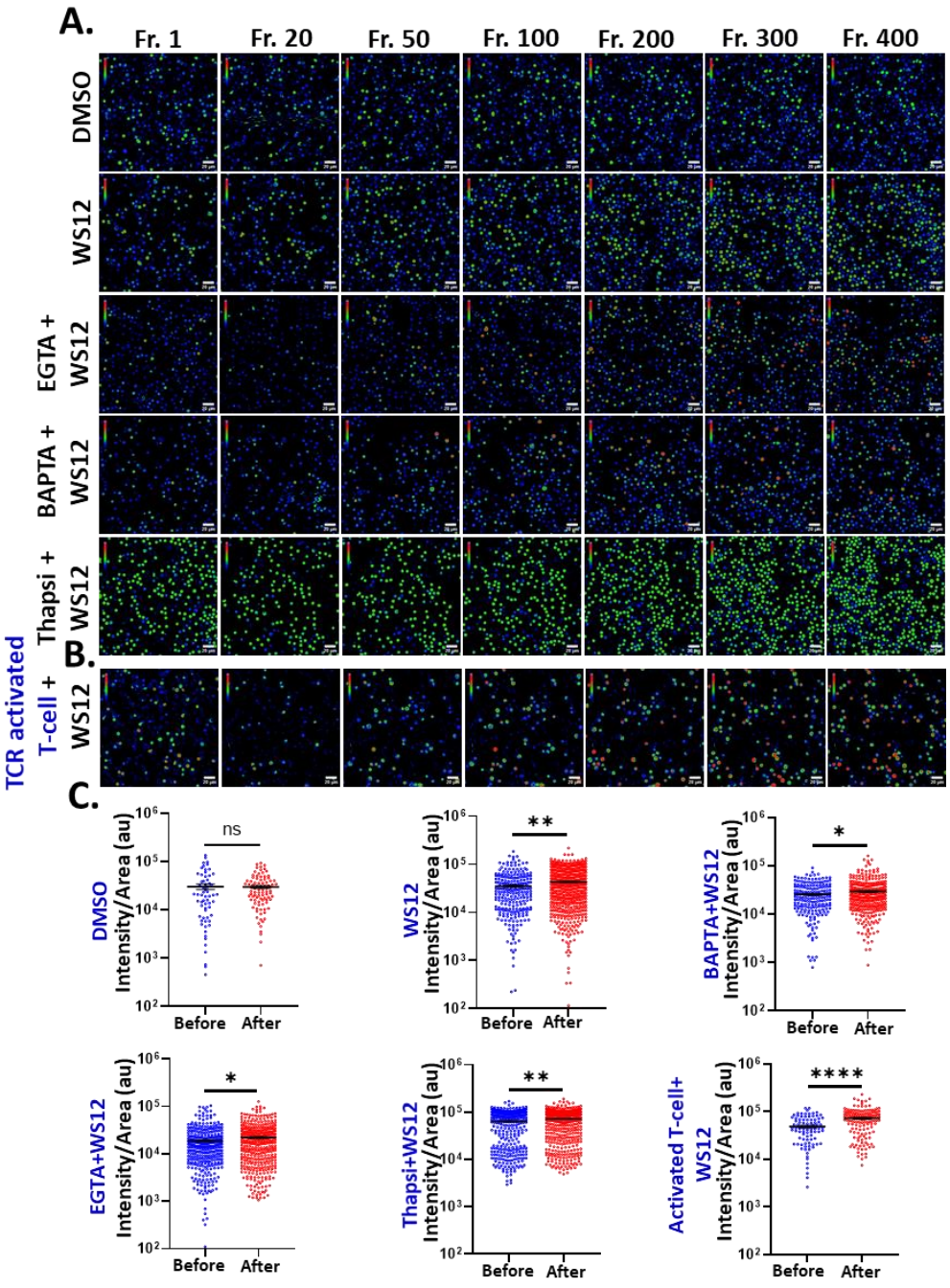


Fig. 85. TRPM8 activation by specific synthetic activator increases mitochondrial Ca^{2+}-status in murine $CD3^+$ Tcells. A-B. Representative images acquired during time series imaging of mitochondrial Ca^{2+} in murine $CD3^+$ Tcells are shown. Mitochondrial Ca^{2+}-levels (represented in intensity scale coded blue to red) increase upon addition of specific TRPM8 agonist WS12 (5 µM) at the 20th frame either in resting and TCR treated cells. The time series imaging was performed for 400th frame (~7min). Cells Where indicated cells were incubated with BAPTA-AM (cytosolic Ca^{2+}-chelator, 5 µM), EGTA (extracellular

Ca^{2+} chelator, 5 µM) and Thapsigargin (SERCA inhibitor and ER Ca^{2+}-chelator, 1 µM). Scale bar is 20µm. **C,** Quantification of Rhod-2-AM (mitochondrial Ca^{2+}-level) fluorescence intensities in Tcells. Fluorescence intensities of individual cells from the initial frame and final frame of the time series experiment are represented. (n ≥100 cells in each condition were quantified, Students t-test, * = p<0.05, ** = p<0.01, **** = p<0.0001, ns = non-significant). (Un-published figure).

We found that in all these conditions, the mitochondrial Ca^{2+} increases significantly after stimulation of TRPM8, suggesting that TRPM8 contributes in mitochondrial Ca^{2+}-level increment and use Ca^{2+} from diverse sources (**Fig. 85C**).

Furthermore, we performed the similar experiment by using a Menthol which is a natural activator of TRPM8. We also want to mention that Menthol has some off-targets in addition to TRPM8. Menthol activates several other ion channels along with TRPM8, which points to the nonspecific activation of TRPM8 by Menthol (Oz M, 2017). With this in mind, we examined the impact of Menthol on mitochondrial Ca^{2+} in resting, and TCR treated Tcells. We observed that upon the addition of Menthol in cells, the mitochondrial Ca^{2+}-level rises. To check the source of the Ca^{2+} we again pre-treated the cells with BAPTA-AM, EGTA and Thapsigargin for 1hr and subsequently monitored the Ca^{2+}-influx by Menthol treatment. Interestingly the propensity of Ca^{2+}-rise decreases in BAPTA and Thapsigargin treated cells but the Ca^{2+}-level significantly increased in EGTA treated cells which infers that Menthol possibly activates the store operated Ca^{2+}-channels to increase mitochondrial Ca^{2+}-level. (**Fig. 86A-B**). The fluorescence intensity of Rhod-2-AM from individual Tcells in different conditions considering the initial and final frame of the time series were quantified and represented in **Fig. 86C**.

We further quantified the basal Ca^{2+}-level, fold change in Ca^{2+}-level and delta change in Ca^{2+}-level (final intensity - initial intensity) in these different experimental conditions (**Fig. 86D-F**). The basal mitochondrial Ca^{2+}-load is high in TCR-treated cells and in other conditions the basal mitochondrial Ca^{2+}-load is less compared to the control condition. The fold change and delta

change value also suggest higher mitochondrial Ca^{2+}-load in TCR-treated cells and contribution of TRPM8 in building higher mitochondrial Ca^{2+}-levels

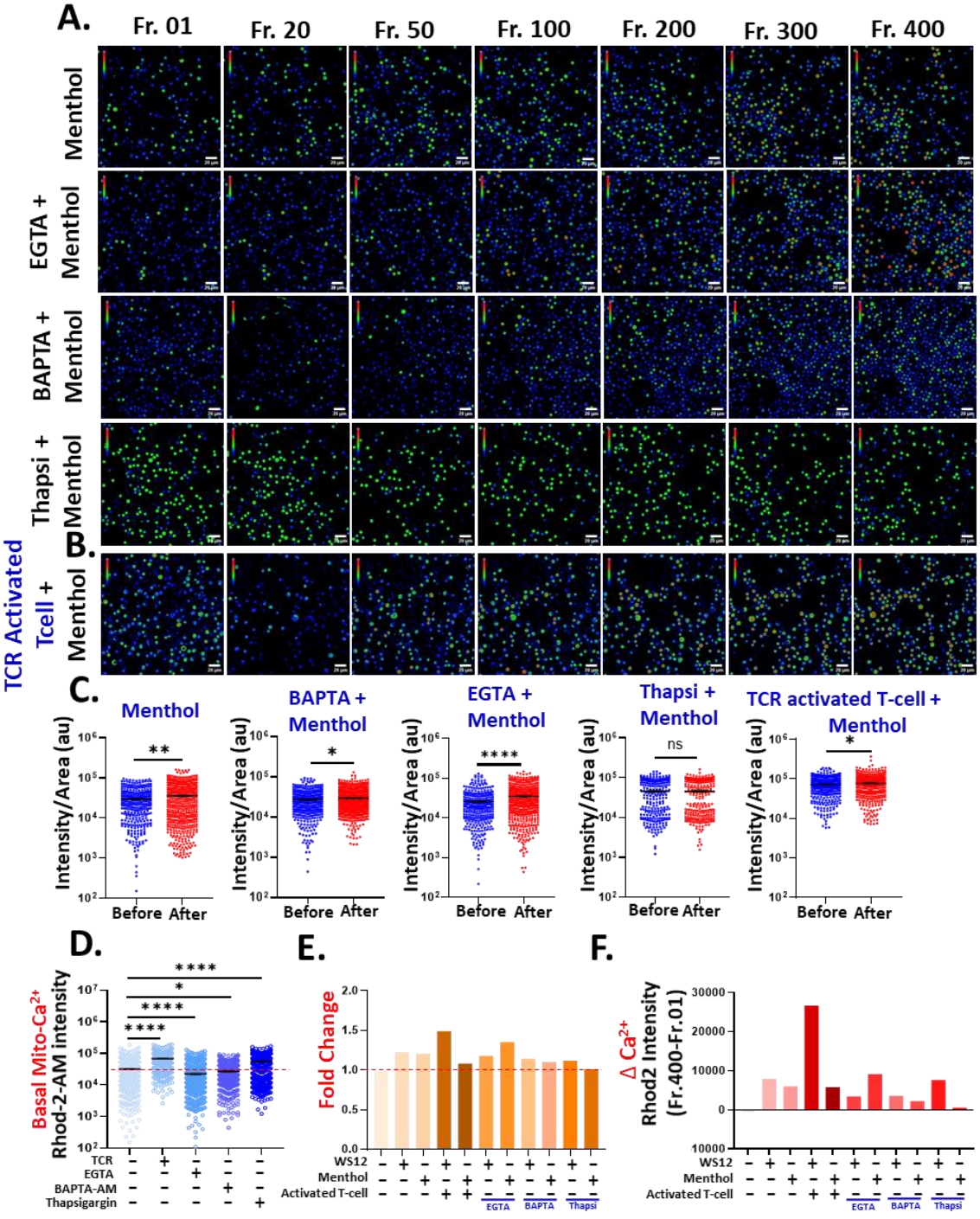


Fig. 86. TRPM8 activation by Menthol, a natural activator increases mitochondrial Ca^{2+}-status in murine $CD3^{+}$Tcells. A-B. Representative images acquired during time series imaging of mitochondrial Ca^{2+} in murine $CD3^{+}$ Tcells are shown. Mitochondrial Ca^{2+}-levels (represented in intensity scale coded

blue to red) increase upon addition of specific TRPM8 agonist Menthol (50 µM) at the 20th frame either in resting and TCR treated cells. Cells were incubated with BAPTA-AM (cytosolic Ca^{2+}-chelator, 5 µM), EGTA (extracellular Ca^{2+}-chelator, 5 µM) and Thapsigargin (SERCA inhibitor and ER Ca^{2+}-chelator, 1 µM). Scale bar is 20µm. **C**. Quantification of Rhod-2-AM (mitochondrial Ca^{2+}-level) fluorescence intensities in Tcells. Fluorescence intensities of individual cell from initial frame and final frame of the time series experiment are represented. (n ≥100 cells in each condition were quantified, Students t-test, * = p<0.05, ** = p<0.01, **** = p<0.0001, ns = non-significant). **D**. Basal mitochondrial Ca^{2+} in different conditions were quantified and TCR-treated cells have higher basal level of Ca^{2+}, **E**. Fold change in Ca^{2+} compared to control condition were quantified and represented. **F.** Delta change in Ca^{2+} (final intensity-initial intensity) in different conditions were calculated and represented (n ≥100 cells in each condition were quantified, one way ANOVA, * = p<0.05, **** = p<0.0001, ns = non-significant). (Un-published figure).

2.7.4 TRPM8 modulation increases basal mitochondrial and cytosolic Ca^{2+}-level:

It is generally known that mitochondria play a pivotal role in of cellular Ca^{2+} management and have an excellent Ca^{2+}-buffering capabilities. We checked if the basal Ca^{2+}-load between mitochondria and cytosol differs after long term activation of TRPM8. Here the resting or TCR treated Tcells were further treated with WS12, Menthol and AMTB for 1 hour. We measured the basal Ca^{2+}-load. We observed that in resting Tcells mitochondrial Ca^{2+}-level increases by any modulation of TRPM8 agonist and antagonist. In contrast, the cytosolic Ca^{2+}-level is not increased by the activation of TRPM8, but there is a slight increase in cytosolic Ca^{2+} when TRPM8 is inhibited by AMTB (**Fig. 87A, C**). Similarly, we checked the mito and cyto Ca^{2+}-level in TCR treated Tcells. We observed that by modulation of TRPM8, mitochondrial Ca^{2+}-level goes up and in contrast, the cytosolic Ca^{2+}-level remains unchanged by TRPM8 agonist and antagonist (**Fig. 87B, D**). The individual cell quantification data of Fluo-4-AM and Rhod-2-AM are plotted (**Fig.87 E-H**). In all the cases, we found that in the AMTB-treated cells, the amount of mitochondrial and cytosolic Ca^{2+} is high. The possible explanation might be the inhibition of TRPM8 impairs the Ca^{2+}-buffering ability of mitochondria which allows mitochondria to accumulate more Ca^{2+} inside it.

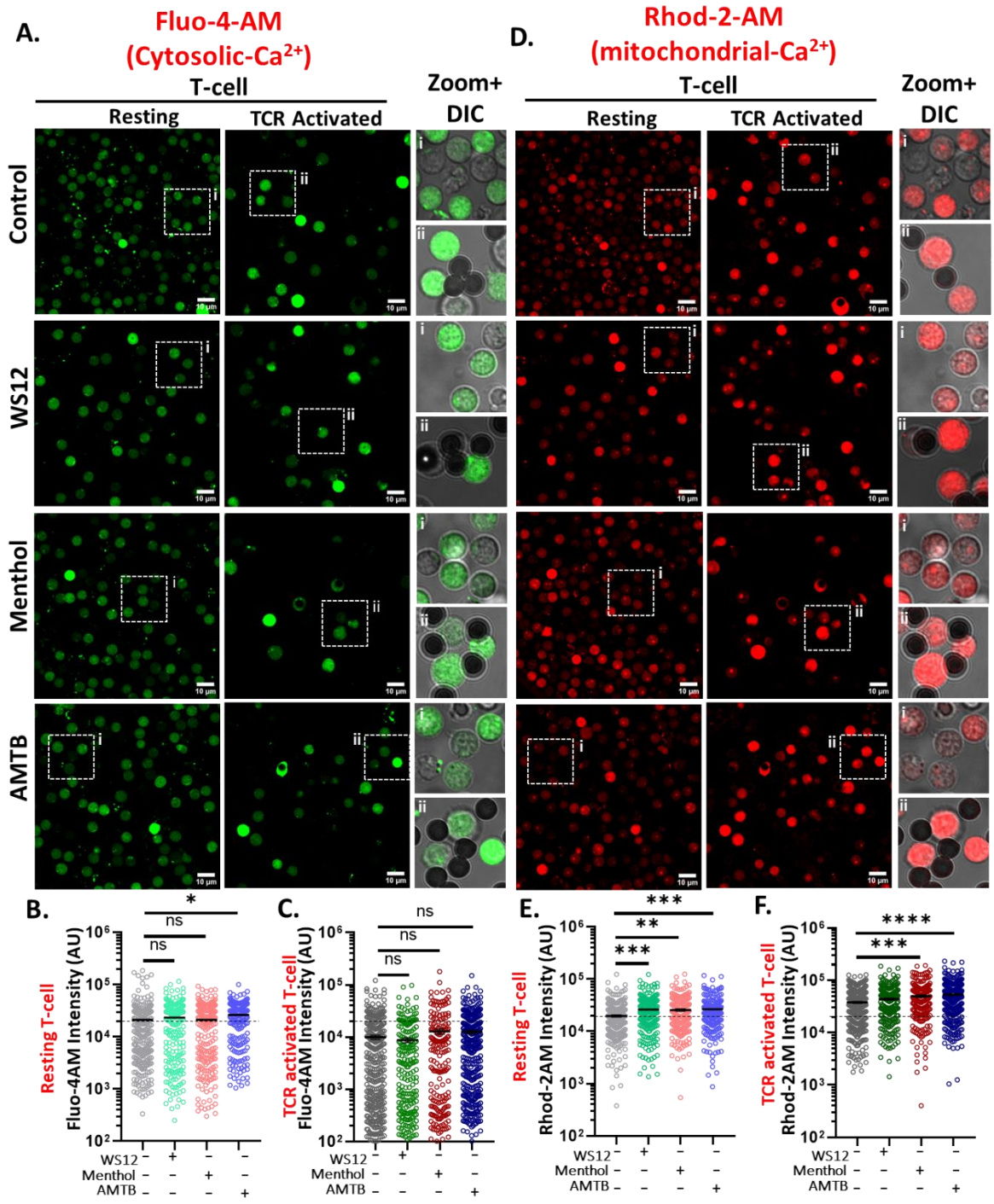


Fig. 87. TRPM8 modulation increases basal cytosolic and mitochondrial Ca^{2+} in murine $CD3^{+}$Tcells. **A-D.** Representative images of basal cytosolic and mitochondrial Ca^{2+} in murine $CD3^{+}$ Tcells are shown. Resting and TCR-treated cells were treated with TRPM8 modulators for 1 hour. and basal cytosolic Ca^{2+} was measured by Fluo-4-AM and mitochondrial Ca^{2+} was measured by using Rhod-2-AM. Images are represented in an intensity scale coded blue to red. Scale bar is 10µm. **E-H.** Quantification of basal Fluo-4-AM (Cytosolic Ca^{2+}-level) and Rhod-2-AM (mitochondrial Ca^{2+}-level) fluorescence intensities in resting and TCR-treated Tcells. (n ≥100 cells in each condition were quantified, one way ANOVA, * = $p<0.05$, ** = $p<0.01$, **** = $p<0.0001$, ns = non-significant). (Un-published figure).

To get a better insight in to the interplay between mitochondrial Ca^{2+} and cytosolic Ca^{2+} we quantified the ratio of mitochondrial Ca^{2+} and cytosolic Ca^{2+} in resting and TCR-treated cells. The ratio is very high in TCR-treated cells when compared to resting cells (**Fig. 88A-B**).

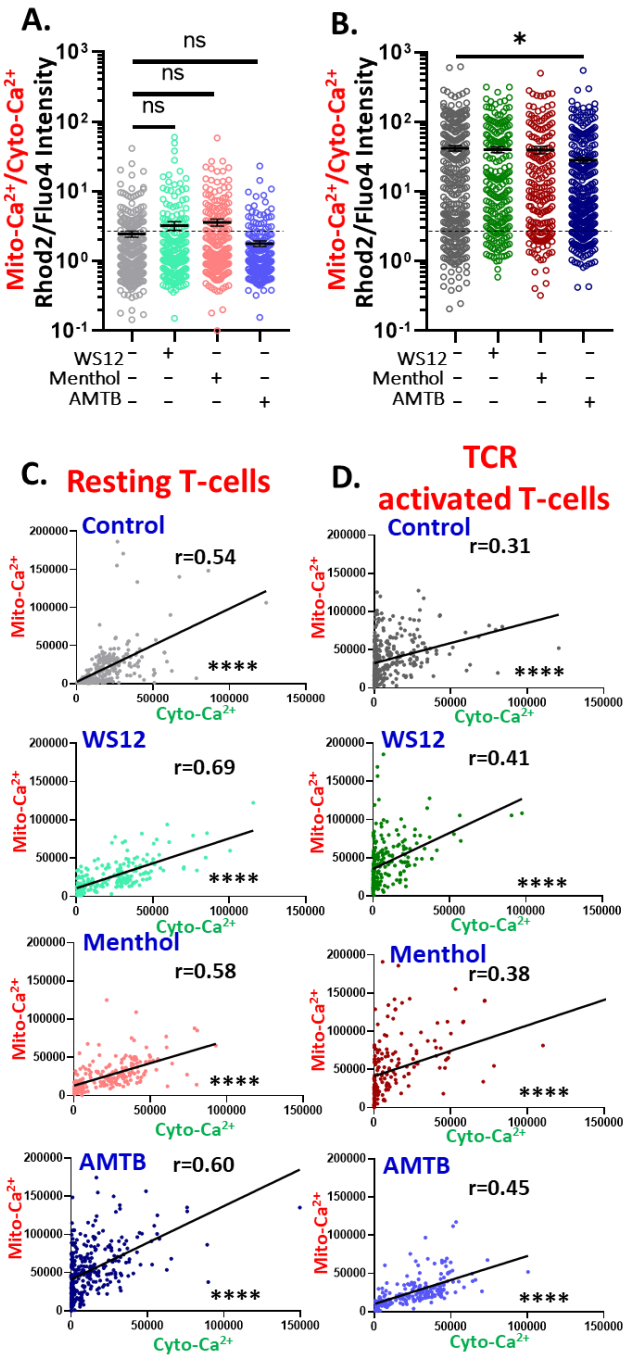


Fig. 88. Correlation study between basal Cytosolic Ca^{2+} and mitochondrial Ca^{2+}. A-B. Graph represented the ratio of mito Ca^{2+}-intensity and cyto Ca^{2+}-intensity in resting as well as TCR-treated conditions. The ratio is high in TCR-treated cells as compared to resting cells. In both conditions (resting

as well as in TCR-treated conditions), AMTB reduces the spontaneous activity of TRPM8 causing reduced mitochondrial Ca^{2+}/cytosolic Ca^{2+} ratio. **C.** In resting $CD3^+$ Tcells the co-relation between mitochondrial Ca^{2+} and cytosolic Ca^{2+} in different experimental condition is represented. In TRPM8 activated cells, the co-relation is high whereas in AMTB treated cells the co-relation is reduced. ($n \geq 100$ cells in each condition were quantified, one way ANOVA, * = $p<0.05$). **D.** The co-relation between cytosolic Ca^{2+} and mitochondrial Ca^{2+} in TCR-treated $CD3^+$ Tcells is represented. In TCR-treated cells, the trend is opposite, TRPM8 activated cells have less co-relation, but inhibited cells have high co-relation. (Un-published figure).

We further tested co-relation between mitochondrial and cytoplasmic Ca^{2+} in different conditions. We observed high co-relation between mitochondrial Ca^{2+} with cytosolic Ca^{2+} in WS12 and Menthol-treated Tcells and the co-relation is decreased in AMTB-treated cells (**Fig. 88C**). In contrast, in the TCR-treated Tcells, there is less co-relation between mitochondrial-Ca^{2+} and cytosolic Ca^{2+} in WS12 and Menthol-treated cells and in the AMTB-treated cells the co-relation increased (**Fig. 88D**). This data depicts the dependence of mitochondrial Ca^{2+} on cytosolic Ca^{2+} and *vice versa*, indicating the importance of TRPM8 in cellular and sub-cellular Ca^{2+}-buffering. In resting cells the mitochondrial Ca^{2+} and cytosolic Ca^{2+} increase simultaneously upon activation of TRPM8 by WS12, whereas in the AMTB-treated cells, the mitochondrial Ca^{2+} increases instead of cytosolic Ca^{2+}. In TCR-treated cells, upon activation of TRPM8 allows accumulation of more Ca^{2+} in mitochondria, but in AMTB treated cells the mitochondrial Ca^{2+} decreases and cyto Ca^{2+}-level increases.

2.7.5 TRPM8 regulates mitochondrial ATP production and membrane potential:

To evaluate the role of TRPM8 in ATP production, we used ATP-Red dye. Activation of TRPM8 by either WS12 or Menthol do not affect the ATP production whereas inhibiting TRPM8 using AMTB results in enhanced ATP production. Similarly, ATP-levels were evaluated in TCR treated T cells (mediated by TCR-beads) where basal ATP-level is increased as compared to

resting T cells. In TCR treated T cells also, TRPM8 activation doesn't affect the ATP-levels significantly, although a slight increase is seen.

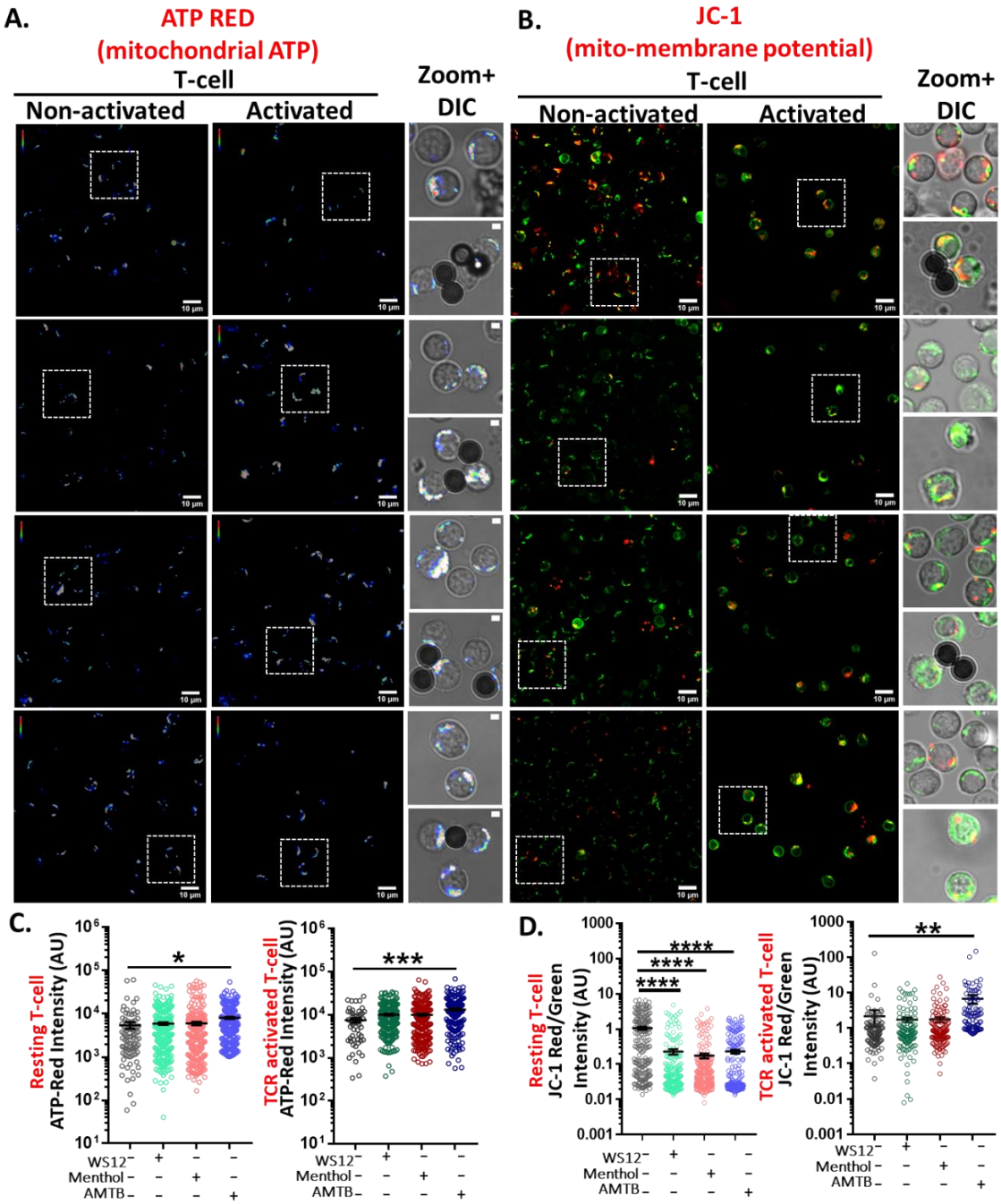


Fig. 89. TRPM8 regulates mitochondrial ATP and membrane potential. **A.** Murine $CD3^+$ T cells at resting and TCR-treated conditions were treated with TRPM8 agonist WS12 (5 µM), Menthol (50 µM), and TRPM8 antagonist AMTB (10 µM). The mitochondrial ATP level was measured by using ATP red dye (5 µM). ATP level is high in TCR-treated cells as compared to resting cells. AMTB-treated cells increase mitochondrial ATP levels in both resting and TCR treated T cells. Scale bar: 10µm. (n ≥100 cells in each condition were quantified). **B.** Both resting and TCR-treated cells were treated with TRPM8

modulators and subsequently stained with JC1 dye (5 µM). In resting T cells, both TRPM8 agonist or antagonist decreases the membrane potential, whereas in TCR-treated cells, the membrane potential increased in all condition (but in AMTB-treated consition, the level increases significantly). Scale bar: 10µm. **C-D**, Quantification of fluorescence intensities of ATP-red and JC1 in resting and TCR treated cells. (n ≥100 cells in each condition were quantified, One way ANOVA, * = p<0.05, ** = p<0.01, *** = p<0.001, **** = p<0.0001, ns = non-significant). (Un-published figure).

Inhibition of TRPM8 results in significant rise in ATP-levels in TCR-treated T cells. This data can be related to the mitochondrial Ca^{2+} and cellular Ca^{2+}-load as in AMTB treated cells, the mitochondrial Ca^{2+} is high. Taken together, our data suggest that inhibition of TRPM8 leads to an increased ATP production and TCR-treated T cells have more ATP-levels (**Fig. 89A, C**).

In resting T cells, WS12 or Menthol leads to a sharp decrease in the mitochondrial membrane potential as analyzed by JC-1 dye. Inhibiting TRPM8 by AMTB also shows a similar effect. This suggest that at control condition, the mitochondrial membrane potential remain high and modulating TRPM8 interferes with the maintenance of higher mitochondrial membrane potential. Significant increase in basal mitochondrial membrane potential is observed in TCR-treated T cells (as compared tp the resting conditions). In TCR-treated cells also, TRPM8 activation by WS12 or Menthol reduces mitochondrial membrane potential to some extent. In a comparative manner, TRPM8 inhibition by AMTB in TCR-treated conditions provides higest mitochondrial membrane potential, suggesting that in TCR-treated conditions, spontaneous activity of TRPM8 is crucial for the maintenance of mitochondrial membrane potential. Therefore, pharmacological inhibition of TRPM8 affects the T cells differently depending on their immunological state (**Fig. 89B, D**).

2.7.6 Regulating TRPM8 affects Cardiolipin and mitochondrial superoxides levels:

We used NAO dye to investigate the levels of Cardiolipin as a factor of TRPM8 modulation (**Fig. 90A, C**). NAO is a membrane potential-independent dye that specifically binds to the mitochondrial phospholipids; mostly, it detects the Cardiolipin level in mitochondria (Mileykovskaya E, 2001). In resting T cells, activation of TRPM8 by WS12 causes a decrease in

Cardiolipin levels. But, this reduction is not seen in case of TRPM8 activation by another agonist, namely Menthol (discussed later). In addition, TRPM8-specific antagonist AMTB escalates the Cardiolipin levels significantly.

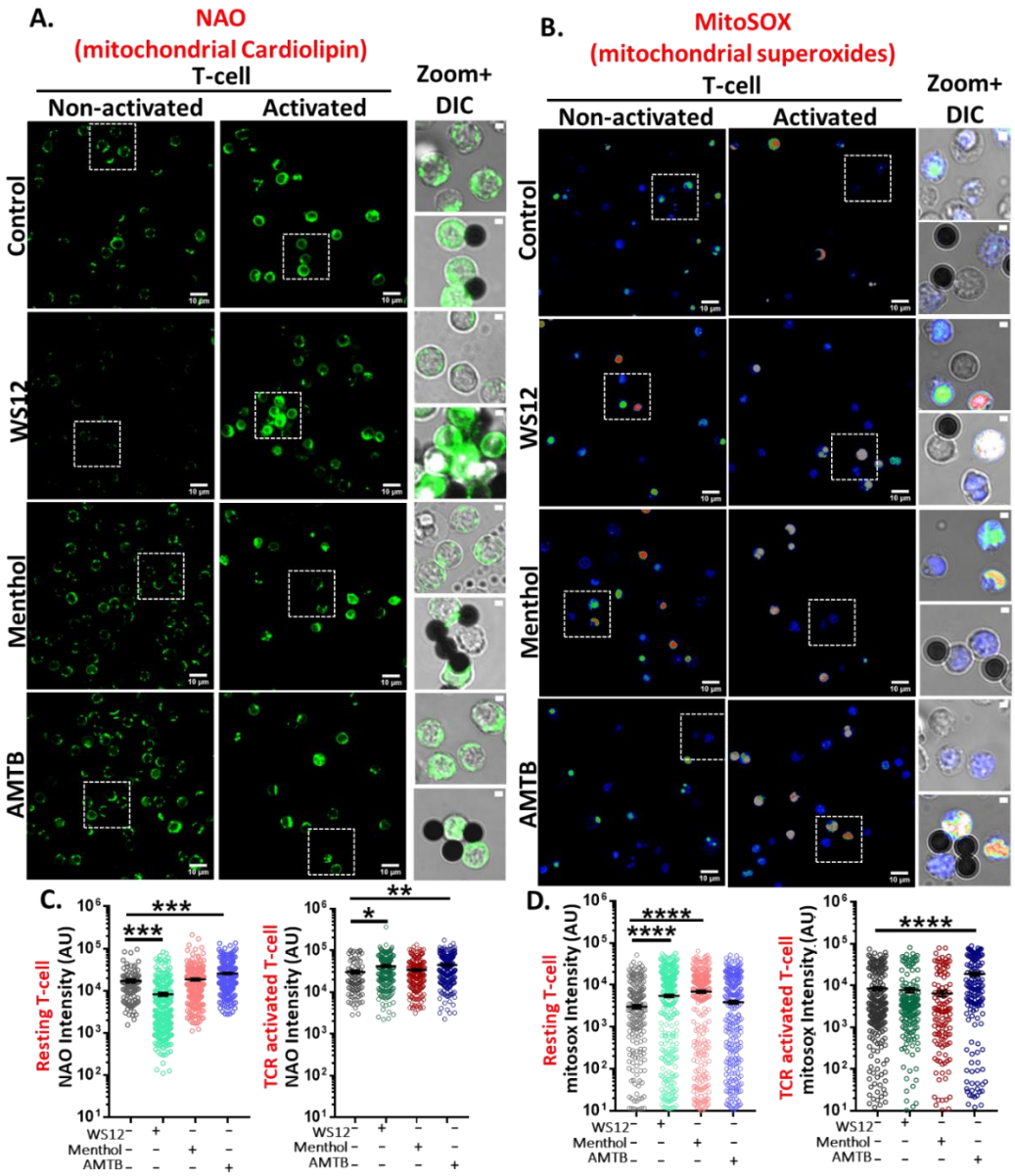


Fig. 90. TRPM8 regulates mitochondrial Cardiolipin and ROS levels. A. Resting and TCR-treated $CD3^{+}$T cells were treated with TRPM8 agonist WS12 (5 µM), Menthol (50 µM), and TRPM8 antagonist AMTB (10 µM). The mitochondrial Cardiolipin was measured by using NAO (5 µM). Scale bar is 10µm. **B.** Both resting and TCR-treated cells were treated with different TRPM8 modulators and subsequently stained with MitoSOX red (2.5 µM). In TCR-treated cells, the ROS level is elevated by the presence of AMTB. Scale bar is 10µm. **C-D**. Quantification of fluorescence intensities of NAO and MitoSOX is represented. (n ≥100 cells in each condition, One way ANOVA, * = $p<0.05$, ** = $p<0.01$, *** = $p<0.001$, **** = $p<0.0001$, ns = non-significant). (Un-published figure).

Next, we evaluated the Cardiolipin levels in TCR-stimulated T cells. In TCR-treated conditions, the basal level of Cardiolipin is high in comparison to resting cells. TCR-treated condition, TRPM8 activation by WS12 results in further increment in Cardiolipin levels. In TCR-treated condition, Menthol doesn't affect the Cardiolipin profile, whereas inhibition of TRPM8 resulted in an increase in Cardiolipin levels similar to that of resting T cells. Altogether, results suggest that inhibiting TRPM8 results in more Cardiolipin levels. Activation by WS12 affects Cardiolipin levels differently in activated and resting T cells.

We investigated whether TRPM8 affects mitochondrial superoxides (mtROS), an important regulator of immunological response (Sena L, 2013). We used MitoSOX dye to detect the the level of mitochondrial superoxides (mtROS) due to TRPM8 in Tcells (**Fig. 90B, D**). In resting T cells, activation of TRPM8 by either WS12 or Menthol results in a rise in mitochondrial ROS levels. In the case of TRPM8 inhibition by AMTB, the mitochondrial ROS levels match well to resting condition. Interestingly, in case of TCR-treated conditions, the level of mitochondrial ROS increases significantly than resting T cells. In TCR-treated T cells, activation of TRPM8 does not induce further increment in mitochondrial ROS. Even in contrast to resting T cells, inhibiting TRPM8 by AMTB leads to more mitochondrial ROS in TCR treated T cells. In summary, mitochondrial ROS levels are regulated by the spontaneous activity of TRPM8, especially in a context-dependent manner.

2.7.7 Mitochondrial and ER temperature are regulated by TRPM8 specific modulations:

Mitochondrial temperature is critical for its metabolism and activity, which inturn guides the T cell activation. In order to assess the effects of TRPM8 on mitochondrial temperature, we used MTY dye (**Fig. 91A, C**). In resting T cells, the application of WS12 or AMTB results in a decrease in MTY intensity, suggesting an increase in mitochondrial temperature.

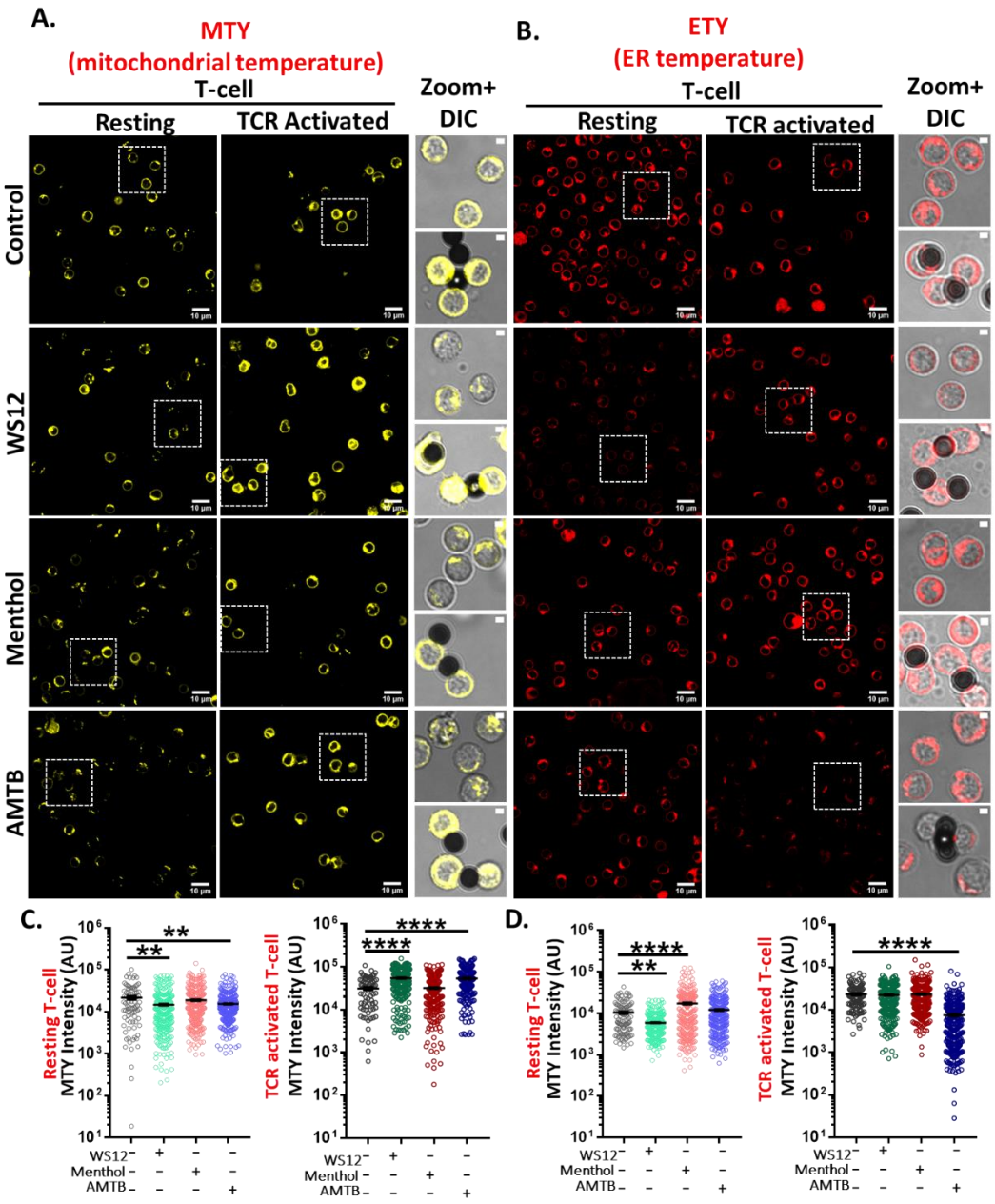


Fig. 91. TRPM8 regulates mitochondrial and ER-temperature. A&C. Resting and TCR-treated murine $CD3^{+}$T cells were treated with TRPM8 agonist WS12 (5 µM), Menthol (50 µM), and TRPM8 antagonist AMTB (10 µM). The mitochondrial temperature was measured by MTY (0.5 µM). In resting cells, the mitochondrial temperature increased with the addition of WS12 and AMTB (decrease in intensity). In TCR-treated cells, the mitochondrial temperature decreased in WS12 and AMTB treatment (increase in intensity). Scale bar 10µm. **B, D.** Both resting and TCR-treated cells were treated with different TRPM8 modulators and subsequently stained with ETY (0.5 µM). In resting T cells, the ER temperature was increased by WS12, whereas TRPM8 inhibition by AMTB does not change the ER temperature. In TCR-treated cells, the ER-temperature is increased (decrease in temperature) due to AMTB, whereas the temperature remains unchanged in the case of agonist treatments. Scale bar 10µm. Fluorescence intensities of individual cells were represented in the graph (n ≥100 cells in each condition, One way ANOVA, ** = $p<0.01$, **** = $p<0.0001$, ns = non-significant). (Un-published figure).

Whereas no change in mitochondrial temperature is observed due to the application of Menthol. Interestingly, in TCR-treated T cells, the mitochondrial temperature is less (as the fluorescence intensity is more) as compared to resting T cells. However, in TCR-treated cells, activation of TRPM8 by WS12 or inhibition of TRPM8 by AMTB results in fluorescence (thus decreases the mitochondrial temperature). In TCR-treated T cells, Menthol shows no effect (discussed later). Altogether, our data suggest that TRPM8 affects the mitochondrial temperature differently in different conditions.

It is well known that mitochondria are physically and functionally associated with ER for the better and easy exchange of Ca^{+2} and other metabolites (Rizzuto R, 2009). We used ETY dye to evaluate the effects of TRPM8 on ER temperature (**Fig. 91B, D**). ETY is a temperature-specific dye which exclusively accumulates at the ER, andan increment in ETY intensity indicates a lowering of ER temperature. In resting T cells, WS12 causes decreased ETY intensity (i.e. increased ER temperature). However, in the Menthol-treated cells, the ETY intensity increased (discussed later) and AMTB showed no effect. In case of TCR-treated T cells, the basal ETY intensity increases greatly as compared to resting T cells. This suggests that the ER temperature is lower in TCR treated T cell than that of the resting conditions. In TCR-treated cells, further TRPM8 activation by either WS12 or Menthol doesn't show any changes in ER temperature whereas TRPM8 inhibition by AMTB increases the ER temperature (decrease in ETY fluorescence intensity), suggesting that spontaneous activity of TRPM8 keeps the ER temperature low.

2.7.8 ER-mito contact points increase upon TRPM8 inhibition:

ER-mito contact is essential for maintaining Ca^{2+}-homeostasis and Ca^{2+}-buffering inside cells (Rizzuto R, 2009). ER-mito contact points are also important for the exchange of other ions

and metabolites. The flow of metabolites from these two compartments are dependant on the extent of ER-mito contact areas (Zhang P, 2021). To test if TRPM8 affects the ER-mito contacts in T cells, we performed particle-based quantification and estimated the total ER, total mitochondria and total colocalized particles (**Fig. 92A-B**).

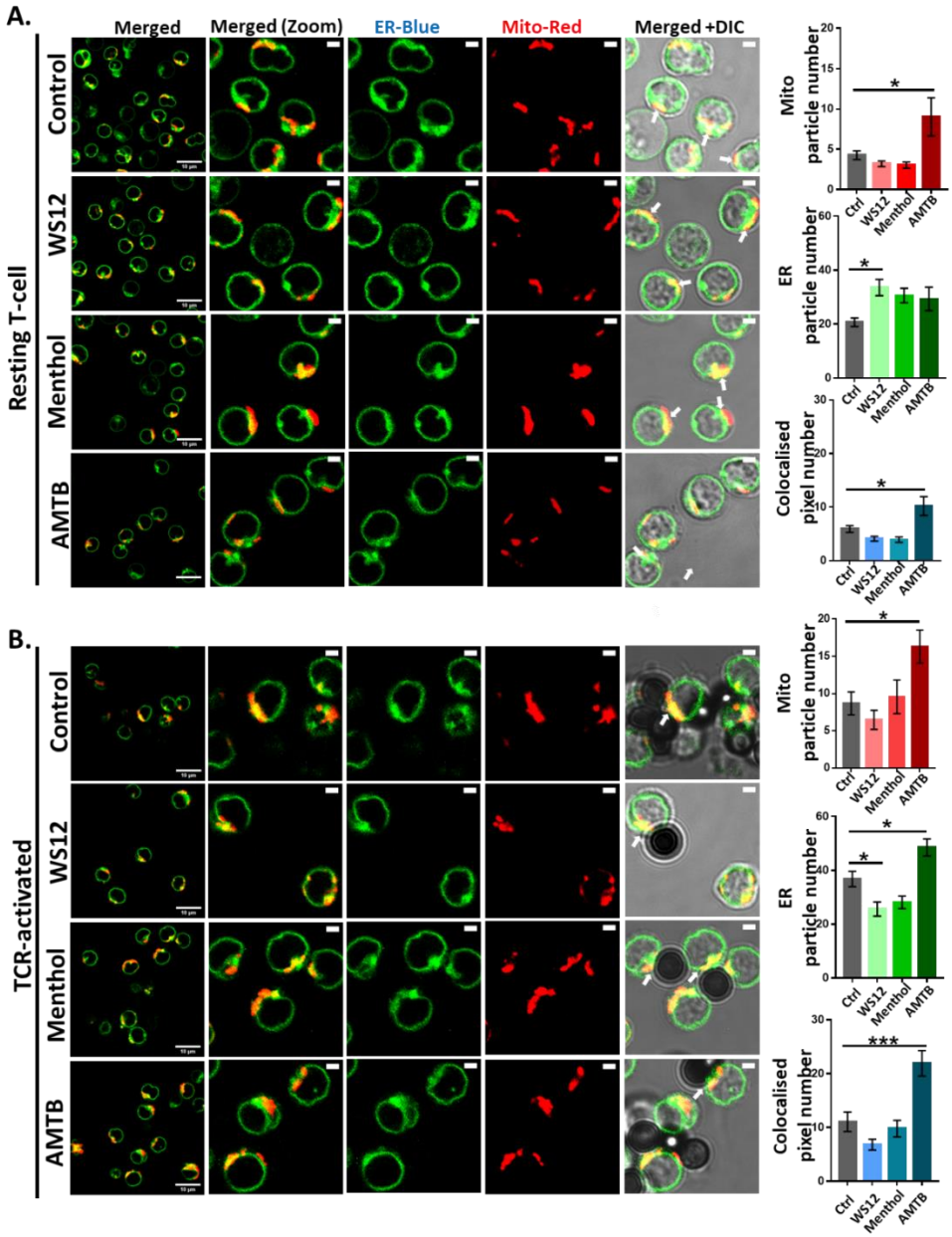


Fig. 92. TRPM8 regulates ER-mito contact sites. A. Resting and TCR-treated CD3^{+}T cells were treated with WS12 (5 µM), Menthol (50 µM), AMTB (10 µM) and were labelled by mitoCMXros (0.5 µM) and ER-tracker blue (0.5 µM). The total mitochondrial, total ER and colocalized particles were quantified by ImageJ. In resting T cell, the mitochondria particle increased in AMTB-treated condition and the ER-

particle increased in the WS12-treated condition. The total colocalized particle number is increased at the AMTB-treated cells. Scale bar 2µm. **B**. In TCR-treated cells, both mitochondrial and ER-particle numbers increased as compared to resting T cells. In this condition, the colocalized particle number increased significantly in the AMTB treated cells. Scale bar 2µm. (n ≥30 cells in each condition were quantified). The quantified graphs are represented on the right side of the images.ER –Tracker blue is represented in pseudocolor green in the representative images. One way ANOVA * = $p<0.05$, *** = $p<0.001$, ns = non-significant. (Un-published figure).

In resting condition, the addition of WS12 or Menthol cause no changes in the number of mitochondria, but the ER particle number increases specifically. In resting T cells, inhibition of TRPM8 by AMTB, the number of mitochondria increases significantly as compared to untreated cells. This correlates well with the increased ER-mito colocalization upon TRPM8 inhibition. A similar trend was seen in the case of TCR-treated T cells, where activation of TRPM8 doesn't have any effect. However, in TCR-treated cells, TRPM8 inhibition causes highest mitochondrial particles (even more than resting T cells treated with AMTB). This also accords well that TRPM8 inhibition causes more ER-mito contact points. In TCR-treated T cells, WS12 or Menthol treatment leads to a decrease in ER particles and in contrast, AMTB increases the ER particles. In general, the numbers of mitochondrial particles in TCR-treated conditions (with or without TRPM8 modulation) are greater than resting T cells. Nonetheless, in TCR treated T cells the total ER particles are more when compared to resting T cells. Thus, activation of T cells causes an increase in the ER and mitochondrial numbers in T cells and also ER-mito colocalization.

Summary: TRPM8 is a non-selective cation channel that can conduct Ca^{2+}-influx upon activation. Previously we have shown that TRPM8 is endogenously expressed in the T cell and is involved in its activation process. In this work, we demonstrate that TRPM8 specifically regulates the physiology of two important sub-cellular compartments. i.e. for mitochondrial and ER. TRPM8 regulates mitochondrial Ca^{2+}-status, ATP-levels, mitochondrial membrane potential, cardiolipin levels and mitochondrial temperature in a context-dependent manner, i.e. by its pharmacological modulation and/or in TCR-activated conditions. Similarly, TRPM8 also regulates the ER temperature. TRPM8 regulates ER-mito contact points, especially in the immunological synapse, suggesting that it has an important role in Ca^{2+}-buffering. We also demonstrate the enrichment of TRPM8 in the immunological synapse. We propose that TRPM8 is an important regulator of T cell functions.

2.8 Characterization of TRPV4-mediated channelopathies in the context of mitochondrial abnormalities:

2.8.1 Mitochondrial morphology is altered by TRPV4 mutants:

TRPV4 is expressed at higher levels in bone cells, chondrocytes, and in cartilage cells (Nilius B, 2013). So far, there is a large number of TRPV4 mutations and variations in the human population that have been reported (Nilius B, 2013, Verma P, 2010, Ghosh A, 2016), many of which lead to skeletal and bone disorders. To date, the functional aspects of these mutants have not been studied well. We transiently expressed TRPV4 mutants (L596P, R616Q, F617L, L618P and V620I) as GFP-tagged proteins in Saos-2 cells (human osteosarcoma cell line) and explored if these mutants affect the mitochondrial structure. We noted that the mitochondrial structure became abnormal and became rounded in cells where these mutants are expressed. We quantified various mitochondrial morphometric parameters of cells expressing WT or different mutants of TRPV4. We quantified mitochondrial numbers, average area and perimeter, area-to-perimeter ratio, percentage of area covered (i.e. mitochondrial distribution within the cell), average circularity and solidity in different cells. The data suggest that the presence of TRPV4-WT or its mutants regulate all these morphology- and distribution-related parameters, often in a cell-specific manner (**Fig. 93A-G**).

We explored the level of translocation of TRPV4-WT and different mutants within the mitochondria (**Fig. 93H-J**). We quantified individual mitochondria and compared the fluorescence intensities of WT and mutant TRPV4 within the mitochondria. The absolute fluorescence intensity of TRPV4-WT and mutants differ significantly. To confirm if these aberrations were truly due to differences in the TRPV4 sequence, we explored the translocation of mitoDsRed within the mitochondria of cells expressing TRPV4-WT or mutants.

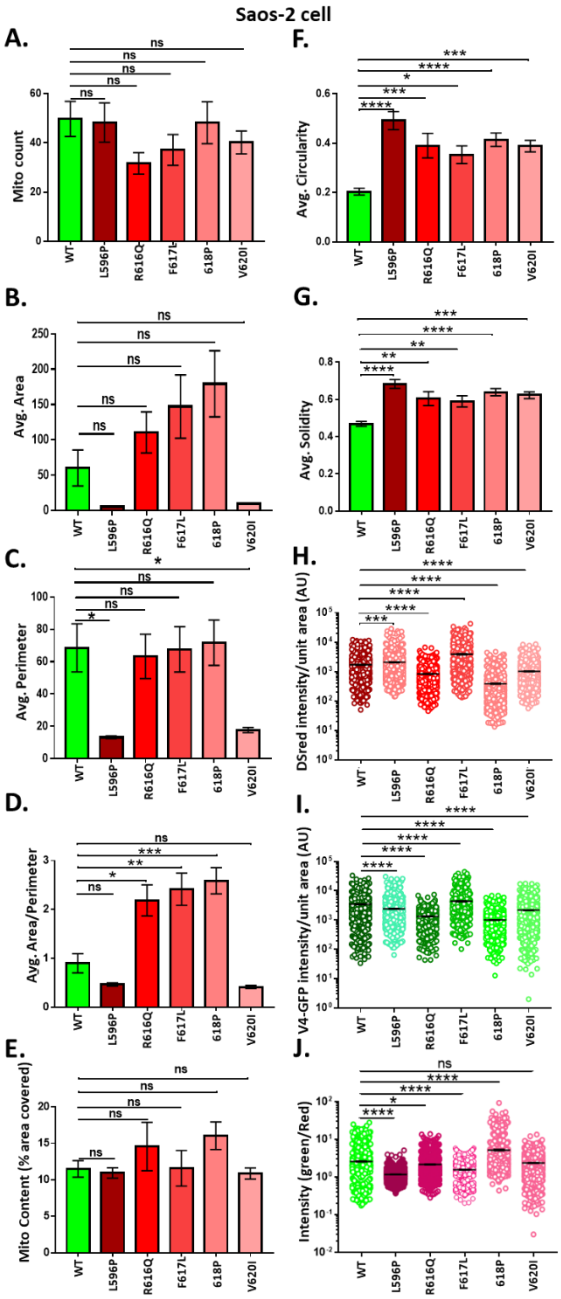


Fig. 93. TRPV4 mutants affect mitochondrial morphology-based parameters and have different translocation efficiencies. A-G. TRPV4-WT-GFP or different mutants were expressed along with mitoDsRed in Saos-2 cells and average mitochondrial number (**A**), average area (**B**), average perimeter (**C**), average area/perimeter (**D**), % of cellular area covered by mitochondria (**E**), average circularity (**F**), and average solidity (**G**) were quantified. **H-J.** mitoDsRed, TRPV4-GFP intensity quantified from the cells expressing TRPV4-WT and TRPV4 mutants. Enrichment of TRPV4 over each mitochondrion was analyzed by quantifying the ratio of TRPV4-GFP intensity over mitoDsRed in each cell. (n = ~1000 mitochondria from ~10 cells). One-way ANOVA, ns = non-significant, ** = p<0.01, *** = p<0.001, **** = p<0.0001. (Published figure, Acharya TK.et al. 2022, *Mitochondrion*).

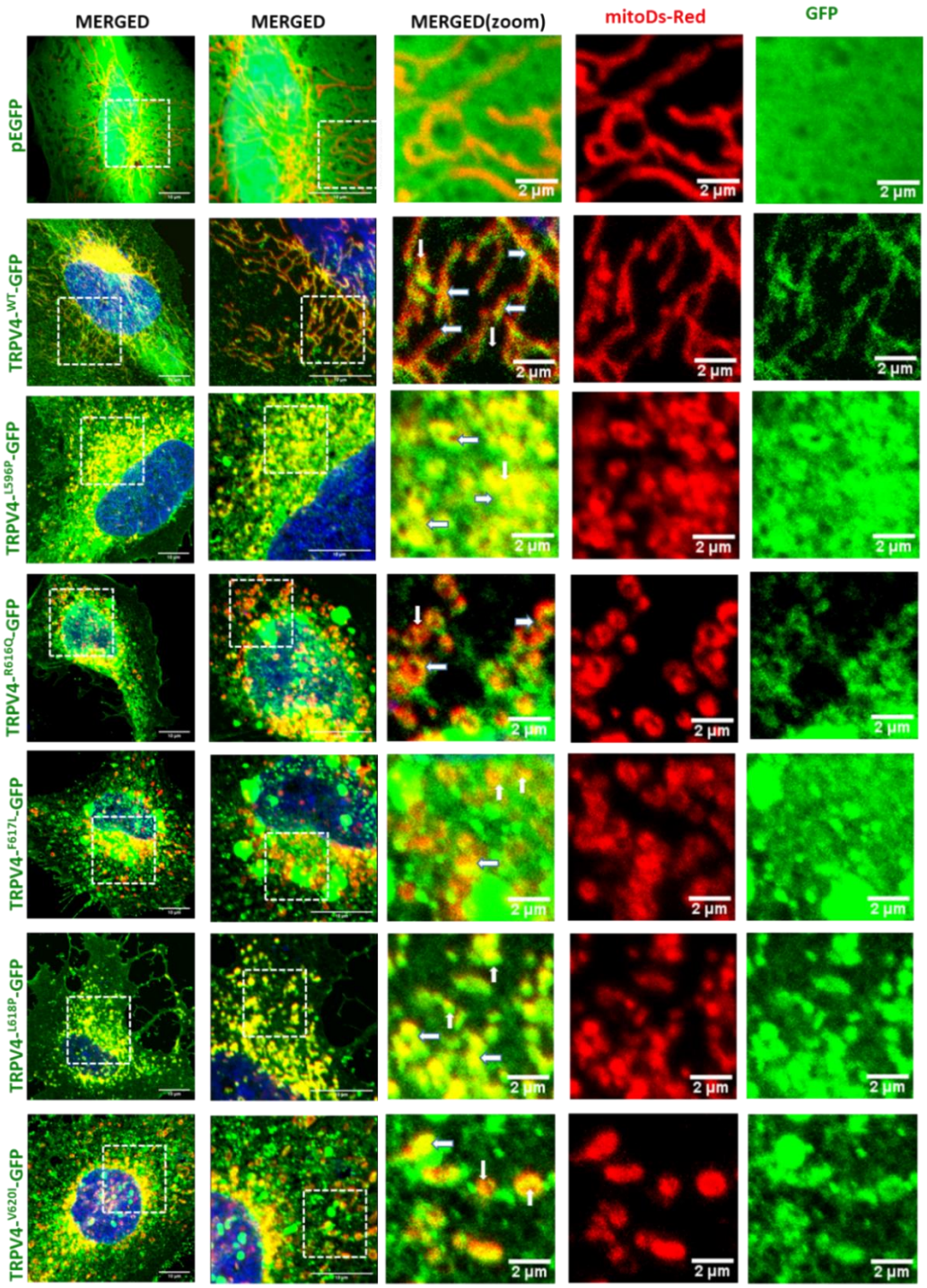


Fig. 94. TRPV4 mutants alter mitochondria shape and size. Human osteosarcoma (Saos-2) cells were co-transfected with GFP-tagged TRPV4-WT or different TRPV4 mutants along with mitoDsRed as a mitochondrial marker. Mitochondrial shape becomes abnormal (mostly spherical) in cells expressing these mutants. Mitochondrial shapes remain elongated in cells that express TRPV4-WT or only EGFP. The arrow indicates the point of localization of TRPV4 at the mitochondria. (N = 3), scale bar is 2µm. (Published figure, Acharya TK.et al. 2022, *Mitochondrion*).

For that purpose, the fluorescence intensities of mitoDsRed were quantified and the ratio of fluorescence intensities of TRPV4-GFP with respect to mitoDsRed were also calculated. The absolute fluorescence intensity of mitoDsRed and the ratio of TRPV4/mitoDsRed suggests that WT and different mutants have distinct characteristics of mitochondrial translocation and enrichment, also in a cell-specific manner (**Fig. 93H-J**).

In case of TRPV4-WT and EGFP control cells, the mitochondria remained normal and elongated. In most cases, all these TRPV4 mutants could be detected in the mitochondria too (**Fig. 94**). The results collectively suggest that functional TRPV4 localizes in mitochondria and play diverse functions there. In order to assess the impact of TRPV4 mutations on the mitochondrial function in bone cells, we co-expressed full-length wild-type (WT) or a series of TRPV4 point mutants (R616Q, F617L, L618P, V620I, L596P) along with a marker for mitochondria (i.e. mitoDsRed) in another murine derived pre-osteoblast cell line, i.e. in MC3T3-E1 cells by transient transfection. In all these cases, colocalization of TRPV4 with mitoDsRed was observed albeit with variable extent. We then quantified the parameters, including mitochondrial number, size, distribution, roundness and protein import that determine mitochondrial health. Mitochondrial number and distribution in osteoblasts altered with the altered TRPV4 function (**Fig. 95A**). However, both area and perimeter of the mitochondria were reduced in the presence of most of the TRPV4 mutants (**Fig. 95C, E**). The overall area-perimeter ratio was also calculated (**Fig. 95G**). Both the solidity and circularity of mitochondria, indicative of their morphology, were affected in the presence of specific mutants. L596P, L618P, and V620I mutations increased the solidity of mitochondria (**Fig. 95B, D**), whereas L596P and L618P mutations increased mitochondrial circularity (**Fig. 95B**).

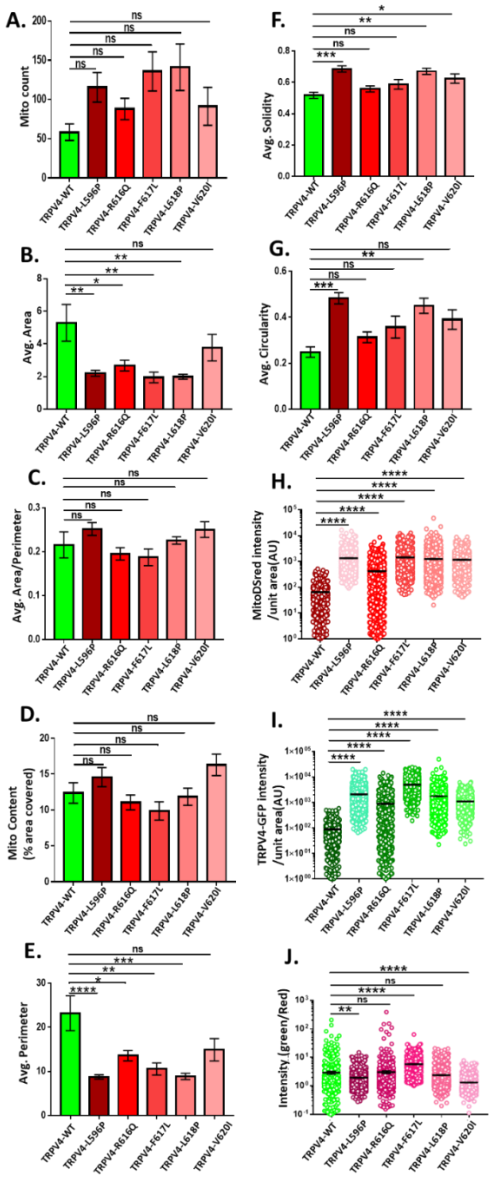


Fig. 95. TRPV4 mutants differentially affect mitochondrial function in MCT3-E1 cells. A-G. Different parameters of mitochondria in cells expressing TRPV4-WT or different mutants were compared. **H**. TRPV4 enrichment in mitochondria was analyzed by quantifying the ratio of TRPV4-GFP intensity over mitoDsRed in each mitochondrion (n = ~1000 individual mitochondria from ~10 cells). The values were compared as one-way ANOVA, ns: non-significant, * = p<0.05, ** = p<0.01, *** = p<0.001, **** = p<0.0001, ns = non-significant. **I-J.** Import of mitoDsRed or TRPV4 were analyzed by quantifying the intensity of TRPV4-GFP-WT or different mutants and mitoDsRed in each mitochondrion (n = ~1000 individual mitochondria from ~10 cells). The values are one-way ANOVA, ns: non-significant, ** = p<0.01, *** = <0.001, **** = <0.0001, ns = non-significant. (Published figure, Acharya TK, et al. 2023, *Frontiers in Cell and Developmental Biology*).

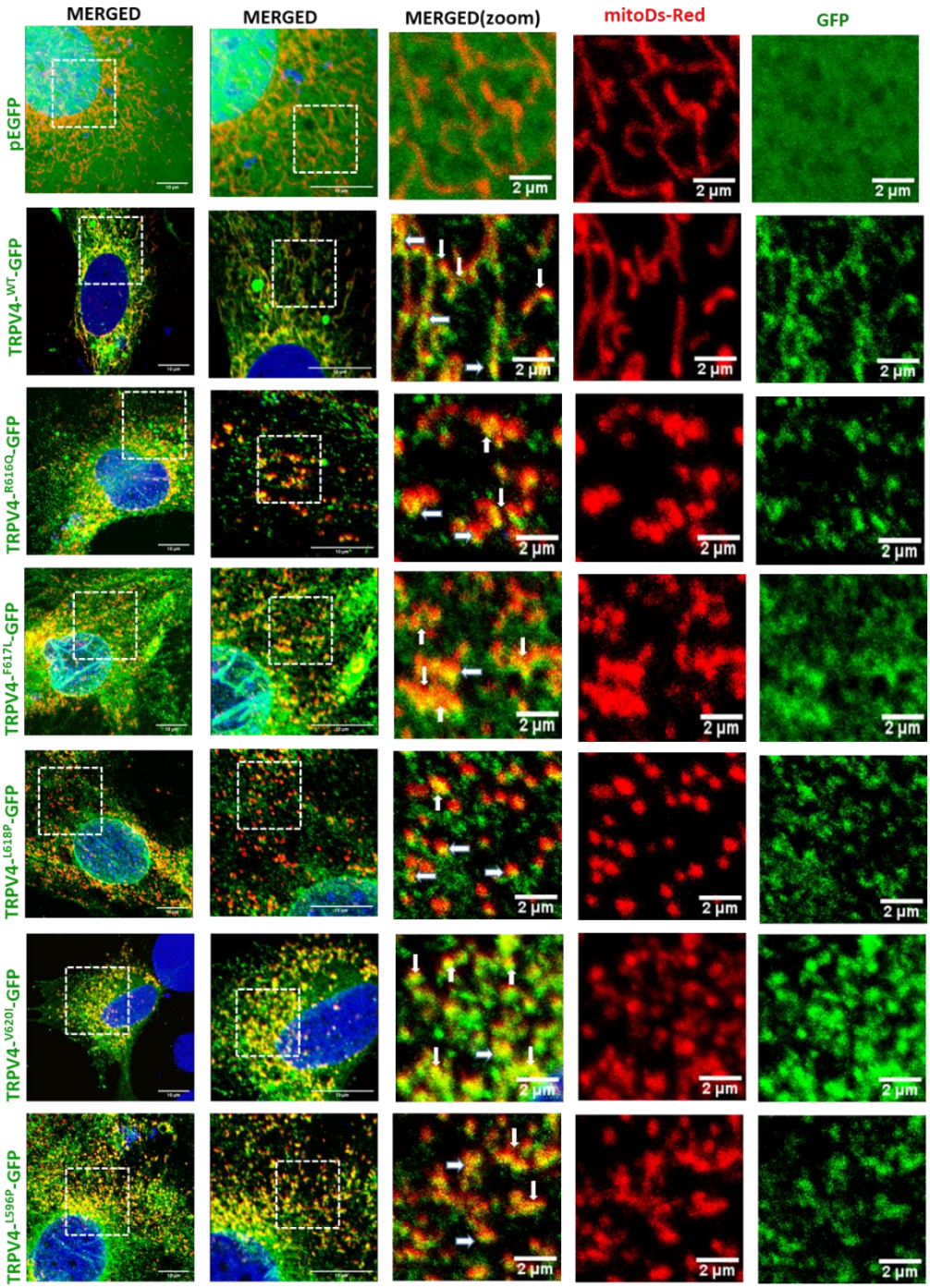


Fig. 96. TRPV4 mutants alter mitochondria shape and size. Murine pre-osteoblast cells (MC3T3-E1) were co-transfected with GFP-tagged TRPV4-WT or different TRPV4 mutants along with mitoDsRed as a mitochondrial marker. Mitochondrial shape becomes abnormal (mostly spherical) in cells expressing these mutants. Mitochondrial shapes remain elongated in cells that express TRPV4-WT or only EGFP. The arrow indicates the point of localization of TRPV4 at the mitochondria. (N = 3), scale bar is 2µm. (Published figure, Acharya TK, et al. 2023, *Frontiers in Cell and Developmental Biology*).

To understand the mitochondrial translocation/import, we measured the intensity of TRPV4 as well as mitoDsRed for cells expressing TRPV4-WT or different mutants. Both mitoDsRed and TRPV4 fluorescence intensities were increased in the presence of mutations (**Fig. 95H-J**). The ratio of TRPV4-GFP intensity with mitoDsRed intensity, however, was increased only in the presence of F617L, while it was decreased in L596P and V620I mutations, suggesting that different mutants affect the mitochondrial import in different extent (**Fig. 95H-J**).

The mitochondria in TRPV4-WT and EGFP control cells remained healthy and elongated. Most of the cases, TRPV4 mutants could also be found in the mitochondria. (**Fig. 96**). The results collectively suggest that functional TRPV4 localizes in mitochondria and play diverse functions there.

2.8.2 Expression of different TRPV4 mutations induce mitochondrial ROS:

The degree of mitochondrial ROS generation in the mutant expressing cells were investigated. This is relevant as TRPV4 mutations alter the shape of the mitochondria. We co-expressed full-length wild-type (WT) or a series of TRPV4 point mutants (R616Q, F617L, L618P, V620I, L596P) in Saos-2 and in MC3T3-E1 cells. These cells were labelled with MitoSOXred for the detection of mitochondrial ROS. In Saos-2 cells, we observed that all the mutants have elevated mtROS level and V620I mutant expressing cells have highest ROS production is observed (**Fig. 97**).

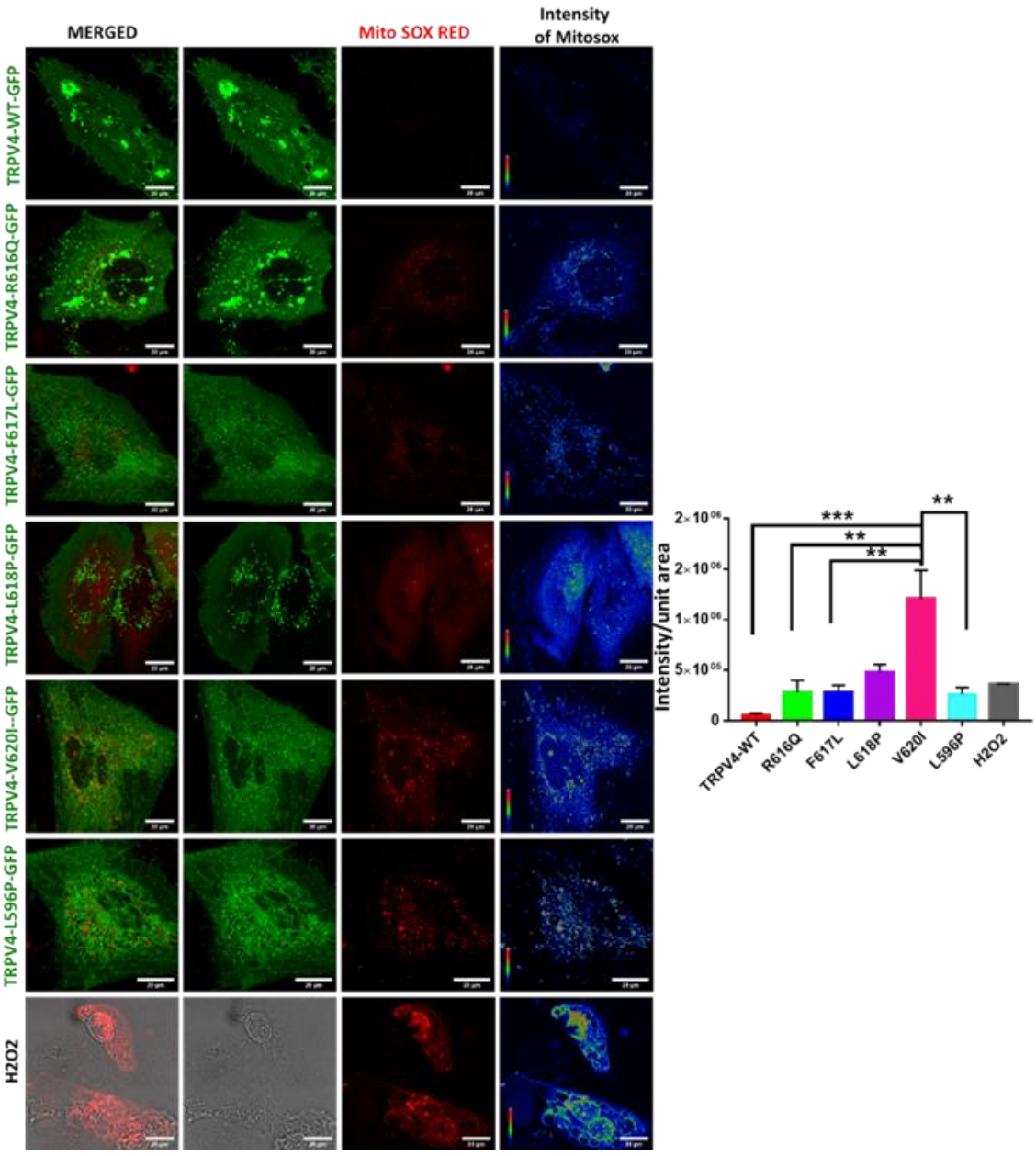


Fig. 97. TRPV4 mutants increase mitochondrial ROS in Saos-2 cells. Human osteosarcoma cell Saos-2 cells were co-transfected with GFP-tagged TRPV4-WT or different TRPV4 mutants and simultaneously labelled with MitoSOXred for detection of mitochondrial ROS. TRPV4 mutants increased mitochondrial ROS production compared to the control condition. ≥10 cells were quantified in each condition. The values were compared as one-way ANOVA, ** = $p<0.01$. *** = $p<0.001$, ns = non-significant, (Un-published figure).

We again checked the similar phenomenon in murine pre-osteoblast cell MC3T3-E1. For that also, we expressed wild type and mutants and simultaneously labelled the cells with MitoSOXred. We

noticed no significant increment of mtROS level in the cells expressing these mutants. In most of the mutant expressing cells, the ROS level is lower except the R616Q mutant, where the ROS production is higher than the wild type (**Fig. 98**).

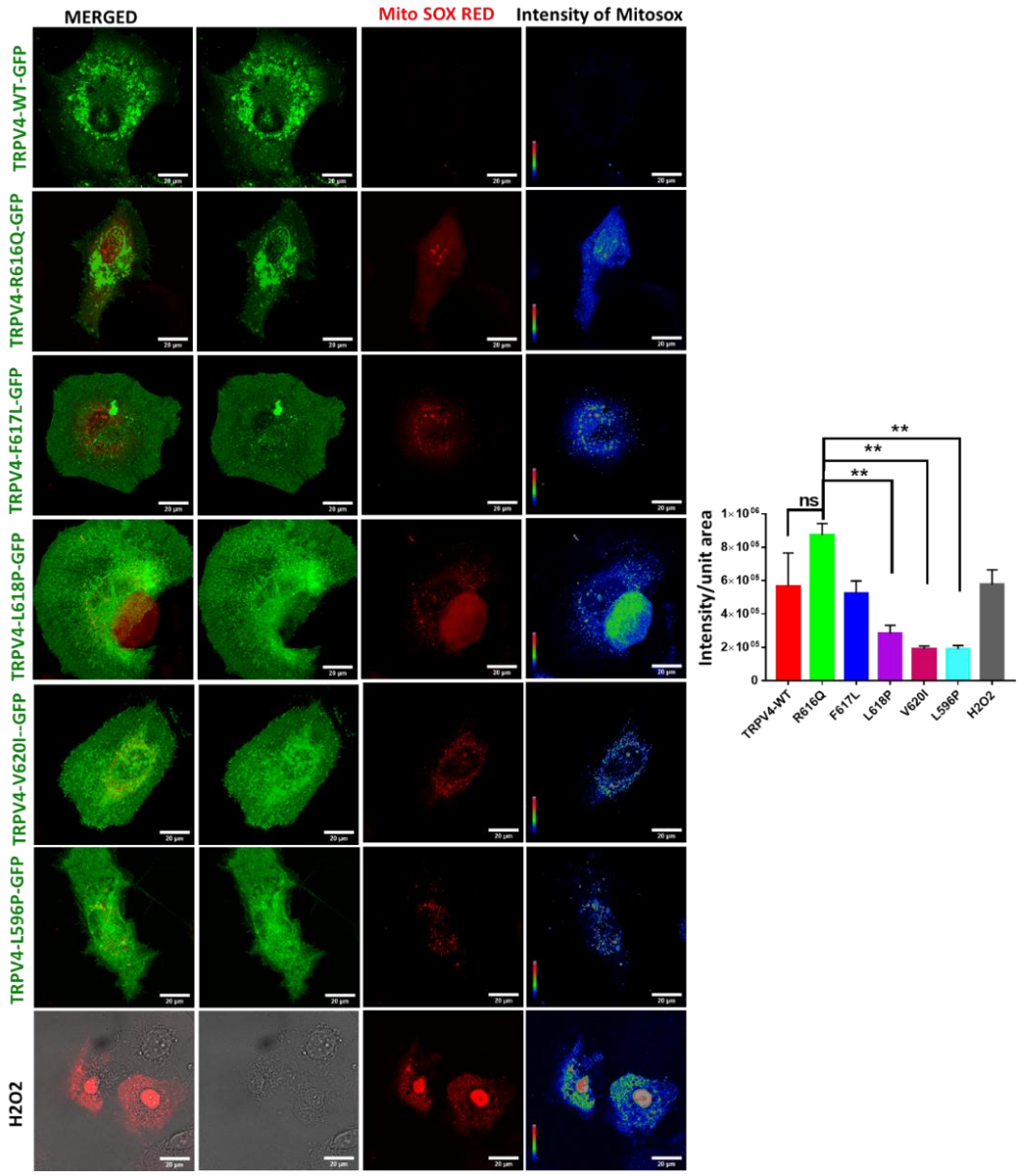


Fig. 98. TRPV4 mutants increase mitochondrial ROS in MC3T3-E1 cells. Murine pre-osteoblast cells MC3T3-E1 were co-transfected with GFP-tagged TRPV4-WT or different TRPV4 mutants and simultaneously labelled with MitoSOXred for detection of mitochondrial ROS. Mitochondrial ROS production decreased in TRPV4 mutants compared to control conditions. R616Q mutant cells have higher ROS then control condition. ≥10 cells were quantified in each condition. The values were compared as one-way ANOVA, ns: non-significant, ** = $p<0.01$, ns = non-significant. (Un-published figure).

2.8.3 Novel mutation at the N-terminal of TRPV4 alters mitochondrial structure and metabolism:

Recently we came across a novel mutation in TRPV4, the exact location of the point mutation is p.S372L (c.1115C>T) position which indicates that this mutation affects the ankyrin repeat domain of TRPV4 (**Fig.99**). This point mutation has also been listed in the COSMIC data base (https://cancer.sanger.ac.uk/cosmic/mutation/overview?id=125022295) and https://www.ncbi.nlm.nih.gov/clinvar/variation/536857/. The tissue distribution of this mutant is mostly at the skin and endometrium. However, the functional significance of this mutation is not known.

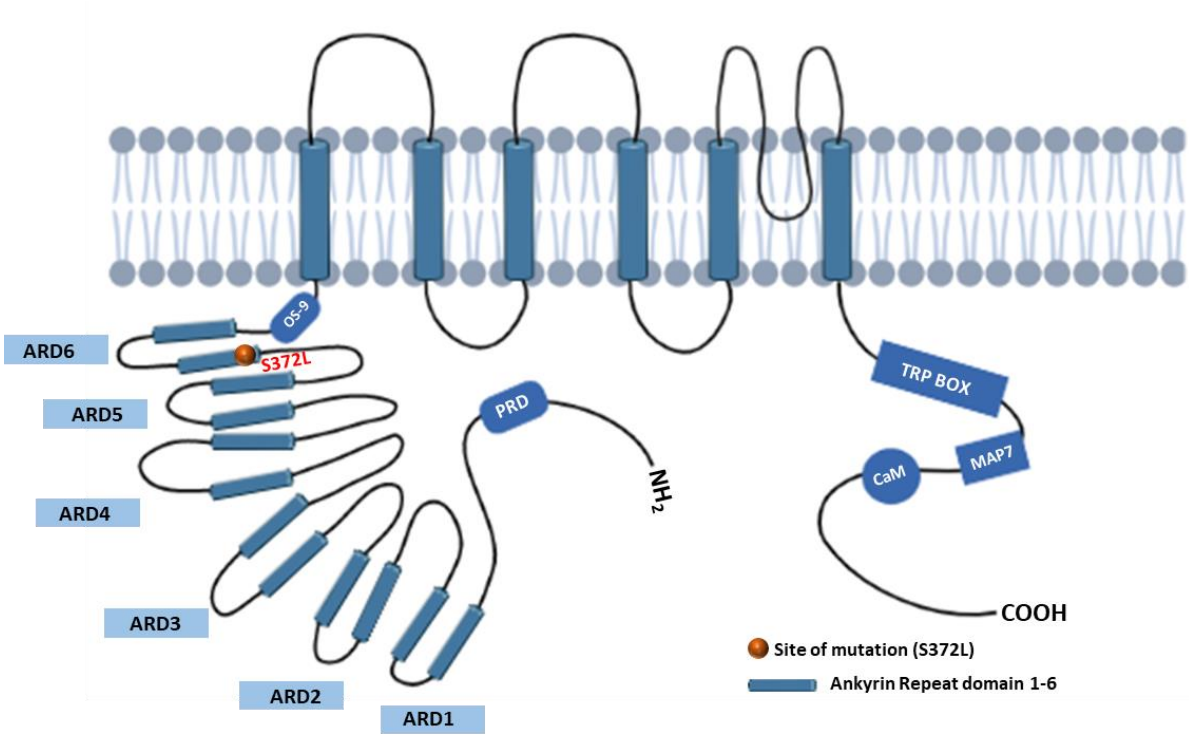


Fig. 99. Schematic representation of the site of occurrence of the S372L point mutation. The mutation lies on the ankyrin repeat domain of the channel at the N-terminal cytosolic region. (Un-published figure).

The S372L mutation was generated by site-directed mutagenesis using the TRPV4-WT sequence as a template. Subsequently, we expressed S372L mutant plasmid in various cell lines from different origins i.e. Saos-2 cell (Human osteosarcoma cell), MC3T3-E1 (Murine pre-osteoblast cell), K7M2 (Mouse osteo sarcoma cell), F-11 (Mouse DRG neuron derived cell), HaCaT (Human epidermal keratinocyte cell), 3T3-L1 (Mouse fibroblast cell). The TRPV4-WT and TRPV4-S372L construct were co-expressed with mitoDSRed in these cells to check the change in mitochondrial morphological parameters in TRPV4-S372L Expressing cells (**Fig. 100, 102**). We noticed that different cells expressing this mutant develop atypical mitochondrial shape. An intriguing finding was made in the human osteosarcoma cell Saos-2, which exhibits mitochondrial aggregation in cells specifically expressing S372L mutant but have normal mitochondria in cells expressing TRPV4-WT (**Fig. 100A**). In accordance, mitochondrial morphology remains normal in the MC3T3-E1 cell (a murine osteoblast cell line), and no mitochondrial aggregation is observed in these cells (**Fig. 100B**). However, in another mouse osteosarcoma cell K7M2, the mitochondrial shape changes are observed where mitochondria become more circular and aggregated in cells expressing S372L mutant (**Fig. 100C**). When we examined the mitochondrial morphology in three more cell lines (F-11, HaCaT, and 3T3L-1) with various lineages, we observed that the mitochondria become circular and aggregated in cells expressing mutant (**Fig. 102A-C**)

Additionally, we quantified various mitochondria morphometric analyzes using the “mito morphology” plugin of Image J. We quantified mitochondrial number, mitochondrial content (% of cytosol covered by mitochondria), mitochondrial area, mitochondrial perimeter, mitochondrial circularity and solidity in six different cells. We compared cells expressing TRPV4-WT with TRPV4-S372L mutant. We found that in Saos-2 cells expressing S372L mutant, the mitochondrial

area, perimeter, and area/perimeter reduced in cells expressing mutant, but the number and solidity of the mitochondria remained unaltered (**Fig. 101A**).

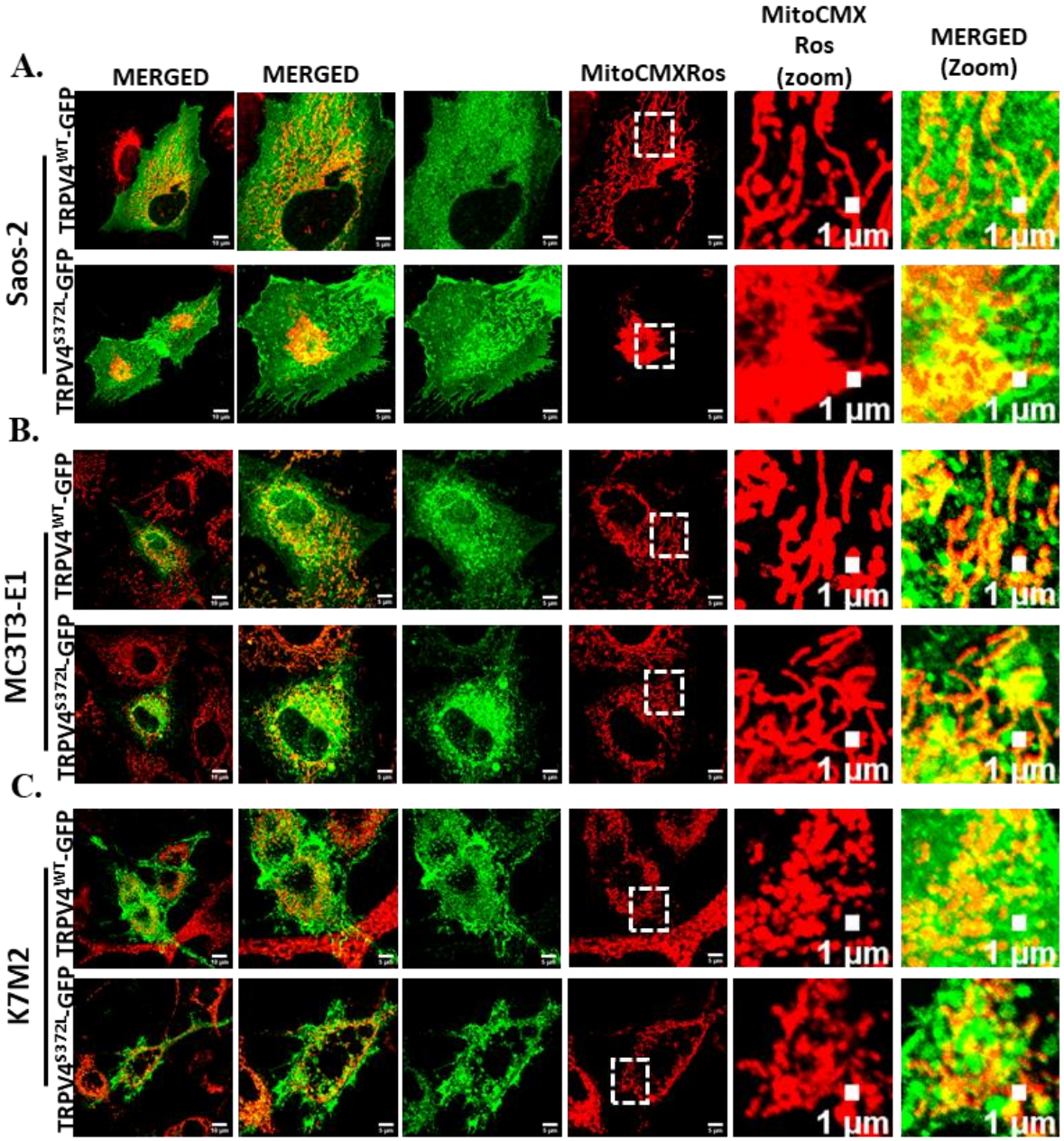


Fig. 100. TRPV4-S372L mutation changes mitochondrial morphology in bone cells. A-C: Human osteosarcoma (Saos-2) cells, murine pre-osteoblast cell (MC3T3-E1) cells, mouse osteosarcoma cell (K7M2) were transfected for transient expression of GFP-tagged TRPV4-WT or TRPV4-S372L. MitoCMXRos were used as a mitochondrial marker. Mitochondrial shape becomes abnormal (mostly spherical) and aggregated in cells expressing these mutants. Mitochondrial shapes remain elongated in cells that express TRPV4-WT. (Un-published figure).

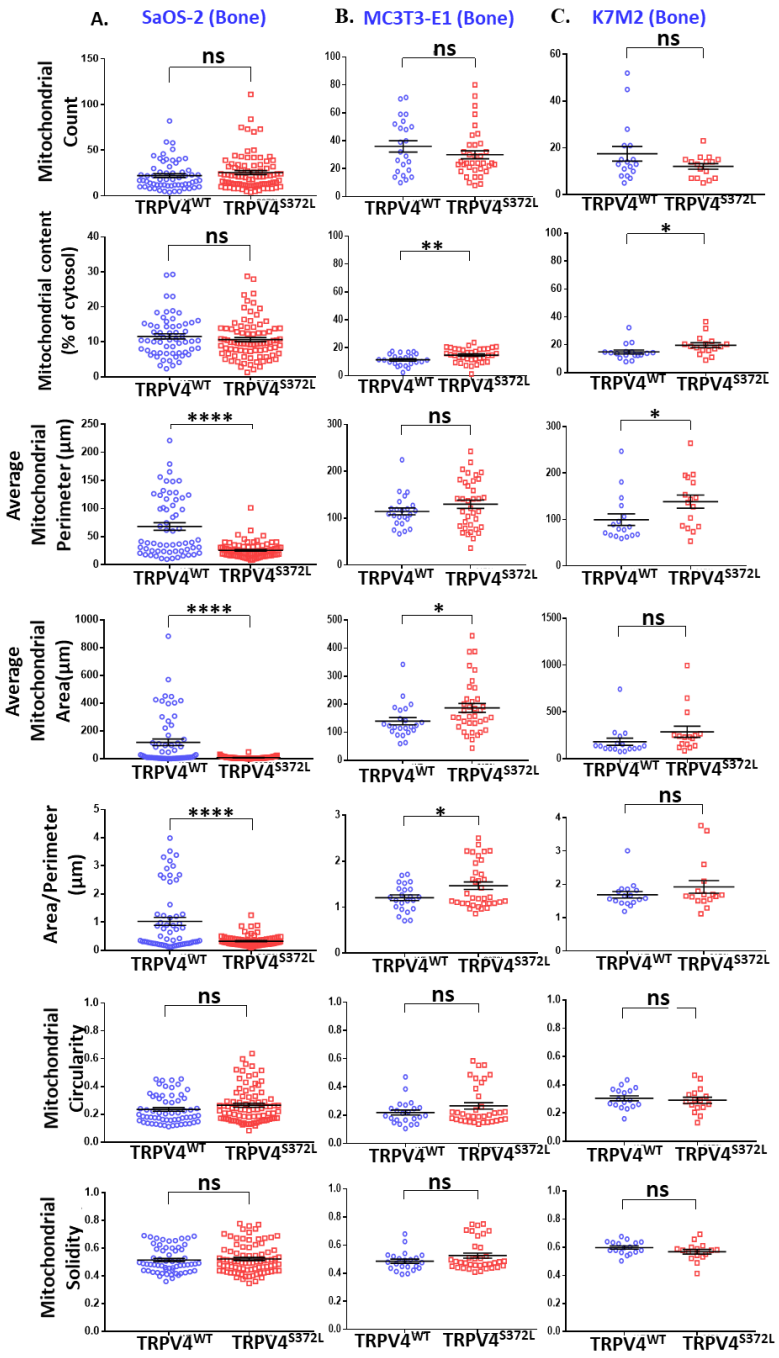


Fig. 101. TRPV4-S372L mutant differentially affects mitochondrial function in bone cells. A. Different parameters of mitochondria in Saos-2 cells expressing TRPV4-WT or S372L mutants were quantified. Significant reductions in mitochondrial area, perimeter and area/perimeter were observed (n≥80 cells). **B**. However, in MC3T3-E1 cells, the area and are/perimeter values increased (n≥20 cells). **C.** In K7M2 cells, the mitochondrial perimeter and mitochondrial content are increased and no significant changes are observed in other parameters (n≥20 cell). The values were compared by student's t-test. ns: non-significant, * = $p<0.05$, ** = $p<0.01$, **** = $p<0.0001$. (Un-published figure).

In MC3T3-E1 cells the mitochondrial area and area/perimeter (inter connectivity) increased and there is no significant change observed in other parameters in S372L mutant expressing cells (**Fig. 101B**). Similarly, in K7M2 cells, there is an increment observed in mitochondrial perimeter and mitochondrial content in mutant cells (**Fig. 101C**). In DRG neuron-derived cell line F-11 cells the mitochondrial circularity and solidity increase in cells expressing S372L mutant. Increased mitochondrial inter-connectivity is also observed, which suggests mitochondrial aggregation in cells expressing S372L mutant (**Fig. 103A**). When we checked these parameters in human keratinocyte cell HaCaT we found that there is a significant reduction in mitochondrial interconnectivity, mitochondrial circularity and solidity in the mutant cells. These results are different from other cell line data (**Fig. 103B**). Interestingly we could not find any significant changes in mitochondrial morphology in 3T3-L1 cells expressing WT or mutant (Mouse fibroblast cell) (**Fig. 103C**).

In a nutshell, the features of this novel mutation, i.e. S372L, is variable in different cells. Therefore, this needs further experiments to understand the effect of this mutation in different cells.

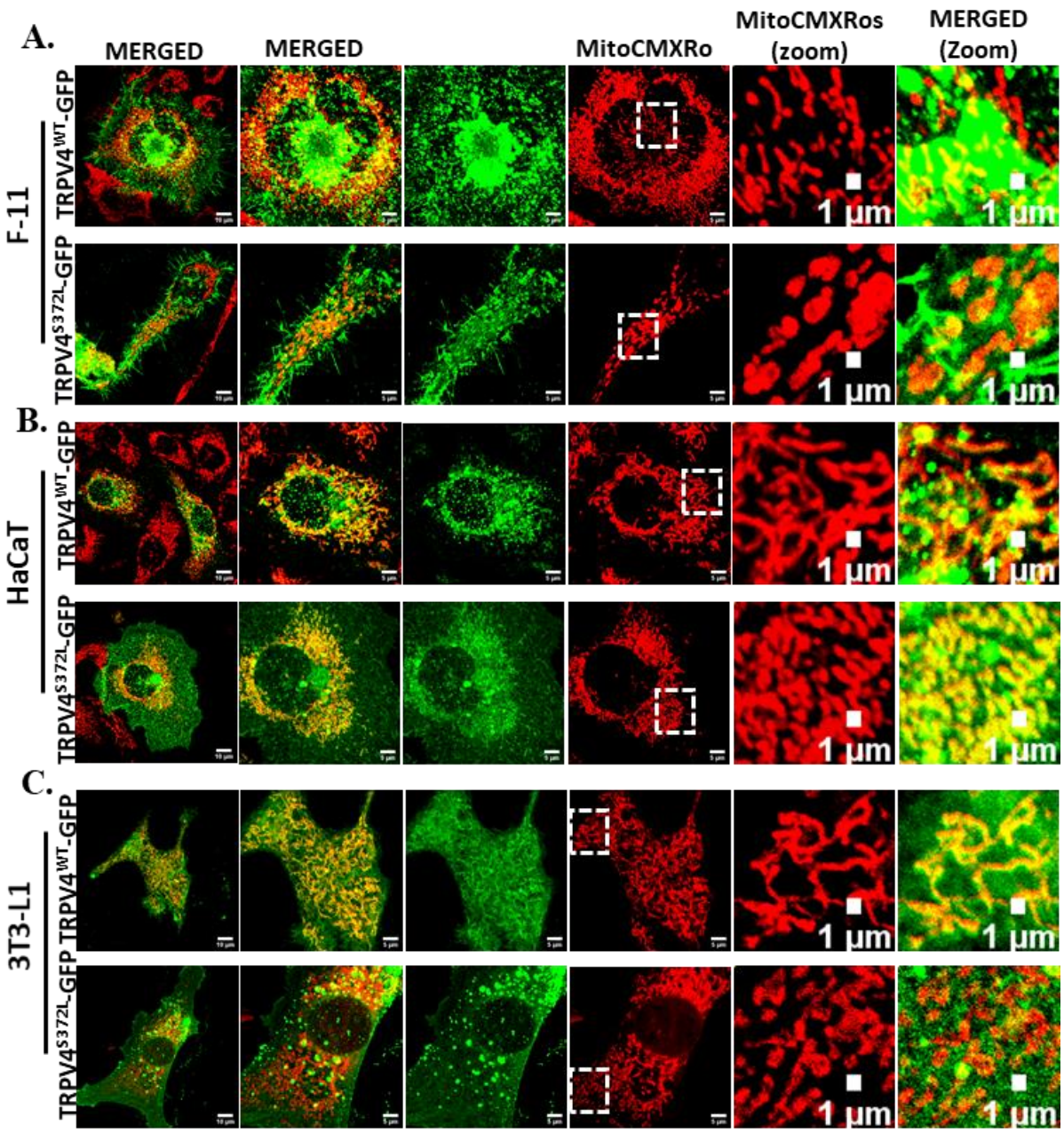


Fig. 102: TRPV4-S372L mutation changes mitochondrial morphology in neuronal, keratinocyte and fibroblast cells. A-C. Mouse DRG neuron-derived cells (F-11), Human keratinocyte cells (HaCaT) cells, mouse fibroblast cells (3T3-L1) were transiently transfected for the expression of GFP-tagged TRPV4-WT or TRPV4-S372L mutant. MitoCMXRos was used as a mitochondrial marker. Mitochondrial shape becomes abnormal (mostly spherical) and aggregated in cells expressing TRPV4-S372L mutant. Mitochondrial shapes remain elongated in cells that express TRPV4-WT. (Un-published figure).

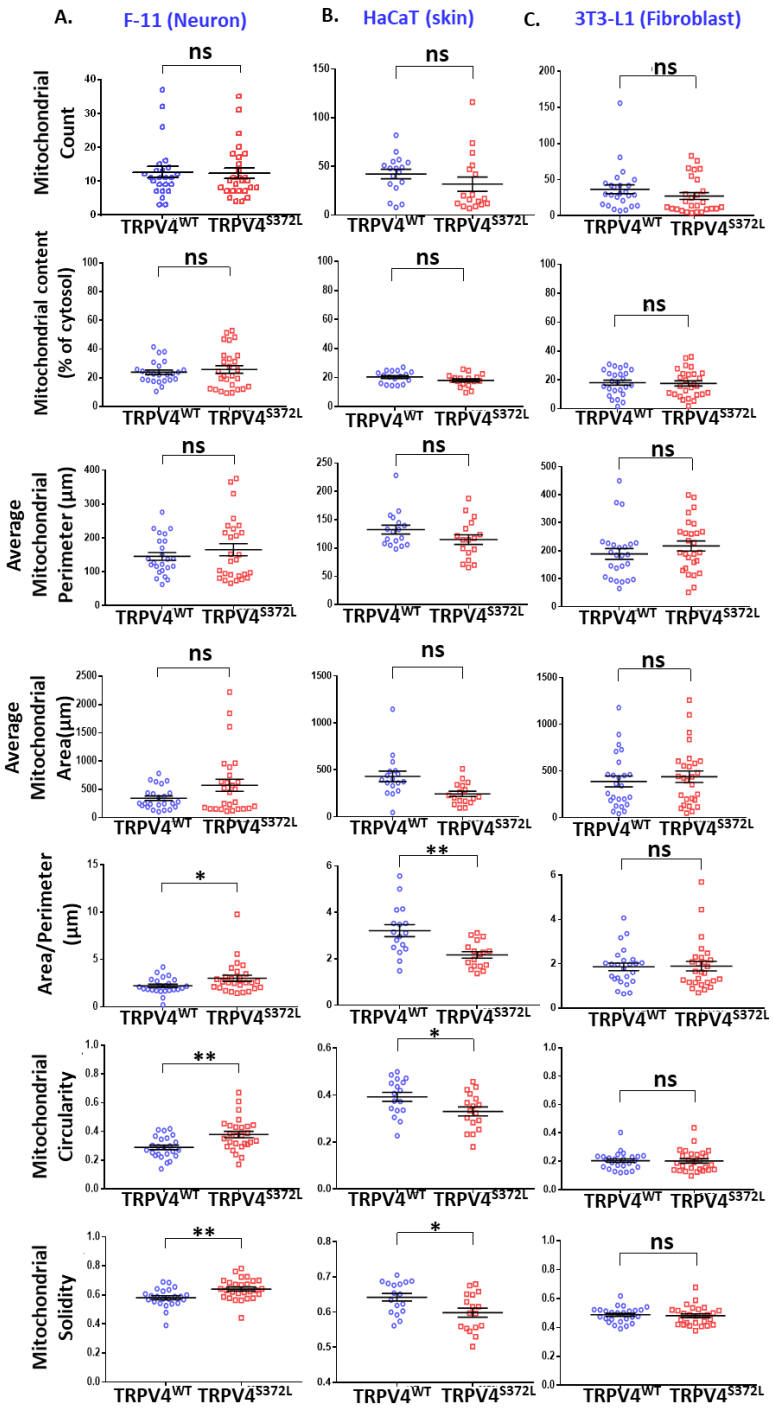


Fig. 103. TRPV4-S372L mutant differentially affects mitochondrial function in neuronal, keratinocyte and fibroblast cells. A. Different parameters of mitochondria in F-11 cells expressing TRPV4-WT or TRPV4-S372L mutants were quantified. Significant increament in mitochondrial area/perimeter, circularity and solidity was observed (n≥20 cell). **B**. In HaCaT cells, the are/perimeter, circularity and solidity values decreased (n≥20 cells). **C.** In 3T3-L1 cells, no significant changes were observed in mitochondrial parameters. The values were compared by student's t-test. ns: non-significant, * = $p<0.05$, ** = $p<0.01$. (Un-published figure).

2.8.4 TRPV4-S372L mutation regulates cytosolic Ca^{2+}-level:

To check the ability of ion conductance of the mutant TRPV4, we performed a cytosolic Ca^{2+}-imaging experiment. We have used TRPV4 agonist 4αPDD (5 µM) as a specific modulator of TRPV4 and compared the extent of Ca^{2+}-influx in cells expressing the wild type and the mutant. We have performed live cell time series Ca^{2+}-imaging (up to 200 frames, ~7 min) by using a genetically encoded cytosolic Ca^{2+}-sensor (GCaMP) for measurement of changes in the cytosolic Ca^{2+}-level. We found that upon addition of 4αPDD at 20th frame, the extent of Ca^{2+}-influx is more in mutant cells (**Fig. 104A-B**). We further checked the Ca^{2+}-influx in conditions where cytosolic Ca^{2+} is chelated by BAPTA-AM. We treated the cells with BAPTA-AM (5µM) for 1 hour and subsequently checked the Ca^{2+}-influx in response to 4αPDD. Here also we noticed unchecked and sustained Ca^{2+}-surge in the mutant cells compared to wild type cells (**Fig. 104C-D**). Interestingly in mutant expressing cells, we observed early and sustained Ca^{2+}-influx as compared to wild type cells. We next intended to check the Ca^{2+}-influx by incubating the cells with EGTA for 1hr. to chelate the extracellular Ca^{2+}-source. In this condition, also we observed uncontrolled and sustained Ca^{2+} escalation in mutant cells (**Fig. 104E-F**). Notably, the rise in Ca^{2+}-influx is always higher in the mutant cells and the uncontrolled and sustained rise of calcium suggests abnormal/abolished Ca^{2+}-buffering ability of these cells. Furthermore, we checked the Ca^{2+}-influx in these cells by adding TRPV4 antagonist RN1734 (10 µM) at the 20th frame and we observed reduced calcium influx in both wild-type and mutant cells (**Fig. 104G-H**).

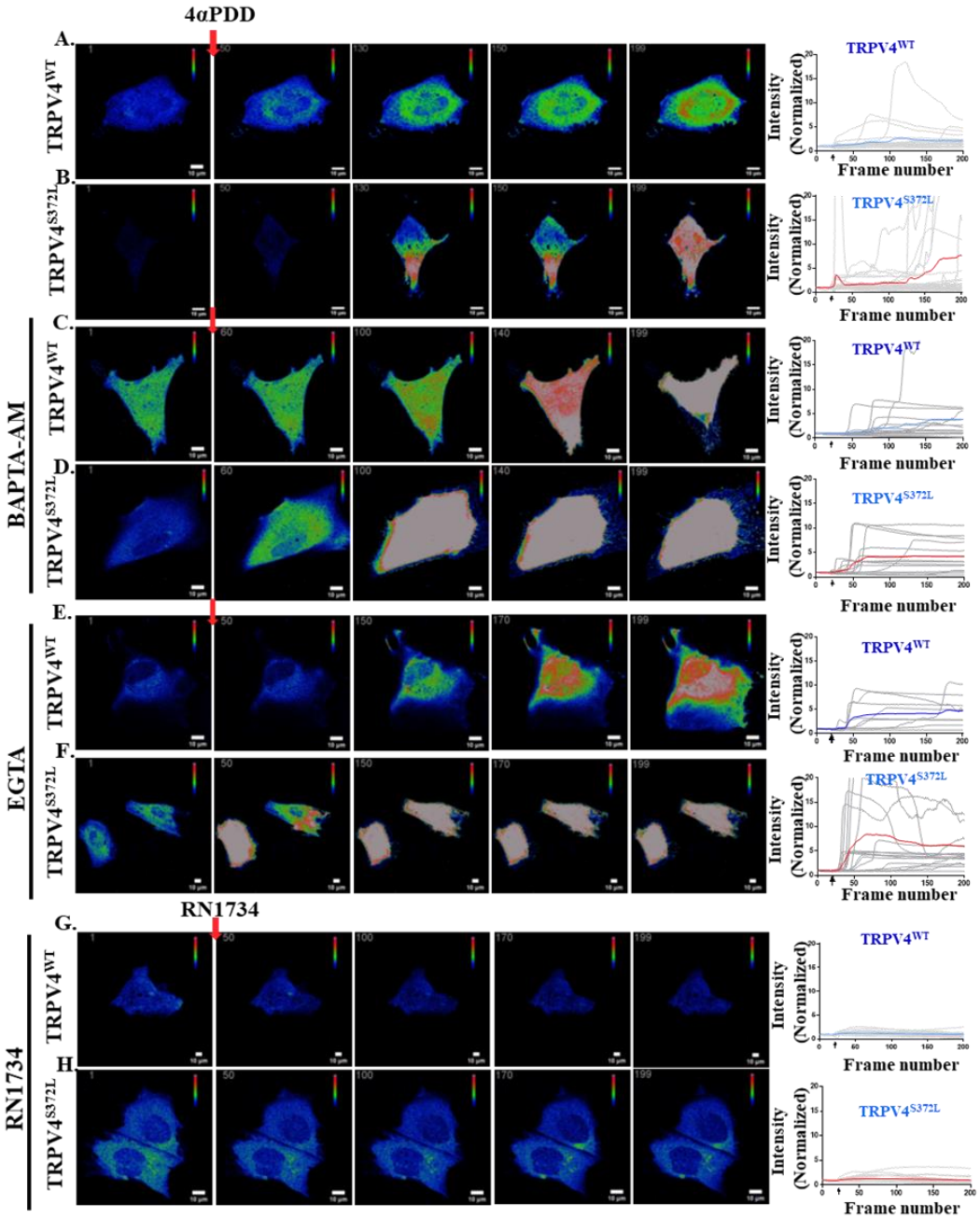


Fig. 104. TRPV4-S372L mutant modulates cytosolic Ca^{2+}-influx in human osteosarcoma cells (Saos-2). A-B. Saos-2 cells were co-transfected with GCaMP and TRPV4-WT-mcherry or TRPV4-S372L-mcherry. Transfected cells were treated with 4αPDD at the 20th frame and live cell time series was performed up to 200 frames. Mutant cells influx more Ca^{2+} inside the cell (n≥10 cell). **C-D**. Ca^{2+}influx was measured after chelating the cytosolic calcium by BAPTA-AM. The propensity of Ca^{2+}-influx is more in mutant cells with compared to wild type cells. **E-F.** In a similar manner, the cells were treated with Thapsigargin and cytosolic Ca^{2+}-level was checked. In mutant cells, the Ca^{2+}-level rose to a larger extent. **G-H.** When the TRPV4 antagonist RN1734 was applied to the cells, both wild-type and mutant cells experienced a decrease in the rate of Ca^{2+}-influx. (Un-published figure).

2.8.5 TRPV4-S372L mutation alters mitochondrial Ca^{2+}-level:

Cellular Ca^{2+}-homeostasis is mainly maintained by mitochondrial and other subcellular organelles and their individual Ca^{2+}-levels. After checking the changes in cellular Ca^{2+}-level in the mutant cell which intrigued us to check the change in mitochondrial Ca^{2+}-level upon treatment of TRPV4 activator 4αPDD in Saos-2 cells. We have used a genetically modified ratio metric construct, i.e. Mito-Pericam for the detection of mitochondrial Ca^{2+}-level. From this experiment we observed sustained Ca^{2+}-rise in mutant cells compared to wild type cells (**Fig. 105**). However, this experiment needs detailed investigation and measurement of individual mitochondrial Ca^{2+}-level will give greater insight into the regulation of mitochondrial Ca^{2+}-level in mutant cells.

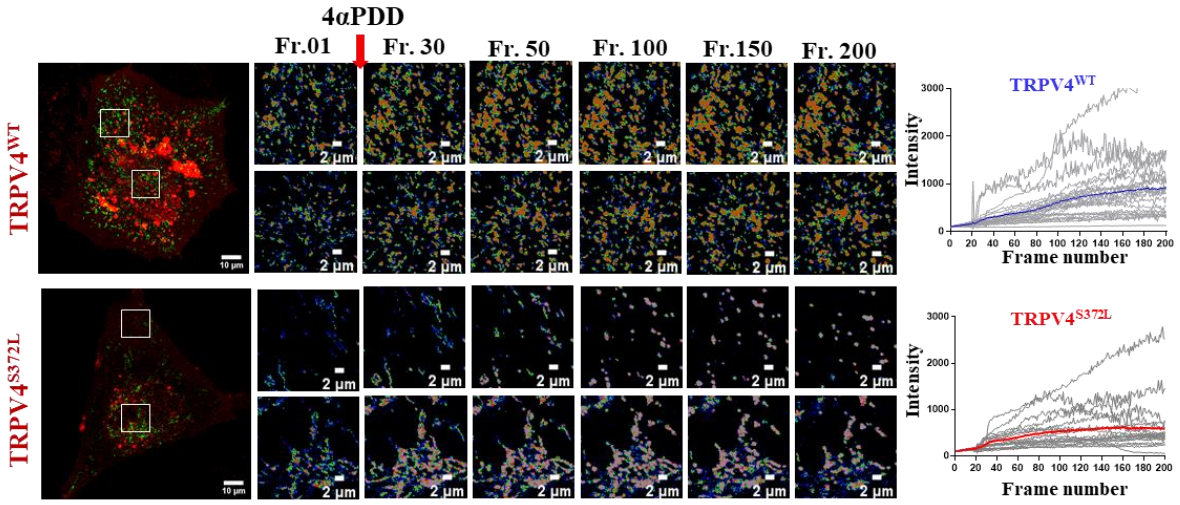


Fig. 105. TRPV4-S372L mutant modulates mitochondrial Ca^{2+}-influx in human osteosarcoma cells (Saos-2). Saos-2 cells were co-transfected with Mito-Pericam and TRPV4-WT-mcherry or TRPV4-S372L-mcherry. Transfected cells were treated with 4αPDD at the 20th frame and live cell time series was performed up to 200 frames. Mutant cells influx more Ca^{2+} inside the mitochondria (n≥10 cells). (Un-published figure).

2.8.6 TRPV4-S372L mutation alters mitochondrial ROS and ATP level:

Mitochondrial ROS and ATP are the crucial indicators of mitochondrial health. We checked the mitochondrial ROS production and ATP generation in cells that express this mutant. For this experiment, Saos-2 cell (human osteosarcoma cell) was used. After transfection of the TRPV4-WT and TRPV4-S372L construct in Saos-2, cells were labelled with MitoSOXred dye for mitochondrial superoxide measurement and ATP-red dye for quantification of mitochondrial

ATP level. We observed an increment in mitochondrial ROS and ATP levels in cells expressing S372L mutant when compared to TRPV4-WT (**Fig. 106A-D**).

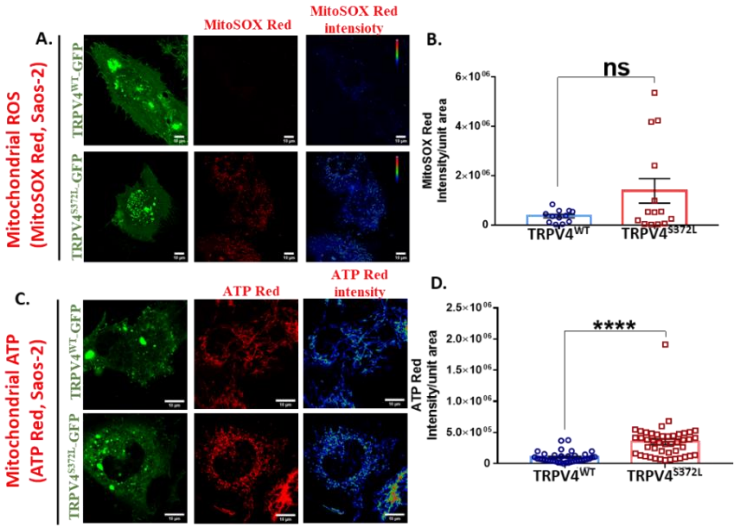


Fig. 106. TRPV4-S372L mutant increases mitochondrial ROS and ATP-level in human osteosarcoma cells (Saos-2). A-B. Saos-2 cells were transfected for transient expression of TRPV4-WT and TRPV4-S372L. The levels of mitochondrial ROS were monitored by using MitoSOX Red dye. TRPV4-S372L-expressing cells produce higher mtROS (n≥10 cells). **C-D**. The wild-type and mutant expressing cells were labelled with ATP red dye for the detection of mitochondrial ATP levels. The mitochondrial ATP-level is higher in cells expressing S372L mutant (n≥10 cell). The values were compared by student's t-test. ns: non-significant, **** = p<0.0001, ns = non-significant. (Un-published figure).

2.8.7 Expression of TRPV4-S372L mutation regulates mitochondrial Cardiolipin and ER temperature level:

Cardiolipin is a phospholipid exclusively present in the inner mitochondrial membrane. Cardiolipin maintains the mitochondrial membrane integrity and makes the respiratory complexes stable. As the patient having this mutation have a diverse range of lipid and steroid related problems, we explored the changes in the mitochondrial Cardiolipin level, especially in the cells expressing the S372L mutation. The Cardiolipin was measured by using NAO dye (Nonyl Acridine Orange). From this experiment, we observed that there is no change in the Cardiolipin level in WT and mutant cells, at least in ~50 cell lines and in our experimental conditions (**Fig. 107A-B**).

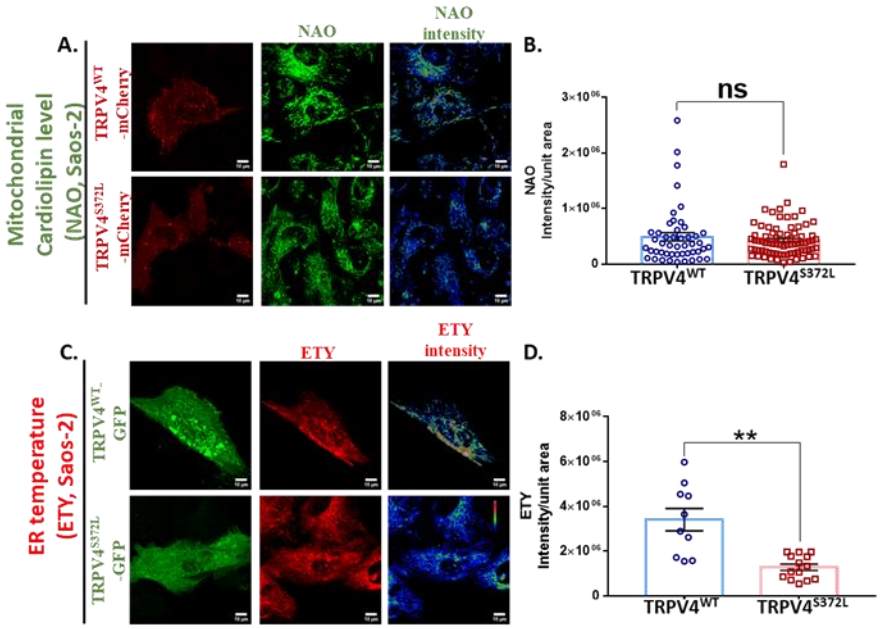


Fig. 107. TRPV4-S372L mutant alters mitochondrial Cardiolipin and ER temperature level in human osteosarcoma cells (Saos-2). A-B. Saos-2 cells were transfected for transient expression of TRPV4-WT and TRPV4-S372L. The level of mitochondrial Cardiolipin was monitored by using NAO dye. Mitochondrial Cardiolipin is not significantly altered in wild type and mutant cells.(n≥10 cells). **C-D**. The wild type and mutant expressing cells were labelled with ETY dye for detection of ER temperature level. The ER temperature is higher in mutant cells (decrease in ETY intensity).(n≥10 cell). The values were compared by student's t-test. ns: non-significant, * = $p<0.05$, ** = $p<0.01$, ns = non-significant. (Un-published figure).

Mitochondria is highly dependent on ER for various metabolism Ca^{2+}, steroids, and other crucial metabolites are exchanged between ER and mitochondria. Till now, we have observed various changes in the mitochondrial morphological and physiological parameters. We further explored if the S372L mutant can cause any changes in ER function. By using ETY (ER temperature sensing dye), we characterized the changes in ER temperature in mutant cells. The ER temperature is inversely proportional to ETY dye intensity. When we quantified the ETY intensity in mutant cells, we noticed a reduction of ETY intensity (increase in ER temperature) in mutant expressing cells compared to wild type cells. This suggests that the S372L mutation alters ER temperature and, thus, ER metabolism (**Fig. 107C, D**).

Summary: Several point mutants of TRPV4 affect mitochondrial structure, distribution and morphology in a variable manner and have different levels of mitochondrial translocation. In this study we have observed morphological alteration of mitochondria in TRPV4 mutant expressing cells. The mitochondria of human osteosarcoma cells Saos-2 cells and mouse pre-osteoblast cell MC3T3-E1 cells expressing various TRPV4 mutations (R616Q, F617L, L618P, V620I, and L596P) become circular and aggregated. We also characterize another mutation of TRPV4, namely S372L in different cell lines, especially in the context of cellular and mitochondrial parameters.

Chapter 3

Discussion

3.1 Physical presence of TRP channels in the mitochondria:

3.1.1 Localization of TRPV4 channel in mitochondria:

The importance of mitochondria in the intracellular Ca^{2+}-buffering is well established (Budd SL, 1996; Duchen MR, 1999; Jouaville LS, 1995). The temperature-sensing ability even in isolated conditions, also remain as a unique property of mitochondria. However, the molecular players involved in this feature are currently unknown (Chrétien D. 2018; Johnston IA, 1994; Kang SH, 2008). TRPV4 is involved in various physiological responses and mutations in TRPV4 cause severe pathophysiological disorders that are often lethal. Many "gain-of-function" mutations cause bone-related disorders like skeletal dysplasia (Das R, 2019; Nilius, B, 2013). In this work, we demonstrate that TRPV4 localizes to a sub-population of mitochondria in various cell types, including bone cells. TRPV4 localization in mitochondria is almost ubiquitous in nature. TRPV4 localization in the mitochondria is also observed in mature spermatozoa from different vertebrates (Kumar A, 2018). Thus, TRPV4-mediated mitochondrial regulation seems to be universal in nature. In this context, it is important to note that TRPV4 knock out animal survives without any major problem, at least in laboratory conditions. In contrast, point mutations in TRPV4 are mostly pathogenic and often become lethal and sometimes embryonic lethal (Verma P, 2010). Notably, all vertebrates retain at least one copy of the TRPV4 gene and so far there is not a single vertebrate known that do not have the TRPV4 gene, suggesting that TRPV4 is indispensable in the natural system and also suggest that the presence of TRPV4 offers additive benefit during vertebrate evolution. Therefore, regulations of mitochondrial structure and functions by TRPV4 are very important to understand, especially in the context of disease and health.

Though initially it was assumed that all TRP channels are primarily localized in the plasma membrane, later reports have confirmed that different TRP channels have diverse yet specific distributions to subcellular membranes, including ER, lysosomes or endosomes, where these channels participate complex tasks such as regulation of membrane trafficking, signal transduction, maintenance of ion- and pH-homeostasis (Dong XP, 2010; Yadav M, 2017; Majhi R, 2011). For example, in DRG neurons, TRPV1 is present in the ER, where it regulates the Ca^{2+}-wave at distinct microdomains, which may cause Ca^{2+}-overload at ER-associated mitochondria and subsequent damage of these mitochondria (Gallego-Sandín S, 2009; Olah Z, 2001). Indeed, TRPV1 is also reported to be present in mitochondria (Lang H, 2015). Similarly, TRPC3 is present in mitochondria and regulates membrane potential as well as Ca^{2+}-oscillation inside these mitochondria (Feng S, 2013). However, the molecular identities of various Ca^{2+} channels (and particularly TRPs) present in mitochondrial membranes are still lacking. Recently we demonstrated that TRPV4 interacts with Cytochrome C, a mitochondrial protein (Das R, 2022). Here, we demonstrate that TRPV4, a temperature-sensitive channel is endogenously present in mitochondria. Our work also provides molecular mechanisms that link TRPV4-mediated functions in the regulation of mitochondrial structure-function relationship as its activation results in Ca^{2+}-influx into the mitochondria. This observation is in full agreement with our previous report demonstrating that the Ca^{2+}-pattern in the mitochondria-enriched neck region of mature spermatozoa is altered upon TRPV4 activation (Kumar A, 2016). Moreover, the presence of TRPV4 that can act as a thermo-sensitive ion channel (Güler A, 2002). It agrees well with the reports that mitochondria maintain a higher temperature than the cytosol (Chrétien D, 2018; Lane N, 2018).

3.1.2 TRPV4 as a part of MAM:

The interaction of MFN1 and MFN2 with TRPV4 strongly suggests that TRPV4 can be present in mitochondria-associated ER membrane (MAM) fraction, the very specialised region which maintains ER-mitochondrial contact sites, i.e. the micro-domain relevant for Ca^{2+}-dynamics in a range of 20-200 nm distance (Patergnani S, 2011). This is in accordance with our findings demonstrating that TRPV4 is present in the ER-mito contact points. This is also consistent with the observation that TRPV4-positive mitochondria are primarily localized in the perinuclear regions (Acharya TK, 2022a). MAM is closely connected to ER and thus may facilitate the direct sorting of TRPV4 from ER to mitochondria (Raturi A, 2013). Notably, MFN2 is known to be involved in the regulation of ER-mitochondrial contact regions (Sugiura A, 2013), and thus, the TRPV4-MFN2 complex may be relevant for Ca^{2+}-dependent regulation of mitochondrial functions (De Brito OM, 2008; Qi H, 2015). In this context, it is essential to mention that mitochondria have sensitivity for recognising microdomains of high cytoplasmic Ca^{2+}, which dissipates high influx and efflux of Ca^{2+} across the mitochondrial membrane. Because of this notion, most of the mitochondria are in close proximity with ER (in fact, connected through MAM) and mediate easy exchange of divalent cations such as Ca^{2+}. Recent reports also suggest that MAM regions are relevant for several neurological disorders, as mitochondrial functions are related to critical processes, such as lipid homeostasis, cholesterol biogenesis, mitochondrial Ca^{2+}-signaling, mitochondrial morphology and mitochondrial dynamics (Krols M, 2016). Our previous study demonstrated that TRPV4 has the ability to interact with different sterols, sterol-precursors and their derivatives (Kumari S, 2015). These findings also support the notion that the presence of TRPV4 in the MAM can be of functional importance for transport and metabolism (of sterols and its intermediates) between ER and mitochondria (Kumari S, 2015). Altogether, our results suggest

that TRPV4 is present in the MAM region and regulates ER-mito associated functions significantly. Our findings also link TRPV4 as a major candidate to understand the mitochondrial diseases. Notably recent reports suggest that not only TRPV4, but also other TRP members, i.e. TRPV1 and TRPM8 are present in MAM (Ortíz-Rentería M, 2018; Bidaux G, 2018).

3.1.3 Localization of TRPM8 channel in mitochondria:

TRPM8 channel is a cold-sensing non-selective cation channel. TRPM8 was initially discovered in the prostate tissue and has gradually been found in other cellular and tissue systems. TRPM8 is detected not only at the plasma membrane but also in the other intracellular organelles like ER where it supports cold/Menthol/icilin-induced Ca^{2+}-release from the ER (Thebault S, 2005). There is a report which demonstrates the localization of an isotype of full-length TRPM8 (i.e. 4TM-TRPM8) in the ER and ER-mito contact region. They have also shown an increment of the Ca^{2+}-level at the MAM region and mitochondria as well due to the activation of this channel (Bidaux G, 2015). This thesis work investigated the mitochondrial localization of TRPM8. The results demonstrated the localization TRPM8 in the mitochondria in endogenous bone marrow derived Mesenchymal stem cells, human osteosarcoma cell Saos-2 cells and in the cell-free isolated mitochondria also. Moreover, the presence of thermosensitive TRPM8 in mitochondria supports the previous observations about the thermosensing behavior of mitochondria.

3.1.4 Functional characterisation of TRP channels in mitochondrial function in T cell:

So far, several reports have confirmed that different TRP channels, such as TRPV1, TRPV4, TRPM8, TRPA1 are expressed endogenously in the resting T cell, and their expression pattern alters during T cell activation (Majhi RK, 2015; Acharya TK, 2021; Sahoo SS, 2019). Accordingly, applications of different pharmacological activators specific for different TRP channels increase cytosolic Ca^{2+}-levels in T cells, often in a dose-dependent and time-dependent

manner (Majhi RK, 2015; Acharya TK, 2021; Sahoo SS, 2019). However, the entire Ca^{2+}-dynamics is mostly assumed to be "primarily cytosolic in nature" and mediated by the ion channels present at the surface, i.e. in plasma-membrane. However, in this work, we demonstrate that changes in mitochondrial parameters are intimately associated with the T cell activation process and TRPV4, an ion channel plays important role in the regulation of several of these mitochondrial parameters, such as membrane potential, ATP-levels, ROS, and Cardiolipin-levels. In this thesis work, the mitochondria and ER temperature as well as the extent of ER-mitochondrial contact points, were also compared. This work indicates that the changes in the mitochondrial parameters are relevant for T cell activation process and also sheds light on several important issues which are discussed below.

3.1.5 Presence of endogenous TRPV4 in the mitochondria of T cells has immunological consequences:

Upon antigen recognition, the T cell drives the cellular organelles, such as mitochondria, secretary apparatus and other signaling molecules to the "immune synapse" (Desdín-Micó G, 2018). It has been reported that mitochondria translocate primarily to the "IS" during the process of T cell activation (Quintana A, 2007). This translocation of large number of mitochondria to the IS is not only for supplying more ATP to the specific sub-cellular site, but also is relevant for controlling cellular and subcellular Ca^{2+}-level (Desdín-Micó G, 2018). It has been noted that during T cell activation (as a process of TCR-bead-mediated signaling events), mitochondrial Ca^{2+}-level goes significantly high as compared to the resting T cells. This data accords well with previous report which also suggested that at IS, enhances mitochondrial Ca^{2+}-level is linked to ATP production (Ledderose C, 2014). It has been noted that the increased mitochondrial Ca^{2+}-level is irrespective of TRPV4 activation or inhibition, suggesting that TCR-signaling is upstream

of TRPV4-medaited mitochondrial signaling. Inhibition of TRPV4 by RN1734 does not prevent translocation of mitochondria, neither the formation of IS mediated by TCR-beads treatment. Thus, TCR-signaling seems to be dominant over TRPV4-mediated mitochondrial signaling. However, our data indicate that increased mitochondrial Ca^{2+}-can be a key prerequisite for T cell activation. This accords well with the fact that perturbing mitochondrial Ca^{2+} affects IS formation (Trebak M, 2019).

3.1.6 TRPM8 regulates mitochondrial function in Tcells:

The surface expression of TRPM8 increases due to activation by Con A (Acharya TK, 2021; Kume H, 2019). In this study, the effect of TRPM8 modulation by pharmacological means on subcellular organelles in a comparative manner between resting and TCR-treated T cells has been tested. In activated cells, mitochondria translocate to the immediate vicinity of immune synapse (IS) and maintains the Ca^{2+}-level high and helps in Ca^{2+}-dependant T cell activation (Quintana A, 2007). Translocation of mitochondria to the "IS" not only regulates Ca^{2+}-level but also supplies higher ATP to mediate the T cell activation process and cytokine production (Desdín-Micó G, 2018). It is noteworthy to mention that so far presence of several TRP ion channels in mitochondria have been reported (Acharya TK, 2022a; Acharya TK, 2022b). In a similar manner, TRPM8 has also been reported to be localized at the MAM (Mitochondria Associated Membrane) (Bidaux G, 2016). Nevertheless, the detailed localization and complex functionality of TRPM8 in mitochondria of T cell is not known yet. This work establishes the colocalization of TRPM8 with mitochondrial markers in resting as well as activated Tcells for the first time. TRPM8 regulates Ca^{2+}-influx, both in the cytosol and in mitochondria, though the exact regulation and mode seems to be different. Notably, the activation of TRPM8 by its agonist elevates both cytosolic and mitochondrial Ca^{2+}. Mitochondrial Ca^{2+}-uptake plays a crucial role in the fundamental events

involved in cellular Ca^{2+}-signaling. Mitochondrial Ca^{2+}-level is a cumulative effect of cytosolic Ca^{2+}-source and store operated Ca^{2+}-sources which are mainly the ER and other organelles. It is known that mitochondria make close contacts with ER for Ca^{2+} and other metabolite exchange. This phenomenon prompted to check the probable Ca^{2+}-source of mitochondria in T cells in the context of TRPM8 modulation. Two different agonists of TRPM8, i.e. WS12 and Menthol, have been used for that purpose.

3.2 Importance of TRP channels in mitochondria: Regulation of mitochondrial Ca^{2+}-homeostasis:

3.2.1 TRPV4 regulates mitochondrial Ca^{2+}-influx and mitochondrial membrane potentiality:

Intracellular Ca^{2+} plays a major role in mitochondrial heterogeneity. Impaired mitochondrial Ca^{2+}-buffering can lead to various pathophysiological situations. Subcellular Ca^{2+}-level promotes changes in mitochondrial morphology as well as motility (Kremneva E, 2013). Our results confirm that TRPV4 agonists and antagonists play a critical role in the regulation of mitochondrial Ca^{2+}-levels. Ca^{2+}-ions also affect the mitochondrial structure, membrane potential, and its energetics. The increment in the mitochondrial Ca^{2+}-levels after 4αPDD treatment, both in whole cell as well in isolated mitochondria, correlates well with the presence of TRPV4 in mitochondria. Similar effects of 4αPDD in CHO-K1-V4 strongly argue for a functional contribution of TRPV4 in mitochondrial membranes, causing increased Ca^{2+}-influx into mitochondria. Considering that Ca^{2+}-buffering by mitochondria is an important aspect of cell function and health, abnormality in mitochondrial Ca^{2+}-buffering can cause compromised cell functions that in turn, may cause serious health hazards. However, the complexity of multiple mitochondrial functions that are actually linked with mitochondrial Ca^{2+}-level needs detail

analysis and needs novel technical approaches to monitor these functions in real-time. Here using specific fluorescence probes, we demonstrate that TRPV4 regulates mitochondrial Ca^{2+}, temperature, and other metabolism as well. Our studies in stable cell lines as well as in endogenous systems indicate that TRPV4-medaited mitochondrial Ca^{2+} regulation is most-likely linked with the mitochondrial numbers. In general, increased mitochondrial Ca^{2+} leads to reduced mitochondrial numbers.

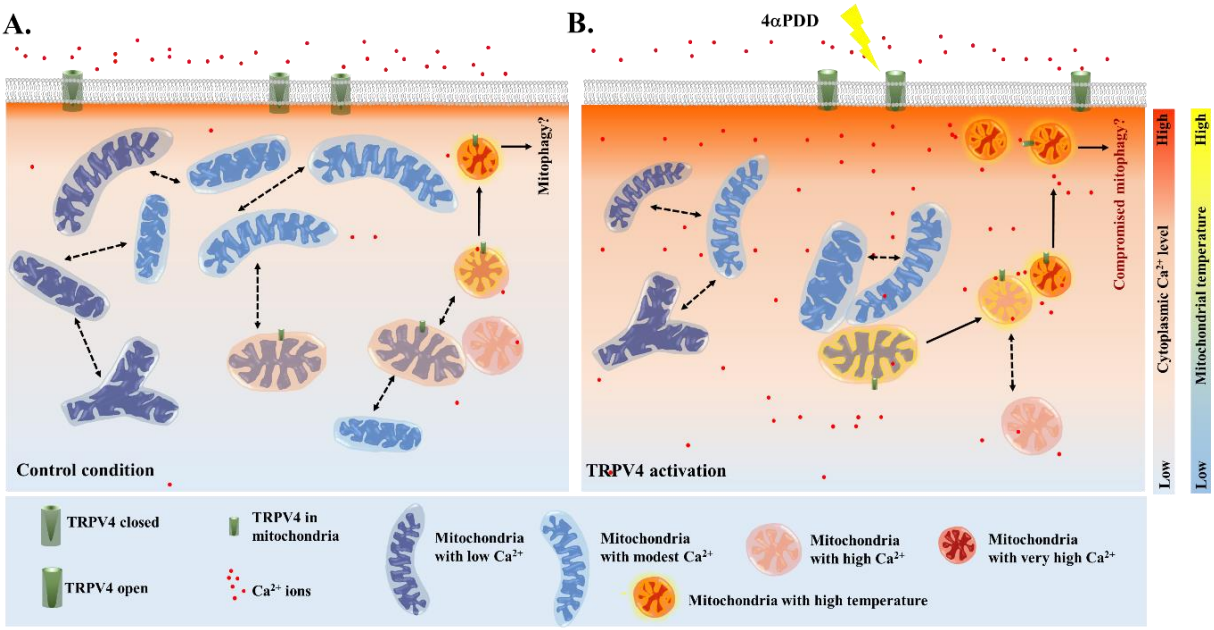


Fig. 108. Schematic model depicting the TRPV4- and Ca^{2+}-dependent regulation of mitochondrial structures, numbers and temperature. Intracellular Ca^{2+} is buffered by mitochondria which can be classified in multiple subpopulations that have low, moderate, high and very high levels of intra-mitochondrial Ca^{2+}. Majority of these particles have capacity to exchange mitochondrial Ca^{2+} (indicated by double headed arrows) to each other and only a limited percentage of particles fails to do so. It seems that the mitochondria with moderate and low amount of Ca^{2+} have a better buffering ability whereas mitochondria having high and very high Ca^{2+}-levels are functionally inferior, probably have compromised buffering capacity and regulated by complex mitophagy. **A.** In control conditions (as shown in left side), the cytoplasm contains modest amount of Ca^{2+} which can be buffered efficiently by the high number of mitochondria (with low and moderate levels of Ca^{2+}) that are also well-distributed throughout the cell. These mitochondria have good shape, size, proper functions, and have capacity to exchange mitochondrial Ca^{2+} with each other effectively resulting in proper quality control of the cells. In this condition, only a very small fraction of mitochondria have high-levels of Ca^{2+}, suggesting that only limited particles fail to buffer-out their Ca^{2+}-content (indicated by unidirectional arrows) and probably controlled by regulated mitophagy. **B.** In case of TRPV4 activation, the intracellular Ca^{2+} concentration increases quickly to several

fold. This escalates the Ca^{2+}-level drastically in mitochondria that contains higher amount of TRPV4. This also creates different levels of Ca^{2+}-load to each mitochondrion. This in turn causes mitochondrial heterogeneity and mitochondrial aggregation causing rapid reduction in the mitochondrial number. In this condition, majority of the mitochondria becomes circular and often fused with each other which subsequently decreases the mitochondrial distribution within the cell leading to a situation where cytosolic Ca^{2+}-buffering by mitochondria is compromised. In case of over stimulation of TRPV4 (also in case of several gain-of-function mutants), higher fraction of mitochondria become less functional and have compromised ability to buffer cytosolic Ca^{2+}. This leads to altered state of cell function and signaling that need further investigation. Increase in the mitochondrial Ca^{2+} may also cause elevated mitochondrial temperature. (Published figure. Acharya TK.et al. 2022, *Mitochondrion*).

Excess of Ca^{2+} in mitochondria may regulate the energetics in several manners. First, initiation of dissipation of mitochondrial membrane potential; second, induction of changes in mitochondrial morphology; third, alteration of mitochondrial metabolite exchange, ATP production and/or ETCs; and fourth, induction of MPT through which excess Ca^{2+} can be removed; and fifth, eventually the mitochondria having high Ca^{2+}-overload can be degraded by mitophagy (Ngo J, 2021). TRPV4 expressing cells have a subpopulation of mitochondria with high amount of Ca^{2+} across the time series, which suggests that TRPV4 expression above a certain level itself impairs the mitochondrial Ca^{2+}-buffering ability (**Fig. 108**). In this context, mitochondria may have other TRP channels as well for Ca^{2+}-buffering under different conditions, which needs further studies. The fate of the mitochondria having higher Ca^{2+}-overload will need to be investigated further. This is in accordance with report showing that cardiomyocytes having TRPM4 decrease mitochondrial membrane potential; however, in the TRPM4 knockout cells, mitochondrial membrane potential restores normally (Wang C, 2021)

3.2.2 TRPV4 as a positive regulator for mitochondrial Ca^{2+} and negative regulator for ER-mito contact points:

Mitochondria are highly dynamic organelles that can rapidly change their morphology. They shape their morphology by going through fusion and fission events. Ca^{2+} is an essential

factor that regulates mitochondrial fission and fusion (Hom J, 2010). The fusion of mitochondria requires the merger of both the outer (MOM) and the inner mitochondrial membranes (IMM). Mitofusin1 (MFN1) and Mitofusin 2 (MFN2) are essential for MOM fusion (Rojo M, 2002), while Optic atrophy 1 (OPA1) mediates the fusion of the IMM (Griparic L, 2004). Ca^{2+} is an essential mediator of mitochondrial homeostasis too. In a highly energy-dependant condition, mitochondria make close contact with ER. The specific mitochondria-ER contact sites are called endoplasmic reticulum–mitochondria contact sites (ERMCSs) or mitochondria-associated membranes (MAM). It is known that the exchange of lipids, Ca^{2+}, reactive oxygen species takes place through MAMs (Rieusset J, 2018). The molecular mechanism of the formation of MAMs is, however, still unknown. Mainly MFN2 acts as a tethering protein and helps in making close association between ER and mitochondria and in the transportation of Ca^{2+} from ER to mitochondria.

The data generated in this work suggests that TRPV4 activation leads to rapid reduction in mitochondrial numbers. In this work, we demonstrate that cells with slightly higher level expression of TRPV4 has mitochondria that have higher Ca^{2+}-levels within as basal level. In different conditions, such as in control condition as well as in cytosolic Ca^{2+}-chelated (BAPTA-AM treated condition) or ER Ca^{2+}-depleted conditions (by Thapsigargin), enhanced level of mitochondrial Ca^{2+} is observed, suggesting that the mere presence of TRPV4 mostly results in higher intra-mitochondrial Ca^{2+}. Notably, pharmacological inhibition of TRPV4 by antagonist reduces this intra-mitochondrial Ca^{2+}. Interestingly, the presence of TRPV4 also results in less ER-mito contact formation almost in all conditions tested in this work. Collectively, this can suggest that slightly higher level expression of TRPV4 enhances higher mitochondrial Ca^{2+}, thus result in less ER-mito contact formation. This aspect might be very well regulated by TRPV4-MFN2 complex, and in a both Ca^{2+}-dependent as well as Ca^{2+}-independent manner. Such inverse

relationship may also suggest that higher mitochondrial Ca^{2+}-level leads to more mitochondrial aggregate formation and reduced ER-mito contact formation. However, if this inverse relationship is universal or cell, tissue and context specific, that needs further investigation.

3.2.3 Mitochondrial Ca^{2+} as a factor for determining the ER-mito contact points:

So far there are several studies conducted that indicate cytosolic Ca^{2+} as an important factor for ER-mito contact points. In general, these reports suggest that increase in cytosolic Ca^{2+} results in increased ER-mito contacts. However, our data indicates a complementary information which suggest that ER-mito contact points are inversely related to the mitochondrial Ca^{2+}-levels. This is mainly because values derived from CHO-K1-Mock and CHO-K1-V4 cells in control condition, and 4αPDD-treated as well as RN1734-treated conditions indicate this inverse relationship. The values derived from BAPTA-treated or Thapsigargin-treated conditions are not exactly comparable to this inverse relationship as in these conditions, Ca^{2+} is depleted either cytoplasmic or ER pools. However, the exact nature of this inverse relationship needs further experiments.

We also noted that there is also a difference in the expression of MFN2 in CHO-K1-Mock and CHO-K1-V4 cells. Notably, the functions of MFN1 and MFN2 are dependent on the cellular GTP. Recently we have also reported that there is a change in the GTP level in CHO-K1-Mock and CHO-K1-V4 cells in control, activated and inhibited conditions (Acharya TK, 2022a). Taken together, the data strongly indicate that TRPV4 forms complex with MFN1/MFN2 and/or the TRPV4-MFN2 complex activity is subject to regulation by relative presence as well as activity of TRPV4.

The importance of mitochondrial Ca^{2+} in ER-mito contact points is explained in a graphical model (**Fig. 109B-C**). This schematic representation indicates the fluctuation in cytosolic and mitochondrial Ca^{2+}-level as a factor of the extent of ER-mito contact points.

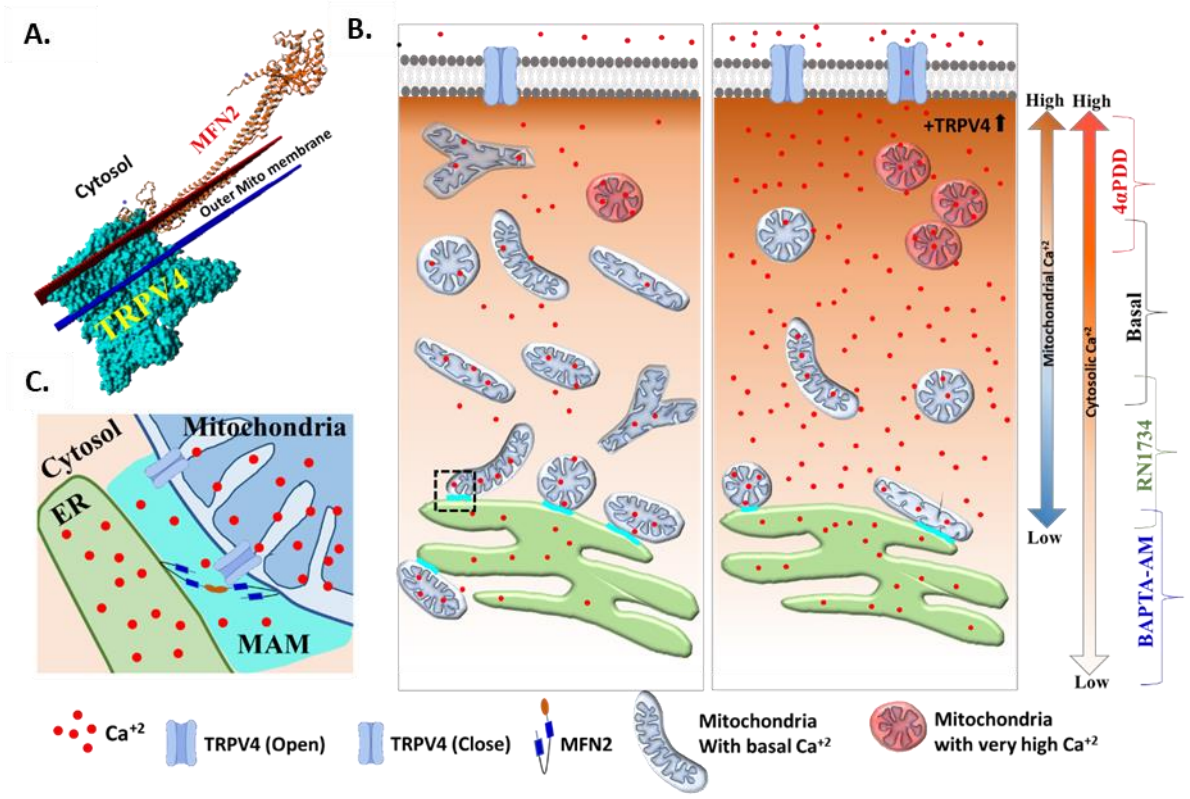


Fig. 109. Involvement of TRPV4 in the ER-mitochondria contact mediated Ca^{2+}-buffering. A. Molecular docking between MFN2 and TRPV4 tetramer depicts that there is a strong possibilities of interaction between TRPV4 and MFN2 on the mitochondrial outer membrane. **B.** Schematic model representing that the cells with different levels of TRPV4 can cause fluctuating levels of cytosolic Ca^{2+} at various experimental conditions, where mitochondria are challenged for Ca^{2+}-buffering at different extent. **C.** TRPV4-MFN2 complex can be present in the MAM region and may help in Ca^{2+}-buffering through ER-mito contact points. (Published Acharya TK.et al. 2022, *Life Sciences*).

3.2.4 TRPV4 makes close contact with lysosome for Ca^{2+}-mobilization too:

The importance of inter-organelle contact sites in maintaining cellular equilibrium is becoming more widely recognised. Actively forming junctions between two different types of organelles in nearby have been demonstrated to serve a number of feature, including the capacity to serve as platforms for the direct transfer of Ca^{2+} ions (Han Y, 2017). Apart from ER, for the maintenance of cellular Ca^{2+}-homeostasis, mitochondria and lysosomes also plays a critical role. Recently, the interaction between mitochondria and lysosomes has been investigated, indicating the existence of a novel mechanism for cross-talk between these two organelles and their

significance in different diseases (Deus CM, 2020). However, the exact mechanism of interaction between these two organelles has not been elucidated. Interestingly recently by using live-cell microscopy with a high level of spatial and temporal resolution, the release of Ca^{2+} from lysosomes by TRPML1 into the mitochondria has been established. Ca^{2+} transfer from mitochondria–lysosome interactions change the way lysosomes communicate to mitochondria. Contact site tethering is generally controlled by the outer and inner mitochondrial membrane proteins, voltage-dependent anion channel 1 (VDAC1) and mitochondrial calcium uniporter (MCU), respectively (Peng W, 2020). It has been shown that by activating TRPML1 by its specific agonist, the mitochondrial Ca^{2+}-level increased at the point of mito-lyso junction (Peng W, 2020). These reports intrigued us to investigate the reliance of TRPV4 on lysosome as a potential Ca^{2+}-source. Therefore, we examined the alteration of mito-lyso contact sites induced by TRPV4 modulation. For this purpose, we treated the CHO-K1-Mock and CHO-K1-V4 cells with 4αPDD (5 µM) and RN1734 (10 µM) for 1 hour and 6 hours respectively. We quantified the colocalized points by using "colocalization" plugin by ImageJ. We observed that in CHO-K1-V4 cells the mitochondria and lysosomal contact sites increased in TRPV4 inhibited state (**Fig. 110**). In contrast, the number of colocalized points are less in TRPV4 activated condition. This observation may suggest that inhibition of TRPV4 induces mitochondria more vulnerable to use lysosomes as a potential source of Ca^{2+}. To better understand the function of TRPV4 in mitochondrial-lysosomal contact point regulation, additional experiments are needed with more control conditions. Thus the findings also suggest new pathways of regulation of intracellular Ca^{2+}-dynamics via mitochondria–lysosome contact sites, which has further implications in various pathophysiology.

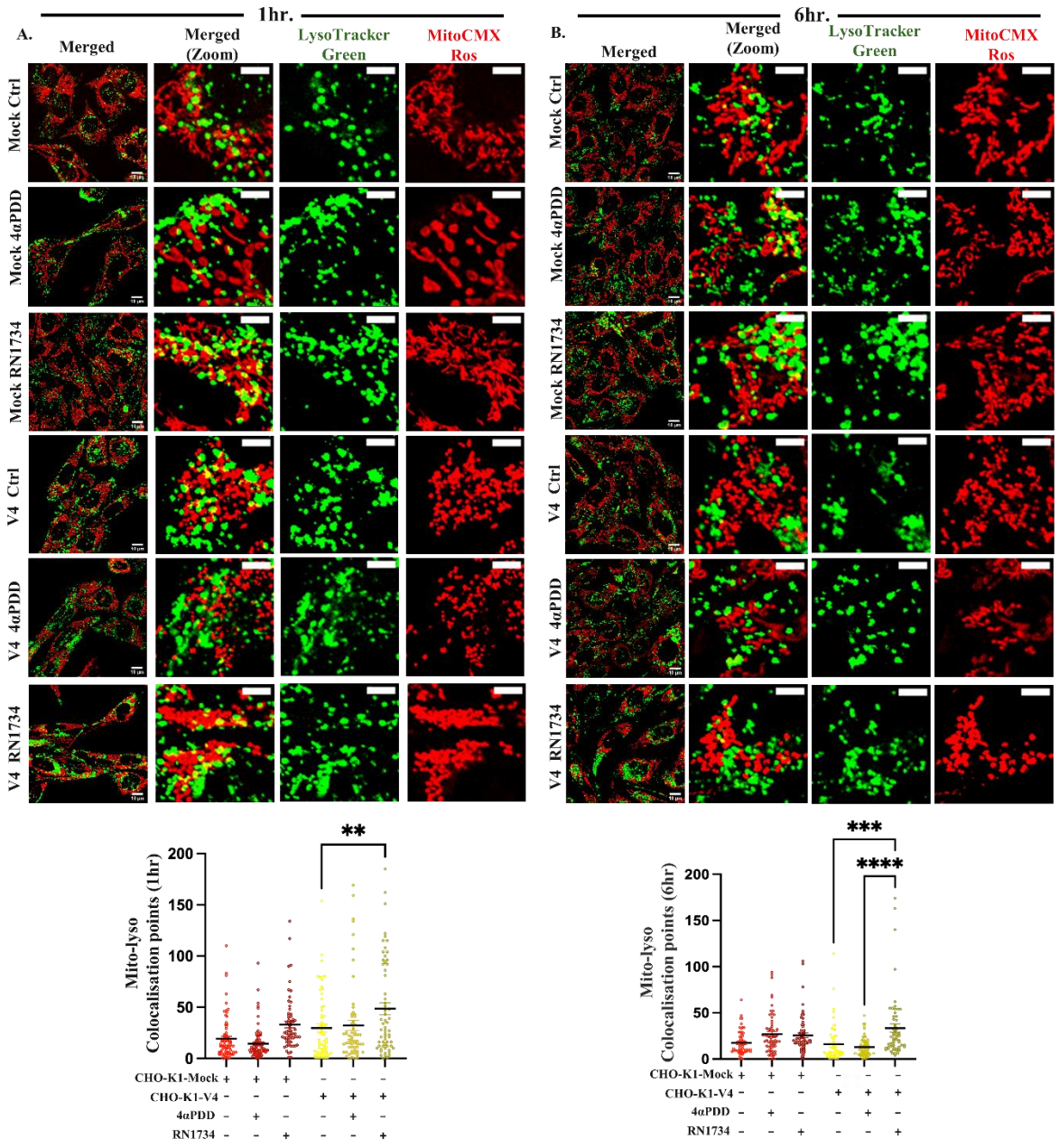


Fig. 110. TRPV4 inhibition increases mitochondria-lysosomal contact sites. A-B. CHO-K1-Mock and CHO-K1-V4 cells were treated with TRPV4 agonist and antagonist for 1 hour (A) and 6 hours (B), respectively. Quantification of colocalization points reveals that inhibition of TRPV4 elevates the mitochondrial-lysosome contact points. ≥50 cells were quantified in each condition. Scale bar is 5µm. One-way ANOVA was performed. ** = $p<0.01$, *** = $p<0.001$, **** = $p<0.0001$, ns = non-significant. (Unpublished figure).

After understanding the significance of TRPV4 in mitochondrial Ca^{2+}-metabolism, we examined the effect of the natural TRP channel modulator Menthol on mitochondrial Ca^{2+}-regulation.

3.2.5 Menthol regulates mitochondrial Ca^{2+} and metabolism in osteogenic cells:

ER-mito contact points are of functional importance as through this contact points exchange of ions and other metabolites between ER and mitochondria takes place (Tubbs E, 2017). Our data suggests that Menthol application increases this ER-mito contact points (~1.13 folds), though total ER particle as well as total mitochondrial particle numbers remain mostly same or marginally different. Increased ER-mito contact points can also be beneficial, especially in terms of ATP-efflux from Mito to ER as ER acts as a major sink for cellular ATP (Depaoli MR, 2019; Yong J, 2019). This increased extent of ER-mitochondrial contact points due to Menthol treatment is mostly due to micro-level changes in the mitochondrial morphology. Indeed, Menthol application increases mitochondrial circularity but decreases interconnectivity and perimeter. So the increased ER-mitochondrial contact can be a result of less mitochondrial interconnectivity and reduced perimeter or *vice versa*.

3.2.6 TRPM8 regulates mitochondrial Ca^{2+}-metabolism:

Mitochondrial Ca^{2+}-level is highly dependent on cytosolic and ER Ca^{2+}-level. Cellular Ca^{2+}-level plays a very crucial role in mitochondrial heterogeneity inside the cell. Any abnormality in the Ca^{2+}-metabolism leads to various pathophysiological situations. So far, several additional ion channels other than these canonical mitochondrial Ca^{2+}-uniporters have been identified. This work also confirms that TRPM8 activation by natural and synthetic agonists elevates the mitochondrial Ca^{2+}-level. As our detailed analysis suggests reduction of mitochondrial number upon activation of TRPM8. This is intriguing as increment of mitochondrial Ca^{2+}-load increases mitochondrial heterogeneity inside a cell. Upon treatment with TRPM8 agonist, the cells develop

a population of mitochondria having very high Ca^{2+}-load, and another population carries basal or low Ca^{2+}-load. However, upon chelation of cytosolic and ER Ca^{2+}, the population having very high Ca^{2+} decreases, and the overall mitochondria having basal and low Ca^{2+}-load increases within the cell. This finding mostly confirms that mitochondrial heterogeneity can be regulated by their respective Ca^{2+}-load, and TRPM8 modulation can in turn, regulate this process. However, the fate of the mitochondria having very high Ca^{2+}-load need to be investigated further

3.2.7 TRPM8 activation decreases ER-mito contact sites:

Mitochondria-associated membrane (MAM), which are the contact sites between mitochondria and endoplasmic reticulum are emerged as the signaling hub to maintain cellular and organelle homeostasis. Mitochondria imports Ca^{2+} and other metabolites from ER (Zhang P, 2021). Furthermore, we tried to identify the change in ER-mito contact points with respect to change in TRPM8 function. Notably, cells treated with WS12 have less ER-mito contact sites with compared to control. In contrast, there is no change in ER-mito contact sites in case of AMTB-treated cells. This data indicates that an increase in mitochondrial Ca^{2+} most likely decreases the propensity of mitochondria to make a closer contact with ER. Till now there are several reports suggest increase in cytosolic Ca^{2+} increases ER-mito contact points but no reports shows the change in ER-mito contact points due to mitochondrial Ca^{2+}-load.

Taken together, these results suggest that TRPM8 is physically present in mitochondria and functionally regulates mitochondrial Ca^{2+}-level. It might be possible that TRPM8 also regulates mitochondrial temperature. Our findings suggest that TRPM8 might be a crucial candidate in mitochondrial physiology and relevant for mitochondrial disease.

3.2.8 TRPV4 is involved in the maintenance of mitochondrial Ca^{2+}-level in Tcell:

Ca^{2+} is a crucial compound for Tcell activation and proliferation. Using different cellular systems (such as MSC, osteogenic cells), we have shown TRPV4 is physically present in a sub-set of mitochondria and activation of TRPV4 elevates mitochondrial Ca^{2+}-level. We further checked the impact of TRPV4 on Tcell function and regulation. Notably, data obtained in this work suggests that in T cell, activation of TRPV4 by 4αPDD always causes increased mitochondrial Ca^{2+}, both in resting as well as TCR-beads treated cells. This probably suggests that the presence of TRPV4 in mitochondria provides an "additive benefit" required for the T cell activation.

Though generally believed that cytosolic Ca^{2+}-level regulates mitochondrial Ca^{2+}-level, data generated in this thesis work indicates that the mitochondrial Ca^{2+}-level is not fully dependent on the cytosolic Ca^{2+} and the ratio of mitochondrial Ca^{2+} to cytosolic Ca^{2+} is different in different experimental conditions. In that context, TRPV4 seems to play a role in the maintenance of cytosolic as well as mitochondrial Ca^{2+}, yet at different extent. The extent of changes in the mitochondrial Ca^{2+}-level due to TRPV4 activation also varies in different cellular conditions. For example, when different Ca^{2+}-sources are fully or partially blocked by using different agents such as EGTA, BAPTA-AM, or Thapsigargin, the ratio of mitochondrial Ca^{2+} to cytosolic Ca^{2+} at basal condition as well as Δ mitochondrial Ca^{2+} values due to TRPV4 activation are altered. In BAPTA- and EGTA-treated cells the cytosolic Ca^{2+}-level decreases and mitochondrial Ca^{2+}-level increases. The Δ mitochondrial Ca^{2+} value is reduced in case of BAPTA, EGTA and Thapsigargin pre-treated cells whereas the values remain high in control and TCR-treated cell. Our data also indicates that in addition to the absolute Ca^{2+}-level in the cytosol, relative Ca^{2+} of cytosol to mitochondria might also be relevant for several parameters which are relevant for T cell activation. Considering the

average mitochondrial Ca^{2+}-levels from different conditions of T cell activation and/TRPV4 modulation, data suggests that both mitochondrial membrane potential as well as mitochondrial ATP-production positively correlates with the mitochondrial Ca^{2+}-levels (**Fig. 111**). This strongly supports that TRPV4 is involved in the regulation of mitochondrial parameters relevant for T cell activation.

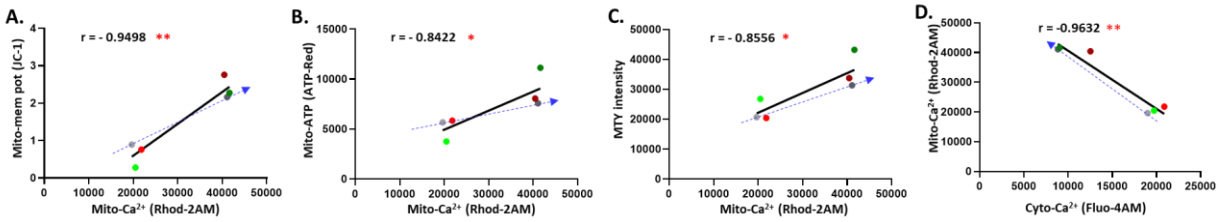


Fig. 111. Correlation study among different mitochondrial parameters. **A**. The correlation between mitochondrial membrane potential and mitochondrial Ca^{2+} is shown. **B**. Correlation between mito-ATP and mitochondrial Ca^{2} is shown**. C**. Correlation between MTY and mitochondrial Ca^{2+} is shown. **D**. Correlation between mitochondrial Ca^{2+} and cytosolic Ca^{2+}. * = $p<0.05$, ** = $p<0.01$. (Published figure. Acharya TK.et al. 2023, *Life Sciences*).

3.2.9 TRPV4 regulates ER-mito contact points in Tcells:

The contact site between mitochondria and ER (known as mitochondria-associated membrane, i.e. MAM) allows inter organelle exchange of lipids, Ca^{2+}, other ions, steroids and other signaling molecules (Aoyama-Ishiwatari S, 2021). Though the nature of MAM and its functions are well established in different cellular systems, the importance of the same in resting- and TCR-activated T cells are still largely uncharacterized. The extent of ER-mito contact points seems to be dependent on both cellular Ca^{2+}-status and mitochondrial Ca^{2+}-level, at least in other cellular systems. Indeed, this work indicates that both TCR-signaling as well as TRPV4 modulation alters ER-mito contact sites. The data also indicates that in T cells, the contact sites are reduced due to TRPV4-activation, in both resting as well as in TCR-activated cells as compared to the control condition. As TRPV4 activation mostly causes more mitochondrial Ca^{2+},

it seems that increase in mitochondrial Ca^{2+} enforces mitochondria to make less contact with ER. Our data suggest that the ER-mito contact point is more dependent on the mitochondrial particle numbers than the ER numbers. However, this aspect needs further detailed study to understand this relationship.

3.2.10 TRPM8 activation increases cellular and mitochondrial Ca^{2+} in T cells:

The change (by subtracting the initial value from the final value) in Ca^{2+}-levels in each condition was also calculated. The delta value (ΔCa^{2+}) is lower in Menthol-treated cells as compared to WS12-treated cells. In accordance with that, the ΔCa^{2+} is very high in TCR+WS12 treated cells as compared to TCR+Menthol treated condition. This suggests the specific activation of TRPM8 by WS12 increases the Ca^{2+}-load in TCR-treated cells. In the TCR+WS12 condition, mitochondrial Ca^{2+}-levels are higher than in the WS12 condition alone. In Ca^{2+}-chelated condition, the situation is a little bit different. Overall, ΔCa^{2+} is low in all the Ca^{2+}-compromised situations. When the impact of WS12 and Menthol on ΔCa^{2+} were compared, it was noted that in EGTA+WS12 treated cells, the ΔCa^{2+} is low. This suggests that cells are highly dependent on extracellular Ca^{2+}-sources. However, in EGTA+Menthol treated cells, the ΔCa^{2+} is high which might be due to the nonspecific activation of Menthol. Menthol also has many other off targets other than TRPM8. In BAPTA-AM-treated condition, the ΔCa^{2+} is low in the presence of both Menthol and WS12, which depicts that cells are also dependent on store operated Ca^{2+}-channels as well. The effect of ER Ca^{2+}-store on mitochondrial Ca^{2+} were also investigated. For that ΔCa^{2+} in Thapsigargin-treated cells were investigated. Thapsigargin acts as a SERCA inhibitor. There are reports suggesting that upon treatment of Thapsigargin, mitochondrial Ca^{2+}-level increases, mitochondria become fragmented and prolonged exposure of Thapsigargin causes cell death (Hom JR, 2007). Accordingly, when ΔCa^{2+} between Thapsi+WS12 and Thapsi+Menthol were

compared, it was noted that in the presence of WS12, the ΔCa^{2+} remains high and in Menthol-treated cells, the ΔCa^{2+} is reduced. This also indicates to WS12 as a specific activator, which activates TRPM8 at ER, and thus in turn, raises the mitochondrial Ca^{2+}. In contrast, Menthol, being as a non-specific activator, is not able to maintain the mitochondrial Ca^{2+}-load as such.

3.2.11 TRPM8 activation increases ER-mito contact points in resting and TCR treated cells:

TRPM8 is reported as a protein present at the ER-mito contact points and regulates mitochondrial Ca^{2+}-level. (Bidaux G, 2016). The establishment of MAM and its function in various cellular systems have been illustrated by various groups (Hayashi T, 2009). However, in Tcells, how the ER-mito contact site appears and changes in TCR activation is still not known. Therefore, it was intriguing to check the change/s in ER-mito contact sites due to TRPM8 modulation in both resting and activated cells. By using a unique methodology and particle-based quantification adopted in this work, the total mitochondrial particle, total ER particle and total colocalized particles were quantified and compared. This data indicates that in TRPM8-activated conditions, the number of mitochondrial particle decreases in both resting and activated conditions. However, the ER particle level remains mostly unaltered. The decrease in mitochondrial number, in turn, decreases the ER-mito contact points. By contrast, in AMTB-treated cells (both in resting and activated T cell), the mitochondrial number increases significantly as compared to the control condition. Notably, the number of ER-mito contact points are highly dependent on mitochondrial number instead of ER number. The process of increment of mitochondrial number and, subsequently ER-mito contact sites seems to be dependent on both cytosolic Ca^{2+} and mitochondrial Ca^{2+}-load. However, detailed mechanisms need to be studied to get a better understanding of organellar contact point regulation in T cells and in other cells as well.

Taken together, our results suggest that indeed TRPM8 is present at the Tcell immunological synapse and regulates mitochondrial and ER physiology differentially in resting and TCR-activated conditions. This study may have a broad implication in paving the path for future understanding of mitochondria and ER regulation in Tcells by different TRP ion channels.

3.3 Importance of TRP channels in the regulation of mitochondrial metabolism:

3.3.1 TRPV4 interacts with mitochondrial proteins:

Recently we demonstrated that the TM4-Loop-TM5 region of TRPV4 interacts with Cytochrome C, a mitochondrial protein (Das R, 2022). In this work, we demonstrate that the C-terminus of TRPV4 interacts with key mitochondrial proteins, i.e. with MFN1 and MFN2. This allowed us to propose that TRPV4 may contribute to essential mitochondrial functions, including fusion and fission. These findings are relevant for the understanding of diseases involving mitochondrial abnormalities. To date, several pathophysiological conditions are known that are associated with mitochondrial abnormalities (Nunnari J, 2012). Involvement of TRPV4 in different tissue functions is well established and mutations and/or abnormalities in TRPV4 are associated with a variety of pathophysiological conditions commonly referred to as channelopathies (Verma P, 2010). For example, more than 20 genes, including TRPV4 and MFN2, are considered to be involved in the development of Charcot Marie Tooth 2 disease (defects in sensory/motor neurons), suggesting that TRPV4 is physiologically and functionally linked with MFN2 (Bird TD, 2008). Indeed, our experiments confirm that TRPV4 interacts with MFN1 and MFN2 directly and thus support as well as establish the evidence of genetic interaction at the protein level too. To characterize this interaction between TRPV4 and MFN2 in detail, we performed a molecular docking analysis with the available structures of TRPV4 and MFN2. This

analysis suggests a possible interaction of TRPV4 and MFN2 at the mitochondrial outer membrane (**Fig. 110A**). Considering that MFN2 has some other conformation also, a more complex interaction of TRPV4 with MFN2 can also be possible (Mattie S, 2018). However, the detailed nature of TRPV4 and MFN2 interaction needs further investigation. Notably, a series of mutations in MFN2 are reported that cause different diseases, many of these diseases matches well with TRPV4-mediated pathophysiologies (Filadi R, 2018). Mutations in the MFN2 also cause mitochondrial defects, such as Charcot–Marie–Tooth type IIa (CMTIIa) disease, a peripheral sensorimotor neuropathy (De Brito OM, 2008).

3.3.2 TRPV4 activation regulates mitochondrial protein level:

As modulation of TRPV4 changes ER-mito contact points, changes in the mitochondrial protein level as a factor of TRPV4 alteration were explored. For that purpose, CHO-K1-V4 cells were treated with 4αPDD and RN1734 for 24 hours, and the whole cell extracts were prepared. By performing Western blot analysis, we checked the expression of HSP60, MFN1 and DRP1 in Mock cell extract and TRPV4 cell extract. We observed that in the TRPV4 cell extract, apart from the expected band of HSP60 at 60 kDa, MFN1 at 80 kDa, and DRP1 at 80kDa, some low molecular weight bands were also observed in all the experimental conditions. These low molecular bands are not detected in Mock cell extract, suggesting that the presence of TRPV4 is linked with the formation of these bands, most likely due to the mitochondrial protease activity (**Fig. 112A-D**).

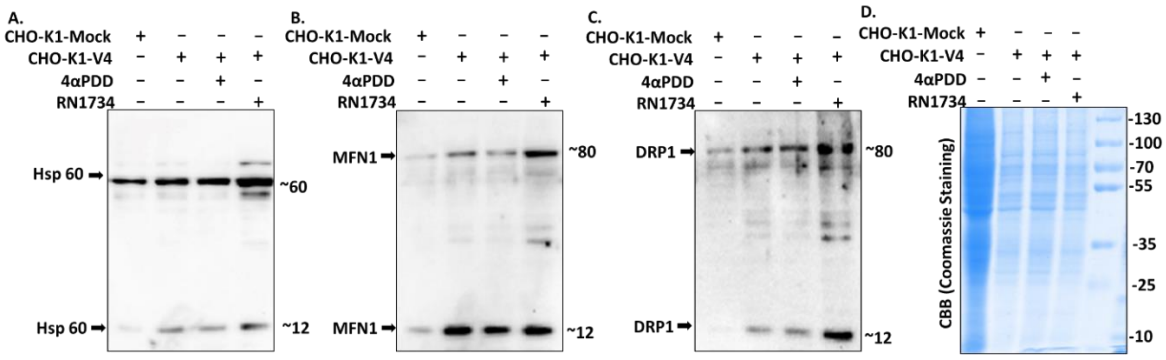


Fig. 112. TRPV4 regulates HSP60, MFN1, DRP1 levels. A-C. TRPV4 expressing cells were treated with TRPV4 agonist (4αPDD) for 24 hours, and total cellular fractions were extracted and probed by western blot analysis by using specific antibodies for HSP60, MFN1, and DRP1. Apart from the expected band of HSP60 at 60 kDa, MFN1 at 80 kDa, and DRP1 at 80 kDa, some smaller bands were observed, especially in the fraction purified from CHO-K1-V4 cells but not from CHO-K1-Mock cells. **D**. Corresponding CBB gel is shown. (Un-published figure).

In a similar manner, we examined the degradation pattern of the MFN2 protein. MFN2 is located at the outer mitochondrial membrane and acts as a tethering protein for ER-mito contact establishment. To check the protein degradation pattern of MFN2 in purified mitochondria from mouse brains were used. The purified mitochondria were treated with 4αPDD and RN1734 at different time intervals (0, 05, 10, 30 and 60minutes). We observed that at different time points, the degradation pattern changes. In addition to the predicted band of MFN2 at 80kDa, we detected other low molecular weight bands, predominantly at ~12kDa, in all experimental conditions. At the 60 minutes, the degradation is high. However, in the RN1734 treated condition the degradation lesser when compared 4αPDD treated condition **(Fig. 113**). This is a very interesting observation and need further investigation to get a better understanding.

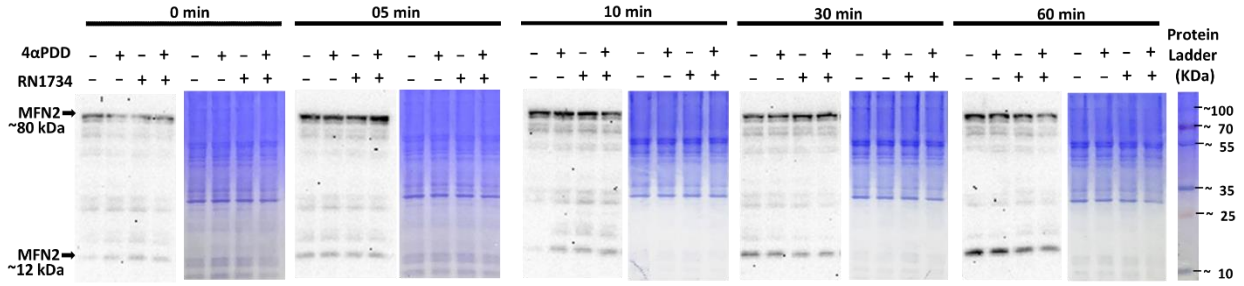


Fig. 113. TRPV4 regulates MFN2 degradation. Shown are the comparative levels of endogenous MFN2 in a representative Mitochondria purified from mouse brain were treated with TRPV4 agonist (4αPDD) and antagonist RN1743 for different time duration (05, 10, 30 and 60 minutes). Subsequently, the fractions were extracted and probed by Western blot analysis by using specific antibodies for MFN2. Apart from the expected band of MFN2 at 80 kDa, some smaller bands were observed (~12 kDa), especially in the fraction treated for 60 minutes. The corresponding CBB gel is shown. (Un-published figure).

3.3.3 To counteract mitochondrial stress, TRPV4 triggers the UPR pathway:

Higher amount of Ca^{2+}-influx inside the mitochondria causes mitochondrial stress which induces reduction of membrane potential and generation of ROS (Görlach A, 2015). Excessive production of ROS causes the misfolding of mitochondrial protein, which leads to mitochondrial stress and cell death (Papa L, 2014). Consequently, mechanisms to reduce mitochondrial stress is required. Recently it has been reported that mitochondrial unfolded protein response is triggered by the accumulation of unfolded proteins in mitochondria (UPR^{mt}). There are certain markers which are activated during UPR^{mt}, i.e. CHOP (C/EBP homologous protein), ERα (Estrogen receptor alpha) and mitochondrial deacetylase SirT3. SirT3 orchestrates antioxidant machinery and mitophagy pathway. Whereas CHOP activates heat shock proteins, such as Hsp10 and Hsp60. Similarly, ERα induces proteasome and protease omi to prevent the accumulation of misfolded proteins in mitochondria (Papa L, 2014). It has been observed that TRPV4 expressing cells have high mitochondrial Ca^{2+}-load and compromised membrane potential, which intrigued to check the marker for UPR^{mt}. For this experiment, CHO-K1-Mock and CHO-K1-V4 cells were treated with 4αPDD (5 µM) and RN1734 (10 µM) for 24 hours and made a whole cell extract. By immunoblotting, the expression of SirT3 and CHOP was checked by using specific antibodies. Higher expression of SirT3 and CHOP in TRPV4 expressing cells compared to Mock cells was observed (**Fig. 114**). This data inferred that TRPV4 expression induces UPR^{mt} to overcome the stress response.

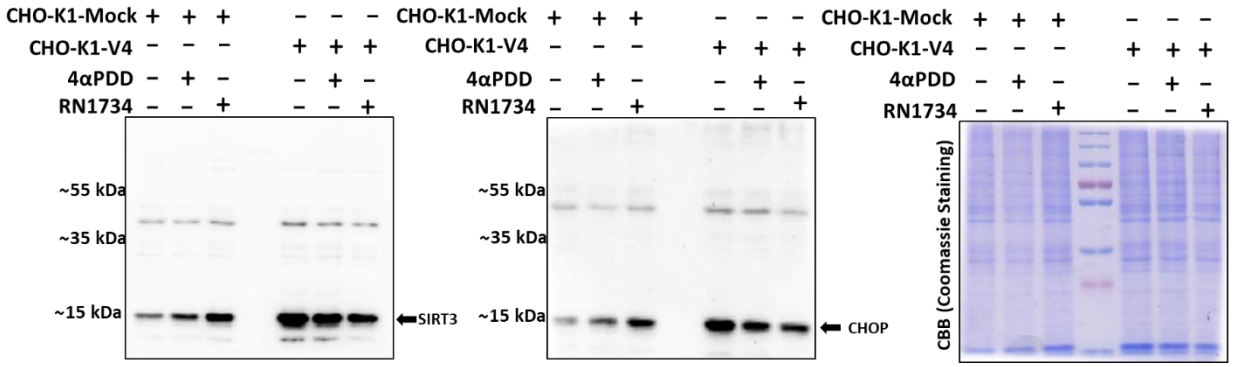


Fig. 114. TRPV4 induces Mitochondrial UPR. CHO-K1-Mock and CHO-K1-V4 cells were treated with agonist (4αPDD) and antagonist RN1743 for 24 hours. Subsequently, the whole cell fractions were extracted and probed by Western blot analysis by using specific antibodies for SirT3 and CHOP. The expression of these proteins is higher in TRPV4 expressing cells. The corresponding CBB gel is shown. (Un-published figure).

3.3.4 Menthol regulates mitochondrial metabolism:

A major source of cellular ROS is mitochondria. ROS were previously thought to be undesired by-products of OXPHOS. However, numerous reports in diverse model systems indicated that decreasing oxidative stress increases lifespan and delays cellular aging. As a result, both natural and synthetic substances referred as antioxidants that interact with ROS and render them inactive have been thoroughly studied. However, numerous of these compounds unexpectedly failed at the clinical trial having no health promoting effects. Contrary, several reports suggest that antioxidants may actually induce cancer in humans and may reduce the lifespan (Bjelakovic G, 2007; Bjelakovic G, 2004; Vivekananthan DP, 2003). Recent concept, namely “mitohormesis” suggests that a moderate amount of ROS delays the ageing phenotype. Moderate increment of ROS have been linked to extension of longevity in *Drosophila melanogaster* and mice as well (Giorgi C, 2018; Ristow M, 2010). We have observed moderate level of ROS production due to Menthol, which might be linked to beneficial for lifespan expansion and can be used as anti-aging therapy. This also accords well with the fact that Menthol

increases energy expenditure relevant for health benefits (Khare P, 2019; Sanders OD, 2021). We have observed Menthol treatment raises Cardiolipin levels in mitochondria. Cardiolipins are important indicators of mitochondrial and cellular health (Hwang MS, 2014). Increased Cardiolipin level due to Menthol also suggests possible changes in the mitochondrial morphology towards more circularity (Matsumura A, 2018). Indeed, this data also matches well with findings that the inactivation of Cardiolipin synthase leads to the formation of more elongated mitochondria (Matsumura A, 2018) Higher Cardiolipin levels due to Menthol suggests better mitochondrial health in general. Notably, Cardiolipins are mitochondrial phospholipid which also affects mitochondrial Ca^{2+}-levels by modulating MCU (Ghosh S, 2020). A large number of mitochondrial functions including ETC are regulated by the mitochondrial Ca^{2+}-levels. Therefore, this data accords well with the fact that Menthol induces mitochondrial ROS and high ATP production (Nazıroğlu M, 2018).

3.3.5 Menthol has some indirect effects independent of TRPM8:

While most of the Menthol-treated functions are generalized as TRPM8-mediated primarily, our data suggest that increased mitochondrial Ca^{2+}-level and a series of mitochondrial changes are more due to Menthol application rather than TRPM8 activation *per se*. A large number of reports have suggested physiological, behavioral, and metabolic changes due to Menthol application (Albishi FM, 2020; Sakellariou P, 2016). Often such effects are not exclusively through TRPM8, and in fact, TRPM8-independent effect of Menthol is also reported. This aspect matches well with previous reports, which suggest that there are cellular responses, such as oxidative stress, that are independent of TRPM8 (Nazıroğlu M, 2018). TRPM8-independent effect/s of Menthol is/are also observed in PC-3 prostate cancer cells (Kim SH, 2009). Even,

Menthol effects have been seen in Zebra fish, which does not have TRPM8 in its genome (Carneiro P, 2022; Majhi RK, 2015).

We noted that in several cases, WS12 and Menthol act very differently. The difference between these two agonists may be due to their chemical properties and/or global action. The dose requirement of Menthol (50 μM) to activate TRPM8 is much high than WS12 (5 μM). Notably, the effect of Menthol can also be TRPM8-independent manner in some cases (Turrens JF, 2003). Thus some of the effects of Menthol may be due to its targets other than TRPM8. While TRPM8 represent a cold-activated ion channel and the ligands used in this study are exogenous in nature, it is worth mentioning that there are several endogens ligands (such as 3-Iodothyronamine) that can act on TRPM8 (Khajavi N, 2017).

3.3.6 TRPM8 regulates mitochondrial membrane potential and ATP level:

ATP is the prime source of energy in the cell and acts as an allosteric effector in various physiological processes inside cell. Mitochondrial Ca^{2+}-homeostasis plays a major role in the generation of ATP as most of the enzymes of the Krebs cycle are modulated by Ca^{2+} (Jouaville LS, 1999). In accordance to the fact that mitochondrial Ca^{2+}-level modulates the ATP level, so far, several mitochondrial Ca^{2+}-ion channels have been studied, especially in the context of ATP generation. This study also suggests that activation of TRPM8 increases mitochondrial Ca^{2+}-level and mitochondrial ATP. These findings support the previous results where TRPM8 knock out cells show less ATP generation (Bidaux G, 2015). However, interestingly prolonged inhibition of TRPM8 by AMTB results more mitochondrial ATP synthesis, and this might be due to other mitochondrial Ca^{2+}-channels which complement the Ca^{2+}-level of the mitochondria.

Mitochondrial membrane potential is also regulated by the mitochondrial Ca^{2+}-level. It is a well demonstrated fact that an increase in mitochondrial Ca^{2+} decreases mitochondrial

membrane potential. We have also checked the change in mitochondrial membrane potential with respect to the modulation of TRPM8. These results also show that in case of TRPM8 activation, mitochondrial membrane potential decreases significantly. This result also supports the results demonstrating that activation of TRPM8 by a hydrogel-based drug delivery system in mouse bone marrow derived Mesenchymal stem cells decreases mitochondrial membrane potential (Acharya TK, 2021).

3.3.7 TRPM8 induces mitochondrial ROS and changes Cardiolipin level:

Interactions between mitochondrial ROS and mitochondrial Ca^{2+} can be considered bidirectional, where ROS can regulate Ca^{2+}-signaling and Ca^{2+}-signaling is required for ROS production (Görlach A, 2015). The cellular systems used in this work, it was observed that mtROS increases in both the TRPM8 activated as well as inhibited conditions. The increase in mtROS might be regulated by the elevated Ca^{2+}-level inside the mitochondria. Cardiolipin is a mitochondrial phospholipid present inner mitochondrial membrane and comprises ~20% of the total mitochondrial lipids (Corrado M, 2020). Change in the level of Cardiolipin gives an insight of the mitochondrial health and energetics. Moreover, our result depicts that activation of TRPM8 increases mitochondrial Cardiolipin level, and the inhibition does not change the Cardiolipin level, which in turn suggests that TRPM8 modulation does not alter the Cardiolipin content in mitochondria.

3.3.8 TRPV4 regulates mitochondrial metabolism relevant for T cell activation:

Supply if ATP is a rate-limiting step involved in the T cell activation process, and the prime metabolic output of mitochondrial function is ATP production. Indeed, blocking the mitochondrial ATP level decreases the mitochondrial Ca^{2+}-uptake and subsequently reduces Tcell activation (Ledderose C, 2014). It has been observed that the mitochondrial ATP level is increased

in TCR activated Tcells. However, TRPV4 activation in resting Tcells has reduced ATP level, whereas in TCR activated cells, it causes more mitochondrial ATP production. This also accords with the fact that the presence and activation of TRPV4 during T cell activation provides additional metabolic benefit, which might also have a larger consequence in terms of survival of the species.

Mitochondrial membrane potential is a hallmark of mitochondrial health. It has been observed that upon TRPV4 activation, the mitochondrial membrane potential increases in TCR-activated cells, whereas the membrane potential decreases in resting T cells. These results accord well with previous results describing hyperpolarisation of mitochondrial membrane potential in TCR-activated T cells (Nagy G, 2003). Ca^{2+} stimulates many of the enzymes involved in mitochondrial metabolism and ETC (Electron Transport Chain) which leads to the generation of ROS (Murphy MP, 2013). We observed that in TCR-activated T cells, the level of mtROS is high irrespective of TRPV4 modulation. This data accords well with the concept of Ca^{2+}-mediated ROS generation, which suggests the involvement of mitochondrial TRPV4 in mitochondria-mediated ROS generation.

3.3.9 TRPV4 regulates Cardiolipin levels in Tcells through complex Ca^{2+}-signaling:

Cardiolipin maintains $CD8^+$ T cell function, and T cells deficient in Cardiolipin have responded poorly to T cell activation (Corrado M, 2020). Cardiolipin depends on mitochondrial Ca^{2+} for the proper functioning of mitochondrial energetics and T cell function as well. Mitochondrial Ca^{2+}-overload prompts the disintegration of complex II, which generates excessive ROS and can cause cell death (Hwang MS, 2014). Mitochondrial Cardiolipin is known to be associated with complex II, and upon Ca^{2+}-binding, it coalesces into clusters (Hwang MS, 2014). It has been reported that complex II dissociation cannot be observed when Cardiolipin is replaced by a lipid lacking of Ca^{2+}-binding capacity. (Hwang MS, 2014). It was found that in resting cells,

the Cardiolipin level decreases due to TRPV4 activation, whereas the level restores in inhibition. But the scenario completely changed in TCR-activated condition where the Cardiolipin level increases in all different treatment conditions. Notably, the Cardiolipin levels remain high in activated T cells. This data also suggest that TRPV4 activation helps Cardiolipin restoration and increases the activity in TCR-activated T cells. Considering the average values from different experimental conditions, the data suggests that in general, the amount of mitochondrial Cardiolipin positively correlates with mitochondrial Ca^{2+}-levels.

Taken together, the data suggest that TRPV4 is present in the mitochondria of T cell and such presence is beneficial for the formation of immune synapse and/or T cell activation process (**Fig. 115**). This presence of TRPV4 in the mitochondria and its involvement in the regulation of mitochondrial Ca^{2+} and function might have evolutionary significance as well. This study may have a broad implication to understand the Tcell functions and contribution of different TRP ion channels in overall immunity

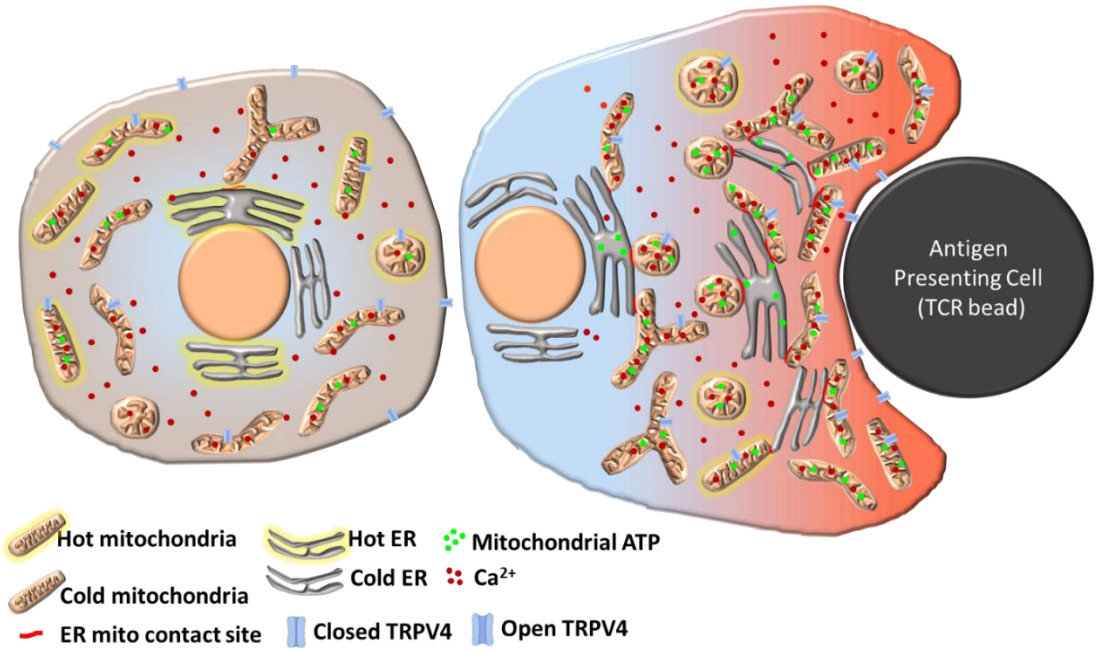


Fig. 115. Regulation of mitochondrial physiology and heterogeneity by TRPV4: The model represents the difference of mitochondrial Ca^{2+}, ATP and temperature in resting and TCR treated T cells.

Translocation of mitochondria to the immunological synapse and increased interaction between mitochondria and ER are both observed in TCR-treated cells. T cell activation and activity are aided by an increase in mitochondrial Ca^{2+} due to the presence of TRPV4 in mitochondria. (Published figure. Acharya TK.et al. 2023, *Life Sciences*).

3.3.10 TRPM8 regulates mitochondrial function in Tcells:

The surface expression of TRPM8 increases due to activation by Con A (Acharya TK, 2021; Kume H, 2019). In this study, the effect of TRPM8 modulation by pharmacological means on subcellular organelles in a comparative manner between resting and TCR-treated T cells has been tested. In activated cells, mitochondria translocate to the immediate vicinity of the immune synapse (IS) and maintain the Ca^{2+}-level high and helps in Ca^{2+}-dependant T cell activation (Quintana A, 2007). Translocation of mitochondria to the "IS" not only regulates Ca^{2+}-level but also supplies higher ATP to mediate the T cell activation process and cytokine production (Desdín-Micó G, 2018). It is noteworthy to mention that so far presence of several TRP ion channels in mitochondria have been reported (Acharya TK, 2022a; Acharya TK, 2022b). In a similar manner, TRPM8 has also been reported to be localized at the MAM (Mitochondria Associate Membrane) (Bidaux G, 2016). Nevertheless, the detailed localization and complex functionality of TRPM8 in the mitochondria of T cell is not known yet. This work establishes the colocalization of TRPM8 with mitochondrial markers in resting as well as activated Tcells for the first time. TRPM8 regulates Ca^{2+}-influx, both in cytosol and in mitochondria, though the exact regulation and mode seems to be different. Notably, the activation of TRPM8 by its agonist elevates both cytosolic and mitochondrial Ca^{2+}. Mitochondrial Ca^{2+}-uptake plays a crucial role in the fundamental events involved in cellular Ca^{2+}-signaling. Mitochondrial Ca^{2+}-level is a cumulative effect of cytosolic Ca^{2+}-source and store operated Ca^{2+}-sources which are mainly the ER and other organelles. It is known that mitochondria make close contact with ER for Ca^{2+} and other metabolite exchange. This phenomenon prompted to check the probable Ca^{2+}-source of mitochondria in T cells in the

context of TRPM8 modulation. Two different agonists of TRPM8, i.e. WS12 and Menthol, have been used for that purpose.

3.3.11 TRPM8 increases mitochondrial ATP level in TCR treated T cell:

Upon antigen recognition, mitochondria translocate to the immune synapse, a process that facilitates intracellular Ca^{2+}-buffering and ATP production, which mediates downstream signaling pathway relevant for T cell activation and proliferation (Desdín-Micó G, 2018). We demonstrate that during the activation by TCR, the ATP-level increases as compared to the resting T cell. However, further addition of WS12, Menthol, or AMTB in the TCR-activated condition, the ATP-level does not low further. Notably, in the presence of AMTB, the ATP-level goes further high. This result can be explained by considering the mitochondrial Ca^{2+}-load. As we discussed earlier that in AMTB-treated cells, the mitochondria accumulate more Ca^{2+} inside it, and the effect of mitochondrial Ca^{2+} on ATP generation cannot be avoided. This data further supports the previous reports demonstrating increased ATP-level in case of TCR activation (Desdín-Micó G, 2018).

3.3.12 Regulation of mitochondrial membrane potential and Cardiolipin level by TRPM8:

TCR activation by CD3/CD28 co-stimulation cause mitochondrial hyperpolarisation by elevating mitochondrial membrane potential. Changes in membrane potential are highly dependent upon cytosolic and mitochondrial Ca^{2+}-levels (Nagy G, 2003). Our results accord well as TCR-activation increases mitochondrial membrane potential, but in the resting T cell, the membrane potential is reduced with the treatment of TRPM8 modulators. However, in the TCR+AMTB treated cells, the mitochondria become significantly more hyperpolarised.

For effective T cell activation, not only the mitochondrial metabolism is essential but also the mitochondrial membrane lipid composition and integrity are indispensable. Cardiolipin is the indicator of mitochondrial health as mislocalization of Cardiolipin to the outer mitochondrial

membrane promotes apoptosis and triggers inflammation (Dudek J, 2017). It has been shown that in the resting T cell, treatment of WS12 results in lowering the Cardiolipin level, whereas in case of treatment with Menthol or AMTB, the level remained unchanged. Notably, in general, the Cardiolipin level is high in TCR-activated conditions (and become highest in WS12-treated condition) as compared to the resting conditions. This also suggests that TRPM8 activation provides additional benefits during T cell activation.

3.3.13 TRPM8 regulates mitochondrial ROS level in Tcells:

Mitochondrial ROS is generated by complex-I, II and III of electron transport chain (Bidaux G, 2016). During the process of T cell activation, the mtROS level increases and this induction is mainly regulated by Ca^{2+}-influx (Sena LA, 2013). In this context, our data suggest that the mtROS level is elevated in the presence of TRPM8 agonists (WS12), reduced due to the presence of AMTB, in resting as well as in TCR-activated cells. This probably also indicates the direct involvement of TRPM8 in the ETC functions. This data accords well with the general concept of Ca^{2+}-mediated generation of mtROS. TRPM8 has been reported to be present at the ER-mito contact points and regulates mitochondrial Ca^{2+}-level (Mahieu F, 2007; Khajavi N, 2017). Our data accords well with that, especially in activated T cells.

3.4 TRP channels as regulators of mitochondrial temperature and quality:

3.4.1 TRPV4 as a mitochondrial temperature sensor:

It is known that mitochondrial respiratory activities and other metabolism re-adjust as a factor of fluctuating temperature (Scot KY, 2019). Mitochondria-mediated Ca^{2+}-uptake is temperature-dependent, at least in some biological systems that operate high Ca^{2+}-dynamics (Lemieux H, 2017; David G, 2000). In this work, we used the mitochondria-specific fluorescence dye that changes its fluorescence with respect to temperature. This study indicates that TRPV4

activation, in general, increases the mitochondrial temperature. With some minor differences, TRPV4 activation or inhibition-mediated changes in the mitochondrial temperature can also be observed in isolated mitochondria in a cell-free system. This may indicate that TRPV4, being present in the mitochondria, is involved in the mitochondrial "heating up-cooling down" process. Indeed, our results suggest that both TRPV4 activation and inhibition by pharmacological means (over a time period of a few minutes) can generate a sharp change in mitochondrial temperature, often in a range of ~25 °C. Our observations are in agreement with the reports indicating that mitochondria are at least 10 °C hotter than the cytoplasm (Chrétien D, 2018; Lane N, 2018). Considering that TRPV4 gets activated at 37 °C, i.e. at core body temperature, the presence of TRPV4 in mitochondrial is extremely meaningful. It may suggest that TRPV4 act as a mitochondrial temperature sensor (**Fig. 108**). The Ability of TRPV4 to affect the ETC and other metabolisms corroborates the same. It is known that disruption of mitochondrial ETC by uncouplers can induce heat in a transient manner (Rajagopal MC, 2019). Theoretical calculations suggest that in a single mitochondrion, this heat production can cause a temperature increase at a rate of ~4.8 K/sec, especially at the initial phase (Kang JS, 2018). It could be possible that TRPV4 plays a similar role during this sharp temperature increase due to uncoupling in ETC.

In spite of changes due to the molecular evolution, the thermal stabilities of protein complexes remain fairly stable during the evolutionary time scale. In that context, members of the respiratory chain present in the mitochondria have robust higher T_m values (median T_m of 60 °C) suggesting that mitochondrial temperature can reach to 60 °C or go even higher (Jarzab A, 2020). This is supported by the fact that we could detect conditions where mitochondrial temperature change (Δ°C) can be even as high as +30 °C. This is logical, as heat dissipation within the cytosol is not that quick or effective. In fact, recent studies with different non-excitable and excitable cells,

both at resting and active conditions, demonstrate that heat produced by intracellular organelles acts very locally and does not increase the temperature of the total cells drastically but results in a very small change in the temperature gradient on the order of ~1 °C just proximal to a heat source (Oyama K, 2020). Taken together, the results suggest that TRPV4 in the mitochondria can be a part of its own temperature regulatory machineries.

3.4.2 TRPV4 at mitochondria is relevant for the regulation of body temperature:

In endothermic animals, the regulation of temperature is a fundamental process. The subcellular management of temperature production and propagation is still elusive. Mitochondria are well known for the management of heat generation and thermogenesis by controlling metabolism. TRPV4 is a thermosensitive ion channel that is activated in the physiological range. Here we report that TRPV4 is localized in mitochondria and plays a key role in maintaining mitochondria-mediated cellular thermogenesis. Recently, ER has recognized as an important organelle for production of heat, mediated by Sarcoplasmic Reticulum Calcium ATPase (SERCA) (Arai S, 2014). Though TRPV4 is also present in the ER, it has a minimal role in the thermal regulation of ER (Haustrate A, 2020).

3.4.3 Menthol decreases mitochondrial temperature:

Multiple reports have confirmed that the cancer cells have a higher temperature than healthy cells. (Dou R, 2022; Ruan L, 2022; Wang D, 2019a; Wang D, 2019b). By using MTY dye, Wang et al. demonstrated that murine bladder cancer cell MB49 have a higher mitochondrial temperature when compared with RAW 264.7 cells and human umbilical vein endothelial cells (HUVEC) cells (Wang D, 2019b). Several therapeutic medicines that target mitochondria specifically have been created by utilising the benefit of tumor intrinsic mitochondrial overheating (TIMO) (Dou R, 2022). It was demonstrated experimentally that the mitochondrial temperature is

maintained at 48 °C in murine breast cancer cells (Ruan L, 2022; Ruan L, 2019). The altered temperature of mitochondria can also be used for efficient drug delivery. It has been shown that the release of the anticancer drug PTX (Paclitaxel loaded in thermosensitive nanocarriers) into the mitochondria is efficient when the lower critical temperature was raised to 48 °C (Ruan L, 2022; Ruan L, 2019). In a similar notion, recently, we have shown that mitochondria remain mostly at hot conditions, and TRPV4 (a thermosensitive ion channel which is present in mitochondria) can regulate the mitochondrial temperature. Activation of TRPV4 by pharmacological agonist 4αPDD elevates mitochondrial temperature further and inhibition of TRPV4 decreases the temperature (Acharya TK, 2022a). In this investigation, we also used MTY, a thermosensitive dye-based method to track the temperature change of the mitochondria. We demonstrate that Menthol treatment on osteo-sarcoma cells lowers the temperature of the mitochondria. Based on this observation, we propose that Menthol can be used as a cooling agent for the mitochondria too.

However, the Menthol-mediated cooling of mitochondria is fully TRPM8-dependent (or partially dependent) or completely-independent of TRPM8, that remains to be explored. While in most cases, Menthol-mediated cellular functions can be interpreted as due to cytosolic Ca^{2+}-influx (including TRPM8 activation) followed by cytosolic Ca^{2+}-signaling, our data indicate that these functions need to be evaluated in the context of changes in the mitochondrial functions also (**Fig. 116**). However, Menthol-mediated mitochondrial functions can also be cell- and tissue-specific, which needs further investigation. We propose that careful application of Menthol can improve the mitochondrial health relevant for several diseases. Our findings can be useful for the application of Menthol in food, ointments and in different medicines keeping mitochondrial health in consideration. So far, numerous studies have pointed Menthol as a potent anticancer and osteoprotective drug. Our findings open a new and realistic possibility of using Menthol along

with novel nano-carrier/s for targeted delivery of Menthol to the hot mitochondria in order to cool them for health benefit. Mitochondria is the prime organelle which plays a pivotal role in maintenance of cellular Ca^{2+}-homeostasis (Contreras L, 2010). Apart from Ca^{2+}-metabolism mitochondria have a unique ability to sense the temperature. Recent reports suggest that mitochondria could normally function at a higher temperature, even at 50 °C (El-Gammal Z, 2022; Chrétien D, 2018; Fahimi P, 2020). Mitochondrial Ca^{2+} and temperature regulation is closely associated. However, the detailed mechanism of the temperature-sensing ability of mitochondria is still an enigma. Following the identification of thermosensitive ion channels, it was shown that these channels were also localised within several intracellular organelles.

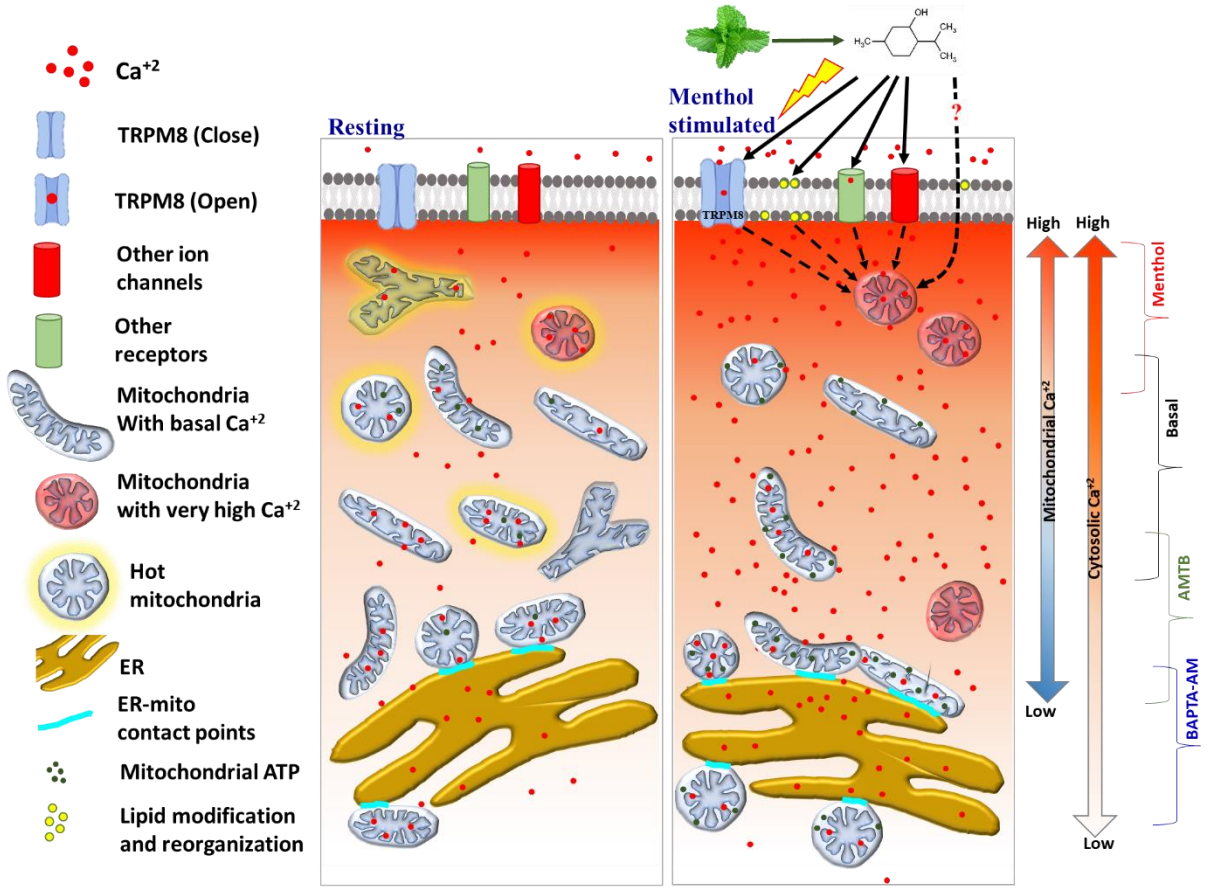


Fig. 116. Plausible molecular mechanism of Menthol-mediated mitochondrial Ca^{2+}-increment. Menthol increases cytosolic Ca^{2+}-levels, mitochondrial Ca^{2+}-levels, ER-mito contact points, mitochondrial ATP levels, decreases mitochondrial membrane potential and cools mitochondrial temperature. Menthol increases mitochondrial Ca^{2+}-level by both TRPM8-dependent as well as TRPM8-independent manners

(possibly also by involving other ion channels and receptors, by membrane alteration, and by other unidentified mechanisms) and this can be partially prevented by blocking different sources by which intracellular Ca^{2+}-mobilization takes place. (Un-published figure).

There are several thermosensitive ion channels such as TRPC3, TRPV1, TRPV4 and truncated 4TM-TRPM8 have been discovered (Feng S, 2013; Lang H, 2015; Acharya TK, 2022a). The detection of these channels in mitochondria sheds light on the thermo-sensing ability of mitochondria. Never-the-less, the regulation of these channels changes the mitochondrial metabolism and Ca^{2+}-buffering ability. The detailed functional characterisation of these channels is less studied. This thesis work characterized the localization of TRPM8 in mitochondria and attempted to characterize the function of this channel in mitochondrial Ca^{2+}-metabolism.

3.4.4 TRPM8 activation increases mitochondrial temperature but not ER temperature:

Mitochondria is the prime organelle specialised in converting free energy from the oxidation of nutrients into adenosine triphosphate (ATP) and heat. The heat produced from metabolic process is used by endothermic organisms to maintain a stable body temperature independent to their external condition (Chrétien D, 2020). Recently it has been reported that mitochondria maintain temperature at 50 ºC, i.e. ~10 ºC hotter than the body temperature. This conclusion has been drawn by using a novel thermosensitive fluorescent probe (i.e. MTY) which is targeted to mitochondria and can sense mitochondrial temperature. The fluorescence of MTY decreases by around 2.7% for 1 ºC rise in temperature (Lane N 2018; Chretien D, 2018). The presence of thermosensitive ion channels like TRPV1 and TRPV4 in mitochondria establishes that mitochondria might also be "sensing the temperature" constantly and/or mitochondrial temperature might be regulated by these groups of thermosensitive ion channels. Recently we have demonstrated that by activation of TRPV4 using specific agonist, the mitochondrial temperature increases in CHO cells (Acharya TK, 2022a). Calculating the change in fluorescence intensity (i.e.

~43%) also suggests that TRPM8 activation by WS12 increases the mitochondrial temperature further in MSCs (~10-15 ºC more) (Liu X, 2022). Our data also suggests that TRPM8 activation by WS12 significantly increase ER temperature (decrease in ETY intensity) in Saos-2 cells. Considering the ETY fluorescence change with respect to temperature in different conditions and buffers, our data indicate that WS12 treatment increases the ER temperature ~8-16 °C (Arai S, 2014). Inhibition of TRPM8 by AMTB increases the fluorescence slightly, thus decreases the temperature of the ER (~3-7 ºC less). Considering the change in temperature of ER and mitochondria induced by TRPM8 modulation (both activation and inhibition), respectively, it might be possible that TRPM8 modulation actually may alter the effectiveness of the "dynamic thermal gradient" between ER and mitochondria. This loss of thermal gradient is also expected to affect the metabolite flow from mito to ER and exchange between these two organelles. Indeed, more ATP levels in mitochondria due to TRPM8 modulation actually support that. It is worthy to mention that these effects of TRPM8 on mitochondria can be cell-type specific and also a context-dependent phenomenon.

Taken together, our results suggest that TRPM8, a cold-sensitive ion channel is indeed present in mitochondria and regulates mitochondrial Ca^{2+}-level as well as other parameters (**Fig. 117**). Our findings suggest that TRPM8 might be a crucial candidate relevant for understanding mitochondrial physiology and mitochondria-mediated diseases. Presence of TRPM8 in mitochondria may also be relevant for mitochondrial temperature sensing and thermoregulation.

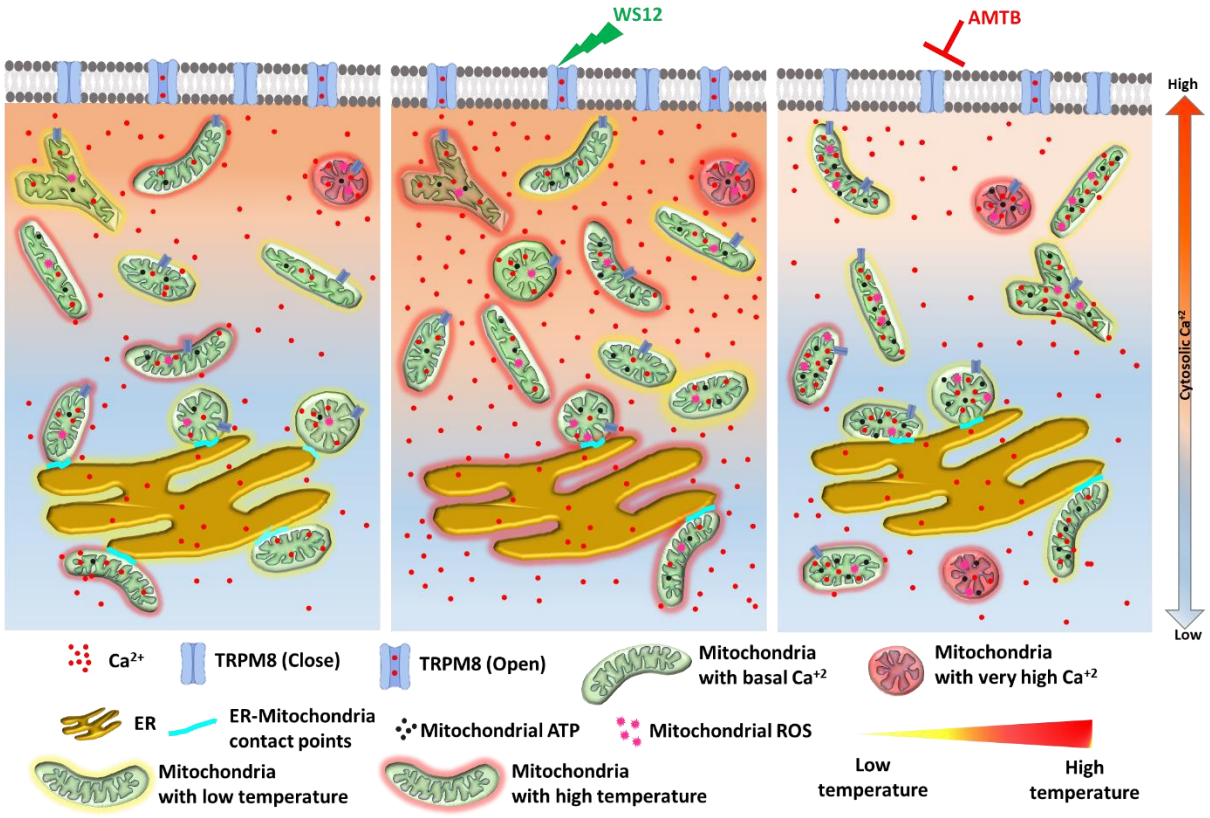


Fig 117: Schematic model depicting the TRPM8-mediated mitochondrial regulation. TRPM8 is localized on subset of mitochondria where its activation causes instantaneous mitochondrial Ca^{2+}-influx. TRPM8 modulation affects the mitochondrial-metabolism related properties such as ATP, ROS and changes the ER-mitochondria contact sites. TRPM8 also regulates the ER and mitochondrial temperature, where pharmacological inhibition of TRPM8 cools mitochondria and ER. Moreover, TRPM8 influences the "dynamic thermal-gradient" between mitochondria and ER that may impact the flow of metabolites such as Ca^{2+}, ATP, and ROS between the two organelles. (Un-published figure).

3.4.5 TRPV4 regulates temperature of subcellular organelles of T cell in context-dependent manner:

Elevation in body temperature during infection and inflammation is an integral part of the innate immune system. Change in body temperature makes several thermos-sensitive ion channels including TRPV4, relevant for immune regulation. The Maintenance of cellular temperature is mostly governed by mitochondria. The "thermoregulation of mitochondria" is highly dependent

on the metabolism and respiration activities performed by mitochondria. Using a thermosensitive dye MTY and ETY (whose intensity is inversely proportional to the rise in temperature of the ER), we monitored the changes in the mitochondrial and ER temperature due to TRPV4 modulation. However, we observed that the mitochondrial temperature does not increase and mostly remains constant in resting as well as activated T cells. Considering the average values of MTY and ETY fluorescence, we explored if mitochondrial temperature has any relationship with mitochondrial parameters. We noted that MTY fluorescence positively correlates with the mitochondrial Ca^{2+}-level, suggesting that in general, increased mitochondrial Ca^{2+} results in lowering the mitochondrial temperature (**Fig. 111**). This data also suggest that the mitochondrial thermoregulation is cell-specific and context dependent phenomenon.

3.4.6 TRPM8 modulates mitochondrial and ER temperature in Tcells:

Elevation of basal body temperature is an integral part of the activation of the innate immune system. Slight change in body temperature makes thermosensitive TRP channels as a potential candidate for immune regulation. In the cellular level, mitochondria is maintained at ~10 °C hotter than the cytoplasm (Chretien D, 2018). Using MTY (a fluorescence dye that changes its intensity with temperature), our study indicates that TRPM8 activation by WS12 increases mitochondrial temperature in resting T cells, but decreases mitochondrial temperature in TCR-activated cells. TRPM8 affects the ER temperature also in a context-dependent manner, which can also be linked with the efficient synthesis and trafficking of specific membrane proteins required for T cell activation. The data also indicates that in a given condition, TRPM8 modulation can cause differential temperature regulation between ER and Mitochondria, a process that might be important for the regulation of "thermal gradient" within the cell and relevant for the diffusion of metabolites.

3.5 TRP channels at mitochondria: Implications in health and pathophysiology:

3.5.1 Importance of TRPV4 in ER-mitochondrial contact point regulation in neuropathic pain and other diseases:

Importance of mitochondria in different forms of pain is well established (Flatters SJ, 2015; Van Den Ameele J, 2020). Even mitochondrial distribution has been linked with the development with the different forms of pain (Guo BL, 2013). Notably, chronic pain is common in majority of the patients suffering from mitochondrial disorders. For example, majority of the disease and pathophysiological conditions where mitochondrial abnormalities are reported, chronic pain and different forms of mechanical hyperalgesia remain common symptoms in such disorders (Van Den Ameele J, 2020). Not only mitochondria as an organelle entity but also the ER-mitochondrial contact points are relevant for different forms of pain (Yousuf MS, 2020). Importance of TRPV4 in the different forms of pain, including chronic and neuropathic pain are well established (Dai Y, 2016). These also accords well with the previously proposed theory of mitochondrial toxicity as pain inducting factor (Van Den Ameele J, 2020). The importance of ER-mito contact points have been implicated to different physiological and metabolic activities, such as in glucose metabolism, steroid metabolism, insulin resistance etc. (Rieusset J, 2018; Rieusset J, 2016; Sun Y, 2020).

3.5.2 Importance of mitochondrial TRPV4 in pathophysiology;

Mitochondrial dysfunction in neuronal cells (or other cells) may cause the production of Reactive Oxygen Species (ROS), Nitric Oxide (NO) and excesses of Ca^{2+}-influx, which in turn leads to the generation of neuropathic and chronic pain (Kim HY, 2009). It seems plausible that due to TRPV4 activation, the Ca^{2+}-level increases in TRPV4 containing mitochondria, which in turn may increase the production of ROS and NO and ultimately results in neuropathic or chronic

pain. An *in vivo* study also revealed that in the case of neuropathic or inflammatory pain, several parameters, such as mitochondrial position, number, and its morphology are altered (Guo BL, 2013). Mitochondrial aggregation or clustering in the perinuclear region is increased, especially in the presence of inflammatory molecules inducing neuropathic pain. In another report it has been shown that mutation on TRPV4 ($TRPV4^{R269C}$) induces axonal degeneration and which can be reversed by genetic and pharmacological inhibition of TRPV4. Moreover, TRPV4 activation hinders axonal mitochondrial transport and the Ca^{2+}-binding mitochondrial GTPase Miro regulates TRPV4-mediated neurotoxicity (Woolums BM, 2020). These studies strongly suggests that TRPV4 is physically present in mitochondria located in the perinuclear region and contributes significantly to the regulation of mitochondrial structure-function relationship. These reports also indicate that TRPV4 modulation can alter ATP and GTP levels. Collectively, the role of TRPV4 in mitochondrial abnormality is relevant in neuropathic pain and several other pathophysiological conditions.

3.5.3 TRPV4 mutants alter mitochondrial morphology:

There are several reports that describe that mutations in TRPV4 causing a broad range of skeletal disorders and neurodegenerative disorders as well. Mutations in TRPV4 cause several major bone-related diseases and defects in bone ossification (Nilius B, 2013). TRPV4 is also involved in Charcot-Marie-Tooth (CMT) disease (Nilius B, 2013), but the underlying mechanism/s of these mutants remain largely unknown. Notably, most of these mutations are "gain-of-function" in nature and thus cause more Ca^{2+}-influx to the cell. Mitochondria of cells expressing these mutants become round-shaped and aggregated. Previously we reported that TRPV4-WT interacts with cholesterol, its precursor mevalonate, and its derivatives such as steroids through the loop region located between TM4 and TM5 (Kumari S, 2015). In this regard,

it is also important to mention that loss-of-interaction of cholesterol has been suggested as one of the characteristics of such mutants, at least for the R616Q mutant (Das R, 2019). In the context of bone formation and Ca^{2+}-deposition, TRPV4 seems to involve in terms of steroid-signaling, intracellular Ca^{2+}-buffering, and mitochondrial functions in a pleiotropic manner (Carson JA, 2015; Velarde MC, 2014; Kumar A, 2015). Here we show that in osteoblast lineage cells, the mitochondrial structure and function is regulated upon the expression of different TRPV4 mutants. However, a detailed characterization of TRPV4 and its mutants needs to be performed, especially in the context of mitochondrial functions and bone deformities.

3.6 Fine regulation of TRP channel as a future therapeutics:

3.6.1 Regulation of bone mineralization *in vitro* and *in vivo*: TRPV4 and TRPM8 as suitable targets for bone tissue engineering:

Different types of bone defects, mainly due to injury, infections, genetic conditions or underlying diseases, possess substantial clinical challenges due to bone's limited self-healing ability, slow tissue formation and high bioenergetics demands (Wan Z, 2020). Recently, biomaterials which provide biomechanical and biochemical responses has been recommended for bone defect repair, particularly in the case of critical size bone defects (Wei Y, 2020). Bone tissue repair incorporates tight regulation of Ca^{2+}-signaling and high metabolic states (i.e., mitochondrial homeostasis) of cells (Zhao Y, 2022; Novicoff WM, 2008; Wan Z, 2020). Migration, proliferation and differentiation of osteogenic cells are decisive for tissue repair, wherein an increase in oxidative metabolism (mitochondrial bioenergetics) grants the greater bioenergetic capabilities necessary to awaken dormant cells and speed up this process. Ample evidences are present which confers the critical role of TRPV4 ion channels in maintaining the of Ca^{2+}-homeostasis in cells (Khan SN, 2005; Giannoudis PV, 2009). Functional TRPV4 ion channel is present in

mitochondria, and upon pharmacological modulation, it regulates the mitochondrial number, morphologies, temperature, and Ca^{2+}-level (Acharya TK, 2022a). Further, for therapeutic delivering purposes, a hydrogel-based approach has gained a lot of attraction due to their sustained and localized delivering ability. For example, CMT: HEMA (Carboxy methyl tamarind grafted 2-Hydroxyethyl methacrylate) hydrogel facilitates the adherence and proliferation of skin and bone cells in an *in vitro* model, and it can also deliver pharmacological modulators of transient receptor potential (TRP) ion channels (Sanyasi S, 2014; Chakraborty R, 2022; Acharya TK, 2021).

3.6.2 TRPV4 modulator-encapsulated hydrogel can be used as a possible target for bone tissue engineering:

Modulation of TRPV4 activity and bioenergetics state of cells at bone defect site through a TRPV4 modulator containing biomaterial has not been investigated previously. Inspired by this, it was hypothesized that regulation of TRPV4 activity at the defect site through TRPV4 modulators containing hydrogel might enhance the bone tissue repair. This can be achieved by gaining primary stability (physiochemical cues) from hydrogel and inducing Ca^{2+}-signaling for enhanced bioenergetics effects due to TRPV4 activity. To this, pharmacological modulators of TRPV4 were infused in CMT: HEMA hydrogel to develop a physicochemical and biochemical functional scaffold. This scaffold is expected to mimic the ECM-like microenvironment and regulates the TRPV4 activity by sustained release of TRPV4 modulators at defect sites and accelerate bone regeneration.

TRPV4 is also known to physically interact with the actin cytoskeleton and also has been detected in the focal adhesion points (Goswami C, 2010). In this present investigation, expression of TRPV4 in murine bone marrow-derived MSCs is observed. As TRPV4 is mechanosensitive and present in focal adhesion points, its expression is reported to be stiffness-dependent, at least

in certain cases. Expression of TRPV4 in MSCs cultured on hydrogel (soft surface) is less as compared to glass surface (stiff surface), as observed. Notably, both expression level and functionality of TRPV4 channels can be modulated by using hydrogel infused with TRPV4 agonist (4αPDD) and antagonist (RN1734). Sustained release of TRPV4 agonist and antagonist from hydrogel significantly alters the cytosolic Ca^{2+}-level in MSCs. MSCs and osteoblasts are anchorage-dependent osteogenic cells, and their interactions with implant surface are critical for osteointegration (Wei Y, 2020). In most of the cases adhesion of osteogenic cells to the implant surface is achieved through formation of focal adhesion complexes. In this context, TRPV4-mediated Ca^{2+}-signaling regulates the expression level of vinculin in MSCs cultured on TRPV4 agonist and/or antagonist containing hydrogel. Previously it has been reported that cytosolic Ca^{2+} regulates the shape and fate of differentiation of MSCs, and these activities are heavily relied on the reorganisation of actin filaments by several actin binding proteins (Dang M, 2018). Furthermore, the elevation of intracellular Ca^{2+} influences the activity of protein kinases which effect actin dynamics (He C, 2010). In the current investigation, TRPV4 activation and inhibition doesn't alter the cellular morphology of MSCs, but upon activation, significantly enhance the actin filament organization. As TRPV4 is permeable towards Ca^{2+} and its activation causes a local spike in Ca^{2+}-transient levels, which likely regulates the actin polymerization and status of stress fibers in MSCs.

3.6.3 TRPV4-modulatory drug-based hydrogel provides a suitable microenvironment for bone differentiation:

One of the main reasons for implant failure is ROS accumulation in implantology, which promotes biomaterial corrosion and cell dysfunction (Willie BM, 2010). TRPV4 acts as a mechano-sensor on the cell surface and plays a critical role in energy metabolism. Most of the

TRP channels senses ROS by extracellular cysteine residues present in their loop regions (Wu M, 2022). Several studies have reported that activation of TRPV4 in human coronary arterioles and coronary artery endothelial cells resulted in elevated levels of ROS (Lieben L, 2012). However, our data suggest that activation of TRPV4 in osteogenic differentiated MSCs through hydrogel-mediated drug release protects cells from oxidative stress through down regulation of ROS production whereas inhibition of its activity results in increases generation of ROS. These differences could be due to the long-term modulation of TRPV4 activity through slow release of agonist/antagonist from hydrogel.

3.6.4 TRPV4 regulates ossification *in vitro* by modulating the mitochondrial activity:

In case of bone repair, mitochondrial bioenergetics is important, as differentiation of MSCs and repairing of tissue are highly energy-demanding process. Enhanced mitochondrial OxPhos activity satisfy the higher energy-demand supply hence, closely related with tissue repair. Osteoblasts are termed as “bone builders” and their enhanced activity during bone formation increases the frequency, size and area of mitochondria (Nilius B, 2011). TRPV4 is endogenously present in mitochondria, activation of TRPV4 results in the development of circular and aggregated mitochondria. TRPV4 activation alters the mitochondrial potential, whereas inhibition of TRPV4 does not cause any alteration in mitochondrial morphology (Acharya TK, 2022a; Acharya TK, 2022b). Gambini et al. has shown that human MSCs containing higher mitochondrial potential possess enhanced ATP synthesis ability and deposition of calcium or Ca^{2+}-complex in osteogenic medium (Gambini E, 2020). MSCs grown on TRPV4 agonist containing hydrogel generally exhibited higher mitochondrial potential, low level of cytosolic ROS and enhanced mineral deposition in cellular matrix. Further, in a rat defect model, optical and radiography

analysis revealed that TRPV4 antagonist containing hydrogel induces increased bone formation than antagonist containing hydrogel or self-healing condition.

3.6.5 Involvement of TRPV4 activator encapsulated hydrogel in *in vivo* bone repair:

In vivo investigation demonstrates remarkable formation of hard tissue, collagen deposition and expression of osteogenic repair markers in condition where TRPV4 agonist is present. These findings related to *in vitro* metabolism and enhanced "*in vivo* femur defect" healing observations indicate that activation of TRPV4 activity rather than physico-chemical properties of hydrogel may have led to the accelerated bone repair via uplifting the metabolic state of cells. These observations are consistent with the idea that TRPV4 channel activity regulates the mitochondrial homeostasis, ROS level. TRPV4 alters all these, possibly by regulating SIRT3 activity and the metabolic state of cells. This aspect is supported by the experimental data of *in vitro* osteogenic differentiation and enhanced *in vivo* bone repair activity as observed in case of TRPV4 activation.

3.6.6 TRPM8 inhibitor encapsulated hydrogel as a tunable surface for bone tissue engineering:

Bone structure and integrity are fine-tuned by continuous large-scale anabolism and catabolism events depending on the relative number as well as activity of osteoblasts and osteoclasts, respectively (Chen X, 2018). Mineralization by osteoblasts is a complex and slow process, stochastic in nature and dependent on many intracellular and extracellular factors. However, selective ion channels can overcome these bottlenecks and TRPM8 channel turns out to be a key regulatory molecule involved in the differentiation of BM-MSCPs to osteoblasts and the subsequent bio-mineralization process. These findings allowed us to use BM-MSCPs directly for the enhanced bio-mineralization *in vitro*, yet in a tunable manner using CMT: HEMA hydrogel

and long-term pharmacological inhibition of TRPM8 in a slow-release and dose-dependent manner.

3.6.7 TRPM8 drug encapsulated hydrogels regulate cellular Ca^{2+}-level and organellar function in MSCs:

In this work, we demonstrate that cells with osteogenic properties respond to agonist for TRPM8 and results in a rise in intracellular Ca^{2+}. In contrast, inhibition of TRPM8 results in no change in Ca^{2+}-levels, at least quickly. In case of TRPM8 inhibition, the intracellular Ca^{2+}-levels reduce gradually and in a slow manner. Such rise and fall of intracellular Ca^{2+}-levels matches well with the general Ca^{2+}-oscillation pattern observed in osteogenic cells which is relatively slower than other excitatory cells such as neurons (Collins TJ, 2000). The Ca^{2+}-imaging experiment conducted here measures total change in intracellular Ca^{2+}-levels in single cells and from such changes firing pattern of single ion channels can be predicted but cannot be concluded. In addition, endoplasmic reticulum, other intracellular organelles such as mitochondria and lysosome also play a major role in the regulation of intracellular Ca^{2+}-homeostasis and Ca^{2+}-metabolism, which are essential for bone mineralization. Mitochondria act as a major Ca^{2+}-storage and transport organelle during osteoblast development (Boonrungsiman S, 2012). Mitochondria act as localized Ca^{2+}-buffering units and modulate intracellular Ca^{2+}-levels by initiating feedback-inhibition or activation mechanisms relevant for bone cell functions (Lieben L, 2012). Bone cells consume a lot of energy and the production of ATP is largely dependent on Ca^{2+}. The mitochondrial F_1F_0-ATP synthase is stimulated by Ca^{2+} (Territo PR, 2000), the uptake of which changes the mitochondrial membrane polarity. In the same manner, it was recently shown that Reactive Oxygen Species (ROS) play a major role in both osteoclasts and osteoblasts (Ha H, 2004). Cells produce more ROS when it comes under stress and ROS-signaling plays a significant role in cell

differentiation process, while excessive ROS production may cause disruption in homeostasis (Bhattacharyya A, 2014). In these contexts, CMT: HEMA encapsulated with different TRPM8 modulators offers materials where both mitochondrial, and lysosomal functions, as well as ROS levels which, can be finely controlled.

3.6.8 TRPM8 drug-encapsulated hydrogel acts as a suitable surface for the growth of osteogenic cells:

We have previously shown CMT: HEMA as a suitable biomaterial for the successful adhesion and growth of osteoclasts and keratinocytes (Sanyasi S, 2014; Choudhury P, 2018). We now demonstrate that the same hydrogel is suitable for osteoblasts and Mesenchymal stem cells. The CMT: HEMA hydrogel has an undulating surface, porous structure and fibrous connectivity, properties that are suitable for drug encapsulation and cell growth. Osteoblasts prefer surfaces that are relatively hard for proper adhesion (Olivares-Navarrete R, 2017). The results suggest that in case of WS12-encapsulated hydrogel, the number of cells in unit area is low, yet the attached cells have increased length, increased perimeter and increased area. Together the data suggest for a better "cell spreading" event on the WS12 containing hydrogel surface. This is justified by the fact that cell adhesion and cell spreading depend on the effective focal adhesion points, which is very much dependent on the Ca^{2+}-dynamics and Ca^{2+}-signaling events. This could also explain the presence of lesser number of cells per unit area on the CMT: HEMA surface. However, the total mineralization levels on CMT: HEMA is similar to that on a glass surface, suggesting that this hydrogel itself (without any drug encapsulation) supports basal mineralization rates. Taking advantage of the fact that CMT: HEMA represents nano-fibrous structure and is also suitable for encapsulation of pharmacological drugs and their sustained release, enhanced bio-mineralization in CMT: HEMA encapsulated with TRPM8 inhibitor AMTB is achieved. The extent of

mineralization is tuneable, mediated by the long-term release of TRPM8-specific pharmacological compounds in a dose-dependent manner. In this context, it is important to consider that CMT: HEMA alone supports basal level of osteoblast growth and mineralization. However, CMT: HEMA-mediated sustained release of TRPM8-specific drugs enhance differentiation, mineralization of osteoblasts. This is also by one-time application of these drugs in the hydrogel which bypasses the requirement of administrating the drugs in large quantities' in every alternate day for bone healing.

3.6.9 Differential expression of TRPV4 and TRPM8 in Mesenchymal stem cells growing over the TRPM8 drug encapsulated hydrogel surface:

TRPM8 is not the only Ca^{2+}-permeable channel which is expressed in bone cells and importance of other ion channels in osteogenesis and bio-mineralization cannot be ruled out. However, as a proof-of-principle we have explored the relative expression of TRPV4 (another ion channel that is also known to express in several cells with osteogenic properties) when cells are grown on different surfaces with or without TRPM8-specific pharmacological agents. We found that there is significant upregulation of TRPV4 expression when cells are grown on only hydrogel surface as compared to glass surface. On the contrary, there is no change in the TRPV4 expression when cells were grown on hydrogel with TRPM8-specfic drugs" as compared to glass as a surface. Therefore, it suggests that expression of other channels may or may not be affected by prolonged activation or inhibition of TRPM8 and such understandings need further detailed work.

3.6.10 TRPM8 inhibitor AMTB-loaded hydrogels promote osteogenesis in MSCs *in vitro:*

In this work, we demonstrate that TRPM8 offers a suitable molecular route for bio-mineralization. TRPM8 has added advantages over any other ion channels for several reasons. First, TRPM8 is not essential as knockout animals also survive without major bone problems. This

may also suggest that pharmacological inhibition of TRPM8 will not cause any major or deleterious physiological problems *in vivo*. Besides, the drug release by the hydrogels will produce a more localized effect rather than a systemic effect. At physiological temperatures (i.e. 35-37 °C), there are high possibilities of spontaneous activation of other thermosensitive ion channels such as TRPV3 or TRPV4 (activation temperature ~27 °C and ~37 °C). This essentially means that in the standard culture conditions/physiological conditions, TRPM8 will not be activated unless influenced by pharmacological compounds. Therefore, TRPM8 offers a more specific molecular route that can be utilized for osteogenesis by pharmacological means and without having any deleterious side effects. The pharmacological agents used in this process are easily available, often from natural sources and are of relatively low cost.

TRPM8 inhibitor, namely AMTB at very low concentrations could provide an opportunity for their therapeutic use in enhancing osteogenesis and could be relevant for treatment of different bone-related disorders such as osteoporosis, where more bio-mineralization is required. The CMT: HEMA, being a slowly degrading hydrogel, can be a useful tool in slow but sustained delivery of TRPM8 inhibitors at sites of injury. Such prospects need further investigation. Taken together, all these suggest that inhibition of TRPM8 affects bone formation and such findings may have broad implications in bio-medical applications.

Chapter 4

Conclusion

Conclusion and future prospects:

While this work demonstrates the presence of endogenous TRPV4 in the mitochondria, the nature of localization of TRPV4 in the mitochondria (inner membrane or outer membrane or both) is not well understood yet. The precise localization of TRPV4 in mitochondria, and subsequent mitochondrial morphological changes may vary with cells and tissue types as well. Also, the exact topology of TRPV4 in the mitochondrial membrane needs further investigation. This is especially important to know the gating mechanism of TRPV4 in mitochondrial membrane and related conductance of different metal ions in different conditions. The "ionic conductance" ability of TRPV4 being in plasma-membrane or in mitochondrial membrane, may differ and can also be regulated by various modulators, such as lipids present in these two different microenvironments.

ER-mito contact points are also relevant for Ca^{2+}-buffering, which helps to cell survival. We observed that TRPV4 expression as well as activation increases a percentage of mitochondria with Ca^{2+}-overload. The possible fate of those Ca^{2+}-overloaded mitochondria remains uncharacterized. Therefore, TRPV4-mediated mitochondrial functions may be involved in cell survival and death process that need further investigation. It is also known that certain mutants of TRPV4 are "constitutive on" in nature and cause more cell death.

The presence of the TRPM8 channel in mitochondria is also explored in this work. TRPM8 is a cold-sensitive ion channel. Notably, TRPM8 is also reported at the mitochondria associated membrane (MAM). Activation of TRPM8 by specific agonist modulates mitochondrial Ca^{2+}, ATP, ROS and other metabolites. So far, several somatic mutations of TRPM8 has been reported, all mainly in the context of different cancers. However, so far, no germline mutations have been reported in TRPM8. As an evolutionary possibility, this indicates that any alterations in the genetic

sequence of this channel could be deleterious to natural selection and could have serious consequences for the thermal regulation of an organism.

Mitochondria is a cellular thermostat and is maintained at a higher temperature than cytosol. Mitochondria regulates the body temperature of an organism. Recent developments in mitochondrial thermal biology suggest that the mitochondrial temperature become very high in cancer, inflammation, pain and possibly in many other pathophysiological conditions. Considering this concept, advanced therapeutics have been proposed where drugs can be targeted based on the mitochondrial temperature for treating cancer and other disorders, and in this context, mitochondrial temperature also plays a role in the effectiveness of these medications (Ruan L, 2022; Ruan L, 2019).

Moreover, the fundamental question is, what are the factors that regulate mitochondrial temperature? As per our understanding, this process is well regulated and various TRP channels may be involved in this process. We have explored two TRP ion channels, TRPV4 (a hot channel) and TRPM8 (a cold channel) in mitochondrial temperature regulation. We observed that in general, TRPV4 expression, as well as activation increases the mitochondrial temperature (indicating possible mitochondria heating up) (**Fig. 118**). In contrast, activation of TRPM8 directly or indirectly decreases mitochondrial temperature (indicating possible mitochondria cooling down). This suggests a possibilities where both TRPV4 and TRPM8 (and maybe other factors as well) as molecular switch for regulating mitochondrial temperature, may be dependent- or independent to each other. Arguably function of other factors, metabolites, ion channels need to be investigated further to give a comprehensive understanding of this critical process.

As potential future applications of this study, mitochondrial TRP channels can be targeted for the development of therapeutics relevant for cancer, inflammation, pain and other

mitochondria-mediated diseases. This can also be relevant for TRPV4-mutation induced channelopathies.

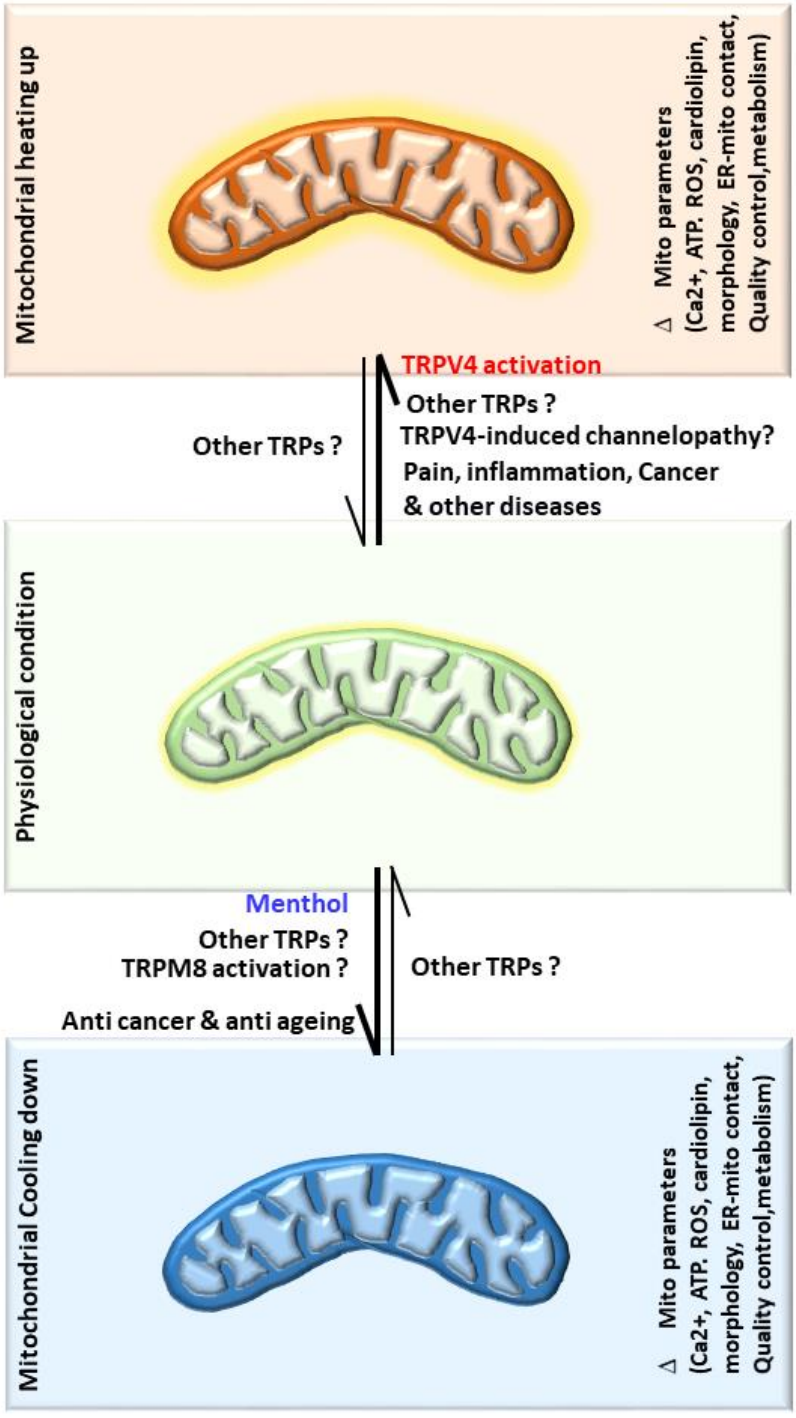


Fig. 118. Schematic model of possible involvement of both "hot and cold-sensitive TRP channels" in mitochondrial "heating up" and "cooling down" processes. (Un-published figure).

Chapter 5

Material and methods

5.1 Materials:

5.1.1 Chemicals used:

Reagents used	Source
4αPDD	Sigma - Aldrich
Acrylamide	Sigma-Aldrich
Acrylamide	Sigma-Aldrich
Agar agar, Type I	Himedia
Alizarin Red stain	Sigma-Aldrich
Alizarin Red stain	Sigma-Aldrich
Ammonium Persulphate	Sigma-Aldrich
Amphotericin B	Sigma-Aldrich
Amphotericin B	MP Biomedicals
Ampicillin	Sigma-Aldrich
AMTB	Tocris
Antibiotic Solution	Himedia
Antimycin	Sigma-Aldrich
ATP-Red	Dr. Young-Tae Chang Department of Chemistry, POSTECH, Korea
BAPTA-AM	Sigma-Aldrich
Bovine Serum Albumin	MP Biomedicals
Bradford Reagent	Sigma-Aldrich
Bromophenol Blue	Sigma-Aldrich
Calcium Cholride Dihydrate	Sigma-Aldrich
CCCP	Sigma-Aldrich
CMT-HEMA	Hindustan gum Pvt.Ltd.
Complete Protease Inhibitor Cocktail	Sigma-Aldrich
Coomassie Brilliant Blue G250	MP Biomedicals
Coverslips (12 mm and 18 mm)	VWR/Fisher Scientific
Coverslips (25 mm)	VWR/Himedia
DAPI	Invitrogen
Dexamethasone	Sigma-Aldrich
Dimethyl Sulfoxide (DMSO)	Sigma-Aldrich
DMEM Media	GIBCO
EDTA	Sigma-Aldrich
EGTA	Sigma-Aldrich
ER Thermo Yellow	Dr. Young-Tae Chang Department of Chemistry, POSTECH, Korea
ER-Tracker blue	Invitrogen
Ethanol (Molecular Grade)	Merck Millipore
Ethidium bromide	Sigma-Aldrich
F-12 Ham's Media	Himedia
Fetal Bovine Serum	GIBCO
Fluo-4-AM	Invitrogen
Fluoromount-G	Southern Biotech
Glacial Acetic Acid	MP Biomedicals
Glass bottom dish	IBIDI
Glucose	MP Biomedicals
Glycerol	Sigma-Aldrich
Glycine	MP Biomedicals

GTP-green	Dr. Young-Tae Chang Department of Chemistry, POSTECH, Korea
H_2DCFDA	Invitrogen
HEPES	MP Biomedicals
Ionomycin	Sigma-Aldrich
JC1	Invitrogen
Kanamycin	Sigma-Aldrich
Lactic Acid	Himedia
L-Ascorbic Acid	Sigma-Aldrich
L-Glutamine	Himedia
Lipofectamine	Invitrogen
LysoTracker Green	Invitrogen
LysoTracker Red	Invitrogen
Magnesium Chloride	MP Biomedicals
McCoys	PAN Biotech/GIBCO
Methanol	Sigma-Aldrich
Mito Thermo Yellow	Dr. Young-Tae Chang Department of Chemistry, POSTECH, Korea
MitoSOXred	Invitrogen
MitoTracker Red	Invitrogen
MitoTracker Red CMXros	Invitrogen
N,N′-Methylenebis (acrylamide)	Sigma-Aldrich
Nonyl Acridine Orange	Sigma-Aldrich
Oligomycin	Sigma-Aldrich
Phalloidin-AF488	Invitrogen
Phosphate Buffer Saline (10X)	Himedia
Potassium Acetate	MP Biomedicals
Potassium Chloride	MP Biomedicals
Potassium Hydroxide	MP Biomedicals
Rhod-2-AM	Invitrogen
Rhod-3-AM	Invitrogen
RN1734	Tocris
Rotenone	Sigma-Aldrich
RPMI Media	PAN Biotech/GIBCO
Rubidium Chloride	MP Biomedicals
Skimmed Milk Powder	Himedia
Sodium Bicarbonate	Sigma-Aldrich
Sodium Chloride	MP Biomedicals
Sodium Dodecyl Sulphate	Sigma-Aldrich
Sodium Hydroxide	MP Biomedicals
Sodium Pyruvate	Sigma-Aldrich
Sucrose	Sigma-Aldrich
TCR bead	Invitrogen
TEMED (Tetramethylethylenediamine)	Sigma-Aldrich
Thapsigargin	Sigma-Aldrich
TMRM	Invitrogen
Tris	MP Biomedicals
Triton X-100	Triton X-100
Trpytone	Himedia
Tween-20	Sigma-Aldrich
WS12	Tocris
Yeast Extract	Himedia

α-MEM	HIMEDIA/GIBCO
β-Glycero Phosphate	Sigma-Aldrich
β-Mercaptoethanol	Sigma-Aldrich

5.1.2 Kits, Markers and Enzymes:

Kit name	Source
1 kb DNA ladder	Biosphere Corp.
1 kb DNA ladder	Biosphere Corp.
100 bp DNA ladder	Biosphere Corp.
100 bp DNA ladder	Biosphere Corp.
ALP substrate	Sigma
ATP determination kit	Thermo Scientific
Bradford protein estimation kit	Sigma
Dynabead Untouched Mouse T cell isolation kit	Thermo Scientific
Dynabeads Mouse T-activator CD3/CD28 for Tcell expansion and activation	Thermo Scientific
ECL	Thermoscientific
EcoRI-HF	NEB
Gel Extraction Kit	Qiagen
HindIII-HF	NEB
Lipofectamine Cell transfection kit	Invitrogen
Masson Trichome Kit	Sigma
Mitochondria Isolation Kit	Sigma
PageRuler™ Plus Prestained Protein Ladder	Thermo Scientific
Pre-stained protein marker	Thermo Scientific
Q5 DNA Polymerase	NEB
QIAprep Spin Miniprep Kit	Qiagen
QIAquick Gel Extraction Kit	Qiagen
proteome Mitochondria Isolation Kit	Qiagen
QuikChange Site-Directed Mutagenesis Kit	Agilent Technologies
T4-DNA Ligase	NEB

5.1.3 Primary Antibodies:

Antibody	Host	Source	Application	Dilution used
CHOP	Mouse	CST	WB	1:1000
cytochrome c	Mouse	Abcam	WB,IF	1:500
DRP1	Rabbit	Abcam	IF	1:500
Hsp60	Mouse	Abcam	WB,IF	1:500
MFN1	Mouse	Abcam	WB	1:250
MFN1	Rabbit	Novus	IF	1:100
MFN2	Mouse	Abcam	WB	1:250
MFN2	Rabbit	CST	IF	1:100
OPA1	Mouse	Abcam	IF	1:250
Osteocalcin	Mouse	Novus	IF	1:500
Osteopontin	Mouse	Novus	IF	1:500
Runx2	Rabbit	CST	IF	1:1000
Sirt3	Rabbit	CST	WB/IHC	1:200

TRPM8	Rabbit	Alomone lab	IF, WB	1:200
TRPV4	Rabbit	Alomone lab	IF, WB	1: 500
TRPV4	Guineapig	Alomone lab	IF	1:200
Vinculin	Mouse	Sigma Aldrich	IF	1:250

WB: Western Blot, IF: Immunofluorescence, IHC: Immunohistochemistry

5.1.4 Secondary Antibodies:

Antibody	Host	Source	Application	Dilution used
Alexa-488-labelled anti-rabbit	Chicken	Molecular Probes	IF	1:1000
Alexa-488-labelled anti-mouse	Chicken	Molecular Probes	IF	1:1000
Alexa-594- labelled anti-rat	Chicken	Molecular Probes	IF	1:1000
Alexa-594- labelled anti-mouse	Chicken	Molecular Probes	IF	1:1000
Alexa-594- labelled anti-rabbit	Chicken	Molecular Probes	IF	1:1000
HRP labelled anti-mouse	Donkey	GE Healthcare	WB	1:10,000
HRP labelled anti-rabbit	Donkey	GE Healthcare	WB	1:10,000

5.1.4 Constructs Used:

Vector	Expression system	Source
pGP-CMV-GCaMP6f	Mammalian	Addgene
Mito Pericam EYFP	Mammalian	(Nagai T, 2001)
mitoDsRed	Mammalian	Clontech
KDEL-BFP	Mammalian	Addgene
pEGFPN3	Mammalian	Prof. J. Berreiter-Hahn (Frankfurt, Germany)
TRPV4-GFP pEGFPN3	Mammalian	(Becker D, 2009)
TRPV4-L596P-GFP pEGFPN3	Mammalian	Prepared in CG lab
TRPV4-R616Q-GFP pEGFPN3	Mammalian	Dr. D. H. Cohn (UCLA)
TRPV4-F617L-GFP pEGFPN3	Mammalian	Prepared in CG lab
TRPV4-L618P-GFP pEGFPN3	Mammalian	Prepared in CG lab
TRPV4-V620I-GFP pEGFPN3	Mammalian	Dr. D. H. Cohn (UCLA)
TRPV4-S372L-GFP-pEGFPN3	Mammalian	Prepared in CG lab
pmCherry-C1	Mammalian	Prepared in CG lab
TRPV4-FL-WT-pmCherryC1	Mammalian	Prepared in CG lab
TRPV4-L596P- pmCherryC1	Mammalian	Prepared in CG lab
TRPV4-R616Q- pmCherryC1	Mammalian	Prepared in CG lab
TRPV4-F617L- pmCherryC1	Mammalian	Prepared in CG lab
TRPV4-L618P- pmCherryC1	Mammalian	Prepared in CG lab
TRPV4-V620I- pmCherryC1	Mammalian	Prepared in CG lab

5.1.5 Cell lines and primary cells:

CHOK1-Mock	Prof. Jon D Levine (UCSF, USA)
CHOK1-V4	Prof. Jon D Levine (UCSF, USA)
F11	Prof. F. Hucho (FU, Berlin)
HaCaT	Prof. F. Hucho (FU, Berlin)
K7M2	Dr. Mamoni Dash (ILS)
L929	NCCS Pune
MC3T3-E1	ATCC
Mesenchymal stem cells (Mouse)*	NISER, Bhubaneswar, India
Mouse bone marrow macrophage (Mouse)*	NISER, Bhubaneswar, India
Murine splenic T cells (from Balb/c mice)**	NISER-Bhubaneswar, India
Saos-2	ATCC

*IAEC number: NISER-IAEC/SBS-AH- 153 ** IAEC number: NISER-IAEC/SBS-AH-200

5.2 Methods:

5.2.1 Methods related to Molecular Biology:

5.2.1.1 Construct Preparation:

For the generation of desired construct, the specific DNA fragments were amplified by PCR by using specific sets of forward and reverse primers. Overhanging ends were obtained by digesting the PCR product and the vector using restriction enzymes. The restriction enzyme-digested PCR product and vector were extracted from agarose gel using a gel extraction kit. They were ligated and transformed in to competent *E. coli* DH5α strain. The transformed *E. coli* was grown over the LB plates containing suitable antibiotic for selection. The positive colonies that come up were cultured further in LB media containing antibiotics. The plasmid DNA was isolated by using plasmid DNA isolation kit. The isolated DNA was further treated with restriction enzymes to check the desired fragment and was further validated by doing sequencing.

5.2.1.2 Polymerase Chain Reaction (PCR):

For the purpose of preparing various constructs in specific expression vectors, PCR reactions were carried out to amplify the distinct coding regions with specific restriction sites at their ends. The PCR was also used for SDM (Site Directed Mutagenesis) for generation of mutants

(mainly point substitutions). The reaction conditions for both types of PCR were different. For cloning a specific stretch or whole insert from one vector to another, primer sets having specific restriction sites were used. For SDM, primers contained only the required mutations and lacked restriction sites. DNA template, forward and reverse primers, 1X polymerase buffer, DNA polymerase enzyme, dNTP mix, and MilliQ water were used as the components of PCR master mix. Using agarose gel electrophoresis, every PCR-amplified DNA was validated. The necessary conditions for PCR reactions are listed in the table below.

5.2.1.3 Site Directed Mutagenesis and construct preparation:

Full-length human TRPV4-WT-GFP construct cloned in pEGFP-N3 vector was a kind gift from Prof. J. Berreiter-Hahn (Becker D, 2005). Using this as a template one point mutant Serine 372 Leucine (S372L) was made. Site Directed Mutagenesis (SDM) was performed using QuikChange Site- Directed Mutagenesis Kit from Agilent Technologies. The SDM was carried out by following manufacturer's protocol. The primers used are tabulated below.

TRPV4-Ser372Leu	**Forward primer** 5'- CAACGACGGCCTC**TTG**CCCCTCATGATGGC -3' **Reverse primer** 5'- GCCATCATGAGGGG**CAA**GAGGCCGTCGTTG -3'

PCR for Site Directed Mutagenesis:

DNA template (100ng/µl)	0.5 µl
10X reaction buffer	2.5 µl
Forward Primer (25µM)	0.5 µl
Reverse Primer (25µM)	0.5 µl
dNTP mix	0.5 µl
Pfu Turbo DNA polymerase(2.5U/µl)	0.5 µl
Autoclaved MilliQ water	20 µl
Total	25 µl

PCR reaction conditions for SDM:

Segment	Cycles	Temperature	Time
1	1	95 °C	30 seconds
2	16	95 °C	30 seconds
		55 °C	1 minute
		68 °C	6 minutes
3	1	68 °C	10 minutes
4	1	4 °C	∞

4 µl of the PCR product was tested on a 0.8% Agarose gel to confirm the product's size. Upon confirmation, the remaining 21 µl of PCR product was digested for 4 hours at 37 °C with 0.5 µl of SalI and HindIII enzyme (provided in the kit). The digested product was then transformed into colonies using DH5α competent cells. The colonies were cultured overnight in LB medium.

Plasmid was extracted using a Qiagen Miniprep Kit. Sanger DNA sequencing was used to confirm the presence of the intended mutations in the extracted DNA.

5.2.1.4 Agarose Gel Electrophoresis:

Horizontal agarose gel electrophoresis was used to separate double-stranded DNA (dsDNA) in 0.8% or 1% agarose gel in a tank containing 1X TAE. The gel of the desired percentage was made by mixing agarose powder with 1X TAE buffer and heating it in the microwave for 2–3 minutes, until the agarose powder dissolved and the solution become clear. The gel percentage is determined by the expected length of dsDNA to be resolved. For DNA visualization, a final concentration of 0.1-0.5 µg/ml of EtBr (Ethidium Bromide) solution was added to the gel solution. At room temperature, the completed slurry was poured onto a casting tray that already had a comb of the correct thickness. After the solution had hardened, the comb was carefully removed, and the gel and casting tray were placed in an electrophoresis chamber containing electrophoretic buffer (1X TAE). DNA samples were added to each well after being mixed with DNA loading dye (1X final concentration). The electrophoresis device is connected with a power supply source with proper cathode and anode direction. The loading dyes help visualization of the DNA migration. After completion of the DNA migration the electrophoresis was stopped and the DNA bands were visualized under UV transilluminator.

Solutions and buffer required:

(1 X) TAE buffer: 40 mM Tris/Acetic acid, pH 7.8; 1 mM EDTA, pH 8.0

(5 X) DNA loading buffer: 40% (w/v) Sucrose, 240 mM Tris/Acetic acid, pH 7.8, 5 mM EDTA, pH 8, 0.25% (w/v) Bromophenol blue, 0.25% (w/v) Xylene cyanol FF.

5.2.1.5 Restriction digestion:

PCR product and desired vector samples were run on 0.8% or 1% Agarose gel for cloning. The correct-sized bands were excised using a clean scalpel. The DNA fragment was extracted from the agarose gel by using the Qiagen Gel Extraction kit and subjected to restriction digestion for three hours at 37 °C using specific restriction enzyme/s. The restriction digestion reaction was set up using the extracted DNA, restriction enzymes, 1X CutSmart Buffer (NEB) and Autoclaved MilliQ water. Minimum 1µg of DNA was used for this reaction and the reaction volume varies from 10-25 µl.

5.2.1.6 Ligation of insert and vector:

The digested product was electrophoretically separated by using 0.8% agarose gel. The required fragment was excised out by clean scalpel and extracted by using Qiagen Gel Extraction Kit. Using Nanodrop (Thermo Scientific) the concentrations of insert and vector DNA were determined. The ratio of insert to vector in the ligation mixture was maintained mostly at 3:1. Depending on the amount of insert and vector DNA, the reaction volume was set between 10 and 15 µl. The ligation mixture was comprised of 1X T4 Ligation buffer (NEB), T4 DNA Ligase (NEB), and autoclaved MilliQ water. The ligation mixture was incubated overnight at 16 °C.

5.2.1.7. Transformation:

After keeping DH5α competent cells (*E. coli*) on ice for a few minutes, 3.5–4 µl of the ligated product was added to 50 µl of the cells for transformation. After incubating on ice for 10 minutes, the tube was placed in a water bath heated to 42 °C for 45 seconds to induce a heat shock. After that the vial was kept in ice for 5 min and it further incubated in 37 °C for 1 hour at 220 RPM with 900 µl of LB media. Post incubation the bacterial cells were pelleted at 13000 RPM for 1 min. Around 800 µl of the supernatant was discarded and the pellet was re-suspended with the

remaining media. Using glass beads the bacterial pellets were spreaded over the ampicillin (100 mg/ml) and kanamycin (50 mg/ml) antibiotic containing LB plates. These plates were incubated overnight at 37 °C and single colonies were obtained after that.

LB media composition for 1 liter	
Yeast extract	5 gm
Tryptone	10 gm
Sodium Chloride	10 gm

5.2.1.8 Competent Cell Preparation by RbCl method:

For the preparation of *E. coli* competent cells Rubidium chloride method was used. We inoculated 3 ml of LB broth with a single colony of *E. coli* from a freshly streaked LB plate. The culture was grown overnight at 37 °C and 220 RPM. After inoculating 1–2 ml of this culture into sterile LB liquid medium, the mixture was incubated at 37 °C with 220 RPM until the OD at 600 nm was between 0.4 and 0.6. After achieving the desired OD, the culture was placed on ice for 15 minutes. After that the culture was pelleted at 4500 RPM for 10 min at 4 °C. The pellet was re-suspended in 40 ml TFBI buffer and incubated on ice for 15 minutes. Again, the solution was centrifuged for 5 minutes at 4 °C and 4000 RPM. The supernatant was discarded and the pellet was re-suspended in 4 ml of TFBII buffer while keeping the tube in ice. Small amounts (50-100 µl) of this bacterial culture were aliquoted into cold micro centrifuge tubes. Afterwards, the tubes containing the competent cells were snap-frozen in liquid nitrogen and kept at -80 °C until needed.

Composition of TFBI buffer:

For 50 ml	
RbCl (100 mM)	0.725 gm
$MnCl_2$-$4H_2O$ (50 mM)	0.5 gm
Potassium acetate (30 mM)	0.147 gm
$CaCl_2$-$2H_2O$ (10 mM)	0.075 gm
Glycerol (15% final)	7.5 ml
Autoclaved MilliQ water	42.5 ml
pH was adjusted to 5.8 with acetic acid, filter sterilized, and stored at 4 °C away from light.	

Composition of TFBII buffer:

For 15 ml	
MOPS (10 mM)	0.031 gm
RbCl (10 mM)	0.018 gm
$CaCl_2$, $2H_2O$ (75 mM)	0.165 gm
Glycerol (15% final)	2.25 ml
Autoclaved MilliQ water	12 ml
pH was adjusted to 6.5 with KOH, filter sterilized, and stored at 4 °C away from light.	

5.2.2 Biochemical techniques:

5.2.2.1 SDS-PAGE:

SDS-PAGE was used to resolve proteins on polyacrylamide gels (8% or 12%) based on their molecular weight. Sodium Dodecyl Sulfate (SDS) is an anionic detergent used to give all the proteins a consistent negative charge, allowing them to be separated solely by their molecular weight and not by their native charge. For the preparation of protein samples suitable for SDS-PAGE analysis, the protein samples were treated with Laemmli buffer (final concentration 1X) and samples were heated at 95° C for 5 minutes. SDS-PAGE Cassettes were put together by using two clean glass plates that were 7 cm high and 10 cm wide (0.75 mm thickness). Between the glass plates, about 5 ml of resolving gel was poured. A thin layer of 1 ml of water was slowly added to this gel to make the top surface as a smooth surface. The gel was allowed to polymerize at ambient temperature. After polymerization, the water was decanted so that the stacking gel could be poured. Approximately 2 ml of stacking gel was added, followed by the insertion of 10 or 15 well combs for well formation. After the polymerisation of stacking gel, the comb was gradually extracted. The cassettes were vertically inserted into the electrophoresis chamber, which was then filled with the electrophoresis running buffer, and denatured protein samples were loaded using a Hamilton syringe into the wells. For electrophoresis, the device was coupled to a continuous current source (10mAmp). Bromophenol blue, a tracking dye in the Laemmli buffer, makes it possible to see proteins that have moved in the gel. Electrophoresis run is stopped when the dye front reaches close to the bottom of the gel. Coomassie Blue was used to visualize the separated proteins in the gel. Proteins were transferred from non-fixed SDS gel to a PVDF membrane for Western Blot analysis if and when needed.

12% SDS-PAGE gel composition			
Resolving		**Stacking**	
30% Acrylamide Solution	1.9 ml	30% Acrylamide Solution	500 µl
Autoclaved MilliQ water	1.7 ml	Autoclaved MilliQ water	2.1 ml
Tris (pH=8.8)	1.3 ml	Tris (pH=6.8)	380 µl
10% SDS	50 µl	10% SDS	30 µl
APS	50 µl	APS	30 µl
TEMED	8 µl	TEMED	4 µl

10X SDS Running buffer (500 ml)	
Tris Base	15.1 gm
Glycine	94 gm
SDS	5 gm
The volume was made up to 500 ml by addition of double distilled water	

5X Laemmli buffer (for 10 ml)	
0.5 M TrisHCl (pH=6.8)	1.25 ml
β-Mercaptoethanol	0.5 ml
Glycerol	5 ml
20% SDS	1 ml
Bromophenol Blue	0.01 gm
Autoclaved Milli Q water	2.6 ml

5.2.2.2 Coomassie staining:

After electrophoresis, the SDS-PAGE gels were stained in a staining solution overnight. The dye stains the entire gel but permanently sticks to the proteins present in the gel. The stained gels were further treated in a destaining solution for about 2 hours with constant shaking. Blue protein bands could be seen on a clear background after effective destaining.

Composition of staining solution (for 500 ml)	
Coomassie Brilliant Blue G-250	0.5 gm
Methanol	250 ml
Glacial Acetic Acid	50 ml
Autoclaved milli Q water	200 ml

Composition of de-staining solution (for 500 ml)	
Methanol	250 ml
Glacial Acetic Acid	50 ml
Autoclaved milli Q water	200 ml

5.2.2.3 Western blot analysis:

Semi-dry transfer of proteins to a PVDF membrane was performed to carry out Western blotting. After the proteins were separated by SDS-PAGE, the gels were incubated briefly for few minutes in western transfer buffer. For the transfer, Whattman paper pad soaked in transfer buffer was placed in semidry apparatus. The methanol-activated PVDF membrane were set on top of the transfer pad and rolled with a glass rod to evenly distribute the buffer and eliminate trapped air bubbles if any. The poly acrylamide gel was immersed in the transfer buffer for a while and placed over the pad. A Western Blot Transfer buffer-soaked Whatman paper pad was placed on top of this gel, and the whole thing was gently rolled with a glass rod. The semi-dry transfer unit was

closed and connected to a power source. The transfer was set at 25 volts for 35 minutes. After transfer, the PVDF membrane was stained with Ponceau dye (optional) and submerged in a blocking solution (1X TBS-T containing either 5% NFDM or 5% BSA). After an hour of blocking, the membrane was incubated overnight at 4 °C with the primary antibody. After that, it was washed three times with 1X TBS-T and then left at room temperature for an hour with the secondary antibody. The blot was then washed three times with 1X TBST and developed using a detection reagent (Thermo Scientific Super Signal™ West Femto Maximum Sensitivity Substrate) and a ChemiDoc machine (BioRad).

Composition of TBS (5X) for 500 ml	
20 mM Tris Base	6.05 gm
150 mM NaCl	21.915 gm
Adjust volume to 500 ml with MilliQ water	

Composition of Western Blot Transfer Buffer (for 1 liter)	
Tris	3.04 gm
Glycine	14.42 gm
Methanol	200 ml
SDS	0.373 gm
The volume was made up to 1 litre by addition of autoclaved Milli Q water	

5.2.3 Methods related to cell biology:

5.2.3.1 Cell culture, transfection, and pharmacological modulation of TRPV4:

Chinese hamster ovary (CHO-K1) cells stably selected for TRPV4 (cloned in pcDNA3.1 vector, termed as CHO-K1-V4 cells) or empty pcDNA3.1 vector-only (termed as CHO-K1-Mock cells) were grown in F-12 Ham's medium containing FBS (10% v/v), L-glutamine (2 mM), Streptomycin (100 µg/ml), Penicillin (100 U/ml). Cells were maintained in a humidity-controlled incubator set at 5% CO_2 and 37 °C. F11 cells [peripheral dorsal root ganglion (DRG) neuron-derived cell line] were cultured on F-12 Ham's medium. HaCaT (Human epidermal keratinocyte cell), HeLa and COS-7 cells were cultured in DMEM media supplemented with FBS (10% v/v), L-glutamine (2 mM), Streptomycin (100 µg/ml), Penicillin (100 U/ml), and Amphotericin-B in a humidity-controlled incubator set at 37°C and 5% CO_2. Saos-2 cells were procured from ATCC and were cultured in McCoy's 5A (modified) media (PAN Biotech, Germany) supplemented with FBS (10% v/v), L-glutamine (2 mM), Streptomycin (100 µg/ml), Penicillin (100 U/ml). Other cell lines, such as K7M2 and L929 were culture in RPMI media supplemented with FBS (10% v/v), L-glutamine (2 mM), Streptomycin (100 µg/ml), Penicillin (100 U/ml) and Amphotericin-B. Cells were maintained in a humidity-controlled incubator at 37 °C. Transient transfection was performed by Lipofectamine 3000 Plus reagent (Invitrogen) according to the manufacturer's protocol. Typically, 24-36 hours after transfection, the cells were used for live-cell imaging or immunocytochemistry.

5.2.3.2 Immunocytochemistry, live-cell imaging, and microscopy:

Cells were grown and transfected on 12 mm glass coverslips. Two days after seeding or transfection, cells were fixed with 4% PFA at RT. Cells were permeabilized with 0.1% Triton-X 100 in PBS for 5 minutes, followed by washing twice with 0.1% PBS-T (0.1% Tween-20 in 1 X

PBS). Cells were blocked with 5% bovine serum albumin (BSA) in PBS-T. Thereafter, cells were incubated with different primary antibodies, such as HSP60 (1:800), and TRPV4 (1:500) in different dilutions for overnight at 4 °C. Thereafter, cells were washed thrice with PBS-T. Cells were further incubated for 1 hour with Alexa dye labelled secondary antibody (anti-mouse or anti-rabbit) diluted (1:1000) in PBS-T and 5% bovine serum albumin (BSA) in 1:1 ratio. Cells were incubated with DAPI (5 μM) in PBS-T for 30 minutes at RT. Subsequently, cells were washed with PBS two times and coverslips were mounted on to glass slides with Fluoromount G (Southern Biotech). The cells were imaged by using confocal microscope (Zeiss, LSM780, 63 X objectives; Olympus FV3000). All images were taken under the same conditions for comparative analysis. Images were analyzed and processed by using LSM Image examiner software and by ImageJ.

5.2.3.3 Isolation of mitochondria from mammalian brain and CHO-K1 cells:

For Ca^{2+}-imaging in cytosol-free condition, mitochondria were purified from the mouse brain by using Qproteome Mitochondria isolation kit (Qiagen, Germany). Mitochondria were purified by following the manufacturer's protocol. The efficiency and activity of the purified mitochondria was analyzed by staining with MitoTracker Red (1 μM). For the Ca^{2+}-imaging of isolated mitochondria, the purified mitochondria pellet is resuspended in mitochondrial storage buffer (Qiagen).

For isolation of mitochondria from CHO-K1 cells, 90% confluent cells were seeded in 100 mm dishes and grown for 24 hours. Mitochondrial fraction and cytoplasmic fraction from the cells were isolated by using a mitochondrial isolation kit according to the manufacturer's protocol (Sigma Aldrich).

5.2.3.4 Mitochondrial Ca^{2+}-imaging:

Mitochondrial Ca^{2+}-imaging was performed with ratiometric mitochondrial Pericam constructs (A gift from Dr. Atsushi Miyawaki, Saitama, Japan). Ratiometric Pericam is a Ca^{2+}-indicator made by fusion of the yellow fluorescent protein (YFP) and calmodulin which is able to enter mitochondria (Nagai T, 2001). Binding of Ca^{2+} to Mito-Pericam changes its excitation wavelengths from 415 nm and 494 nm, while its emission spectrum is maintained at 515 nm. Mito-Pericam was expressed in CHO-K1-Mock and CHO-K1-V4 cells by transient transfection and 24 hours after transfection, cells were imaged with confocal microscope. Cells expressing moderate levels of the sensor were considered for Ca^{2+}-imaging because these cells allow very well the qualitative as well as quantitative analysis of both increase and decrease in intensities. Ca^{2+}-imaging was performed by using drugs at different concentrations- 4αPDD (5 µM), RN1734 (10 µM), BAPTA-AM (10 µM), Ruthenium Red (10 µM)). In case of pre-treatment conditions, cells were pre-incubated with RN1734, BAPTA-AM or Ruthenium Red for 1 hour and the Ca^{2+}-influx was recorded by using TRPV4 activator 4αPDD (5 µM). For mitochondrial Ca^{2+}-imaging in an endogenous system, Saos-2 cell (human osteosarcoma cell) were used and plasmid encoding Mito-Pericam was expressed. The cells were stimulated with 4αPDD (5 µM) and Ca^{2+}-influx was recorded by time series live cell imaging. In another experiment cells were pre-treated with RN1734 (10 µM) and subsequently activated by 4αPDD. Similarly to check the activity of TRPM8 on mitochondrial Ca^{2+}, TRPM8-specific agonist and antagonist such as WS12 (5 µM), AMTB (10 µM) or Menthol (100 µM) were used.

For Ca^{2+}-imaging in cytosol-free condition, mitochondria were purified from the mouse brain by using Qproteome Mitochondria isolation kit (Qiagen, Germany). Mitochondria were purified by following the manufacturer's protocol. The efficiency and activity of the purified

mitochondria was analyzed by staining with MitoTracker Red (1 μM). For the Ca^{2+}-imaging of isolated mitochondria, the purified mitochondria pellet is resuspended in mitochondrial storage buffer (Qiagen). Purified mitochondria were incubated with Ca^{2+}-sensing dye Rhod-3-AM (10 μM) for 1 hour along with different concentrations of drugs- 4αPDD (5 μM, 0.5 μM, 0.05 μM), RN1734 (10 μM), Ionomycin (5 μM), and CCCP (carbonyl cyanide m-chlorophenyl hydrazine; 100 μM) at 37 °C. After 1 hour of incubation, unbound dyes were washed and mitochondria were taken for imaging. The whole mitochondrial Ca^{2+}- imaging for 720 seconds (3.6 seconds per image in 512x512 pixels) had been performed in temperature controlled live cell imaging system (OKO lab). Similarly to check the impact of TRPM8 in mitochondrial Ca^{2+}-level in isolated mitochondria, purified mitochondria was labelled with Rhod-3-AM dye (10 μM) for 1 hour along with either WS12 (5 μM), AMTB (10 μM) or Antimycin A (10 μM). In case of "cold shock", purified mitochondria were kept on ice for an hour. After 1-hour incubation, the labelled mitochondria were then washed and then taken for imaging. The purified mitochondria were re-suspended in the mitochondria storage buffer (Qiagen). In all the Ca^{2+}-imaging experiment, no extra Ca^{2+} was added other than what is present in the complete media in which cells were growing. In case of isolated mitochondria, the Ca^{2+}-source is the mitochondrial storage buffer (Qiagen) where the mitochondrial pellet is re-suspended.

5.2.3.5 Fluorescence labelling and antibody staining of Mesenchymal stem cells & isolated mitochondria:

Freshly purified mitochondrial pellet was fixed with 2% glutaraldehyde for 1 hr at 37°C. For immunofluorescence staining mitochondria were labelled with primary antibodies, namely with anti-HSP60 (Abcam, 1:500) anti-MFN1 (Novus, 1:100), anti-MFN2 (CST, 1:100) and anti-TRPV4 (Guineapig, Alomone, 1:200) for overnight. Thereafter mitochondria were washed three

times with PBS and were further incubated for 1 hour with Alexa dye labelled secondary antibody (anti-Guineapig for TRPV4 and anti-rabbit for MFN1 and MFN2). The secondary antibodies were diluted at 1:500 in PBS supplemented with 5% bovine serum albumin (BSA). Isolated mitochondria were imaged with confocal microscope (FV3000) using the 63X objective. All images were taken under same conditions for comparative analysis. Images were analyzed and processed by using LSM Image examiner software and by ImageJ. Mesenchymal stem cells (MSCs) from mouse bone marrow were isolated and cultured as mentioned before (Watanabe H, 2003). The purified MSCs were fixed by 4% PFA. Anti-MFN1 (Novus, 1:100), MFN2 (CST, 1:100) and TRPV4 (Alomone, 1:200) were used for immunostaining.

5.2.3.6 JC-1 (Ratiometric dye) staining in adherent cells and isolated mitochondria:

Mitochondrial potential detection in the adherent cell (CHO-K1-V4 and CHO-K1-Mock) was performed by using 5, 5, 6, 6-tetrachloro-1, 1, 3, 3-tetraethylbenzimidazolylcarbocyanine iodide (JC-1) cationic dye. JC-1 dye exhibits potential-dependent accumulation inside the mitochondria and also has fluorescence emission properties that shift from green (525 nm) to red (590 nm) region (Reers M, 1995). 4αPDD (5 μM) and RN1734 (10 μM) were added for 6 hours, followed by staining with JC-1 (5 μM) for 40 minutes. Subsequently, cells were washed with PBS and live-cell imaging was performed by confocal microscopy (Zeiss LSM780). JC1 staining was also performed in isolated mitochondria. Mitochondrial purification and resuspension in mitochondria storage buffer (Qiagen) were performed as mentioned before. The re-suspended mitochondrial sample was incubated with 4αPDD (5 μM), RN1734 (10 μM), Antimycin (20 μM) along with JC1 dye (5 μM) for 1 hour at 37 °C. After incubation, spectroscopic absorbance was taken for green to the red range (525-590 nm).

In some experiments (such as in Saos-2 cells) the mitochondrial membrane potential was determined by using TMRM dye (Invitrogen). Saos-2 cells were seeded on 25 mm glass coverslips. Cells were then treated with WS12 (5 μM), Menthol (100 μM) and AMTB (10 μM) for 6 hours and subsequently labelled with TMRM dye (50 μM) for 30 minutes. After that confocal imaging was performed to check the changes in membrane potential.

5.2.3.7 Labelling of Mito Thermo Yellow (MTY) and ER Thermo Yellow (ETY):

MTY and ETY sensors were used as described before (Arai S, 2014; Arai S, 2015). These are mitochondria- and ER-targeted compounds that show changes in fluorescence intensity in a temperature-dependent manner. The fluorescence excitation and emission range of MTY are used at 530 nm/570 nm (Arai S, 2015). Similarly, the excitation and emission range for ETY is set at 560 nm/585 nm (Arai S, 2014). For using these sensors, the cells were grown in 25 mm glass coverslips and were treated with either 4αPDD (5 μM), RN1734 (10 μM), or Antimycin (20 μM) for 6 hours or left untreated. After drug treatment, cells were incubated with MTY (0.5 μM) and ETY (0.5 μM) for 15 minutes. Subsequently, cells were washed with fresh media and taken for live-cell imaging.

In order to analyze the changes in mitochondrial temperature due to the modulation of endogenous TRPV4, two different systems, i.e. mouse bone marrow-derived Mesenchymal stem cells (MSC) and mitochondria isolated from mouse brain were used. MSCs were treated with 4αPDD (5 μM), or RN1734 (10 μM) for 6 hour and subsequently loaded with MTY (0.5 μM) for 15 min and live cell imaging was performed. Similarly, isolated mitochondria were incubated with drugs for 1 hour and last 15 min with MTY (0.5 μM) at 37 °C. After incubation, unbound dyes were washed out and the mitochondria were taken for imaging. The fluorescence intensities of MTY in MSCs were measured by Image J (200 cells were considered in each group). In case of

isolated mitochondria, the fluorescence intensity was measured by using 'analyze particle' function in Image J.

To check the effect of TRPM8 on mitochondrial and ER temperature Cells were grown in 25 mm glass coverslips and treated with WS12 (5 μM), AMTB (10 μM) and Menthol (100 μM) for 6 hours. Before completion of 6 hours, cells were labelled with either MTY or ETY dye at concentration of 0.5 μM for 15 minutes and subsequently taken for live cell confocal imaging after washing. The isolated mitochondria from mouse brain were treated with WS12 (5 μM), AMTB (10 μM) and Menthol (5 μM) for 1hr and subsequently labelled by MTY (0.5 μM) for 15 minutes and the unbound dyes were washed out by centrifugation. Multiple view fields were imaged by confocal microscope. The MTY intensities of each mitochondrion were quantified by 'Analyze Particle' function of Image J.

5.2.3.8 Mitochondrial image analysis and quantification:

Quantification of mitochondrial Ca^{2+} and the mitochondrial number were performed by Image J. For that purpose, total 200 time-series images (total time 720 seconds and the pharmacological modulators were added at 72nd seconds in each experiment) were acquired. In some experiments, cells pre-treated with different pharmacological agents [such as RN1734 (10 μM); BAPTA-AM (10 μM); Ruthenium Red (10 Mm), Menthol (100 μM) for 6 hours] were used. Images at different time points (01, 108, 180, 360, 540 and 720 seconds) were used for detailed analysis of Ca^{2+}-level dependent group-wise particle number quantification.

For this analysis, the confocal images were first converted in to 8 bit images and image threshold was set for the individual ROIs (equivalent to individual cell). In each case, the image threshold was kept constant in all ROIs irrespective of the conditions. From this, total particle

numbers as well as the Ca^{2+}-intensity of respective particles were derived. This data set was further analyzed numerically and statistically.

For the quantification of mitochondrial morphological parameters, we used mitochondria morphology plugin as described before (Dagda RK, 2009): https://imagejdocu.tudor.lu/plugin/morphology/mitochondrial_morphology_macro_plug-in/start).

The quantification of ratio of mitoDsRed intensity with GFP intensity (of TRPV4-WT and TRPV4 mutants) in individual mitochondria were performed by Image J. Here individual mitochondria were quantified and more than 1000 mitochondrial ROIs per group were considered. For the analysis of change in morphological parameters in different experimental condition in Saos-2 cells the cells were treated with TRPM8 activator WS12 (5 µM), AMTB (10 µM) and Menthol (100 µM) for six hours. Post drug incubation cells were stained with MitoTracker Red CMXRos (0.5 µM) for 20 minutes and multiple images were taken by using confocal microscope (FV3000, OLYMPUS).

5.2.3.9 Measurement of Mitochondrial ATP level and ATP release assay:

Mitochondrial ATP release was quantified by using a luciferase-based assay (kit from Invitrogen). Mitochondria was isolated from CHO-K1-Mock and CHO-K1-V4 cells. The mitochondria pellet was suspended with 100 µl of Mitochondria storage buffer from Qiagen. The mitochondrial suspension was incubated with TRPV4 activator 4αPDD (5 µM), TRPV4 inhibitor RN1734 (10 µM) and antimycin (20 µM) for 1 hour at 37 °C. After incubation, amount of ATP released was quantified by using luciferase ATP assay kit by following manufacture's protocol. Luminescence was measured by using Varioskan multimode multiplate reader (Thermo Fisher Scientific). In another set of experiment, we have measured mitochondrial ATP level by using an

ATP-binding dye, i.e. ATP red. This dye specifically binds to mitochondrial ATP and thus its level can be monitored by live cell imaging (Wang L, 2016). The fluorescence intensity of the dye increases with increase in the ATP level. We treated CHO-K1-Mock and CHO-K1-V4 cells with 4αPDD (5 µM) and RN1734 (10 µM) for 6 hours. After the treatment, the cells were incubated with ATP-Red dye (5 µM) for 20 minutes and subsequently live cell imaging was performed by confocal microscope (Olympus, FV3000).

To check the effect of TRPM8 in mitochondrial ATP level the Ssos-2 cells were treated with WS12 (5 µM), Menthol (100 µM) and AMTB (10 µM) for 6 hour and subsequently labelled with ATP red (5 µM) for 20 min and live cell imaging was performed.

5.2.3.10 Measurement of GTP level:

For the measurement of cytosolic GTP level cells were treated with 4αPDD (5 µM) and RN1734 (10 µM) for 6 hour and subsequently loaded with GTP green (10 µM) for 30 minutes and cells were imaged by confocal microscopy (Olympus, FV3000). The dye recognises the cytosolic GTP specifically as described before (Wang S, 2006).

5.2.3.11 Hypotonic treatment to the cell and ER-mito contact point quantification:

Cells were left untreated (control) or treated with 4αPDD (5 µM), RN1734 (10 µM), WS12 (5 µM), Menthol (100 µM) and AMTB (10 µM) for 6 hours. In some experiments, Thapsigargin (1 µM) or BAPTA-AM (5 µM) were treated for 1 hour at the last. Before hypotonic stimulus, the cells were treated with 0.5 µM Mito Tracker Red CMXRos (Invitrogen) and 0.5 µM ER-Tracker Blue-White DPX (Invitrogen) and incubated for 30 minutes at 37 °C. The incubated cells were treated with 5% hypotonic media (5% F-12 Ham media in diH_2O) and kept for 5 minutes in 5% CO_2 at 37 °C to allow the cells to generate ER and mitochondria-derived Large Intracellular Vesicles (LICV). Treatment of cells with hypotonic medium was based on the methodology

established before (Jaiswal A, 2019; King C, 2020). After the generation of LICVs multiple images were taken immediately (within 2-5 minutes) by using confocal microscope (FV3000, Olympus). The live cell imaging was performed by using CO_2 and temperature-controlled live cell imaging set up (Okolab).

For the quantification of ER-mito contact points, we followed the detailed protocol described before (Chidawanyika T, 2021). Co-localization of ER and Mitochondria was performed by using 'Co-localization' plugin in Image J. For quantification of ER-mito contact points, "particle-based quantification" was performed. The images were converted into binary format and 'Analyze Particle' function of Image J was used to quantify total mitochondrial particle, total ER particle and total colocalized particle in individual cells. Values from different cells were clubbed together and the graphs were plotted using GraphPad Prism 7. In all the conditions minimum of 40 cells were quantified. The colocalized pixels in different conditions are plotted on a percentage scale. For the percentage quantification the average colocalized pixel number of mock control is taken as a hundred percent.

5.2.3.12 Docking of MFN2 with TRPV4:

Human TRPV4 (PDB id: 7AA5) (Botte M, 2020) structure was downloaded from RCSB PDB. Human Mitofusion protein-2 (MFN2) was taken from Alpha-fold 2 (ID: O95140). The proteins were imported in YASARA and energy minimization was carried to fill any gaps present in the downloaded structure (Krieger E, 2009). Further, ClusPro2.0 (Kozakov D, 2017) was used to perform protein-protein docking, taking TRPV4 as receptor and MFN2 as ligand with default parameters. Model with the lowest energy was selected. The docked model was then uploaded to OPM PPM3.0 server to embed it in outer mitochondrial membrane with other settings as default. YASARA was then employed for representation and snap capturing.

5.2.3.13 Detection of mitochondrial superoxides and Cardiolipin:

MitoSOX-Red and NAO dye were used for labelling of mitochondrial superoxides and mitochondrial Cardiolipins respectively. Saos-2 cells were seeded on 25 mm glass coverslips and subsequently treated with WS12 (5 µM), Menthol (100 µM) and AMTB (10 µM) for 6 hours. Before completion of 6 hours, either MitoSOX-Red dye was used at 2.5 µM for 30 minutes or NAO dye was used at 0.5 µM concentration for 15mins. Post labelling, cells were washed with warm media and taken for live cell imaging.

5.2.3.14 Animal procurement and Primary cell isolation:

Animals used for this work were procured either from NISER animal house facility. Experiments were performed as per the ethical approval (NISER/SBS/IAEC/AH-55, NISER/SBS/IAEC/AH-77, and NISER-IAEC/SBS-AH-200). All methods were performed in accordance with the relevant guidelines and regulations of IAEC (Institutional Animal Ethical Committee). For isolation of Mesenchymal stem cells, adult BALB/c mice (4-6 weeks old) were sacrificed by CO_2 asphyxiation. Bone marrow was flushed out from tibia and femur with chilled culture media (α-MEM supplemented with 10% FBS). After passing through 70µm cell strainer (SPL Labs), bone marrow cells were subjected to RBC lysis and centrifuged. Cells were resuspended in α-MEM supplemented with 10% FBS and plated in 90 mm dishes (CORNING Corporation).The detailed procedure has been followed as described before (Siddiqui JA, 2010; Bhattacharyya A, 2014; Ullah F, 2018).

After 1 day of incubation, the non-adherent cells (containing primarily hematopoietic cells) are removed, the adherent cells are washed twice with PBS and cultured up to a week in CO_2 incubator in α-MEM supplemented with 10% FBS. These cells are enriched in BM-MSCs, and proliferate rapidly. After 1-2 passages, sufficient cells were visually examined to be fibroblast-

like morphology and are obtained for experimentation. These cells, primarily represent BM-MSCs and are subsequently seeded on hydrogel-coated or uncoated coverslips or plates for functional studies.

5.2.3.15 Growing cells on hydrogel-coated surface:

The prepared drug-gel combination is applied to 18 mm coverslip, coating it evenly and subsequently left for air drying in aseptic conditions. Simultaneously the coverslips are UV-irradiated in 12 well culture plates. Mouse bone marrow-derived Mesenchymal stem cells are seeded in each well (approx. 1x 10^5 cells/well) over hydrogel-drug-coated coverslips and left to adhere for at least 24 hours. After a sufficient number of cells have adhered to the coverslips, old media was discarded and new media supplemented with L-Ascorbic Acid and beta-glycerophosphate is added. Fresh media is added in every 4 days keeping half amount of the old media in well. For ARS the experiment was continued for 15-21 days for mineralization.

5.2.3.16 Quantification of Reactive Oxygen Species (ROS):

Quantification of ROS generation was performed by microscopic analysis using intracellular oxidation of a cell-permeable dye, i.e. 2', 7'-dichlorodihydrofluorescein diacetate (H_2DCFDA) (INVITROGEN). The H_2DCFDA measures reactive oxygen species (ROS) activity within the cell. Approximately 10,000 bone marrow-derived Mesenchymal stem cell population was seeded on glass cover slips and on hydrogel-coated cover slips. Cells were incubated with 10μm H_2DCFDA at 37 °C for 20 min. In a similar manner 50 μm H_2O_2 (MERCK) treated cells were taken as a positive control. Subsequently the fluorescence signals of ROS were observed under confocal microscope (FV 3000). Images were processed in Image J software.

5.2.3.17 Mineralization assay:

Mineralization assay was performed by seeding the equal number of cells in 12-well plates and cultured in mineralization media for 21 days in presence or absence of TRPV4 and TRPM8 modulators. After 21 days, media was aspirated, cells were washed with PBS and equal amount of Alizarin Red-S (ARS 2%) dye was added to each well. After 30 minutes of incubation, the ARS dye was washed with water and micrographs were taken to qualitatively assess the extent of mineralization. The extent of mineralization was quantified by extracting ARS dye by 10% Cetyl Peridynium Chloride (CPC, MP Biomedicals) and spectrophotometric reading was taken at 595 nm as mentioned above.

5.2.3.18 Implantation of hydrogel in rat femur:

12 male rats (aged between 7-8 weeks and weight range between ~290-340g) were taken and divided randomly into three groups PBS (control) and TRPV4 agonist (4αPDD 50 nM) and antagonist (RN1734 100 nM) encapsulated hydrogel treated group. The animals were anesthetized by inhalation of 2-5% isoflurane method. The respective region ofoperation was shaved by electric trimmer and aseptically prepared for operation. For implantation of hydrogel in femur, a single hole in proximal femur was marked and then expanded into a round metaphyseal bone injury using a blunt electric drill bit. Further, bone debris was removed by washing the bone defect by sterile saline solution. Hydrogel discs containing TRPV4 agonist and antagonist were lyophilized, sliced into desired shape and then, subsequently sterilized by exposing to ultraviolet light for 30 minutes, and then the hydrogel disc was implanted into the bone injury site of the femur. After surgery, all animals were allowed to recover on a warm sheet and then transferred to their respective cages for post-operative care. To prevent potential infection, all animals received drinking water including trimethoprim-sulfamethoxazole for 7 days. After 8 weeks of hydrogel implantation, rats were

sacrificed by CO_2 asphyxiation. Hydrogel implanted femurs were collected and visuallymonitored for new bone formation and possible toxic effect of hydrogel surrounding the damaged tissue. Subsequently, the femur was fixed in 4% formaldehyde. For histopathological analysis collected bone samples were washed in running tap water overnight for removing fixative solution and decalcified in 10% EDTA solution for 4 weeks at room temperature, at every 4 day intervals, the decalcification agent was changed. After complete decalcification, samples were dehydrated in increasing concentrations of ethanol solution (50-100%), subsequently cleared by xylene solution and finally embedded in wax. Further, samples were sliced in 5μm thin sections by microtome and fixed on charged slide for further examination. For H&E (Hematoxylin & Eosin) and Masson's Trichome staining samples were deparaffinized in xylene solution and hydrated with graded series of ethanol solution and stained with H&E and Masson's Trichome staining as per products manual. Stained samples were observed under light microscope and images were taken for further analysis.

Animals used for this study were procured from National Centre for Animal Research and Experimentation (NCARE), NISER with approval of the Institution Animal Ethics Committee (IAEC) under (NISER/SBS/IAEC/AH-199). All methods performed were in accordance with the guidelines and regulations set by the IAEC.

5.2.3.19 Histopathological study of organs:

All the collected vital organs (Liver, Kidney and Spleen) of animals were fixed in 10% buffered formaldehyde solution for 7 days. After fixation, all the organs were dehydrated by using series of alcohol solutions and then kept into xylene solutions. These organs were then fixed in paraffin wax and sliced into thin sections by microtome. For histopathological analysis, thin sections of organs were stained by haematoxylin and eosin stain and their photographs were recorded by light microscopy equipped with digital camera.

5.2.3.20 Assessment of newly formed at defect site by SEM (Scanning Electron Microscopy):

TRPV4 agonist and antagonist encapsulated hydrogels were implanted in defect rat femur as per protocol described above. For SEM analysis, bone samples after 8 weeks of implantation were isolated and fixed in 4% PFA solution. Before SEM analysis all bone samples were washed in running tap water and dehydrated in graded series of ethanol (40-100%). After that desire area of bone samples was taken out by diamond saw and coated with platinum for better resolution. Images of defect area in SEM was acquired at accelerated voltage of 6 Kv and further processed by Image J software.

5.2.3.21 RAMAN Spectroscopic analysis:

Raman spectral measurement was performed using LabRAM HR Evol (HORIBA Scientific, France), fitted with a 532 nm laser (laser spot size ~150 microns). Before performing Raman measurements, all wavelength spectra were calibrated against the silicon wafer's wavelength dependency of a standard 520 cm-1 vibrational peak. 50X objective was used to focus the laser onto the defect site of the bone surface. An integration time of 15 seconds with 15 accumulation was fixed for spectral measurement over a spectral range of 200-2000 cm^{-1}. The Raman scattering from the sample surface was collected by TE cooled (-59 °C CCD camera (Sincerity OE Horiba). Raman spectra obtained from different samples were acquired and analyzed by Lab spec 6 software package.

5.2.3.22 Isolation and activation of murine Tcell:

Isolation and culturing of T cells were done as previously described (Acharya TK, 2021). Briefly, spleen was harvested from 4-6 weeks old male BALB/c mice as per the approval of Institutional Animal Ethics Committee (IAEC protocol no. NISER/SBS/IAEC/AH-245). Spleens were minced into smaller pieces and single cell suspension of spleenocytes was made by passing

through syringes and finally filtering using a 70-µm cell strainer. Out of the whole spleenocytes population, T cells were purified using the Dynabeads^{TM} Untouched Mouse T Cells Kit according to the manufacturer's guidelines. Isolated T cells were cultured in RPMI1640 (GIBCO) media supplemented with 10% FBS (GIBCO, Streptomycin (100µg/ml), and Penicillin (100U/ml) in humidity-controlled incubator maintained at 37 ^{o}C and 5% CO_2. T cell activation was carried out by using 'Dynabeads^{TM} Mouse T-Activator CD3/CD28 for TCell Expansion and Activation' as per the manufacturer's instructions. T cell activation was carried out for 12 hours by then activated T cell blasts were visible. The TCR-treated cells were incubated with TRPV4 and TRPM8 agonist and antagonist for 1 hour.

5.2.3.23. Live cell mitochondrial and cellular Ca^{2+}-imaging of T cells:

Live cell Ca^{2+}-imaging of T cells was performed as previously described (Sahoo SS, 2019). For intra-cellular Ca^{2+}-imaging, T cells were incubated with Ca^{2+}-sensitive dye Fluo-4-AM (1 µM for 30 minutes). For mitochondrial Ca^{2+}-imaging, T cells were labelled with Rhod-2-AM dye (5 µM for 1 hour) and subsequently, washed and kept for 1 hour at 37 °C to reduce its cellular signal. For chelation of extra-cellular Ca^{2+}, EGTA (5 µM) was used. Intracellular Ca^{2+}-chelation, or ER Ca^{2+}-depletion was done by using BAPTA-AM (5 mM) or Thapsigargin (1 µM) respectively. In each case, cells were pre-incubated with either EGTA, BAPTA-AM or Thapsigargin for 1 hour. Subsequently, live cell time series imaging was done for 400 frames (~7.5 mins) using confocal microscope (Olympus FV3000). TRPV4 and TRPM8 agonist were added at the 20th frame of imaging. ImageJ was used to analyze the images and fluorescence intensity of cells was quantified at different time points (at frame 1 and frame 400).

5.2.3.24 Basal cytosolic and mitochondrial Ca^{2+}-detection in T cell:

In order to evaluate the levels of cytosolic and mitochondrial Ca^{2+}, Fluo-4-AM and Rhod-2-AM dye was used in same cell respectively. Both resting and non-activated T cells were grown in 35mm glass bottom dish and labelled by Rhod-2-AM (5 μM) for 1 hour and then washed and kept for 1 hour at 37 °C to reduce its background signal. Cells were then treated with either 4αPDD, RN1734, WS12, Menthol and AMTB for 1 hour. Before completion of 1 hour, cells were loaded with Fluo-4-AM dye (1 μM) and Rhod-2-AM for 30 minutes. Cells were then washed to remove excess dye and taken for live cell confocal imaging.

5.3 Statistical tests and correlation analysis:

GraphPad Prism 8 was used for performing the statistical and correlational analysis. One-way ANOVA test with multiple comparison were done for comparing two or more experimental groups. Student's t test was performed for comparing two experimental conditions in case of calcium imaging. P-value less than 0.05 is considered statistically significant. **** represent p value ≤ 0.0001; *** represents p value <0.001; ** represents p value <0.01; * represents p value <0.05. For correlation analysis, mean of intensities of different experimental groups (each mean value is of >100 different cells) were plotted together and Pearson Co-efficient was evaluated to test the dependence of two parameters on each other.

Chapter 6

Bibliography

Abadir, P.M., Foster, D.B., Crow, M., Cooke, C.A., Rucker, J.J., Jain, A., Smith, B.J., Burks, T.N., Cohn, R.D., Fedarko, N.S. and Carey, R.M., 2011. Identification and characterization of a functional mitochondrial angiotensin system. *Proceedings of the National Academy of Sciences*, *108*, pp.14849-14854.

Acharya, T.K., Pal, S., Ghosh, A., Kumar, S., Kumar, S., Chattopadhyay, N., Goswami, C., 2023. TRPV4 regulates osteoblast differentiation and mitochondrial function that are relevant for channelopathy. *Frontiers in Cell and Developmental Biology. 11*, 1066788

Acharya, T.K., Kumar, A., Kumar, S. and Goswami, C., 2022a. TRPV4 interacts with MFN2 and facilitates endoplasmic reticulum-mitochondrial contact points for Ca^{2+}-buffering. *Life Sciences*, *310*, p.121112.

Acharya, T.K., Kumar, A., Majhi, R.K., Kumar, S., Chakraborty, R., Tiwari, A., Smalla, K.H., Liu, X., Chang, Y.T., Gundelfinger, E.D. and Goswami, C., 2022b. TRPV4 acts as a mitochondrial Ca^{2+}-importer and regulates mitochondrial temperature and metabolism. *Mitochondrion*, *67*, pp.38-58.

Acharya, T.K., Kumar, S., Tiwari, N., Ghosh, A., Tiwari, A., Pal, S., Majhi, R.K., Kumar, A., Das, R., Singh, A. and Maji, P.K., 2021. TRPM8 channel inhibitor-encapsulated hydrogel as a tunable surface for bone tissue engineering. *Scientific Reports*, *11*, pp.1-16.

Acharya, T.K., Sahu, R.P., Kumar, S., Rokade, T.P., Chakraborty, R., Dubey, N.K., Shikha, D., Chawla, S. and Goswami, C., 2022c. Function and regulation of thermosensitive ion channel TRPV4 in the immune system. *Current Topics in Membranes*, *89*, pp.155-188.

Acharya, T.K., Tiwari, A., Majhi, R.K. and Goswami, C., 2021. TRPM8 channel augments T-cell activation and proliferation. *Cell Biology International*, *45*, pp.198-210.

Adam-Vizi, V. and Starkov, A.A., 2010. Calcium and mitochondrial reactive oxygen species generation: how to read the facts. *Journal of Alzheimer's Disease*, *20*(s2), pp.S413-S426.

Akopian, A.N., Ruparel, N.B., Patwardhan, A. and Hargreaves, K.M., 2008. Cannabinoids desensitize Capsaicin and mustard oil responses in sensory neurons via TRPA1 activation. *Journal of Neuroscience*, *28*, pp.1064-1075.

Albishi, F.M., Albeshi, S.M., Alotaibi, K., Alhussain, N., Kamal, A., Sultan, A.A. and Aljishi, M.J., 2020. The Effect of Menthol on Anxiety and Related Behaviors in Mice. *Bahrain Medical Bulletin*, *42*(4). pp. 277-282.

Andre, E., Campi, B., Materazzi, S., Trevisani, M., Amadesi, S., Massi, D., Creminon, C., Vaksman, N., Nassini, R., Civelli, M. and Baraldi, P.G., 2008. Cigarette smoke–induced neurogenic inflammation is mediated by α, β-unsaturated aldehydes and the TRPA1 receptor in rodents. *The Journal of Clinical Investigation*, *118*, pp.2574-2582.

Aoyama-Ishiwatari, S. and Hirabayashi, Y., 2021. Endoplasmic Reticulum–Mitochondria Contact Sites—Emerging Intracellular Signaling Hubs. *Frontiers in Cell and Developmental Biology*, *9*. p.1040.

Arai, S., Lee, S.C., Zhai, D., Suzuki, M. and Chang, Y.T., 2014. A molecular fluorescent probe for targeted visualization of temperature at the endoplasmic reticulum. *Scientific Reports*, *4*, pp.1-6.

Arai, S., Suzuki, M., Park, S.J., Yoo, J.S., Wang, L., Kang, N.Y., Ha, H.H. and Chang, Y.T., 2015. Mitochondria-targeted fluorescent thermometer monitors intracellular temperature gradient. *Chemical Communications*, *51*(38), pp.8044-8047.

Aryaman, J., Johnston, I.G. and Jones, N.S., 2019. Mitochondrial heterogeneity. *Frontiers in Genetics*, *9*, p.718.

Asuthkar, S., Elustondo, P.A., Demirkhanyan, L., Sun, X., Baskaran, P., Velpula, K.K., Thyagarajan, B., Pavlov, E.V. and Zakharian, E., 2015. The TRPM8 protein is a testosterone receptor: I. Biochemical evidence for direct TRPM8-testosterone interactions. *Journal of Biological Chemistry*, *290*, pp.2659-2669.

Audano, M., Pedretti, S., Ligorio, S., Crestani, M., Caruso, D., De Fabiani, E. and Mitro, N., 2020. "The Loss of Golden Touch": Mitochondria-Organelle Interactions, Metabolism, and Cancer. *Cells*, *9*, p.2519.

Bai, V.U., Murthy, S., Chinnakannu, K., Muhletaler, F., Tejwani, S., Barrack, E.R., Kim, S.H., Menon, M. and Reddy, G., 2010. Androgen regulated TRPM8 expression: a potential mRNA marker for metastatic prostate cancer detection in body fluids. *International Journal of Oncology*, *36*, pp.443-450.

Bajpai, P., Koc, E., Sonpavde, G., Singh, R. and Singh, K.K., 2019. Mitochondrial localization, import, and mitochondrial function of the androgen receptor. *Journal of Biological Chemistry*, *294*, pp.6621-6634.

Bandell, M., Story, G.M., Hwang, S.W., Viswanath, V., Eid, S.R., Petrus, M.J., Earley, T.J. and Patapoutian, A., 2004. Noxious cold ion channel TRPA1 is activated by pungent compounds and bradykinin. *Neuron*, *41*, pp.849-857.

Bang, S., Kim, K.Y., Yoo, S., Lee, S.H. and Hwang, S.W., 2007. Transient receptor potential V2 expressed in sensory neurons is activated by probenecid. *Neuroscience Letters*, *425*, pp.120-125.

Baratchi, S., Keov, P., Darby, W.G., Lai, A., Khoshmanesh, K., Thurgood, P., Vahidi, P., Ejendal, K. and McIntyre, P., 2019. The TRPV4 agonist GSK1016790A regulates the membrane expression of TRPV4 channels. *Frontiers in Pharmacology*, *10*, p.6.

Baratchi, S., Knoerzer, M., Khoshmanesh, K., Mitchell, A. and McIntyre, P., 2017. Shear stress regulates TRPV4 channel clustering and translocation from adherens junctions to the basal membrane. *Scientific Reports*, *7*, pp.1-9.

Bautista, D.M., Movahed, P., Hinman, A., Axelsson, H.E., Sterner, O., Högestätt, E.D., Julius, D., Jordt, S.E. and Zygmunt, P.M., 2005. Pungent products from garlic activate the sensory ion channel TRPA1. *Proceedings of the National Academy of Sciences*, *102*, pp.12248-12252.

Bautista, D.M., Siemens, J., Glazer, J.M., Tsuruda, P.R., Basbaum, A.I., Stucky, C.L., Jordt, S.E. and Julius, D., 2007. The Menthol receptor TRPM8 is the principal detector of environmental cold. *Nature*, *448*, pp.204-208.

Beck, A., Kolisek, M., Bagley, L.A., Fleig, A., Penner, R., Beck, A., Kolisek, M., Bagley, L.A., Fleig, A. and Penner, R., 2006. Nicotinic acid adenine dinucleotide phosphate and cyclic ADP-ribose regulate TRPM2 channels in T lymphocytes. *The FASEB Journal*, *20*, pp.962-964.

Becker, D., Bereiter-Hahn, J. and Jendrach, M., 2009. Functional interaction of the cation channel transient receptor potential vanilloid 4 (TRPV4) and actin in volume regulation. *European Journal of Cell Biology*, *88*, pp.141-152.

Becker, D., Blase, C., Bereiter-Hahn, J. and Jendrach, M., 2005. TRPV4 exhibits a functional role in cell-volume regulation. *Journal of Cell Science*, *118*(11), pp.2435-2440.

Becker, D., Müller, M., Leuner, K. and Jendrach, M., 2008. The C-terminal domain of TRPV4 is essential for plasma membrane localization. *Molecular Membrane Biology*, *25*, pp.139-151.

Behrendt, H.J., Germann, T., Gillen, C., Hatt, H. and Jostock, R., 2004. Characterization of the mouse cold-Menthol receptor TRPM8 and vanilloid receptor type-1 VR1 using a fluorometric imaging plate reader (FLIPR) assay. *British Journal of Pharmacology*, *141*, pp.737-745.

Belikov, A.V., Schraven, B. and Simeoni, L., 2015. T cells and reactive oxygen species. *Journal of Biomedical Science*, *22*, pp.1-11.

Belvisi, M.G., Dubuis, E. and Birrell, M.A., 2011. Transient receptor potential A1 channels: insights into cough and airway inflammatory disease. *Chest*, *140*, pp.1040-1047.

Bénard, G., Massa, F., Puente, N., Lourenço, J., Bellocchio, L., Soria-Gómez, E., Matias, I., Delamarre, A., Metna-Laurent, M., Cannich, A. and Hebert-Chatelain, E., 2012. Mitochondrial CB1 receptors regulate neuronal energy metabolism. *Nature Neuroscience*, *15*, pp.558-564.

Berrout, J., Jin, M., Mamenko, M., Zaika, O., Pochynyuk, O. and O'Neil, R.G., 2012. Function of transient receptor potential cation channel subfamily V member 4 (TRPV4) as a mechanical transducer in flow-sensitive segments of renal collecting duct system. *Journal of Biological Chemistry*, *287*, pp.8782-8791.

Bezzerides, V.J., Ramsey, I.S., Kotecha, S., Greka, A. and Clapham, D.E., 2004. Rapid vesicular translocation and insertion of TRP channels. *Nature Cell Biology*, *6*, pp.709-720.

Bhattacharyya, A., Chattopadhyay, R., Mitra, S. and Crowe, S.E., 2014. Oxidative stress: an essential factor in the pathogenesis of gastrointestinal mucosal diseases. *Physiological Reviews*, *94*, pp.329-354.

Bidaux, G., Borowiec, A.S., Dubois, C., Delcourt, P., Schulz, C., Abeele, F.V., Lepage, G., Desruelles, E., Bokhobza, A., Dewailly, E. and Slomianny, C., 2016. Targeting of short TRPM8 isoforms induces 4TM-TRPM8-dependent apoptosis in prostate cancer cells. *Oncotarget*, *7*, p.29063.

Bidaux, G., Borowiec, A.S., Gordienko, D., Beck, B., Shapovalov, G.G., Lemonnier, L., Flourakis, M., Vandenberghe, M., Slomianny, C., Dewailly, E. and Delcourt, P., 2015. Epidermal TRPM8 channel isoform controls the balance between keratinocyte proliferation and differentiation in a cold-dependent manner. *Proceedings of the National Academy of Sciences*, *112*, pp.E3345-E3354.

Bidaux, G., Gordienko, D., Shapovalov, G., Farfariello, V., Borowiec, A.-S., Iamshanova, O., Lemonnier, L., Gueguinou, M., Guibon, R., Fromont, G., Paillard, M., Gouriou, Y., Chouabe, C., Dewailly, E., Gkika, D., L´opez-Alvarado, P., Carlos Men´endez, J., H´eliot, L., Slomianny, C., Prevarskaya, N., 2018. 4TM-TRPM8 channels are new gatekeepers of the ER-mitochondria Ca^{2+} transfer, *Biochimica et Biophysica Acta (BBA)-Molecular Cell Res*. 1865, 981–994

Bidaux, G., Roudbaraki, M., Merle, C., Crépin, A., Delcourt, P., Slomianny, C., Thébault, S., Bonnal, J.L., Benahmed, M., Cabon, F. and Mauroy, B., 2005. Evidence for specific TRPM8 expression in human prostate secretory epithelial cells: functional androgen receptor requirement. *Endocrine-Related Cancer*, *12*, pp.367-382.

Bird, T.D., 2008. Excerpt from Charcot–Marie–Tooth. Hereditary Neuropathy Overview. *CMT Facts*, *6*, pp.8-9.

Bisogno, T., Hanuš, L., De Petrocellis, L., Tchilibon, S., Ponde, D.E., Brandi, I., Moriello, A.S., Davis, J.B., Mechoulam, R. and Di Marzo, V., 2001. Molecular targets for cannabidiol and its synthetic analogues: effect on vanilloid VR1 receptors and on the cellular uptake and enzymatic hydrolysis of anandamide. *British Journal of Pharmacology*, *134*, pp.845-852.

Desai, B.N. and Clapham, D.E., 2005. TRP channels and mice deficient in TRP channels. *Pflügers Archiv*, *451*, pp.11-18.

Bjelakovic, G., Nikolova, D., Gluud, L.L., Simonetti, R.G. and Gluud, C., 2007. Mortality in randomized trials of antioxidant supplements for primary and secondary prevention: systematic review and meta-analysis. *Jama*, *297*, pp.842-857.

Bjelakovic, G., Nikolova, D., Simonetti, R.G. and Gluud, C., 2004. Antioxidant supplements for prevention of gastrointestinal cancers: a systematic review and meta-analysis. *The Lancet*, *364*, pp.1219-1228.

Boonrungsiman, S., Gentleman, E., Carzaniga, R., Evans, N.D., McComb, D.W., Porter, A.E. and Stevens, M.M., 2012. The role of intracellular calcium phosphate in osteoblast-mediated bone apatite formation. *Proceedings of the National Academy of Sciences*, *109*, pp.14170-14175.

Botte, M., Ulrich, A.K., Adaixo, R., Gnutt, D., Brockmann, A., Bucher, D., Chami, M., Bocquet, N., Ebbinghaus-Kintscher, U., Puetter, V. and Becker, A., 2020. Cryo-EM structural studies of the agonist complexed human TRPV4 ion-channel reveals novel structural rearrangements resulting in an open-conformation. *bioRxiv*. 2020.10.13.334797.

Boulay, G., Zhu, X., Peyton, M., Jiang, M., Hurst, R., Stefani, E. and Birnbaumer, L., 1997. Cloning and Expression of a Novel Mammalian Homolog of *Drosophila* Transient Receptor Potential (Trp) Involved in Calcium Entry Secondary to Activation of Receptors Coupled by the Gq Class of G Protein. *Journal of Biological Chemistry*, *272*, pp.29672-29680.

Brauchi, S., Krapivinsky, G., Krapivinsky, L. and Clapham, D.E., 2008. TRPM7 facilitates cholinergic vesicle fusion with the plasma membrane. *Proceedings of the National Academy of Sciences*, *105*, pp.8304-8308.

Bravo, R., Vicencio, J.M., Parra, V., Troncoso, R., Munoz, J.P., Bui, M., Quiroga, C., Rodriguez, A.E., Verdejo, H.E., Ferreira, J. and Iglewski, M., 2011. Increased ER–mitochondrial coupling promotes mitochondrial respiration and bioenergetics during early phases of ER stress. *Journal of Cell Science*, *124*, pp.2143-2152.

Brinkmeier, H., 2011. TRP channels in skeletal muscle: gene expression, function and implications for disease. *Transient Receptor Potential Channels*, *Advances in Experimental Medicine and Biology*, *Springer, Dordrecht*, 704, pp.749-758. (Book)

Brookes, P.S., Yoon, Y., Robotham, J.L., Anders, M.W. and Sheu, S.S., 2004. Calcium, ATP, and ROS: a mitochondrial love-hate triangle. *American Journal of Physiology-Cell Physiology*, *287*, pp.C817-C833.

Brooks, C.A., Barton, L.S., Behm, D.J., Brnardic, E.J., Costell, M.H., Holt, D.A., Jolivette, L.J., Matthews, J.M., McAtee, J.J., McCleland, B.W. and Patterson, J.R., 2019. Discovery of GSK3527497: A candidate for the inhibition of transient receptor potential vanilloid-4 (TRPV4). *Journal of Medicinal Chemistry*, *62*, pp.9270-9280.

Budd, S.L. and Nicholls, D.G., 1996. A reevaluation of the role of mitochondria in neuronal Ca^{2+} homeostasis. *Journal of Neurochemistry*, *66*, pp.403-411.

Cai, X. and Clapham, D.E., 2012. Ancestral Ca^{2+} signaling machinery in early animal and fungal evolution. *Molecular Biology and Evolution*, *29*, pp.91-100.

Carneiro, P., Vieira, R., Venâncio, C. and Félix, L., 2022. Oxidative stress as the trigger for Menthol-induced developmental alterations in zebrafish (*Danio rerio*) model. *Journal of Environmental Chemical Engineering*, *10*, p.108323.

Carson, J.A. and Manolagas, S.C., 2015. Effects of sex steroids on bones and muscles: Similarities, parallels, and putative interactions in health and disease. *Bone*, *80*, pp.67-78.

Case, A.J., McGill, J.L., Tygrett, L.T., Shirasawa, T., Spitz, D.R., Waldschmidt, T.J., Legge, K.L. and Domann, F.E., 2011. Elevated mitochondrial superoxide disrupts normal T cell development, impairing adaptive immune responses to an influenza challenge. *Free Radical Biology and Medicine*, *50*, pp.448-458.

Caterina, M.J., Rosen, T.A., Tominaga, M., Brake, A.J. and Julius, D., 1999. A Capsaicin-receptor homologue with a high threshold for noxious heat. *Nature*, *398*, pp.436-441.

Caterina, M.J., Schumacher, M.A., Tominaga, M., Rosen, T.A., Levine, J.D. and Julius, D., 1997. The Capsaicin receptor: a heat-activated ion channel in the pain pathway. *Nature*, *389*, pp.816-824

Chakraborty, R., Acharya, T.K., Tiwari, N., Majhi, R.K., Kumar, S., Goswami, L. and Goswami, C., 2022. Hydrogel-Mediated Release of TRPV1 Modulators to Fine Tune Osteoclastogenesis. *ACS Omega*, *7*(11), pp.9537-9550.

Chalmers, S. and McCarron, J.G., 2008. The mitochondrial membrane potential and Ca^{2+} oscillations in smooth muscle. *Journal of Cell Science*, *121*, pp.75-85.

Chen, X., Wang, Z., Duan, N., Zhu, G., Schwarz, E.M. and Xie, C., 2018. Osteoblast–osteoclast interactions. *Connective Tissue Research*, *59*, pp.99-107.

Chidawanyika, T., Chakrabarti, R., Beauchemin, K.S., Higgs, H.N. and Supattapone, S., 2021. SEC24A facilitates colocalization and Ca^{2+} flux between the endoplasmic reticulum and mitochondria. *Journal of Cell Science*, *134*, p.jcs249276.

Choudhury, P., Kumar, S., Singh, A., Kumar, A., Kaur, N., Sanyasi, S., Chawla, S., Goswami, C. and Goswami, L., 2018. Hydroxyethyl methacrylate grafted carboxy methyl tamarind (CMT-g-HEMA) polysaccharide based matrix as a suitable scaffold for skin tissue engineering. *Carbohydrate Polymers*, *189*, pp.87-98.

Chretien, D., Bénit, P., Ha, H.H., Keipert, S., El-Khoury, R., Chang, Y.T., Jastroch, M., Jacobs, H.T., Rustin, P. and Rak, M., 2018. Mitochondria are physiologically maintained at close to 50 C. *PLoS Biology*, *16*, p.e2003992.

Chrétien, D., Bénit, P., Leroy, C., El-Khoury, R., Park, S., Lee, J.Y., Chang, Y.T., Lenaers, G., Rustin, P. and Rak, M., 2020. Pitfalls in monitoring mitochondrial temperature using charged thermosensitive fluorophores. *Chemosensors*, *8*, p.124.

Chung, M.K., Lee, H. and Caterina, M.J., 2003. Warm temperatures activate TRPV4 in mouse 308 keratinocytes. *Journal of Biological Chemistry*, *278*, pp.32037-32046.

Clapham, D.E., 2003. TRP channels as cellular sensors. *Nature*, *426*, pp.517-524.

Clapham, D.E., Runnels, L.W. and Strübing, C., 2001. The TRP ion channel family. *Nature Reviews Neuroscience*, *2*, pp.387-396.

Colburn, R.W., Lubin, M.L., Stone Jr, D.J., Wang, Y., Lawrence, D., D'Andrea, M.R., Brandt, M.R., Liu, Y., Flores, C.M. and Qin, N., 2007. Attenuated cold sensitivity in TRPM8 null mice. *Neuron*, *54*, pp.379-386.

Collins, T.J., Berridge, M.J., Lipp, P. and Bootman, M.D., 2002. Mitochondria are morphologically and functionally heterogeneous within cells. *The EMBO Journal*, *21*, pp.1616-1627.

Collins, T.J., Lipp, P., Berridge, M.J., Li, W. and Bootman, M.D., 2000. Inositol 1, 4, 5-trisphosphate-induced Ca^{2+} release is inhibited by mitochondrial depolarization. *Biochemical Journal*, *347*, pp.593-600.

Contreras, L., Drago, I., Zampese, E. and Pozzan, T., 2010. Mitochondria: the calcium connection. *Biochimica et Biophysica Acta (BBA)-Bioenergetics*, *1797*, pp.607-618.

Corrado, M., Edwards-Hicks, J., Villa, M., Flachsmann, L.J., Sanin, D.E., Jacobs, M., Baixauli, F., Stanczak, M., Anderson, E., Azuma, M. and Quintana, A., 2020. Dynamic cardiolipin synthesis is required for CD8+ T cell immunity. *Cell Metabolism*, *32*, pp.981-995.

Cosens, D.J. and Manning, A., 1969. Abnormal electroretinogram from a Drosophila mutant. *Nature*, *224*, pp.285-287.

Dagda, R.K., Cherra, S.J., Kulich, S.M., Tandon, A., Park, D. and Chu, C.T., 2009. Loss of PINK1 function promotes mitophagy through effects on oxidative stress and mitochondrial fission. *Journal of Biological Chemistry*, *284*, pp.13843-13855.

Dai, Y., 2016, May. TRPs and pain. In *Seminars in Immunopathology* (Vol. 38, No. 3, pp. 277-291). Springer Berlin Heidelberg. (Book)

Dang, M., Saunders, L., Niu, X., Fan, Y. and Ma, P.X., 2018. Biomimetic delivery of signals for bone tissue engineering. *Bone Research*, *6*, pp.1-12.

Das, R. and Goswami, C., 2019. TRPV4 expresses in bone cell lineages and TRPV4-R616Q mutant causing Brachyolmia in human reveals “loss-of-interaction” with cholesterol. *Biochemical and Biophysical Research Communications*, *517*, pp.566-574.

Das, R. and Goswami, C., 2022. Role of TRPV4 in skeletal function and its mutant-mediated skeletal disorders. *Current Topics in Membranes*, *89*, pp.221-246.

Das, R., Kumar, A., Dalai, R. and Goswami, C., 2022. Cytochrome C interacts with the pathogenic mutational hotspot region of TRPV4 and forms complexes that differ in mutation and metal ion-sensitive manner. *Biochemical and Biophysical Research Communications*, *611*, pp.172-178.

Dash, R.K. and Beard, D.A., 2008. Analysis of cardiac mitochondrial Na^+–Ca^{2+} exchanger kinetics with a biophysical model of mitochondrial Ca^{2+} handing suggests a 3: 1 stoichiometry. *The Journal of Physiology*, *586*, pp.3267-3285.

David, G. and Barrett, E.F., 2000. Stimulation-evoked increases in cytosolic [Ca^{2+}] in mouse motor nerve terminals are limited by mitochondrial uptake and are temperature-dependent. *Journal of Neuroscience*, *20*, pp.7290-7296.

De Brito, O.M. and Scorrano, L., 2008. Mitofusin 2 tethers endoplasmic reticulum to mitochondria. *Nature*, *456*, pp.605-610.

De Jong, P.R., Takahashi, N., Peiris, M., Bertin, S., Lee, J., Gareau, M.G., Paniagua, A., Harris, A.R., Herdman, D.S., Corr, M. and Blackshaw, L.A., 2015. TRPM8 on mucosal sensory nerves regulates colitogenic responses by innate immune cells via CGRP. *Mucosal Immunology*, *8*, pp.491-504.

De Logu, F., Patacchini, R., Fontana, G. and Geppetti, P., 2016, May. TRP functions in the broncho-pulmonary system. *Seminars in Immunopathology* (Vol. 38, No. 3, pp. 321-329). Springer Berlin Heidelberg. (Book)

Demonacos, C., Djordjevic-Markovic, R., Tsawdaroglou, N. and Sekeris, C.E., 1995. The mitochondrion as a primary site of action of glucocorticoids: the interaction of the glucocorticoid receptor with mitochondrial DNA sequences showing partial similarity to the nuclear glucocorticoid responsive elements. *The Journal of Steroid Biochemistry and Molecular Biology*, *55*, pp.43-55.

Deng, Z., Paknejad, N., Maksaev, G., Sala-Rabanal, M., Nichols, C.G., Hite, R.K. and Yuan, P., 2018. Cryo-EM and X-ray structures of TRPV4 reveal insight into ion permeation and gating mechanisms. *Nature Structural & Molecular Biology*, *25*, pp.252-260.

Denis, V. and Cyert, M.S., 2002. Internal Ca^{2+} release in yeast is triggered by hypertonic shock and mediated by a TRP channel homologue. *The Journal of Cell Biology*, *156*, pp.29-34.

Depaoli, M.R., Hay, J.C., Graier, W.F. and Malli, R., 2019. The enigmatic ATP supply of the endoplasmic reticulum. *Biological Reviews*, *94*, pp.610-628.

Desdín-Micó, G., Soto-Heredero, G. and Mittelbrunn, M., 2018. Mitochondrial activity in T cells. *Mitochondrion*, *41*, pp.51-57.

Deus, C.M., Yambire, K.F., Oliveira, P.J. and Raimundo, N., 2020. Mitochondria–lysosome crosstalk: from physiology to neurodegeneration. *Trends in Molecular Medicine*, *26*, pp.71-88.

Dhaka, A., Murray, A.N., Mathur, J., Earley, T.J., Petrus, M.J. and Patapoutian, A., 2007. TRPM8 is required for cold sensation in mice. *Neuron*, *54*, pp.371-378.

Diogo, C.V., Yambire, K.F., Mosquera, L.F., Branco, T. and Raimundo, N., 2018. Mitochondrial adventures at the organelle society. *Biochemical and Biophysical Research Communications*, *500*, pp.87-93.

Diver, M.M., Cheng, Y. and Julius, D., 2019. Structural insights into TRPM8 inhibition and desensitization. *Science*, *365*, pp.1434-1440.

Dong, X.P., Cheng, X., Mills, E., Delling, M., Wang, F., Kurz, T. and Xu, H., 2008. The type IV mucolipidosis-associated protein TRPML1 is an endolysosomal iron release channel. *Nature*, *455*, pp.992-996.

Dong, X.P., Wang, X. and Xu, H., 2010. TRP channels of intracellular membranes. *Journal of Neurochemistry*, *113*, pp.313-328.

Dou, R., Cai, X., Ruan, L., Zhang, J., Rouzi, A., Chen, J., Chai, Z. and Hu, Y., 2022. Precision nanomedicines: Targeting hot mitochondria in cancer cells. *ACS Applied Bio Materials*, *5*, pp.4103-4117.

Duchen, M.R., 1999. Contributions of mitochondria to animal physiology: from homeostatic sensor to calcium signalling and cell death. *The Journal of Physiology*, *516*, pp.1-17.

Dudek, J., 2017. Role of cardiolipin in mitochondrial signaling pathways. *Frontiers in Cell and Developmental Biology*, *5*, p.90.

Dussor, G. and Cao, Y.Q., 2016. TRPM8 and migraine. *Headache: The Journal of Head and Face Pain*, *56*, pp.1406-1417.

El-Gammal, Z., Nasr, M.A., Elmehrath, A.O., Salah, R.A., Saad, S.M. and El-Badri, N., 2022. Regulation of mitochondrial temperature in health and disease. *Pflügers Archiv*, 474: 1043-1051

Elokely, K., Velisetty, P., Delemotte, L., Palovcak, E., Klein, M.L., Rohacs, T. and Carnevale, V., 2016. Understanding TRPV1 activation by ligands: Insights from the binding modes of Capsaicin and resiniferatoxin. *Proceedings of the National Academy of Sciences*, *113*, pp.E137-E145.

Everaerts, W., Nilius, B. and Owsianik, G., 2010. The vanilloid transient receptor potential channel TRPV4: from structure to disease. *Progress in Biophysics and Molecular Biology*, *103*, pp.2-17.

Fahimi, P., Nasr, M.A., Castanedo, L.M., Cheng, Y., Toussi, C.A. and Matta, C.F., 2020. A note on the consequences of a hot mitochondrion: Some recent developments and open questions. *Biophys. Bull.*, *43*, pp.14-21.

Fan, M., Zhang, J., Tsai, C.W., Orlando, B.J., Rodriguez, M., Xu, Y., Liao, M., Tsai, M.F. and Feng, L., 2020. Structure and mechanism of the mitochondrial Ca^{2+} uniporter holocomplex. *Nature*, *582*, pp.129-133.

Feng, S., Li, H., Tai, Y., Huang, J., Su, Y., Abramowitz, J., Zhu, M.X., Birnbaumer, L. and Wang, Y., 2013. Canonical transient receptor potential 3 channels regulate mitochondrial calcium uptake. *Proceedings of the National Academy of Sciences*, *110*, pp.11011-11016.

Fernández-Peña, C. and Viana, F., 2013. Targeting TRPM8 for pain relief. *The Open Pain Journal*, *6* (Supplementary 1). pp. 154-164

Filadi, R., Pendin, D. and Pizzo, P., 2018. Mitofusin 2: from functions to disease. *Cell Death & Disease*, *9*, pp.1-13.

Filosa, J.A., Yao, X. and Rath, G., 2013. TRPV4 and the regulation of vascular tone. *Journal of Cardiovascular Pharmacology*, *61*, p.113.

Finkel, T., Menazza, S., Holmström, K.M., Parks, R.J., Liu, J., Sun, J., Liu, J., Pan, X. and Murphy, E., 2015. The ins and outs of mitochondrial calcium. *Circulation Research*, *116*, pp.1810-1819.

Flatters, S.J., 2015. The contribution of mitochondria to sensory processing and pain. *Progress in Molecular Biology and Translational Science*, *131*, pp.119-146.

Fonfria, E., Murdock, P.R., Cusdin, F.S., Benham, C.D., Kelsell, R.E. and McNulty, S., 2006. Tissue distribution profiles of the human TRPM cation channel family. *Journal of Receptors and Signal Transduction*, *26*, pp.159-178.

Fujiu, K., Nakayama, Y., Iida, H., Sokabe, M. and Yoshimura, K., 2011. Mechanoreception in motile flagella of Chlamydomonas. *Nature Cell Biology*, *13*, pp.630-632.

Gallego-Sandín, S., Rodríguez-García, A., Alonso, M.T. and García-Sancho, J., 2009. The endoplasmic reticulum of dorsal root ganglion neurons contains functional TRPV1 channels. *Journal of Biological Chemistry*, *284*, pp.32591-32601

Gambini, E., Martinelli, I., Stadiotti, I., Vinci, M.C., Scopece, A., Eramo, L., Sommariva, E., Resta, J., Benaouadi, S., Cogliati, E. and Paolin, A., 2020. Differences in mitochondrial membrane potential identify distinct populations of human cardiac mesenchymal progenitor cells. *International Journal of Molecular Sciences*, *21*, p.7467.

Gao, J., Feng, Z., Wang, X., Zeng, M., Liu, J., Han, S., Xu, J., Chen, L., Cao, K., Long, J. and Li, Z., 2018. SIRT3/SOD2 maintains osteoblast differentiation and bone formation by regulating mitochondrial stress. *Cell Death & Differentiation*, *25*, pp.229-240.

Gasperini, R.J., Hou, X., Parkington, H., Coleman, H., Klaver, D.W., Vincent, A.J., Foa, L.C. and Small, D.H., 2011. TRPM8 and Nav1. 8 sodium channels are required for transthyretin-induced calcium influx in growth cones of small-diameter TrkA-positive sensory neurons. *Molecular Neurodegeneration*, *6*, pp.1-12.

Gaudet, R., 2006. Structural Insights into the Function of TRP Channels. *TRP Ion Channel Function in Sensory Transduction and Cellular Signaling Cascades*, (Taylor and Francis, Book) pp. 349-360.

Georgiadou, E. and Rutter, G.A., 2020. Control by Ca^{2+} of mitochondrial structure and function in pancreatic β-cells. *Cell Calcium*, *91*, p.102282.

Gevaert, T., Vriens, J., Segal, A., Everaerts, W., Roskams, T., Talavera, K., Owsianik, G., Liedtke, W., Daelemans, D., Dewachter, I. and Van Leuven, F., 2007. Deletion of the transient receptor potential cation channel TRPV4 impairs murine bladder voiding. *The Journal of Clinical Investigation*, *117*, pp.3453-3462.

Ghosh, A., Kaur, N., Kumar, A. and Goswami, C., 2016. Why individual thermo sensation and pain perception varies? Clue of disruptive mutations in TRPVs from 2504 human genome data. *Channels*, *10*, pp.339-345.

Ghosh, S., Basu Ball, W., Madaris, T.R., Srikantan, S., Madesh, M., Mootha, V.K. and Gohil, V.M., 2020. An essential role for cardiolipin in the stability and function of the mitochondrial calcium uniporter. *Proceedings of the National Academy of Sciences*, *117*, pp.16383-16390.

Giannoudis, P.V. and Einhorn, T.A., 2009. Bone morphogenetic proteins in musculoskeletal medicine. *Injury*, *40*, pp.S1-S3.

Giorgi, C., Marchi, S. and Pinton, P., 2018. The machineries, regulation and cellular functions of mitochondrial calcium. *Nature Reviews Molecular Cell Biology*, *19*, pp.713-730.

Giorgi, C., Marchi, S., Simoes, I.C., Ren, Z., Morciano, G., Perrone, M., Patalas-Krawczyk, P., Borchard, S., Jędrak, P., Pierzynowska, K. and Szymański, J., 2018. Mitochondria and reactive oxygen species in aging and age-related diseases. *International Review of Cell and Molecular Biology*, *340*, pp.209-344.

González-Muñiz, R., Bonache, M.A., Martín-Escura, C. and Gómez-Monterrey, I., 2019. Recent progress in TRPM8 modulation: an update. *International Journal of Molecular Sciences*, *20*, p.2618.

Görlach, A., Bertram, K., Hudecova, S. and Krizanova, O., 2015. Calcium and ROS: A mutual interplay. *Redox Biology*, *6*, pp.260-271.

Goswami, C., Kuhn, J., Heppenstall, P.A. and Hucho, T., 2010. Importance of non-selective cation channel TRPV4 interaction with cytoskeleton and their reciprocal regulations in cultured cells. *PloS One*, *5*, p.e11654.

Gottlieb, P., Suchyna, T.M., Bowman, C.L. and Sachs, F., 2006. The mechanosensitive TRPC1 ion channel activity is modulated by cytoskeleton and inhibited by the peptide GsMTx4. *Biophys. J*, *90*, p.1545.

Griparic, L., Van Der Wel, N.N., Orozco, I.J., Peters, P.J. and Van Der Bliek, A.M., 2004. Loss of the intermembrane space protein Mgm1/OPA1 induces swelling and localized constrictions along the lengths of mitochondria. *Journal of Biological Chemistry*, *279*, pp.18792-18798.

Grolez, G.P., Hammadi, M., Barras, A., Gordienko, D., Slomianny, C., Völkel, P., Angrand, P.O., Pinault, M., Guimaraes, C., Potier-Cartereau, M. and Prevarskaya, N., 2019. Encapsulation of a TRPM8 agonist, WS12, in lipid nanocapsules potentiates PC3 prostate cancer cell migration inhibition through channel activation. *Scientific Reports*, *9*, pp.1-15.

Gualdani, R., Seghers, F., Yerna, X., Schakman, O., Tajeddine, N., Achouri, Y., Tissir, F., Devuyst, O. and Gailly, P., 2020. Mechanical activation of TRPV4 channels controls albumin reabsorption by proximal tubule cells. *Science Signaling*, *13*, p.eabc6967.

Güler, A., Lee, H., Shimizu, I. and Caterina, M.J., 2002. Heat-evoked activation of TRPV4 (VR-OAC). *J Neurosci*, *22*, pp.6408-6414.

Gunter, K.K., Zuscik, M.J. and Gunter, T.E., 1991. The Na (+)-independent Ca^{2+} efflux mechanism of liver mitochondria is not a passive $Ca^{2+}/2H^{+}$ exchanger. *Journal of Biological Chemistry*, *266*, pp.21640-21648.

Guo, B.L., Sui, B.D., Wang, X.Y., Wei, Y.Y., Huang, J., Chen, J., Wu, S.X., Li, Y.Q., Wang, Y.Y. and Yang, Y.L., 2013. Significant changes in mitochondrial distribution in different pain models of mice. *Mitochondrion*, *13*, pp.292-297.

Ha, H., Kwak, H.B., Lee, S.W., Jin, H.M., Kim, H.M., Kim, H.H. and Lee, Z.H., 2004. Reactive oxygen species mediate RANK signaling in osteoclasts. *Experimental Cell Research*, *301*, pp.119-127.

Hamano, K.I., Kawanishi, T., Mizuno, A., Suzuki, M. and Takagi, Y., 2016. Involvement of Transient Receptor Potential Vanilloid (TRPV) 4 in mouse sperm thermotaxis. *Journal of Reproduction and Development*, *62*, pp.415-422.

Han, Y., Li, M., Qiu, F., Zhang, M. and Zhang, Y.H., 2017. Cell-permeable organic fluorescent probes for live-cell long-term super-resolution imaging reveal lysosome-mitochondrion interactions. *Nature Communications*, *8*, pp.1-9.

Harteneck, C. and Gollasch, M., 2011. Pharmacological modulation of diacylglycerol-sensitive TRPC3/6/7 channels. *Current Pharmaceutical Biotechnology, 12*, pp.35-41.

Harteneck, C., Klose, C. and Krautwurst, D., 2011. Synthetic modulators of TRP channel activity. *Transient Receptor Potential Channels*, *Advances in Experimental Medicine and Biology*, Springer, Dordrecht.704. pp. 87-106.

Haustrate, A., Prevarskaya, N. and Lehen'kyi, V.Y., 2020. Role of the TRPV channels in the endoplasmic reticulum calcium homeostasis. *Cells*, *9*, p.317.

Hayashi, T., Rizzuto, R., Hajnoczky, G. and Su, T.P., 2009. MAM: more than just a housekeeper. *Trends in Cell Biology, 19*, pp.81-88.

He, C., Xiao, G., Jin, X., Sun, C. and Ma, P.X., 2010. Electrodeposition on nanofibrous polymer scaffolds: rapid mineralization, tunable calcium phosphate composition and topography. *Advanced Functional Materials*, *20*, pp.3568-3576.

Henao, J.C., Grismaldo, A., Barreto, A., Rodríguez-Pardo, V.M., Mejía-Cruz, C.C., Leal-Garcia, E., Pérez-Núñez, R., Rojas, P., Latorre, R., Carvacho, I. and Torres, Y.P., 2021. TRPM8 Channel Promotes the Osteogenic Differentiation in Human Bone Marrow Mesenchymal Stem Cells. *Frontiers in Cell and Developmental Biology*, *9*, p.592946.

Himmel, N.J. and Cox, D.N., 2020. Transient receptor potential channels: current perspectives on evolution, structure, function and nomenclature. *Proceedings of the Royal Society B*, *287*, p.20201309.

Hofmann, T., Schaefer, M., Schultz, G. and Gudermann, T., 2002. Subunit composition of mammalian transient receptor potential channels in living cells. *Proceedings of the National Academy of Sciences*, *99*, pp.7461-7466.

Hom, J., Yu, T., Yoon, Y., Porter, G. and Sheu, S.S., 2010. Regulation of mitochondrial fission by intracellular Ca^{2+} in rat ventricular myocytes. *Biochimica et Biophysica Acta (BBA)-Bioenergetics*, *1797*, pp.913-921.

Hom, J.R., Gewandter, J.S., Michael, L., Sheu, S.S. and Yoon, Y., 2007. Thapsigargin induces biphasic fragmentation of mitochondria through calcium-mediated mitochondrial fission and apoptosis. *Journal of Cellular Physiology*, *212*, pp.498-508.

Hoppe, U.C., 2010. Mitochondrial calcium channels. *FEBS Letters*, *584*, pp.1975-1981.

https://www.nobelprize.org/uploads/2021/10/press-medicineprize2021.pdf

Hu, F., Zhao, Y., Hui, Z., Xing, F., Yang, J., Lee, I., Zhang, X., Pan, L. and Xu, J., 2019. Regulation of intracellular Ca^{2+}/CaMKII signaling by TRPV4 membrane translocation during osteoblastic differentiation. *Biophysics Reports*, *5*, pp.254-263.

Huffer, K.E., Aleksandrova, A.A., Jara-Oseguera, A., Forrest, L.R. and Swartz, K.J., 2020. Global alignment and assessment of TRP channel transmembrane domain structures to explore functional mechanisms. *Elife*, *9*, p.e58660.

Hurt, C.M., Lu, Y., M. Stary, C., Piplani, H., Small, B.A., Urban, T.J., Qvit, N., Gross, G.J., Mochly-Rosen, D. and Gross, E.R., 2016. Transient receptor potential vanilloid 1 regulates mitochondrial membrane potential and myocardial reperfusion injury. *Journal of the American Heart Association*, *5*, p.e003774.

Hüser, J., Blatter, L.A. and Sheu, S.S., 2000. Mitochondrial calcium in heart cells: beat-to-beat oscillations or slow integration of cytosolic transients?. *Journal of Bioenergetics and Biomembranes*, *32*, pp.27-33.

Hwang, M.S., Schwall, C.T., Pazarentzos, E., Datler, C., Alder, N.N. and Grimm, S., 2014. Mitochondrial Ca^{2+} influx targets cardiolipin to disintegrate respiratory chain complex II for cell death induction. *Cell Death & Differentiation*, *21*, pp.1733-1745.

Inada, H., Procko, E., Sotomayor, M. and Gaudet, R., 2012. Structural and biochemical consequences of disease-causing mutations in the ankyrin repeat domain of the human TRPV4 channel. *Biochemistry*, *51*, pp.6195-6206.

Iwasaki, Y., Morita, A., Iwasawa, T., Kobata, K., Sekiwa, Y., Morimitsu, Y., Kubota, K. and Watanabe, T., 2006. A nonpungent component of steamed ginger—[10]-shogaol—increases adrenaline secretion via the activation of TRPV1. *Nutritional Neuroscience*, *9*, pp.169-178.

Jaiswal, A., Hoerth, C.H., Zúñiga Pereira, A.M. and Lorenz, H., 2019. Improved spatial resolution by induced live cell and organelle swelling in hypotonic solutions. *Scientific Reports*, *9*, pp.1-13.

Janas, S., Seghers, F., Schakman, O., Alsady, M., Deen, P., Vriens, J., Tissir, F., Nilius, B., Loffing, J., Gailly, P. and Devuyst, O., 2016. TRPV4 is associated with central rather than nephrogenic osmoregulation. *Pflügers Archiv-European Journal of Physiology*, *468*, pp.1595-1607.

Janssen, D.A., Hoenderop, J.G., Jansen, K.C., Kemp, A.W., Heesakkers, J.P. and Schalken, J.A., 2011. The mechanoreceptor TRPV4 is localized in adherence junctions of the human bladder urothelium: a morphological study. *The Journal of Urology*, *186*, pp.1121-1127.

Jarzab, A., Kurzawa, N., Hopf, T., Moerch, M., Zecha, J., Leijten, N., Bian, Y., Musiol, E., Maschberger, M., Stoehr, G. and Becher, I., 2020. Meltome atlas—thermal proteome stability across the tree of life. *Nature Methods*, *17*, pp.495-503.

Jia, Y., McLeod, R.L., Wang, X., Parra, L.E., Egan, R.W. and Hey, J.A., 2002. Anandamide induces cough in conscious guinea-pigs through VR1 receptors. *British Journal of Pharmacology*, *137*, pp.831-836.

Johnston, I.A., Guderley, H., Franklin, C.E., Crockford, T. and Kamunde, C., 1994. Are mitochondria subject to evolutionary temperature adaptation?. *The Journal of Experimental Biology*, *195*, pp.293-306.

Jordt, S.E., Bautista, D.M., Chuang, H.H., McKemy, D.D., Zygmunt, P.M., Högestätt, E.D., Meng, I.D. and Julius, D., 2004. Mustard oils and cannabinoids excite sensory nerve fibres through the TRP channel ANKTM1. *Nature*, *427*, pp.260-265.

Jouaville, L.S., Ichas, F., Holmuhamedov, E.L., Camacho, P. and Lechleiter, J.D., 1995. Synchronization of calcium waves by mitochondrial substrates in Xenopus laevis oocytes. *Nature*, *377*, pp.438-441.

Jouaville, L.S., Pinton, P., Bastianutto, C., Rutter, G.A. and Rizzuto, R., 1999. Regulation of mitochondrial ATP synthesis by calcium: evidence for a long-term metabolic priming. *Proceedings of the National Academy of Sciences*, *96*, pp.13807-13812.

Jung, D.W., Baysal, K. and Brierley, G.P., 1995. The Sodium-Calcium Antiport of Heart Mitochondria Is Not Electroneutral (∗). *Journal of Biological Chemistry*, *270*, pp.672-678.

Kang, J.S., 2018. Theoretical model and characteristics of mitochondrial thermogenesis. *Biophysics Reports*, *4*, pp.63-67.

Kang, S.H., Carl, A., McHugh, J.M., Goff, H.R. and Kenyon, J.L., 2008. Roles of mitochondria and temperature in the control of intracellular calcium in adult rat sensory neurons. *Cell Calcium*, *43*, pp.388-404.

Kanki, H., Kinoshita, M., Akaike, A., Satoh, M., Mori, Y. and Kaneko, S., 2001. Activation of inositol 1, 4, 5-trisphosphate receptor is essential for the opening of mouse TRP5 channels. *Molecular Pharmacology*, *60*, pp.989-998.

Karbowski, M., Arnoult, D., Chen, H., Chan, D.C., Smith, C.L. and Youle, R.J., 2004. Quantitation of mitochondrial dynamics by photolabeling of individual organelles shows that mitochondrial fusion is blocked during the Bax activation phase of apoptosis. *The Journal of Cell Biology*, *164*, pp.493-499.

Khajavi, N., Mergler, S. and Biebermann, H., 2017. 3-Iodothyronamine, a novel endogenous modulator of transient receptor potential melastatin 8. *Frontiers in Endocrinology*, *8*, p.198.

Khalil, M., Babes, A., Lakra, R., Försch, S., Reeh, P.W., Wirtz, S., Becker, C., Neurath, M.F. and Engel, M.A., 2016. Transient receptor potential melastatin 8 ion channel in macrophages modulates colitis through a balance-shift in TNF-alpha and interleukin-10 production. *Mucosal Immunology*, *9*, pp.1500-1513.

Khan, S.N., Cammisa Jr, F.P., Sandhu, H.S., Diwan, A.D., Girardi, F.P. and Lane, J.M., 2005. The biology of bone grafting. *JAAOS-Journal of the American Academy of Orthopaedic Surgeons*, *13*, pp.77-86.

Khare, P., Chauhan, A., Kumar, V., Kaur, J., Mahajan, N., Kumar, V., Gesing, A., Chopra, K., Kondepudi, K.K. and Bishnoi, M., 2019. Bioavailable Menthol (Transient Receptor Potential Melastatin-8 agonist) induces energy expending phenotype in differentiating adipocytes. *Cells*, *8*, p.383.

Kim, H.Y., Wang, J., Lu, Y., Chung, J.M. and Chung, K., 2009. Superoxide signaling in pain is independent of nitric oxide signaling. *Neuroreport*, *20*, pp.1424-1428.

Kim, S.H., Nam, J.H., Park, E.J., Kim, B.J., Kim, S.J., So, I. and Jeon, J.H., 2009. Menthol regulates TRPM8-independent processes in PC-3 prostate cancer cells. *Biochimica et Biophysica Acta (BBA)-Molecular Basis of Disease*, *1792*, pp.33-38.

King, C., Sengupta, P., Seo, A.Y. and Lippincott-Schwartz, J., 2020. ER membranes exhibit phase behavior at sites of organelle contact. *Proceedings of the National Academy of Sciences*, *117*, pp.7225-7235.

Kiselyov, K., Chen, J., Rbaibi, Y., Oberdick, D., Tjon-Kon-Sang, S., Shcheynikov, N., Muallem, S. and Soyombo, A., 2005. TRP-ML1 is a lysosomal monovalent cation channel that undergoes proteolytic cleavage. *Journal of Biological Chemistry*, *280*, pp.43218-43223.

Kitaguchi, T. and Swartz, K.J., 2005. An inhibitor of TRPV1 channels isolated from funnel Web spider venom. *Biochemistry*, *44*, pp.15544-15549.

Klinge, C.M., 2017. Estrogens regulate life and death in mitochondria. *Journal of Bioenergetics and Biomembranes*, *49*, pp.307-324.

Koivisto, A.P., Belvisi, M.G., Gaudet, R. and Szallasi, A., 2022. Advances in TRP channel drug discovery: From target validation to clinical studies. *Nature Reviews Drug Discovery*, *21*, pp.41-59.

Kowaltowski, A.J., Menezes-Filho, S.L., Assali, E., Gonçalves, I.G., Abreu, P., Miller, N., Nolasco, P., Laurindo, F.R., Bruni-Cardoso, A. and Shirihai, O., 2019. Mitochondrial morphology regulates organellar Ca^{2+} uptake and changes cellular Ca^{2+} homeostasis. *BioRxiv*, p.624981.

Kozakov, D., Hall, D.R., Xia, B., Porter, K.A., Padhorny, D., Yueh, C., Beglov, D. and Vajda, S., 2017. The ClusPro web server for protein–protein docking. *Nature Protocols*, *12*, pp.255-278.

Krapivinsky, G., Mochida, S., Krapivinsky, L., Cibulsky, S.M. and Clapham, D.E., 2006. The TRPM7 ion channel functions in cholinergic synaptic vesicles and affects transmitter release. *Neuron*, *52*, pp.485-496.

Kremneva, E., Kislin, M., Kang, X. and Khiroug, L., 2013. Motility of astrocytic mitochondria is arrested by Ca^{2+}-dependent interaction between mitochondria and actin filaments. *Cell Calcium*, *53*, pp.85-93.

Krieger, E., Joo, K., Lee, J., Lee, J., Raman, S., Thompson, J., Tyka, M., Baker, D. and Karplus, K., 2009. Improving physical realism, stereochemistry, and side-chain accuracy in homology modeling: Four approaches that performed well in CASP8. *Proteins: Structure, Function, and Bioinformatics*, *77*(S9), pp.114-122.

Krols, M., Van Isterdael, G., Asselbergh, B., Kremer, A., Lippens, S., Timmerman, V. and Janssens, S., 2016. Mitochondria-associated membranes as hubs for neurodegeneration. *Acta Neuropathologica*, *131*, pp.505-523.

Kumar, A., Kumari, S., Majhi, R.K., Swain, N., Yadav, M. and Goswami, C., 2015. Regulation of TRP channels by steroids: implications in physiology and diseases. *General and Comparative Endocrinology*, *220*, pp.23-32.

Kumar, A., Majhi, R.K., Acharya, T.K., Smalla, K.H., Gundelfinger, E.D. and Goswami, C., 2018. TRPV4 interacts with mitochondrial proteins and acts as a mitochondrial structure-function regulator. *BioRxiv*, p.330993.

Kumar, A., Majhi, R.K., Swain, N., Giri, S.C., Kar, S., Samanta, L. and Goswami, C., 2016. TRPV4 is endogenously expressed in vertebrate spermatozoa and regulates intracellular calcium in human sperm. *Biochemical and Biophysical Research Communications*, *473*, pp.781-788.

Kumari, S., Kumar, A., Sardar, P., Yadav, M., Majhi, R.K., Kumar, A. and Goswami, C., 2015. Influence of membrane cholesterol in the molecular evolution and functional regulation of TRPV4. *Biochemical and Biophysical Research Communications*, *456*, pp.312-319.

Kume, H. and Tsukimoto, M., 2019. TRPM8 channel inhibitor AMTB suppresses murine T-cell activation induced by T-cell receptor stimulation, concanavalin A, or external antigen re-stimulation. *Biochemical and Biophysical Research Communications*, *509*, pp.918-924.

Lane, N., 2018. Hot mitochondria?. *PLoS Biology*, *16*, p.e2005113.

Lang, H., Li, Q., Yu, H., Li, P., Lu, Z., Xiong, S., Yang, T., Zhao, Y., Huang, X., Gao, P. and Zhang, H., 2015. Activation of TRPV1 attenuates high salt-induced cardiac hypertrophy through improvement of mitochondrial function. *British Journal of Pharmacology*, *172*, pp.5548-5558.

Lange, I., Yamamoto, S., Partida-Sanchez, S., Mori, Y., Fleig, A. and Penner, R., 2009. TRPM2 functions as a lysosomal Ca^{2+}-release channel in β cells. *Science Signaling*, *2*, pp.ra23-ra23.

Lange, M., Weihmann, F., Schliebner, I., Horbach, R., Deising, H.B., Wirsel, S.G. and Peiter, E., 2016. The Transient Receptor Potential (TRP) channel family in Colletotrichum graminicola: a molecular and physiological analysis. *PloS One*, *11*, p.e0158561.

Lavender, V., Chong, S., Ralphs, K., Wolstenholme, A.J. and Reaves, B.J., 2008. Increasing the expression of calcium-permeable TRPC3 and TRPC7 channels enhances constitutive secretion. *Biochemical Journal*, *413*, pp.437-446.

Ledderose, C., Bao, Y., Lidicky, M., Zipperle, J., Li, L., Strasser, K., Shapiro, N.I. and Junger, W.G., 2014. Mitochondria are gate-keepers of T cell function by producing the ATP that drives purinergic signaling. *Journal of Biological Chemistry*, *289*, pp.25936-25945.

Lee, Y.X., Lin, P.H., Rahmawati, E., Ma, Y.Y., Chan, C. and Tzeng, C.R., 2019. Mitochondria Research in Human Reproduction. *The Ovary* (pp. 327-335). Academic Press. (Book)

Lemieux, H., Blier, P.U. and Gnaiger, E., 2017. Remodeling pathway control of mitochondrial respiratory capacity by temperature in mouse heart: electron flow through the Q-junction in permeabilized fibers. *Scientific Reports*, *7*, pp.1-13.

Leuner, K., Kazanski, V., Muller, M., Essin, K., Henke, B., Gollasch, M., Harteneck, C. and Müller, W.E., 2007. Hyperforin—a key constituent of St. John's wort specifically activates TRPC6 channels. *The FASEB Journal*, *21*, pp.4101-4111.

Li, M., Jiang, J. and Yue, L., 2006. Functional characterization of homo-and heteromeric channel kinases TRPM6 and TRPM7. *The Journal of General Physiology*, *127*, pp.525-537.

Lieben, L. and Carmeliet, G., 2012. The involvement of TRP channels in bone homeostasis. *Frontiers in Endocrinology*, *3*, p.99.

Liedtke, W., Choe, Y., Martí-Renom, M.A., Bell, A.M., Denis, C.S., Hudspeth, A.J., Friedman, J.M. and Heller, S., 2000. Vanilloid receptor–related osmotically activated channel (VR-OAC), a candidate vertebrate osmoreceptor. *Cell*, *103*, pp.525-535.

Liu, J., Que, K., Liu, Y., Zang, C. and Wen, J., 2020. Tumor necrosis factor-α regulates the TRPA1 expression in human odontoblast-like cells. *Journal of Pain Research*, *13*, p.1655

Liu, L., Guo, M., Lv, X., Wang, Z., Yang, J., Li, Y., Yu, F., Wen, X., Feng, L. and Zhou, T., 2021. Role of transient receptor potential vanilloid 4 in vascular function. *Frontiers in Molecular Biosciences*, *8*, p.677661.

Liu, X., Yamazaki, T., Kwon, H.Y., Arai, S. and Chang, Y.T., 2022. A palette of site-specific organelle fluorescent thermometers. *Materials Today Bio*, *16*, p.100405.

Liu, Y. and Qin, N., 2011. TRPM8 in health and disease: cold sensing and beyond. *Transient Receptor Potential Channels*, *Advances in Experimental Medicine and Biology*, Springer, Dordrecht, 704. pp. 185-208. (Book)

Lo, I.C., Chan, H.C., Qi, Z., Ng, K.L., So, C. and Tsang, S.Y., 2016. TRPV3 channel negatively regulates cell cycle progression and safeguards the pluripotency of embryonic stem cells. *Journal of Cellular Physiology*, *231*, pp.403-413.

Lorenzo, I. M., Liedtke, W., Sanderson, M. J. & Valverde, M. A. (2008) TRPV4 channel participates in receptor-operated calcium entry and ciliary beat frequency regulation in mouse airway epithelial cells, *Proceedings of the National Academy of Sciences*. 105, 12611-6.

Lorton, D., Lubahn, C., Engan, C., Schaller, J., Felten, D.L. and Bellinger, D.L., 2000. Local application of Capsaicin into the draining lymph nodes attenuates expression of adjuvant-induced arthritis. *Neuroimmunomodulation*, *7*, pp.115-125.

Lu, J., Lee, Y.K., Ran, X., Lai, W.H., Li, R.A., Keung, W., Tse, K., Tse, H.F. and Yao, X., 2017. An abnormal TRPV4-related cytosolic Ca^{2+} rise in response to uniaxial stretch in induced pluripotent stem cells-derived cardiomyocytes from dilated cardiomyopathy patients. *Biochimica et Biophysica Acta (BBA)-Molecular Basis of Disease*, *1863*, pp.2964-2972.

Lucius, A., Khajavi, N., Reinach, P.S., Köhrle, J., Dhandapani, P., Huimann, P., Ljubojevic, N., Grötzinger, C. and Mergler, S., 2016. 3-Iodothyronamine increases transient receptor potential melastatin channel 8 (TRPM8) activity in immortalized human corneal epithelial cells. *Cellular Signalling*, *28*(3), pp.136-147.

Lykhmus, O., Gergalova, G., Koval, L., Zhmak, M., Komisarenko, S. and Skok, M., 2014. Mitochondria express several nicotinic acetylcholine receptor subtypes to control various pathways of apoptosis induction. *The International Journal of Biochemistry & Cell Biology*, *53*, pp.246-252.

M Knowlton, W. and D McKemy, D., 2011. TRPM8: from cold to cancer, peppermint to pain. *Current Pharmaceutical Biotechnology*, *12*, pp.68-77.

Mahieu, F., Owsianik, G., Verbert, L., Janssens, A., De Smedt, H., Nilius, B. and Voets, T., 2007. TRPM8-independent Menthol-induced Ca^{2+} release from endoplasmic reticulum and Golgi. *Journal of Biological Chemistry*, *282*, pp.3325-3336.

Majhi, R., Sardar, P., Goswami, L. and Goswami, C., 2011. Right time-right location-right move: TRPs find motors for common functions. *Channels*, *5*, pp.375-381.

Majhi, R.K., Saha, S., Kumar, A., Ghosh, A., Swain, N., Goswami, L., Mohapatra, P., Maity, A., Sahoo, V.K., Kumar, A. and Goswami, C., 2015. Expression of temperature-sensitive ion channel TRPM8 in sperm cells correlates with vertebrate evolution. *PeerJ*, *3*, p.e1310.

Majhi, R.K., Sahoo, S.S., Yadav, M., Pratheek, B.M., Chattopadhyay, S. and Goswami, C., 2015. Functional expression of TRPV channels in T cells and their implications in immune regulation. *The FEBS Journal*, *282*, pp.2661-2681.

Malfait, A.M., Gallily, R., Sumariwalla, P.F., Malik, A.S., Andreakos, E., Mechoulam, R. and Feldmann, M., 2000. The nonpsychoactive cannabis constituent cannabidiol is an oral anti-arthritic therapeutic in murine collagen-induced arthritis. *Proceedings of the National Academy of Sciences*, *97*, pp.9561-9566.

Matsumura, A., Higuchi, J., Watanabe, Y., Kato, M., Aoki, K., Akabane, S., Endo, T. and Oka, T., 2018. Inactivation of cardiolipin synthase triggers changes in mitochondrial morphology. *FEBS Letters*, *592*, pp.209-218.

Mattie, S., Riemer, J., Wideman, J.G. and McBride, H.M., 2018. A new mitofusin topology places the redox-regulated C terminus in the mitochondrial intermembrane space. *Journal of Cell Biology*, *217*, pp.507-515.

Matuz-Mares, D., González-Andrade, M., Araiza-Villanueva, M.G., Vilchis-Landeros, M.M. and Vázquez-Meza, H., 2022. Mitochondrial Calcium: Effects of Its Imbalance in Disease. *Antioxidants*, *11*, p.801.

McCoy, D.D., Zhou, L., Nguyen, A.K., Watts, A.G., Donovan, C.M. and McKemy, D.D., 2013. Enhanced insulin clearance in mice lacking TRPM8 channels. *American Journal of Physiology-Endocrinology and Metabolism*, *305*, pp.E78-E88.

McCray, B.A., Schindler, A., Hoover-Fong, J.E. and Sumner, C.J., 2020. Autosomal dominant TRPV4 disorders. Book from University of Washington, Seattle. PMID: 24830047.

McKemy, D.D., 2005. How cold is it? TRPM8 and TRPA1 in the molecular logic of cold sensation. *Molecular Pain*, *1*, pp.1744-8069.

McKemy, D.D., 2007. TRPM8: the cold and Menthol receptor. *TRP ion channel function in sensory transduction and cellular signaling cascades*. (1st Ed.) CRC Press. (Book).

McKemy, D.D., Neuhausser, W.M. and Julius, D., 2002. Identification of a cold receptor reveals a general role for TRP channels in thermosensation. *Nature*, *416*, pp.52-58.

McNamara, F.N., Randall, A. and Gunthorpe, M.J., 2005. Effects of piperine, the pungent component of black pepper, at the human vanilloid receptor (TRPV1). *British Journal of Pharmacology*, *144*(6), p.781.

Messina, A., Reina, S., Guarino, F. and De Pinto, V., 2012. VDAC isoforms in mammals. *Biochimica et Biophysica Acta (BBA)-Biomembranes*, *1818*, pp.1466-1476.

Mileykovskaya, E., Dowhan, W., Birke, R.L., Zheng, D., Lutterodt, L. and Haines, T.H., 2001. Cardiolipin binds nonyl acridine orange by aggregating the dye at exposed hydrophobic domains on bilayer surfaces. *FEBS Letters*, *507*, pp.187-190.

Minke, B., Wu, C.F. and Pak, W.L., 1975. Induction of photoreceptor voltage noise in the dark in Drosophila mutant. *Nature*, *258*, pp.84-87.

Mistretta, F.A., Russo, A., Castiglione, F., Bettiga, A., Colciago, G., Montorsi, F., Brandolini, L., Aramini, A., Bianchini, G., Allegretti, M. and Bovolenta, S., 2016. DFL23448, A Novel Transient Receptor Potential Melastin 8–Selective Ion Channel Antagonist, Modifies Bladder Function and Reduces Bladder Overactivity in Awake Rats. *Journal of Pharmacology and Experimental Therapeutics*, *356*, pp.200-211.

Miyake, T., Shirakawa, H., Nakagawa, T. and Kaneko, S., 2015. Activation of mitochondrial transient receptor potential vanilloid 1 channel contributes to microglial migration. *Glia*, *63*, pp.1870-1882.

Mochizuki, T., Wu, G., Hayashi, T., Xenophontos, S.L., Veldhuisen, B., Saris, J.J., Reynolds, D.M., Cai, Y., Gabow, P.A., Pierides, A. and Kimberling, W.J., 1996. PKD2, a gene for polycystic kidney disease that encodes an integral membrane protein. *Science*, *272*, pp.1339-1342.

Montell, C. and Rubin, G.M., 1989. Molecular characterization of the Drosophila trp locus: a putative integral membrane protein required for phototransduction. *Neuron*, *2*, pp.1313-1323.

Montell, C., 2005. The TRP superfamily of cation channels. *Science's STKE*, *2005*(272), pp.re3-re3.

Montell, C., 2011. The history of TRP channels, a commentary and reflection. *Pflügers Archiv-European Journal of Physiology*, *461*, pp.499-506.

Montell, C., Jones, K., Hafen, E. and Rubin, G., 1985. Rescue of the Drosophila phototransduction mutation trp by germline transformation. *Science*, *230*, pp.1040-1043.

Moqrich, A., Hwang, S.W., Earley, T.J., Petrus, M.J., Murray, A.N., Spencer, K.S., Andahazy, M., Story, G.M. and Patapoutian, A., 2005. Impaired thermosensation in mice lacking TRPV3, a heat and camphor sensor in the skin. *Science*, *307*, pp.1468-1472.

Morenilla-Palao, C., Planells-Cases, R., García-Sanz, N. and Ferrer-Montiel, A., 2004. Regulated exocytosis contributes to protein kinase C potentiation of vanilloid receptor activity. *Journal of Biological Chemistry*, *279*(24), pp.25665-25672.

Morgan, D.J., Poolman, T.M., Williamson, A.J., Wang, Z., Clark, N.R., Ma'ayan, A., Whetton, A.D., Brass, A., Matthews, L.C. and Ray, D.W., 2016. Glucocorticoid receptor isoforms direct distinct mitochondrial programs to regulate ATP production. *Scientific Reports*, *6*, pp.1-10.

Mosselman, S., Polman, J. and Dijkema, R., 1996. ERβ: identification and characterization of a novel human estrogen receptor. *FEBS Letters*, *392*, pp.49-53.

Murphy, M.P. and Siegel, R.M., 2013. Mitochondrial ROS fire up T cell activation. *Immunity*, *38*, pp.201-202.

Naert, R., López-Requena, A., Voets, T., Talavera, K. and Alpizar, Y.A., 2019. Expression and functional role of TRPV4 in bone marrow-derived CD11C+ cells. *International Journal of Molecular Sciences*, *20*, p.3378.

Nagai, T., Sawano, A., Park, E.S. and Miyawaki, A., 2001. Circularly permuted green fluorescent proteins engineered to sense Ca^{2+}. *Proceedings of the National Academy of Sciences*, *98*, pp.3197-3202.

Nagy, G., Koncz, A. and Perl, A., 2003. T cell activation-induced mitochondrial hyperpolarization is mediated by Ca^{2+}-and redox-dependent production of nitric oxide. *The Journal of Immunology*, *171*, pp.5188-5197.

Nakano, M., Arai, Y., Kotera, I., Okabe, K., Kamei, Y. and Nagai, T., 2017. Genetically encoded ratiometric fluorescent thermometer with wide range and rapid response. *PloS One*, *12*, p.e0172344.

Namer, B., Seifert, F., Handwerker, H.O. and Maihöfner, C., 2005. TRPA1 and TRPM8 activation in humans: effects of cinnamaldehyde and menthol. *Neuroreport*, *16*(9), pp.955-959.

Nazıroğlu, M., Blum, W., Jósvay, K., Çiğ, B., Henzi, T., Oláh, Z., Vizler, C., Schwaller, B. and Pecze, L., 2018. Menthol evokes Ca^{2+} signals and induces oxidative stress independently of the presence of TRPM8 (Menthol) receptor in cancer cells. *Redox Biology*, *14*, pp.439-449.

Neeper, M.P., Liu, Y., Hutchinson, T.L., Wang, Y., Flores, C.M. and Qin, N., 2007. Activation properties of heterologously expressed mammalian TRPV2: evidence for species dependence. *Journal of Biological Chemistry*, *282*, pp.15894-15902.

Nesin, V., Tsiokas, L. (2014). TRPC1. *Mammalian Transient Receptor Potential (TRP) Cation Channels. Handbook of Experimental Pharmacology*, vol 222. Springer, Berlin, Heidelberg (Book).

Ngo, J., Osto, C., Villalobos, F. and Shirihai, O.S., 2021. Mitochondrial Heterogeneity in Metabolic Diseases. *Biology*, *10*, p.927.

Nicholls, D.G. and Locke, R.M., 1984. Thermogenic mechanisms in brown fat. *Physiological Reviews*, *64*, pp.1-64.

Nilius, B. and Owsianik, G., 2011. The transient receptor potential family of ion channels. *Genome Biology*, *12*, pp.1-11.

Nilius, B. and Voets, T., 2013. The puzzle of TRPV4 channelopathies. *EMBO Reports*, *14*, pp.152-163.

Nilius, B., 2012. Transient receptor potential (TRP) channels in the brain: the good and the ugly. *European Review*, *20*, pp.343-355.

Novicoff, W.M., Manaswi, A., Hogan, M.V., Brubaker, S.M., Mihalko, W.M. and Saleh, K.J., 2008. Critical analysis of the evidence for current technologies in bone-healing and repair. *Journal of Bone and Joint Surgery*, *90* (Supplement_1), pp.85-91.

Nunnari, J. and Suomalainen, A., 2012. Mitochondria: in sickness and in health. *Cell*, *148*, pp.1145-1159.

O'Sullivan, D., Stanczak, M.A., Villa, M., Uhl, F.M., Corrado, M., Klein Geltink, R.I., Sanin, D.E., Apostolova, P., Rana, N., Edwards-Hicks, J. and Grzes, K.M., 2021. Fever supports CD8+ effector T cell responses by promoting mitochondrial translation. *Proceedings of the National Academy of Sciences*, *118*, p.e2023752118.

Olah, Z., Szabo, T., Karai, L., Hough, C., Fields, R.D., Caudle, R.M., Blumberg, P.M. and Iadarola, M.J., 2001. Ligand-induced dynamic membrane changes and cell deletion conferred by vanilloid receptor 1. *Journal of Biological Chemistry*, *276*, pp.11021-11030.

Olivares-Navarrete, R., Lee, E.M., Smith, K., Hyzy, S.L., Doroudi, M., Williams, J.K., Gall, K., Boyan, B.D. and Schwartz, Z., 2017. Substrate stiffness controls osteoblastic and chondrocytic differentiation of mesenchymal stem cells without exogenous stimuli. *PloS One*, *12*, p.e0170312.

Ortíz-Rentería, M., Juárez-Contreras, R., González-Ramírez, R., Islas, L.D., Sierra-Ramírez, F., Llorente, I., Simon, S.A., Hiriart, M., Rosenbaum, T. and Morales-Lázaro, S.L., 2018. TRPV1 channels and the progesterone receptor Sig-1R interact to regulate pain. *Proceedings of the National Academy of Sciences*, *115*, pp.E1657-E1666.

Oyama, K., Gotoh, M., Hosaka, Y., Oyama, T.G., Kubonoya, A., Suzuki, Y., Arai, T., Tsukamoto, S., Kawamura, Y., Itoh, H. and Shintani, S.A., 2020. Single-cell temperature mapping with fluorescent thermometer nanosheets. *Journal of General Physiology*, *152*, pp. e201912469

Oz, M., El Nebrisi, E.G., Yang, K.H.S., Howarth, F.C. and Al Kury, L.T., 2017. Cellular and molecular targets of Menthol actions. *Frontiers in Pharmacology*, *8*, p.472.

Pairet, N., Mang, S., Fois, G., Keck, M., Kühnbach, M., Gindele, J., Frick, M., Dietl, P. and Lamb, D.J., 2018. TRPV4 inhibition attenuates stretch-induced inflammatory cellular responses and lung barrier dysfunction during mechanical ventilation. *PloS One*, *13*, p.e0196055.

Palazzo, E., Rossi, F., de Novellis, V. and Maione, S., 2013. Endogenous modulators of TRP channels. *Current Topics in Medicinal Chemistry*, *13*, pp.398-407.

Palmer, C.P., Zhou, X.L., Lin, J., Loukin, S.H., Kung, C. and Saimi, Y., 2001. A TRP homolog in Saccharomyces cerevisiae forms an intracellular Ca^{2+}-permeable channel in the yeast vacuolar membrane. *Proceedings of the National Academy of Sciences*, *98*, pp.7801-7805.

Palmer, J.W., Tandler, B. and Hoppel, C.L., 1985. Biochemical differences between subsarcolemmal and interfibrillar mitochondria from rat cardiac muscle: effects of procedural manipulations. *Archives of Biochemistry and Biophysics*, *236*, pp.691-702.

Palty, R., Ohana, E., Hershfinkel, M., Volokita, M., Elgazar, V., Beharier, O., Silverman, W.F., Argaman, M. and Sekler, I., 2004. Lithium-calcium exchange is mediated by a distinct potassium-independent sodium-calcium exchanger. *Journal of Biological Chemistry*, *279*, pp.25234-25240.

Papa, L. and Germain, D., 2014. SirT3 regulates the mitochondrial unfolded protein response. *Molecular and Cellular Biology*, *34*, pp.699-710.

Paradies, G., Paradies, V., Ruggiero, F.M. and Petrosillo, G., 2019. Role of cardiolipin in mitochondrial function and dynamics in health and disease: molecular and pharmacological aspects. *Cells*, *8*, p.728.

Parenti, A., De Logu, F., Geppetti, P. and Benemei, S., 2016. What is the evidence for the role of TRP channels in inflammatory and immune cells?. *British Journal of Pharmacology*, *173*, pp.953-969.

Parnas, M., Peters, M., Dadon, D., Lev, S., Vertkin, I., Slutsky, I. and Minke, B., 2009. Carvacrol is a novel inhibitor of Drosophila TRPL and mammalian TRPM7 channels. *Cell Calcium*, *45*, pp.300-309.

Patergnani, S., Suski, J.M., Agnoletto, C., Bononi, A., Bonora, M., De Marchi, E., Giorgi, C., Marchi, S., Missiroli, S., Poletti, F. and Rimessi, A., 2011. Calcium signaling around mitochondria associated membranes (MAMs). *Cell Communication and Signaling*, *9*, pp.1-10.

Pedersen, S.F., Owsianik, G. and Nilius, B., 2005. TRP channels: an overview. *Cell Calcium*, *38*, pp.233-252.

Peier, A.M., Moqrich, A., Hergarden, A.C., Reeve, A.J., Andersson, D.A., Story, G.M., Earley, T.J., Dragoni, I., McIntyre, P., Bevan, S. and Patapoutian, A., 2002. A TRP channel that senses cold stimuli and Menthol. *Cell*, *108*, pp.705-715.

Peier, A.M., Reeve, A.J., Andersson, D.A., Moqrich, A., Earley, T.J., Hergarden, A.C., Story, G.M., Colley, S., Hogenesch, J.B., McIntyre, P. and Bevan, S., 2002. A heat-sensitive TRP channel expressed in keratinocytes. *Science*, *296*, pp.2046-2049.

Peng, W., Wong, Y.C. and Krainc, D., 2020. Mitochondria-lysosome contacts regulate mitochondrial Ca^{2+} dynamics via lysosomal TRPML1. *Proceedings of the National Academy of Sciences*, *117*, pp.19266-19275.

Petersen, O.H. and Verkhratsky, A., 2016. Calcium and ATP control multiple vital functions. *Philosophical Transactions of the Royal Society B: Biological Sciences*, *371*, p.20150418.

Picard, M. and Shirihai, O.S., 2022. Mitochondrial signal transduction. *Cell Metabolism*, *34*, pp.1620-1653.

Plant TD, Strotmann R (2007) TRPV4.*Transient Receptor Potential (TRP) Channels. Handbook of Experimental Pharmacology*, Springer, Berlin, Heidelberg. 179:189–205 (Book)

Poirier, Y., Antonenkov, V.D., Glumoff, T. and Hiltunen, J.K., 2006. Peroxisomal β-oxidation—a metabolic pathway with multiple functions. *Biochimica et Biophysica Acta (BBA)-Molecular Cell Research*, *1763*, pp.1413-1426.

Preti, D., Szallasi, A. and Patacchini, R., 2012. TRP channels as therapeutic targets in airway disorders: a patent review. *Expert Opinion on Therapeutic Patents*, *22*, pp.663-695.

Prevarskaya, N., Zhang, L. and Barritt, G., 2007. TRP channels in cancer. *Biochimica et Biophysica Acta (BBA)-Molecular Basis of Disease*, *1772*, pp.937-946.

Qi, H., Li, L. and Shuai, J., 2015. Optimal microdomain crosstalk between endoplasmic reticulum and mitochondria for Ca^{2+} oscillations. *Scientific Reports*, *5*, pp.1-11.

Quintana, A., Schwindling, C., Wenning, A.S., Becherer, U., Rettig, J., Schwarz, E.C. and Hoth, M., 2007. T cell activation requires mitochondrial translocation to the immunological synapse. *Proceedings of the National Academy of Sciences*, *104*, pp.14418-14423.

Raisinghani, M., Pabbidi, R.M. and Premkumar, L.S., 2005. Activation of transient receptor potential vanilloid 1 (TRPV1) by resiniferatoxin. *The Journal of Physiology*, *567*, pp.771-786.

Rajagopal, M.C., Brown, J.W., Gelda, D., Valavala, K.V., Wang, H., Llano, D.A., Gillette, R. and Sinha, S., 2019. Transient heat release during induced mitochondrial proton uncoupling. *Communications Biology*, *2*, pp.1-6.

Ramsey, I.S., Delling, M. and Clapham, D.E., 2006. An introduction to TRP channels. *Annual Review of Physiology*, *68*, pp.619-647.

Raturi, A. and Simmen, T., 2013. Where the endoplasmic reticulum and the mitochondrion tie the knot: the mitochondria-associated membrane (MAM). *Biochimica et Biophysica Acta (BBA)-Molecular Cell Research*, *1833*, pp.213-224.

Reers, M., Smiley, S.T., Mottola-Hartshorn, C., Chen, A., Lin, M. and Chen, L.B., 1995. Mitochondrial membrane potential monitored by JC-1 dye. *Methods in enzymology*, 260, pp. 406-417.

Rieusset, J., 2018. The role of endoplasmic reticulum-mitochondria contact sites in the control of glucose homeostasis: an update. *Cell Death & Disease*, *9*, pp.1-12.

Rieusset, J., Fauconnier, J., Paillard, M., Belaidi, E., Tubbs, E., Chauvin, M.A., Durand, A., Bravard, A., Teixeira, G., Bartosch, B. and Michelet, M., 2016. Disruption of calcium transfer from ER to mitochondria links alterations of mitochondria-associated ER membrane integrity to hepatic insulin resistance. *Diabetologia*, *59*, pp.614-623.

Ristow, M. and Zarse, K., 2010. How increased oxidative stress promotes longevity and metabolic health: The concept of mitochondrial hormesis (mitohormesis). *Experimental Gerontology*, *45*, pp.410-418.

Rizzuto, R., Marchi, S., Bonora, M., Aguiari, P., Bononi, A., De Stefani, D., Giorgi, C., Leo, S., Rimessi, A., Siviero, R. and Zecchini, E., 2009. Ca^{2+} transfer from the ER to mitochondria: when, how and why. *Biochimica et Biophysica Acta (BBA)-Bioenergetics*, *1787*, pp.1342-1351.

Rodrigues, T., Sieglitz, F. and Bernardes, G.J., 2016. Natural product modulators of transient receptor potential (TRP) channels as potential anti-cancer agents. *Chemical Society Reviews*, *45*, pp.6130-6137.

Rojo, M., Legros, F., Chateau, D. and Lombès, A., 2002. Membrane topology and mitochondrial targeting of mitofusins, ubiquitous mammalian homologs of the transmembrane GTPase Fzo. *Journal of Cell Science*, *115*, pp.1663-1674.

Rosencrans, W.M., Rajendran, M., Bezrukov, S.M. and Rostovtseva, T.K., 2021. VDAC regulation of mitochondrial calcium flux: From channel biophysics to disease. *Cell Calcium*, *94*, p.102356.

Ruan, L., Chen, J., Du, C., Lu, H., Zhang, J., Cai, X., Dou, R., Lin, W., Chai, Z., Nie, G. and Hu, Y., 2022. Mitochondrial temperature-responsive drug delivery reverses drug resistance in lung cancer. *Bioactive Materials*, *13*, pp.191-199.

Ruan, L., Zhou, M., Chen, J., Huang, H., Zhang, J., Sun, H., Chai, Z. and Hu, Y., 2019. Thermoresponsive drug delivery to mitochondria *in vivo*. *Chemical Communications*, *55*, pp.14645-14648.

Sabnis, A.S., Shadid, M., Yost, G.S. and Reilly, C.A., 2008. Human lung epithelial cells express a functional cold-sensing TRPM8 variant. *American Journal of Respiratory Cell and Molecular Biology*, *39*, pp.466-474.

Sahoo, S.S., Majhi, R.K., Tiwari, A., Acharya, T., Kumar, P.S., Saha, S., Kumar, A., Goswami, C. and Chattopadhyay, S., 2019. Transient receptor potential ankyrin1 channel is endogenously expressed in T cells and is involved in immune functions. *Bioscience Reports*, *39*. BSR20191437

Sahu, R.P. and Goswami, C., 2022. Presence of TRPV3 in macrophage lysosomes helps in skin wound healing against bacterial infection. *Experimental Dermatology*. 32(1), pp.60-74.

Saito, M., Hanson, P.I. and Schlesinger, P., 2007. Luminal chloride-dependent activation of endosome calcium channels: patch clamp study of enlarged endosomes. *Journal of Biological Chemistry*, *282*, pp.27327-27333.

Sakellariou, P., Valente, A., Carrillo, A.E., Metsios, G.S., Nadolnik, L., Jamurtas, A.Z., Koutedakis, Y., Boguszewski, C., Andrade, C.M.B., Svensson, P.A. and Kawashita, N.H., 2016. Chronic l-Menthol-induced browning of white adipose tissue hypothesis: A putative therapeutic regime for combating obesity and improving metabolic health. *Medical Hypotheses*, *93*, pp.21-26.

Sanders, O.D., Rajagopal, J.A. and Rajagopal, L., 2021. Menthol to induce non-shivering thermogenesis via TRPM8/PKA signaling for treatment of obesity. *Journal of Obesity & Metabolic Syndrome*, *30*, p.4.

Sanyasi, S., Kumar, A., Goswami, C., Bandyopadhyay, A. and Goswami, L., 2014. A carboxy methyl tamarind polysaccharide matrix for adhesion and growth of osteoclast-precursor cells. *Carbohydrate Polymers*, *101*, pp.1033-1042.

Scheraga, R.G., Southern, B.D., Grove, L.M. and Olman, M.A., 2017. The role of transient receptor potential vanilloid 4 in pulmonary inflammatory diseases. *Frontiers in Immunology*, *8*, p.503.

Scott, K.Y., Matthew, R., Woolcock, J., Silva, M. and Lemieux, H., 2019. Adjustments in the control of mitochondrial respiratory capacity to tolerate temperature fluctuations. *Journal of Experimental Biology*, *222*, p.jeb207951.

Sena, L., Li, S., Jairaman, A., Prakriya, M., Ezponda, T., Hildeman, D., Wang, C.R., Schumacker, P., Licht, J., Perlman, H. and Bryce, P., 2013. Mitochondria are required for antigen-specific T cell activation through reactive oxygen species signaling. *Immunity*, *38*, pp.225-236.

Shang, S., Zhu, F., Liu, B., Chai, Z., Wu, Q., Hu, M., Wang, Y., Huang, R., Zhang, X., Wu, X. and Sun, L., 2016. Intracellular TRPA1 mediates Ca^{2+} release from lysosomes in dorsal root ganglion neurons. *Journal of Cell Biology*, *215*, pp.369-381.

Shigematsu, H., Sokabe, T., Danev, R., Tominaga, M. and Nagayama, K., 2010. A 3.5-nm structure of rat TRPV4 cation channel revealed by Zernike phase-contrast cryoelectron microscopy. *Journal of Biological Chemistry*, *285*, pp.11210-11218.

Shlykov, S.G., Yang, M., Alcorn, J.L. and Sanborn, B.M., 2003. Capacitative cation entry in human myometrial cells and augmentation by hTrpC3 overexpression. *Biology of Reproduction*, *69*, pp.647-655.

Shoshan-Barmatz, V. and Mizrachi, D., 2012. VDAC1: from structure to cancer therapy. *Frontiers in Oncology*, *2*, p.164.

Siddiqui, J.A., Swarnkar, G., Sharan, K., Chakravarti, B., Sharma, G., Rawat, P., Kumar, M., Khan, F.M., Pierroz, D., Maurya, R. and Chattopadhyay, N., 2010. 8, 8 ″-Biapigeninyl stimulates osteoblast functions and inhibits osteoclast and adipocyte functions: Osteoprotective action of 8, 8 ″-biapigeninyl in ovariectomized mice. *Molecular and Cellular Endocrinology*, *323*, pp.256-267.

Siemens, J., Zhou, S., Piskorowski, R., Nikai, T., Lumpkin, E.A., Basbaum, A.I., King, D. and Julius, D., 2006. Spider toxins activate the Capsaicin receptor to produce inflammatory pain. *Nature*, *444*, pp.208-212.

Singh, B.B., Lockwich, T.P., Bandyopadhyay, B.C., Liu, X., Bollimuntha, S., Brazer, S.C., Combs, C., Das, S., Leenders, A.M., Sheng, Z.H. and Knepper, M.A., 2004. VAMP2-dependent exocytosis regulates plasma membrane insertion of TRPC3 channels and contributes to agonist-stimulated Ca^{2+} influx. *Molecular Cell*, *15*, pp.635-646.

Smith, P.L., Maloney, K.N., Pothen, R.G., Clardy, J. and Clapham, D.E., 2006. Bisandrographolide from Andrographis paniculata activates TRPV4 channels. *Journal of Biological Chemistry*, *281*, pp.29897-29904.

Solakidi, S., Psarra, A.M. and Sekeris, C.E., 2005. Differential subcellular distribution of estrogen receptor isoforms: localization of ERα in the nucleoli and ERβ in the mitochondria of human osteosarcoma SaoS-2 and hepatocarcinoma HepG2 cell lines. *Biochimica et Biophysica Acta (BBA)-Molecular Cell Research*, *1745*, pp.382-392.

Sterling, K., Campbell, G.A. and Brenner, M.A., 1984. Purification of the mitochondrial triiodothyronine (T3) receptor from rat liver. *European Journal of Endocrinology*, *105*, pp.391-397.

Sterling, K., Lazarus, J.H., Milch, P.O., Sakurada, T. and Brenner, M.A., 1978. Mitochondrial thyroid hormone receptor: localization and physiological significance. *Science*, *201*, pp.1126-1129.

Sterling, K., Milch, P.O., Brenner, M.A. and Lazarus, J.H., 1977. Thyroid hormone action: the mitochondrial pathway. *Science*, *197*, pp.996-999.

Storey, N.M. and Lambert, D.G., 2017. Mitochondrial pharmacology turns its sights on the Ca^{2+} uniporter. *Cell Death Discovery*, *3*, pp.1-3.

Strotmann, R., Harteneck, C., Nunnenmacher, K., Schultz, G. and Plant, T.D., 2000. OTRPC4, a nonselective cation channel that confers sensitivity to extracellular osmolarity. *Nature Cell Biology*, *2*, pp.695-702.

Suchyna, T.M., Johnson, J.H., Hamer, K., Leykam, J.F., Gage, D.A., Clemo, H.F., Baumgarten, C.M. and Sachs, F., 2000. Identification of a peptide toxin from Grammostola spatulata spider venom that blocks cation-selective stretch-activated channels. *The Journal of General Physiology*, *115*, pp.583-598.

Sugiura, A., Nagashima, S., Tokuyama, T., Amo, T., Matsuki, Y., Ishido, S., Kudo, Y., McBride, H.M., Fukuda, T., Matsushita, N. and Inatome, R., 2013. MITOL regulates endoplasmic reticulum-mitochondria contacts via Mitofusin2. *Molecular Cell*, *51*, pp.20-34.

Sun, Y. and Ding, S., 2020. ER–Mitochondria Contacts and Insulin Resistance Modulation through Exercise Intervention. *International Journal of Molecular Sciences*, *21*, p.9587.

Suofu, Y., Li, W., Jean-Alphonse, F.G., Jia, J., Khattar, N.K., Li, J., Baranov, S.V., Leronni, D., Mihalik, A.C., He, Y. and Cecon, E., 2017. Dual role of mitochondria in producing melatonin and driving GPCR signaling to block cytochrome c release. *Proceedings of the National Academy of Sciences*, *114*, pp.E7997-E8006.

Takaishi, M., Fujita, F., Uchida, K., Yamamoto, S., Sawada, M., Hatai, C., Shimizu, M. and Tominaga, M., 2012. 1, 8-cineole, a TRPM8 agonist, is a novel natural antagonist of human TRPA1. *Molecular Pain*, *8*, pp.1744-8069.

Talbot, J., Barrett, J.N., Barrett, E.F. and David, G., 2007. Stimulation-induced changes in NADH fluorescence and mitochondrial membrane potential in lizard motor nerve terminals. *The Journal of Physiology*, *579*, pp.783-798.

Tarasov, A.I., Griffiths, E.J. and Rutter, G.A., 2012. Regulation of ATP production by mitochondrial Ca^{2+}. *Cell Calcium*, *52*, pp.28-35.

Territo, P.R., Mootha, V.K., French, S.A. and Balaban, R.S., 2000. Ca^{2+} activation of heart mitochondrial oxidative phosphorylation: role of the F0/F1-ATPase. *American Journal of Physiology-Cell Physiology*, *278*, pp.C423-C435.

Thebault, S., Lemonnier, L., Bidaux, G., Flourakis, M., Bavencoffe, A., Gordienko, D., Roudbaraki, M., Delcourt, P., Panchin, Y., Shuba, Y. and Skryma, R., 2005. Novel role of cold/Menthol-sensitive transient receptor potential melastatine family member 8 (TRPM8) in the activation of store-operated channels in LNCaP human prostate cancer epithelial cells. *Journal of Biological Chemistry*, *280*, pp.39423-39435.

Tian, W., Salanova, M., Xu, H., Lindsley, J.N., Oyama, T.T., Anderson, S., Bachmann, S. and Cohen, D.M., 2004. Renal expression of osmotically responsive cation channel TRPV4 is restricted to water-impermeant nephron segments. *American Journal of Physiology-Renal Physiology*, *287*, pp.F17-F24.

Togashi, K., Hara, Y., Tominaga, T., Higashi, T., Konishi, Y., Mori, Y. and Tominaga, M., 2006. TRPM2 activation by cyclic ADP-ribose at body temperature is involved in insulin secretion. *The EMBO Journal*, *25*, pp.1804-1815.

Togashi, K., Inada, H. and Tominaga, M., 2008. Inhibition of the transient receptor potential cation channel TRPM2 by 2-aminoethoxydiphenyl borate (2-APB). *British Journal of Pharmacology*, *153*, pp.1324-1330.

Tominaga, M. and Caterina MJ. 2004. Thermosensation and pain. *J Neurobiol*, *61*, pp.3-12.

Trebak, M. and Kinet, J.P., 2019. Calcium signalling in T cells. *Nature Reviews Immunology*, *19*, pp.154-169.

Tsavaler, L., Shapero, M.H., Morkowski, S. and Laus, R., 2001. Trp-p8, a novel prostate-specific gene, is up-regulated in prostate cancer and other malignancies and shares high homology with transient receptor potential calcium channel proteins. *Cancer Research*, *61*, pp.3760-3769.

Tubbs, E. and Rieusset, J., 2017. Metabolic signaling functions of ER–mitochondria contact sites: role in metabolic diseases. *Journal of Molecular Endocrinology*, *58*, pp.R87-R106.

Turner, H., Fleig, A., Stokes, A., Kinet, J.P. and Penner, R., 2003. Discrimination of intracellular calcium store subcompartments using TRPV1 (transient receptor potential channel, vanilloid subfamily member 1) release channel activity. *Biochemical Journal*, *371*, pp.341-350.

Turrens, J.F., 2003. Mitochondrial formation of reactive oxygen species. *The Journal of Physiology*, *552*, pp.335-344.

Ullah, F., Javed, F., Othman, M.B.H., Khan, A., Gul, R., Ahmad, Z. and Md. Akil1, H., 2018. Synthesis and functionalization of chitosan built hydrogel with induced hydrophilicity for extended release of sparingly soluble drugs. *Journal of Biomaterials science, Polymer edition*, *29*, pp.376-396.

Valero, M., Morenilla-Palao, C., Belmonte, C. and Viana, F., 2011. Pharmacological and functional properties of TRPM8 channels in prostate tumor cells. *Pflügers Archiv*, *461*, pp.99-114.

Van de Graaf, S.F., Chang, Q., Mensenkamp, A.R., Hoenderop, J.G. and Bindels, R.J., 2006. Direct interaction with Rab11a targets the epithelial Ca^{2+} channels TRPV5 and TRPV6 to the plasma membrane. *Molecular and Cellular Biology*, *26*, pp.303-312.

Van Den Ameele, J., Fuge, J., Pitceathly, R.D., Berry, S., McIntyre, Z., Hanna, M.G., Lee, M. and Chinnery, P.F., 2020. Chronic pain is common in mitochondrial disease. *Neuromuscular Disorders*, *30*, pp.413-419.

Velarde, M.C., 2014. Mitochondrial and sex steroid hormone crosstalk during aging. *Longevity & Healthspan*, *3*, pp.1-10.

Vellino, S., Oddou, C., Rivier, P., Boyault, C., Hiriart-Bryant, E., Kraut, A., Martin, R., Coute, Y., Knölker, H.J., Valverde, M.A. and Albigès-Rizo, C., 2021. Cross-talk between the calcium channel TRPV4 and reactive oxygen species interlocks adhesive and degradative functions of invadosomes. *Journal of Cell Biology*, *220*. e201910079

Venkatachalam, K., Hofmann, T. and Montell, C., 2006. Lysosomal localization of TRPML3 depends on TRPML2 and the mucolipidosis-associated protein TRPML1. *Journal of Biological Chemistry*, *281*, pp.17517-17527.

Vennekens, R., Vriens, J. and Nilius, B., 2008. Herbal compounds and toxins modulating TRP channels. *Current Neuropharmacology*, *6*, pp.79-96.

Verma, P., Kumar, A. and Goswami, C., 2010. TRPV4-mediated channelopathies. *Channels*, *4*, pp.319-328.

Vetter, I. and Lewis, R.J., 2011. Natural product ligands of TRP channels. *Adv Exp Med Biol*.; 704, pp. 41-85.

Vincent, F., Acevedo, A., Nguyen, M.T., Dourado, M., DeFalco, J., Gustafson, A., Spiro, P., Emerling, D.E., Kelly, M.G. and Duncton, M.A., 2009. Identification and characterization of novel TRPV4 modulators. *Biochemical and Biophysical Research Communications*, *389*, pp.490-494.

Vivekananthan, D.P., Penn, M.S., Sapp, S.K., Hsu, A. and Topol, E.J., 2003. Use of antioxidant vitamins for the prevention of cardiovascular disease: meta-analysis of randomised trials. *The Lancet*, *361*, pp.2017-2023.

Voets, T., Talavera, K., Owsianik, G. and Nilius, B., 2005. Sensing with TRP channels. *Nature Chemical Biology*, *1*, pp.85-92.

Vriens, J., Owsianik, G., Janssens, A., Voets, T. and Nilius, B., 2007. Determinants of 4α-phorbol sensitivity in transmembrane domains 3 and 4 of the cation channel TRPV4. *Journal of Biological Chemistry*, *282*, pp.12796-12803.

Wan, Z., Zhang, P., Lv, L. and Zhou, Y., 2020. NIR light-assisted phototherapies for bone-related diseases and bone tissue regeneration: A systematic review. *Theranostics*, *10*, p.11837.

Wang, C., Chen, J., Wang, M., Naruse, K. and Takahashi, K., 2021. Role of the TRPM4 channel in mitochondrial function, calcium release, and ROS generation in oxidative stress. *Biochemical and Biophysical Research Communications*, *566*, pp.190-196.

Wang, D., Huang, H., Zhou, M., Lu, H., Chen, J., Chang, Y.T., Gao, J., Chai, Z. and Hu, Y., 2019a. A thermoresponsive nanocarrier for mitochondria-targeted drug delivery. *Chemical Communications*, *55*, pp.4051-4054.

Wang, D., Zhou, M., Huang, H., Ruan, L., Lu, H., Zhang, J., Chen, J., Gao, J., Chai, Z. and Hu, Y., 2019b. Gold nanoparticle-based probe for analyzing mitochondrial temperature in living cells. *ACS Applied Bio Materials*, *2*, pp.3178-3182.

Wang, H., Chen, Q., Zhang, S. and Lu, L., 2021. A Transient Receptor Potential-like Calcium Ion Channel in the Filamentous Fungus Aspergillus nidulans. *Journal of Fungi*, *7*, p.920.

Wang, L., Yuan, L., Zeng, X., Peng, J., Ni, Y., Er, J.C., Xu, W., Agrawalla, B.K., Su, D., Kim, B. and Chang, Y.T., 2016. A multisite-binding switchable fluorescent probe for monitoring mitochondrial ATP level fluctuation in live cells. *Angewandte Chemie International Edition*, *55*, pp.1773-1776.

Wang, S. and Chang, Y.T., 2006. Combinatorial synthesis of benzimidazolium dyes and its diversity directed application toward GTP-selective fluorescent chemosensors. *Journal of the American Chemical Society*, *128*, pp.10380-10381.

Watanabe, H., Davis, J.B., Smart, D., Jerman, J.C., Smith, G.D., Hayes, P., Vriens, J., Cairns, W., Wissenbach, U., Prenen, J. and Flockerzi, V., 2002. Activation of TRPV4 channels (hVRL-2/mTRP12) by phorbol derivatives. *Journal of Biological Chemistry*, *277*, pp.13569-13577.

Watanabe, H., Vriens, J., Prenen, J., Droogmans, G., Voets, T. and Nilius, B., 2003. Anandamide and arachidonic acid use epoxyeicosatrienoic acids to activate TRPV4 channels. *Nature*, *424*, pp.434-438.

Wei, Y., Shi, M., Zhang, J., Zhang, X., Shen, K., Wang, R., Miron, R.J., Xiao, Y. and Zhang, Y., 2020. Autologous versatile vesicles-incorporated biomimetic extracellular matrix induces biomineralization. *Advanced Functional Materials*, *30*, p.2000015.

Willie, B.M., Petersen, A., Schmidt-Bleek, K., Cipitria, A., Mehta, M., Strube, P., Lienau, J., Wildemann, B., Fratzl, P. and Duda, G., 2010. Designing biomimetic scaffolds for bone regeneration: why aim for a copy of mature tissue properties if nature uses a different approach?. *Soft Matter*, *6*, pp.4976-4987.

Wolf, D.M., Segawa, M., Kondadi, A.K., Anand, R., Bailey, S.T., Reichert, A.S., van der Bliek, A.M., Shackelford, D.B., Liesa, M. and Shirihai, O.S., 2019. Individual cristae within the same mitochondrion display different membrane potentials and are functionally independent. *The EMBO Journal*, *38*, p.e101056.

Woolums, B.M., McCray, B.A., Sung, H., Tabuchi, M., Sullivan, J.M., Ruppell, K.T., Yang, Y., Mamah, C., Aisenberg, W.H., Saavedra-Rivera, P.C. and Larin, B.S., 2020. TRPV4 disrupts mitochondrial transport and causes axonal degeneration via a CaMKII-dependent elevation of intracellular Ca^{2+}. *Nature Communications*, *11*, p.2679.

Wrutniak-Cabello, C., Casas, F. and Cabello, G., 2001. Thyroid hormone action in mitochondria. *Journal of Molecular Endocrinology*, *26*, pp.67-77.

Wu, M., Zhang, Y., Wu, P., Chen, F., Yang, Z., Zhang, S., Xiao, L., Cai, L., Zhang, C., Chen, Y. and Deng, Z., 2022. Mussel-inspired multifunctional surface through promoting osteogenesis and inhibiting osteoclastogenesis to facilitate bone regeneration. *NPJ Regenerative Medicine*, *7*, pp.1-20.

Wu, S.N., Wu, P.Y. and Tsai, M.L., 2011. Characterization of TRPM8-like channels activated by the cooling agent icilin in the macrophage cell line RAW 264.7. *The Journal of Membrane Biology*, *241*, pp.11-20.

Xia, M., Zhang, Y., Jin, K., Lu, Z., Zeng, Z. and Xiong, W., 2019. Communication between mitochondria and other organelles: a brand-new perspective on mitochondria in cancer. *Cell & Bioscience*, *9*, pp.1-19.

Xing, H., Chen, M., Ling, J., Tan, W. and Gu, J.G., 2007. TRPM8 mechanism of cold allodynia after chronic nerve injury. *Journal of Neuroscience*, *27*, pp.13680-13690.

Xu, H., Blair, N.T, Clapham, D.E., 2005. Camphor activates and strongly desensitizes the transient receptor potential vanilloid subtype 1 channel in a vanilloid-independent mechanism. *J. Neurosci.*, 25, pp.8924-8937.

Xu, H., Delling, M., Jun, J.C. and Clapham, D.E., 2006. Oregano, thyme and clove-derived flavors and skin sensitizers activate specific TRP channels. *Nature Neuroscience*, *9*, pp.628-635.

Xu, H., Ramsey, I.S., Kotecha, S.A., Moran, M.M., Chong, J.A., Lawson, D., Ge, P., Lilly, J., Silos-Santiago, I., Xie, Y. and DiStefano, P.S., 2002. TRPV3 is a calcium-permeable temperature-sensitive cation channel. *Nature*, *418*, pp.181-186.

Xu, S.Z., Zeng, F., Boulay, G., Grimm, C., Harteneck, C. and Beech, D.J., 2005. Block of TRPC5 channels by 2-aminoethoxydiphenyl borate: a differential, extracellular and voltage-dependent effect. *British Journal of Pharmacology*, *145*, p.405.

Yadav, M. and Goswami, C., 2017. TRPV3 mutants causing Olmsted Syndrome induce impaired cell adhesion and nonfunctional lysosomes. *Channels*, *11*, pp.196-208.

Yadav, M., Saha, S., Kumar, A. and Goswami, C., 2019. Plant and natural products as modulators of TRP channels. *Biological Research & Reviews*, *2*, pp.e1363-e1363.

Yang, B.H., Piao, Z.G., Kim, Y.B., Lee, C.H., Lee, J.K., Park, K., Kim, J.S. and Oh, S.B., 2003. Activation of vanilloid receptor 1 (VR1) by eugenol. *Journal of Dental Research*, *82*, pp.781-785.

Yang, S.H., Liu, R., Perez, E.J., Wen, Y., Stevens Jr, S.M., Valencia, T., Brun-Zinkernagel, A.M., Prokai, L., Will, Y., Dykens, J. and Koulen, P., 2004. Mitochondrial localization of estrogen receptor β. *Proceedings of the National Academy of Sciences*, *101*, pp.4130-4135.

Yee, N.S., 2015. Roles of TRPM8 ion channels in cancer: proliferation, survival, and invasion. *Cancers*, *7*, pp.2134-2146.

Yin, Y., Le, S.C., Hsu, A.L., Borgnia, M.J., Yang, H. and Lee, S.Y., 2019. Structural basis of cooling agent and lipid sensing by the cold-activated TRPM8 channel. *Science*, *363*, p.eaav9334.

Yin, Y., Wu, M., Zubcevic, L., Borschel, W.F., Lander, G.C. and Lee, S.Y., 2018. Structure of the cold- and Menthol-sensing ion channel TRPM8. *Science*, *359*, pp.237-241.

Yong, J., Bischof, H., Burgstaller, S., Siirin, M., Murphy, A., Malli, R. and Kaufman, R.J., 2019. Mitochondria supply ATP to the ER through a mechanism antagonized by cytosolic Ca^{2+}. *Elife*, *8*, p.e49682.

Yousuf, M.S., Maguire, A.D., Simmen, T. and Kerr, B.J., 2020. Endoplasmic reticulum–mitochondria interplay in chronic pain: The calcium connection. *Molecular Pain*, *16*, p.1744806920946889.

Yu, X., Yu, M., Liu, Y. and Yu, S., 2016, TRP channel functions in the gastrointestinal tract. *Seminars in Immunopathology* (Vol. 38, No. 3, pp. 385-396). Springer Berlin Heidelberg. (Book)

Zhang, P., Konja, D., Zhang, Y. and Wang, Y., 2021. Communications between mitochondria and endoplasmic reticulum in the regulation of metabolic homeostasis. *Cells*, *10*, p.2195.

Zhang, X., Hu, M., Yang, Y. and Xu, H., 2018. Organellar TRP channels. *Nature Structural & Molecular biology*, *25*, pp.1009-1018.

Zhao, C., Xie, Y., Xu, L., Ye, F., Xu, X., Yang, W., Yang, F. and Guo, J., 2022. Structures of a mammalian TRPM8 in closed state. *Nature Communications*, *13*, pp.1-11

Zhao, Y., Huang, H., Jiang, Y., Wei, H., Liu, P., Wang, W. and Niu, W., 2012. Unusual localization and translocation of TRPV4 protein in cultured ventricular myocytes of the neonatal rat. *European Journal of Histochemistry*, *56*, pp.e32-e32.

Zhao, Y., McVeigh, B.M. and Moiseenkova-Bell, V.Y., 2021. Structural pharmacology of TRP channels. *Journal of Molecular Biology*, *433*, p.166914.

Zhao, Y., Xing, Y., Wang, M., Huang, Y., Xu, H., Su, Y., Zhao, Y. and Shang, Y., 2022. Supramolecular Hydrogel Based on an Osteogenic Growth Peptide Promotes Bone Defect Repair. *ACS Omega*, *7*, pp.11395-11404.

Zheng, J., 2013. Molecular mechanism of TRP channels. *Comprehensive Physiology*, *3*, p.221.

Zholos A, Johnson C, Burdyga T, Melanaphy D. 2011, TRPM channels in the vasculature. *Advances in Experimental Medicine and Biology*. 704:pp. 707-729.

Zhou, X.L., Batiza, A.F., Loukin, S.H., Palmer, C.P., Kung, C. and Saimi, Y., 2003. The transient receptor potential channel on the yeast vacuole is mechanosensitive. *Proceedings of the National Academy of Sciences*, *100*, pp.7105-7110.

Zorova, L.D., Popkov, V.A., Plotnikov, E.Y., Silachev, D.N., Pevzner, I.B., Jankauskas, S.S., Babenko, V.A., Zorov, S.D., Balakireva, A.V., Juhaszova, M. and Sollott, S.J., 2018. Mitochondrial membrane potential. *Analytical Biochemistry*, *552*, pp.50-59.

Zuo, X., Ling, J.X., Xu, G.Y. and Gu, J.G., 2013. Operant behavioral responses to orofacial cold stimuli in rats with chronic constrictive trigeminal nerve injury: effects of Menthol and capsazepine. *Molecular Pain*, *9*, pp.1744-8069.